

2011

## Discrete element methods for asphalt concrete : development and application of user-defined microstructural models and a viscoelastic micromechanical model

Yu Liu

*Michigan Technological University*

Follow this and additional works at: <https://digitalcommons.mtu.edu/etds>



Part of the [Civil and Environmental Engineering Commons](#)

Copyright 2011 Yu Liu

---

### Recommended Citation

Liu, Yu, "Discrete element methods for asphalt concrete : development and application of user-defined microstructural models and a viscoelastic micromechanical model ", Dissertation, Michigan Technological University, 2011.

<https://digitalcommons.mtu.edu/etds/253>

Follow this and additional works at: <https://digitalcommons.mtu.edu/etds>



Part of the [Civil and Environmental Engineering Commons](#)

DISCRETE ELEMENT METHODS FOR ASPHALT CONCRETE: DEVELOPMENT  
AND APPLICATION OF USER-DEFINED MICROSTRUCTURAL MODELS AND A  
VISCOELASTIC MICROMECHANICAL MODEL

By

Yu Liu

A DISSERTATION

Submitted in partial fulfillment of the requirements for the degree of

DOCTOR OF PHILOSOPHY

(Civil Engineering)

MICHIGAN TECHNOLOGICAL UNIVERSITY

2011

© 2011 Yu Liu

This dissertation, “Discrete Element Methods for Asphalt Concrete: Development and Application of User-defined Microstructural Models and a Viscoelastic Micromechanical Model,” is hereby approved in partial fulfillment of the requirements for the DEGREE OF DOCTOR OF PHILOSOPHY IN CIVIL ENGINEERING.

Department of Civil and Environmental Engineering

Signatures:

Dissertation Advisor: \_\_\_\_\_  
Zhanping You

Department Chair: \_\_\_\_\_  
David Hand

Date: \_\_\_\_\_

# Table of Contents

List of Figures .....	xi
List of Tables .....	xv
Preface.....	xvi
Acknowledgements.....	xix
Abstract.....	xx
Chapter 1. Introduction.....	1
1.1. Background .....	1
1.2. Problem Statement .....	2
1.3. Objectives.....	3
1.4. Scopes and Methodology .....	4
1.5. Hypotheses .....	6
1.6. Organization of This Dissertation .....	7
Chapter 2. Literature Review.....	14
2.1. Overview .....	14
2.2. Introduction .....	14
2.3. AC Mixture Composition Characteristics .....	15
2.3.1. Mineral Aggregate Sizes .....	16
2.3.2. Aggregate Morphology .....	19
2.3.3. Asphalt Binder Rheological Properties .....	20
2.3.4. Anisotropic Microstructure of AC Mixture.....	20
2.4. Impact of Mix Composition I: Experiment-Based Methods .....	22
2.5. Impact of Mix Composition II: Micromechanical Models .....	26
2.5.1. Mechanics of Composite Materials .....	26
2.5.2. Micromechanical Models for AC Mixtures .....	29
2.5.3. Summary of Micromechanical Models .....	30
2.6. Impact of Mix Composition III: FE and DE Models .....	31
2.6.1. FE Model Developments and Applications.....	31
2.6.2. DE Model Developments and Applications .....	35
2.6.3. Summary of DE and FE Models .....	40
2.7. Summary and Recommendations.....	40

2.8. Acknowledgements .....	42
Chapter 3. Aspects for Simulating Asphalt Concrete Materials with PFC2D/3D.....	43
3.1. Overview .....	43
3.2. Modeling Concrete-like Materials with PFC2D/3D .....	43
3.3. Reconstruction of AC Geometry with PFC2D/3D.....	44
3.4. Mechanics of DE Model for Concrete Materials .....	46
3.5. Links between Model Inputs and Material Physical Properties.....	46
3.6. Boundary, Initial, and Loading Conditions .....	49
3.7. Simulation and Result Interpretation.....	50
3.7.1. Is It a Static or Dynamic Problem? .....	50
3.7.2. Mechanical Time step Determination .....	51
3.7.3. Mechanical Damping Determination .....	52
3.7.4. Interpretation of Modeling Results.....	53
3.8. Size Effects of Discrete Elements on Modeling Results.....	55
3.8.1. Discrete Element Model of Asphalt Concrete.....	56
3.8.2. Analysis of Mineral Aggregate Shapes .....	57
3.8.3. Discrete Element Modeling of Creep Stiffness .....	59
3.8.4. Summary and Conclusion .....	62
Chapter 4. A Randomly-generated Two-dimensional Model for Simulating AC Microstructure and Mechanical Behavior under Cyclic Loads .....	64
4.1. Overview .....	64
4.2. Introduction .....	64
4.3. Lab Tests and Burger's Model Parameters .....	65
4.3.1. Lab Tests .....	65
4.3.2. Burger's Model parameters.....	65
4.4. Random Polygon Algorithm and DE Geometry Model.....	66
4.5. DE Micromechanical Model .....	66
4.6. Input Parameters.....	68
4.7. DE Modeling .....	69
4.8. Summary and Conclusion .....	71
4.9. Acknowledgement.....	72
Chapter 5. A Randomly Generated 3D Model for Simulation and Visualization of AC Microstructures .....	73

5.1. Abstract .....	73
5.2. Introduction .....	73
5.3. Objectives and Scopes .....	74
5.4. 3D Digital Samples and Mechanical Models .....	74
5.4.1. Digital Samples: a Randomly Generated Model .....	76
5.4.2. Mechanical Models .....	80
5.5. Visualization and Analysis of Asphalt Mixture Structure.....	81
5.5.1. Visualization of Asphalt Mixture Structure .....	82
5.5.2. Analysis of Asphalt Mixture Internal Structure .....	83
5.6. Micromechanical Analysis .....	86
5.6.1. Visualizing Contact Forces and Displacements during Simulation .....	86
5.6.2. Micromechanical Analysis .....	88
5.7. Macro-scale Analysis .....	90
5.8. Summary and Future Study .....	91
5.9. Acknowledgements .....	92
 Chapter 6. Two Idealized Models for Simulating AC Microstructures and Studying Aggregate Morphology .....	 93
6.1. Abstract .....	93
6.2. Research Background.....	93
6.3. Objective and Scope.....	95
6.4. Discrete Element Model Geometry .....	96
6.4.1. Discrete Element R-model .....	97
6.4.2. Discrete Element A-model .....	99
6.5. Discrete Element Model Mechanics.....	102
6.6. DE Simulation of Uniaxial Creep Compliance Tests.....	104
6.7. Observations and Discussion.....	105
6.7.1. Effects of Aggregate Sphericity and Orientation .....	105
6.7.2. Effects of Aggregate Fractured Faces with a DE A-model.....	109
6.8. Summary and Conclusion .....	111
6.9. Acknowledgements .....	112
 Chapter 7. A Viscoelastic Model for Simulating AC Time- and Temperature dependency.....	 113
7.1. Abstract .....	113

7.2. Introduction .....	113
7.2.1. Discrete Element Method.....	113
7.2.2. Review of Current Research Efforts .....	114
7.3. Objectives and Scopes.....	115
7.4. Discrete Element Viscoelastic Model .....	117
7.4.1. Micromechanical Behaviors within Asphalt Mixtures.....	117
7.4.2. Determine Micro-scale Model Parameters.....	119
7.5. Macro-Scale Parameters of Burger Model.....	127
7.5.1. Burger’s Model Under Haversine Loading Condition.....	127
7.5.2. Determine Burger’s Model Parameters .....	129
7.6. Laboratory Tests.....	129
7.7. Discrete Element Simulation of Asphalt Mixture .....	131
7.8. Computation Speed for Viscoelastic Modeling.....	133
7.9. Summary, Conclusions, And Further Research Work .....	134
7.10. Acknowledgements .....	135
 Chapter 8. Determination of Burger’s Model Parameters using Creep-recovery Testing Data.....	 136
8.1. Abstract .....	136
8.2. Introduction .....	136
8.3. Burger’s Model Constitutive Equation.....	137
8.4. Determination of Burger’s model parameters .....	139
8.5. Viscoelastic Analysis of asphalt binder and mastic .....	140
8.6. Summary and Conclusions.....	146
8.7. Acknowledgements .....	147
 Chapter 9. Discrete Element Modeling through User-written C++ Codes .....	 148
9.1. Abstract .....	148
9.2. Introduction .....	148
9.3. Discrete Element Package: Particle Flow Codes .....	149
9.4. User-written C++ Code for Discrete Element Modeling .....	149
9.4.1. Build Digital Samples .....	150
9.4.2. Defining Material Properties .....	150
9.4.3. Loading Conditions .....	151
9.5. Laboratory Tests and Discrete Element Simulation.....	151

9.6. Timing Test: Comparison between C++ and FISH Codes.....	153
9.7. Summary and Conclusions.....	154
9.8. Acknowledgements .....	155
Chapter 10. Accelerated Discrete Element Modeling of Dynamic Modulus Tests with the Frequency-temperature Superposition Principle .....	156
10.1. Abstract: .....	156
10.2. Introduction .....	156
10.3. Objectives and Scopes .....	158
10.4. Experimental Tests and Burger’s Model Parameters .....	160
10.4.1. Dynamic Modulus Test .....	160
10.4.2. Burger’s Model Parameters under Sinusoidal Loads .....	161
10.5. Methodology: Application of Frequency-Temperature Superposition .....	166
10.6. Simulation of Asphalt Mastic Using the 2D DE Model.....	167
10.7. Predict Dynamic Behaviors of Asphalt Mixture .....	171
10.8. Geometric and Mechanical Models.....	172
10.8.1. DE Modeling with Different Random Seeds .....	173
10.8.2. Predict Dynamic Behaviors with 2D and 3D DE Models.....	176
10.9. Computation Time for Viscoelastic DE Modeling.....	178
10.10. Summary and Conclusions .....	180
10.11. Acknowledgements.....	181
Chapter 11. Discrete Element Simulation of Creep Tests using Time-Temperature Superposition .....	182
11.1. Abstract .....	182
11.2. Introduction .....	182
11.3. Objective and Roadmap .....	184
11.4. Reconstruction of an Asphalt Mixture Microstructure.....	185
11.5. Discrete Element Micromechanical Models .....	187
11.6. Time-Temperature Superposition Used in the DE Viscoelastic Model .....	189
11.7. Simulation of Creep Responses with the DE Viscoelastic Model .....	191
11.8. Creep Response Simulation with Microstructural-based DE Elastic Model .....	196
11.9. Comparison and Analysis.....	196
11.10. Summary and Conclusions .....	199
11.11. Acknowledgments.....	200



Chapter 12. 3D Discrete Element Modeling of Asphalt Concrete under Haversine Loading	201
12.1. Abstract .....	201
12.2. Introduction .....	201
12.3. Objectives and Scopes .....	203
12.4. Preliminary Studies .....	204
12.4.1. Reconstruction of Asphalt Mixture Microstructure .....	204
12.4.2. Time-dependent Constitutive Model.....	205
12.4.3. Experimental Measurement.....	206
12.4.4. Acceleration Techniques for DE modeling.....	206
12.5. Three-dimensional Discrete Element Modeling.....	207
12.5.1. Strain Responses under Dynamic Loading .....	207
12.5.2. DE Prediction of Dynamic Modulus and Phase Angle .....	209
12.6. Sensitivity and Effects of DE Modeling under Amplified Frequencies.....	211
12.6.1. Sensitivity Analysis of DE Modeling under Amplified Frequencies..	211
12.6.2. Computation Time of 3D DE Modeling.....	213
12.7. Summary and Conclusions.....	215
12.8. Acknowledgments .....	216
Chapter 13. Discrete Element Simulation for Linking Aggregate Morphological Parameters to AC Creep Stiffness .....	217
13.1. Abstract .....	217
13.2. Introduction .....	217
13.3. Discrete Element Models .....	219
13.4. Creep Testing Simulation and Results .....	221
13.5. Conclusions .....	223
13.6. Acknowledgements .....	224
Chapter 14. 3D Discrete Element Modeling for Stiffness of Sand Mastic versus Stiffness of Asphalt Binder .....	225
14.1. Abstract .....	225
14.2. Introduction .....	225
14.3. Discrete Element Models Of Sand Mastics.....	226
14.4. DE Simulation and Results.....	228
14.5. Discussion: Micromechanical Basis.....	230
14.6. Summary and Conclusion .....	234

14.7. Acknowledgments .....	234
Chapter 15. 3D DE Simulation to Formulate Asphalt Concrete Stiffness for Specific AC Microstructures .....	235
15.1. Abstract .....	235
15.2. Introduction .....	235
15.3. Microstructure-Based Discrete Element Models .....	237
15.4. Microstructure-Based Discrete Element Modeling .....	239
15.5. Formulation of Asphalt Concrete Stiffness .....	240
15.6. Example Application .....	242
15.7. Conclusions .....	244
15.8. Acknowledgements .....	245
Chapter 16. Discrete Element Models of Pavement under a Rolling Wheel .....	246
16.1. Abstract .....	246
16.2. Background .....	246
16.3. Problem Statement .....	248
16.4. Objectives and Scope .....	249
16.5. DE Model for Asphalt Pavement Analyzer (APA) .....	249
16.5.1. Geometry of the DE Model .....	249
16.5.2. Simulation of Wheel Loading .....	250
16.5.3. Mechanics in the APA Model .....	252
16.5.4. Challenges in Simulating Rutting with the APA DE Model .....	253
16.6. DE Model of Pavement under a Rolling Wheel .....	253
16.6.1. Geometry of the DE Model .....	253
16.6.2. Simulation of Wheel Loading .....	254
16.6.3. Mechanics in the Rutting Model .....	254
16.6.4. Challenges in Applying the Rutting Model .....	254
16.7. Normal and Shear Forces under the Rolling Wheel .....	257
16.8. Comparison with Boussinesq Theory .....	258
16.9. Impact of Stiffness Ratio on Poisson Ratio .....	259
16.10. Summary .....	262
Chapter 17. Modeling and Analysis of Dynamic Traffic Loads: An Idealized Discrete Element Model for Pavement-wheel Interaction .....	264
17.1. Abstract .....	264

17.2. Background .....	264
17.3. Objectives and Scopes .....	268
17.4. Discrete Element Model for Pavement-wheel Interaction .....	269
17.4.1. Hypotheses .....	269
17.4.2. Geometry of the DE Model .....	270
17.4.3. Mechanical Model .....	270
17.4.4. Loading Conditions .....	271
17.5. Discrete Element Simulation with different Critical Damping Ratio .....	272
17.5.1. DEM Simulation Result: Horizontal and Angular Velocities .....	274
17.5.2. DEM Simulation Result: Vertical Compressive Force .....	274
17.5.3. DEM Simulation Result: Contact Frictional Force .....	278
17.5.4. DEM Simulation Result: Vertical Velocity of the Rolling Wheel .....	282
17.6. Discrete Element Simulation under Various Rotational Velocities .....	286
17.6.1. DEM Simulation Result: Horizontal Velocity .....	286
17.6.2. DEM Simulation Result: Vertical Compressive Force .....	288
17.6.3. DEM Simulation Result: Frictional Force .....	289
17.7. Summary and Conclusion .....	291
References .....	293
Appendix A: Copyright Clearance .....	307
Appendix B: Computer Programs .....	320
Computer Program 1: Randomly-generated Polygon Model for 2D Microstructure of AC Mixtures .....	320
Computer Program 2: Randomly-generated Polyhedron Model for 3D Microstructure of AC Mixtures .....	326
Computer Program 3: Randomly-generated Ellipsoid Model for 3D Microstructure of AC Mixtures .....	332
Computer Program 4: Viscoelastic DE Modeling of Dynamic /Creep Tests .....	339
Yu Liu's Vita .....	355

# List of Figures

Figure 1.1 Illustration of a possible hybrid method .....	6
Figure 1.2 Organization of this dissertation .....	8
Figure 2.1 Schematics of the AC composition.....	18
Figure 2.2 Demonstration of a composite material design philosophy.....	27
Figure 2.3 Spatial distributions for the example micromechanical models .....	27
Figure 2.4 Summary of DEM models for simulating AC mixtures .....	38
Figure 3.1 Contact Models in PFC2D/3D.....	46
Figure 3.2 Equilibrium of particle-particle contact to beam (RA, RB are radius of particle A and B, respectively, while W, L, and H are three dimensions of the beam).....	48
Figure 3.3 A bending beam test—an illustration of determination between static and dynamic problems	50
Figure 3.4 Calculation cycle in PFC2D/3D .....	52
Figure 3.5 Geometry of the four digital samples for the asphalt concrete .....	55
Figure 3.6 Mineral Aggregate Microstructures of the four AC digital samples ('R' denotes .....	59
Figure 3.7 DE simulation results of creep compliance tests.....	62
Figure 4.1 Burger's model .....	67
Figure 4.2 Virtual sample of asphalt mixture .....	67
Figure 4.3. Calibration for input parameters of Burger's contact model fitted with lab testing data .....	69
Figure 4.4 The applied stress and strain response of the specimens .....	71
Figure 4.5 Comparison of the predicted and measured moduli and phase angles .....	71
Figure 5.1 Procedure for a randomly generated model.....	75
Figure 5.2 Aggregate gradations for three mixtures.....	76
Figure 5.3 Sketch for a randomly generated model .....	77
Figure 5.4 A reference plane for generation of a polyhedron.....	78
Figure 5.5 Examples of randomly created polyhedrons.....	80
Figure 5.6 Visualization of an asphalt mixture sample .....	82
Figure 5.7 Aggregate structures for the three gradations .....	83
Figure 5.8 Normal distribution of mastic, air voids, and aggregate contents .....	85
Figure 5.9 Tensile force distributions within mastic or between aggregates and mastic of the region .....	88
Figure 5.10 Tensile forces vs. Iterative steps: in the figure, K represents one thousand; and M represents one million. ....	90
Figure 5.11 Stress and strain vs time .....	91
Figure 6.1 Definition of the three rotation angles: $\alpha$ , $\beta$ , $\gamma$ .....	98
Figure 6.2 An example of the DE R-Model and individual particles with different SP values .....	98
Figure 6.3 Examples of 3D digital mix specimens .....	102
Figure 6.4 DE simulation results and comparison with the upper and lower bounds .....	104
Figure 6.5 Sphericity index vs. Creep stiffness.....	107
Figure 6.6 Demonstration of the equivalence of the DE R-model to the Voigt model and the Reuss model .....	108
Figure 6.7 Creep stiffness vs. Sample ID (the sample ids are listed in Table 6.2, while legends indicate creep loading time).....	109
Figure 6.8 Creep stiffness ratio vs. Loading time.....	110
Figure 7.1 Digital sample with image-based model.....	116

Figure 7.2 Sketch of interactions and the corresponding constitutive models within the digital sample of asphalt mixtures.....	119
Figure 7.3 Conversion of Burger’s model parameters between mastic and aggregate balls.....	125
Figure 7.4. Burger’s model .....	126
Figure 7.5 Conversion of Burger’s model parameters of two contacting mastic balls.....	126
Figure 7.6. The applied stress and strain response.....	132
Figure 7.7 Dynamic modulus and phase angle .....	133
Figure 8.1 Burger’s Model.....	138
Figure 8.2 Shear compliances vs. Time of the binder and mastics .....	143
Figure 8.3 Phase angles vs. Temperatures of the binder and mastics .....	143
Figure 8.4 Ratio of the viscous flow to the elasticity vs. Creep time of binder and mastics.....	146
Figure 9.1. Digital samples of asphalt mixture with user-written C++ code.....	150
Figure 9.2 Speed ratio vs. Loading time for 5 samples (legend shows the number of discrete elements)	152
Figure 9.3 Average speed ratio of 7 hours’ loading simulation time vs. Sizes of samples.....	154
Figure 10.1 Dynamic moduli and phase angles from measurement of asphalt mastic .....	159
Figure 10.2 Dynamic moduli and phase angles from measurement of asphalt mixture .....	161
Figure 10.3 Burger’s model.....	163
Figure 10.4 M-K circle to determine Burger’s model parameters .....	165
Figure 10.5 Procedure to determine Burger’s model parameters under a real dynamic modulus test loading condition .....	165
Figure 10.6 Stress & strain vs. Time curve from a simulation output data .....	169
Figure 10.7 Comparison between prediction and measurement of dynamic moduli and phase angles....	171
Figure 10.8 Example of asphalt mixture microstructure (the white elements represent the asphalt sand mastic while the others represent coarse aggregates of different sizes).....	172
Figure 10.9 Configuration of the DE viscoelastic model (Liu et al. 2009).....	173
Figure 10.10 Comparison between prediction and measurement of different random seeds.....	176
Figure 10.11 2D and 3D modeling vs. Laboratory results of asphalt mixture.....	178
Figure 11.1 Reconstructed three-dimensional microstructure of an asphalt mixture (dark-colored elements represent the upper and lower loading platens; white elements represent the asphalt sand mastic; grey elements symbolize mineral aggregates).....	186
Figure 11.2 Sketch of interactions and the corresponding constitutive models within the digital sample of asphalt mixtures (Liu et al. 2009) .....	188
Figure 11.3 Research methodology flow chart for modeling with the DE elastic model.....	189
Figure 11.4. Research methodology flow chart for modeling with the DE viscoelastic model.....	192
Figure 11.5 Creep stiffness of the asphalt sand mastic .....	193
Figure 11.6 Results of DE viscoelastic modeling with different shifting factors (the legends represent shifting factors, for example, 1000 means the shifting factor=1000).....	194
Figure 11.7 Predicted creep stiffness at the reference temperature vs. The logarithmic reduced time (‘T’ in the legend is the real temperature, not the reference temperature) .....	194
Figure 11.8 Predicted creep stiffness at the real temperature vs. The logarithmic loading time.....	195
Figure 11.9 Predicted creep stiffness vs. The logarithmic loading time .....	195
Figure 11.10 Measured creep stiffness of the asphalt mixture vs. The logarithmic loading time .....	197
Figure 11.11 Comparisons of DE modeling with the experimental measurements.....	199
Figure 12.1. Three-dimensional visualization of X-ray Computed Tomography images .....	204
Figure 12.2. Strain responses of laboratory testing and DE modeling at 13°C (under an amplified frequency of 25000Hz).....	209

Figure 12.3. Dynamic Modulus and Phase Angle comparison between 3D prediction and the measurement (under an amplified frequency of 25000Hz) .....	210
Figure 12.4. Predicted dynamic modulus vs. Amplified frequencies at 21°C .....	212
Figure 12.5. Comparison of predicted dynamic moduli with laboratory values at 21°C .....	213
Figure 12.6. Sensitivity analysis of DE modeling under amplified frequencies .....	213
Figure 13.1 Definition of the three rotation angles: $\alpha$ , $\beta$ , and $\gamma$ .....	220
Figure 13.2 A DE R-model (SP=0.7; $\beta=0$ , $\gamma=0$ , $\alpha=30$ ) .....	220
Figure 13.3 Typical DE simulation results .....	223
Figure 14.1 Gradation graphs of coarse and fine sands .....	228
Figure 14.2: Examples of the digital coarse sand mastics .....	228
Figure 14.3 Sand mastics stiffness VS. Stiffness ratio of sands to asphalt (asphalt content: 42.15%, 52.4%, 61.8%, 70.8%, 80.3%, and 90%).....	230
Figure 14.4 Curves of $R_m$ vs. $R_s$ for the Voigt and Ruess models ( $R_m$ is the ratio of sand mastic to asphalt, $R_s$ is the ratio of sands to asphalt).....	232
Figure 14.5 Curves of stiffness ratios of sand mastics to asphalt vs. Those of sands to asphalt. ....	233
Figure 15.1 Examples of microstructures for two-phase micromechanical models .....	237
Figure 15.2 Reconstructed three-dimensional microstructure and air void distribution .....	238
Figure 15.3 DE modeling results of model-I and model-II.....	240
Figure 15.4 Strain concentration factor versus stiffness ratio for various models.....	241
Figure 15.5 Comparisons of different models as well as laboratory measurements .....	243
Figure 16.1 APA Rutting-model Setting-up Demonstration .....	250
Figure 16.2 APA rutting testing in laboratory .....	251
Figure 16.3 APA Rutting-model and Contact Forces under the Rolling Wheel .....	252
Figure 16.4 Interaction between an elastic element and a viscoelastic element.....	252
Figure 16.5 DE model of pavement under a rolling wheel .....	255
Figure 16.6 Demonstration of rutting simulation under the rolling wheel: horizontal velocity vs. Computational cycles.....	255
Figure 16.7 Demonstration of a challenge in using the Rutting Model .....	256
Figure 16.8 Newly developed elements with more contacts .....	256
Figure 16.9 Stresses under the rolling wheel.....	258
Figure 16.10. Absolute error between the simulation results and those calculated from Boussinesq theory (Unit: %).....	259
Figure 16.11 Setting-up for a triaxial test .....	260
Figure 16.12 Views of the Testing Specimen from Different Angles .....	261
Figure 16.13 Poisson ratio vs. Stiffness ratio .....	261
Figure 17.1 Illustration of the idealized discrete element model.....	269
Figure 17.2 Typical motion feature of the rolling wheel.....	271
Figure 17.3 Typical motion feature of the rolling wheel (the different colors of the curves indicate that different motion features: acceleration, steadily moving, and deceleration).....	272
Figure 17.4 Vertical compressive force vs. Loading time when the wheel rolling along pavement surface (peak rotational velocity=10rad/s; the different colors of the curves indicate that different motion features: acceleration, steadily moving, and deceleration) .....	276
Figure 17.5 Average, maximum, and minimum values of the vertical force vs. Critical damping ratio during the wheel accelerating, steadily moving, and decelerating .....	278
Figure 17.6 Frictional force vs. Loading time when the wheel rolling along pavement surface (peak rotational velocity=10rad/s; the different colors of the curves indicate that different motion features: acceleration, steadily moving, and deceleration).....	280

Figure 17.7 Average, maximum, and minimum values of the frictional force vs. Critical damping ratio during the wheel accelerating, steadily moving, and decelerating..... 282

Figure 17.8 Vertical velocity vs. Loading time when the wheel rolling along pavement surface (peak rotational velocity=10rad/s; the different colors of the curves indicate that different motion features: acceleration, steadily moving, and deceleration)..... 284

Figure 17.9 Average, maximum, and minimum values of the vibration vs. Critical damping ratio during the wheel accelerating, steadily moving, and decelerating ..... 286

Figure 17.10 Horizontal velocity vs. Loading time when the wheel rolling along pavement surface (*peak rotational velocity=10, 20, and 100rad/s and damping ratio=0.5*; the different colors of the curves indicate that different motion features: acceleration, steadily moving, and deceleration)..... 288

Figure 17.11 Vertical compressive force vs. Loading time when the wheel rolling along pavement surface (*peak rotational velocity=10, 20, and 100rad/s and damping ratio=0.5*; the different colors of the curves indicate that different motion features: acceleration, steadily moving, and deceleration)... 289

Figure 17.12 Vertical compressive force vs. Loading time when the wheel rolling along pavement surface (*peak rotational velocity=10, 20, and 100rad/s and damping ratio=0.5*; the different colors of the curves indicate that different motion features: acceleration, steadily moving, and deceleration)... 291

# List of Tables

Table 2.1	superpave aggregate testing protocols .....	19
table 2.2	research effects with the experiment-based methods .....	23
table 2.3	formulations of a2 for some micromechanical models .....	28
table 2.4	summary of the models for rebuilding ac microstructures .....	38
table 3.1	three types of elements for building a pfc2d/3d model.....	45
table 3.2	boundary conditions in pfc2d/3d .....	49
table 3.3	determination of mechanical timestep in pfc2d/3d .....	51
table 3.4	selection of mechanical damping in pfc2d/3d .....	53
table 3.5	indicators for interpretation of a pfc2d/3d modeling results .....	54
table 3.6	input parameters of the discrete element simulation .....	60
table 3.7	volumetric percentages and time_steps for the four ac digital samples .....	62
table 6.1	mineral aggregate gradation used in the 108 de models .....	99
table 6.2	18 digital mix specimens prepared with the de a-model .....	101
table 6.3	inputs of the de viscoelastic model used in this study .....	105
table 7.1	gradation of the asphalt mixture .....	130
table 7.2	laboratory test results of aggregates, asphalt mastic and mixture .....	130
table 7.3	burger’s model parameters fitted using lab data .....	130
table 8.1	average absolute errors (aaes) for fitting creep-recovery test datum (%).....	144
table 8.2	burger’s model parameters under creep-recovery tests .....	144
table 9.1	gradation of the asphalt mixture (dai and you 2008; liu and you 2008; you and buttlar 2006)..	152
table 9.2	laboratory test results of aggregates, asphalt mastic and mixture .....	153
table 9.3	burger’s model parameters fitted using lab data .....	153
table 10.1	aggregate gradation for asphalt mixture .....	158
table 10.2	the fitted burger’s model parameters of asphalt mastic.....	169
table 10.3	average errors of dynamic moduli and phase angles .....	177
table 10.4	computation times for the 2d and 3d de models with traditional method .....	179
table 11.1	an incomplete international review of the dem study in pavement area.....	183
table 11.2	aggregate gradation .....	185
table 11.3	real burger’s model parameters of the three temperatures in viscoelastic models.....	193
table 11.4	computation time comparison .....	199
table 12.1	an incomplete summary of methodologies used in the studies with dem.....	202
table 12.2	computational time required for de modeling using laboratory frequencies .....	214
table 13.1	inputs of the de viscoelastic model used in this study.....	220
table 14.1	inputs for the de model.....	229
table 15.1	aggregate gradation .....	239
table 15.2	dynamic modulus of the asphalt sand mastic (mpa).....	242
table 15.3	dynamic modulus of the asphalt concrete (mpa) .....	243
table 16.1	loading conditions.....	262
table 17.1	inputs for dem simulation under different damping ratios.....	273



## Preface

This dissertation is organized as a collection of journal and conference articles. A total of 13 articles are included in this dissertation. Followed is the basic information of those articles including journal or conference names, article titles, authorship, and etc.

Chapter 2 of this dissertation is from an article published by Taylor & Francis in the International Journal of Pavement Engineering, Vol 12, No. 4 in 2011. The title of this paper is “Review of Advances in Understanding Impacts of Mix Composition Characteristics on Asphalt Concrete (AC) Mechanics”, by Yu Liu, Zhanping You, Qingli Dai, and Julian Mills-Beale. The dissertation author (Yu Liu) collected literatures, analyzed them, and wrote this article with Dr. Zhanping You, Dr. Qingli Dai, and Mr. Julian Mills-Beale.

Chapter 4 of this dissertation is from an article published by American Society of Civil Engineers (ASCE) as a conference proceeding paper in 2008. The title of this paper is “Simulation of Cyclic Loading Tests for Asphalt Mixtures Using User Defined Models within Discrete Element Method”, by Yu Liu and Zhanping You. The dissertation author (Yu Liu) developed the programming codes, collected the simulation data, analyzed the data, and wrote this article with Dr. Zhanping You.

Chapter 5 of this dissertation is from an article published by American Society of Civil Engineers (ASCE) in Journal of Computing in Civil Engineering, Vol. 23, Issue 340, in 2009. The title of this paper is “Visualization and Simulation of Asphalt Concrete with Randomly Generated Three-Dimensional Models”, by Yu Liu and Zhanping You. The dissertation author (Yu Liu) developed the method, collected simulation data, and analyzed the data, and wrote this article with Dr. Zhanping You.

Chapter 6 of this dissertation is from an article published by American Society of Civil Engineers (ASCE) in Journal of Engineering Mechanics. The article was posted ahead of print in October 2010. The title of this paper is “Discrete Element Modeling: Impacts of Aggregate Sphericity, Orientation, and Angularity on Creep Stiffness of Idealized Asphalt Mixtures”, by Yu Liu and Zhanping You. The dissertation author (Yu Liu) developed the programming codes, collected the simulation data, analyzed the data, and wrote this article with Dr. Zhanping You.

Chapter 7 of this dissertation is from an article published by American Society of Civil Engineers (ASCE) in Journal of Engineering Mechanics, Vol. 135, No. 324, in 2009. The title of this paper is “Viscoelastic Model for Discrete Element Simulation of Asphalt Mixtures”, by Yu Liu, Qingli Dai, and Zhanping You. The dissertation author (Yu Liu) developed the method collected the simulation data, analyzed the data, and wrote this article with Dr. Qingli Dai and Dr. Zhanping You.

Chapter 8 of this dissertation is from an article published by American Society of Civil Engineers (ASCE) as a conference proceeding paper in 2008. The title of this paper is “A method to determine Burger’s Model Parameters using Creep-recovery Testing Data”, by Yu Liu and Zhanping You. The dissertation author (Yu Liu) developed the method, collected the data, analyzed the data, and wrote this article with Dr. Zhanping You.

Chapter 9 of this dissertation is from an article published by American Society of Civil Engineers (ASCE) as a conference proceeding paper in 2008. The title of this paper is “Speed Up Discrete Element Simulation of Asphalt Mixtures with User-written C++ Codes”, by Yu Liu and Zhanping You. The dissertation author (Yu Liu) wrote this article with Dr. Zhanping You.

Chapter 10 of this dissertation is from an article published by American Society of Civil Engineers (ASCE) in Journal of Engineering Mechanics. The article was posted ahead of print on November 2010. The title of this paper is “Accelerated Discrete Element Modeling of Asphalt-based Materials with the Frequency-temperature Superposition Principle”, by Yu Liu and Zhanping You. The dissertation author (Yu Liu) developed the method, collected the simulation data, analyzed the data, and wrote this article with Dr. Zhanping You.

Chapter 11 of this dissertation is from an article published by American Society of Civil Engineers (ASCE) in Journal of Materials in Civil Engineering, Vol. 23, Issue 79, in 2011.. The title of this paper is “Three-Dimensional Microstructural-based Discrete Element Viscoelastic Modeling of Creep Compliance Tests for Asphalt Mixtures”, by Zhanping You, Yu Liu, and Qingli Dai. The dissertation author (Yu Liu) developed the method, collected the simulation data, analyzed the data, and wrote this article with Dr. Zhanping You and Dr. Qingli Dai.

Chapter 12 of this dissertation is from an article published by LAVOISIER in Journal of Road Materials and Pavement Design, Vol. 11, Issue 2, in 2010. The title of this paper is “Three-Dimensional Simulation of Asphalt Concrete Subjected to Haversine Loading: An Application of Frequency-temperature Superposition Technique”, by Zhanping You and Yu Liu. The dissertation author (Yu Liu) developed the method, collected the simulation data, analyzed the data, and wrote this article with Dr. Zhanping You.

Chapter 13 of this dissertation is from an article published by American Society of Civil Engineers (ASCE) as a conference proceeding paper in 2010. The title of this paper is “Discrete Element Simulation of Aggregate Sphericity and Orientation: An Approach to Improving the Understanding of Asphalt Concrete”, by Yu Liu and Zhanping You. The dissertation author (Yu Liu) developed the programming codes, collected the simulation data, analyzed the data, and wrote this article with Dr. Zhanping You.

Chapter 14 of this dissertation is from an article published by American Society of Civil Engineers (ASCE) as a conference proceeding paper in 2010. The title of this paper is “Stiffness of Sand Mastic versus Stiffness of Asphalt Binder Using Three-Dimensional Discrete Element Method”, by Yu Liu, Zhanping You, and Qingli Dai. The dissertation

author (Yu Liu) developed the method, collected the data, analyzed the data, and wrote this article with Dr. Zhanping You and Dr. Qingli Dai.

Chapter 15 of this dissertation is from an article published by American Society of Civil Engineers (ASCE) as a conference proceeding paper in 2010. The title of this paper is “Formulization of Asphalt Concrete Stiffness for Specific Microstructures Based on Discrete Element Method”, by Yu Liu and Zhanping You. The dissertation author (Yu Liu) developed the method, collected the data, analyzed the data, and wrote this article with Dr. Zhanping You.

## Acknowledgements

I would like to express my special thanks and sincere appreciation to my advisor, Dr. Zhanping You, who has brought me a continuous motivation, research enthusiasm, encouraged supervision, and strong support. His continued guidance, patience, friendly attitude, and financial support provided me the inspiration and confidence to achieve my research goal. I express the deepest respect and sincere admiration for him.

I wish to extend my sincere thanks to Dr. Jacob Hiller, Dr. Gregory M. Odegard, and Dr. Qingli Dai for serving as committee members and providing me good suggestions during my Ph.D. study. I wish to extend my special thanks to Dr. Zhanping You, Dr. Jacob Hiller, and Dr. Qingli Dai for suggestions and help in my job hunting. I wish to extend my special thanks to my M.S. advisor Prof. Zhaoran Xiao and my former employer Dr. Xianguang Hu for their advisory and support before I came to United States for my Ph.D. study.

I would like to acknowledge the National Science Foundation of the United States, Michigan Department of Transportation (MDOT), and Graduate School of Michigan Technological University for financial support. I wish to extend my special thanks to Ms. Neil V. Hakala who endowed the finishing fellowship through the Graduate School of Michigan Technological University in Fall of 2010.

I am indebted to my colleagues Shu Wei Goh, Julian Mills-Beale, Baron Colbert, Sanjeev Adhikari, Haizhu Lu, Hui Yao, Hainian Wang, Chris DeDene, Qian Zhang, Zhixi Yang, Yinhong Qin, Marliana Azura for their kindness and precious discussion.

Finally, I heartily appreciate my wife Yunhuan Liu, daughter Sara Liu, son Alex Liu, father Jiming Liu, mother Jingying Duan for their endless love, huge patience, and strong support.

## Abstract

As an important Civil Engineering material, asphalt concrete (AC) is commonly used to build road surfaces, airports, and parking lots. With traditional laboratory tests and theoretical equations, it is a challenge to fully understand such a random composite material. Based on the discrete element method (DEM), this research seeks to develop and implement computer models as research approaches for improving understandings of AC microstructure-based mechanics. In this research, three categories of approaches were developed or employed to simulate microstructures of AC materials, namely the randomly-generated models, the idealized models, and image-based models. The image-based models were recommended for accurately predicting AC performance, while the other models were recommended as research tools to obtain deep insight into the AC microstructure-based mechanics. A viscoelastic micromechanical model was developed to capture viscoelastic interactions within the AC microstructure. Four types of constitutive models were built to address the four categories of interactions within an AC specimen. Each of the constitutive models consists of three parts which represent three different interaction behaviors: a stiffness model (force-displace relation), a bonding model (shear and tensile strengths), and a slip model (frictional property). Three techniques were developed to reduce the computational time for AC viscoelastic simulations. It was found that the computational time was significantly reduced to days or hours from years or months for typical three-dimensional models. Dynamic modulus and creep stiffness tests were simulated and methodologies were developed to determine the viscoelastic parameters. It was found that the DE models could successfully predict dynamic modulus, phase angles, and creep stiffness in a wide range of frequencies, temperatures, and time spans. Mineral aggregate morphology characteristics (sphericity, orientation, and angularity) were studied to investigate their impacts on AC creep stiffness. It was found that aggregate characteristics significantly impact creep stiffness. Pavement responses and pavement-vehicle interactions were investigated by simulating pavement sections under a rolling wheel. It was found that wheel acceleration, steadily moving, and deceleration significantly impact contact forces. Additionally, summary and recommendations were provided in the last chapter and part of computer programming codes were provided in the appendixes.

# Chapter 1. Introduction

The purpose of this chapter is to give an introduction of this dissertation which includes research background, problem statement, objectives, scopes and methodology, hypotheses, organization of this dissertation.

## 1.1. Background

As described in the literature (Schwartz and Carvalho 2007), a pavement basic geometry is quite simple, but its material composition, mechanical properties, and loading conditions are challenging for pavement engineers or researchers. First of all, pavement materials have complex microstructure and mechanical properties. For example, asphalt concrete (AC) is one of the typically used pavement materials which is composed of mineral aggregates, asphalt binder, additives, and air voids. Mineral aggregates have a wide range of sizes (from as large as 37.5mm to as small as several micrometers), irregular shapes, and various values of roughness, frictional properties, and other characteristics. Asphalt has time- and temperature-dependency: at a high temperature (over 100C), it can be as soft as a liquid; while at a low temperature (below 0C), it can be as hard as a stone. Secondly, there are many factors which can influence the pavement responses under traffic loads, such as stress state, stress magnitude, temperature, moisture, loading time, and loading rate. Additionally, traffic loading conditions are impacted by vehicle axle types, axle loads, motion features (acceleration, steadily moving, or deceleration), and other factors (pavement surface textures, frictional properties).

Due to the complexity of pavement system, the majority of the public roads in the United States have been built with empirical methods. For instance, the American Association of State Highway and Transportation Officials (AASHTO) design guides (AASHTO 1962, 1972, 1986, and 1993) were the most widely used empirical design methods for pavement structures in the past decades. The Superpave mix design method is the most commonly used empirical design method for AC mixtures. It is worth noting that the AASHTO design guides were developed from the AASHTO Road Test which was conducted in the late 1950s. Superpave mix design method was also developed from a large amount of tests in the laboratory or field. Obviously, the differences have been becoming larger and larger from year to year in terms of traffic volumes, construction materials, vehicle types, and others. Even though adjustments and modifications were made over years using the performance data from existing pavements, empirical methods as design tools for pavement structures or AC mixtures are still very limited (Schwartz and Carvalho 2007).

As mentioned in the literature (Sun and Deng 1998), high speeds, heavy loads, and large traffic volume had become the three most significant characteristics of modern transportation. In order to meet the rapid changing reality, improved methods are needed for pavement structural and material design. Even though empirical methods may exhibit good accuracy sometimes, they are valid only for the materials and climate conditions similar to those for which they were developed. The need to upgrade those empirical

methods is also very time-consuming and expensive. Therefore, an empirical approach was often employed as an expedient for both pavement material and structure design when the precise cause-and-effect relationships were too difficult to be defined theoretically. With advances in computational mechanics and computer technologies, it becomes possible to predict the precise cause-and-effect relationships by incorporating more realistic features such as material nonlinearities, rate effects, and microstructures. Therefore, it is the time to move one step forward from currently used empirical methods for both pavement structure and material design.

## 1.2. Problem Statement

As demonstrated in the comprehensive literature review of Chapter 2, a) testing equipments (Superpave mix tests, binder tests, aggregate tests) were developed to measure both AC and its constituents' properties; b) imaging technologies were newly applied for characterizing AC microstructures; c) advanced computer modeling methods (finite element methods and discrete element methods) were developed and verified for simulating microstructure-based mechanics of AC materials; d) close-form equations were implemented to formulate the link of the microstructural parameters of a composite (such as proportions, properties, and distributions of its constituents) to its overall mechanical properties (such as stiffness, strength). Additionally, from the literature review, the following issues were recognized:

- 1) Research efforts have been made in the past hundred years with purpose to characterize the AC materials with experimental methods. Their observations, however, sometimes were conflicting due to the following reasons:
  - a) Since most experimental testing methods were developed for certain practical uses other than particularly designed for research purposes, they had very limited capabilities to characterize the links between AC and its components.
  - b) Researchers utilized different testing methods for various material resources. As a result, their observations or conclusions were difficult to be prepared, even though in most of the cases they seemed similar to each other.
  - c) Their observations were combinations of many impact factors (eg. asphalt properties, aggregate sizes, shapes, angularities, air voids, etc.) instead of those (eg. aggregate shapes, orientation angles, etc.) which the researchers intended to investigate.
- 2) The existing close-form equations were too simple to represent the complex microstructural and micromechanical features of an AC mixture. To extend the usefulness of the existing equations, researchers usually modified them with the laboratory or field testing data. The modified versions of the equations were often referred to as empirical equations. Those empirical equations were useful for the particular material resources and testing conditions in which they had been developed. However, they have to be updated when the material resources and the testing conditions are different.

- 3) In the past two decades, many researchers utilized both computer modeling and imaging techniques to predict AC mechanical properties. Those existing research efforts were important since they verified the accuracy of computer modeling models and provided additional approaches to characterize AC materials. However, it is challenging to expect that the existing computer model can be utilized as a prediction tool to provide design data in practical projects due to the following reasons:
  - a) They are expertise-required. In other words, special knowledge or skills are required for performing a computer modeling.
  - b) They are time-consuming if both microstructural features and time-dependent mechanical properties are simulated. As demonstrated in this dissertation, some modeling work may take several months or years if both complex geometrical information and mechanical behaviors are considered without advanced techniques utilized.
  - c) They cannot be perfect no matter how much effort researchers contribute: Simple models are easy-understood, but they provide very limited information. By contrast, a complex model may provide more accurate information, but it may be not as useful as it is expected. The reason is that the complexity of the complex model is comparable to its counterpart in the reality. As a result, few people can understand the model except the researchers who have developed the model.

In summary, experiment-based approaches are the most direct and persuasive tools to provide design data in practical projects of pavement engineering. However, they have limited capabilities in studying fundamentals of AC materials at microscopic levels. Close-form equations are often theory-based and the most accurate solutions to problems whose conditions are identical to those in which the equations were developed. In structural engineering, analytical equations are often employed for preliminary design of complex structures or for final design of simple structures. However, in pavement engineering, it is still challenging to apply the exiting analytical solutions for providing design data in practical projects. Alternatively, computer modeling approaches are becoming more and more popular for solving engineering problems through providing deeper insights of the target problems. However, it is still challenging to implement computer models as prediction tools even though their accuracy has been proved.

### **1.3. Objectives**

Instead of utilizing computer modeling models as prediction tools for practical use, this dissertation seeks to develop and implement them as research approaches for improving understandings of AC microstructure-based mechanics. Followed are the three main objectives of this dissertation:

- 1) The first objective is to develop user-defined computer models to construct AC microstructures based on the discrete element method (DEM). In most of the existing studies, the image-based models were utilized to reconstruct AC microstructure through processing the real AC mixture's images. Apparently, they are the most accurate approaches to represent AC microstructural features. However, the process



of preparing an image-based model is much more complex and time-consuming than that of preparing an AC sample in the laboratory. By contrast, the newly developed user-defined microstructural models in this dissertation can bring the following benefits:

- a) They are lab-independent. Users can easily build a digital sample to simulate AC microstructure through controlling the given parameters, such as gradation, shape, angularity, orientation, and volumetric proportion of mineral aggregates, sizes, volumetric percentage, and gradation of air voids, and asphalt content.
  - b) They allow users to emphasize certain microstructural parameters and minimize influences of other factors. For instance, users are able to build a set of digital samples which have different aggregate shapes and identical values of the other volumetric and mechanical parameters.
- 2) The second objective is to develop a viscoelastic model for simulating the micromechanical interactions within the AC microstructures. Four typical interactions are considered in the newly developed model: interactions between individual aggregate particles, those between an individual particle and asphalt mastic, those within an individual aggregate particle, and those within the asphalt mastic. The four interactions are simulated with the four constitutive models which are built at individual contacts of discrete elements. The corresponding approaches were also developed to convert the microscopic parameters of the viscoelastic model to those from the regular laboratory tests. Additionally, three approaches were developed to reduce the computational time of the viscoelastic modeling of AC mechanics.
- 3) The third objective is to implement those developed microstructural and micromechanical models to simulate dynamic and creep stiffness, pavement responses under a rolling wheel load, and pavement-wheel interaction. Through analyzing simulation results, the ultimate goal of this research is to link microstructural parameters to overall mechanical behaviors/parameters of AC under different loading conditions.

## **1.4. Scopes and Methodology**

The scope of this dissertation is mainly limited to computer modeling of AC materials using DEM. Even though both the finite element method (FEM) and the DEM were recommended to characterize AC materials in the literature review of Chapter 2, the DEM was selected in this dissertation study due to its efficiency in simulating AC materials:

- a) DEM has been widely used for studying geo-materials (soils, rocks, and granular materials) as an efficient approach. In a typical asphalt concrete sample, granular materials compose the majority of the mass or volume.
- b) With DEM, simple constitutive models can simulate complex mechanical behaviors. For instance, particle flow and particle-particle interaction are complex mechanical problems which can be simulated with linear-elastic contact model in DEM.

c) With DEM, it is nature and straightforward to simulate the dynamic behaviors of pavement materials under traffic loads. As demonstrated in Chapters 16 and 17 of this dissertation, the wheel-pavement dynamic interaction behaviors were directly simulated with DEM.

There are a few commercial DEM codes available, such as PFC2D&3D, EDEM, UDEC, etc. PFC2D and PFC3D were selected in this study due to their accuracy and efficiency in simulating AC materials. The PFC2D and PFC3D stand for Particle Flow Codes in two-dimensional (2D) and three-dimensional (3D), respectively. Additionally, both the laboratory testing and analytical solutions of composite mechanics are also involved as auxiliaries to provide inputs, verification, and theoretical basis. Figure 1.1 shows the general methodology of this study. In the figure, the solid arrows connect topics related to numerical modeling approaches which play the primary roles in this research. The dotted arrows connect topics related to experimental tests and analytical equations which play auxiliary roles. This study starts from measuring asphalt or mastic properties in the laboratory, developing numerical models, and setting up loading conditions. Then, it is followed by a series of numerical simulations which are categorized into three groups:

- 1) First of all, simulation results are compared with those from the experimental tests of AC mixtures. The objective is to verify or calibrate the numerical models. It is obviously important: only validated numerical models are able to produce reliable or reasonable predictions which can be further utilized to improve understandings of AC materials.
- 2) Secondly, simulation results are utilized to modify the existing analytical equations. The objective is to develop numerical modeling-based ‘empirical’ models through modifying the analytical equations with numerical modeling results. On the one hand, analytical equations are simple and theory-based. Therefore, they are easy to be accepted by engineers or designers. On the other hand, numerical modeling can provide more complex information which is beyond of capabilities of simple analytical equations. Traditionally, researchers usually modified analytical equations using experimental testing data. As discussed in previous sections, those traditional empirical methods are highly dependent on testing conditions, material resources, and testing methods. Different from the traditional empirical methods, the numerical modeling-based ‘empirical’ models are less lab-dependent and can be served as universal solutions for predicting AC performance from its microstructural features and components’ mechanical properties.
- 3) Thirdly, simulation results are directly analyzed. After the simulation results are analyzed, there are two directions: the first one is to predict AC behaviors for providing design data. Usually complex model is needed to accurately represent AC microstructural and mechanical properties. The second one is to study microstructure-based mechanics of AC materials for research purpose. In this case, AC can be simulated with idealized models in order to emphasize certain special parameters as demonstrated in Chapter 6 of this dissertation.

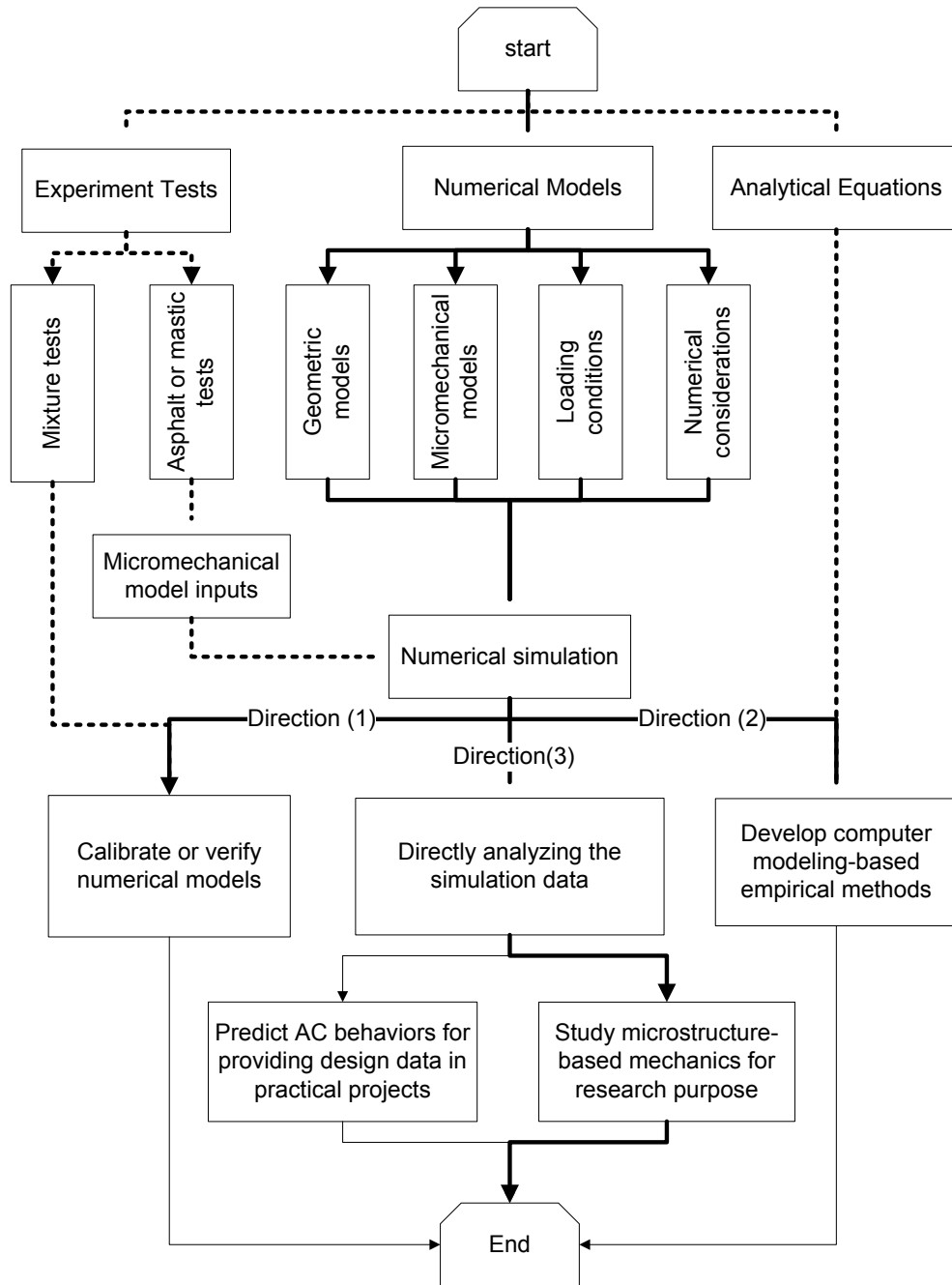


**Figure 1.1 Illustration of a possible hybrid method**

## 1.5. Hypotheses

As mentioned in the section 1.2, no perfect models are available. On the one hand, a simple model cannot exactly represent its counterpart, but it is easy to be understood and accepted by engineers or researchers with limited knowledge. Additionally, a simple model can be used to emphasize certain features with less influence of unnecessary interference factors. On the other hand, a complex model is accurate, but it is not easy to

be implemented due to its complexity. Additionally, it could be as complex as or more complex than its counterpart. If that is the case, it is unnecessary to develop such a complex model. Therefore, it is necessary to balance advantages and disadvantages of complex and simple models at the beginning of this dissertation research. In order to fulfill the objectives and scopes above, followed are five hypotheses for this dissertation research:

- 1) The image-based model can be utilized to calibrate the discrete element mechanical models with more accuracy. The randomly-created polyhedron or polygon models can be used to predict the AC mechanical properties, such as dynamic modulus and phase angles. The idealized R-model and A-model can be used to understand the isolated impacts of mineral aggregate morphology characteristics on creep stiffness of AC materials
- 2) The newly developed viscoelastic model can be used to simulate time-dependent properties of AC materials. The accelerated discrete element modeling techniques are able to significantly reduce the computational time which is required for simulating time-dependent properties of AC materials.
- 3) The newly developed computer modeling techniques in this dissertation can be served as useful research tools for understanding AC material mechanical behaviors with its constituents' properties and microstructure considered. They can be used to develop simple computer modeling-based 'empirical' models.
- 4) The newly developed approaches for determining model input parameters are reasonable and reliable for the discrete element simulation.
- 5) The newly developed model for wheel-pavement interaction is rational and can be used for further studies.

## **1.6. Organization of This Dissertation**

This dissertation is organized as a collection of published, submitted, or ongoing technical articles. The individual chapters consist of individual journal or conference articles which have been published, submitted, or going to be submitted for publication. Figure 1.2 shows the organization of chapters and appendices which are related to different research topics: Chapter 1 gives a introduction of this dissertation, chapter 2 reports literature review results, chapter 3 gives a introduction of PFC2D/3D which are the two commercial DEM codes utilized in this study, chapters 4~6 are linked to objective 1, Chapters 7~11 are linked to objective 2, Chapter 12~17 are linked to objective 3, and Chapter 18 gives summary and recommends future works.

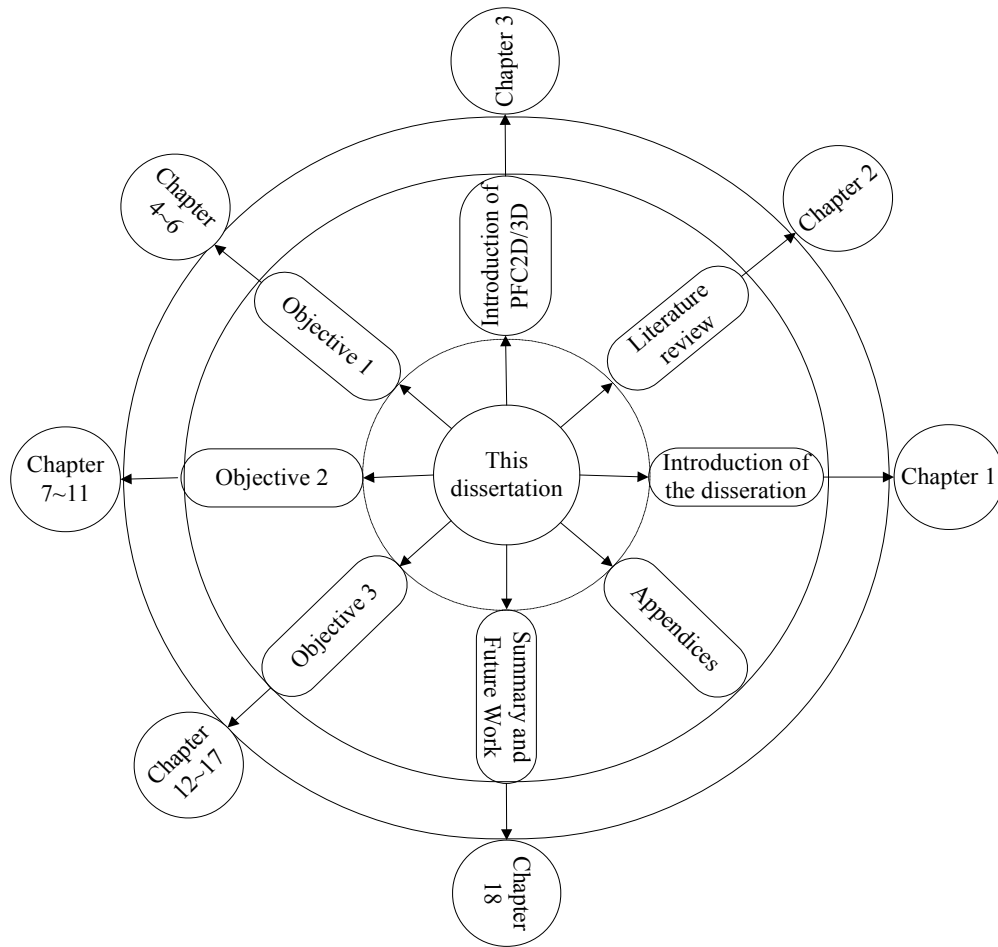


**Figure 1.2 Organization of this dissertation**

Followed is a brief introduction of each chapter:

Chapter 1 presents an introduction of this dissertation, which includes research background, hypothesis, objectives, scopes, and organization of this dissertation.

Chapter 2 presents a comprehensive review of the advances in understanding the mix composition characteristics and their impact on AC mechanics. This review focused on the links between mix composition and the overall properties and contains a brief background of this study, followed by a discussion of four typical mixture composition characteristics; namely aggregate size, aggregate morphology, asphalt matrix time-dependent properties, and anisotropic AC micro-structural characteristics. Furthermore, three kinds of methods were reviewed for understanding the links between the composition characteristics and the AC behaviors: the experiment-based methods, multiphase micromechanical models, and numerical models. The numerical models include discrete element (DE) models and finite element (FE) models.

Chapter 3 provides a general introduction on problem solving with PFC2D/3D for simulating asphalt concrete or relevant materials. The objective is to provide readers with a general background of the research tool used in this dissertation. The whole content of this chapter is split into six sections. Each of them is designed for one unique issue which is important for one to perform DEM simulation with PFC2D/3D. Even though this chapter is oriented toward modeling AC materials, the content could be used by researchers in any other relevant areas.

Chapter 4 introduces development and implementation of a user-defined 2D DE model for the simulation of a cyclic loading test (i.e., dynamic modulus test) of asphalt mixtures. In the 2D DE model, mineral aggregate particles were simulated with polygons and asphalt materials were represented with the viscoelastic Burger's model. The dynamic moduli of asphalt were predicted by conducting the DE simulation under a cyclic loading condition. It was found that the simulation results were very promising in terms of predicted dynamic moduli and the phase angles.

Chapter 5 introduces development and implementation of a randomly-generated 3D model for simulation and visualization of asphalt concrete. In the newly developed model, the microstructure of an AC sample was composed of three ingredients: coarse aggregates, sand mastic (a combination of fines, fine aggregates and asphalt binder), and air voids. Coarse aggregates were represented with the irregular polyhedron particles which were randomly created with an algorithm developed for this study. The gaps among the irregular particles were filled with air voids and discrete elements of sand mastic. The mechanical behaviors of the three ingredients were simulated with specific constitutive models at different contacts of discrete elements. Based on the geometric and mechanical models, visualization and simulation of asphalt mixtures were conducted.

Chapter 6 introduces development and implementation of two user-defined 3D idealized microstructural models for AC mixtures to study mineral aggregate morphology properties and their impacts on AC creep stiffness. The two models were the R-model and A-model, short for a user-defined rounded aggregate model and a user-defined angular aggregate model, respectively. Hot Mix Asphalt (HMA) contains a significant amount of mineral aggregates, approximately 95% by weight and 85% by volume. The aggregate sphericity, orientation, and angularity are very important in determining HMA mechanical behaviors. The objective of this study is to investigate the isolated effects of aggregate sphericity index, fractured faces, and orientation angles on the creep stiffness of HMA mixtures. A total of 102 digital samples were prepared with the two user-defined models to simulate creep compliance tests. Of the 102 digital specimens, 84 were prepared with the R-Model in order to investigate the effects of aggregate sphericity and orientation, while the remaining 18 were built with the A-model to address the effect of aggregate angularity. A viscoelastic model was used to capture the interactions within the mix specimens. It was observed that: 1) as sphericity increased, creep stiffness of the HMA mixture increased or decreased, which was dependent on the angles of aggregate orientation. 2) As the angle of aggregate orientation increased, creep stiffness of the HMA mixture increased, with the rate depending on the sphericity index values. 3)

Compared with sphericity index and orientation angles, the influence of aggregate fractured faces was insignificant.

Chapter 7 introduces development and implementation of a viscoelastic model of asphalt mixtures with DEM. In the newly developed model, the viscoelastic behaviors of asphalt mastics (fine aggregates, fines and asphalt binder) were represented by the Burger's model. Aggregates were simulated with irregular shape particles consisting of balls bonded together by elastic contact models, and the inter-places between aggregates were filled with balls bonded with viscoelastic Burger's model to represent asphalt mastic. Digital samples were prepared with the image analysis technique. The micromechanical model was composed of four constitutive models developed herein to represent the interactions at contacts of discrete elements (balls) within an individual aggregate particle, within asphalt mastic, between an individual aggregate particle and asphalt mastic, and between two adjacent individual aggregate particles. Each of four constitutive models consists of three parts: a stiffness model, a slip model, and a bonding model. The stiffness model provides a relationship between the contact force and relative displacement, the slip model describes slipping behaviors at the contact, and the bonding model represents tensile strengths at the contact. The relationship between the micro-scale model inputs and macro-scale material parameters was derived, and an iterative procedure was developed to fit the dynamic modulus test data of asphalt mastic with Burger's model. It was observed that the viscoelastic DE model developed in this study is very capable of simulating constitutive behavior of asphalt mixtures due to the good agreement between the prediction results and the lab test results.

Chapter 8 presents a method for determining Burger's model parameters using creep-recovery data of asphalt materials. With the determined Burger's model parameters, the viscoelastic behaviors of an asphalt binder (PG64-28) and its two mastics (a binder PG64-28 blended with mineral fines passing the ASTM 100# sieve and 200# sieve, respectively) were investigated. The total deformation of the mastics was separated into three parts: the instantaneous elasticity, delayed elasticity, and viscous flow. The ratios of the viscous flow to the elasticity were calculated and analyzed. It was found the proposed method is promising where the average errors of the creep section are 3.53%, 5.28% and 8.02% for the three materials, and the values are 0.69%, 1.286% and 1.80% for the recovery section.

Chapter 9 introduces development and implementation of a user-written C++ code to reduce the computational time required for simulating AC materials. The user-written C++ code is an advanced application and can improve simulation speeds. Both 2D and 3D DE simulation of AC materials were conducted with both the user-written C++ code and the traditional embedded programming language "FISH". It was found that the newly developed approach speeded up the DE simulation by 3.74 times the "FISH" code in average.

Chapter 10 introduces development and implementation of an approach to reduce the computational time for the DE modeling of AC dynamic modulus tests based on the frequency-temperature superposition principle. It was found that the proposed approach

could significantly accelerate the DE viscoelastic elastic simulation of AC dynamic modulus tests: The modeling work which took several months or years using the traditional methods only took a few hours or less with the proposed approach.

Chapter 11 introduces development and implementation of an approach to reduce computation time required for simulating creep tests of AC materials based on the time-temperature superposition. The primary objective of this paper is to simulate and analyze creep responses of an asphalt mixture with a 3D microstructural-based DE viscoelastic model. A key task in this study is to develop an approach to reduce the computation time with the Time-Temperature Superposition (TTS) Principle. Using this developed approach, creep compliance tests of an asphalt mixture under temperatures of 0, -10, and -20°C, were simulated with a microstructural-based DE viscoelastic model. Additionally, a DE elastic model was also employed and compared with the viscoelastic model. It was observed that: 1) the computation time was reduced to several hours from several decades; 2) the DE viscoelastic model, the DE elastic model, and the experimental measurements yielded similar results.

Chapter 12 describes an implantation of the developed computer modeling techniques to simulate time-dependent behaviors of AC materials subjected to sinusoidal loads. 3D DE models of asphalt mixtures under dynamic loads were developed with the assistance of X-ray Computed Tomography (X-ray CT) and the frequency-temperature superposition. The X-ray CT images were used to reconstruct the microstructure of asphalt concrete, while a time-dependent model was built by taking into consideration micro-scale interactions within the models. Through this study, it was observed that the dynamic modulus and phase angles of asphalt mixtures could be well-predicted from the component properties of those mixtures. It is anticipated that the techniques developed in this study can be used to simulate full scale pavements when the computation power is available.

Chapter 13 introduces an implementation of the developed computer modeling approaches to investigate impacts of mineral aggregate shapes and orientations on creep stiffness of AC mixtures. The R-model, the A-model, and time-temperature superposition were utilized in this study. It was found that that: 1) aggregate sphericity and orientation have significant impact on AC creep stiffness; 2) the effects of aggregate sphericity indices were correlated with that of aggregate orientation angles and vice versa.

Chapter 14 introduces an implementation of the developed computer modeling approaches to predict and interpret the stiffness ratios of sand mastics to asphalt binder at a broad range of temperatures. The purpose of this study is to develop an approach which could be utilized to determine asphalt sand mastic stiffness from its components (asphalt binder, sands, and minerals). Both fine and coarse sand mastics were studied using DEM. Twelve samples were prepared in this study, including six fine sand mastics, and six coarse sand mastics. The six fine sand mastics were prepared by blending fine sands (diameters ranging from 0.075mm to 0.3mm) with the 42.15%, 52.4%, 61.8%, 70.8%, 80.3%, 90% of asphalt binders by volume. The six coarse sand mastics were fabricated by blending coarse sands (diameters ranging from 0.3mm to 2.36mm) with the 42.15%,



52.4%, 61.8%, 70.8%, 80.3%, 90% of asphalt binders by volume. The previously developed DE model was employed to consider the interactions in the digital specimens of the 12 sand mastics. The DE simulations were conducted by varying the asphalt binder stiffness values with the constant stiffness value of sands. The stiffness ratios of mineral aggregates to asphalt binders were varied from 1 to  $1 \times 10^{10}$ . The outputs of the simulations were the predicted stiffness of the sand mastics. Finally, the outputs were analyzed to evaluate the impacts of asphalt binder stiffness values and volumetric fractions on the stiffness values of the asphalt sand mastics. Through this study, it was observed that 1) the DE simulation results agreed well with the micromechanical models; 2) the stiffness ratios of sand mastics to asphalt binders ranged from 1 to  $1.18 \times 10^9$  for fine sand mastics and from 1 to  $3.76 \times 10^8$  for coarse sand mastics.

Chapter 15 demonstrates an implementation of the developed computer modeling techniques to formulate asphalt concrete stiffness for specific microstructures. An asphalt concrete was designed on the basis of the Superpave mix design method. Its images were obtained from X-ray Computed Tomography (X-ray CT). Through processing those X-ray CT images, two microstructure-based models, namely the Model-I and the Model-II were rebuilt on the basis of the discrete element (DE) method. In Model-I, no air void was included, while in Model-II, the air void level was 3.1%. The DE simulation of the asphalt concrete was conducted with those two models whose primary inputs were the stiffness values of both coarse aggregate and asphalt sand mastic. The asphalt sand mastic was defined as a sub-mix of fines, fine aggregate (less than 2.36mm), and asphalt binder. Through regression analysis of the DE simulation results, the asphalt concrete stiffness values were formulated into two analytical equations for Model-I and Model-II, respectively. A potential application of those two equations is to predict effective stiffness values of the asphalt concrete at various temperatures and different loading conditions. At the end of this study, an application example is provided. It was found that the formulated equations were able to predict AC stiffness at various temperatures and frequencies.

Chapter 16 introduces development of DE models for studying pavement responses under a rolling wheel. Advantages, challenges, and limitations were identified for the developed modeling approaches. Through this study, It was observed that the numerical results were comparable with the theoretical calculation and it was still challenging to simulate a pavement section with a 3D model.

Chapter 17 presents an idealized DE model for simulating pavement-wheel interaction. The idealized model consists of three parts: a smooth surface for simulating a pavement surface, a wheel for simulating one of vehicle wheels, and a mass for simulating vehicle mass. An elastic contact model and a slip model are utilized to simulate the force-displacement relation and the frictional property at contacts between the pavement surface and the wheel. Additionally, the mechanical damping is simulated through a viscous contact damping model. The wheel is rotated through applying a torsion force and a vertical compressive force. When the wheel starts rolling on the pavement surface, the reaction forces and motion parameters of the rolling wheel are monitored. The

simulation results are compared with those from the existing literatures, it was observed that they agreed well to each other.

Chapter 18 provides a summary of this dissertation research and viewpoints for future research.

# Chapter 2. Literature Review<sup>1</sup>

## 2.1. Overview

The overall performance of an asphalt concrete (AC) mixture is dependent on its composition including the properties, proportions and distributions of the ingredients. For existing asphalt mix design methods, however, there is a missing link between the mix composition and the overall properties or performance. In order to improve the fundamental understanding of AC mixtures, this paper presents a comprehensive review of the advances in understanding the mix composition characteristics and their impact on AC mechanics. This review focused on the links between mix composition and the overall properties. The review contains a brief background of this study, followed by a discussion of four typical mixture composition characteristics; namely aggregate size, aggregate morphology, asphalt matrix time-dependent properties, and anisotropic AC micro-structural characteristics. Furthermore, three types of methods were reviewed for understanding the links between the composition characteristics and the AC behaviors: the experiment-based methods, multiphase micromechanical models, and numerical models. The numerical models include discrete element (DE) models and finite element (FE) models. Finally, a brief summary and further research needs are provided.

## 2.2. Introduction

The overall objective of asphalt concrete (AC) mix design is to determine an economical blend of selected materials that will eventually yield a pavement with desired performance under a variety of loading and environmental conditions. AC mix design involves selecting, proportioning and distributing its component materials to achieve the required strength and desired qualities of the finished product. Theoretically, to select the constituents, it is essential for the designer to know the role of each constituent in the contribution to the field performance of the AC mixture. It is also critical for the designer to understand the correlation between the constituent's volumetric properties and the overall composite mechanics. Furthermore, the overall mix performance is significantly impacted by the spatial distributions of its constituents. In general, the three major challenges of AC mix design are: 1) Understanding the impact of component material properties; 2) Understanding the impact of component volumetric or weight percentages; 3) Understanding the impact of mix compaction methods such as gyratory compaction, field compaction, and etc.

It is noteworthy that the traditional asphalt mix design methods have focused on the properties of the composite AC mix without any consideration for how the individual

---

<sup>1</sup> The full text reused with permission from Taylor & Francis: “Yu Liu, Zhanping You, Qingli Dai, and Julian Mills-Beale (2011), Review of Advances in Understanding Impacts of Mix Composition Characteristics on Asphalt Concrete (AC) Mechanics, International Journal of Pavement Engineering, First published on: 13 June 2011(iFirst), Final published on Vol 12, No. 4 (2011). See Copyright Clearance in Appendix A. Link to Taylor & Francis: <http://www.informaworld.com>

component materials contribute to the composite properties. The Marshall mix design method, for instance, uses the number of compaction blows, stability and flow to evaluate the mixture's properties without considering how much the individual aggregate, asphalt binder and any additive properties may be contributing towards the overall mixture performance. In the Superpave mix design method, both asphalt binder and aggregate properties are considered, the SHRP researchers, however, focused on the asphalt binder properties and gave less attention to mineral aggregates. Researchers believed that it is the asphalt sand mastic rather than the asphalt cement alone that bonds the larger size aggregates together (Shashidhar and Romero 1998b). Additionally, as mentioned in the technical report (Papagiannakis et al. 2002), the Superpave volumetric mixture design method alone is insufficient to guarantee reliable mixture performance over a wide range of traffic and climatic conditions. In the same report, the researchers emphasized the importance of developing a simple performance tests for asphalt mixtures. In addition to the simple performance tests, there are many other performance tests of asphalt mixtures such as the asphalt pavement analyzer (APA) test, the beam fatigue tests, a repeated triaxial test. Those laboratory tests can be used to measure AC performance in terms of dynamic modulus, flow number, rutting depth and fatigue life, etc. However, it is a challenging task to build the theoretically rational link between the measured performance results and the volumetric properties of a mix. Research studies have been published to understand the impact of mix composition characteristics on AC performances (Chen et al. 2001; Huber and Heiman 1987; Masad et al. 2007a; Stephens and Sinha 1978; Yue and Morin 1996). However, these observations were based on very limited amount of laboratory test results. Therefore, further studies are needed to improve the fundamental understanding of AC mixtures and build on the body knowledge of AC compositional characteristics and its effect on field performances. Special emphasis should be given for a better understanding of the impact of the mix composition characteristics on AC mechanics.

The main objectives of this study are to: 1) review the existing studies in understanding mix composition characteristics; 2) review advances in understanding the impact of the mix composition on the AC mechanics; 3) provide recommendations for future studies. A total of four topics were involved in this review as demonstrated in the subsequent sections in this paper:

- 1) AC mixture composition characteristics
- 2) Impact of mix composition I: experiment-based methods
- 3) Impact of mix composition II: micromechanical models
- 4) Impact of mix composition III: numerical models

### **2.3. AC Mixture Composition Characteristics**

A typical AC mixture is composed of mineral aggregates, asphalt binder and air voids. Both the mineral aggregate and asphalt binder have complex properties which play an integral role in determining the AC behavior. For example, the mineral aggregates have a wide range of sizes and complex morphological properties that influence greatly the AC mixture's response to traffic wheel loads, environmental conditions and climatic changes.

Asphalt binder has the time- and temperature dependent properties which further influence the AC mixture performances. Additionally, the size, distribution and amount of air voids also significantly impact the AC performance. The following is a brief discussion of mineral aggregate sizes, aggregate morphology, asphalt binder and anisotropic distributions of the three AC constituents.

### 2.3.1. Mineral Aggregate Sizes

Aggregates in AC are usually classified by size as coarse aggregates, fine aggregates and mineral fillers. The American Society for Testing and Materials (ASTM) defines coarse aggregates as particles retained on a No. 4 (4.75mm) sieve and fine aggregates as those passing a No. 4 sieve. It goes further to define mineral filler as an aggregate material with at least 70 percent passing the No. 200 (75 $\mu$ m) sieve. Other agencies may use different definitions. The Asphalt Institute, for instance, uses the No. 8 (2.36mm) sieve as the dividing line between coarse and fine aggregates. The Bailey method (Vavrik et al. 2002) gives a specific definition, where coarse aggregates is defined as large aggregate particles that create voids, while the fine aggregate is defined as smaller aggregate particles that fill the voids created by the coarse aggregates. The sieve which distinguishes coarse aggregates from fine aggregates is known as the primary control sieve (PCS). Instead of a constant sieve size (4.75mm or 2.36mm), the PCS in the Bailey method is dependent on the nominal maximum particle size (NMPS). The PCS is defined as the sieve size closest to the results of the PCS formula below:

$$PCS = NMPS \times 0.22 \qquad 2.1$$

Even though there are some inconsistent definitions of the control sieve sizes, a general agreement is that the mineral aggregates in a typical AC mixture can be separated into three categories: coarse aggregates, fine aggregates and mineral fillers. These three types of aggregates play different roles in determining the AC mixture performance at the micro-level as demonstrated by researchers below.

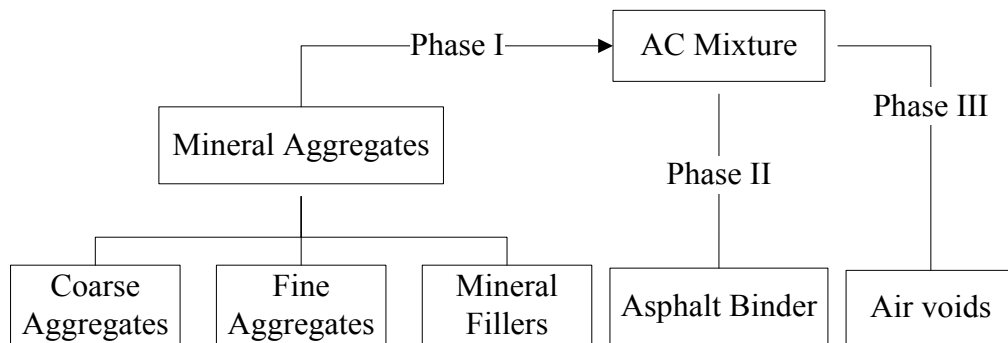
A number of researchers believed that mineral fillers exhibited an affinity with asphalt binder. The mix of asphalt binder and mineral filler was called asphalt mastic. On the basis of a microscopic consideration of AC, researchers believed that the AC binder is not pure asphalt cement but instead a asphalt mastic consisting of mineral fillers and asphalt cement (Anderson et al. 1992). In other words, asphalt mastic is an individual and integrated component that interacts with larger aggregate particles (fine and coarse aggregates) in the mixture. This hypothesis was also held by other researchers (Anderson 1971; Buttlar et al. 1999; Kim and Little 2004).

Another group of researchers had the similar idea, but they considered that fine aggregate, mineral filler and asphalt binder are mixed as an integrated component to interact with coarse aggregate particles in the mixture (Li and Metcalf 2005a). The integrated component called as asphalt sand mastic is a fine aggregate-filler-binder mixture (Dai and You 2007; Liu et al. 2009; You and Dai 2007a). Similarly, researchers pointed out that the three components can be visually observed in cross-sections of AC

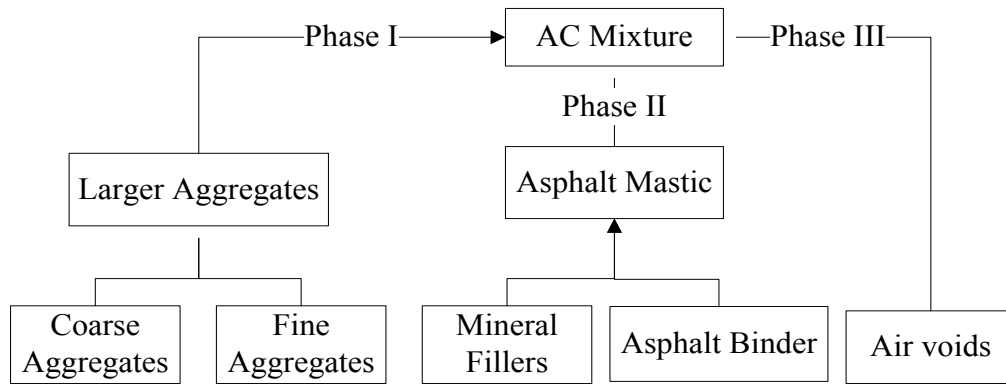
samples (Shashidhar and Romero 1998b). These are coarse aggregates, air voids, and fine aggregate-filler-binder mixture. Researchers similarly considered that an asphalt mixture is a coarse aggregate assembly coated by asphalt binder mortar that are composed of fine aggregates, mineral filler, and asphalt binder (Zhu and Nodes 2000).

Evidently, in term of the roles to interact with the asphalt binder, the AC mixture composition may be understood through the three different ways as illustrated in Figure 2.1. In Figure 2.1, coarse aggregates, fine aggregates, mineral fillers, and asphalt binder are the raw materials. Figure 2.1(a), (b), and (c) illustrate the three different ways to understand the AC mixture composition in terms of relation to the asphalt binder. The following are the explanations:

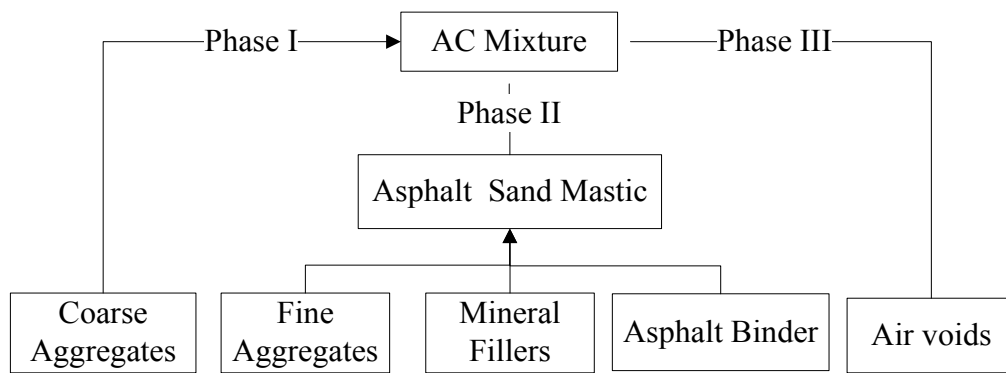
- 1) The first approach is shown in Figure 2.1(a): the asphalt binder alone is regarded as the bonding material to glue mineral aggregate particles which include coarse aggregates, fine aggregates, and mineral fillers. In this case, the AC mixture can be understood as a three-phase mix of mineral aggregates (including mineral fillers, fine aggregates, and coarse aggregates), asphalt binder, and air voids.
- 2) The second approach is shown in Figure 2.1(b): Mineral fillers are distinguished from the aggregate system and mixed with asphalt binder as an integrated component (the asphalt mastic). The asphalt mastic is considered as the bonding material to glue the larger aggregates (fine and coarse aggregates). In this case, the three phase of AC mixture are larger aggregate particles, the asphalt mastic, and air voids.
- 3) The third approach is shown in Figure 2.1(c): Both mineral fillers and fine aggregate are isolated from the aggregate system. They are mixed with asphalt binder into an individual component (asphalt sand mastic). The sand mastic is regarded as the bonding material to glue the coarse aggregate particles. In this case, the AC mix is the three-phase composite of coarse aggregates, asphalt sand mastic, and air voids.



(a) Schematic I



(b) Schematic II



(c) Schematic III

**Figure 2.1 Schematics of the AC composition**

In the Superpave mix design method, several test protocols are included to evaluate the physical and mechanical properties of the coarse aggregates, fine aggregates and mineral fillers. Also, in the design of aggregate gradation, the control points and the restricted zone are used to consider the percentages of aggregates of different sizes. However, the protocols, control points and restricted zones were developed on the basis of empirical methods, and the underlying theories have not been clearly determined. Furthermore, the focus of Superpave is tests on asphalt binder instead of asphalt mastic or asphalt sand mastic. However, the asphalt sand mastic or asphalt mastic directly impacts the mixture mechanics instead of the asphalt binder in the mixture system, if the AC composition can be understood by 3) or 2).

In summary, although many studies (as mentioned above) have been performed in the past decades, additional efforts are still needed to: 1) improve the understanding of the role of mineral aggregates at the micro-level; 2) validate whether the asphalt mastic or asphalt sand mastic is more important than the asphalt binder in directly impacting the AC mixture performance.

### 2.3.2. Aggregate Morphology

By conducting interviews and interactions with pavement experts, Strategic Highway Research Program (SHRP) researchers concluded that: 1) there was a general agreement that aggregate properties played an integral role in overcoming pavement permanent deformation; 2) fatigue cracking and low-temperature cracking were less affected by aggregate characteristics. Instead of comprehensively evaluating aggregate properties, the SHRP researchers used their survey results to identify some aggregate properties which needed to be used in the Superpave system. Those aggregate properties included coarse aggregate angularity, fine aggregate angularity, flatness and elongation as well as clay content and some source aggregate properties. Table 2.1 provides three typical testing protocols used to measure aggregate morphology properties in the Superpave system. It should be noted the testing methods listed in Table 2.1 are intended to be applied to a proposed aggregate blend rather than individual components.

Some researchers believed that the Superpave methods for characterizing aggregate morphological properties are imprecise and cannot be applied across the broad range of aggregate materials without ambiguity (Pan et al. 2006). Therefore, standard methods for directly measuring aggregate morphology properties were desired. The aggregate image system (AIMS) was recommended to measure both coarse and fine aggregate shape, angularity, and texture under NCHRP Project 4-30A, reported in NCHRP Report 555. Additional direct methods include X-ray computed tomography (X-ray CT) (Garboczi 2002), LADAR (Garboczi et al. 2006), optical method (Giordano Jr et al. 2006), neural network method (Garboczi 2002; Garboczi et al. 2006; Giordano Jr et al. 2006; Pan and Tutumluer 2006), and University of Illinois Aggregate Image Analyzer (UIAIA) (Pan and Tutumluer 2006). With these direct methods, researchers can quantify the morphological properties of aggregate and relate them to mixture or pavement performance (Chen et al. 2001; Masad et al. 2007a; Pan et al. 2005; 2006; Tutumluer et al. 2005). Details of these testing methods can be found in the references. Clearly, quite a few methods and testing equipments are able to quantify aggregate morphological properties. The major challenge, however, is how to use the existing resources to improve the understanding of the relationship between aggregate morphology and the overall mixture performances. For instance, if the aggregate angularity is quantified, how can the designer know the impact of this parameter on the performance of AC mixtures?

**Table 2.1**  
**Superpave Aggregate Testing Protocols**

Aggregate Morphology	Coarse Aggregate Angularity	Fine Aggregate Angularity	Flatness and Elongation
Testing Protocol	ASTM D5821	AASHTO T304	ASTM D4791



### **2.3.3. Asphalt Binder Rheological Properties**

Asphalt binder is another basic component of the AC mixture. The rheological properties of asphalt binders are so important that a key target of SHRP researchers was to evaluate asphalt binder properties and their contributions to pavement performance. The typical Superpave binder tests include the Dynamic Shear Rheometer (DSR), Bending Beam Rheometer (BBR), Direct Tension Tester (DTT), Rotational Viscometer (RV), Rolling Thin Film Oven (RTFO) and Pressure Aging Vessel (PAV). DSR and RV tests can be used to measure the asphalt binder's linear viscoelastic properties. RTFO and PAV tests can simulate the asphalt binder aging that occurs during the manufacturing and construction process, and 5 to 10 years after paving. BBR and DTT tests can indicate asphalt binder resistances to lower temperature cracking even though they cannot accurately quantify tensile strengths of asphalt binder. In other words, most of asphalt binder properties can be measured using the Superpave binder testing equipments.

In addition to the routine testing methods above, a number of research projects were conducted in the past decade to address the issues related to asphalt binder properties. For example, some researchers utilized the laboratory or field testing results to understand the rheological properties of asphalt binders (Bahia and Kamel 1994; Billiter et al. 1997; Giuliani and Merusi 2009; Khalid et al. 1998; Marateanu and Anderson 1996; Newman 1998), while other researchers tried to correlate asphalt binder properties with the AC properties and evaluated the impact of asphalt binders on AC mixture performance (Bouldin and Collins 1990; Soleymani et al. 2004; Stuart 2002; Tayebali et al. 1990; Tsai et al. 2005). Since many existing test methods and theories are available to measure and evaluate asphalt binder properties as mentioned above, relating the asphalt binder properties to AC mixture performance has been achieved to a large extent. However, it should be noted that the problem becomes much more complicated when the asphalt binder is blended with mineral aggregates to form an AC mixture. For example, when one intends to correlate asphalt binder properties with AC mixtures, the complicated effects resulting from the aggregate physical properties, aggregate morphological characteristics, air voids, gradations, etc. have to be considered. Otherwise, the resulting conclusions are the combination of many impacting factors instead of the targeted asphalt binder property.

### **2.3.4. Anisotropic Microstructure of AC Mixture**

As mentioned above, mineral aggregates have irregular shapes and a broad range of sizes. When the mineral aggregates are mixed with asphalt binder, they are randomly distributed and create randomly-distributed air voids. The spatial distribution of mineral aggregates and air voids depends on the compaction method, temperature, and loading condition. On one hand, it can be easily understood that the AC mixture has a very complex microstructure with an arbitrary and anisotropic nature. On the other hand, the performance of the AC mixture is influenced by its internal structure. Theoretically, the mix designer needs to know the internal structural effects on the final product before he can design an AC mixture. Unfortunately, none of the existing mix design methods is able to achieve that. The existing mix design methods, including the Superpave system, were developed based on observations from many experimental tests, or from the

experiences of pavement experts without knowledge of the AC internal structure. However, more and more researchers have realized the importance of the internal structure and have started to focus their work on this area in the last ten years. According to existing studies shown below, researchers have succeeded in:

- 1) Quantifying and analyzing some characteristics of AC mixture's internal structures by using digital imaging process techniques. For example, researchers were able to characterize air void distribution in asphalt mixtures using X-ray CT (Arambula et al. 2007; Kelleher and Markow 2009; Masad et al. 2002a). Masad et al (1999a) were able to quantify and analyze the internal structure of AC in terms of aggregate orientations, aggregate gradations and internal air void distributions with two-dimensional (2D) optical or X-ray CT imaging process. Additionally, Li et al. (2009b) presented methods for computation of size, location, contact points, and orientations of the aggregates in an AC mixture.
- 2) Evaluating the effects of laboratory compaction behavior on AC internal structures by analyzing digital images of mixture specimens. With X-ray CT and computer automated image analysis techniques, Tashman et al. (2002) quantified the AC internal structure: a) to evaluate the ability of the Superpave Gyratory Compactor (SGC) in simulating the internal structure of asphalt pavements; and b) to investigate the influence of different field compaction patterns on the produced internal structure. Masad et al (1999b) evaluated the effects of laboratory compaction methods on the AC internal structure. In this study, the AC internal structures were quantified in terms of aggregate orientation, aggregate contacts and air void distribution through processing X-ray CT images. Specimens compacted with the SGC and the linear kneading compactors (LKC) were studied.
- 3) Simulating AC micromechanics with numerical methods by providing geometric inputs which are needed in the numerical models.

The recent advances listed above may help researchers or engineers to understand the link between AC mechanics and geometry. Additional efforts are still needed for making another stride in understanding the correlation between AC internal structure and its performance:

- 1) Additional parameters are needed to represent AC composition characteristics, especially distributions of AC constituents. As discussed in the introduction section, an AC composition can be characterized by properties, proportions, and distributions of constituents. In the Superpave laboratory, properties and proportions of constituents can be easily measured, such as properties of asphalt binder and aggregates, and volumetric proportions of asphalt binder, aggregates, air voids, etc. Currently, limited information was provided in the Superpave system to address distributions of AC constituents. With rapid development of imaging techniques, researchers utilized imaging techniques to study internal structural features of AC materials (Arambula et al. 2007; Chandan et al. 2004; Masad 2004; Masad et al. 2002a). Those existing studies demonstrated that imaging techniques could be potential methods for quantifying distributions of AC constituents. Additional research efforts are needed to develop certain parameters which can typically

- represent AC mixture internal structures. With those parameters, one can easily reconstruct AC microstructures without repeating the laboratory testing and imaging processing. Those reconstructed microstructures can closely represent their counterparts in the reality and be utilized in computer modeling for micromechanical analysis.
- 2) Additional research is needed to advance the understanding of the correlation between AC mixture internal microstructure and overall performance. The ultimate goal of microstructural analysis is to improve the AC mix performance. The Superpave system emphasizes the volumetric characteristics, but less information is presented in the system about the links between volumetric characteristics and mixture or pavement performance. With rapid development of computational mechanics and computer technologies, it becomes possible to perform computer simulation with considering complex microstructural and micromechanical features. Additional research efforts should be made to link the microstructural characteristics to mixture or pavement performance in a more fundamental manner instead of empirical equations.

## **2.4. Impact of Mix Composition I: Experiment-Based Methods**

Experimental tests are important to understand or interpret the performance of engineering materials. Compared with other engineering materials, a remarkable feature of the AC mixtures is the complex and arbitrary nature of its composition, which makes it difficult to correlate the component properties to the composite behaviors. Even though the links between AC and its components have been ambiguous until today, hundreds of experimental-based studies have been conducted in this direction since as early as the 1920's. Nicholson (1927) have investigated the stability of mineral aggregates with different shapes in asphalt pavements from different parts of the country. Furthermore, bituminous mortars have been tested to investigate their effects on the stability of the mixes (Vaswani and Shukla 1963). Other research work was conducted to investigate impacts of asphalt cements and air void contents on the AC fatigue life and stiffness (Harvey and Tsai 1996). An attempt was made by Pan and Tutumluer (2005) to use the UIAIA to determine aggregate morphological shape indices and link those indices to the laboratory and field performances of asphalt mixtures. Li et al (2008b) have addressed the effects of reclaimed asphalt pavement (RAP) and binder grade on dynamic modulus of asphalt mixtures .

It is interesting that conflicting observations were obtained in some of these previous studies. As shown in Table 2.2, researchers in Group I believed that aggregate, binder, mastic and air voids might significantly impact AC properties or could be correlated with AC mixture performance, while those in Group II had different observations.

There may have been many reasons for those conflicting observations. To better explain these reasons, the following important concerns should be taken into account:

- 1) Different methods were used to measure pavement or mixture properties;
- 2) Different methods were used to measure aggregate properties;

- 3) Different types of aggregates and mixtures were used for experimental tests;
- 4) Researchers were unable to isolate the effects of one aggregate characteristic from the other.

**Table 2.2**  
**Research effects with the experiment-based methods**

Research focus	Selected studies and their conclusions in Group I	Selected studies and their conclusions in Group II
Coarse and fine aggregate	(Oduroh et al. 2000): Crushed coarse aggregate particles could significantly impact AC permanent deformation properties.	(Shklarsky and Livneh 1964): The asphalt mix properties were not significantly improved by crushed coarse aggregate particles.
	(Asphalt-Institute 2001): SHRP researchers believed that flat or elongated particles could be easily broken during construction or under normal traffic loading. Therefore, they are undesirable for producing AC mixtures.	(Li and Kett 1967): flat and elongated particles did not have adverse effect on AC strength. Therefore, they could be permitted in producing AC mixtures.  (Stephens and Sinha 1978): flat particles and rod-like particles are desirable to achieve optimum strength.  (Huber and Heiman 1987): The mix volumetric properties were not adversely impacted by crushed aggregate with 19% flat and elongated particles.
	(Bennert et al. 2006): As the FAA increased, the APA rutting decreased.  (Johnson et al. 2007): APA rutting resistance was significantly influenced by the aggregate blend FAA.	(Huber et al. 1998): 1) the rate of rutting on couch wheel tracker did not correlate well with the fine aggregate angularity (FAA); 2) rut depths measured on the asphalt pavement analyzer (APA) did not have a good correlation with FAA values; 3) dynamic modulus of mixtures measured on the Superpave shear tester did not vary with different FAA.

**Table 2.2 Continued**

Research focus	Selected studies and their conclusions in Group I	Selected studies and their conclusions in Group II
Asphalt binder	<p>(Asphalt-Institute 2001): SHRP researchers believed that asphalt binder properties could be correlated with those of the corresponding asphalt mixtures. That is one of the very important reasons why their focus was on asphalt binder properties.</p> <p>(Zeng and Huang 2006): 1) Within the material linearity, the AC complex modulus and phase angle could be represented by the similar parameters of the binder. 2) For typical dense graded asphalt mixtures, the relationship between mixture and binder was not significantly influenced by the characteristics of both asphalt binder and aggregate. 3) The relationship was independent on temperatures and frequencies.</p> <p>(Wasage et al. 2008): mixtures prepared with susceptible asphalt binders are more prone to rutting.</p> <p>(Soleymani et al. 2004): There are phenomenological relationships between modified binders and the corresponding mixtures. It was found that 1) Simple power law function of asphalt binder's <math>G^*</math> could represent asphalt mixture's <math>G^*</math>. 2) Binder rutting rate of mixtures was approximately 20% that of binders. 3) Mixture fatigue life was changed by 20% as a result that asphalt binder fatigue life was changed by 100%.</p>	<p>(Shenoy et al. 2003): the properties of the mixtures for evaluating permanent deformation appear to have poor correlation with rheological properties of binders.</p> <p>(Stuart 2002): 1) the correlation between repeated shear at constant height (RSCH) and <math>G^*/\sin\delta</math> depended on loading frequency of DSR tests; 2) compared with the high-temperature PG's of the asphalt binders, <math>G^*/\sin\delta</math> at 0.1 rad/s did not clearly present an improved correlation to RSCH.</p> <p>(Stuart and Mogawer 2002): A weak correlation was found using the French PRT.</p>

**Table 2.2 Continued**

Research focus	Selected studies and their conclusions in Group I	Selected studies and their conclusions in Group II
Asphalt mastic	<p>(Li and Metcalf 2005a; Shashidhar and Romero 1998a; Zhu and Nodes 2000): 1) asphalt mastic play a very important role in determine asphalt mixture properties. 2) Asphalt mixture stiffness could be predicted from those of asphalt mastic.</p>	<p>(Shenoy et al. 2003): the properties of the mixtures for evaluating permanent deformation appear to have no correlation with rheological properties of asphalt mastics.</p>
Air voids	<p>(Arambula et al. 2007): air void distribution has the influence on moisture susceptibility. Mixtures with the smaller range of air void content and air void radius were more susceptible to moisture damage.</p> <p>(Harvey et al. 1994): better designed air voids could reduce the propensity for fatigue cracking in asphalt concrete pavements.</p> <p>(Li et al. 2008a): the air voids affect the cohesion between aggregates and asphalt remarkably. The damage pictures show that the fracture of mixtures with lower air voids (less than 4.5%) occurred with breakage of aggregates while mixtures with larger percentage of air voids (larger than 8.0%) were damaged with the parting of interface between aggregate and binder.</p> <p>(Masad et al. 2006): permeability could be expressed as a function of statistical parameters of the air void distribution.</p>	<p>(Mohammad et al. 2004): a good correlation was found between the complex shear moduli of SGC samples and field cores which had different air void distributions. In other words, air void distributions played a minor role in correlation between shear moduli of SGC samples and field cores.</p>

Among the four concerns above, the first three of them could be easily solved by using the same material sources and testing methods, but it is extremely hard for a researcher to

isolate one aggregate characteristic parameter from the other impacting factors. For example, researchers have used measurable indices to link aggregate morphology properties to permanent deformation behavior and resilient modulus of hot-mix asphalt (Pan et al. 2005; 2006). In their studies, there were a total of 18 Superpave asphalt mixture specimens prepared in the laboratory from ten state highway agencies. The imaging-based morphological indices of coarse aggregate materials were determined using the UIAIA. They concluded that the effects of aggregate angularity and surface texture indices on permanent deformation were especially significant. The actual effects, however, were not only from the angularity index or surface texture index, but also others such as aggregate orientation, gradation, air voids, and asphalt properties. Therefore, the observations in those studies were not the isolated effect from a single factor (angularity or texture), but the combined effect from many factors.

## 2.5. Impact of Mix Composition II: Micromechanical Models

Micromechanical analysis of composite materials provides an approach to predict the composite overall behaviors from the known properties of the individual constituents and their interactions. Compared with experiment-based methods, two advantages of micromechanical analysis are that: 1) only constituent properties need to be used for the analysis; 2) the impact of constituents on the overall composite behaviors can be easily and directly evaluated. In the past century, a considerable number of studies have been undertaken on the mechanical analysis of composite materials. This review herein is intended not to be exhaustive in its coverage, but to provide a representative cross-section which may be helpful in understanding AC micromechanics. As mentioned in the previous sections, AC is a typical composite with complex microstructure. Therefore, the review of this section starts from reviewing mechanics of composite materials, followed by micromechanical models for prediction of asphalt-aggregate mixtures.

### 2.5.1. Mechanics of Composite Materials

The fundamentals of micromechanics of two-phase composites and the previously developed models before 1991 were presented or reviewed by Aboudi (Aboudi 1991); According to this book, under homogenous boundary conditions, the overall stiffness tensor of a two-phase composite can be derived on the basis of average stress and strain theorems or the energy approach. The overall stiffness tensor ( $C^*$ ) is given by

$$C^* = C^{(1)} + c_2 A_2 (C^{(2)} - C^{(1)}) \quad 2.2$$

where  $C^{(1)}$  and  $C^{(2)}$  are stiffness values of the two constituents (the phase 1 and the phase 2, respectively) in the composite;  $c_2$  is volumetric fraction of the phase 2;  $A_2$  is the strain concentration matrix of the phase 2, which is written as

$$A_2 = \bar{\varepsilon}^{(2)} / \bar{\varepsilon} \quad 2.3$$

Where  $\bar{\varepsilon}^{(2)}$  and  $\bar{\varepsilon}$  are average strains in the phase 2 and the composite, respectively.

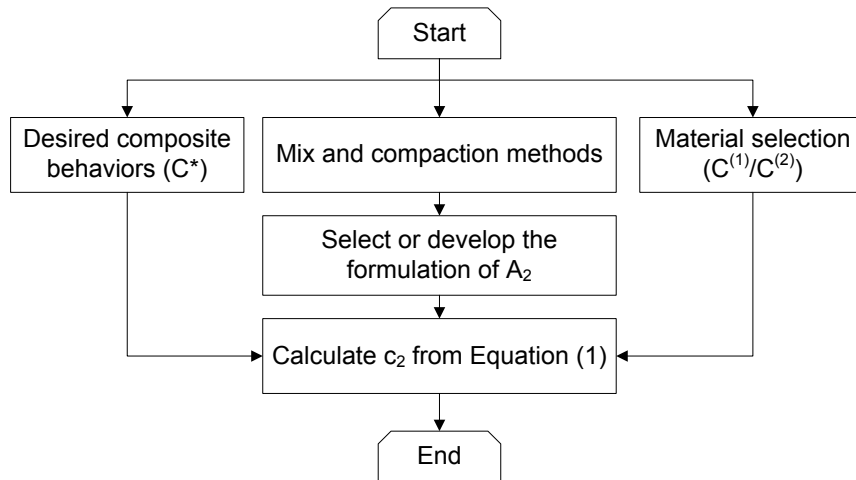


**Figure 2.2 Demonstration of a composite material design philosophy**

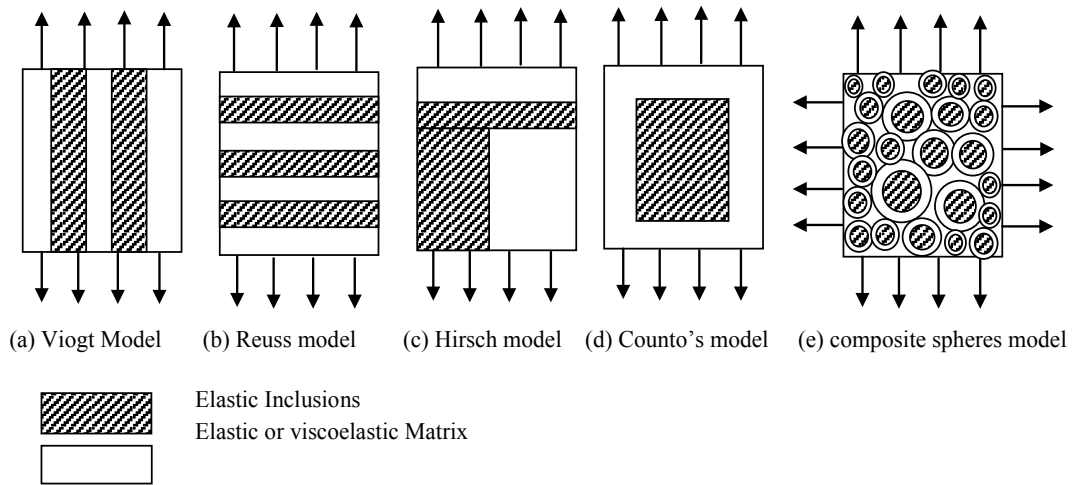


**Figure 2.3 Spatial distributions for the example micromechanical models**

In the Equations 2-2 and 2-3, phase 1 is for the asphalt binder and phase 2 for mineral aggregates herein. Theoretically, three key factors which are used to determine the behaviors of a composite are properties, proportions, and distributions of its constituents. Those three factors are represented in Equation 2-2 by  $C^{(1)}$  and  $C^{(2)}$ ,  $c_2$ , and  $A_2$ , respectively. Figure 2.2 demonstrates a basic design philosophy of any two-phase composite. As shown in the figure,  $C^{(1)}$  and  $C^{(2)}$  are stiffness values of selected constituent materials which are easy to be quantified. Stiffness of the composite,  $C^*$ , is usually pre-determined on the basis of its application conditions. Therefore, if  $A_2$  can be formulated with  $C^{(1)}$  and  $C^{(2)}$ , and  $C^*$ , the volumetric fraction of the phase 2,  $c_2$  can be determined from Equation 2-2. Actually, a number of micromechanical models have been developed in the past century. The only difference in those micromechanical models is the formulation of  $A_2$ . In other words, it is the formulations of  $A_2$  that have defined a number of micromechanical models. Table 2.3 shows some of them, in which the first and second



columns show the micromechanical models and their formulations of  $A_2$ , respectively, while the third one lists the assumptions for each model. Figure 2.3 shows the spatial distribution of the example micromechanical models. In the same book (Aboudi 1991), a number of micromechanical models were reviewed. Ten of them were discussed in detail. They are: 1) the Voigt approximation (Voigt 1889); 2) Ruess approximation (Reuss 1929); 3) the Dilute approximation (Christensen 1979; Christensen and Lo 1979), 4) the composite spheres model (Hashin 1965); 5) the self-consistent scheme; 6) generalized self-consistent scheme (Christensen and Lo 1979); 7) the differential scheme; 8) the Mori-Tanaka theory (Tanaka and Mori 1973); 9) Eshelby equivalent inclusion method and; 10) the micromechanical method of cells.

**Table 2.3**  
**Formulations of  $A_2$  for some micromechanical models**

Models	$A_2$	Assumptions
Parallel model (Voigt 1889)	1	The composite is subject to uniform strain. Figure 2.3(a) is an application example.
Series model (Reuss 1929)	$\frac{C^{(1)}}{c_2 C^{(1)} + c_1 C^{(2)}}$	The composite is subject to uniform stress. Figure 2.3(b) is an application example.
Simple Hirsch model (Hirsch 1962)	$\frac{x C^U + (1-x) C^L}{(C^{(2)} - C^{(1)}) c_2}$ where: $C^U$ and $C^L$ are effective stiffness predicted from Voigt (1889) and Reuss (1929), respectively.	Hirsch model is a combination of the parallel model and series model. The composite is subject to uniform stress. Figure 2.3(c) is an application example.
Counto's model (Counto 1964)	$\frac{\left[ \frac{1}{\sqrt{c_2}} C^{(1)} - 1 + \frac{1}{1 - \sqrt{c_2}} C^{(2)} \right] C^{(1)}}{(C^{(2)} - C^{(1)}) c_2}$	Elastic conclusions are dispersed in elastic matrix as shown in Figure 2.3(d)
Composited Spheres model (Hashin 1962)	Predict bulk modulus: $\frac{(4G^{(1)} + 3C^{(1)})c}{[4G^{(1)} + 3C^{(2)} + 3(C^{(1)} - C^{(2)})c]c_2}$ Where: $G^{(1)}$ , $G^{(2)}$ are shear moduli of the two phases. $c$ is volume concentration of inclusions = $\left(\frac{a}{b}\right)^3$ . It should be noted that $C^{(1)}$ , $C^{(2)}$ are bulk moduli of the two phases.	Graded spherical particles are embedded in a continuous matrix as shown in Figure 2.3(e)

Based on the extreme principles of minimum potential and minimum complimentary energy, Paul (1960) derived bounds for effective bulk and shear moduli of two-phase and irregular geometry composite materials. The formulations of the bounds are the Ruess and Voigt approximations in terms of bulk and shear moduli. Hill (Hill 1952) rigorously proved that the actual overall moduli lie somewhere in the interval between the Ruess and Voigt approximations, irrespective of the geometry. In other words, the upper and lower bounds of the true effective elastic moduli are the Voigt and Ruess approximations for any two-phase composite.

Aboudi (1991) believed that the upper and lower bounds represented by Voigt and Ruess approximations are of practical significance only for small volume fractions and slight mismatch of elastic moduli of the two component materials. To improve the bounds, Hashin (1962) derived the composite spheres model and Hashin and Shtrikman (1963) developed the arbitrary phase geometry model. The arbitrary phase geometry model was further improved by other researchers (Hashin 1965; Hill 1963; Walpole 1966). Apparently, those improved models could provide more accurate prediction of the upper and lower bounds, but their accuracy for predicting AC mix properties are still limited as demonstrated in the following section.

### **2.5.2. Micromechanical Models for AC Mixtures**

Buttlar (1995) reviewed and evaluated theoretical binder-to-mixture stiffness relationships at low temperatures. The review covered the Paul's equations (Paul 1960), the arbitrary phase geometry model (Hashin and Shtrikman 1963), the composite spheres model (Hashin 1962), the generalized self-consistent scheme (Christensen and Lo 1979) and the Mori-Tanaka theory (Tanaka and Mori 1973). It was concluded that: 1) the Paul's equations and the arbitrary phase geometry model could successfully envelope the measured values, but the bounds from those two models were so wide that they essentially provide no useful information. 2) The composite spheres model could not envelope the measured values: both lower and upper bounds of the composite spheres model were found to greatly under predict the measured mixture stiffness. 3) The remaining two models (the generalized self-consistent scheme and Mori-Tanaka theory) also greatly under-predicted mixture stiffness. In order to explain the discrepancies between the measured and the predicted stiffness, the researcher performance sensitivity analysis of those five models to input properties. It was concluded that a rational explanation was not achieved by estimating aggregate stiffness and Poisson's ratios of the asphalt binder. As mentioned above, A2 is related to the component geometry and plays a crucial role in determining a two-phase composite. Those five models, however, have relatively simple geometries which cannot properly simulate AC complex internal structure. Therefore, the prediction from those five models had greatly mismatched the measured mixture stiffness.

Wu (1966) performed an analytical study to compare the effective properties between composites with spherical inclusions and those with needle and disk-shaped inclusions. It was found that the shape of spherical inclusions can have significant effect on the

computation of effective properties over a wide range of inclusion volume concentrations. When the volumetric concentrations exceeded 0.8, however, the effect of inclusion shape was found to be almost negligible. This conclusion looks suitable for AC which has more than 80% of mineral aggregates. It should be noted that mineral aggregates have a wide range of sizes from 0.075mm to 37.5mm in a typical AC mixture. As mentioned in the introduction, different sizes of aggregates play different roles in determining the overall properties of mixes. If an AC mixture is considered as a three-phase composite of coarse aggregate, asphalt sand mastic, and air voids, the coarse aggregate particles are inclusions which usually count less than 80% of AC mass (about 50% in a typical AC mixture). Therefore, Wu's conclusion needs to be re-examined before it could be used for such kinds of materials.

As mentioned by You (2003) in his dissertation, a number of models may be appropriate for modeling AC mixtures. Buttlar and You (2001) classified different micromechanical models into three categories: 1) models with non-interacting particles and unspecified geometry (Hashin and Shtrikman 1963; Paul 1960; Reuss 1929; Voigt 1889); 2) models with non-interacting particles and geometry specified (Christensen and Lo 1979; Hashin 1965; Hirsch 1962) and; 3) models with interacting particles, such as discrete element (DE) method developed by Cundall (Cundall and Strack 1979b) and finite element (FE) method developed by Cook (Cook 1974). It was believed that models with non-interacting particles have the advantage of simplicity and efficiency, but cannot be accurately applied to most asphaltic materials which involve interacting particles. You (2003) believed that DE and FE models could more accurately simulate particle-particle interactions, but they are time-consuming and expertise-required. Details about DE and FE models will be discussed in the subsequent section. For more information on the micromechanical models with non-interacting particles and unspecified geometry, readers can refer to the literature (You 2003)

Other researchers (Druta et al. 2007) estimated the shear stiffness of mastics using the complex shear modulus of binder and Hirsch model based on binder modulus and the volumetric composition of filler. The predicted mastic shear moduli showed very good agreement with R2 values around 0.8 or higher.

### **2.5.3. Summary of Micromechanical Models**

The importance of AC composition characteristics has been studied by many researchers. Several developed micromechanical models have been used to predict effective properties of AC mixtures by inputting those of its constituents. However, it was found that none of them could reasonably predict AC overall behaviors from asphalt binder and mineral aggregates. Even though some micromechanical models, such as the Paul's equations and the arbitrary phase geometry model could act as mix laws to provide bounds of AC stiffness values, the bounds were so wide that they essentially provided no useful information. The authors of this paper believe that the following two concerns should be taken into account in explaining the mismatch:

- 1) Currently, most researchers considered mineral aggregates to act as inclusions, which count for around 84% of the overall mixture volume. Most micromechanical models,

- however, may be suitable for the composite with a smaller volumetric fraction of the inclusions.
- 2) Mineral aggregate system has a wide range of particle sizes from less than 0.075mm to as large as 37.5mm. The roles of different sizes of aggregate particles are varied, but they were not emphasized in the existing micromechanical models. Followed is a simple mathematic calculation which indicates the roles of different sizes of particles: Usually, mineral fillers are less than 0.075mm and the cut-off size between coarse and fine aggregates is 2.36mm. It is assumed that the average size of mineral fillers is 0.0375mm and the average size of fine aggregates is 1.18mm, while the average size of coarse aggregate is 9.5mm. If the mineral aggregate particle is spherical, the volumetric ratio between a fine aggregate particle and a mineral filler particle is about 31,157 and the volumetric ratio between fine and coarse aggregate is about 522. In other words, more than 31,157 mineral filler particles are equivalent to one fine aggregate particle and 522 fine aggregate particles are equivalent to one coarse aggregate. When an individual mineral filler particle interacts with a fine or coarse aggregate, the reaction force is so small that it can be neglected. In other words, a single mineral filler particle alone has negligible influences on larger sizes of aggregates, even though millions of the tiny particles together can significantly impact the motion of the larger aggregate particles and the mix performances. In this case, it is reasonable that mineral fillers should be considered as an integrated component instead of individual particles. If one considers the aggregate system is a particle system, mineral fillers do not belong to the system. However, most of the existing micromechanical models did not consider the size impacts of different mineral aggregates.

## **2.6. Impact of Mix Composition III: FE and DE Models**

Since an AC mixture has a very complex microstructure with arbitrary and anisotropic natures, accurate analytical solutions usually are not available. The simplified micromechanical models as discussed in the previous section are too simple to provide enough useful information. Experimental tests are persuasive and direct, but the observations are usually from specific projects where the material resources and testing conditions are specified. When the observations are going to be used in other projects, their accuracies may be different. Numerical solutions obtained using a high-speed computer are very useful for engineering problems, especially when the geometry of the object (such as AC mixture) is irregular or the boundary conditions are nonlinear. The commonly used numerical methods include finite element (FE) method, discrete element (DE) method, finite difference (FD) method, boundary element (BE) method, and element-free (EF) method. In modeling of AC mixtures, FE and DE methods were more popular than the others. The following is an introduction of the developments and applications of the DE and FE models.

### **2.6.1. FE Model Developments and Applications**

The FE method is a numerical technique for finding approximate solutions of partial differential equations and integral equations. It originated from the need for a method to solve complex elasticity and structural analysis problems in civil or aeronautical

engineering. In modeling of AC microstructure with the FE method, the early development may be traced back to the work by K. Sepehr and his colleagues at the national research council of Canada (Sepehr et al. 1994). In this early study, the aggregate particles were modeled as elastic, randomly shaped and distributed solids surrounded by an elastic asphalt matrix. Instead of elastic-plasticity, the constant material properties (such as Young's modulus) were used as inputs. Results of the FE analysis clearly demonstrated that a FE model constructed using a microstructure mesh was much more realistic than when a linear mesh is employed. This early study was followed by many others in the past ten years.

Bahia et al. (1999) performed the FE analysis to estimate the binder strain distribution inside the mix with a simplified model, where the aggregate particles were represented by circular objects. The asphalt binder and aggregate phases were simulated with elastic models. It was found that the shear strains in the asphalt binder were much higher than the bulk strain of the mixtures. For example, when the asphalt mixture model was subjected to 1% strain, the shear strain in the asphalt binder could be as high as 46%.

Kose et al. (2000b) applied the imaging and FE techniques to investigate the distribution of strains within the AC mixtures. In their study, the tomography, digital scanning, and video imaging methods were used to capture the AC images. Those three aforementioned imaging methods were evaluated in order to determine the most accurate, precise and feasible technique for AC analysis. The digital images of the AC mixtures were converted to FE mesh such that each pixel represents one finite element. The FE analysis was conducted using the commercial FE computer package (ABAQUS) by inputting linear elastic properties for both asphalt mastic and aggregate phases. They concluded that the high optical resolution scanning was effective in capturing images and could provide accurate images that gave a reasonable match with the actual aggregate size distribution. Additionally, it was found from the FE analysis that: 1) the binder strain could be as high as 1.8 times the mastic strain; 2) the strain in the binder can range between an average of 7.8 times and a maximum of 510 times the bulk strain of the AC mixture.

Masad et al. (2001) utilized experimental measurements, micromechanical analysis, and FE modeling to investigate the strain distribution in asphalt mixes. An image correlation technique was used herein to experimentally measure the strain distribution in the AC specimens. A FE model of the AC internal structure was developed to calculate the strain distribution under loading conditions similar to those used in experimental measurements. Due to limitations imposed by image resolution, the FE analysis provided the strain distribution in the asphalt mastic phase rather than the binder phase. Therefore, a micromechanical model was presented in order to determine strain distribution in the binder phase. By comparing the results from the experimental measurements with the FE modeling, it was found that the computed and measured strain distribution compared well. The FE and micromechanical analysis indicated: 1) the mastic strains were about 3-4 times the bulk strains in the AC mixtures while the binder strains were about 3 times the mastic strain; 2) the binder maximum strain was as high as 90 times that of the overall mix strain although the average binder strain was estimated to be in the range of 9-12

times the mix strain. The aforementioned observations were similarly observed by other Masad and Somadevan (2002)

Masad et al (2002b) launched a study with the purpose of deriving micromechanics-based models that link the internal structure properties to the stiffness anisotropy of AC mixtures. Experimental procedures based on image analysis techniques were presented in this study to quantify the internal structure and provide the models' parameters. FE analysis of the mixture's internal structures was performed to provide insight into the AC stiffness anisotropy. It was determined that: 1) the AC specimens were shown to have higher stiffness in the horizontal direction compared to the vertical one; 2) the mixture stiffness anisotropy decreased with a decrease in temperature

Papagiannakis et al (2002) presented a methodology for describing the constitutive behavior of AC mixtures. In their study, mechanistic models of asphalt binders were developed and the rheological model parameters were determined from frequency-sweep Dynamic Shear Rheometer (DSR) tests. Asphalt binder nonlinearity was treated in a piece-wise linear fashion, whereby the binder model constants were assigned as a function of strain level. The FE geometry was built by translating two-dimensional AC images. The FE model was considered as a two-phase system of larger-size aggregates and mastic. The mastic was defined as a mix of asphalt binder and smaller-size aggregates. The aggregates were treated as linear elastic, while the mastic was treated as viscoelastic. The stiffness of the mastic was estimated to be 3 to 30 times larger than the stiffness of the binder. The proposed FE model was verified by comparing the predicted shear moduli with Simple Shear Test (SST) measurements.

Sadd *et al.* 2003 (2003) undertook the simulation of indirect tension tests (IDT) of AC mixtures using FE micromechanical model with damage mechanics. The AC mixtures were simulated with an equivalent FE network which represented the load-carrying behavior between aggregates in the multiphase material. Each of the elements in the network was specially developed from an elasticity solution for cemented particulates. According to this study, reasonable qualitative relationships were observed between the FE model damage evolution and the experimental photographic data. It should be mentioned that the AC specimens were numerically generated with the idealized microstructures. Later on, researchers (Dai 2010; Dai et al. 2005) further improved the FE modeling technique by exploring the use of real AC microstructures. In their study, the AC microstructures were numerically generated from scanned images of the real AC samples.

Abbas et al. (2004) described a convolution integral-based approach to simulate asphalt binder stress-strain behavior. Compared with the similar method used in ABAQUS (one FEM software), the proposed method allowed changeable model constants depending on the level of strain and hence could model nonlinear viscoelastic behavior. The FE model was a two-dimensional system consisting of coarse aggregates and mastic. The largest size of aggregates in the mastic was dependent on the image resolution. The model was tested by comparing AC shear modulus  $G^*$  predictions to measurements obtained with a simple shear tester. It was revealed that the mastics were 3 to 30 times stiffer than the

binders. Additionally, the relationship between the dynamic axial modulus  $E^*$  and the dynamic shear modulus  $G^*$  of AC mixtures was studied. Hooke's law was employed to relate  $G^*$  and  $E^*$ . It was observed that the predicted Poisson's ratio was unreasonably high, which ranged from 1.1 to 1.5.

Kim et al. (2005) presented a cohesive FE modeling to predict damage-induced mechanical response of AC mixtures. A cohesive damage FE model was formulated for analyzing AC mixtures that were composed of elastic aggregate particles and a viscoelastic binder matrix. The heterogeneous geometric characteristics of the AC mixtures were represented by randomly oriented grain structures which were constructed using the Voronoi tessellation approach. The FE simulation results indicated that the inputting model parameters significantly influenced the mechanical behaviors of the overall AC mixtures.

To predict the compressive complex modulus and creep stiffness of AC mixtures, some researchers have explored the use of the FE models (Dai 2009; Dai and You 2007; You and Dai 2007a; You et al. 2006). In their studies, the AC mixture was considered as a two-phase system which consisted of coarse aggregate (larger than 2.36mm) and asphalt sand mastic (mineral fillers, fine aggregate, and asphalt). The AC microstructures were generated from the 2D images of cross sections of mixture specimens. Uniaxial compression test simulations were conducted on the FE models, inputting Young's moduli of the coarse aggregate and the asphalt sand mastic at a specific time or frequency. The comparative studies indicated that the FE models were able to predict the complex modulus and creep stiffness of AC mixtures.

Briefly, FE models have been developed, verified, and implemented for microscopic analysis to improve the understanding of AC mixture mechanical behaviors. The research efforts in the past decades can be summarized as follows:

- 1) To build the digital microstructure of AC mixture, two types of approaches were typically utilized, namely the user-made models and the image-based models. The examples of the user-made models are: a) the randomly shaped and distributed solids surrounded by an elastic asphalt matrix (Sepehr et al. 1994); b) the general elliptical particles surrounded by binder cement (Sadd et al. 2003) and; c) the randomly oriented grain structure constructed using a Voronoi tessellation approach (Kim et al. 2005). The image-based models were built from the AC mixture images, which could be captured from a digital camera (Masad and Somadevan 2002), a scanner (Abbas et al. 2004), or X-ray CT (Kose et al. 2000b).
- 2) To simulate interactions in the AC digital microstructures, different mechanical models were developed including a) the elastic models (Sepehr et al. 1994), b) the linear and nonlinear viscoelastic models, c) the damage-induced models and d) the viscoelasto-plastic or viscoelasto-viscoplastic models.
- 3) The developed FE models have been utilized to a) predict AC stiffness, b) investigate localized strain distribution (Bahia et al. 1999);(Kose et al. 2000b), c) estimate stiffness anisotropy (Masad et al. 2002b) and simulate damage behaviors.

Although there have been many achievements in microstructure-based FE modeling of AC mixtures, additional focus is still needed on the following issues:

- 1) Most existing FE models were built on the basis of the assumption that: an AC microstructure was considered as a two-phase system of larger size aggregates surrounded by asphalt mastic. Although more and more researchers believed that the large size aggregates are intended to interact with asphalt mastic instead of asphalt binder alone, the theoretical basis for this assumption was not clearly reported.
- 2) In most studies, asphalt mastic properties were estimated from those of asphalt binders with an amplified coefficient. Usually, the amplified coefficient is referred to the stiffness ration of mastic to binder. Unfortunately, the coefficient was varied in a broad range and different researchers used different values. For example, researcher (Papagiannakis et al. 2002) conducted micromechanics analysis and yielded the stiffness ratio of mastic to binder ranging from 3 to 5, while other researchers (Abbas et al. 2004) observed that the value ranges from 3 to 30.
- 3) FE analysis provided the mastic strains rather than the asphalt binder strains. In order to estimate the stains in asphalt binder, micromechanical models were usually used. However, the micromechanical model was too simple to represent the real microstructure of the asphalt mastic. Therefore, the so-called binder strains may not be true after all.
- 4) Effects of mix composition were not considered. The influences of aggregate gradation, aggregate particle shapes, air voids, and stiffness ratio of aggregate to asphalt binder, for instance, may turn the conclusions in the opposite direction. In a mixture with a well interlocked aggregate structure, the major load is transformed through the aggregate structure and the asphalt binder or mastic takes a very small fraction of the load. Thus, the strain in the asphalt or mastic may be not as large as what was observed in the previous studies. Therefore, for future study: a) more accurate micromechanical models or FE analysis are needed to capture asphalt binder strains; b) it is necessary to consider the effects of mix composition.

### **2.6.2. DE Model Developments and Applications**

The DE method (DEM) is a family of numerical methods for computing the motion of a large number of particles of micron-scale or above. As of today, DEM is widely accepted as an effective method for addressing engineering problems in granular materials as well as in solids with discontinuities. The discontinuities in AC microstructure include: a) discontinuities of material properties at interfaces between aggregates and asphalt matrix; b) disconnections between adjacent aggregate particles and; c) air voids. Although continuum mechanical models, such as FE models, may be able to simulate AC mixtures' discontinuities, additional assumptions are needed. Since DEM was developed to simulate material discontinuities, Meegoda and Chang (1993) believed that a DE model is a very intuitive approach in modeling AC mixture mechanics.

In the early 1990's, Meegoda and Chang described their initial attempt to model the behavior of asphalt concrete under different loading conditions using DEM. Change and Meegoda (1999b; 1997b) continued their studies using the same DE model subsequently.



In their studies, a microscopic model for AC mixtures, ASBAL was developed by modifying TRUBAL program (an open DEM code). The modified version was called ASBAL as it modeled the Asphalt concrete based on the TRUBAL. In the ASBAL model, AC mixture specimen was reconstructed with a given number of aggregates coated with asphalt cement. The aggregates were simulated with discrete elements (balls), while the asphalt cement was microscopically represented by two sets of viscoelastic elements in normal and tangential directions at each contact of two adjacent discrete elements. The viscoelastic elements could be Maxwell, Kelvin-Voigt, or Burger's elements. It was believed that the Burger's elements were the most promising for modeling asphalt binder behaviors. Simulations based on ASBAL were performed under varied types of loadings such as monotonic loading and cyclic loading with considering temperature effects. It was found that the simulations compared well with experimental results. The ASBAL model, however, was: 1) unable to simulate mineral aggregate gradation, shape, and distribution; 2) unable to consider the asphalt film thickness between aggregates and; 3) unable to simulate deformations in aggregate particles and asphalt cement. Additionally, it was hard to determine the ASBAL model parameters in the laboratory since there was contact stiffness between particles.

Although the ASBAL was developed in the earlier 1990's, few literatures have been found till today to discuss the implements of the ASBAL by other researchers. Instead, most researchers utilized the commercial DEM codes, Particle Flow Codes in two-dimension and three-dimension (PFC2D and PFC3D). Both PFC2D and PFC3D were first released in 1994, which had friendly interfaces and many useful features for modeling granular and solid-like materials. At the very beginning of the 21st century, Buttlar and You (2001) developed a microfabric discrete element modeling (MDEM) approach and implemented the new approach to simulate indirect tension tests with diametrically loaded cylindrical specimens. In their study, the mineral aggregate system was broken into two parts: the coarse and fine aggregates plus mineral fillers. The fine aggregates plus mineral fillers with the asphalt binder were integrated into the asphalt matrix (asphalt sand mastic).. Both asphalt sand mastic and coarse aggregates were modeled with clusters of small discrete elements (balls or discs). It should be mentioned herein that in ASBAL model, each coarse aggregate particle was simulated with a single ball while the asphalt matrix geometry was not simulated with visible discrete elements. Obviously, compared with ASBAL, the MDEM has the following advantages: 1) aggregate morphology characteristics, such as shape, angularity, and orientation can be simulated; 2) deformation and strength properties of coarse aggregates and the asphalt matrix can be modeled. After the early model development, the same researchers continued their studies to improve the MDEM and utilize the model to predict the stiffness of AC mixtures from 2001 to 2006. For example, in 2004, they developed a technique to calibrate the MDEM model by dilating aggregates to create additional aggregate contacts (You and Buttlar 2004). In 2005, they published an article to apply the MDEM for use in predicting the complex modulus of asphalt-aggregate hollow cylinders subjected to internal pressure. It was observed that the 2D DEM models under predicted the mixture modulus. Additionally, in that article, the key technique of the MDEM, clustered discrete element modeling technique, was introduced. In 2006, they published another article to apply the MDEM for predicting the AC mixture complex modulus

under uniaxial loads. It was similarly observed that the MDEM approach provides a low prediction compared with the experimental tests.

The overall constitutive behaviors of a solid-like material can be simulated in PFC2D or PFC3D by assigning a local constitutive law at each particle contact. The local constitutive law consists of three parts: a stiffness model, a slip model, and a bonding model. The stiffness model provides the links between the contact forces and relative displacements of contacting discrete elements. The slip model and bonding model describe the strength properties at the given contact. The slip model enforces a relation between shear and normal contact forces, such that the two contacting discrete elements may experience frictional sliding. The bonding model serves to limit the total normal or shear force that the contact can carry by enforcing bond-strength limits. The slip model is an intrinsic property of the two entities in contact, while the bonding model is also easily defined using one of the available models in the PFC2D or PFC3D. Therefore, the local constitutive law is usually distinguished by its stiffness model. In the MDEM model, aggregates and asphalt mastic can be assigned using different stiffness models even though the developers of the MDEM utilized the same model for both aggregates and mastic, a simple linear elastic contact stiffness model which is a built-in model in the PFC2D (Buttlar and You 2001; You and Buttlar 2004; You and Buttlar 2005). It should be mentioned herein that different values of model parameters were assigned to mineral aggregates and asphalt mastic even though the same stiffness model was used. Recently, the MDEM model was improved by researchers through employing a linear viscoelastic Burger's model as the stiffness model to simulate the time-dependent behaviors of the asphalt mastic (Abbas et al. 2007; Liu et al. 2009) and utilizing an energy-based bilinear cohesive zone model to simulate the crack initiation and propagation (Kim and Buttlar 2009; Kim et al. 2008). When the viscoelastic Burger's model was used, the computation time was very long. To accelerate the simulation of AC mixture with the viscoelastic model, researchers introduced several techniques by using user-written C++ codes (Liu et al. 2008) and utilizing the frequency- or time-temperature superposition principles (Liu and You 2011a; b; You et al. 2011a; You and Liu 2010). According to their studies, the between 2 to 5 times the simulation time could be saved by using the user-written C++ codes and around 1,000 times by using the frequency-temperature superposition principle. In other words, the DE viscoelastic simulation of AC mixtures which took several years or months could be completed within several days or hours.

In addition to the MDEM models discussed above, Collop et al. (2007; 2006a) utilized the PFC3D to simulate the viscoelastic deformation and dilation behaviors of an idealized AC mixture under uniaxial and triaxial compressive creep loading. For convenience, the authors call the DE model used in their studies the idealized PFC model. In the idealized PFC model, the highly idealized mixture was composed of single-sized spherical particles mixed with asphalt binder. The principal reasons for choosing this form of idealized asphalt mixture were: 1) the packing characteristics could be known (dense random packing); 2) the behavior of the mixture would be dominated by the asphalt binder and; 3) complex influence of aggregate interlock would be minimized. The overall constitutive model in the idealized PFC model had concepts similar to the ASBAL: aggregates were simulated with discrete elements, but the bitumen film geometry was not modeled with

visible discrete elements. It's difference from the ASBAL was that: 1) a technique was presented in this study to consider the bitumen film geometry; 2) aggregates were simulated with spherical particles.

Figure 2.4 shows a brief summary of the DEM models for AC mixtures. As mentioned above, the early DEM model is called ASBAL which was developed in 1993 by modifying an open DEM code, TRUBAL. After the ASBAL model, the PFC2D or PFC3D was utilized and a series of studies were conducted. Buttlar and You developed the MDEM in 2001. Initially, both asphalt matrix and mineral aggregates were simulated with the simple linear elastic model. Later on, the linear viscoelastic Burger's model and the bilinear cohesive model were employed to simulate AC mixture's time-dependent and fracture properties. The idealized PFC model was developed to simulate AC mixture with PFC3D, but its concept was much closer to the ASBAL model.

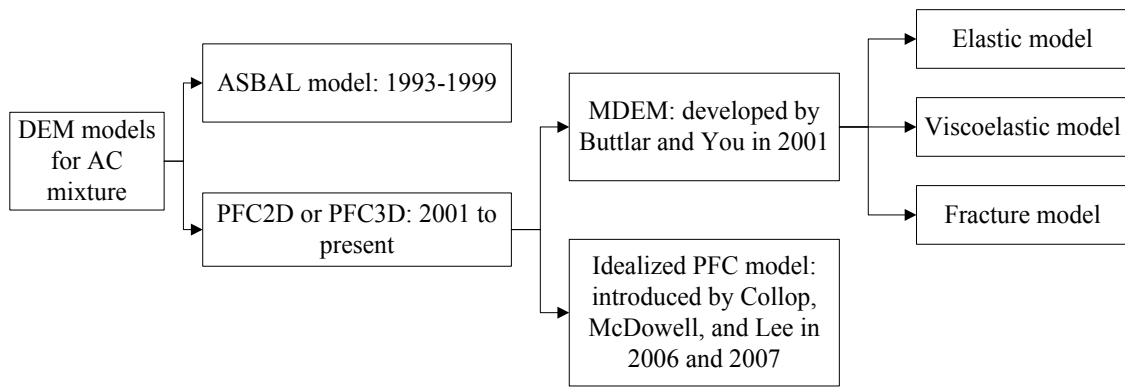


**Figure 2.4 Summary of DEM models for simulating AC mixtures**

**Table 2.4  
Summary of the models for rebuilding AC microstructures**

Geometric models		References
Image-based models	2D	(Adhikari and You 2008; Adhikari et al. 2008a; Buttlar and You 2001; You 2003; You et al. 2008d; You and Buttlar 2006); (Kim and Buttlar 2005; Kim et al. 2008);(Abbas et al. 2007; Liu et al. 2009)
	3D	(Adhikari and You 2008; Adhikari et al. 2008a; Fu et al. 2008; Wang et al. 2007a; You et al. 2008d)
User-defined models	2D	(Liu and You 2008; Liu et al. 2008; You et al. 2008a)
	3D	(Liu and You 2011a; Liu and You 2009; Tian et al. 2007a; You et al. 2008a)

Unlike the ASBAL and the idealized PFC models, the MDEM allows users to rebuild AC mixture microstructure. Generally, two kinds of geometric models were utilized to rebuild the AC mixture microstructure, namely image-based models and user-defined models. An image-based model is built from real images of an asphalt mixture. With current imaging techniques, such as X-ray Computed Tomography (X-ray CT), most of the real micro-structural features of AC mixture could be characterized (Abbas et al. 2007; Masad 2004; Wang et al. 2007a; You and Adhikari 2008). The major advantage of an image-based model is that it is able to exactly represent the AC microstructure if the resolution of the images is high enough. Therefore, most researchers utilized image-based models to build the AC digital microstructures. The disadvantage, however, is its laboratory dependency, which gives users limited options to choose different microstructures unless the AC images are redone. In order to overcome the disadvantages of image-based models, the authors of this paper developed and implement user-defined models to predict AC dynamic or creep stiffness (Liu and You 2011b; Liu and You 2009). Compared with the imaged based models, a major advantage of the user-defined models is its lab-independency. For example, when researchers try to investigate the effects of aggregate shapes on AC performances, they need to minimize the influences from aggregate orientation, gradation, air voids, and asphalt properties. If an image-based model is employed, they are not supposed to change the AC microstructures until a new AC specimen is prepared and its images are taken. In this situation, the researchers may need a user-defined model where users are able to build their own AC microstructures for particular research purposes. Table 2.4 lists recent advances in the development or implementation of models for rebuilding digital AC microstructures.

- 1) Briefly, three kinds of DE models were developed and implemented to predict AC mixture performances. All the three models compared well with the experimental testing results. The most popularly used the DE model is the MDEM. Currently, after improvements by several researchers the MDEM approach is able to simulate viscoelastic behaviors and fracture behaviors. Although there have been many achievements in the DE modeling of AC mixtures, additional attention is still needed in the following issues:
- 2) Most existing DE models considered AC mixture as an asphalt mastic (or asphalt sand mastic) and mineral aggregates as well as air voids. However, the theoretical basis for this assumption was not clearly reported.
- 3) Most researchers utilized DE models to predict AC stiffness or investigate fracture properties. Few of them applied the DE models to understand the impacts of AC composition on its mechanics.
- 4) Few researchers considered Poisson ratio in their DE models even though this is one very important parameters, especially for a typical three-dimensional problems, For example, if one tries to simulate pavement responses under the rolling wheels, the Poisson ratio in the DE model has to be considered in order to accurately predict the stresses and strains in the horizontal directions.

### **2.6.3. Summary of DE and FE Models**

Both FE and DE models were developed for modeling AC mixture microstructures in the early 1990s. Subsequently, those models were further verified through comparisons with experimental testing results and implemented for microscopic analysis and prediction of stiffness, rutting, and fracture properties. According to recent studies, the FE and DE models compared well in prediction of creep stiffness (Dai and You 2007; You 2011) and mixture specimen compactions (Wang et al. 2007c).

To build the digital microstructure of AC mixture, two techniques were typically utilized, namely the user-defined models and the image-based models. The major advantage of the image-based models is that they were able to represent relatively accurate AC microstructure. The disadvantage is their lab-dependency nature. For example, before building the image-based model, the images of the pre-prepared AC specimen are required and imaging processing is needed. The user-defined models have less accuracy, but they are independent of the laboratory tests. Therefore, an image-based model is recommended when particular AC mixture and its images are available or easily obtained. A user-made model is recommended when the researchers want to know general conclusions.

To simulate interactions in the AC digital microstructures, different mechanical models were developed. The FE models include: a) the elastic models (Sepehr et al. 1994); b) the linear and nonlinear viscoelastic models; c) the damage-induced models and; d) the viscoelasto-plastic models. The DE models include the ASBAL, the MDEM, and the idealized PFC model.

Both the FE and DE models can be used to improve the fundamental understanding of AC mixtures. Few studies, however, have focused on the impact of the mix composition characteristics on AC mechanics.

## **2.7. Summary and Recommendations**

This study has reviewed the advances in understanding AC mixture composition and methods to investigate the impact of mixture composition on AC mechanicals. The following observations were summarized:

- 1) Although several researchers have pointed out that mineral aggregate of different sizes play different roles in determining the asphalt mixture mechanics, more evidence is needed to validate this assumption.
- 2) Based on the roles of mineral fillers, fine aggregates, and coarse aggregates, there are at least three different ways to understand the composition of an AC mixture as shown in Figure 2.1. With the rapid developments of the imaging processing techniques and computer modeling approaches, a deeper insight of the AC composition characteristics is expected in the near future. For example, additional parameters will be developed to characterize distribution features of AC mixtures using imaging techniques. With those microstructural parameters, one can perform complex computer simulation to understand the links between AC microstructure

- composition and its performance. Eventually, the developed parameters and the links can improve the existing design method for AC mixtures.
- 3) Many techniques and testing equipments are available to quantify aggregate morphology properties. The major challenge, however, is how to use the existing resources for improving the fundamental understanding of aggregate morphology properties.
  - 4) Most of asphalt binder properties can be measured using the Superpave binder equipment except the accurate tensile strength.
  - 5) With digital imaging techniques, researchers are able to reconstruct an AC microstructure for further analysis and develop certain parameters to quantify the AC micro structural features. However, additional studies are needed before those techniques can be put to routine use. Parameters are needed to link the AC mixture's internal structural characteristics with its global mechanical behaviors.
  - 6) Although studies have been done to understand the impact of AC mixture composition with experiment-based methods, the conclusions were sometimes conflicting.
  - 7) Even though some micromechanical models, such as the Paul's equations and the arbitrary phase geometry model could act as mix laws to provide bounds of AC stiffness values, the bounds were so wide that they essentially provided no useful information. On one hand, most micromechanical models are suitable for the composite with a smaller volumetric fraction of the inclusion phase instead of as large as 84% in the AC mixture. On the other hand, mineral aggregates with different sizes may play different roles in determining the effective properties, but most researchers did not consider aggregate sizes.
  - 8) Numerical models, such as the FE and DE models, have been developed, validated, and implemented in modeling AC stiffness, rutting, and fracture behaviors. However, few studies have focused on implementing the FE or DE models to understand the impact of AC mixture composition characteristics on its global mechanical performances.

Based on the observations above, the authors believed that additional studies are needed to:

- 1) Improve the understanding of the roles of mineral aggregates with different sizes in determining AC performances;
- 2) Improve the understanding of how the AC mixture composition characteristics impact mechanical behaviors. The AC mixture composition characteristics may include aggregate gradation, morphology, asphalt binder time-dependent properties, and distributions of the aggregates, asphalt matrix, and air voids.
- 3) Develop certain structural parameters which can be used to link the AC composition or microstructure characteristics to its certain global mechanical behaviors.

For the future studies, the authors would recommend numerical models as research tools to understand the impact of AC composition on its mechanics due to their advantages over analytical models and experiment-based methods. Both the FE models and the DE

models are recommended. The advantages of FE models include: 1) The FE method is the most popularly used numerical method. The FE modeling results are accepted by a larger population of researchers, designers, and practitioners; 2) There are very powerful and user-friendly commercial FE codes, such as ABAQUS, ANSYS. 3) The existing studies have developed complex viscoelastic-viscoplastic constitutive models which can simulate AC time-dependent behaviors. The disadvantages of an FE model includes: 1) Advanced constitutive models are needed to simulate the nonlinear, time-dependent, and plastic deformation of asphalt materials; 2) particular elements are needed to simulate the interactions at the surfaces between individual aggregate particles or an aggregate particle and asphalt mastic. By contrast, the advantages of DE models include: 1) It was developed to simulate a system which consists of particles. An AC sample is a composite of aggregate particles glued with asphalt binder or mastic. Therefore, a DE model is closer to the AC composition and can be considered as a straightforward and intuitional approach; 2) The AC complex mechanical behaviors can be simulated with very simple linear elastic and viscoelastic contact models. The disadvantages include: 1) a DE model has limited capability to simulate asphalt binding materials (asphalt binder, asphalt mastic, or asphalt sand mastic) which is not particles in nature. In order to accurately simulate asphalt binding materials, a DE model requires a larger number of elements which causes the inefficiency of the DE simulation; 2) The existing DE codes have less powerful than the FE codes.

## **2.8. Acknowledgements**

This material is based in part upon work supported by the National Science Foundation under grants 0701264. Any opinions, findings, and conclusions or recommendations expressed in this material are those of the author's and do not necessarily reflect the views of the National Science Foundation.

## **Chapter 3. Aspects for Simulating Asphalt Concrete Materials with PFC2D/3D<sup>2</sup>**

### **3.1. Overview**

PFC2D/3D, short for Particle Flow Codes in two-dimensions and three-dimensions, are two of the commercially available DEM software packages, commonly utilized for geotechnical engineering problems. As mentioned in Chapter 2, researchers recently applied those two codes to modeling AC materials due to their advantages over the continuum codes. This dissertation employs the two DEM codes for predicting and interpreting AC micromechanics and pavement-wheel interactions. The main objective of this chapter is to describe the methodology which was utilized in this research to simulate AC materials. It should be noted that even though this chapter is oriented toward modeling asphalt concrete materials, most of the discussions and conclusions are also suitable to any other concrete-like materials. Followed are the seven sections of this chapter: section 3.2 gives a general outline of steps for simulating asphalt concrete materials, sections 3.3 through 3.7 provide specific aspects in modeling, and section 3.8 concludes this chapter.

### **3.2. Modeling Concrete-like Materials with PFC2D/3D**

As mentioned in the chapter 2, there are many factors which can govern the overall performance of AC materials. Additionally, those factors become entangled together, which makes it very challenging to isolate one from the others. Since there is massive uncertainty in both AC structural and mechanical properties at micro-levels, it is a challenge to expect that the prediction from a microstructure-based computer model can be utilized to provide design data in practical projects. However, computer models such as the DE and FE models are still useful in providing a picture of the mechanisms that may occur in particular situations. A computer model can be very simple or extremely complicated for simulating AC materials. Generally, a complicated model provides more accurate microstructural and mechanical information, but it is time consuming, expensive, and less efficient. Sometimes, it is a waste of effort to construct a very large and complicated model that may be just as difficult to understand as the real case. By contrast, a simple model provides less information in term of microstructural or mechanical features, but such a simple model has more efficiency and sometimes provides a clearer picture than a complicated model does. Evidently, both simple and complicated models are useful in different circumstances. The author believes that:

- 1) A large and complicated model may be very useful in a) providing more detailed information which is beyond the current experimental testing capabilities; b) validating or calibrating simple models.

---

<sup>2</sup> Part of this chapter will be submitted for publication.



- 2) A simple or idealized model is helpful in a) understanding concrete material fundamentals in a fast, simple, and clear way; 2) providing preliminary data which can be used to develop a guidance for more complicated numerical or experimental research.

In order to simulate AC materials with PFC2D/3D, five steps must be considered and will be discussed in sections 3.3 through 3.6. The five steps are listed below:

- 1) Create AC geometry which is constructed with fundamental elements (discs in PFC2D or spheres in PFC3D);
- 2) Develop constitutive models at each contact between fundamental elements or walls;
- 3) Link constitutive model parameters to physical material properties;
- 4) Apply boundary and initial conditions;
- 5) Perform simulation and interpret the results.

### **3.3. Reconstruction of AC Geometry with PFC2D/3D**

A computer modeling usually starts from a geometry generation. No matter which method is chosen to perform the modeling, a geometry model can be considered as a container which holds the mechanical model, material properties, and loading conditions.

In PFC2D/3D, material geometry is constructed with a finite number of fundamental elements (discs in 2D model and balls in 3D model). Evidently, if the physical problem is concerned with the movement and interaction of spherical or circular particles, it can be directly simulated with the fundamental elements (discs or balls). However, mineral aggregates in concrete have blocky shapes which are completely different from the spherical shapes.

In PFC2D/3D, there are two approaches for modeling blocky shapes, namely the cluster logic and the clump logic. The cluster logic allows users to create a cluster which consists of two or more spherical particles bonded together with bonding contact models. The clump logic allows user to create a clump by modifying a group of slaved fundamental elements. Followed are differences between a clump and a cluster:

- 1) According to clump logic, the slaved particles in a clump remain at a fixed distance from each other and contacts internal to the clump are skipped during the calculation cycle. In other words, no internal deformation occurs in a clump and a clump behaves as a rigid body which never breaks and deforms only at its boundary. By contrast, a cluster behaves as a solid which can have internal deformation or fracture.
- 2) The fundamental elements within a clump can overlap to any extent and contact forces are not generated between those particles. By contrast, elements within a cluster cannot overlap too much since contact forces will be generated.

As discussed above, a clump and a cluster can be considered as advanced elements which are composed of a finite number of the fundamental elements. Therefore, there are three

types of elements for constructing geometry of a PFC2D/3D model. Table 3.1 lists the three types of elements and their potential applications.

There are two commands that can be used to create the fundamental elements in PFC2D/3D: BALL and GENERATE. The BALL command creates a single particle and place it at the specified location, while the GENERAL command creates a specified number of particles and randomly place them within the specified area (2D) or volume (3D). See more details about those two commands in the manuals of PFC2D/3D. After the fundamental elements have been created, clumps or clusters are formed through using CLUMP command and the bonding models, respectively, to simulate blocky shapes in a concrete sample. In this dissertation, both 2D and 3D DE models were utilized to simulate AC microstructures.

**Table 3.1**  
**Three types of elements for building a PFC2D/3D model**

Physical Particle Shapes	Elements in PFC2D/3D
Spherical or Circular Shapes	Fundamental elements: balls in 3D and circles in 2D
Blocky Shapes	Clusters which behaves as a solid
	Clumps which behaves as a rigid body

**Table 3.2**  
**Shows the DE models versus chapters.**

Model Category	Chapters	Notes
2D Randomly-generated Polygon	4, 9	Aggregate particle are simulated with randomly-created polygonal particles
3D Randomly-generated polyhedron	5, 9, 10, 14	Aggregate particle are simulated with randomly-created polyhedron particles
3D Idealized Model I: R-model	6, 13	Aggregate particles are simulated with ellipsoidal particles. All the particles have the same orientation angle throughout the entire specimen
3D Idealized Model II: A-model	6	Aggregate particles are simulated with ellipsoidal particles with fractured surfaces. All the particles have the same orientation angle throughout the entire specimen
2D image-based model	7	The microstructure is reconstructed from a 2D image of the laboratory-prepared AC specimens.
3D image-based model	11, 12, 15	The microstructure is reconstructed from 154 X-ray scanned 2D images of the laboratory-prepared AC specimens.

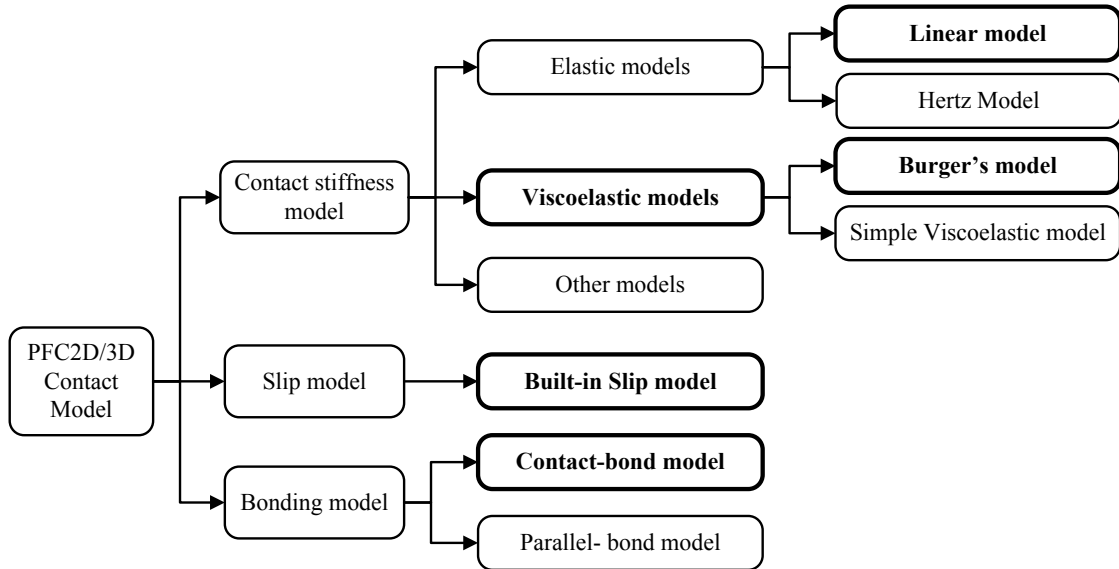


**Figure 3.1 Contact Models in PFC2D/3D**

### **3.4. Mechanics of DE Model for Concrete Materials**

Geometry of a DE model tells how the elements listed in Table 3.1 are distributed in a certain volume or area, while mechanics of the DE model describes how those elements interact with each other. In PFC2D/3D, the discrete elements interact with other elements, or with walls (usually serve as boundaries) through forces that develop at their contacts. PFC2D/3D utilizes the term “contact” to denote the mechanical interaction and the term “contact model” to describe the physical behavior occurring at a contact. In an AC digital specimen, there are at least four interactions, including interactions between mineral aggregate particles, those within a single aggregate particle, those between a particle and cement, and those within cement. In order to model the four interactions, four constitutive models are needed. Each of them may have three parts: a contact-stiffness model, a slip model, and a bonding model (Kim et al. 2009b). Figure 3.1 shows contact models which are available in PFC2D/3D. In this dissertation, both the linear elastic model and the Burger’s model were selected as the contact stiffness models to simulate mineral aggregates and asphalt cement. The built-in slip model and the contact-bond model were chosen to simulate the strength properties in the asphalt concrete system. Chapter 7 will provide more details about the mechanical model of AC materials.

### **3.5. Links between Model Inputs and Material Physical Properties**

As mentioned above, a PFC2D/3D model can easily simulate complicated systems without advanced constitutive models. However, it is often difficult to choose such model parameters that the behavior of the synthetic material resembles that of an intended physical material. In other words, compared with FE models, one challenge for using a PFC2D/3D model is to choose material properties. In typical FE programs, the input

parameters (such as modulus and strength) can be directly derived from those measured in the laboratory. By contrast, in a PFC2D/3D model, the macro-scale material behavior is synthesized from the micro-scale interactions of its components (discrete elements). The input properties of the microscopic components are usually unknown and also difficult or impossible to be obtained from regular experimental tests. In this situation, the person who performs the simulation has to understand not only the PFC2D/3D program itself, but also the system which he/she studies on. In other words, he or she must first understand the relevant behaviors of the intended physical system and the responses that best characterize those behaviors. Then, the appropriate microscopic properties can be determined to best represent the responses of the synthetic material which are comparable directly with the relevant measured responses of its physical counterpart. In the PFC2D/3D manuals, a calibration process is recommended for determining the appropriate microscopic properties. Followed are the brief summary of the process.

The target of the calibration process is to relate the deformability and strength micro-parameters (particle and bond stiffness, particle friction coefficients, and bond strengths) to their corresponding set of macro-responses (such as elastic constants, material friction angle, and peak-strength envelope). In the process, the microscopic parameters at a level of a single particle-particle contact are derived by comparing the behaviors of the contact to that of an elastic beam with its ends at the particle center. Figure 3.2 illustrates the equilibrium between the particle-particle contact to the beam. The Equations as follows are utilized in the process to formulate the links between the two sides of the equilibrium:

$$L = W = R_A + R_B \quad 3.1$$

$$H = \begin{cases} t & (PFC2D) \\ L & (PFC3D) \end{cases} \quad 3.2$$

$$A = \begin{cases} Lt & (2D) \\ L^2 & (3D) \end{cases} \quad 3.3$$

$$I = \frac{1}{12} \begin{cases} L^3 t & (2D) \\ L^4 & (3D) \end{cases} \quad 3.4$$

Where:

$t$  = the circular element thickness and can be set by PFC2D command “set disk  $t$ ”;

$A, I$  = cross-sectional area and inertia of the beam, respectively;

$R_A, R_B$  = radius of particle A and B, respectively;

$W, L,$  and  $H$  = three dimensions of the beam.

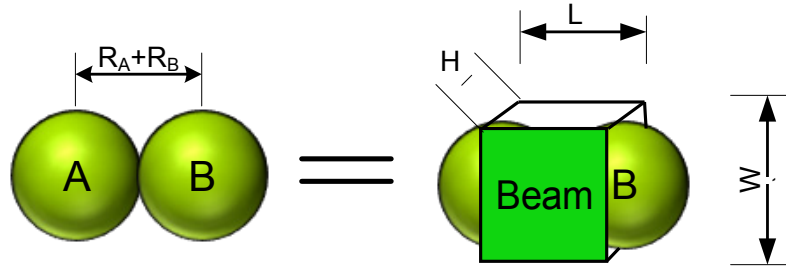


**Figure 3.2 Equilibrium of particle-particle contact to beam ( $R_A$ ,  $R_B$  are radius of particle A and B, respectively, while  $W$ ,  $L$ , and  $H$  are three dimensions of the beam)**

In terms of mechanical properties, the following equations can be derived for expressing the equilibrium between the contact and the beam:

$$K_n = \frac{EA}{L} = E \begin{cases} t & (PFC2D) \\ L & (PFC3D) \end{cases} \quad 3.5$$

$$K_s = \frac{12IG}{L^3} = \begin{cases} Gt & (PFC2D) \\ GL & (PFC3D) \end{cases} \quad 3.6$$

$$\varphi_n = \sigma_c A = \sigma_c \begin{cases} tL & (PFC2D) \\ L^2 & (PFC3D) \end{cases} \quad 3.7$$

$$\varphi_s = \tau_c A = \tau_c \begin{cases} tL & (PFC2D) \\ L^2 & (PFC3D) \end{cases} \quad 3.8$$

Where:

$K_n, K_s$  = Normal and shear contact stiffness values at the contact, respectively;

$\varphi_n, \varphi_s$  = Normal and shear contact bond strength values at the contact.

$E, G$  = Young's modulus and shear modulus of the beam, respectively;

$\sigma_c, \tau_c$  = normal and shear strength values of the beam, respectively.

It should be noted that Chapter 7 will provide more details on the relationship between the model inputs and their corresponding material properties.

**Table 3.2**  
**Boundary conditions in PFC2D/3D**

Boundary Category	Applied Velocities	Applied Forces
Wall as Boundary	<p>Directly apply specified velocities on walls:</p> <p>1) Walls act as boundary constraints if the applied velocities are equal to zero;</p> <p>2) Walls may move at specified velocities to load samples or perform compaction.</p>	<p>Forces cannot directly applied on walls, but there are indirect way:</p> <p>1) Apply velocities and reaction forces are monitored</p> <p>2) Control wall velocities by a numerical servomechanism in order to maintain some prescribed forces</p>
Particle as Boundary	Directly apply specified velocities on the boundary elements (particles)	Directly apply specified forces on the boundary elements
Mixed Boundary	The above boundary conditions can be mixed to solve a more complex problem.	

### 3.6. Boundary, Initial, and Loading Conditions

After the geometry and mechanics done, the next step is to set up boundary, initial, and loading conditions for solving certain engineering or scientific problems. To apply boundary conditions, there are three categories of methods available in PFC2D/3D. As listed in Table 3.2, the three categories are: 1) walls as boundary conditions, 2) particles as boundary conditions, and 3) mixed boundary conditions. Readers may refer to the manual for more detailed information.

The Initial Conditions herein particularly refer to the spatial distribution mode of discrete elements, initial internal stress, and initial porosity in the targeted assembly (the synthetic material). Obviously, different initial conditions results in different material behaviors. Detailed discussion is available in the PFC2D/3D manual.

There are two broad categories of loading conditions in PFC2D/3D: passive loading and active loading. Examples of passive loading are 1) excavation of a void in a model cause loads to be transferred within the model; 2) a gravitational force is applied on each particle according to its density and radius. Passive loading happens automatically and internally to the synthetic material. By contrast, the active loading usually is applied on boundaries. Two commonly used active loading methods are 1) controlling walls as

boundary conditions; 2) Controlling particles by applying forces or velocities on the boundary elements. More details are referred to the PFC2D/3D manual.

### **3.7. Simulation and Result Interpretation**

In order to correctly perform a simulation and interpret the modeling results, this section presents four important aspects in a PFC2D/3D simulation. The author believes those four aspects may impact the computational time or accuracy of the simulation result. Followed are the four sub-sections which summarize those four aspects, respectively.

#### **3.7.1. Is It a Static or Dynamic Problem?**

In a PFC2D/3D model, the interaction of particles is treated as a dynamic process, which easily makes most people believe that the solution of a PFC2D/3D is dynamic instead of static. In fact, a PFC2D/3D model can solve both static and dynamic problems. For a static problem, the solution is achieved whenever the internal forces balance. For a dynamic problem, the solution is constituted with the time histories of quantities of interest. Figure 3.3 shows a bending beam test which is usually considered as a static problem. However, the bending beam test is also can be considered as a dynamic problem if one is more interested in monitoring the beam response in the process of applying the load.

For a static problem, the final steady-state solution is more important than the transitory states. Therefore, an internal damping is usually applied by default in order to cause the equilibrium of the simulated system in a minimum number of cycles. Sometimes, one may choose a proper approach to determine his or her time step which also impacts the computational time and the accuracy of the final simulation results. Details about the damping and time stepping will be discussed in sections 3.7.2 an 3.7.3, respectively.

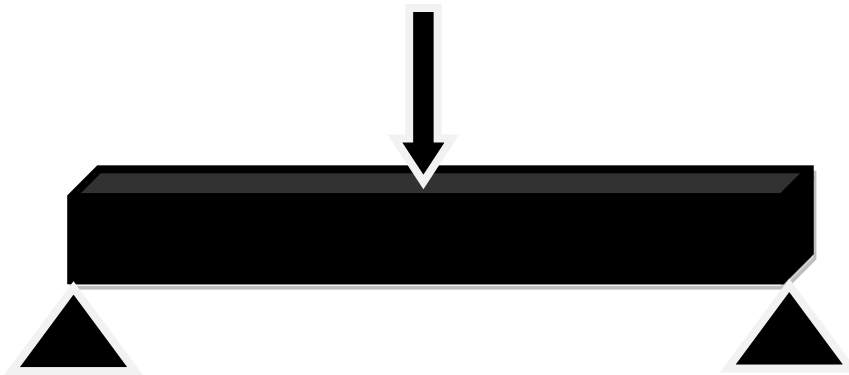


**Figure 3.3 A bending beam test—an illustration of determination between static and dynamic problems**

For a dynamic problem, the emphasis is on the transitory states more than the final steady-state. In this case, both damping and time step should be carefully determined in order to correctly simulate the real material behavior. The damping has to be reduced to a physical realistic value, while the time step has to be small enough. Again, details about the damping and time stepping will be discussed in sections 3.7.2 and 3.7.3, respectively.

### 3.7.2. Mechanical Time step Determination

The solution of a PFC2D/3D model is achieved by the repeated application of the law of motion to each particle, a force-displacement law to each contact, and a constant updating of wall positions. Figure 3.4 is borrowed from the PFC2D/3D manual to illustrate one of the repeated calculation cycles. The calculation cycle starts from updating the set of contacts from known particle and wall position. Then, the contact forces are updated using the force-displacement law based on the relative motion between the two contacting entities and the contact constitutive law. Next, the locations of particle are updated using the law of motion which requires acceleration ratio and an incremental time to calculate the relative displacements of each particle. The acceleration ratio can be calculated from the contact forces while the incremental time is known as the time step which is determined by the system or specified a specific value by user. In a dynamic simulation, the time step value means realistic physical time, which cannot exceed a critical time step that is related to the minimum eigen-period of the total system. By default, the PFC2D/3D system automatically determines the critical time step. This default value of the time step provides a true dynamic solution that is valid for both dynamic and static problems, but it is usually very small and inefficient for a static problem.

**Table 3.3**  
**Determination of mechanical timestep in PFC2D/3D**

Category	PFC2D/3D Commands	Application Limitations
The default option	Set safety_fac	Applicable for both static and dynamic problems;
Differential density scaling	Set dt dscale	Applicable only for static problem to save the computational time
Uniform density scaling	Set dt value	Used for a problem which has a characteristic timescale much longer than that of inertial response



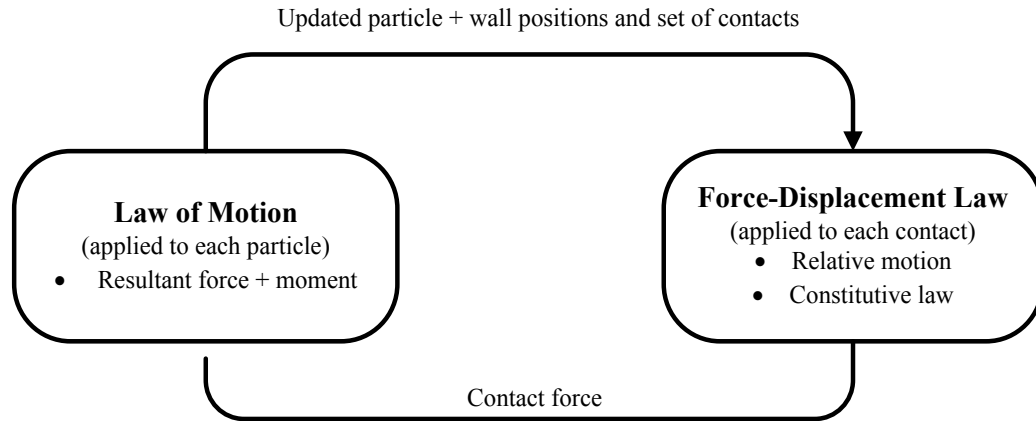


**Figure 3.4 Calculation cycle in PFC2D/3D**

If one is interested only in obtaining the final steady-state solution (for a static problem), an alternative option is available in PFC2D/3D to reduce the total number of cycles required to reach the final solution. This option is to invoke the differential density scaling by using the command: *Set dt dscale*, which causes a fictitious inertial mass to be calculated for each particle, such as its stable timestep will be unity. With this option selected, the final solution will converge faster, but the timescale will be meaningless. Therefore, this option is only valid for a static problem. Other than the two options above for calculating the timestep, one may select another type of density scaling option by using the command: *set dt = value*, where *value* is a desired timestep. By using this option, the inertial mass of each particle is scaled to produce the desired timestep. It should be noted this option does not improve the converging efficiency. To summarize, Table 3.3 lists the three options to determine the timestep.

### 3.7.3. Mechanical Damping Determination

Generally, frictional sliding dissipates the excessive energy in a PFC2D/3D model. However, frictional sliding may not be active in a given model or, even if active, may not be sufficient to reach a steady state solution in a reasonable number of cycles. Therefore, damping is necessary for a PFC2D/3D model to dissipate the excessive kinetic energy. There are three options in PFC2D/3D to apply the damping, namely local damping, viscous damping, and hysteretic damping. Table 3.4 lists the three damping options and their application limitations:

Since concrete material is a compact assembly, most relevant simulations can be considered as static or quasi-static problems. Therefore, local damping is the most appropriate form for most of the concrete simulation. However, there are dynamic problems such as concrete structures under earthquake loading. In that case, viscous damping should be selected and the local damping coefficient is reduced to a reasonable level at the same time.

**Table 3.4**  
**Selection of mechanical damping in PFC2D/3D**

Category	PFC2D/3D Commands/Model	Application Limitations
Local damping	Damp local model	For static or quasi-static problems, the default parameter setting is the most appropriate;  For dynamic problems, the local damping coefficient should be set to a low value appropriate to energy dissipation of dynamic waves.  Inappropriate for problems involving free flight of particles and or impacts between particles.
Viscous damping	Damp viscous model	appropriate for dynamic problems as an alternative damping approach;  inappropriate for static or quasi-static problems
Hysteretic damping	Hysteretic-Damping Model	considered for a problem which is dominated by rapid impacts;  not recommended for other problems

### **3.7.4. Interpretation of Modeling Results**

Compared with conventional continuum code which produces a “solution” at the end of its calculation phase, a PFC2D/3D model is a nonlinear system of discrete elements which evolves in time. In other words, the “solution” of a PFC2D/3D model is time-dependent. At different time point, different “solution” is achieved. One who performs the simulation has to determine when and how the simulation results should be collected by using various indicators which are available in PFC2D/3D to assess the state of a given simulation. Table 3.5 is a brief summary of those indicators.

**Table 3.5**  
**Indicators for interpretation of a PFC2D/3D modeling results**

Category	PFC2D/3D Commands	Notes
Diagnostic forces	History diagnostic muf	The mean unbalanced force can be saved as a history and viewed as a graph
	History diagnostic mcf	The mean contact force can be saved as a history and viewed as a graph
	Print info	The ratio of the mean unbalanced force to the mean contact force, and the ratio of the maximum unbalanced force to the maximum contact force can be printed on the screen
	Solve	This command can be used to set a limiting ratio for a run automatically
Histories	History	This command can be used to track important variables during the simulation
Energy tracing	Trace energy on	This command is to activate energy tracing
	History energy	This command is to save the energy terms as histories. The energy terms include body work, bond energy, boundary work, frictional work, kinetic energy, and strain energy.
Measurement spheres	Measure	Porosity, stress, strain rate, coordination number, and sliding fraction can be measured over spherical volumes positioned at selected locations in the model.
Spatial field variables	Plot velocity/disp/cforce/cbond/pbond/ball	Velocities/displacements/contact forces/contact bonds/parallel bonds/balls can be plotted throughout the model

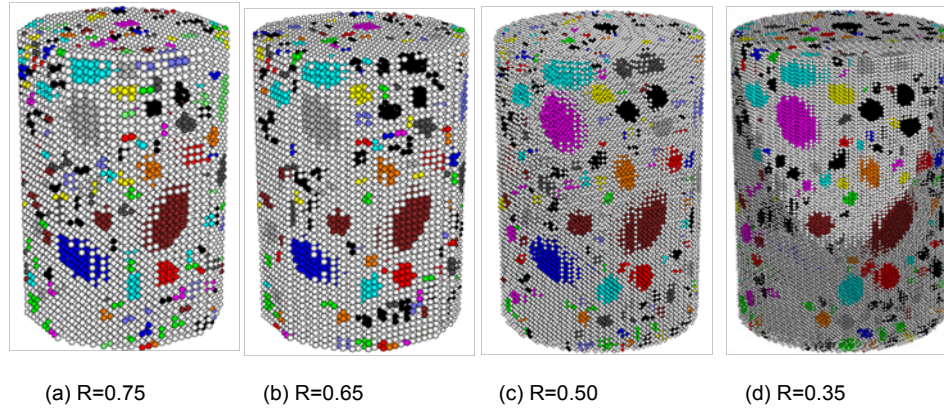


**Figure 3.5 Geometry of the four digital samples for the asphalt concrete**

### **3.8. Size Effects of Discrete Elements on Modeling Results**

The discrete element method (DEM) has been widely accepted as an effective method of addressing engineering problems in granular and discontinuous materials (Cundall and Strack 1979b; Hart et al. 1985; Huang et al. 2008; Kim and Choi 2008; Kim 2008; Taylor et al. 1985). In an asphalt concrete (AC) sample, mineral aggregate particles account for 85% of the total volume and play important roles in determining the overall AC performance. In other words, the majority of an AC volume is occupied by granular particles (aggregates) which result in complex mechanics at discontinuities between individual aggregate particles or those between aggregate and asphalt matrix. Meegoda and Chang (1993) believed that a discrete element model is an intuitive and direct approach in modeling AC mixture mechanics. As discussed in Chapter 2, the early research with DEM can be traced back to the research which was done by Meegoda and Chang (1993). From 1993 to 1999, Meegoda and Chang developed the ASBAL model and used it for studying asphalt concrete viscoelastic behaviors (Chang and Meegoda 1999b; Chang and Jay N 1997; Meegoda and Chang 1994; Meegoda and Chang 1995; Meegoda and Chang 1993). The Particle Flow Codes in two-dimensions and three dimensions (PFC2D/3D) were most commonly used discrete element methods for studying asphalt materials since 2001. The PFC2D/3D models were further categorized into two groups: one of them is the idealized PFC3D model which was developed by Collop et al (2007 ; 2006b) to investigate impacts of asphalt on the AC stiffness. The other is the microfabric discrete element modeling (MDEM) approach which was developed by Buttlar and You (Buttlar and You 2001). From 2001 to present, the MDEM approach has been widely used for simulating asphalt concrete creep tests (Dai and You 2007; You et al. 2011b; Zelelew and Papagiannakis 2010), dynamic modulus test (Buttlar and You 2001; Liu et al. 2009; Liu and You 2011a), and fracture properties (Kim 2007; Kim et al. 2009a). Advantages of the MDEM approach include: 1) the complex behavior of asphalt concrete could be simulated by combining simple contact constitutive models with complex geometric features. 2) Aggregate particles were simulated with clusters of discrete elements. As a result, aggregate particles could be crushable. It should be noted that in a MDEM mode, different sizes of elements could result in different accuracy in

simulating aggregate particle shapes. Additionally, discrete element sizes could further impact computational time-step, computational time, and volumetric proportions of asphalt and aggregates. In order to quantify those potential impacts of discrete element sizes, this section presents a series of three-dimensional discrete element simulations of asphalt concrete as demonstrated in the following sections.

### **3.8.1. Discrete Element Model of Asphalt Concrete**

A computer-generated discrete element model (Liu and You 2011b) was employed in this study to simulate the geometry of an asphalt concrete. Table 11.2 in Chapter 11 shows the aggregate gradation, asphalt content, and air voids in the asphalt concrete. In this study, the asphalt concrete was considered as a two-phase composite of asphalt mastic and mineral aggregates larger than 2.36mm. The volumetric percentages of the asphalt mastic and mineral aggregates larger than 2.36mm were 53% and 47%, respectively. In order to simulate the two-phase system, mineral aggregates were simulated with randomly-created ellipsoid particles. Each ellipsoid particle was a cluster of discrete elements (balls) which were bonded with the contact-bond model. Even though the asphalt mastic was a composite of fines, aggregates less than 2.36mm, asphalt, and air voids in the reality, it was considered as a homogenous media and simulated with a cluster of discrete elements in this study. With the computer-generated model, a total of four digital samples were created to simulate the asphalt concrete. The radiuses of discrete elements in the four digital samples were 0.75mm, 0.65mm, 0.50mm, and 0.35mm, respectively. Figure 3.5 shows the geometry of the four samples.

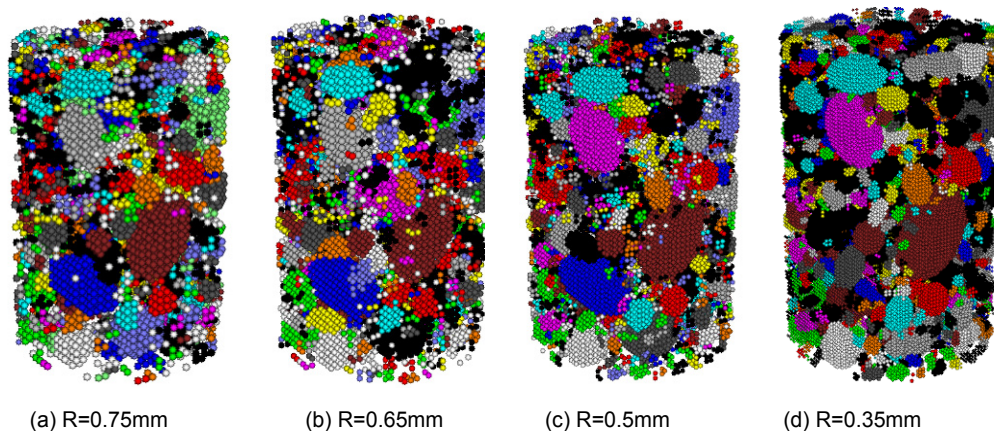
As demonstrated in Figure 3.5, a three-dimensional discrete element model was a system of discrete elements (balls). Apparently, the overall material property of the discrete element model could be simulated through assigning a constitutive model at a certain contact. A homogenous material can be simulated using a single constitutive model for all contacts of discrete elements, while a heterogeneous material needs more than one constitutive models for different contacting interaction behaviors. In asphalt concrete, there are four different contacting interaction behaviors, namely interactions within asphalt mastic, within individual aggregate particles, between asphalt mastic and aggregate particles, and within individual aggregate particles. Therefore, this research utilized four different constitutive models to address the four contacting interactions as demonstrated in Figure 7.2 in Chapter 7. Obviously, each contact model consisted of three parts: a contact stiffness model, a slip model, and a bonding model. The stiffness model expressed the relation between the contacting forces and the corresponding relative displacements of the two contacting elements. The slip model represented the frictional property at a contact, while the bonding model addressed the shear and normal strength at a contact. As shown in the Figure 7.2, the viscoelastic Burger's model (spring-dashpot system) was used as the stiffness model for contacts within asphalt mastic and those between asphalt mastic and aggregates, while the linear contact stiffness model (spring system) was used for other contacts. The slip model was applied for all the contacts but different values were given to the frictional coefficient. The contact-bond model was applied to all the contacts except those between adjacent aggregate particles.

### 3.8.2. Analysis of Mineral Aggregate Shapes

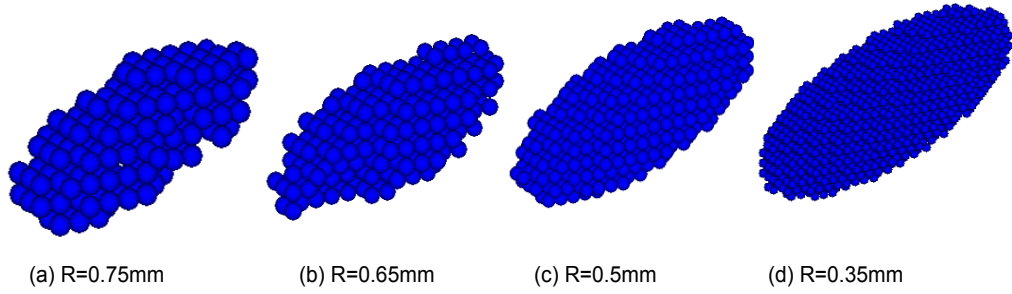
As described in the last section, mineral aggregates were simulated with clusters of discrete elements. Therefore, sizes of discrete elements directly impact accuracy in modeling mineral aggregate shapes. In order to investigate impacts of element sizes on mineral aggregate shapes, mineral aggregates in the four digital samples shown in Figure 3.5 were extracted. Figure 3.6 shows the microstructure of mineral aggregates and individual aggregates of different sizes. From Figure 3.6, it was found that:

- 1) The four digital samples had the similar mineral aggregate microstructures, but they had clear differences in accuracy of mineral aggregate shapes. As shown in Figure 3.6 a), there were many separated balls which simulated fine aggregate particles in the first two samples ( $R=0.75\text{mm}$  and  $R=0.65\text{mm}$ ). Those balls were replaced by clusters of balls in the other two models whose element sizes were smaller. In other words, reducing element sizes could obviously increase the accuracy in simulating mineral aggregate shapes.
- 2) From Figure 3.6 b)~e) shows mineral aggregates whose sieve sizes were larger than  $4.75\text{mm}$ . Apparently, even though their accuracies were dependent on element sizes, the general shapes of those aggregate particles could be simulated. Decreasing element sizes could clearly increase accuracy of shapes of mineral aggregates.
- 3) From Figure 3.6 f) shows mineral aggregates whose sieve size smaller than  $4.75\text{mm}$ . As shown in the figure, in the first two samples ( $R=0.75\text{mm}$  and  $R=0.65\text{mm}$ ) the majority of aggregate particles were simulated with individual balls instead of clusters of discrete elements. With the element size increasing, the individual balls were replaced by clusters of discrete elements. The majority of aggregates were clusters of elements instead of balls when the element size was larger than  $0.5\text{mm}$ .

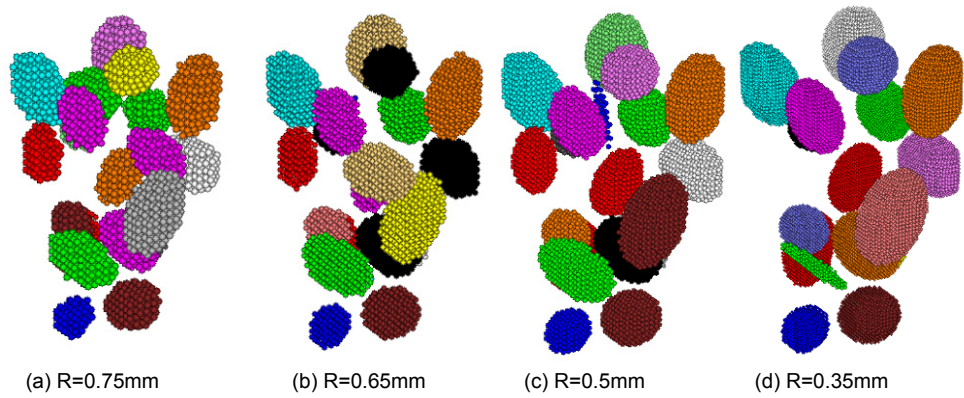
From the findings above, it was concluded that: 1) mineral aggregates larger than  $2.36\text{mm}$  could be simulated with discrete elements whose radius was  $0.5\text{mm}$  or less; 2) Reducing sizes of discrete elements increased accuracy in modeling aggregate shapes.



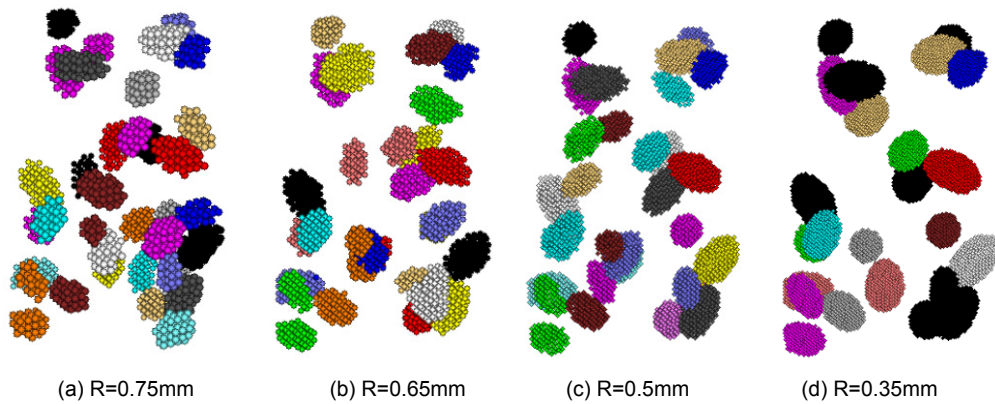
a) Microstructure of Mineral Aggregates



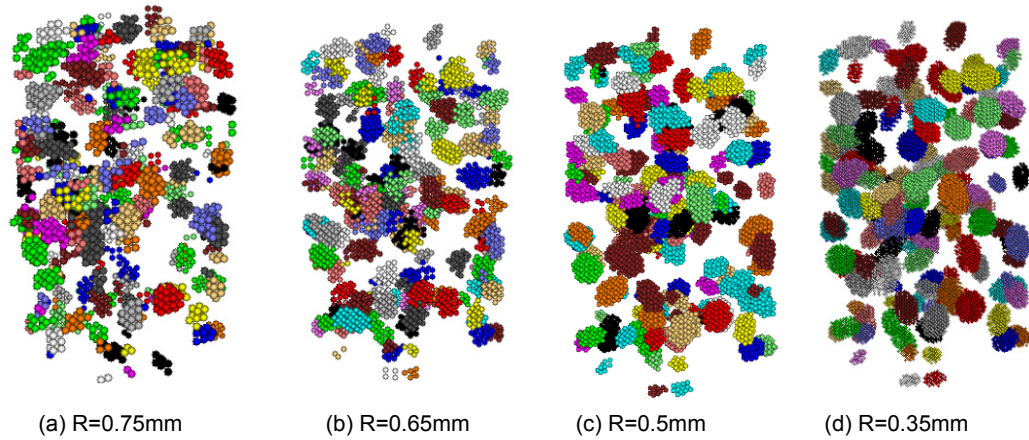
b) Coarse Aggregates ranging from 19mm to 25mm



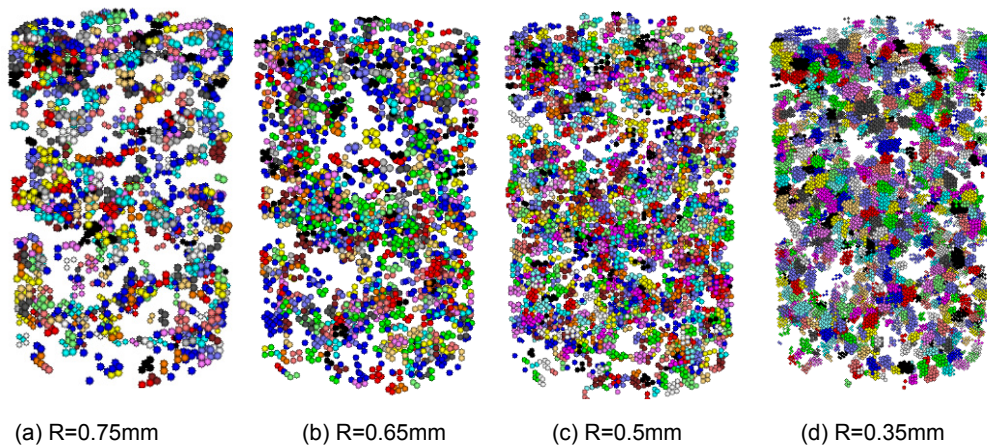
c) Coarse Aggregates ranging 12.5mm to 19mm



d) Coarse Aggregates ranging from 9.5mm to 12.5mm



e) Coarse Aggregates ranging from 4.75mm to 9.5mm



f) Coarse Aggregates ranging from 2.36mm to 4.75mm

**Figure 3.6 Mineral Aggregate Microstructures of the four AC digital samples ('R' denotes**

### 3.8.3. Discrete Element Modeling of Creep Stiffness

Sizes of discrete elements could not only impact mineral aggregate shapes, but also influence computational time, time-step, volumetric percentages of mixture ingredients, and the prediction results of mixture performance. In this study, the four digital samples were used to simulate creep compliance test of the asphalt concrete. The simulation was conducted through applying a constant load on the top of the samples and fixing their bottoms. The inputs of the discrete element simulation include Young's modulus of mineral aggregates and the Burger's model parameters. Table 3.6 shows the values of the inputting parameters. In the table,  $E_m$  and  $\eta_m$  are parameters for the spring and dashpot of the Maxwell element, while the  $E_m$  and  $\eta_k$  are parameters for the spring and dashpot of Kelvin element. Additionally, the time-temperature superposition principle was



employed to accelerate the discrete element simulation. A previous research (You et al. 2011b) shows more details on the time-temperature superposition for simulating asphalt concrete creep tests with discrete element method. During the discrete element simulation, the histories of averaged stress and strain of the asphalt concrete samples were recorded. Through analyzing the simulation results, the creep stiffness was calculated and plotted in Figure 3.7. Figure 3.7 a) and b) show the creep stiffness vs. loading time and element sizes, respectively. it was found that: 1) the curves of creep stiffness vs. creep time were so close to each other that it was difficult to identify their differences; 2) similarly, the curves of creep stiffness vs. element sizes were almost horizontal. Both findings exhibited the fact that discrete element sizes gave negligible impacts on creep stiffness.

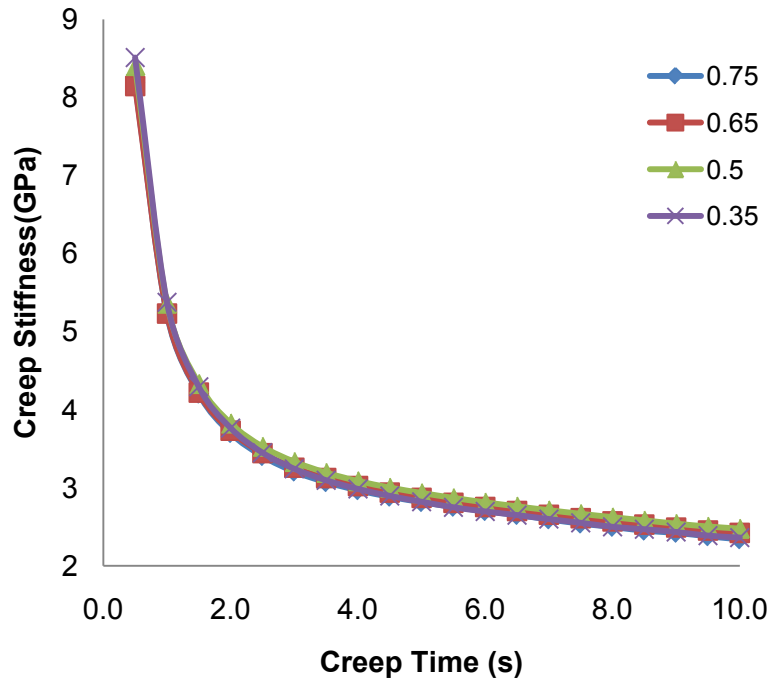
Since it was difficult to distinguish the differences among the four digital samples in terms of stiffness, their relative differences were expressed through stiffness ratios: ratios of stiffness of the four digital samples to that of the fourth digital sample (R=0.35mm). The stiffness ratio was defined as:

$$\text{stiffness ratio} = \frac{\text{stiffness of an AC sample}}{\text{stiffness of the AC sample with } R = 0.35} \quad 13.9$$

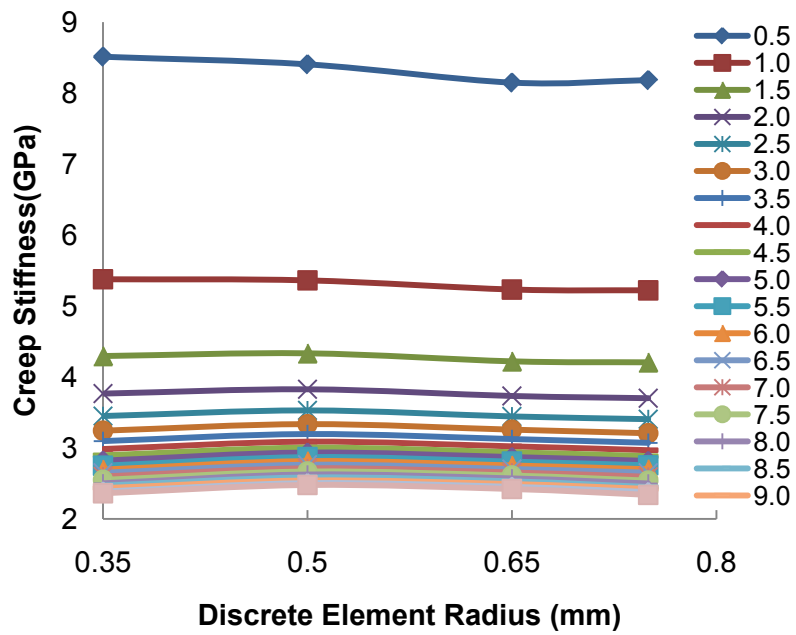
Figure 3.7 c) shows stiffness ratios of the four digital samples vs. element sizes. The following findings were observed: 1) stiffness ratios are various from 0.955 to 1.05. In other words, stiffness differences among the four AC digital samples were within 5%. 2) When creep time is larger than one second, the creep stiffness increased to its peak value at R=0.5mm and then decreased. When the creep time is equal or less than one second, the creep stiffness decreased to its lowest value and then slightly increased. In order to explain the findings above, mineral aggregate shapes were different in the four digital samples. Additionally, volumetric percentages, time steps, and computational times of the four digital samples were also different as shown in Table 3.7. From Table 3.7, it was found that reducing element sizes increased volumetric percentages of mineral aggregates, decreased the time-steps, and increased computational time. The volumetric percentages were slightly impacted by element sizes, which were from 46.69% to 47.41%. Element sizes significantly impacted time-steps and computational time. The time steps decreased from 4.44e-8 to 2.02e-8, while the computational time increased from 0.29 days to 5.61 days.

**Table 3.6**  
**Input parameters of the discrete element simulation**

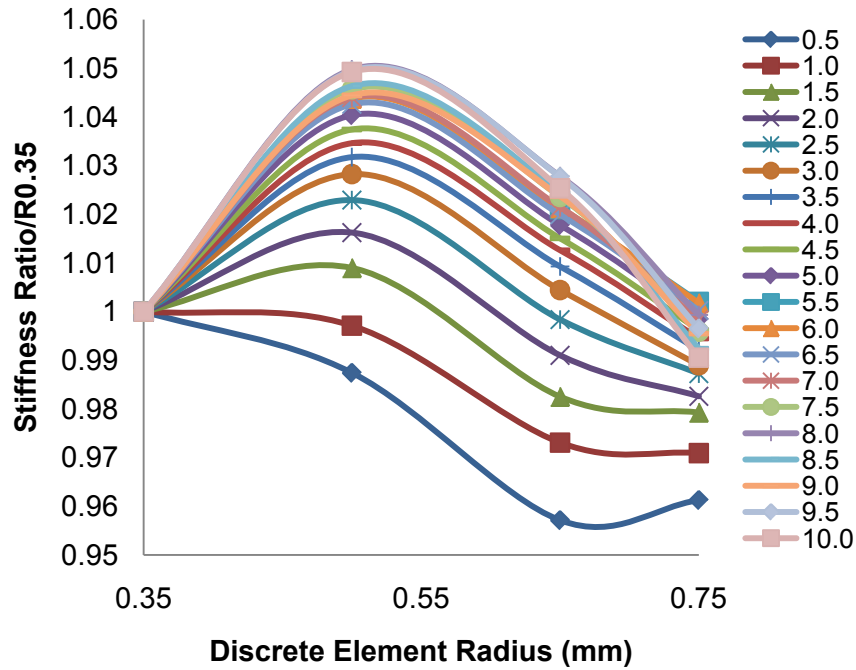
	$E_m$ (GPa)	$E_k$ (GPa)	$\eta_m$ (GPa.s)	$\eta_k$ ((GPa.s)
Burger's Model Parameters	430.9	1.8	35.0	2.2
Young's Modulus	55GPa			



a) Creep stiffness vs. creep time



b) creep stiffness vs. discrete element radius



c) Stiffness ratio vs. discrete element radius

Figure 3.7 DE simulation results of creep compliance tests

**Table 3.7**  
**Volumetric percentages and time steps for the four AC digital samples**

Radius of Discrete Elements (mm)	Volumetric Percentage (%)		Time_step (second/step)	Computational time (days)
	mastic	aggregates		
0.75	53.30841	46.69	4.44E-08	0.29
0.65	53.12034	46.87	3.86E-08	0.63
0.5	52.95264	47.05	2.87E-08	1.71
0.35	52.5917	47.41	2.02E-08	5.61

### 3.8.4. Summary and Conclusion

This paper presents three-dimensional discrete element modeling of an asphalt concrete to investigate effects of discrete element sizes. Four digital samples of the asphalt concrete were produced with a computer-generated discrete element model. All the

inputting parameters were identical except the element sizes to create the digital samples. Through this study, it was found that:

- 1) Reducing sizes of discrete elements could increase the accuracy in modeling the mineral aggregate shapes, vice versa. When element radius was larger than 0.5mm, the smaller aggregate particle shapes could not be simulated.
- 2) In terms of predicted creep stiffness values, the differences among the four digital samples of the asphalt concrete were within 5%. It was not a clear relationship between the predicted stiffness values and the discrete element sizes.
- 3) Discrete element sizes impacted not only aggregate shapes and creep stiffness, but also time-step, volumetric proportions of the asphalt concrete, and computational time. Reducing discrete element sizes resulted in reduced time-steps and longer computational time.

From the findings above, it was recommended that:

- 1) If one's research objective is to predict creep stiffness of an asphalt concrete, it was recommended to select a relatively larger element sizes for reducing the computational time. However, it should be kept in mind that element sizes could give impacts on volumetric proportions of mixture components, time-steps, and aggregate shapes.
- 2) If one's research purpose is to accurately simulate asphalt concrete, it is recommended to select a relatively smaller element sizes for correctly modeling mineral aggregate shapes. However, it should be kept in mind that reducing element sizes could result in longer computational time.

The research findings and conclusions in this paper were based on the limited simulation results. More research efforts are needed to further validate them.

# **Chapter 4. A Randomly-generated Two-dimensional Model for Simulating AC Microstructure and Mechanical Behavior under Cyclic Loads<sup>3</sup>**

## **4.1. Overview**

This paper presents a newly developed model for the simulation of a cyclic loading test (i.e., dynamic modulus test) of asphalt mixtures using user defined material models in the discrete element (DE) method. The DE model was prepared based on a random polygon algorithm instead of the image analysis technique commonly and usually used by many researchers. With this algorithm, the polygonal particles (i.e., aggregates) were created to present aggregates shape and size, and discrete elements (disks or balls) were bonded together with the viscoelastic model to simulate mastics (i.e., asphalt binder mixed with fines). In order to build the constitutive model, four contact models were employed in the asphalt mixture composite including the slip model, linear stiffness-contact model, contact-bond model and Burger's contact model. Lab tests of aggregates and mastics were conducted under dynamic loads to provide the input parameters for DE models of asphalt mixtures. The dynamic modulus and phase angles were measured in the lab were used to calibrate the micro parameters for the DE models so that the micro parameters reflected the viscoelastic behavior of the asphalt mastic. Then, the dynamic moduli of asphalt mixtures (coarse aggregates plus asphalt mastic) were predicted by conducting DE simulation under a cyclic loading algorithm to reflect the viscoelastic behavior of the mixture. The simulation results are very promising when compared the predicted and measured dynamic moduli and the phase angles.

## **4.2. Introduction**

The overall macro-mechanical behaviors of the asphalt mixture are determined by the micromechanics within the cemented particulate system. Based on the heterogeneous multiphase nature of asphalt material, it appears that a micromechanical model would be suited to properly simulate such a material. In fact, over the past 10 years, the use of micromechanics to predict properties of asphalt mixtures and mastics has drawn increasing attention, and a number of researchers have developed micromechanical models with different approaches (You and Dai 2007b). Among these approaches, the discrete element method (DEM) was popularly applied. A few examples of the DEM approach are given here. Zhong and Chang modeled cementitious granular materials with DEM (Zhong and Chang 1999). You and Buttlar developed the micro-fabric discrete element modeling approach (Buttlar and You 2001) and then predicted the asphalt

---

<sup>3</sup>Full text reprinted with permission from ASCE: "Simulation of Cyclic Loading Tests for Asphalt Mixtures using User Defined Models within Discrete Element Method" by Yu Liu and Zhanping You, 2008, GeoCongress 2008: Characterization, Monitoring, and Modeling of GeoSystems (GSP 179), Proceedings of sessions of GeoCongress 2008, pp. 742-749, Copyright © 2008, ASCE. See Copyright clearance in Appendix A.

mixture complex modulus in extension/compression across a range of test temperatures and load frequencies (You and Buttlar 2004; You and Buttlar 2006). These researches listed above had been mainly focused on the linear elastic approach, in which asphalt binder and aggregates were simulated with elastic contact models. With the elastic approach, the stiffness of asphalt mixtures can be predicted, but the viscoelastic properties are difficult to represent. Therefore, in the recent two years, some researchers directed their researches on DE viscoelastic models. Among these researchers, Abbas et al presented a methodology for analyzing the viscoelastic response of asphalt mixtures using DEM (Abbas et al. 2007). However, viscoelastic models for DEM are still needed to further investigate in the following two key areas: 1) input parameters (in micro) for DE models because the micromechanical parameters in DEM are difficult to be obtained from lab tests (not as easy as in finite element models (Dai and You 2007; You and Dai 2007b)); 2) DEM simulation under cyclic loads was not fully addressed in the previous studies. Therefore, the objective of this paper is to present a newly developed model for the simulation of a cyclic loading test (i.e., dynamic modulus test) of asphalt mixtures using user defined material properties in the discrete element (DE) method. The micromechanical parameters for the DEM are defined using lab tests.

### 4.3. Lab Tests and Burger's Model Parameters

#### 4.3.1. Lab Tests

Lab tests were developed in this study to serve two main purposes: 1) to measure the complex modulus and phase angles of mastics and the Young's modulus of coarse aggregates to determine the DE model parameters; and, 2) to measure complex modulus and phase angles of asphalt mixtures for calibration of the micro parameters in DE models. For the asphalt concrete mixture studied in this research, a 19-mm nominal maximum aggregate size mixture was used. It was compacted in a Superpave gyratory compactor to a target air void level of 4.8% by volume. The sand mastic had a nominal maximum aggregate size of 1.18-mm, which was obtained from the mixture's aggregate gradation by eliminating all the aggregates bigger than 2.36mm except the asphalt. The sand mastic had around 14% asphalt content, by weight of mixture. The uniaxial compression test was conducted to obtain the dynamic modulus and phase angles for mastics, aggregate (stones), and mixtures. The test procedure and the results were listed in previous research work (You and Buttlar 2006). The dynamic moduli were measured at 0°C with four frequencies, 0.1, 1, 5, and 10Hz.

#### 4.3.2. Burger's Model parameters

The Burger's model (as shown in Fig.1) was applied in this paper and the parameters were obtained by solving the equation group consisting of Equation (1), (2),(3), and (4):

$$\frac{1}{|E^*|} = \sqrt{\frac{1}{E_1^2} + \frac{1}{\eta_1^2 \omega^2} + \frac{1 + 2(E_2 / E_1 + \eta_2 / \eta_1) \omega^2}{E_2^2 + \eta_2^2 \omega^2}} \quad 4.1$$

$$\tan \Phi = \frac{E_1[E_2^2 + \eta_2(\eta_1 + \eta_2)\omega^2]}{\eta_1\omega(E_2^2 + E_1E_2 + \eta_2^2\omega^2)} \quad 4.2$$

$$E_1 = \lim_{\omega \rightarrow \infty} |E^*| \quad 4.3$$

$$\eta_1 = \lim_{\omega \rightarrow 0} \frac{|E^*|}{\omega} \quad 4.4$$

Where,  $E_1, \eta_1, E_2,$  and  $\eta_2$  represent the parameters of Burger's Model as shown in Fig. 1, and;  $|E^*|$  and  $\Phi$  are dynamic models and phase angle which can be measured from lab tests or obtained from simulation results.

#### 4.4. Random Polygon Algorithm and DE Geometry Model

In this research, the DE software Particle Flow Code in 2 Dimensions (PFC2D) was employed as used in the previous studies (Buttlar and You 2001; You and Buttlar 2004; You and Buttlar 2006). Within this software, only disks or balls are available for discretization of materials. Asphalt mixture is a composite of graded aggregates bound with a mastic mortar and aggregates have different shapes. In order to consider the coarse aggregate shapes, a cluster of disks or balls were bonded together to represent an aggregate in this study. Then asphalt mastic can be treated as a homogenous composite of fines, fine aggregates bound with asphalt binders, and can be simulated with balls bonded with the viscoelastic contact model. In this paper, a newly developed algorithm, namely the random polygon algorithm, was employed. The DE geometry model was built based on this algorithm using the following steps:

- 1) Set a desired aggregate gradation, asphalt mastic content, and sample size;
- 2) Prepare a rectangular sheet filled with balls (or discrete elements);
- 3) Create graded aggregates with the information from Step 1 and 2;
- 4) Obtain the geometry parameters of the model, and;
- 5) Finalize the model and prepare the simulations.

#### 4.5. DE Micromechanical Model

A DE micromechanical model was then prepared and ready for simulation as shown in Fig. 2, where the aggregates were represented with polygonal clusters. The interaction among the discrete particles within the DE model of asphalt mixtures was defined using the following four contact models in this paper, namely the linear contact-stiffness model, the slip model, the contact-bond model and the Burger's contact model. In order to present the micromechanical performances of asphalt mixtures, four interactions were considered and the specific contact models were assigned to the interactions as follows:

- 1) Interaction within an aggregate: a combined model is prepared with a linear contact-stiffness model and a contact-bond model in the aggregate;

- 2) Interaction of aggregates and mastics: a combined model is used with a Burger's viscoelastic contact model, a contact-stiffness model, and a contact-bond model;
- 3) Interaction within mastics: a combined model is developed with a Burger's model and a contact-bond model;
- 4) Interaction between two aggregates: a contact-stiffness model is considered.

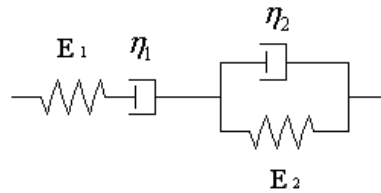


**Figure 4.1 Burger's model**

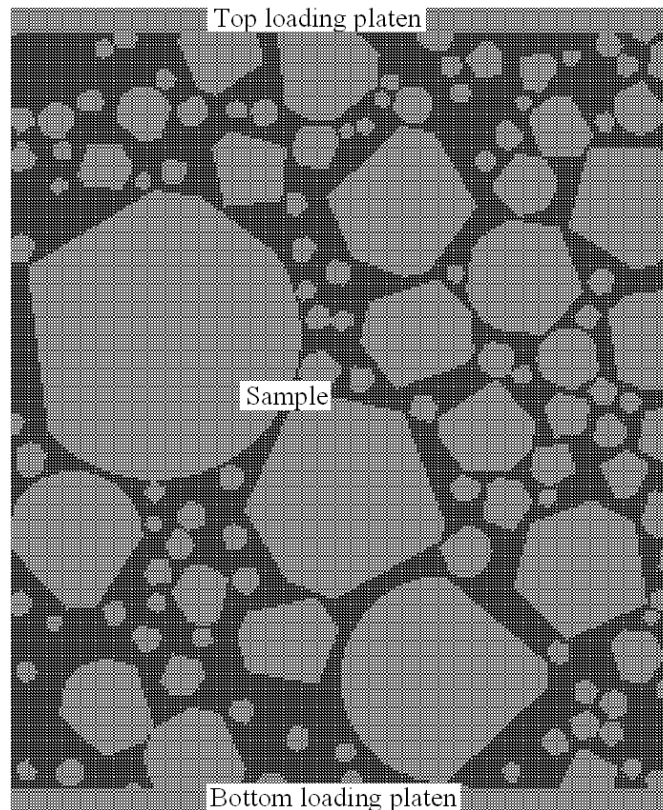


**Figure 4.2 Virtual sample of asphalt mixture**



## 4.6. Input Parameters

According to the DE model described above, the following input parameters were specified:

- (1) The contact stiffness of discrete elements consisting of aggregates

Lab tests were developed to measure the Young's modulus ( $E_c$ ), and the relationship between  $E_c$  and the stiffness ( $k_n, k_s$ ) were listed as follows:

$$k_n = 2E_c t \quad 4.5$$

$$k_s = 2k_n \lambda \quad 4.6$$

Where  $t$  is the disk thickness, and,  $\lambda$  is the ratio  $k_s$  over  $k_n$ . In this study,  $E_c$  was taken as 55Gpa based upon the previous studies (Buttlar and You 2001; You and Buttlar 2004; You and Buttlar 2006), and set  $\lambda = 1$ .

- (2) Burger's contact model parameters for asphalt mastics

The relationship of parameters of the Burger's contact model and general Burger's model were developed as follows:

$$K_n^{BCM} = 2E_c^{GBM} t \alpha \quad 4.7$$

$$K_s^{BCM} = \delta K_n^{BCM} \quad 4.8$$

Where,  $K_n^{BCM}$  represents the parameters of Burger's contact model in the normal direction; and  $E_c^{GBM}$  is the corresponding parameters for  $K_n^{BCM}$  in the general Burger's model.  $K_s^{BCM}$  is the parameters of the Burgers contact model in the shear direction.  $\alpha$  and  $\delta$  are coefficients to adjust the deviations of two groups of parameters.

In this paper, lab tests were developed to measure the dynamic modulus and phase angles of asphalt mastics, and then the parameters of the general Burger's model  $E_c^{GBM}$  were calculated by solving the equation group of (1), (2), (3), and (4). In order to determine the coefficients  $\alpha$  and  $\delta$ , the DE model of asphalt mastics was developed. It was shown that  $\delta$  had little effects on the DE model, and when  $\alpha = 0.88$ , a good agreement between the fitted and measured modulus was obtained as shown in Fig. 3. In addition, the fitted and the measured phase angles are also shown in the figure with good match.

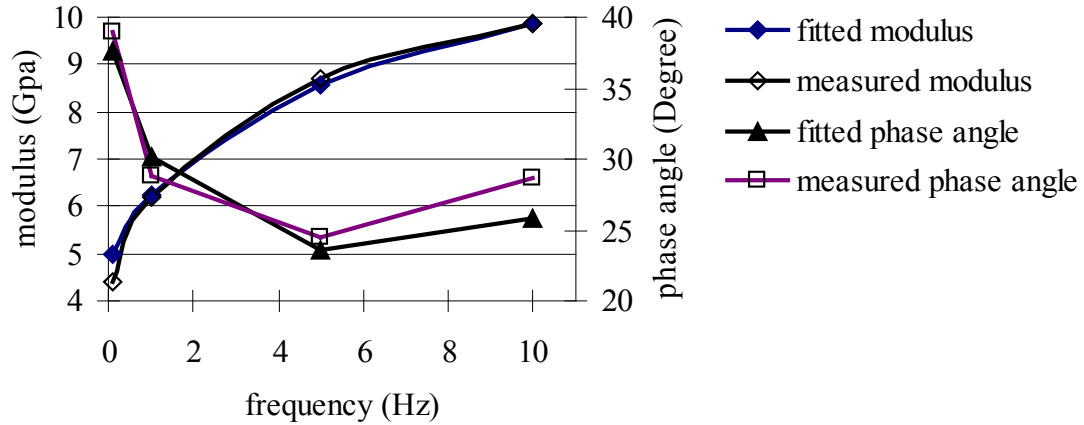


**Figure 4.3. Calibration for input parameters of Burger's contact model fitted with lab testing data**

(3) Parameters for the contact-bond model

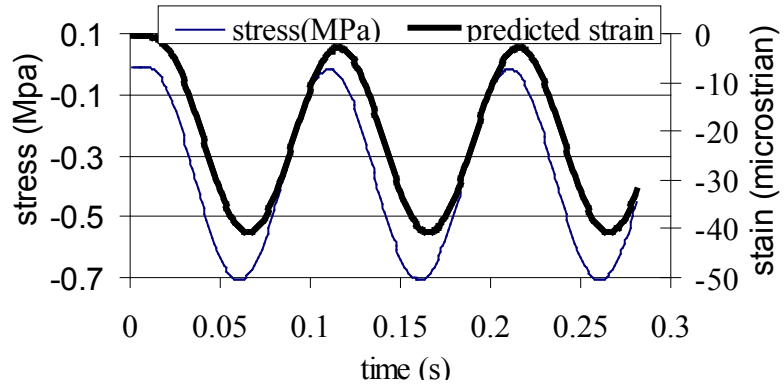
In this study, the main purpose is to simulate the viscoelastic properties of asphalt mixtures. The breakage of the contact bond is not allowed and therefore cracks are not allowed during the simulation. Therefore, a large value (100,000 KN) was set for all the contact-bonds in the aggregate-mastic model.

(4) Parameters for the Slip Model

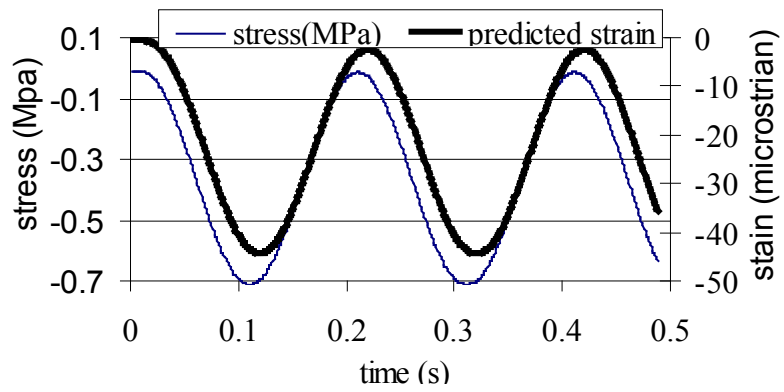
Since the bond was set with a large value, the slip model remained inactive and had little effect on the simulation results in this paper. This prevents excessively large displacements when individual bond break due to large tensile contact forces in a single cycle.

## 4.7. DE Modeling

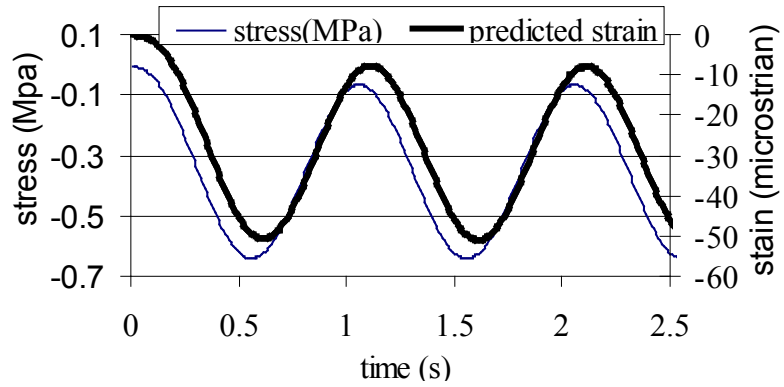
Uniaxial compressive virtual tests of the asphalt mixture were conducted under dynamic cyclic loadings to predict dynamic modulus according to the properties of its constituents. As shown above, the DE model of the asphalt mixture and its input parameters were determined by its constituents. Two loading platens were employed as shown in Fig 2: on the top platen, the dynamic loadings were applied, and the bottom one was fixed in all directions. Sinusoidal applied stress and strain response versus time were plotted in Fig 4 for loading frequencies of 10, 5, 1, and 0.1Hz, respectively. It should be noted that the simulation time using DEM on the viscoelastic model took a large amount of time. Therefore it is very difficult to simulate hundreds of loading cycles as in the lab tests. However, the viscoelastic response can still be obtained in a few loading cycles.



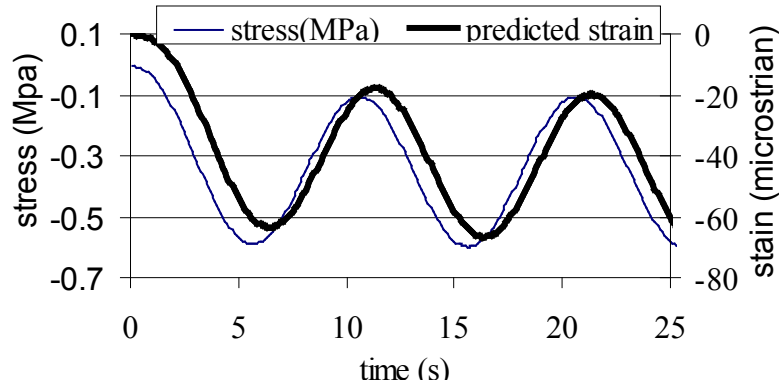
a) Simulation results at 10Hz



b) Simulation results at 5Hz



c) Simulation results at 1Hz



d) Simulation results at 0.1Hz

**Figure 4.4 The applied stress and strain response of the specimens**

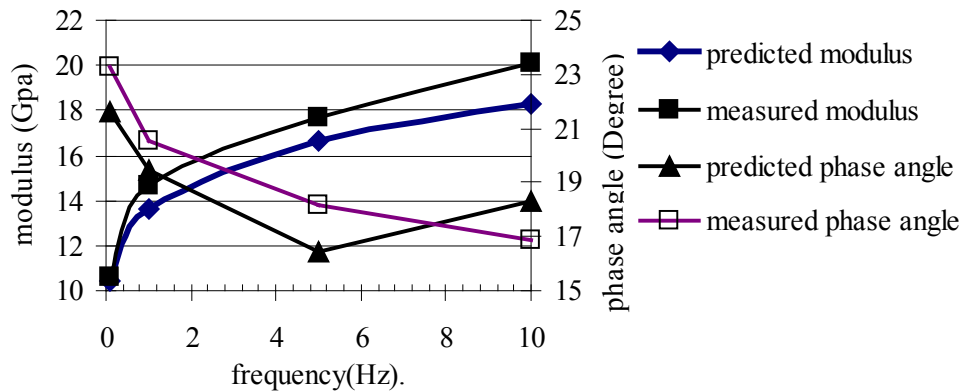


**Figure 4.5 Comparison of the predicted and measured moduli and phase angles**

Then the dynamic moduli and phase angles were obtained from Fig. 4. The predicted results were compared with the lab test results as shown in Fig. 5. In general, the predicted mixture moduli are close to the measurements, the predicted phase angles for the mixture are also comparable with the measurements. It was found that the predicted modulus and phase angles were slightly lower than those from lab tests. This was probably due to the limitation of the 2D models. However, the errors for both dynamic modulus and phase angles were small, where the average error for modulus is about 6%, and for phase angle 8.5%. It is anticipated that the 3D modeling technique will provide a more accurate prediction. At this time, research work is ongoing at Michigan Tech with financial support from the National Science Foundation.

## 4.8. Summary and Conclusion

In this paper, a newly developed method in the simulation of cyclic a loading test (i.e., dynamic modulus test) of asphalt mixtures using user defined material properties in the discrete element (DE) models was developed. The DE model was prepared based on the random polygon algorithm. With this algorithm, the polygonal particles were created to

present aggregates. Lab tests of aggregates and mastics were conducted under dynamic loading to provide the input parameters for DE modeling of asphalt mixtures. In the DE models, the dynamic moduli of asphalt mixtures were predicted under a cyclic loading algorithm. The simulation results are promising, where the predicted dynamic modulus and phase angles were slightly lower than those from lab tests. It is anticipated that the 3D modeling technique with air void content considered will provide a more accurate prediction in an ongoing project at Michigan Tech.

#### **4.9. Acknowledgement**

This material is based in part upon work supported by the National Science Foundation under Grant CMMI 0701264. Any opinions, findings, and conclusions or recommendations expressed in this material are those of the author's and do not necessarily reflect the views of the National Science Foundation.

## **Chapter 5. A Randomly Generated 3D Model for Simulation and Visualization of AC Microstructures<sup>4</sup>**

### **5.1. Abstract**

The objective of this study is to visualize and simulate micro-scale properties of asphalt concrete with three dimensional (3D) discrete element models under mechanical loading. The microstructure of the asphalt concrete sample was composed of three ingredients: coarse aggregates, sand mastic (a combination of fines, fine aggregates and asphalt binder), and air voids. Coarse aggregates were represented with the irregular polyhedron particles which were randomly created with an algorithm developed for this study. The gaps among the irregular particles were filled with air voids and discrete elements of sand mastic. The mechanical behaviors of the three ingredients were simulated with specific constitutive models at different contacts of discrete elements. Based on the geometric and mechanical models, visualization and simulation of asphalt mixtures were conducted in this study.

### **5.2. Introduction**

Asphalt concrete mixture can be regarded as a three-phase material: coarse aggregates, asphalt mastic (fine aggregates, fines and asphalt binder) and air voids. Coarse aggregates are discontinuous and represent the granular properties. Asphalt mastic is considered as a continuum media with viscoelastic properties. The discrete element method (DEM) was originally developed to simulate granular or rock assemblies, and was then extended to perform solids-based modeling, in which a solid is represented as an assembly of particles bonded to one another at their contacts. Therefore, DEM is an ideal method which can simulate not only continuum but also granular properties of AC mixtures.

In the past decade, micro-mechanical models have been developed with DEM. Researchers developed a microfabric discrete element modeling (MDEM) approach for simulating the microstructure of asphalt concretes (Buttler and You 2001; You and Buttler 2004; You and Buttler 2005; 2006). In these studies, the image analysis technique was employed to rebuild the microstructures of asphalt mixtures, and uniaxial and hollow cylinder dynamic modulus and creep tests were conducted to predict stiffness of asphalt mixtures. Additionally, micro-scale fracture modeling of asphalt concrete was conducted with a bilinear cohesive model (Kim and Buttler 2005).

---

<sup>4</sup>Full text reprinted with permission from ASCE: “Visualization and Simulation of Asphalt Concrete with Randomly Generated 3D Models” by Yu Liu and Zhanping You, 2009, Journal of Computing in Civil Engineering, Vol. 23, Issue 6, pp. 340-347, Copyright © 2009, ASCE. See Copyright clearance in Appendix A.

Some researchers conducted elastic and viscoelastic discrete element simulation of asphalt mixtures with a highly idealized model (Collop et al. 2007; Collop et al. 2006a) to simulate the dilation and deformation behaviors of asphalt mixtures. Abbas et al. developed a micromechanical model to simulate the viscoelastic behaviors of asphalt materials of asphalt materials using the Burger's model (Abbas et al. 2007), where the dynamic moduli and phase angles were predicted by the 2D DEM simulation. Recently, researchers simulated asphalt mixtures with a viscoelastic model under cyclic loads (Liu et al. 2009; Liu and You 2008), which provided a unique strain-stress response of asphalt concrete. Additionally, ellipse or ellipsoid particles were applied for granular material modeling (Favier et al. 2001; Mustoe and Miyata 2001).

By summarizing research studies on the models of asphalt concrete in the past, micromechanical models were developed with DEM, but little attention was focused on the visualization of the microstructure of the materials which is very important for updating and improving asphalt mixture design methods. 3D visualization and simulation of the 3D microstructure of asphalt concrete has been used in the previous studies (Papagiannakis et al. 2002; Wang et al. 2007b), where the x-ray computed tomography technique was used. However, those studies were limited by the imaging resolution and costly capital investment of the facility. Therefore, in this study, a 3D visualization and simulation technique is developed by randomly generated particles without using the x-ray technique.

### **5.3. Objectives and Scopes**

The main objective of this study is to visualize and simulate micro-scale properties of asphalt concrete with 3D discrete element models under mechanical loading. Two major tasks are required to accomplish the objective: (1) establish 3D digital samples and micro-mechanical models; and (2) visualize micro-structure, analyze micro-mechanical responses during DE simulations and predict the macro properties of asphalt concrete

Micro-scale analysis of asphalt concrete is a broad topic. This research provides a methodology for visualizing and simulating asphalt concrete with DEM. Digital samples, mechanical models, micro-structural and mechanical analysis, macro-scale property prediction were discussed. The gradations, shapes, distribution of aggregates in the asphalt concrete were considered. It should be noted that the digital samples were randomly created rather than from x-ray images. Additionally, due to the limitation of computation speed, digital samples used herein are smaller than those normally measured in the laboratory.

### **5.4. 3D Digital Samples and Mechanical Models**

In many studies, a digital image based method was used to prepare the digital image samples (Adhikari 2008; You and Adhikari 2008). In a digital image based method, asphalt mixture images are first captured with X-ray Computed Tomography (X-ray CT) or scanners. Then, image-processing techniques are used to process the images. Finally, the digital samples are built using the processed image data. Obviously, a digital image-

based method may give a better correlation to a real mixture specimen, but the following two issues should be noted if an image analysis method is employed. The first key issue is its laboratory-dependency. To prepare a digital sample, a real asphalt mixture should be prepared and scanned. Associated with the key issue, expensive equipment, manpower, and image processing techniques may restrict the utilization of the digital image-based method. For example, only few institutes have the equipments to prepare asphalt mixture samples and acquire images. The second key issue is resolution limitations in processing HMA images. It was found that the image binder thickness was larger than the actual film thickness (Abbas et al. 2007). Limited by these two issues, an image based method can be used for micro-scale analysis, but it is very expensive and time-consuming when a larger number of digital samples are needed with different types of gradations, aggregate shapes, angularities, air voids, asphalt contents, and mechanical properties. Therefore, a lab-independent method is needed. A randomly generated model is presented herein. Additionally, the constitutive models are provided to address the interactions within a digital sample.

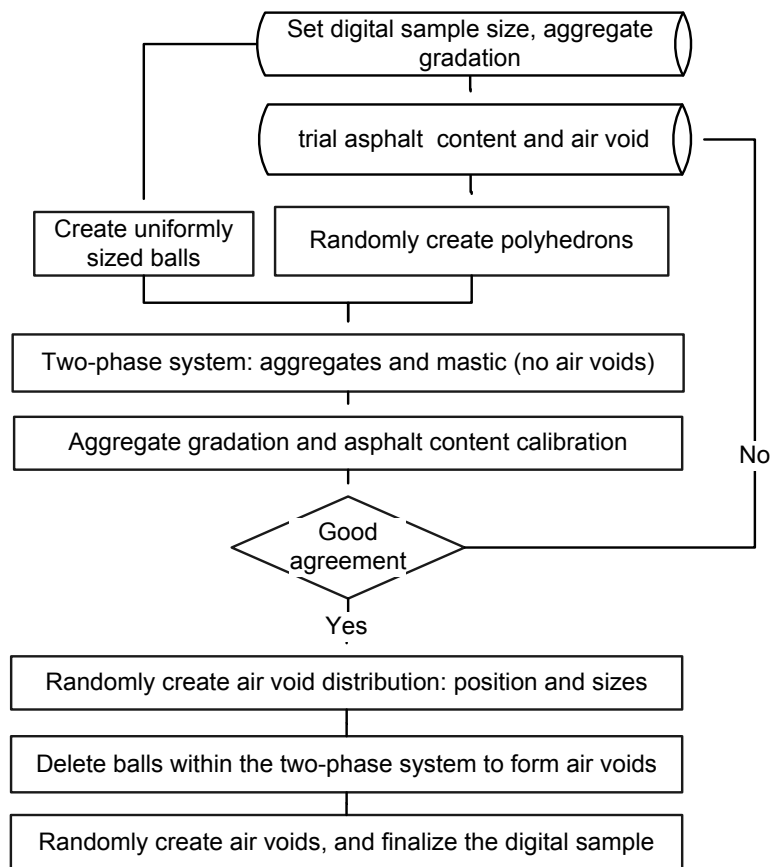


**Figure 5.1 Procedure for a randomly generated model**



### 5.4.1. Digital Samples: a Randomly Generated Model

This section proposes a seven-step-procedure for the randomly generated model as shown in Figure 5.1. With this procedure, digital samples of three gradations will be prepared in the subsequent sections of this paper. The seven-step-procedure is discussed in details with a simple example as follows:

(1) Define digital sample size and aggregate gradation:

In this step, the digital sample size and aggregate gradation are defined based upon the actual aggregate gradation and the available computing resource. In this study, as examples, three aggregate gradations were selected as shown in Figure 5.2. Digital sample for each gradation is a cylindrical sample with diameter and height of 40mm and 60mm, respectively.

(2) Set trial asphalt content and air voids by volume:

In this step, the asphalt content and air voids level are set based upon the volumetric properties of the asphalt mixture. The target asphalt contents for all the three gradations are 10.77% and the air void levels are 4.0%, both by volume. The trial asphalt content and air voids are set to the target values.

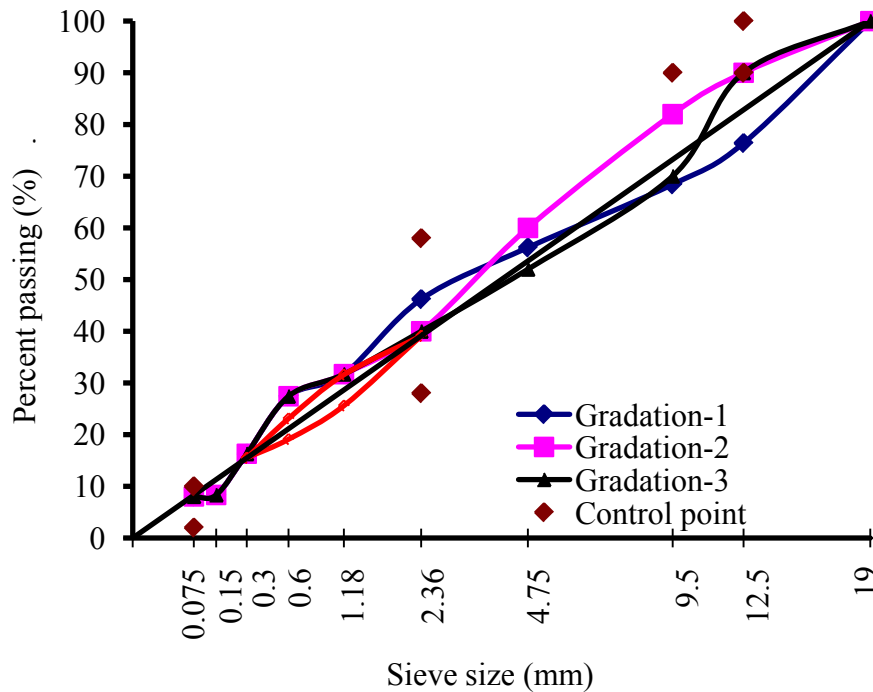
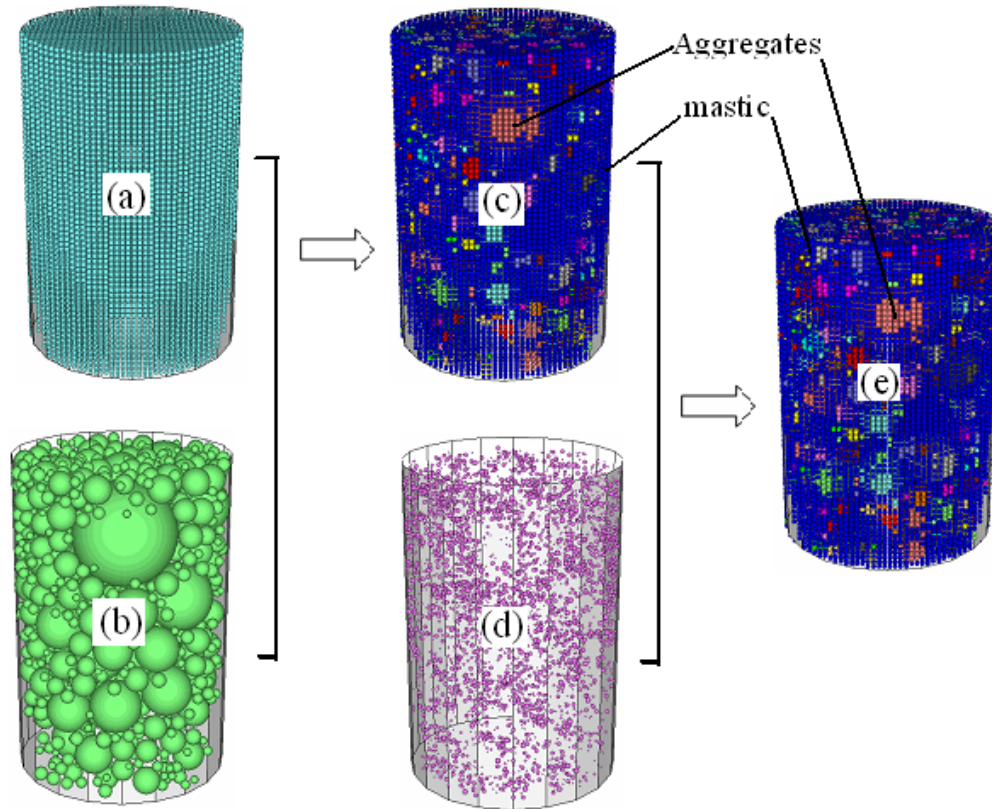


Figure 5.2 Aggregate gradations for three mixtures



Key:

- (a) uniformly sized balls
- (b) graded balls
- (c) two-phase system
- (d) air voids distribution
- (e) finalized digital sample

**Figure 5.3 Sketch for a randomly generated model**

(3) Create uniformly sized balls:

Uniformly sized balls were created within a digital sample boundary (or the pre-defined sample size) as discrete elements of DE model as shown in Figure 5.3 (a).

(4) Randomly create polyhedrons:

In order to randomly create polyhedrons based on the aggregate gradation, graded balls are generated within the cylinder as shown in Figure 5.3 (b), where the diameters of the graded balls represent aggregate sizes and the positions of these graded balls represent the distribution of aggregates. Within each of the graded ball, a polyhedron particle is created with the four steps as follows:

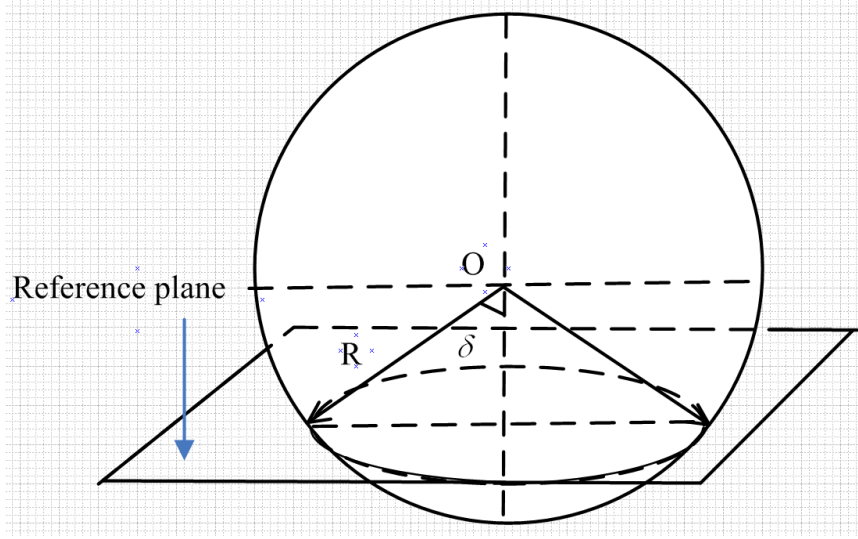


**Figure 5.4 A reference plane for generation of a polyhedron**

(a) A reference plane is created randomly as shown in Figure 5.4:

As shown in Figure 5.4, the center and radius of a graded ball are  $O(x_c, y_c, z_c)$  and  $R$ , respectively. In order to create a reference plane, its normal direction as well as a point on the reference plane is needed. The normal direction of the reference plane is determined by three randomly created numbers  $n_x, n_y, n_z$ , such that

$$\begin{aligned} n_x &= \cos(2\pi \times \text{rand}()) \\ n_y &= \cos(2\pi \times \text{rand}()) \\ n_z &= \cos(2\pi \times \text{rand}()) \end{aligned} \quad 5.1$$

Where  $\text{rand}()$  is a random-number generator. The number from 0.0 to 1.0 is randomly created with the generator.

The coordinates of a point on the reference plane,  $O'(x'_c, y'_c, z'_c)$ , are determined in Equation 5.2.

$$\begin{aligned} x'_c &= x_c + R \times (1 - \zeta) \times \frac{n_x}{\sqrt{n_x^2 + n_y^2 + n_z^2}} \\ y'_c &= y_c + R \times (1 - \zeta) \times \frac{n_y}{\sqrt{n_x^2 + n_y^2 + n_z^2}} \\ z'_c &= z_c + R \times (1 - \zeta) \times \frac{n_z}{\sqrt{n_x^2 + n_y^2 + n_z^2}} \end{aligned} \quad 5.2$$

Where  $n_x, n_y, n_z$  are the three components of the normal direction vector as expressed in Equation 5.1;  $\zeta$  is a cut ratio whose value range from  $l_{min}$  to 1 as shown in Equation 5.3:

$$\zeta = 1 - (1 - l_{min}) \times rand() \quad 5.3$$

Where  $l_{min}$  is the minimum value of  $\zeta$ .  $l_{min}$  is set by users to determine the created particle shapes. A larger  $l_{min}$  results in a larger percentage of elongated or flat particles, and vice versa.

In this approach, a reference plane as shown in Figure 5.4 is created by the point  $O'$  and normal direction vector  $n$  ( $n_x, n_y, n_z$ ).

(b) Several reference planes can be created using the procedure discussed in (a).

(c) A polyhedron is formed by truncating the graded ball with the reference planes.

(d) A polyhedron particle is generated by covering the uniformly sized balls with the polyhedron: balls fallen in the polyhedron belong to the polyhedron particle. All the balls in the polyhedron particle are bonded together to represent an aggregate. Some of the randomly created polyhedrons are shown in Figure 5.5 as examples. Those polyhedrons were created through inputting various cut ratios ( $\zeta$ ):  $\zeta=0.2, 0.4, 0.6, \text{ and } 0.8$ .

(5) Create a two-phase system:

A number of polyhedron particles are generated with the previous five steps. Then, a two-phase system is created: polyhedron particles and the remaining portion as shown in Figure 5.3(c). The polyhedron particles represent aggregates, and the remaining portion composes of asphalt mastic (i.e., a mix of fine aggregates, fines and asphalt binder) and air voids.

(6) Validate volumetric properties (gradation and asphalt binder and air void contents):

The aggregate gradation in the two-phase system and volumetric properties of the synthetic asphalt mixture are calculated, and compared with the desired values. If the desired result is not obtained, the steps above should be repeated until the desired gradation and volumetric properties reach the target.

(7) Randomly create air voids:

Air voids in an asphalt mix are dispersed within asphalt mastic and between aggregates and mastic. The target air voids content is 4% as described in step (2). Air voids formed between aggregates and mastic were assumed as 70% of the total air void content in this study. The rest of the air void is assumed in the mastic phase. The accurate value of air voids (including the distribution) between aggregate and mastic will be recommended based on the laboratory tests (and x-ray computed tomography) in future studies. It should be noted that air voids within asphalt mastic are only used for building the microstructure of mastic. To randomly create air voids between aggregates and mastic, the following two steps are needed:

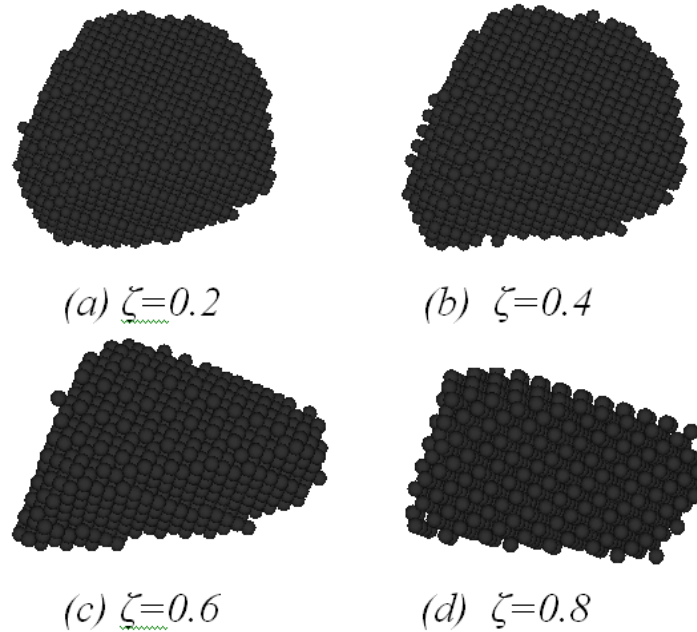


**Figure 5.5 Examples of randomly created polyhedrons**

- 1) Randomly create balls within the cylinder as shown in Figure 5.3(d)
- 2) If the balls in the two-phase system are covered by the randomly created balls, they are deleted to form air voids.

In summary, the randomly created polyhedrons partially reflect the actual geometry of aggregate particles, such as sizes, shapes, fracture surfaces, flat particles, and elongate particles. Sizes and shapes can be controlled by gradation and random distribution functions. Uniform and gauss distribution functions can be used in the codes. Fracture surfaces can be controlled by setting different numbers of reference planes, while flat and elongate particles can be controlled by setting different distances between polyhedron particle centers to the reference planes. In further studies, more geometry and physical properties of aggregates will be considered. With the current version of randomly created polyhedrons, the aggregates with visible angularities are particularly well modeled, while the rounded or rough surface of aggregate particles can be modeled by increasing fracture surface numbers. The correlations between the randomly created polyhedrons and the real aggregates were not established in this paper but in an ongoing research study. In the future version, eight structural indicators will be provided to correlate the computer-based model to the real asphalt mixture microstructure. The eight indicators are aggregate shape, angularity, orientation, distribution, volumetric concentration, and gradation, asphalt binder content, and air void content.

#### **5.4.2. Mechanical Models**

There are four types of contacts within the digital sample built above: contacts within mastic, between aggregates and mastic, within aggregates, and between aggregates. Four different constitutive models are built for these four types of contacts, and each of them

consists of three sections: stiffness model, slip model and bonding model. Stiffness model represents deformation properties at a contact, which expresses the relationship between the relative displacements and the contact forces at a contact. The other two models represent the strength properties at a contact: slip model and the bonding model. The slip model is an intrinsic property of the two entities in contact, which provides no normal strength in tension and allows slip to occur by limiting shear force, while the bonding model provides tensile and shear strengths at a contact.

At contacts within mastic, the constitutive model is built by employing Burger's model (Itasca Consulting Group 2004b) as the stiffness model, as well as setting the bonding strength and friction as the bonding model and slip model (Itasca Consulting Group 2004b). At contacts between aggregates and mastic, the constitutive model is built by employing Burger's model connected with a spring element in series as the stiffness model as well as setting the bonding strength and friction as the bonding model and slip model. At contacts between aggregates, the constitutive model is built by employing the contact-stiffness model (Itasca Consulting Group 2004b) as the stiffness model as well as friction as the slip model. In this case, no bonding model is available. Different from the contacts between aggregates, the constitutive model at contacts within aggregates is built with the contact-stiffness model, slip model, and a bonding model. The detailed information about Burger's model, slip model, contact-stiffness model and bonding model is included in the PFC2D/3D manual (Itasca Consulting Group 2004a; b)

## **5.5. Visualization and Analysis of Asphalt Mixture Structure**

There are many factors which can influence an asphalt mixture structure. Due to their dominant sizes and larger percentage, coarse aggregates usually form the skeleton of an asphalt mixture structure. This section presents the visualization and analysis of an asphalt mixture structure by considering different coarse aggregate gradations. Three digital samples of asphalt mixtures were prepared with three different coarse aggregates, where the coarse aggregates are defined as mineral particles larger than 1.18mm in this study. The same mastic and air voids were used in the three digital samples as described in section 3.1.

In the randomly generated model, the graded balls and reference planes are randomly created. Therefore, the locations, sizes, and shapes are affected by the state of the random-number generator, *rand()*. The random-number generator itself is affected by the random-seeds. The previous literatures (Itasca Consulting Group 2004a; b) used a default random seed of 10,000 and the value specified should be of the same magnitude as the default value. According to a recent study (Liu and You 2011a), when the random seed equals 10,000 (the default value), the predicted dynamic modulus and phase angles can correlate well with those measured in the laboratory. Furthermore, in order to minimize the effects from other factors, the digital samples of the three gradations were prepared with the same random seed: 10,000 in this study.

### 5.5.1. Visualization of Asphalt Mixture Structure

In order to visualize an asphalt mixture structure, each of the three digital samples was “cut” into a few sections, and each section was visualized in different views. In Figure 5.6, the digital sample of gradation-1 is shown as an example. The aggregate structure and asphalt mastic distribution can be separated and visualized vertically and horizontally. These views provided very important information that the conventional laboratory cannot provide. In addition, the visualization of the model provided excellent three-dimensional (3D) information in any selected cross-section, which is much better than a two-dimensional (2D) model. There are two reasons why the 3D model is better than the 2D model. Firstly, more accurate volumetric concentrations of aggregates, air voids, and asphalt binder can be provided in a 3D model than a 2D model. A 3D model is composed of a larger number of 2D slices, which may give extra useful information. Since a 2D model is only one of the slices, it only represents part of the information of a 3D model. Secondly, the three-dimensional interactions within an asphalt mixture, such as coarse aggregate interlocking, can only be addressed in a 3D model. The 3D aggregate interlocking may be examined through calculating the contact forces between aggregates and counting the contact numbers within the system. Research on 3D aggregate interlocking is ongoing in Michigan Technological University.

Using a similar approach, the other two models for Gradation-2 and Gradation-3 were prepared. Figure 5.7 shows the aggregate structures of the three gradations, and the corresponding mastic distributions and more detailed views of them can be visualized if needed.

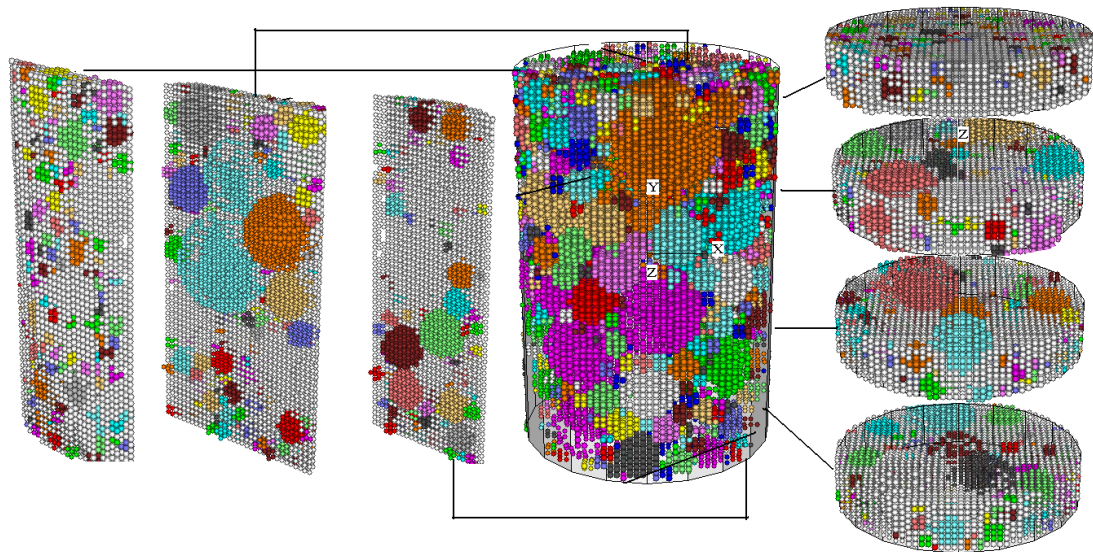
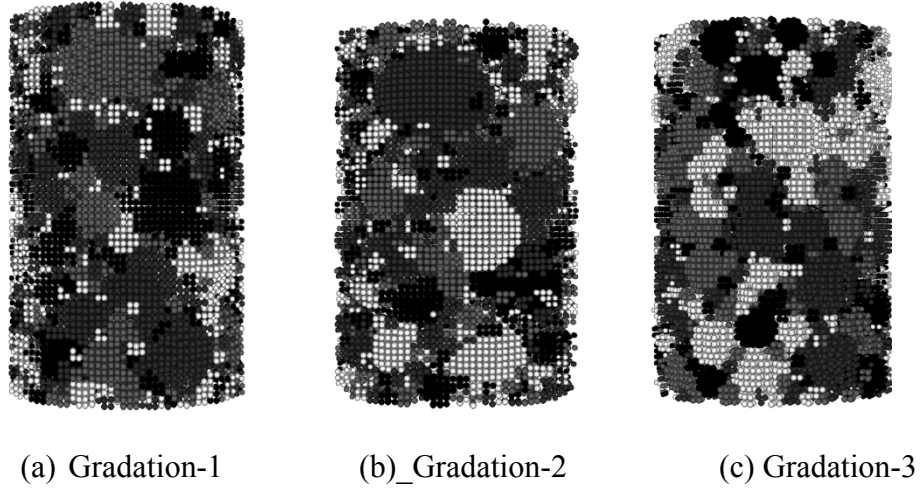


Figure 5.6 Visualization of an asphalt mixture sample



**Figure 5.7 Aggregate structures for the three gradations**

### 5.5.2. Analysis of Asphalt Mixture Internal Structure

The visualization in Section 4.1 gives an optical cognition of the micro-structures of asphalt mixtures, and quantitative analysis is needed to obtain more details of the micro-structures of asphalt mixtures. To achieve this, the digital samples of asphalt mixtures are divided into several sections along the diameter and depth directions. The contents of the aggregates, asphalt mastic, and air voids at each divided section are calculated to investigate the structure of each separate small section. At each separate section of the three gradations, the phase constituent (asphalt mastic, coarse aggregate, or air void) content is defined as the ratio of each phase constituent to mixture by volume. The number and locations of the divided sections are related to sample sizes and the specific situations. Smaller samples have fewer sections and vice versa. In this study, eight sections were chosen in each of the diameter and depth directions based on the sizes of the sample and discrete elements. Therefore, a total of sixteen separate sections were chosen to analyze the asphalt mixture internal structure.

The normal distribution, also called the Gaussian distribution, is an important family of continuous probability distributions. Each member of the family may be defined by two parameters, location and scale: the mean (“average”,  $\mu$ ) and standard deviation squared ( $s_2$ ). The mean,  $\mu$ , standard deviation,  $s$ , and the probability density function,  $f(y)$ , are expressed in.

$$\mu = \frac{1}{N-1} \sum_{i=1}^N y_i \tag{5.4}$$

$$s = \sqrt{\frac{1}{N-1} \sum_{i=1}^N (y_i - \mu)^2} \tag{5.5}$$



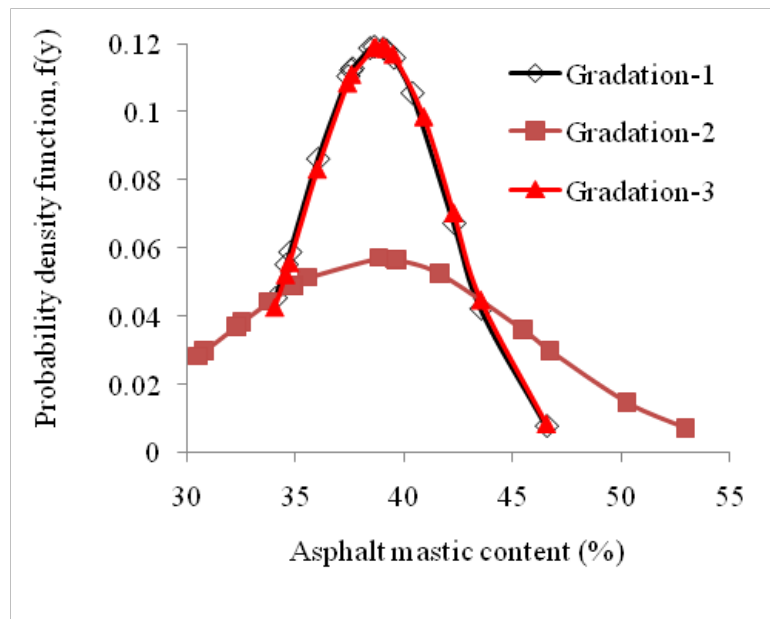
$$f(y) = \frac{1}{s\sqrt{2\pi}} \exp\left(-\frac{(y-s)^2}{2s^2}\right) \quad 5.6$$

Where  $y$  is phase constituent content in this study;  $y_i$ , represents  $i^{th}$  value of  $y$ ;  $N$  is the number of data points;  $f(y)$  is the normal density function.

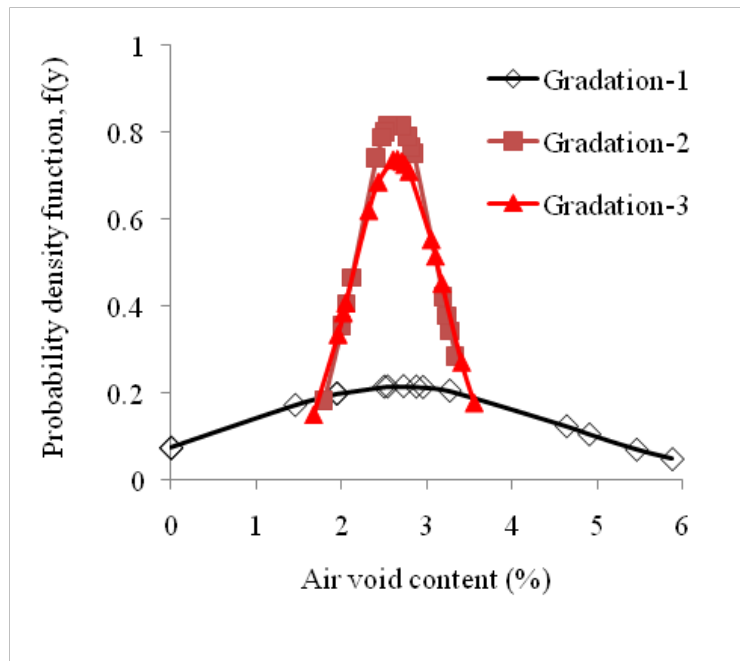
At each separate section, the mean, standard deviation, and the normal density of each phase constituent content was calculated with the Equations 5.4~5.6. The normal distribution curves of the three phase constituents are plotted in Figure 5.8. The following findings were observed:

- 1) The mean value of the three phase constituents in the three digital samples are very close.
- 2) Air void contents of the sixteen sections have a higher deviation for gradation-1 compared with the other two gradations.
- 3) Mastic or coarse aggregate contents of the sixteen sections have a higher deviation for gradation-2 compared with the other two gradations.

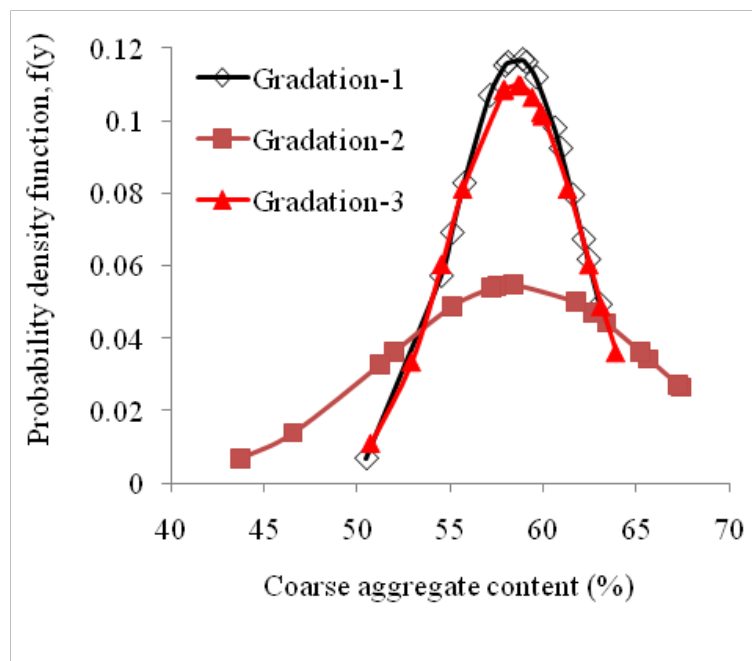
Based on the observations, all the three phase constituents of gradation-3 have smaller deviations. Therefore, gradation-3 is expected to have a better performance.



(a) Mastic



(b) air voids



(c) Coarse aggregates

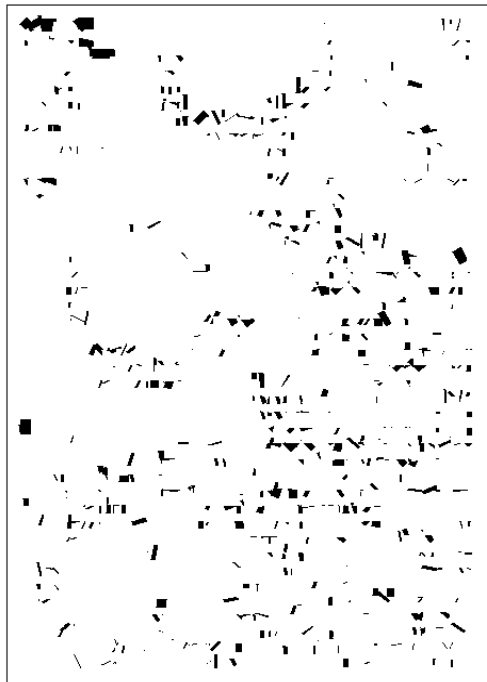
**Figure 5.8 Normal distribution of mastic, air voids, and aggregate contents**

## 5.6. Micromechanical Analysis

### 5.6.1. Visualizing Contact Forces and Displacements during Simulation

Micro-mechanical characteristics can be visualized during the discrete element simulation process. With the visualized micro-mechanical features, the micro-scale behaviors of asphalt mixture can be analyzed optically. These micro-mechanical characteristics include contact forces, relative displacements, and relative velocities. Tensile contact force chains within asphalt mastic and between aggregates and mastic are very important for characterizing fractures within asphalt mixtures. By visualizing these tensile contact force chains at specified regions, fracture features can be analyzed during the simulation. As an example, the asphalt mix of Gradation-1 was simulated under a sinusoidal load. As shown in Figure 5.9, the tensile forces within mastic and between aggregates and mastic were visualized at the iterative steps of 2000 and 500,000. The following findings were observed:

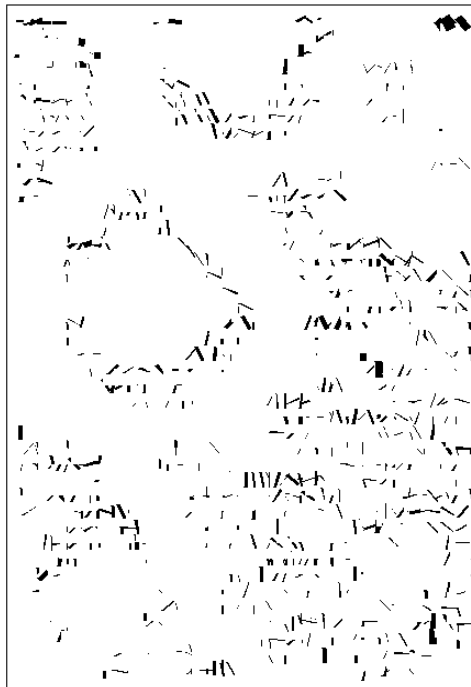
- (1) The tensile force magnitude within mastic or between aggregates and mastic increases from  $4.131 \times 10^{-2}$  to  $1.863 \times 10^{-1}$ , from  $3.534 \times 10^{-2}$  to  $1.322 \times 10^{-1}$ , respectively, with the iterative steps from 2,000 to 500,000.
- (2) The maximum tensile forces can be visualized clearly: thicker lines in the Figure 5.9 represent larger tensile force magnitude, and vice versa. The direction of the lines represents the contact force direction along two contacted balls.



(a) Tensile forces between aggregate and mastic at iterative steps = 2,000  
(Maximum =  $4.131 \times 10^{-2}$ )



(b) Tensile forces within mastic at iterative steps = 2,000  
(Maximum =  $3.534 \times 10^{-2}$ )



(c) Tensile forces between aggregate and mastic at iterative steps = 500,000  
(Maximum =  $1.863 \times 10^{-1}$ )



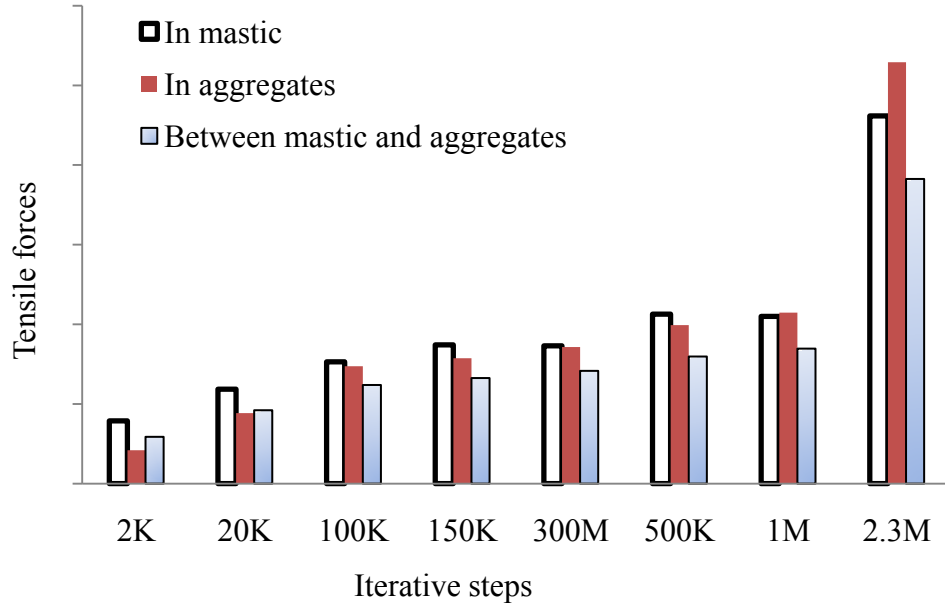
(d) Tensile forces within mastic at iterative steps = 500,000  
(Maximum =  $1.302 \times 10^{-1}$ )

**Figure 5.9 Tensile force distributions within mastic or between aggregates and mastic of the region**

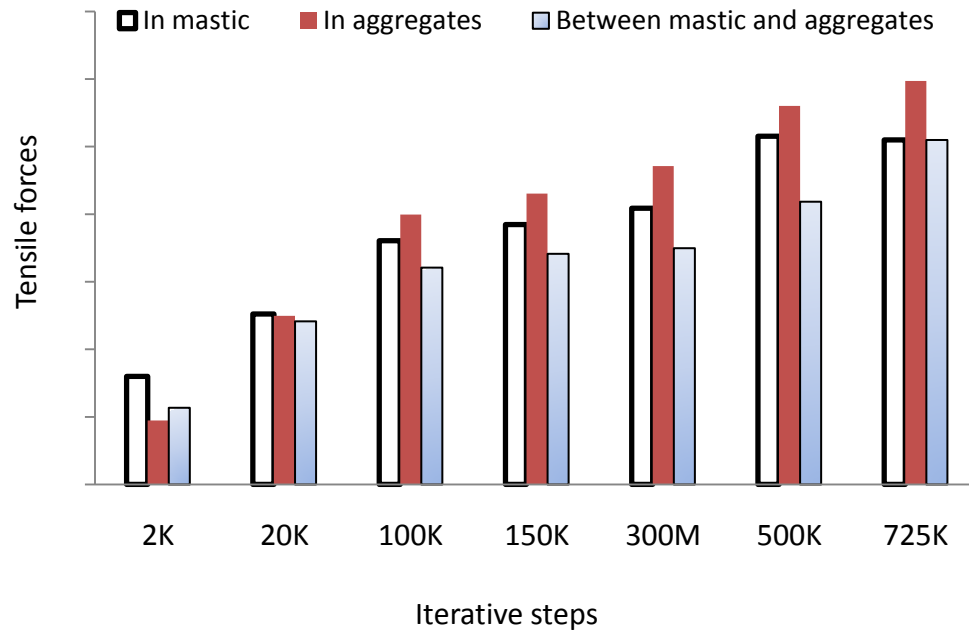
In addition to the tensile forces within mastic and between aggregates and mastic, there are other micro-scale properties which are very important. For example, tensile forces within aggregates may indicate the fracture in aggregates. Compressive forces between two separate aggregates may indicate the interlock forces between aggregates. Relative displacements or velocities indicate the steady state: a larger displacement represents an unbalanced status. All these micro-scale characteristics can be visualized during simulation if they are needed.

**5.6.2. Micromechanical Analysis**

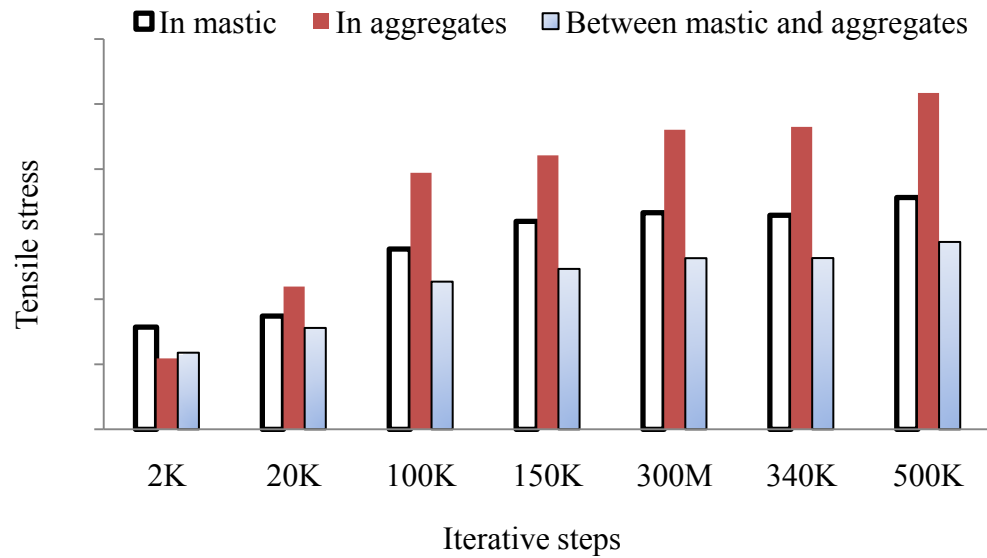
Compared with compressive forces, tensile forces play a more important role in asphalt mixture behaviors, especially at a lower temperature. Therefore, the objective of this section is to present an analysis of tensile force within asphalt mixtures. The average tensile contact forces within mastic, within aggregates, and between mastic and aggregates were calculated during the simulation of asphalt mixture.



(a) Gradation-1



(b) Gradation-2



(c) Gradation-3

**Figure 5.10 Tensile forces vs. iterative steps: in the figure, K represents one thousand; and M represents one million.**

The average contact tensile forces vs. the iterative steps are plotted in Figure 5.10. The following findings were observed: 1) Tensile forces increase with iterative steps increasing. 2) When the iterative steps are smaller, tensile forces in asphalt mastic are larger than those in aggregates or between aggregates and mastic. When the iterative steps become larger, the tensile forces in asphalt mastic become smaller than those in aggregates or equal to those between mastic and aggregates. This finding indicates the contact forces are transferring from asphalt mastic to aggregates. 3) The tensile forces in the aggregates exceed those in the asphalt mastic when the iterative steps equal to one million for Gradation-1, 0.1 million for Gradation-2, and 0.02 million for Gradation-3. Because aggregates have a higher stiffness and higher strength, Gradation-3 is expected to have a higher modulus based on this finding, while Gradation-1 is expected to have a smaller modulus.

## 5.7. Macro-scale Analysis

Macro-scale performances of a material include the deformation and strength properties as a whole. In this research study, deformation properties were investigated by conducting simulation of uniaxial dynamic modulus tests. Viscoelastic parameters of asphalt mastic and elastic modulus of aggregates were measured as input model parameters. Asphalt mixture samples of the three gradations were simulated under the same applied haversine stress as shown in Figure 5.11. The corresponding micro-strains of the three gradations were calculated and plotted in Figure 5.11. From the stress and strain curves in Figure 5.11, the dynamic modulus and phase angles were calculated.

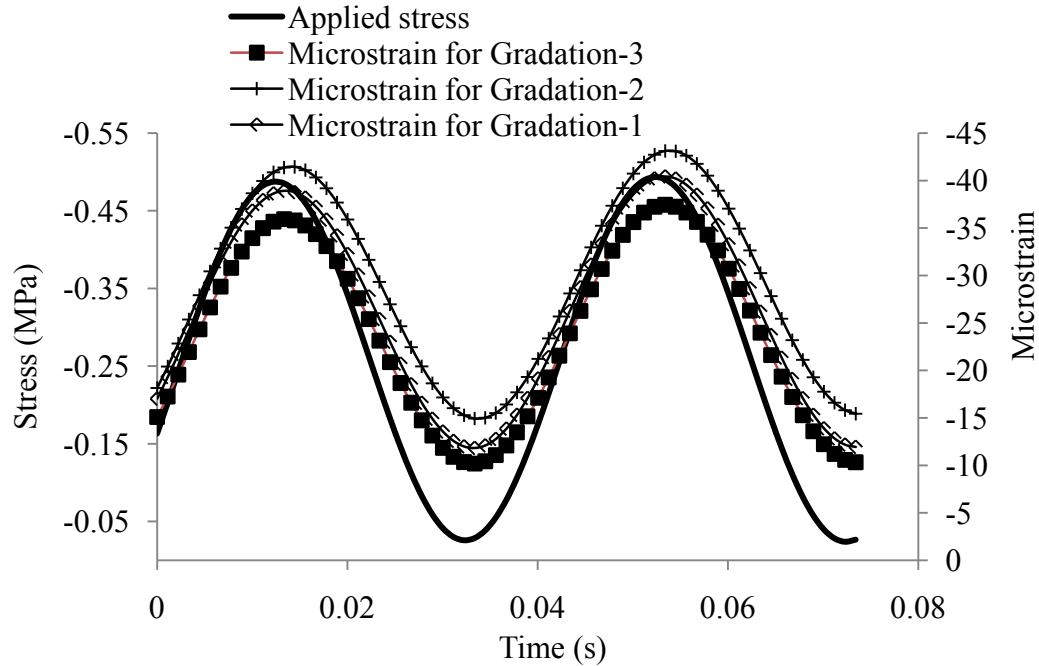


**Figure 5.11 Stress and strain vs time**

They are 16.8GPa/8.6° for Gradation-1, 16.6GPa/16.7° for Gradation-2, 17.8GPa/9.7° for Gradation-3. Obviously, Gradation-3 has the largest modulus while Gradation-1 and Gradation-2 have the similar modulus. Therefore, from both macro-scale and micro-scale analysis, the same observation was obtained: Gradation-3 has the largest modulus. Therefore, Gradation-3 has a best performance compared with the other two. Of course, more micro- and macro-scale analysis should be given to get a more reliable conclusion. The analysis used herein can be employed in asphalt mixture computer design without much involvement of laboratory testing. Therefore a possible application of the visualization of the asphalt mixture is the computer design, which leads to time saving and more accurate results.

## 5.8. Summary and Future Study

The objective of this study is to visualize and simulate micro-scale properties of asphalt concrete through three dimensional (3D) discrete element methods. In this research, the randomly generated models were developed for the purpose of visualization and simulation. Although the randomly generated model only partially represents actual geometry of aggregate particles, it is a lab-independent method. Furthermore, with this kind of model, the accurate volumetric properties can be represented. With the visualization and analysis of the microstructures and micromechanics, the fundamental understanding of asphalt mixtures can be achieved.

Micro-scale analysis of asphalt mixtures is a difficult topic due to the complicated nature of the asphalt concrete material microstructure. This paper provided a successful



visualization and simulation method. There are many issues to be addressed in future research study:

- 1) Aggregate shapes are randomly created in this study. Therefore, it is necessary to develop a technique to build mixture digital sample using the real shapes of aggregates by preparing a database of aggregates.
- 2) A new technique is needed to improve the computation speed of discrete element simulation. The model scale in this paper is small, however, the current computational time required for the simulation normally exceed a few weeks with a high speed personal computer for higher loading frequencies. It is estimated that quite a few years will be required when a low frequency loading simulation is performed. Therefore, with large scale models, the simulation will be very challenging and a the computation speed shall be addressed.
- 3) The distributions of aggregates and air voids in this paper are not correlated to those in the laboratory nor field well. An approach in prepare a better digital samples are needed so that the sample represents the true distributions of aggregates and air voids.
- 4) Field and laboratory validation of the digital sample preparation and performance will be needed when computational power is available

## **5.9. Acknowledgements**

This material is based in part upon work supported by the National Science Foundation under Grant CMMI 0701264. Any opinions, findings, and conclusions or recommendations expressed in this material are those of the authors' and do not necessarily reflect the views of the National Science Foundation.

## **Chapter 6. Two Idealized Models for Simulating AC Microstructures and Studying Aggregate Morphology<sup>5</sup>**

### **6.1. Abstract**

Hot Mix Asphalt (HMA) contains a significant amount of mineral aggregates, approximately 95% by weight and 85% by volume. The aggregate sphericity, orientation, and angularity are very important in determining HMA mechanical behaviors. The objective of this study is to investigate the isolated effects of aggregate sphericity index, fractured faces, and orientation angles on the creep stiffness of HMA mixtures. The discrete element method was employed to simulate creep compliance tests on idealized HMA mixtures. Two user-defined models were used to build 102 idealized asphalt mix digital specimens. They were the R-model and A-model, short for a user-defined rounded aggregate model and a user-defined angular aggregate model, respectively. Of the 102 digital specimens, 84 were prepared with the R-Model in order to investigate the effects of aggregate sphericity and orientation, while the remaining 18 were built with the A-model to address the effect of aggregate angularity. A viscoelastic model was used to capture the interactions within the mix specimens. It was observed that: 1) as sphericity increased, creep stiffness of the HMA mixture increased or decreased, which was dependent on the angles of aggregate orientation. 2) As the angle of aggregate orientation increased, creep stiffness of the HMA mixture increased, with the rate depending on the sphericity index values. 3) Compared with sphericity index and orientation angles, the influence of aggregate fractured faces was insignificant.

### **6.2. Research Background**

Mineral aggregate constitutes approximately 95% of the total weight and about 85% of the total volume of hot mix asphalt (HMA) mixture. Due to the significant amount of mineral aggregate, its morphology properties, such as sphericity, fractured surface, texture, orientation, and size, were believed to have a dramatic influence on HMA performance and serviceability (Pan et al. 2005; 2006; Stakston et al. 2002). Researchers (Masad et al. 2005a) gave a comprehensive review of aggregate characteristics affecting pavement performance. It was concluded that aggregate properties, such as sphericity, angularity, and texture play important roles in controlling performances of HMA mixtures, hydraulic cement concrete mixtures, and unbound layers. Although a general agreement has been achieved on the importance of aggregate characteristics in controlling mixture performances, traditional mix design methods have been focused on properties of the composite rather than the component materials (Leahy and McGennis 1999). Effects of mineral aggregate properties on permanent deformation have also been

---

<sup>5</sup>Full text reprinted with permission from ASCE: “Discrete Element Modeling: Impacts of Aggregate Sphericity, Orientation, and Angularity on Creep Stiffness of Idealized Asphalt Mixtures” by Yu Liu and Zhanping You, 2011, *Journal of Engineering Mechanics*, Vol 137, No. 4, pp. 294-303, Copyright © 2010, ASCE. See Copyright clearance in Appendix A.

recognized by the Strategy Highway Research Program (SHRP), but the major target of SHRP is the asphalt binder properties and their contribution to pavement performance. Instead of performing detailed investigations of aggregate contribution to pavement performance, SHRP researchers surveyed pavement experts to determine which aggregate properties were most important. Then, they used the survey results to identify aggregate properties that needed to be used in the Superpave system.

Although the practical mix design procedures, such as the Marshall mix design method and the Superpave system, have not given enough emphasis on mineral aggregate characteristics, a considerable number of studies have been done on investigating the effects of aggregates on mixture performances. It was interesting that some observations from those previous studies were conflicting: On the one hand, researchers observed (Shklarsky and Livneh 1964) that Crushed coarse aggregate did not significantly improve the asphalt mix properties. The researcher (Foster 1970) concluded that HMA mixtures containing crushed coarse aggregates showed no better performance than a mix with uncrushed aggregates. Researchers (Li and Kett 1967) concluded that flat and elongated particles could be permitted in a mixture without an adverse effect on its strength. Researchers (Huber et al. 1998) observed that: 1) the rate of rutting on a couch wheel tracker did not correlate well with the fine aggregate angularity (FAA); 2) rut depths measured on the asphalt pavement analyzer (APA) did not correlate well with FAA; 3) dynamic modulus of mixtures measured on the Superpave shear tester did not vary with different FAA. On the other hand, however, researchers (Oduroh et al. 2000) believed crushed coarse aggregate particles had a significant effect on HMA permanent deformation properties. Researchers (Asphalt-Institute 2001; Kandhal and Parker Jr 1998) believed that flat or elongated particles are undesirable since they have a tendency to break during construction and under traffic. Researchers (Bennert et al. 2006) concluded that as the FAA increased, the APA rutting decreased. Researchers (Johnson et al. 2007) observed that APA rutting resistance was significantly influenced by the aggregate blend FAA. To better explain the reasons why those conflicting observations happened, the following important concerns should be taken into account:

- a) Different methods were used to measure pavement or mixture properties;
- b) Different methods were used to measure aggregate properties;
- c) Different types of aggregates and mixtures were used for experimental tests;
- d) Researchers were unable to isolate one aggregate characteristic from the others.

Due to the four concerns above, the observations of the previous studies were results from the combined effects of many factors instead of a single isolated aggregate index. For example, researchers have used measurable indices to link aggregate morphology properties to permanent deformation behaviors and resilient modulus of hot mix asphalt (Pan et al. 2005; 2006). In their studies, there were a total of 18 Superpave asphalt mixture specimens prepared in the laboratory from ten state highway agencies. They concluded that the effects of aggregate angularity and surface texture indices on permanent deformation were especially significant. Their observations, however, were not solely from the effect of the angularity index or surface texture index, but also from a

combined effect of many factors, such as aggregate orientation, gradation, air voids, and asphalt properties.

Evidently, isolating effects of a single aggregate index is very important for a fundamental understanding of the link between performances of a mixture and its composition characteristics. Existing studies, as cited above, were based on experimental tests which are direct and persuasive, but difficult to separate the effects of a single aggregate index from the others. Fortunately, numerical models, such as discrete element (DE) and finite element (FE) models have been developed and applied for simulating asphalt concrete mixture behaviors in the recent ten years (Buttlar and You 2001; Kose et al. 2000b; Liu et al. 2009; Meegoda and Chang 1994). The authors believe that either the FE or DE model is able to build an idealized model to isolate the effects of a single aggregate index from the others. Few existing studies, however, have been focused on isolating the effects of a single aggregate index from the others for a better understanding of the relation between a mixture composition and its mechanics.

### **6.3. Objective and Scope**

The major objective of this study is to investigate the isolated effects of aggregate characteristics on HMA creep stiffness using the discrete element method. Aggregate characteristics may include aggregate size, gradation, sphericity, angularity, texture, orientation, specific gravity, stiffness, and strength. In this study, three of them are involved: sphericity, angularity, and orientation. Aggregate sphericity is represented by sphericity (SP) index which is defined according to NCHRP Report 555 (Masad et al. 2007b). SP index is determined using the shortest, intermediate, and longest dimensions of an aggregate particle which are equivalent to the lengths of the three principal axes of an ellipsoid. Therefore, aggregate particles are simulated with ellipsoids with different orientations in the DE models to consider the effects of aggregate sphericity and orientations. Aggregate orientation is defined with orientation angles which are formed by rotating a standard axis-aligned ellipsoid around its three principal axes. By inputting different values of SP index and orientation angles, a total of 84 digital mixture specimens were built, where the aggregate particles were represented by ellipsoids. To simulate aggregate angularity, a total of 18 digital specimens were built, where the aggregate particles were simulated with ellipsoids having different fractured surfaces.

All the mixture specimens were built with the same aggregate gradation, air voids, and asphalt binder content. A discrete element (DE) viscoelastic model was used to address the mechanical interactions within the specimens. The DE viscoelastic model has been developed and used in a previous study (Liu et al. 2009). Young's modulus of aggregate and Burger's model parameters of asphalt sand mastic are required as inputs of the DE viscoelastic model. The asphalt sand mastic herein is defined as a mix of fines, fine aggregates (less than 2.36mm in diameter), and asphalt binder. To highlight the three aggregate characteristics, all the DE models had the same inputs. The DE simulations were performed by applying uniaxial constant loads on the top of each specimen with the bottom end fixed. The creep stiffness was calculated and recorded during the loading time from 0 to 50 seconds.

## 6.4. Discrete Element Model Geometry

Since mineral aggregates have very complex morphological features, it is very hard to accurately represent their real geometry. In order to simulate the complex aggregate structure in an asphalt concrete specimen, three kinds of techniques have been developed in the past decade, namely the highly idealized model, the randomly-created model, and the image-based model. The highly idealized model was developed by mixing single-sized spherical particles with bitumen to emphasize effects of the bitumen phase: since the packing characteristics were known in the idealized model, the behavior of the mixture would be dominated by the bitumen (Collop et al. 2007; Collop et al. 2006a). The randomly-created model was built by authors in the previous study (Liu and You 2009) for visualization and simulation of asphalt concrete. In the randomly-created model, mineral aggregate gradation, shape, angularity, orientation, and distribution can be randomly created to represent the real asphalt concrete microstructure as much as possible. The advantages of this kind of model are 1) it can more realistically represent asphalt concrete microstructure compared with the highly idealized model; 2) although it is not as accurate as the image-based model, it is lab-independent. The image-based model was built by processing real images of an asphalt specimen and was believed that the most accurate model. In the existing studies, many researchers have used the image-based models for reconstruction of asphalt concrete microstructures (Abbas et al. 2007). However, the image-based model is lab-dependent and very expensive. Some researchers used the image-based model for simulation of granular materials and evaluated the differences between the idealized aggregate particles and the real aggregate particles for DE simulation (Fu et al. 2008; Wang et al. 2007b). They argued that the idealized mineral aggregate particle shapes such as spheres or ellipsoids could only provide very rough quantitative results due to the lack of accuracy in representing the real particles. However, each of the three models has its own advantages over the others: the simplified idealized model (the highly idealized model and the randomly-created model) can be used as tools for preliminary studies to save the costs, and the more accurate model (the image-based model) can serve as a validating tool for advanced studies. Since asphalt concrete has such a complex microstructure and many factors may affect its overall performances, it is impossible to isolate one factor from the others if the image-based model or the randomly created model is used. Therefore, it is necessary to simplify the mixture microstructure with an idealized model as demonstrated in the previous study (Collop et al. 2007; Collop et al. 2006a).

Since the highly idealized model presented by the researchers (Collop et al. 2007; Collop et al. 2006a) is too simple to represent aggregate shape, orientation, and angularity, this paper provide two additional models: the R-model and the A-model, short for a user-defined rounded aggregate model and a user-defined angular aggregate model, respectively. In a digital mix specimen prepared with the R-model, ellipsoids with different orientations represent aggregate particles. For the A-Model specimens, ellipsoids with fractured surfaces were used to simulate aggregate particles. Details of these two newly-developed models are given below.

### 6.4.1. Discrete Element R-model

As mentioned above, the R-model uses ellipsoids to simulate aggregate particles. The ellipsoids are formed by a cluster of discrete elements bonded together. The three principal axes of an ellipsoid represent the longest, intermediate, and shortest dimensions of the corresponding aggregate particle. Aggregate orientations are simulated with three orientation angles. The definitions of an ellipsoid and the orientation angles are given as follows: If an ellipsoid's three principal axes are aligned on the three axes of a xyz-Cartesian coordinate system, the equation of the ellipsoid body is:

$$\frac{x^2}{a^2} + \frac{y^2}{b^2} + \frac{z^2}{c^2} \leq 1 \quad 6.1$$

Where  $a$  and  $b$  are the equatorial radii (along the x and y axes) and  $c$  is the polar radius (along the z-axis). All variables are fixed positive real numbers determining the shape of the ellipsoid. If  $a \geq b \geq c$ ,  $2a$ ,  $2b$ , and  $2c$  are the longest, intermediate, and shortest dimensions of an aggregate particle respectively.

According to NCHRP Report 555 (Masad et al. 2007b), the SP index is formulated as:

$$SP = \sqrt[3]{\frac{2b \times 2c}{(2a)^2}} = \sqrt[3]{\frac{bc}{a^2}} \quad 6.2$$

If the flakiness ratio ( $FR$ ) is:

$$FR = \frac{2b}{2c} = \frac{b}{c} \quad 6.3$$

Assuming the longest dimension of an aggregate particle ( $2a$ ) represents aggregate particle size, the  $b$ , and  $c$  can be determined by Equations 4 and 5 for given SP and FR:

$$c = \sqrt{\frac{SP^3}{FR}} a \quad 6.4$$

$$b = c \times FR = \sqrt{FR \times SP^3} \times a \quad 6.5$$

The particle size ( $2a$ ) can be randomly created using the sieve size for the given gradation shown in Table 6.1. For an example, if the sieve size is 19mm, the particle size ( $2a$ ) is a random number between 19mm and 25mm. Then,  $b$  and  $c$  can be determined in Equations 6.4 and 6.5 for a given SP and FR. Obviously, three input parameters for creating an aggregate particle shape are SP, FR, and aggregate gradation which are utilized to randomly create  $a$ ,  $b$ , and  $c$ .

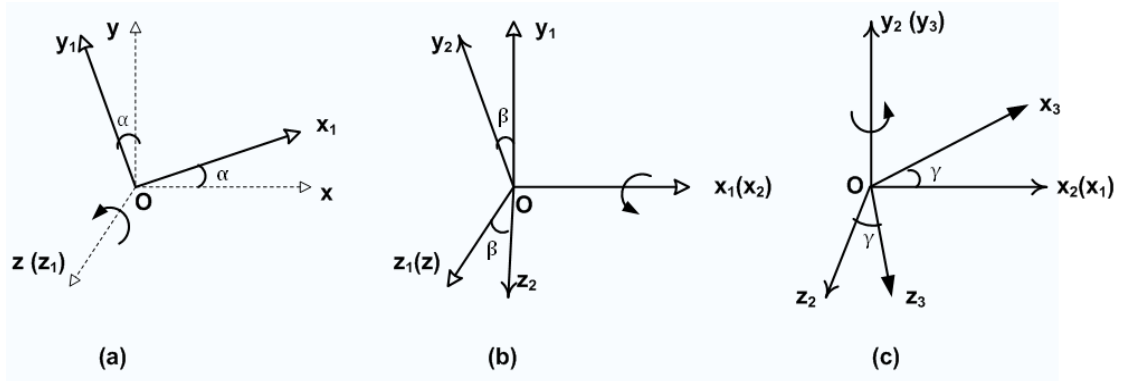
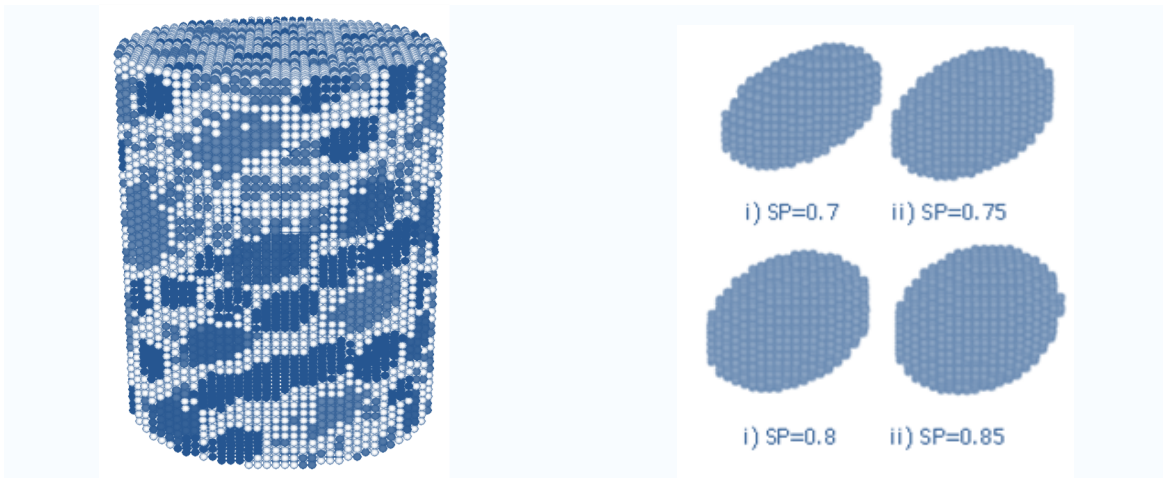


**Figure 6.1 Definition of the three rotation angles:  $\alpha$ ,  $\beta$ ,  $\gamma$**



**(a) DE R-model ( $SP=0.7$ ;  $\alpha = 30^\circ$ ) (b) Individual particles with different SP values**

**Figure 6.2 An example of the DE R-Model and individual particles with different SP values**

After the aggregate shape was determined, aggregate orientation was considered through three orientation angles:  $\alpha$ ,  $\beta$ , and  $\gamma$ . These three angles are defined by rotating the standard axis-aligned ellipsoid (Equation 6.1) around its three principal axes as shown in Figure 6.1: First, the ellipsoid body rotates around its polar radius (along the  $z$ -axis), which results in the orientation angle,  $\alpha$ , shown in Figure 6.1(a). Then, the ellipsoid continues rotating around its equatorial radius (along the  $x_1$ -axis), which results in the orientation angle,  $\beta$ , shown in Figure 6.1(b). It continues rotating around another equatorial radius (along the  $y_2$ -axis), which results in the orientation angle,  $\gamma$ , shown in Figure 6.1(c). By setting different values of  $\alpha$ ,  $\beta$ , and  $\gamma$ , ellipsoid particles with different orientations are created to simulate aggregate orientations.

**Table 6.1**  
**Mineral aggregate gradation used in the 108 DE models**

Sieve Size (mm)	Percentage Passing (%)
25	100
19	98.9
12.5	77.5
9.5	68.4
4.75	56.2
2.36	46.2
1.18	31.7
0.6	20.8
0.3	12.6
0.15	8.3
0.075	5.6

As mentioned above, for a given gradation, particle size (2a) is determined by sieve sizes. If  $SP$ ,  $FR$ ,  $\alpha$ ,  $\beta$  and  $\gamma$  are given, an assembly of ellipsoid particles can be created to simulate aggregate structure in an asphalt mixture specimen. In reality, some mineral aggregate particles may statistically pass through a sieve whose size is smaller than the particle size (2a). However, the above situation did not happen in the current DE models and will be considered in the future study. A total of 84 mixture specimens were prepared with the R-model discussed above. Followed are the input parameters: 1) Sphericity index:  $SP$  ranging from 0.7 to 1. 2) Orientation angle:  $\alpha$  ranging from 0 to 90,  $\beta=0$ , and  $\gamma=0$ . 3) Flakiness ratio:  $FR=1$ . It should be mentioned herein that all the orientation angles are less than 90 even though  $\alpha$  can be a value larger than 90. In the future study, the orientation angles of larger than 90 will be considered. Figure 6.2(a) shows an example of the DE R-model where  $FR = 1$ ,  $SP = 0.7$  and  $\alpha = 30^\circ$ . Figure 6.2(b) shows examples of individual particles with different  $SP$  values. The height and diameter of each cylindrical specimen was 60mm and 40mm, respectively. 68,200 discrete elements were used to build each of the specimens. Of these, 32,190 of them were used to simulate aggregate and the remaining elements were used to simulate asphalt sand mastic. As recommended in National Cooperative Highway Research Program (NCHRP) report 338 (Harold and Quintus 1991), if possible, the sample diameter of asphalt concrete to maximum aggregate size diameter should have ratio greater than 4 in order to minimize the adverse effects. If the ratio of 4 was used in this study, the diameter of cylindrical mixture specimen should be 100mm instead of 40mm. Due to the limited capability of the current computational facility, it is unrealistic to run such a big model.

#### **6.4.2. Discrete Element A-model**

In the DE A-model, ellipsoids with fractured surfaces were used to simulate angular aggregate particles. The fractured surfaces are defined by planes which are formulated mathematically as seen in Equation 6.6.



$$\frac{x}{m} + \frac{y}{n} + \frac{z}{p} = 1 \quad 6.6$$

where  $m$ ,  $n$ , and  $p$  are intercepts at  $x$ -,  $y$ -, and  $z$ -coordinates.

By assigning various values to  $m$ ,  $n$ , and  $p$ , different planes could be defined to simulate different fractured faces of aggregate particles. For example, assuming  $m=m_1$ ,  $n=n_1$ ,  $p=p_1$ .

A standard axis-aligned ellipsoid particle with one fractured face can be defined as:

$$\frac{x}{m_1} + \frac{y}{n_1} + \frac{z}{p_1} \leq 1 \quad \text{and} \quad \frac{x^2}{a^2} + \frac{y^2}{b^2} + \frac{z^2}{c^2} \leq 1 \quad 6.7$$

A standard axis-aligned ellipsoid with two fractured faces can be similarly defined as:

$$\frac{x}{m_1} + \frac{y}{n_1} + \frac{z}{p_1} \leq 1, \quad \frac{x}{m_2} + \frac{y}{n_2} + \frac{z}{p_2} \leq 1, \quad \text{and} \quad \frac{x^2}{a^2} + \frac{y^2}{b^2} + \frac{z^2}{c^2} \leq 1 \quad 6.8$$

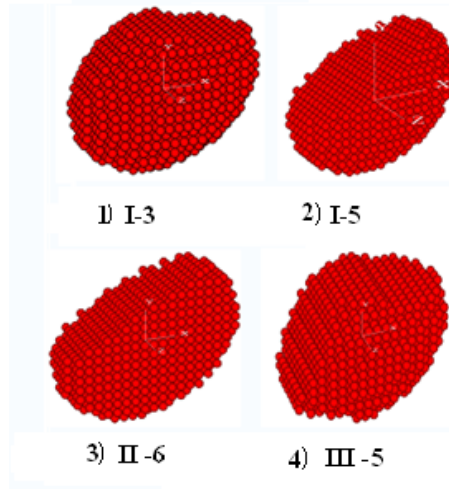
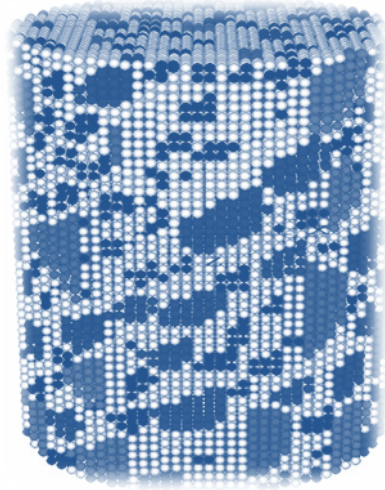
In the same principle, ellipsoid bodies with three or more fractured faces are defined through adding new planes which can be expressed by Equation 6.6. If asphalt mixture volumetric properties and mineral aggregate gradation are given, the inputs for an A-model digital specimen could be categorized into two groups as follows:

- 1) Parameters required for building the R-model: FR, SP,  $\alpha$ ,  $\beta$ , and  $\gamma$ ;
- 2) Parameters required for creating fractured surfaces: a) amount of fractured surfaces, N (N=1,2,or 3 in this study); and b) intercepts at  $x$ -,  $y$ -, and  $z$ -coordinates:  $m$ ,  $n$ , and  $p$ .

As previously mentioned, the A-model was developed to simulate aggregate particles with fractured surfaces. A total of 18 mixture specimens were prepared with different fractured surfaces. In the 18 specimens, all parameters in the first group have the same values: FR=1,  $\alpha=30^\circ$ ,  $\beta=0$ ,  $\gamma=0$ , and SP=0.8, while those in the second group are different as listed in Table 6.2. The first column of Table 6.2 shows the Sample IDs for the 18 digital specimens, where I, II, and III indicate one, two, and three fractured surfaces on the particles in the corresponding digital samples. The other three columns of the Table 6.2 listed the values of intercepts at  $x$ -,  $y$ -, and  $z$ -coordinates ( $m$ ,  $n$ , and  $p$ ). As shown in the table, 6 specimens have one fractured face, 6 have two fractured faces, and 6 have three fractured faces. The height and diameter of each cylindrical specimen was 60mm and 40mm, respectively. 68,200 discrete elements were used to build each of the specimens. Of these, 32,190 of them were used to simulate aggregate and the remaining were used to simulate asphalt sand mastic. Figure 6.3 shows an example of a specimen prepared with the DE A-model whose sample ID is III-6 and several individual particles from samples of I-3, I-5, II-6, and III-5.

**Table 6.2**  
**18 Digital mix specimens prepared with the DE A-model**

Sample ID	Definition of Fractured surfaces								
	Fractured surface I			Fractured surface II			Fractured surface III		
	<i>m</i>	<i>n</i>	<i>p</i>	<i>m</i>	<i>n</i>	<i>p</i>	<i>m</i>	<i>n</i>	<i>p</i>
I-1	<i>a</i>	<i>b</i>	<i>c</i>						
I-2	<i>a</i>	<i>-b</i>	<i>-c</i>						
I-3	<i>a</i>	<i>b</i>							
I-4		<i>b</i>	<i>c</i>						
I-5		<i>b/2</i>							
I-6			<i>c/2</i>						
II-1	<i>a</i>	<i>b</i>	<i>c</i>	<i>-a</i>	<i>b</i>				
II -2	<i>a</i>	<i>b</i>	<i>c</i>		<i>b/2</i>				
II -3	<i>-a</i>	<i>b</i>			<i>b/2</i>				
II -4	<i>a</i>	<i>b</i>	<i>c</i>	<i>-a</i>	<i>-b</i>	<i>-c</i>			
II -5	<i>a</i>	<i>b</i>		<i>-a</i>	<i>-b</i>				
II -6		<i>b/2</i>				<i>c/2</i>			
III-1	<i>a</i>	<i>b</i>	<i>c</i>	<i>-a</i>	<i>b</i>		<i>-a</i>	<i>-b</i>	<i>-c</i>
III -2	<i>a</i>	<i>b</i>	<i>c</i>		<i>b/2</i>		<i>-a</i>	<i>-b</i>	<i>-a</i>
III -3	<i>-a</i>	<i>b</i>			<i>b/2</i>				<i>c/2</i>
III -4	<i>a</i>	<i>b</i>	<i>c</i>	<i>-a</i>	<i>-b</i>	<i>-c</i>		<i>b/2</i>	
III -5	<i>a</i>	<i>b</i>		<i>-a</i>	<i>-b</i>		<i>-a</i>	<i>b</i>	<i>-a</i>
III -6		<i>b/2</i>				<i>c/2</i>	<i>-a</i>	<i>-b</i>	<i>-c</i>



(a) DE A-model (sample ID: III-6)      (b) Individual particles with different fractured surfaces

**Figure 6.3 Examples of 3D digital mix specimens**

## 6.5. Discrete Element Model Mechanics

In terms of discrete element mechanical models, a number of studies have been performed in the past two decades. Researchers developed a micro structural-based discrete element model (MDEM) and applied this model to predict asphalt mixture creep stiffness or dynamic modulus (Buttlar and You 2001; You et al. 2008c; You and Buttlar 2005). In their studies, both asphalt mortar and mineral aggregates are simulated with linear elastic models. Researchers (Abbas et al. 2007) used viscoelastic models to simulate asphalt concrete time-dependent behaviors. In their studies, asphalt mortar was simulated with linear viscoelastic models, such as the Kelvin model and the Burger's model. Authors of this paper developed a DE viscoelastic model to simulate the real time-dependent behaviors of an asphalt mixture (Liu et al. 2009). The research results indicated that the viscoelastic DE model was able to predict dynamic moduli and creep behaviors of asphalt concrete (Liu and You 2008; Liu and You 2009). The study herein employs the DE viscoelastic model to simulate creep stiffness responses of the 102 digital mixture specimens as described in the previous section.

In the viscoelastic model, four contact models were used: the Burger's model, the elastic contact-stiffness model, the contact-bond model, and the slip model. All the four model are available in three-dimensional Particle Flow Code version 4.0 (PFC3D 4.0) (Itasca Consulting Group 2008b). The Burger's model is an alternative contact model in PFC3D 4.0, which is defined by connecting the Kelvin model and the Maxwell model in series in both normal and shear directions, respectively, at a contact point between neighbor elements. The elastic contact-stiffness model is defined by normal and shear stiffness of the two contacting entities. Both the Burger's model and the elastic contact-stiffness model are designed to represent the relationship between contact force and the relative

displacements of two contacting elements at a contact. The contact-bond model and the slip model are two important contact models in PFC3D 4.0 to represent the tensile and shear strengths at a contact. The contact-bond model can be envisioned as a kind of glue joining the two contacting particles, while the slip model allows two contacting elements slip to each other through limiting the shear contact force. The previous research used the four contact models to describe the four kinds of contacting interactions within an asphalt concrete sample. The first kind of contacting interactions may happen between an aggregate and the asphalt sand mastic, which is represented by the Burger's model, the slip model, and the contact-bond model. The second kind of contacting interactions may occur between two adjacent aggregate particles, which is represented by the elastic contact-stiffness model, the slip model, and the contact-bond model. The third kind of contacting interactions is within an individual aggregate particle, which is represented by the elastic contact-stiffness model, the slip model, and the contact-bond model. The fourth kind of interactions is those within the asphalt sand mastic which is simulated using the Burger's model, the slip model, and the contact-bond model. Details about the four contact models and their arrangements were provided in the previous research (Liu et al. 2009). According to the previous study, the viscoelastic model requires the Burger's model parameters of the asphalt sand mastic and Young's modulus of aggregates as input model parameters. Readers may refer to the previous study (Liu et al. 2009) for more details.

In order to emphasize the three aggregate characteristics (SP index, orientation, and fractured surfaces), the same mechanical inputs were used. Table 6.3 lists the mechanical inputs, where  $E_m$ ,  $\eta_m$  are the stiffness and viscosity of the Maxwell element in the Burger's model, and  $E_k$ ,  $\eta_k$  are the stiffness and viscosity of the Kelvin element in the Burger's model. The original experimental data was reported in the previous study (Dai and You 2007). According to that previous study, the creep stiffness of the asphalt sand mastic was tested for up to 100 seconds of loading time at three test temperatures (0, -10, and -20°C). At the same time, aggregate Young's modulus was reported: 55.5GPa. By fitting the testing results of asphalt sand mastic at 0°C, the four Burger's model parameters were achieved in this study as listed in Table 6.3. It should be noted herein that those mechanical parameters in Table 6.3 are not the microscopic contact model parameters, but the macro-scale parameters from the experimental tests. According to the previous study (Liu et al. 2009), the micro-scale contact model parameters for the viscoelastic DE model include stiffness values, friction coefficients, and bond strengths at each contact. The stiffness values could be automatically converted from the parameters in Table 6.3 according to this previous study (Liu et al. 2009). In the current study, it was assumed that the bonds between discrete elements were never broken during the simulation. Therefore, the extremely large values (200 MPa) were given to the bond strengths. Since two adjacent elements could not slip from each other before the bond broke, no friction happened in this study. The friction coefficient can be any value.

## 6.6. DE Simulation of Uniaxial Creep Compliance Tests

As mentioned in the previous two sections, a total of the 102 cylindrical mixture specimens were prepared in this study. All those specimens have the following common features:

- 1) All of them were created by inputting the same aggregate gradation shown in Table 6.1. Therefore, they were supposed to have the same aggregate gradation even though they might be slightly different due to calculation errors.
- 2) Aggregate particles less than 2.36mm were considered as fine aggregates which were integrated into the asphalt sand mastic.
- 3) They had the same asphalt content and no air voids. Therefore, all specimens have the same volumetric properties, where aggregate larger than or equal to 2.36mm counts for 47.2% of the total volume of a mixture specimen, and asphalt sand mastic counts for the other 52.8%.
- 4) They had the same mechanical inputs as shown in Table 6.3.

Uniaxial creep compliance tests were simulated by applying a constant load on the top end of each digital specimen with its bottom end fixed. The test duration was a maximum of 50 seconds and calculation of creep stiffness was recorded during the DE simulation. Figure 6.4 shows the typical outputs of DE simulation and the comparison with the upper bound and the lower bound. The upper bound and the lower bound were predicted through the Voigt model(Voigt 1889) and the Reuss model(Reuss 1929). Clearly, all the prediction results were between the upper and lower bounds. More information about the validation of the DE model used in this study can be found in the previous studies (You and Liu 2010).

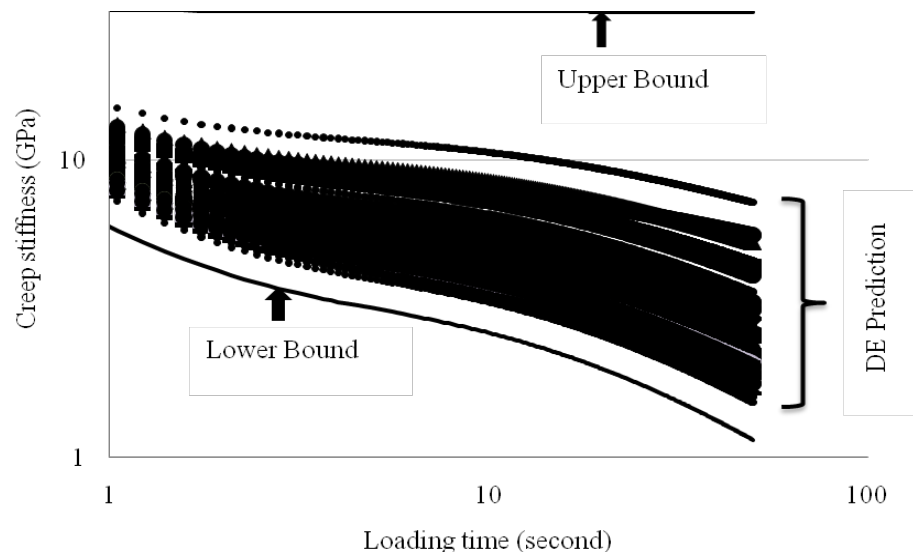


Figure 6.4 DE simulation results and comparison with the upper and lower bounds

**Table 6.3**  
**Inputs of the DE viscoelastic model used in this Study**

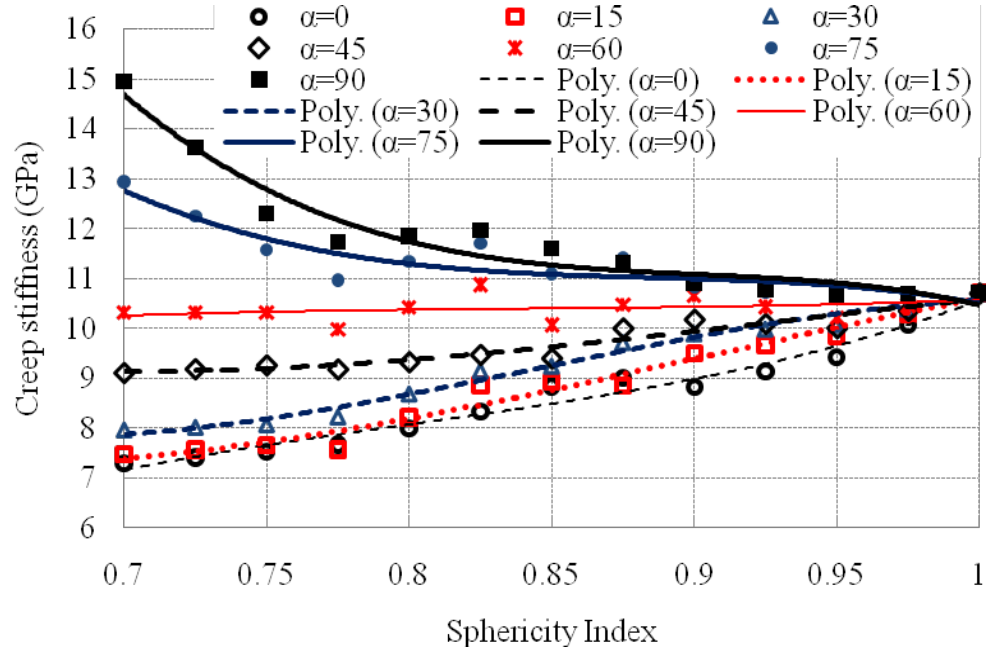
Aggregate	Young's modulus (GPa)			
	55.5			
Asphalt sand mastic	Burger's model parameters (GPa) at 0 °C			
	$E_m$	$\eta_m$	$E_k$	$\eta_k$
	430.9	35.0	1.8	2.2

## 6.7. Observations and Discussion

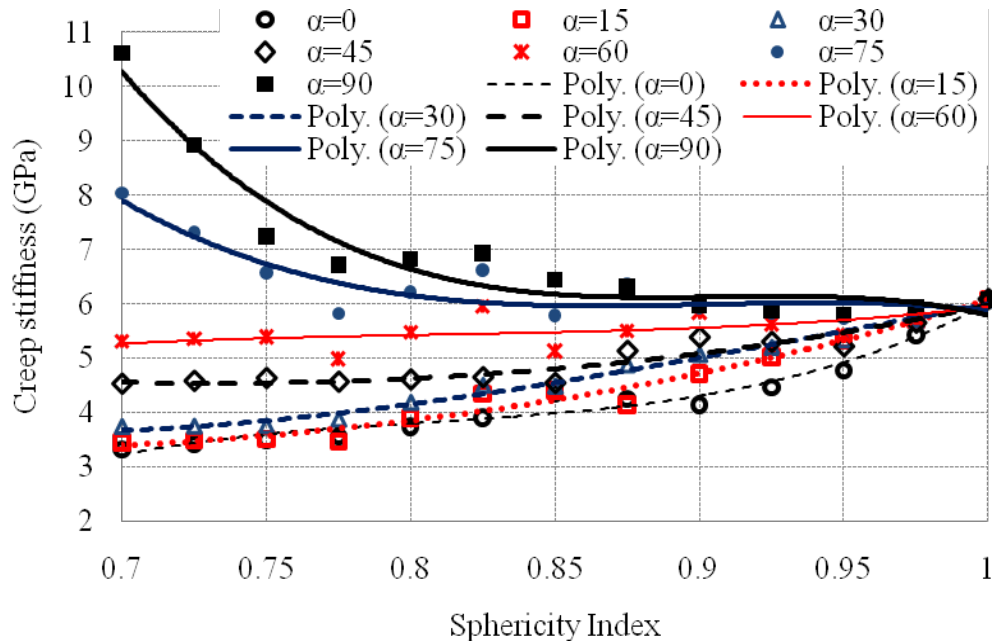
### 6.7.1. Effects of Aggregate Sphericity and Orientation

By analyzing the output data of simulation with the 84 DE R-model mix specimens, effects of aggregate sphericity and orientation were investigated. Creep stiffness values at 1, 10, and 50 seconds were observed. Figure 6.5 shows curves of sphericity index vs. creep stiffness at different orientation angles ( $\alpha = 0, 15, 30, 45, 60, 75, \text{ and } 90^\circ$ ). In order to clarify the underlying principles, the simulation results were fitted with polynomials as shown in the Figure 6.5. From Figure 6.5, it was observed that:

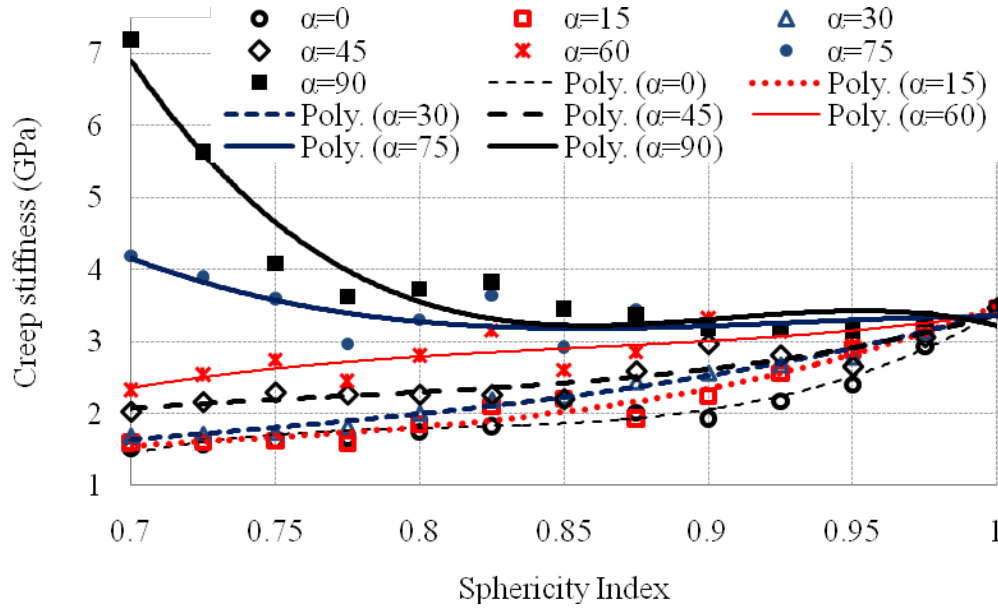
- 1) Influence of sphericity index on creep stiffness is dependent on orientation angles:
  - a) When  $\alpha$  is close to  $60^\circ$ , sphericity index values have slight effects on creep stiffness.
  - b) When  $90^\circ \geq \alpha > 60^\circ$ , influence of sphericity index is significant and creep stiffness values decrease as sphericity index increases.
  - c) When  $60^\circ > \alpha \geq 0^\circ$ , influence of sphericity index is also significant and creep stiffness values increase as sphericity index increases.
  - d) Even though some individual points ran over the curves of  $\alpha=0^\circ$  and  $\alpha=90^\circ$ , most of them were on or between those two curves. Therefore, the authors believed that the curves of  $\alpha=0^\circ$  and  $\alpha=90^\circ$  could be envisioned as the lower and upper bounds of the creep stiffness. The theoretical basis of this assumption is provided after the observation 3).
- 2) Creep stiffness always increases as aggregate orientation angles increase, but the increasing rate is dependent on the sphericity index:
  - a) As sphericity index increases, the rate decreases. For example, the ratios of the highest stiffness to the lowest stiffness are about 15/7, 11/3, and 7/1.5 in Figure 6.5(a), (b), and (c) at SP=0.7 respectively, while the ratios are 11/7.5, 6.2/4, and 3.1/1.8 at SP=0.85.
  - b) When the sphericity index is close to 1, the effects of aggregate orientation can be neglected.
- 3) As creep loading time increases, the ratio between the upper bound ( $\alpha=90^\circ$ ) and lower bound ( $\alpha=0^\circ$ ) increases at lower sphericity indices. For example, when SP=0.7, the ratios are about 15/7, 11/3, and 7/1.5 at the loading time of 1 second, 10 seconds, and 50 seconds, respectively.



(a)  $t=1$  second



(b)  $t=10$  seconds



(c)  $t=50$  seconds

**Figure 6.5 Sphericity index vs. creep stiffness**

The observations above can be explained as follows: according to the composite mechanics, the effective stiffness of a two-phase system is always in the range between the upper bound and lower bound which are predicted with the Voigt model and the Reuss model, respectively. Therefore, the DE R-model is equivalent to the combination of the Voigt and the Reuss models as shown in Figure 6.6. Obviously, when in the DE R-model the aggregate orientation angle increases from  $0^\circ$  to  $90^\circ$ , the contribution of the Voigt model also increases. As a result, the effective stiffness increases correspondingly. Therefore, the curves of  $\alpha=0^\circ$  and  $\alpha=90^\circ$  could be envisioned as the two bounds of effective stiffness, which is the theoretical basis of the observation 1) d). When the orientation angle is equal to  $45^\circ$ , the Voigt model and the Reuss model have the same contribution to the effective stiffness. Therefore, no matter how much the SP index is changed, the effective stiffness of the DE R-model is keeping the same value if the orientation angle is equal to  $45^\circ$  and no aggregate interaction is considered. When the orientation angle is larger than  $45^\circ$ , the increase of the SP index value may increase the contribution of the Reuss model on the effective stiffness. Therefore, the effective stiffness values decrease with the SP values increasing. However, when the orientation angle is less than  $45^\circ$ , the increase of the SP index value may increase the contribution of the Voigt model on the effective stiffness. Therefore, the effective stiffness values increase with the SP values increasing. It was also noted that the principles above are based on the non-interaction between the aggregate particles. However, the interactions between particles were involved in this current study. As a result, it was observed in this study that the dividing orientation angle was  $60^\circ$  instead of the  $45^\circ$  as mentioned above.



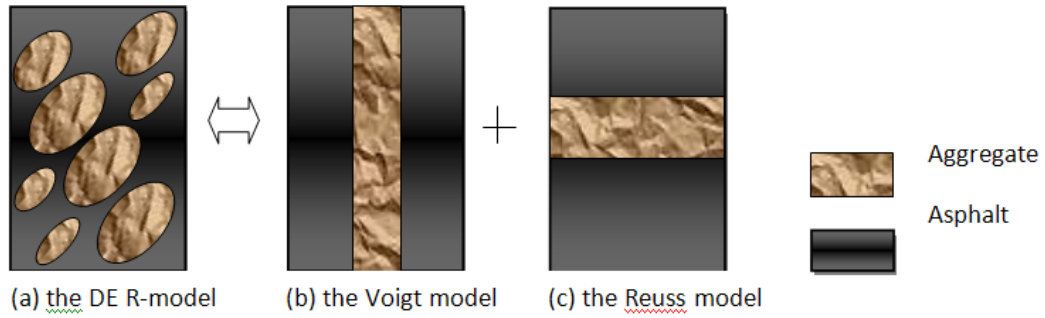


**Figure 6.6 Demonstration of the equivalence of the DE R-model to the Voigt model and the Reuss model**

The observations above may help an asphalt mix designer to select aggregate sources if aggregate orientation angles in the finished mix products are known or can be estimated:

- 1) When  $\alpha$  is close to  $60^\circ$ , the designer may select aggregate sources without considering the aggregate sphericity index;
- 2) When  $90^\circ \geq \alpha > 60^\circ$ , the designer should select aggregate sources with lower sphericity indices;
- 3) When  $60^\circ > \alpha \geq 0^\circ$ , the designer should select aggregate sources with higher sphericity indices.

Actually, several researchers have conducted the studies to estimate and analyze aggregate orientations in a hot-mix asphalt (HMA) mixture. For example, researchers (Masad et al. 1999a) investigate internal structural characterization of asphalt concrete using image analysis. It was observed in their study that the average orientation angle was around  $33^\circ$  in the specimens compacted in the field and anywhere from  $33^\circ$  to  $40^\circ$  for the specimens compacted with a Superpave Gyrotory Compactor (SGC). In other words, orientation angles are from  $33^\circ$  to  $40^\circ$  ( $60^\circ > \alpha \geq 0^\circ$ ) for specimens prepared in the field or SGC. Therefore, aggregate sources with higher sphericity indices are preferred to improve asphalt mixture stiffness according to the observations in the paper.

The observations in this paper may also help mix designers or researchers to optimize the use of the existing aggregate sources by developing new compaction methods. For example, if sphericity indices are very low for some aggregate resources, mix designers and researchers may collaborate to develop a new compaction method which may be able to produce mixes with high aggregate orientation angles. As shown in Figure 6.5, asphalt mixture creep stiffness can be improved significantly by increasing aggregate orientation angles.

It should be noted the observations above were based on several specific conditions: the specific aggregate gradation, asphalt properties at a relatively lower temperature ( $0^\circ\text{C}$ ), and no air voids. Studies of other conditions will be conducted in the ongoing research work. Additionally, the authors tried their best to minimize the impacts from the other

factors on the final simulation results. However, there were still some factors which could impact the simulation results. For example, the digital samples were relative smaller due to limited computational capability. The aggregate gradations and volumetric fractions were slightly different among the 108 digital samples even though they were supposed to be the same values. As a result, some individual points ran over the upper and lower bounds in Figure 6.5. Additionally, the readers may observe that in Figure 6.5(c), the curve of  $\alpha=90^\circ$  was supposed to be always declining with the SP values increasing, but it declined, then slightly increased, and then declined again. Those calculation errors will be fixed in the future study.

### 6.7.2. Effects of Aggregate Fractured Faces with a DE A-model

By analyzing the output data from simulation with the 18 DE A-model mix specimens, the effect of aggregate fractured faces was investigated. Creep stiffness values at 1, 5, 10, 20, and 50 seconds were observed. Figure 6.7 shows creep stiffness vs. sample IDs of DE A-model specimens. The sample IDs were previously shown in Table 6.2. From Figure 6.7, it was found that fractured faces had a slight affect on mixture creep stiffness on average, and the maximum differences of creep stiffness among those 18 A-model specimens were within 10%.

The Superpave mixture design method evaluates coarse aggregates by the percentage of one fractured face and the percentage of two and more fractured faces. To evaluate the difference between aggregate with one fractured face and those with two fractured faces, the stiffness ratio,  $R_{21}$  is defined below:

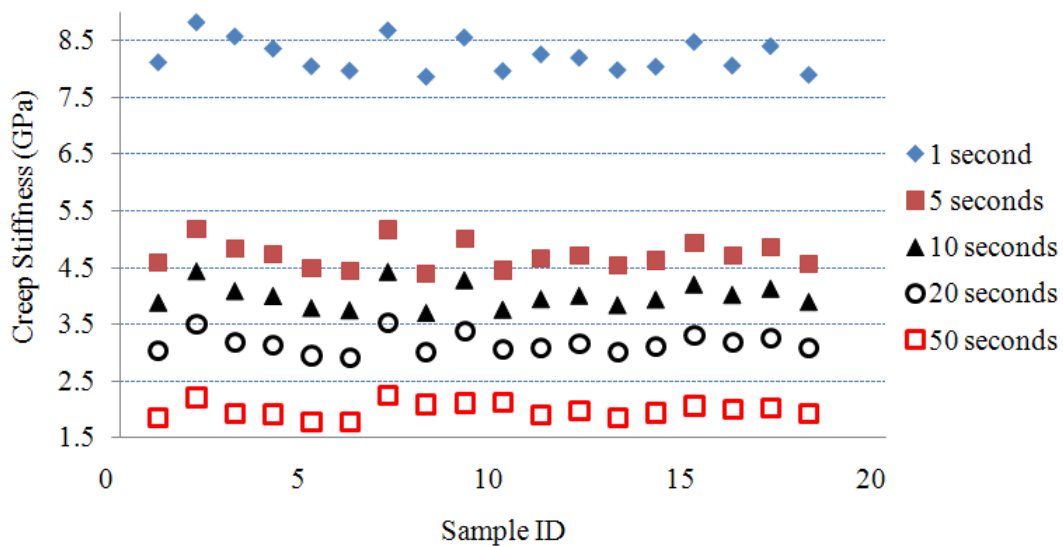


Figure 6.7 Creep stiffness vs. sample ID (the sample IDs are listed in Table 6.2, while legends indicate creep loading time)

$$R_{21} = \frac{E_{II}}{E_I} \quad 6.9$$

To evaluate the difference between aggregate with one fractured face and those with three fractured faces, the stiffness ratio,  $R_{31}$  is defined below:

$$R_{31} = \frac{E_{III}}{E_I} \quad 6.10$$

In 6.9 and 10,  $E_I$  is the average creep stiffness of mixtures in which aggregate particles have only one fractured face (sample IDs from I-1 to I-6 in Table 6.2).  $E_{II}$  is the average creep stiffness of mixtures in which aggregate particles have two fractured faces (sample IDs from II-1 to II-6 in Table 6.2).  $E_{III}$  is the average creep stiffness of mixtures in which aggregate particles have three fractured faces (sample IDs from III-1 to III-6 in Table 6.2). Figure 6.8 shows the creep stiffness ratios vs. the loading time. When the loading time increased from 0 to 50 seconds, it was observed that: 1) Creep stiffness ratios  $R_{21}$  and  $R_{31}$  increased. 2)  $R_{21}$  was slightly larger than  $R_{31}$  initially and then the difference between the two increased with the loading time.

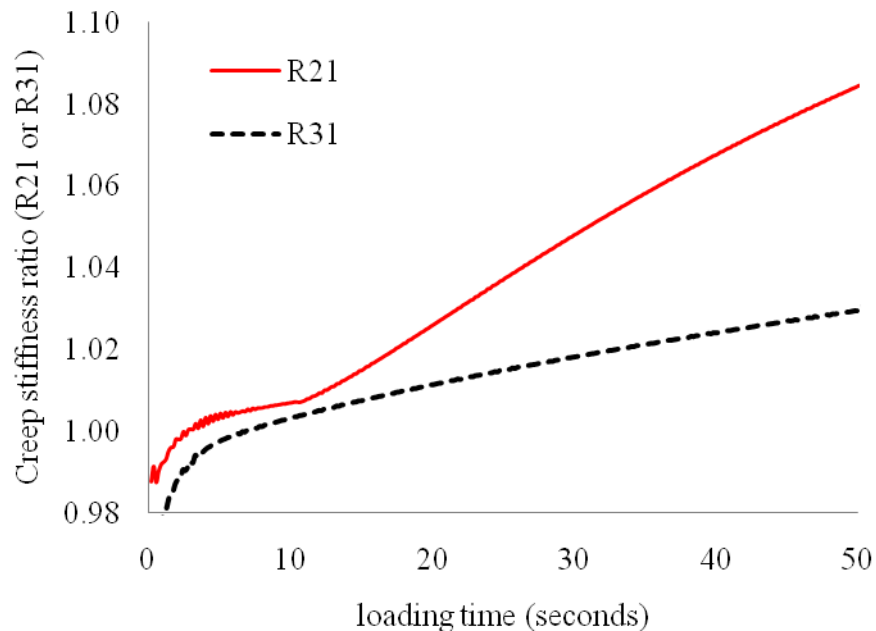


**Figure 6.8 Creep stiffness ratio vs. loading time**

Therefore, it could be concluded that: 1) Aggregate particles with two or three fractured faces can improve asphalt mixture creep stiffness better than those with one fractured face. 2) Aggregates with two fractured faces are much better than those with three fractured faces for improving asphalt mixture creep stiffness. 3) As creep time increases, the fractured aggregates have increasing impacts on asphalt mixture stiffness.

It should be noted herein that the observations and conclusions stated in this paper were based on 18 asphalt mixture specimens with specific fractured faces. Additional studies should be conducted in the future to further verify the findings in this study.

## 6.8. Summary and Conclusion

Although there has been a general understanding of aggregate effects on asphalt mixture performances, a major challenge of existing studies was to isolate the effect of a specific aggregate characteristic from those of other impacting factors. For example, one intends to investigate the influence of aggregate angularity. Aggregate gradation, sphericity index, air void content in the mixture, and asphalt properties may give additional effects simultaneously. Therefore, the combined effect of many other factors should be observed, instead of the isolated effect of aggregate angularity. To address the challenge, this study presents a method to simulate creep tests of idealized HMA mixtures based on discrete element method. A total of the 102 idealized HMA specimens were specially built to model aggregate sphericity, orientation, and angularity with simplified geometries. To minimize the influences of other factors, all the specimens had the same gradation, asphalt content, air voids, and mechanical inputs for the DE simulations. From this study, several interesting findings were observed as shown in the previous section in this paper:

- 1) Influence of sphericity index on creep stiffness was dependent on orientation angles.
- 2) Creep stiffness always increases as aggregate orientation angles increase, but the increasing rate is dependent on the sphericity index
- 3) As creep loading time increases, the ratio between the upper bound ( $\alpha=90^\circ$ ) and lower bound ( $\alpha=0^\circ$ ) increases at lower sphericity indices.
- 4) fractured faces had a slight impact on mixture creep stiffness on average, and the maximum differences of creep stiffness among those 18 A-model specimens were within 10%.
- 5) Aggregate particles with two or three fractured faces can improve asphalt mixture creep stiffness better than those with one fractured face.
- 6) Aggregates with two fractured faces are much better than those with three fractured faces for improving asphalt mixture creep stiffness.
- 7) As creep time increases, the fractured aggregates have increasing impacts on asphalt mixture stiffness.

This study is an initial attempt to investigate the isolated effects of aggregate properties using the discrete element method. The authors tried their best to isolate mineral aggregate shape, orientation, and fractured surfaces from the other impact factors (such as gradation, friction, asphalt, air voids, etc.). However, there were still some factors which

could impact the simulation results. For an example, even though all the DE models were created by inputting the same gradation, the actual gradations in the different digital samples may be slightly different. Additionally, due to the limitation of the current computation capability, the digital sample dimensions were relatively smaller. In reality, aggregate orientation angles range from 0 to 180°, but the orientation angles are within 90°. In the future research, different values and mixed angles will be considered for preparing more AC digital samples. All those impact factors could impact the simulation result. Therefore, the observations and conclusions in this study may be further validated under more comprehensive aggregate packing, gradation, and loading temperature conditions.

## **6.9. Acknowledgements**

This material is based in part upon work supported by the National Science Foundation under grant 0701264. Any opinions, findings, and conclusions or recommendations expressed in this material are those of the author's and do not necessarily reflect the views of the National Science Foundation.

# Chapter 7. A Viscoelastic Model for Simulating AC Time- and Temperature dependency<sup>6</sup>

## 7.1. Abstract

This paper presents a viscoelastic model of asphalt mixtures with the discrete element method, where the viscoelastic behaviors of asphalt mastics (fine aggregates, fines and asphalt binder) are represented by a Burger's model. Aggregates are simulated with irregular shape particles consisting of balls bonded together by elastic contact models, and the inter-places between aggregates are filled with balls bonded with viscoelastic Burger's model to represent asphalt mastic. Digital samples were prepared with the image analysis technique. The micromechanical model is composed of four constitutive laws developed herein to represent the interactions at contacts of discrete elements (balls) within an aggregate, within mastic, between an aggregate and mastic, and between two adjacent aggregates. Each of them consists of three parts: a stiffness model, a slip model, and a bonding model, in order to provide a relationship between the contact force and relative displacement and describe slipping and tensile strength at a particular contact. The relationship between the micro-scale model input and macro-scale material parameters was derived, and an iterative procedure was developed to fit the dynamic modulus test data of asphalt mastic with Burger's model. It was observed that the viscoelastic DE model developed in this study is very capable of simulating constitutive behavior of asphalt mixtures due to the good agreement between the prediction results and the lab test results.

## 7.2. Introduction

### 7.2.1. Discrete Element Method

Discrete element (DE) method is a numerical method, in which Newton's second law and a finite difference scheme are adapted to study the interaction among assemblies of discrete particles. This numerical method is built on successively solving the Newton's second law (law of motion) for each discrete element and applying the force-displacement law for each contacting point. An explicit time stepping scheme is commonly used to integrate the Newton's second law for every discrete element. As a result, contact forces on each element are updated after each time step. Based on the new contact forces, new unbalanced forces are produced and the particles' positions and velocities are calculated. With these new positions, the relative displacements of each pair of elements are updated, and utilized to calculate the next new contact forces. Different materials can be distinguished by applying different force-displacement laws, which is usually called the contact model.

---

<sup>6</sup>Full text reprinted with permission from ASCE. "A Viscoelastic Model for Discrete Element Simulation of Asphalt Mixtures" by Yu Liu, Qingli Dai, and Zhanping You, 2009, Journal of Engineering Mechanics in Civil Engineering, Vol. 135, No. 4, pp. 324-333, Copyright © 2009, ASCE. See Copyright clearance in Appendix A.

Discrete element method was introduced by Cundall (1971) for analysis of rock-mechanics, and then applied to soils by Cundall and Strack (1979). Today, in addition to the granular materials, solid materials can be modeled with bonded contact models. Many computation codes have been developed and applied to granular and solid material simulation with DE method, such as the early problem Ball (Cundall and Strack 1979a; Cundall and Strack 1979b), and revised version of Ball, or Trubal which was used by many researchers (Chen and Hung 1991; Ng and Dobry 1994; Washington and Meegoda 2003), Universal Distinct Element Code (UDEC) (Dickens and Walker 1996; Hart et al. 1985; Idris et al. 2008; Liu et al. 2004a; Liu et al. 2004b; Souley and Homand 1996; Vardakos et al. 2007; Zhang et al. 1999; Zhao et al. 2002; Zhao et al. 2008), Discrete Element Code in three Dimensions (3DEC) (Hart et al. 1988), and Particle Flow Code in two and three dimensions (PFC2D/3D) (Abbas et al. 2007; Buttlar and You 2001; Dai and You 2007; Itasca Consulting Group 2004a; b; Liu et al. 2007; Liu and You 2008; You and Buttlar 2006). For asphalt mixture simulation, however, only PFC2D/3D codes were commonly used due to their following benefits: (1) these coded have higher computation efficiency; (2) these codes can be used to model fracture cracks within aggregates and mastic, and between aggregates and mastic.

### **7.2.2. Review of Current Research Efforts**

The overall macro-mechanical behaviors of the asphalt mixture are determined by micromechanics within the cemented particulate system. Based on the heterogeneous multiphase nature of asphalt materials, it appears that a micromechanical model would be one of the best models to simulate the complex behavior of asphalt materials. Over the past 10 years, the use of micromechanics to predict properties of asphalt mixtures and mastics has drawn increasing attention, and a number of researchers have developed micromechanical models with the discrete element method (You and Buttlar 2004).

Among these research studies, asphalt mastics were usually simulated with elastic models (Abbas et al. 2005; Buttlar and You 2001; Collop et al. 2004; 2007; Collop et al. 2006a; Dai and You 2007; You and Buttlar 2004; You and Buttlar 2005; 2006). With the elastic models, some time-independent properties, such as stiffness at a specified frequency or time, can be predicted, but the real time-dependent behaviors of asphalt mixtures need be investigated. Therefore, viscoelastic models for asphalt mixture were developed, where the viscoelastic behaviors of asphalt mastic (including fines, fine aggregates, and asphalt binder) were represented with Burger's model. Two different methods were used to build the DE constitutive models with Burger's constitutive relations. In one of them, the built-in linear contact model (Itasca Consulting Group 2004a; b) was applied, where the normal and shear stiffness of a discrete element (the linear contact model parameters) change with loading time based on the Burger's constitutive relations (Collop et al. 2007; Collop et al. 2006a). An alternative contact model in PFC2D/3D, the Burger's model, was applied, where the viscoelastic behaviors at a contact are defined with the Burger's constitutive relations and the model parameters are the stiffness or viscosity at a contact (Abbas et al. 2007; Itasca Consulting Group 2004a; b; Liu et al. 2007; Liu and You 2008). With these viscoelastic models, some real time-dependent behaviors of asphalt mixtures were simulated, for instance, dilation,

dynamic modulus and phase angles. In addition to contact models above, the bilinear cohesive model developed by Kim and Buttlar in 2005 for simulating fractures in asphalt mixtures, where the displacement-softening model was employed (Itasca Consulting Group 2004a; b; Kim and Buttlar 2005).

According to the literatures in the past, digital samples for DE simulation of asphalt mixtures were prepared with three following methods: 1) the highly idealized model (Collop et al. 2004; 2007; Collop et al. 2006a); 2) the image-based model (Buttlar and You 2001; You and Buttlar 2004; You and Buttlar 2006); 3) user-defined irregular particle model (Abbas et al. 2007; Tian et al. 2007a; Tian et al. 2007b). The highly idealized model is too simple to represent aggregates' shapes, where aggregates were simulated with balls in three dimensions (3D) or disks in two dimensions (2D). The image-based model is obtained from image of mixtures and the image analysis. Obviously, the image-based model may represent not only shapes but also distributions of aggregates. This kind of model, however, is normally lab-dependent, and also restricted by laboratory conditions. With user-defined irregular particle model, aggregates are represented by randomly created irregular polygons (2D) or polyhedron (3D) particles. The shapes and distributions of aggregates are controlled by user-defined functions which may be from laboratory tests or empirical equations related to properties of aggregates. The advantages of this model are its laboratory independence and time efficiency. At the same time, this model has better simulation prediction of asphalt mixtures than the idealized one.

By summarizing a number of literatures cited above, it was found that DE simulations were conducted for stiffness prediction (Abbas et al. 2007; Dai and You 2007; Liu and You 2008; You and Buttlar 2004; You and Buttlar 2006), fatigue modeling (Carmona et al. 2007), and fracture modeling . Most of the researchers applied PFC2D and PFC3D in discrete element simulation of asphalt mixtures and elastic models were commonly used. Even though viscoelastic models were also used in the recent years, the description of the micromechanical models was insufficient to help understand the mixture behavior of asphalt mixtures. For instance, what are the constitutive models at a specific contact? What are the constitutive model parameters? How do the model parameters be determined? Although general introductions were given in some literatures cited above, a detailed description is needed so that other researchers can implement the work.

### **7.3. Objectives and Scopes**

Based on the research work done in the past, the main objective of this paper is to develop a viscoelastic model for asphalt mixtures, where the Burger's constitutive relations are applied for representing the viscoelastic behaviors of asphalt mastics. Different from the previous studies which gave few details about model development, this paper presents not only the development of the viscoelastic DE model for asphalt mixtures, but also the methodology of determination of the model parameters. A series of equations are developed to express the correlation between micro-scale DE model parameters and the macro-scale material properties of asphalt mastics and aggregates measured in laboratory. Micro-scale model parameters herein are parameters of discrete elements or contacts between two elements. Compared with the micro-scale model



parameters, the macro-scale parameters are material properties of the mastic and aggregates, which can be measured in the laboratory tests or fitted from test results. The conversions between micro-scale model parameters and macro-scale material properties are addressed in this paper. Furthermore, an iterative procedure is applied to fit dynamic modulus laboratory tests with Burger's model.

In this study, digital samples of the asphalt mixture were prepared with the image-based model, where the image-analysis technique was employed. A brief procedure to prepare digital samples with the image analysis technique was developed in the previous research (You and Buttlar 2006). One of the digital samples of asphalt mixtures is shown in Figure 7.1. The model input parameters, including stiffness and viscosities, were calibrated from the material laboratory test data of aggregates and asphalt mastic. The dynamic moduli and phase angles of asphalt mixtures were predicted with two dimensional (2D) discrete element simulations under cyclic loading conditions. By comparing the simulation results with those measured in the laboratory, the predictions of micromechanical model were validated.

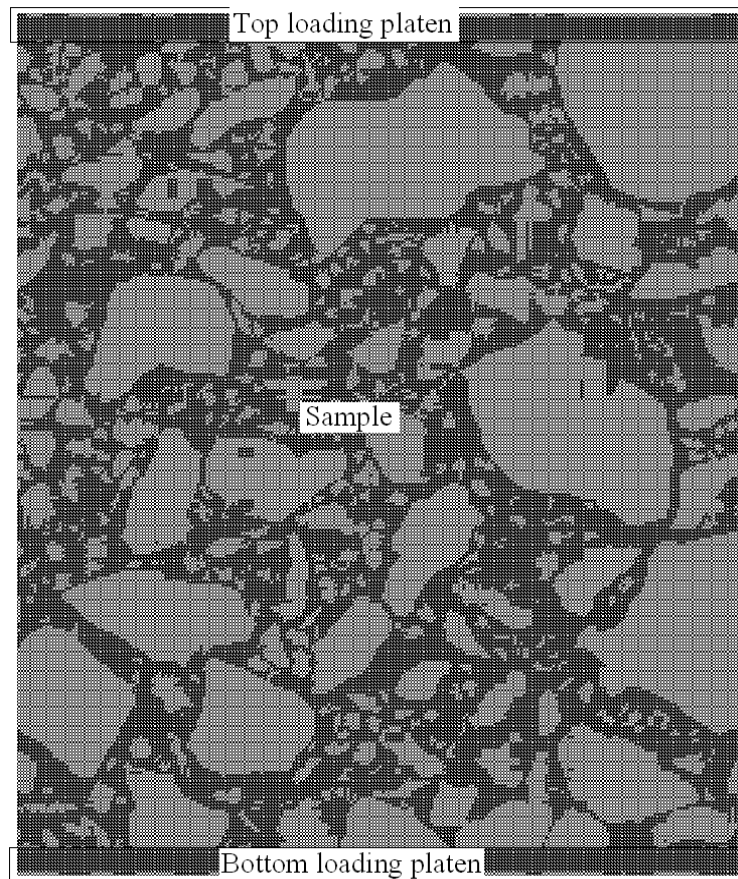


**Figure 7.1 Digital sample with image-based model**

## 7.4. Discrete Element Viscoelastic Model

In *PFC2D* or *PFC3D*, the overall constitutive behavior of a material is modeled through associating constitutive models with the corresponding contacts (Itasca Consulting Group 2004a; b). The constitutive model acting at a particular contact has three parts: a stiffness model, a slip model and a bonding model. The stiffness model provides a relationship between the contact force and relative displacement. The slip model enforces a relationship between shear and normal contact forces, such that the two contacting balls may slip relative to one another. The bonding model is used to limit the total normal and shear forces at the corresponding contact through enforcing bond-strength limits.

### 7.4.1. Micromechanical Behaviors within Asphalt Mixtures

There are four types of contacts to represent four different interactions within the digital sample of asphalt mixture as shown in Figure 7.2: contacts within asphalt mastic, between mastic and aggregates, between adjacent aggregates, and within aggregates. Therefore, four corresponding constitutive models, at contacts, were built to characterize these contact behaviors.

(1) Stiffness model at contacts within asphalt mastic

The viscoelastic behaviors of asphalt mastic at a contact are presented by Burger's model in normal and shear directions. As shown in Figure 7.2(b), Burger's model consists of Maxwell model element (a spring and a dashpot are connected in series) and Kelvin element (a spring and a dashpot are connected in parallel). The constitutive behaviors of Burger's model at a contact can be expressed with the following equations (Itasca Consulting Group 2004a; b):

$$f_n = C_{mn} \dot{u}_{mc} = u_k K_{kn} + \dot{u}_k C_{kn} = K_{mn} u_{mk} \quad 7.1$$

$$f_s = C_{ms} \dot{\delta}_{mc} = \delta_k K_{ks} + \dot{\delta}_k C_{ks} = K_{ms} \delta_{mk} \quad 7.2$$

$$u_n = u_k + u_{mk} + u_{mc} \quad , \quad u_s = \delta_k + \delta_{mk} + \delta_{mc} \quad 7.3$$

where  $f_n$  and  $f_s$ , are the contact forces in normal and shear directions at a contact, respectively;  $u_n$  and  $u_s$  are the relative displacements in normal and shear directions at a contact, respectively;  $u_k$ ,  $\delta_k$  are the normal and shear displacement of the Kelvin model element, respectively;  $u_{mk}$  and  $\delta_{mk}$  are the normal and shear displacements of the isolated spring element of the Maxwell model element;  $u_{mc}$  and  $\delta_{mc}$  are the normal and shear displacements of the isolated dashpot element of the Maxwell model element;  $C_{mn}$ ,  $C_{ms}$ ,  $C_{kn}$ , and  $C_{ks}$  are viscosities of dashpot elements in Figure 7.2(b), and  $K_{mn}$ ,  $K_{ms}$ ,  $K_{kn}$ ,  $K_{ks}$  are stiffness of spring elements in Figure 7.2(b).

(2) Stiffness models at contacts within aggregates and between adjacent aggregates

In this research study, aggregates are considered as a pure elastic material and the spring element is employed to represent the constitutive mechanical behaviors. At a contact within an aggregate or between two adjacent aggregates, the linear contact model was

employed as their stiffness model. As shown in Figure 7.2(d), the linear contact model is defined by connecting two springs in series which represent the two balls in contact. With the spring stiffness ( $k_n^A, k_s^A, k_n^B, k_s^B$ ) in Figure 7.2(d), the normal and shear stiffness ( $K_n, K_s$ ) at a contact can be expressed as (Itasca Consulting Group 2004a; b)

$$K_n = \frac{k_n^A k_n^B}{k_n^A + k_n^B}, \quad K_s = \frac{k_s^A k_s^B}{k_s^A + k_s^B} \quad 7.4$$

Then, the constitutive behaviors of at a contact can be expressed by contact stiffness ( $K_n, K_s$ ) as (Itasca Consulting Group 2004a; b)

$$F_n = U_n K_n, \quad F_s = U_s K_s \quad 7.5$$

### (3) Stiffness model at contacts between aggregates and mastic

At a contact between aggregates and mastic, a stiffness model is built by connecting a spring and Burger's model as shown in Figure 7.2(c). The spring represents aggregates (A), and the Burger's model represents mastic (B). Obviously, Burger's model at a contact can be formed by combining the two spring elements in series in Figure 7.2(c) into one spring element as shown in Figure 7.3. After combination, Burger's model parameters can be expressed as

$$K_{mn} = \frac{k_{mn}^B k_n^A}{k_{mn}^B + k_n^A}, \quad K_{ms} = \frac{k_{ms}^B k_s^A}{k_{ms}^B + k_s^A} \quad 7.6$$

$$\begin{aligned} C_{mn} &= c_{mn}^B & K_{kn} &= k_{kn}^B & C_{kn} &= c_{kn}^B \\ C_{ms} &= c_{ms}^B & K_{ks} &= k_{ks}^B & C_{ks} &= c_{ks}^B \end{aligned} \quad 7.7$$

Where, the parameters in the equations are stiffness and viscosities of the spring and dashpot elements as shown in Figure 7.3. Those at the left side of the equations represent stiffness and viscosity at a contact, while those at the right side of the equations represent stiffness and viscosity of the two balls in contact.

### (4) Slip and bonding models within asphalt mixtures

In addition to the stiffness models above, slip model characterized with friction  $\mu$ , and a bonding model defined with tensile and shear strength are applied at a contact as shown in Figure 7.2 (Itasca Consulting Group 2004a; b).

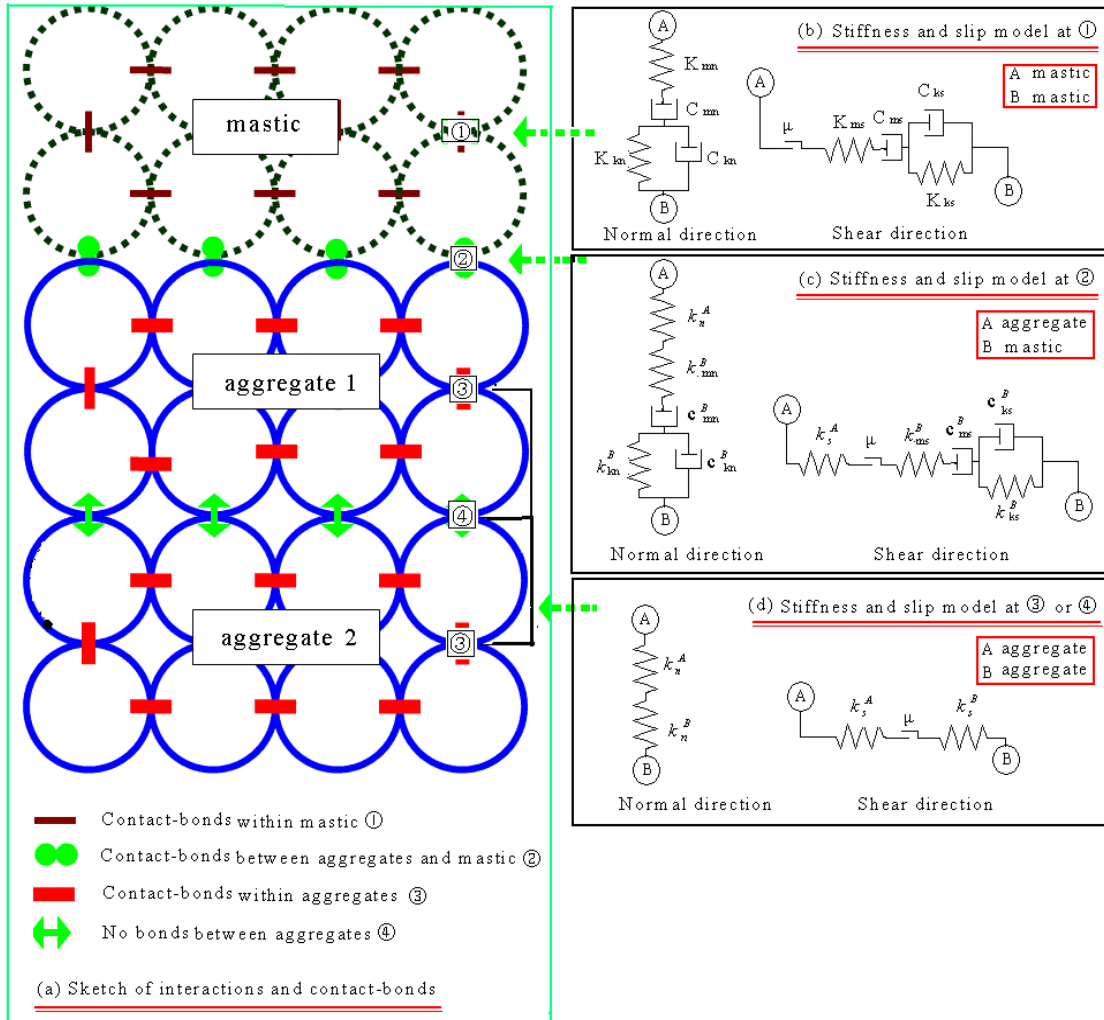


**Figure 7.2 Sketch of interactions and the corresponding constitutive models within the digital sample of asphalt mixtures**

### 7.4.2. Determine Micro-scale Model Parameters

As discussed above, the constitutive models within asphalt mixture are micro-scale mechanical models built by synthesizing macro-scale material behaviors from the interaction of micro-scale components (balls or contacts to represent different material properties). Obviously, these micro-scale mechanical models are easy to represent the micromechanical behaviors, but the micro-scale model parameters are usually difficult to be measured in the laboratory. In order to determine the model parameters, macro-scale properties which can be obtained directly from measurements performed on laboratory specimens are needed. Conversion from macro-scale properties to micro-scale model parameters is developed and illustrated in this paper.

In the laboratory, the following properties can be measured: (1) Young's modulus ( $E$ ) and Poisson ratio ( $\nu$ ) of aggregates; and (2) viscoelastic properties of asphalt mastic such as

dynamic modulus ( $E^*$ ), phase angle ( $\Phi$ ), and creep compliance ( $J_c$ ). Usually, asphalt mastic lab test data is fitted with Burger's model and its four parameters are shown in Figure 7.4. As discussed in the previous section, the corresponding micro-scale model parameters are parameters of discrete elements or contacts (within aggregates, between aggregates, within mastic and between mastic and aggregates). Usually for DE elastic modeling, the behavior of a contact between two discrete elements is related to that of an elastic beam with its ends at the centers of the two discrete elements. And the beam is loaded at its ends by the corresponding force and moment vectors acting at each the discrete element center (Itasca Consulting Group 2004a, 2004b). For viscoelastic simulation, a viscoelastic beam is employed instead of using an elastic beam. In this study, elastic and viscoelastic beams were employed to represent aggregates and mastic properties.

The beam length ( $L$ ), width ( $W$ ) and height ( $H$ ) are expressed as

$$H = \begin{cases} t & (2D) \\ L & (3D) \end{cases}, \quad L = W = R^{[A]} + R^{[B]} \quad 7.8$$

Where,  $R^{[A]}$  and  $R^{[B]}$  is the radius of balls in contact;  $t$  is the disk thickness and can be set by PFC2D command "set disk t".

Therefore, the cross-sectional area ( $A$ ) and inertia of the beam ( $I$ ) can be expressed as

$$A = \begin{cases} Lt & (2D) \\ L^2 & (3D) \end{cases}, \quad I = \frac{1}{12} \begin{cases} L^3 t & (2D) \\ L^4 & (3D) \end{cases} \quad 7.9$$

(1) Parameters for stiffness model within and between aggregates

The macro-scale properties of aggregates ( $E$  and  $\mu$ ) can be measured in laboratory and the corresponding micro-scale model parameters ( $k_n^A, k_s^A, k_n^B, k_s^B$ ) can be expressed with the macro-scale properties.

In normal direction, the following equation can be derived as

$$\left. \begin{aligned} F &= K_n \Delta L \\ F &= E \varepsilon A = \frac{EA \Delta L}{L} \end{aligned} \right\} \Rightarrow K_n = \frac{EA}{L} = E \begin{cases} t & (2D) \\ L & (3D) \end{cases} \quad 7.10$$

Where  $F$  is pure axial loading applied at the two ends of the elastic beam;  $K_n$  is the contact stiffness at a contact point and represents the stiffness of the beam;  $E$  is the Young's modulus of the beam;  $\Delta L$  and  $\varepsilon$  are the increment of relative displacement and strain of the beam under the pure axial loading condition, respectively.

In shear direction, the similar equation can be obtained as

$$K_s = \frac{12IG}{L^3} = \begin{cases} Gt & (2D) \\ GL & (3D) \end{cases} \quad 7.11$$

Where  $K_s$  is shear stiffness at the contact point;  $G$  is the shear modulus can be expressed with Young's modulus  $E$  and Poisson ratio ( $\nu$ ) as

$$E = 2G(1 + \nu) \quad 7.12$$

Because the stiffness of the two balls at a contact in Figure 7.2(d) have the same value. Therefore, according to Equations 7.4, 7.10 and 7.11, the micro-scale model parameters can be expressed as

$$k_n^A = k_n^B = 2E \begin{cases} t & (2D) \\ L & (3D) \end{cases}, \quad k_s^A = k_s^B = 2G \begin{cases} t & (2D) \\ L & (3D) \end{cases} \quad 7.13$$

(2) Parameters for stiffness model within asphalt mastic

As discussed above, a viscoelastic beam is employed to relate the lab-based macro-scale material properties to the micro-scale model parameters for asphalt mastic. The macro-scale response of asphalt mastic under compressive or tensile loading conditions is commonly fitted with Burger's model in Figure 7.4. With the viscoelastic macro-scale material properties, the micro-scale model parameters can be determined as follows.

Under pure axial loading condition, the three sections of displacements of Burger's model ( $u_k, u_{mk}, u_{mc}$ ) can be expressed with their corresponding strains ( $\varepsilon_k, \varepsilon_{mk}, \varepsilon_{mc}$ ) as

$$u_{mc} = \varepsilon_{mc}L, \quad u_k = \varepsilon_kL, \quad u_{mk} = \varepsilon_{mk}L \quad 7.14$$

Substitute (14) to (1) the contact force ( $f_n$ ) can be expressed with strains ( $\varepsilon_k, \varepsilon_{mk}, \varepsilon_{mc}$ ):

$$f_n = \dot{\varepsilon}_{mc} C_{mn} L = L \varepsilon_k K_{kn} + L \dot{\varepsilon}_k C_{kn} = \varepsilon_{mk} K_{mn} L \quad 7.15$$

According to Burger's model as shown in Figure 7.4, the corresponding stress ( $\sigma$ ) can be formulated as follows:

$$\sigma = \dot{\varepsilon}_{mc} \eta_1 = \varepsilon_k E_2 + \dot{\varepsilon}_k \eta_2 = \varepsilon_{mk} E_1 \quad 7.16$$

Where,  $E_1, \eta_1, \eta_2, E_2$  are Burger's model parameters shown in Figure 7.4.  $E_1, \eta_1$ , are modulus and viscosity of the spring and dashpot elements in serial, and  $E_2, \eta_2$ , are modulus and viscosity of the spring and dashpot elements in parallel.

Also, stress ( $\sigma$ ) and force ( $f_n$ ) can be expressed:

$$f_n = \sigma A \quad 7.17$$

Substitute (15)~(16) to (17):

$$\dot{\varepsilon}_{m_C} C_{mn} L = A \dot{\varepsilon}_{m_C} \eta_1 \quad 7.18$$

$$\begin{aligned} L \varepsilon_k K_{kn} + L \dot{\varepsilon}_k C_{kn} &= A \varepsilon_k E_2 + A \dot{\varepsilon}_k \eta_2 \Leftrightarrow \\ \varepsilon_k (L K_{kn} - E_2 A) + \dot{\varepsilon}_k (L C_{kn} - A \eta_2) &= 0 \end{aligned} \quad 7.19$$

$$\varepsilon_{m_K} K_{mn} L = A \varepsilon_{m_K} E_1 \quad 7.20$$

Therefore,

$$K_{kn} = \frac{E_2 A}{L} = E_2 \begin{cases} t & (2D) \\ L & (3D) \end{cases} \quad 7.21$$

$$C_{kn} = \frac{A \eta_2}{L} = \eta_2 \begin{cases} t & (2D) \\ L & (3D) \end{cases} \quad 7.22$$

$$K_{mn} = \frac{E_1 A}{L} = E_1 \begin{cases} t & (2D) \\ L & (3D) \end{cases} \quad 7.23$$

$$C_{mn} = \frac{A \eta_1}{L} = \eta_1 \begin{cases} t & (2D) \\ L & (3D) \end{cases} \quad 7.24$$

Using Equation 7.21 ~ 7.24, the micro-scale parameters of Burger's model can be expressed with lab-based macro-scale properties in normal direction. According to the relation between Young's modulus ( $E$ ) and the shear modulus ( $G$ ):  $E = 2(1+\nu)G$ , the micro-scale parameters for spring elements in shear direction can be expressed with equations 7.26 and 7.28. For dashpot elements, this research assumes the similar relationships exist and they can be expressed with equation 7.25 and 7.27. The sequent calibration with laboratory tests can prove this assumption.

$$C_{ms} = \frac{C_{mn}}{2(1+\nu)} = \frac{\eta_1}{2(1+\nu)} \begin{cases} t & (2D) \\ L & (3D) \end{cases} \quad 7.25$$

$$K_{ks} = \frac{K_{kn}}{2(1+\nu)} = \frac{E_2}{2(1+\nu)} \begin{cases} t & (2D) \\ L & (3D) \end{cases} \quad 7.26$$

$$C_{ks} = \frac{C_{kn}}{2(1+\nu)} = \frac{\eta_2}{2(1+\nu)} \begin{cases} t & (2D) \\ L & (3D) \end{cases} \quad 7.27$$

$$K_{ms} = \frac{K_{mn}}{2(1+\nu)} = \frac{E_1}{2(1+\nu)} \begin{cases} t & (2D) \\ L & (3D) \end{cases} \quad 7.28$$

Where,  $\nu$  is Poisson ratio and is set as 0.5 for asphalt mastic as referred to (Christensen and Anderson 1992).

### (3) Burger's model parameters for a mastic ball

As discussed above, the viscoelastic parameters at a contact between two mastic balls can be expressed with Equation 7.21 ~ 7.28. In order to convert parameters at a contact as listed in Equation 7.21~7.28 into the properties of the two mastic balls in contact, Burger's model at a contact is separated into two identical Burger's model elements as shown in Figure 7.5. The two Burger's model elements represent the two mastic balls in contact. The parameters of the converted model are determined as follows:

$$c_{mn}^B = c_{mn}^A = 2C_{mn} = 2\eta_1 \begin{cases} t & (2D) \\ L & (3D) \end{cases} \quad 7.29$$

$$k_{kn}^B = k_{kn}^A = 2K_{kn} = 2E_2 \begin{cases} t & (2D) \\ L & (3D) \end{cases} \quad 7.30$$

$$c_{kn}^B = c_{kn}^A = 2C_{kn} = 2\eta_2 \begin{cases} t & (2D) \\ L & (3D) \end{cases} \quad 7.31$$

$$k_{mn}^B = k_{mn}^A = 2K_{mn} = 2E_1 \begin{cases} t & (2D) \\ L & (3D) \end{cases} \quad 7.32$$

$$c_{ms}^B = c_{ms}^A = 2C_{ms} = \frac{\eta_1}{(1+\nu)} \begin{cases} t & (2D) \\ L & (3D) \end{cases} \quad 7.33$$



$$k_{ks}^B = k_{ks}^A = 2K_{ks} = \frac{E_2}{(1+\nu)} \left\{ \begin{array}{l} t \quad (2D) \\ L \quad (3D) \end{array} \right. \quad 7.34$$

$$c_{ks}^B = c_{ks}^A = 2C_{ks} = \frac{\eta_2}{(1+\nu)} \left\{ \begin{array}{l} t \quad (2D) \\ L \quad (3D) \end{array} \right. \quad 7.35$$

$$k_{ms}^B = k_{ms}^A = 2K_{ms} = \frac{E_1}{(1+\nu)} \left\{ \begin{array}{l} t \quad (2D) \\ L \quad (3D) \end{array} \right. \quad 7.36$$

(4) Burger's model parameters for stiffness model between aggregates and mastic  
Substitute Equation 7.13, 7.29~7.31, 7.33~7.35 to 7.6~7.7, the Burger's model parameters of the stiffness model between aggregates and mastics as shown in Figure 7.3 can be obtained as

$$K_{mn} = \frac{2EE_1}{E+E_1} \left\{ \begin{array}{l} t \quad (2D) \\ L \quad (3D) \end{array} \right. , \quad K_{ms} = \frac{2GE_1}{G(1+\nu)+E_1} \left\{ \begin{array}{l} t \quad (2D) \\ L \quad (3D) \end{array} \right. \quad 7.37$$

$$K_{kn} = 2E_2 \left\{ \begin{array}{l} t \quad (2D) \\ L \quad (3D) \end{array} \right. , \quad K_{ks} = \frac{E_2}{(1+\nu)} \left\{ \begin{array}{l} t \quad (2D) \\ L \quad (3D) \end{array} \right. \quad 7.38$$

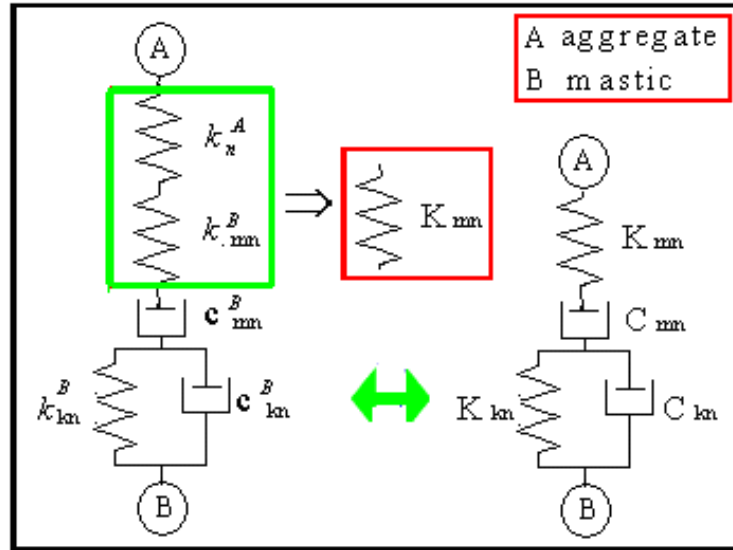
$$C_{mn} = 2\eta_1 \left\{ \begin{array}{l} t \quad (2D) \\ L \quad (3D) \end{array} \right. , \quad C_{ms} = \frac{\eta_1}{(1+\nu)} \left\{ \begin{array}{l} t \quad (2D) \\ L \quad (3D) \end{array} \right. \quad 7.39$$

$$C_{kn} = 2\eta_2 \left\{ \begin{array}{l} t \quad (2D) \\ L \quad (3D) \end{array} \right. , \quad C_{ks} = \frac{\eta_2}{(1+\nu)} \left\{ \begin{array}{l} t \quad (2D) \\ L \quad (3D) \end{array} \right. \quad 7.40$$

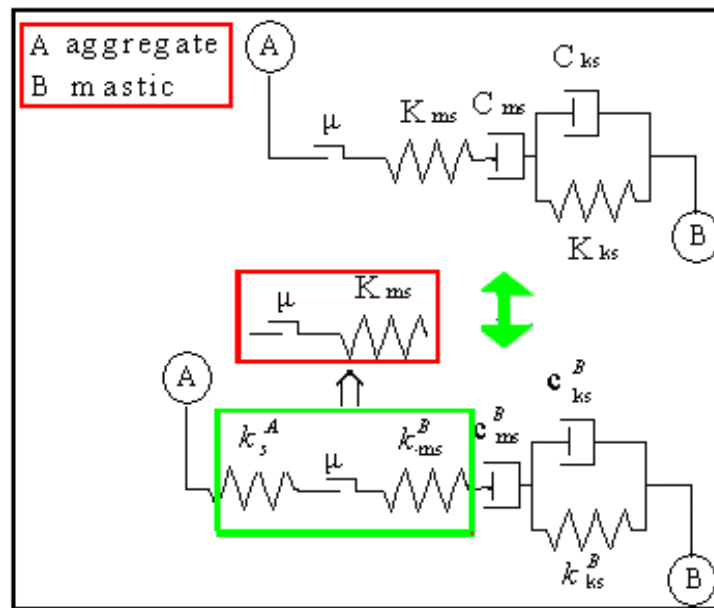
#### (5) Slip and bonding model parameters

The friction  $\mu$  of the slip model at a contact is determined by the maximum value between the frictions of the two contact balls. Supposing the material tensile and shear strengths at a contact are termed with  $\sigma_c, \tau_c$ , then the contact bonds in normal and shear directions can be expressed as

$$\phi_n = \sigma_c A = \sigma_c \left\{ \begin{array}{l} tL \quad (2D) \\ L^2 \quad (3D) \end{array} \right. , \quad \phi_s = \tau_c A = \tau_c \left\{ \begin{array}{l} tL \quad (2D) \\ L^2 \quad (3D) \end{array} \right. \quad 7.41$$



(a) Normal direction



(b) Shear direction

**Figure 7.3 Conversion of Burger's model parameters between mastic and aggregate balls**

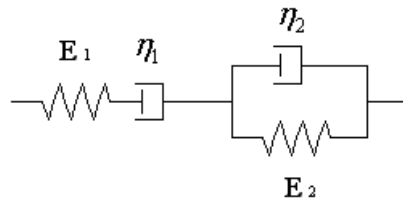
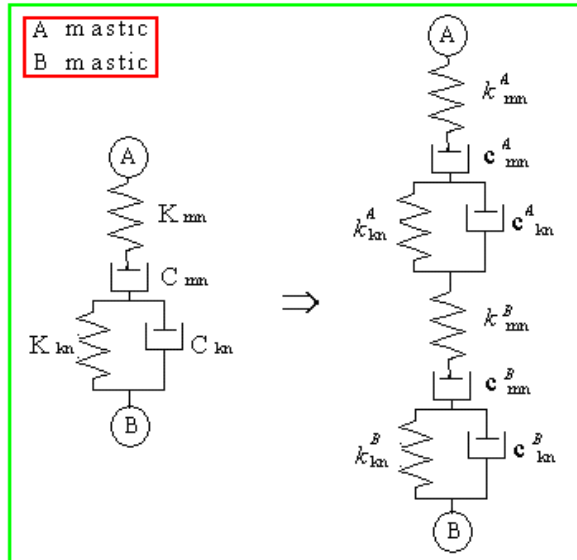
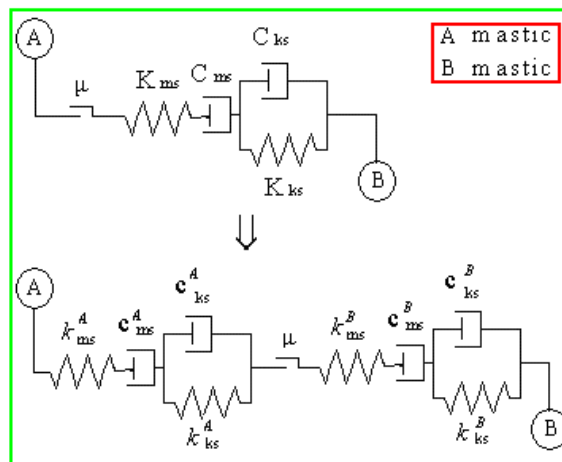


Figure 7.4. Burger's model



(a) Normal direction



(b) Shear direction

Figure 7.5 Conversion of Burger's model parameters of two contacting mastic balls

## 7.5. Macro-Scale Parameters of Burger Model

In this research, dynamic moduli and phase angles of asphalt mastic were measured as discussed later on. Burger's model in Figure 7.4 was employed to fit the lab test data by a procedure as follows.

### 7.5.1. Burger's Model Under Haversine Loading Condition

Burger's model consists of a Maxwell model and a Kevin Model in series, and its constitutive equation can be derived as follows:

$$\begin{aligned}\varepsilon(t) = \varepsilon_{mk} + \varepsilon_{mc} + \varepsilon_k &= \frac{\sigma}{E_1} + \frac{\int \sigma dt + C_1}{\eta_1} + e^{\int \frac{-E_2}{\eta_2} dt} \left( \int \frac{\sigma}{\eta_2} e^{\int \frac{E_2}{\eta_2} dt} dt + C_2 \right) \\ &= \frac{\sigma}{E_1} + \frac{\int \sigma dt + C_1}{\eta_1} + \frac{e^{\frac{-E_2 t}{\eta_2}} \left( \int \sigma e^{\frac{E_2}{\eta_2} dt} dt + C_2 \right)}{\eta_2}\end{aligned}\quad 7.42$$

Where,  $E_1$ ,  $\eta_1$ ,  $\eta_2$  and  $E_2$  are Burger's model parameters as mentioned in the previous section.  $\sigma$  and  $\varepsilon$  are stress and strain;  $C_1$  and  $C_2$  are constants determined by the following equations when  $t=0$ :

$$\frac{\int \sigma dt + C_1}{\eta_1} = 0 \quad , \quad e^{\frac{-E_2}{\eta_2}} \left( \int \frac{\sigma}{\eta_2} e^{\frac{E_2}{\eta_2} dt} dt + C_2 \right) = 0 \quad 7.43$$

In this research, the dynamic modulus tests were conducted by inputting Haversine stress in Equation 7.44.

$$\sigma = \sigma_0 + (\sigma_{\max} - \sigma_0) \sin^2(\omega t / 2) = a + b \cos(\omega t) \quad 7.44$$

Where,  $\sigma_0$  is the pre-compressive stress, and  $\sigma_{\max}$  is the maximum compressive stress.  $\omega$  is angular frequency.  $a$  and  $b$  are expressed as

$$a = \frac{\sigma_{\max} + \sigma_0}{2} \quad , \quad b = \frac{\sigma_{\max} - \sigma_0}{2} \quad 7.45$$

Then, Equation 7.46 as follows can be obtained by solving the equation group (42), (43) and 7.44.

$$\begin{aligned}
\varepsilon(t) &= b\left[\left(\frac{1}{E_1} + \frac{E_2}{E_2^2 + \omega^2\eta_2^2}\right)\cos(\omega t) + \left(\frac{1}{\omega\eta_1} + \frac{\omega\eta_2}{E_2^2 + \omega^2\eta_2^2}\right)\sin(\omega t)\right] + \\
&\quad a\left[\frac{1}{E_1} + \frac{t}{\eta_1} + \frac{(1 - e^{-\frac{E_2 t}{\eta_2}})}{E_2}\right] - \frac{bE_2}{E_2^2 + \omega^2\eta_2^2} e^{-\frac{E_2 t}{\eta_2}} \\
&= b\sqrt{\frac{1}{E_1^2} + \frac{1}{\eta_1^2\omega^2} + \frac{1 + 2(E_2/E_1 + \eta_2/\eta_1)}{E_2^2 + \eta_2^2\omega^2}} \sin(\omega t + \theta) + f(t)
\end{aligned} \tag{7.46}$$

where,

$$f(t) = a\left[\frac{1}{E_1} + \frac{t}{\eta_1} + \frac{(1 - e^{-\frac{E_2 t}{\eta_2}})}{E_2}\right] - \frac{bE_2}{E_2^2 + \omega^2\eta_2^2} e^{-\frac{E_2 t}{\eta_2}} \tag{7.47}$$

$$\tan \theta = \frac{\eta_1\omega(E_2^2 + E_1E_2 + \eta_2^2\omega^2)}{E_1[E_2^2 + \eta_2(\eta_1 + \eta_2)\omega^2]} \tag{7.48}$$

As shown in Equation 7.46, the response strain is composed with two sections: haversine or sinusoidal formulation and  $f(t)$ . Among the two sections,  $f(t)$  can be neglected if the applied stresses are small enough and the loading time is not too long. In this case, the Equation 7.46 can be expressed as follows:

$$\varepsilon(t) = b\sqrt{\frac{1}{E_1^2} + \frac{1}{\eta_1^2\omega^2} + \frac{1 + 2(E_2/E_1 + \eta_2/\eta_1)}{E_2^2 + \eta_2^2\omega^2}} \sin(\omega t + \theta) \tag{7.49}$$

Therefore, the complex compliance ( $1/|E^*|$ ) and phase angle ( $\Phi$ ) can be obtained from Equations 7.44 , 7.48 and 7.49 as follows:

$$\frac{1}{|E^*|} = \frac{\Delta\varepsilon}{\Delta\sigma} = \frac{\varepsilon_{\max} - \varepsilon_{\min}}{\sigma_{\max} - \sigma_{\min}} = \sqrt{\frac{1}{E_1^2} + \frac{1}{\eta_1^2\omega^2} + \frac{1 + 2(E_2/E_1 + \eta_2/\eta_1)}{E_2^2 + \eta_2^2\omega^2}} \tag{7.50}$$

$$\tan \Phi = \frac{1}{\tan(\theta)} = \frac{E_1[E_2^2 + \eta_2(\eta_1 + \eta_2)\omega^2]}{\eta_1\omega(E_2^2 + E_1E_2 + \eta_2^2\omega^2)} \tag{7.51}$$

From equations 7.50 and 7.51, the following two equations can be obtained

$$E_1 = \lim_{\omega \rightarrow \infty} |E^*| \quad , \quad \eta_1 = \lim_{\omega \rightarrow 0} \frac{|E^*|}{\omega} \tag{7.52}$$

### 7.5.2. Determine Burger's Model Parameters

In this research study, an iterative procedure was developed to determine Burger's model parameters by fitting the test data as follows:

(1) Initialize the two parameters of Maxwell element ( $E_1$ , and  $\eta_1$ )

In the laboratory, the loading frequencies commonly used ranges from 0.01 to 25, which are not large enough to determine  $E_1$  (frequency tends to infinite), and not small enough to determine  $\eta_1$  (frequency tends to 0). Therefore, the two parameters are initialized as

$$E_1 = [|E^*|]_{\omega=\omega_{max}} \quad , \quad \eta_1 = \left[ \frac{|E^*|}{\omega} \right]_{\omega=\omega_{min}} \quad 7.53$$

Where,  $\omega_{max}$ ,  $\omega_{min}$  are maximum and minimum values of angle frequencies in lab tests.

(2) Determine the other two parameters ( $E_2$  and  $\eta_2$ ) by substituting Equation 7.53 to Equations (50) and (51), and solving the equation group 7.50 and 7.51.

(3) Then apply (1), (2) above to each frequency.

(4) Keep iterating  $E_1$ ,  $\eta_1$  till both  $E_2$  and  $\eta_2$  have positive values at each frequency.

Finally, the four parameters at the end of the iteration should be substituted to Equation 7.47 and make sure  $f(t)$  is small enough. If  $f(t)$  is not reasonable, the approach developed above will not be applicable. According to this research,  $f(t)$  is small enough at regular frequency range, and low stress levels, where the ratio of  $f(t)/\varepsilon(t)$  is within 1%.

## 7.6. Laboratory Tests

Lab tests were developed in this study to serve two main purposes: 1) to measure the complex modulus and phase angles of mastics and the Young's modulus of coarse aggregates for determining the DE model parameters, and 2) to measure complex modulus and phase angles of asphalt mixtures for calibration and verification of DE modeling. The asphalt mixture specimens were compacted in a Superpave gyratory compactor to a target air void level of 4% by volume, with a nominal maximum aggregate size of 19mm and 4.8% asphalt content by mass as shown in Table 7.1. The sand mastic had a nominal maximum aggregate size of 1.18mm, which came from the mixture's aggregate gradation by eliminating all the aggregate particles larger than 1.18mm except the asphalt (You and Buttlar 2006). The sand mastic had around 14% asphalt content by weight. The uniaxial compression test was performed to obtain the dynamic modulus and phase angles for mastics, aggregate (stones), and mixtures. The test procedure and the results of the mastics and mixtures were listed in previous research work (You and Buttlar 2006). The aggregates test procedure and results were listed in a recent paper. Dynamic moduli and phase angles were measured at 0°C with four frequencies, 0.1, 1, 5, and 10Hz, and the results are listed in Table 7.2.

**Table 7.1**  
**Gradation of the asphalt mixture**

Coarse Aggregates							
Size/mm	25-19	19-12.5	12.5-9.5	9.5-4.75	4.75-2.36	2.36-1.18	<1.18
Mass (%)	1.1	21.4	9.1	12.2	10	14.5	31.7
Volume (%)	0.94	18.24	7.76	10.40	8.52	12.36	27.02
	Asphalt Content		Air Voids		Mastic Content		-
Mass (%)	4.8		0		36.5		-
Volume (%)	10.77		4		41.78		-

**Table 7.2**  
**Laboratory test results of aggregates, asphalt mastic and mixture**

Loading Frequencies		0.1	1	5	10
Dynamic Modulus (GPa)	Mastic	4.40	6.19	8.69	9.86
	Mixture	10.62	14.67	17.67	20.08
Phase Angles (°C)	Mastic	38.93	28.8	24.5	28.65
	Mixture	23.24	20.54	18.16	16.87
Young's Modulus (GPa)	Aggregates	55.5			

**Table 7.3**  
**Burger's model parameters fitted using lab data**

Burger's model parameters	Frequency			
	0.1Hz	1Hz	5Hz	10
$E_1$	901	901	901	901
$\eta_1$	607	607	607	607
$E_2$	3.77	5.64	8.07	8.88
$\eta_2$	3.66	0.41	0.011	0.0067

Then, Burger's model parameters for asphalt mastic was obtained using the procedure developed above, and listed in Table 7.3. As shown in Table 7.3,  $E_2$  is increasing while  $\eta_2$  is decreasing with the loading frequencies.

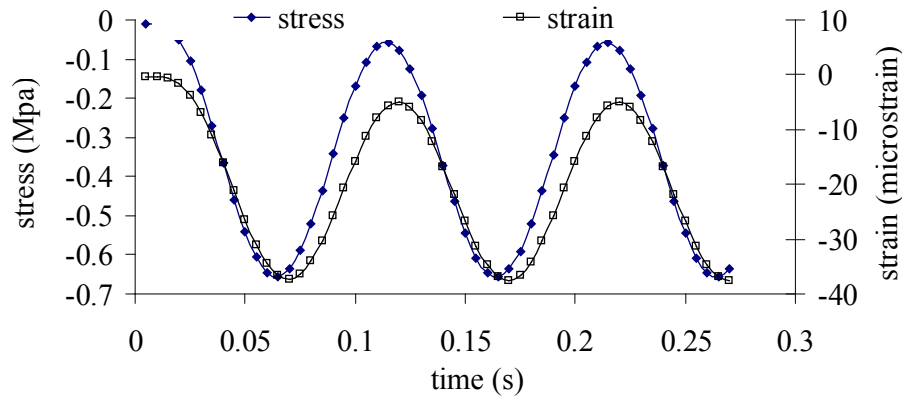
## 7.7. Discrete Element Simulation of Asphalt Mixture

Discrete element (DE) simulations of uniaxial compressive tests were conducted with the viscoelastic model developed in this research study. A digital sample as shown in Figure 7.1 was prepared using the image-based model in the previous research study (You and Buttlar 2006). Model parameters for DE simulation were determined using the procedure of section 3 in this paper. Compressive dynamic loads in the y- direction were applied to the top loading plate of the digital sample as shown in Figure 7.1, while the bottom loading plate of this sample was fixed in all directions.

The viscoelastic DE simulation was conducted on the image sample with the corresponding model parameters under the cyclic uniaxial compression loadings. 9540 discrete elements were included in the image sample. The applied loading frequencies were 25Hz, 10Hz, 5Hz, 1Hz and 0.1Hz. The applied stress and strain response are plotted in Figure 7.6 for each loading frequency. Dynamic modulus ( $E^*$ ) and phase angle ( $\Phi$ ) are calculated from the stress and strain curve in Figure 7.6 using Equation 7.54. The predicted  $E^*$  and  $\Phi$  were plotted in Figure 7.7 along with those measured in laboratory.

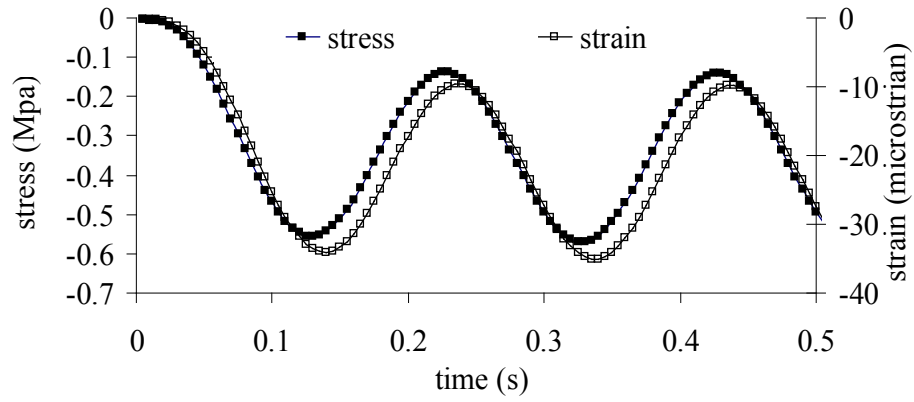
$$E^* = \frac{\sigma_{\max} - \sigma_{\min}}{\varepsilon_{\max} - \varepsilon_{\min}}, \quad \Phi = \frac{\Delta t}{T} \times 360 \quad 7.54$$

Where,  $\sigma_{\max}$ ,  $\sigma_{\min}$ ,  $\varepsilon_{\max}$ ,  $\varepsilon_{\min}$  are the maximum and minimum values of the applied stress and the calculated strain responses.  $\Delta t$  is the time difference between two adjacent peak stress and strain and  $T$  is the loading period which is the inverse of the loading frequency.

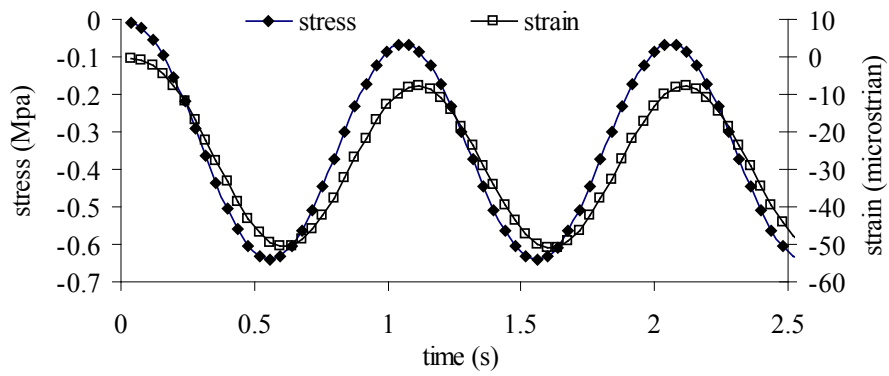


a) Simulation results at 10Hz

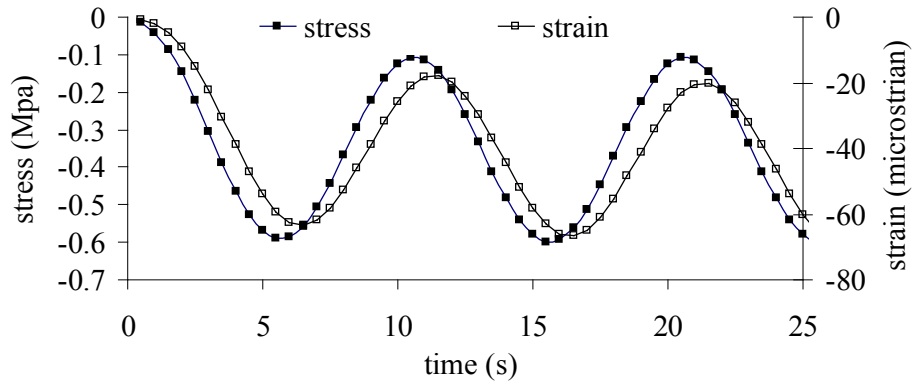




b) Simulation results at 5Hz



c) Simulation results at 1Hz



d) Simulation results at 0.1Hz

**Figure 7.6. The applied stress and strain response**

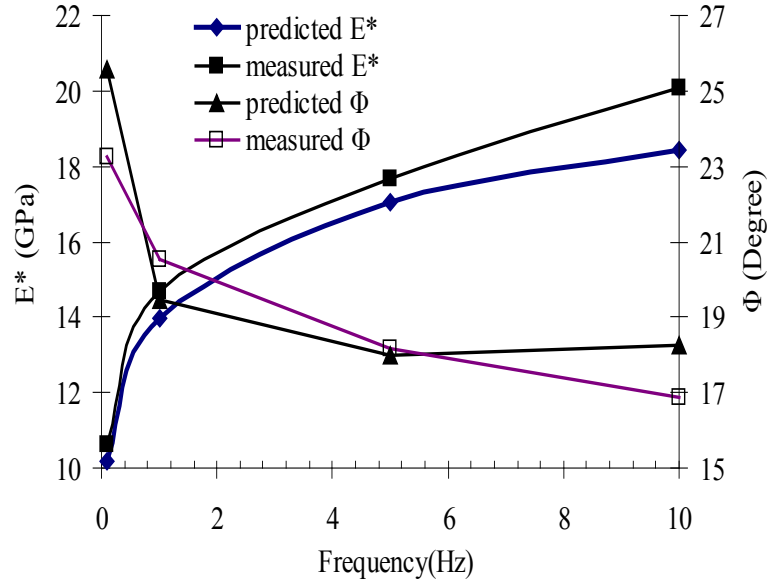


**Figure 7.7 Dynamic modulus and phase angle**

It was found that with the DE viscoelastic model, the predicted dynamic moduli and phase angles were slightly lower than those from the lab tests. The dynamic modulus has a maximum, a minimum and an average prediction error of 8.8%, 1.8% and 5%, respectively. Additionally, the maximum, minimum and average errors for phase angle are 9.4%, 4.6% and 6.4%, respectively. Therefore, the model in this research is able to predict the complex viscoelastic properties of asphalt mixtures with the confidence of more than 90%.

## 7.8. Computation Speed for Viscoelastic Modeling

Compared with elastic DE modeling, viscoelastic DE modeling is time-consuming due to the following two reasons:

Firstly, viscoelastic behaviors of asphalt mixture are time-dependent, and real physical time is needed to represent the time-dependant performances. Discrete Element method is a dynamic iterative method through successively solving the Newton's second law (law of motion) for each contacting elements and applying the force-displacement law for each contact. After many times of iterative calculations, the final results can be obtained. The consuming time for one iterative step is termed with time-step, which is the real physical time per iterative step. The accumulative physical time is determined by the specific problem. For example, the accumulative time ( $t$ ) for modeling dynamic tests at a frequency of 10Hz is 0.1 seconds under one cyclic loading. Therefore, if the time-step ( $t_{del}$ ) is  $10^{-7}$  second/step, the accumulative iterative steps ( $N_{cyc}$ ) determined with Equation 7.55 is  $10^6$  steps:

$$N_{cyc} = \frac{t}{t_{del}} = \frac{0.1}{10^{-7}} = 10^6 \text{ (steps)} \quad 7.55$$

Within one day,  $2 \times 10^6$  iterative steps for the DE model consisting of 100,000 discrete elements can be processed on a personal computer (Processor of Quad Core Extreme Edition) for this case.

Secondly, Burger's model is not the built-in model in PFC. Different from the built-in models which associate stiffness with particles (discrete elements), Burger's model is an alternative model, which associates stiffness directly with the contacts. Therefore, a further consideration when using Burger's model is the way in which the model is installed in new contacts. Usually, FISHcall is set so that the creation of a new contact will automatically trigger the calling of a FISH function which installs Burger's model and its properties dynamically. When a new contact is created, the FISH function will be triggered and all the contact properties within the digital sample will be updated. In this way, the computation speed is lowered. Furthermore, FISH functions are not the built-in standard codes of PFC2D/3D, and have to be interpreted before they are executed. FISH is a programming language embedded within PFC2D/3D that allows users to develop their own variables and functions. FISHcall is an approach with which FISH functions may be called when particular events occur during execution. For example, when a new contact is created, a FISH function may be called automatically with FISHcall (Itasca Consulting Group 2004a; b).

## **7.9. Summary, Conclusions, And Further Research Work**

This paper developed a viscoelastic discrete element simulation approach for asphalt mixture based on the Burger's model. The micro-mechanical behaviors within asphalt mixture were studied, and the corresponding constitutive models were developed to represent different contact behaviors. The micro-scale input parameters of DE model derived from the Burger's constitutive relations were determined by the corresponding lab-based macro-scale material properties. An iterative procedure was developed to calibrate these micro-scale model parameters. Viscoelastic DE simulation with developed models was conducted under uniaxial compression loading with different loading frequencies.

This computation study found that: (1) The viscoelastic performances of asphalt mixtures can be simulated with the viscoelastic model over cyclic loading periods. (2) The viscoelastic model of asphalt mixtures is promising in the prediction of dynamic modulus and phase angle of asphalt mixtures. In the examples shown in this paper, the dynamic modulus has a maximum, a minimum and an average prediction error of 8.8%, 1.8% and 5%, respectively. Additionally, the maximum, minimum and average errors for phase angle are 9.4%, 4.6% and 6.4%, respectively. Therefore, the developed micromechanical viscoelastic models can accurately predict the dynamic modulus and phase angle of asphalt mixtures with the confidence of more than 90%. (3) A procedure presented in this paper is able to fit Burger's model parameters for simulation inputs with dynamic modulus laboratory test data.

The following items should be addressed in the future studies: (1) Simulation of asphalt mixtures under other loading conditions (for example, under static step loading

condition), and; (2) Three dimensional (3D) DE simulation of asphalt mixtures, which can be easily extended with the research herein by developing 3D digital samples and using the viscoelastic model developed in this paper.

### **7.10. Acknowledgements**

This material is based in part upon work supported by the National Science Foundation under grant 0701264. Any opinions, findings, and conclusions or recommendations expressed in this material are those of the author's and do not necessarily reflect the views of the National Science Foundation.

# Chapter 8. Determination of Burger's Model Parameters using Creep-recovery Testing Data<sup>7</sup>

## 8.1. Abstract

this paper proposes a method for determining Burger's model parameters using creep-recovery data. With the determined Burger's model parameters, the viscoelastic behaviors of an asphalt binder (PG64-28) and its two mastics (a binder PG64-28 blended with mineral fines passing the ASTM 100# sieve and 200# sieve, respectively) are investigated. The total deformation of the mastics was separated into three parts: the instantaneous elasticity, delayed elasticity, and viscous flow. The ratios of the viscous flow to the elasticity were calculated and analyzed. It was found the proposed method is promising where the average errors of the creep section are 3.53%, 5.28% and 8.02% for the three materials, and the values are 0.69%, 1.286% and 1.80% for the recovery section.

## 8.2. Introduction

The asphalt mixture has been commonly used to build the surface courses of flexible pavements, where rutting and fatigue distresses of pavement surface courses are caused due to rheological properties of asphalt mixtures. Hundreds of research literatures were published to address the rheological properties of asphalt materials in the past. By summarizing the published literatures in the past a few decades, creep, creep-recovery, and dynamic modulus tests were commonly used as loading modes and the master curves were usually utilized to analyze the test results by using time-temperature superposition principles (Dobson 1969; Marasteanu et al. 2004; Schwartz et al. 2002; Zanzotto and Stastna 1997; Zhao and Kim 2003). Several rheological models were utilized such as the Burger's model, the six-element solid model, the generalized Maxwell model, the generalized Kelvin model, and the power law model. Although a complex model is powerful and gives better fitted results, such as the generalized Maxwell model or the Kelvin model, all rheological models cited above could well fit the laboratory test results. The errors between the fitted and measured are reasonable for engineering purposes. A simple model, however, has its own benefits since its parameters can easily be determined and each of them has a clear physical meaning. For an example, the four parameters of Burger's model represent elastic, viscoelastic, and viscous flow properties of asphalt materials which can be determined using creep-recovery data. In the following sections of this paper, a procedure is presented and the viscoelastic behaviors of an asphalt binder and two mastics are analyzed.

---

<sup>7</sup>Full text reprinted with permission from ASCE. "A Viscoelastic Model for Discrete Element Simulation of Asphalt Mixtures" by Yu Liu, Qingli Dai, and Zhanping You, 2009, Journal of Engineering Mechanics in Civil Engineering, Vol. 135, No. 4, pp. 324-333, Copyright © 2009, ASCE. See Copyright clearance in Appendix A.

### 8.3. Burger's Model Constitutive Equation

Burger's model consists of four mechanical components as shown in Figure 8.1: the two spring elements ( $E_M$ ,  $E_K$ ) which coincide with the Hookean principle and the two dashpots ( $\eta_M$ ,  $\eta_K$ ) which follow the Newtonian principle. According to these two principles, Burger's model constitutive equation can be expressed in Equation 8.1.

$$\varepsilon(t) = \varepsilon_e + \varepsilon_v + \varepsilon_d = \frac{\sigma}{E_M} + \frac{\int \sigma dt + C_1}{\eta_M} + \left( \frac{1}{\eta_K} \int \sigma e^{\frac{E_K}{\eta_K} t} dt + C_2 \right) e^{-\frac{E_K}{\eta_K} t} \quad 8.1$$

Where,  $\varepsilon_e$ ,  $\varepsilon_v$ ,  $\varepsilon_d$ , are three sections of the strain response when a stress,  $\sigma$ , is applied: the instantaneous elastic, the viscous flow and the viscoelastic (delayed elastic) strain.  $C_1$ ,  $C_2$  are constants.

According to the Newtonian principle, both  $\varepsilon_p$  and  $\varepsilon_d$  are zero at  $t=0$  as shown in Equation 8.2 and 8.3.

$$\frac{\int \sigma dt + C_1}{\eta_M} = 0 \Rightarrow C_1 = -\left( \int \sigma dt \right) \Big|_{t=0} \quad 8.2$$

$$\frac{1}{\eta_K} \int \sigma e^{\frac{E_K}{\eta_K} t} dt + C_2 = 0 \Rightarrow C_2 = -\frac{\int \sigma e^{\frac{E_K}{\eta_K} t} dt \Big|_{t=0}}{\eta_K} \quad 8.3$$

A creep-recovery test consists of two sections: a creep under a constant load ( $\sigma=\sigma_0$ ) when  $t < t_1$  and a recovery after the load is removed when  $t > t_1$ . For the creep section ( $t < t_1$ ), a constant load ( $\sigma=\sigma_0$ ) is applied and the two constants ( $C_1$ ,  $C_2$ ) are solved by substituting  $\sigma=\sigma_0$  to 8.2 and 8.3. Therefore, the strain response is expressed in Equation 8.4.

$$\varepsilon(t) = \frac{\sigma_0}{E_M} + \frac{\sigma_0 t}{\eta_M} + \frac{\sigma_0}{E_K} \left( 1 - e^{-\frac{E_K}{\eta_K} t} \right) \quad 8.4$$

After the constant load ( $\sigma_0$ ) is removed ( $t=t_1$ ), the instantaneous elastic strain ( $\varepsilon_e$ ) is recovered immediately, and therefore,

$$\varepsilon(t_1) = \varepsilon_v(t_1) + \varepsilon_d(t_1) = \frac{\sigma_0 t_1}{\eta_M} + \frac{\sigma_0}{E_K} \left( 1 - e^{-\frac{E_K}{\eta_K} t_1} \right) \quad 8.5$$

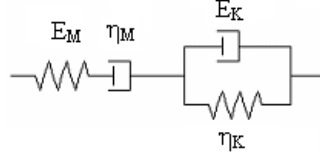


**Figure 8.1 Burger's Model**

During unloading time ( $t > t_l$ ), viscous strain ( $\varepsilon_v$ ) cannot be recovered, and the viscoelastic strain ( $\varepsilon_d$ ) can be recovered, but it is time-dependent as expressed in Equation 8.6.

$$E_K \varepsilon_d + \eta_K \dot{\varepsilon}_d = 0 \quad 8.6$$

By solving Equation 8.6, the viscoelastic strain ( $\varepsilon_d$ ) can be expressed as

$$\varepsilon_d(t) = C e^{-\frac{E_K t}{\eta_K}} \quad 8.7$$

Therefore, the strain response of the recovery section can be expressed in Equation 8.8.

$$\varepsilon(t) = \varepsilon_v(t_1) + \varepsilon_d(t) = \frac{\sigma_0 t_1}{\eta_M} + C e^{-\frac{E_K t}{\eta_K}} \quad 8.8$$

Where  $C$  is a constant which can be determined with Equation 8.8 by applying boundary condition at  $t = t_l$ .

$$C = \frac{\sigma_0}{E_K} (1 - e^{-\frac{E_K t_1}{\eta_K}}) e^{\frac{E_K t_1}{\eta_K}} \quad 8.9$$

By summarizing, the constitutive equation for creep-recovery test condition can be expressed in Equation 8.10.

$$\varepsilon(t) = \begin{cases} \frac{\sigma_0}{E_M} + \frac{\sigma_0 t}{\eta_M} + \frac{\sigma_0}{E_K} (1 - e^{-\frac{E_K t}{\eta_K}}) & (t < t_1) \\ \frac{\sigma_0 t_1}{\eta_M} + \frac{\sigma_0}{E_K} (1 - e^{-\frac{E_K t_1}{\eta_K}}) e^{-\frac{E_K (t-t_1)}{\eta_K}} & (t \geq t_1) \end{cases} \quad 8.10$$

## 8.4. Determination of Burger's model parameters

In order to determine Burger's model parameters, this section presents a procedure where Equation 8.10 are converted into two linear equations and the creep-recovery data is fitted with the two linear equations.

Firstly, for the creep section ( $t < t_l$ ), the nonlinear viscoelastic strain ( $\varepsilon_d$ ) is moved to the left side of the function, the right side is a linear function as written in Equation 8.11.

$$\varepsilon_l(t) = a + bt \quad (t < t_l) \quad 8.11$$

Where  $a$ ,  $b$  are constants;  $t$  is loading time and  $\varepsilon_l$  is the linear strain.  $a$ ,  $b$ , and  $\varepsilon_l$  are formulated in Equations 8.12 and 8.13.

$$a = \frac{\sigma_0}{E_M} \quad \text{and} \quad b = \frac{\sigma_0}{\eta_M} \quad 8.12$$

$$\varepsilon_l = \varepsilon(t) - \frac{\sigma_0}{E_K} \left(1 - e^{-\frac{E_K t}{\eta_K}}\right) \quad 8.13$$

Then, for the recovery section ( $t > t_l$ ), the constitutive equation can also be converted into a linear equation as expressed in Equation 8.14.

$$y = cx \quad (t \geq t_l) \quad 8.14$$

Where,  $c$ ,  $x$ ,  $y$  are expressed as

$$x = t - t_l, \quad y = \ln\left(\frac{\varepsilon - \varepsilon_v(t_l)}{\varepsilon(t_l) - \varepsilon_v(t_l)}\right), \quad c = -\frac{\eta_K}{E_K} \quad 8.15$$

In Equation 8.15,  $\varepsilon(t_l)$  is strain at  $t=t_l$ , which can be obtained from original data of the recovery section;  $\varepsilon_v(t_l)$  is expressed as

$$\varepsilon_v(t_l) = \frac{\sigma_0 t_l}{\eta_M} \quad 8.16$$

With the two linear equations, the creep-recovery data can be fitted with a procedure as follows:

(1) Initialize the viscous strain at  $t=t_l$ ,  $\varepsilon_v(t_l)$ ;

The viscoelastic strain is recovered with time increasing. If the time is infinite, the viscoelastic strain is recovered completely according to Equation 8.7. Based on Equation 8.8, if the time tends to be infinite, the viscous strain can be expressed in Equation 8.17:



$$\varepsilon_v(t_1) = \lim_{t \rightarrow \infty} \varepsilon(t) \quad 8.17$$

Because time cannot be infinite in the laboratory, the viscous strain is initialized as the minimum strain of the recovery data.

(2) Determine constant  $c$  in the linear Equation 8.14

With the recovery data and the initialized viscous strain, the variables,  $x$  and  $y$  can be obtained. Then, the constant,  $c$ , is determined by fitting  $x$ ,  $y$  with the linear equation 8.14.

(3) Determine  $E_K$  and  $\eta_K$ ;

When  $t=t_1$ , Equation 8.17 is obtained from Equations 8.10 and 8.15. With the test data at  $t=t_1$  and the fitted constant,  $c$ ,  $E_K$  is determined by Equation 8.18. Then, the parameter,  $\eta_K$  is determined by submitting the constant,  $c$ , and  $E_K$  to Equation 8.15.

$$\frac{\sigma_0}{E_K} (1 - e^{-ct_1}) = \varepsilon(t_1) - \varepsilon_v(t_1) \quad 8.18$$

Where  $\sigma_0$  is the constant stress;  $\varepsilon(t_1)$  can be obtained from original datum and  $\varepsilon_v(t_1)$  is initialized at the first step.

(4) Determine the constants ( $a$  and  $b$ ) in the linear Equation 8.11;

With calculated parameters,  $E_K$  and  $\eta_K$ , the linear section of the strain at creep section,  $\varepsilon_l(t)$ , is determined with Equation 8.13. Then, the two constants in Equation 8.11 are determined by fitting  $\varepsilon_l(t)$  and  $t$ .

(5) Determine  $E_M$  and  $\eta_M$ ;

The two parameters  $E_M$  and  $\eta_M$  can be determined by substituting the two constants,  $a$  and  $b$ , to Equation 8.12.

(6) Calculate average absolute errors ( $AAE$ );

Average absolute errors of creep and recovery section are calculated in Equation 8.19.

$$AAE = \frac{1}{N} \sum_i^N \frac{\varepsilon_{predicted}(t_i) - \varepsilon_{measured}(t_i)}{\varepsilon_{measured}(t_i)} \quad 8.19$$

Where  $N$  is the total test data of creep or recovery,  $t_i$  is the time of  $i^{\text{th}}$  data.

(7) Finalize the Burger's model parameters

By repeating the previous six steps, the minimum average absolute errors ( $AAEs$ ) are obtained, where the four Burger's model parameters are finally determined.

## 8.5. Viscoelastic Analysis of asphalt binder and mastic

Generally, the mechanical model parameters are determined as input parameters for numerical simulation with the finite element method or the discrete element method (Dai

and You 2007; Liu et al. 2009; Liu et al. 2007; Liu and You 2008). In this paper, however, the viscoelastic properties of an asphalt binder (PG64-28) and its two mastics (mastic-100 and mastic-200) are analyzed with the determined Burger's model parameters. Mastic-100 was made by mixing binder PG64-28 with mineral fines passing the ASTM 100# sieve, while mastic-200 was made by mixing binder PG64-28 with mineral fines passing the ASTM 200# sieve. Creep-recovery tests were conducted with 1000 seconds loading time and 1000 seconds recovery time on Dynamic Shear Rheometer (DSR) at four temperatures: 40°C, 52°C, 64°C, and 70°C, respectively. In addition, the dynamic shear modulus tests at a frequency of 0.01Hz were conducted at the same temperatures as in the creep-recovery tests. The shear compliances  $\varepsilon(t)/\sigma_0$  from the creep and recovery data of the binder and its two mastics are plotted in Figure 8.2. It should be noted that the recovery strain is very small compared with the creep strain for all the tests. Based upon the dynamic shear modulus results, the phase angles vs. temperatures are plotted in Figure 8.3. From Figure 8.3, it was observed that with temperatures increasing, the phase angles of the binder increase with temperatures, and the phase angles of the two mastics decrease and then increase.

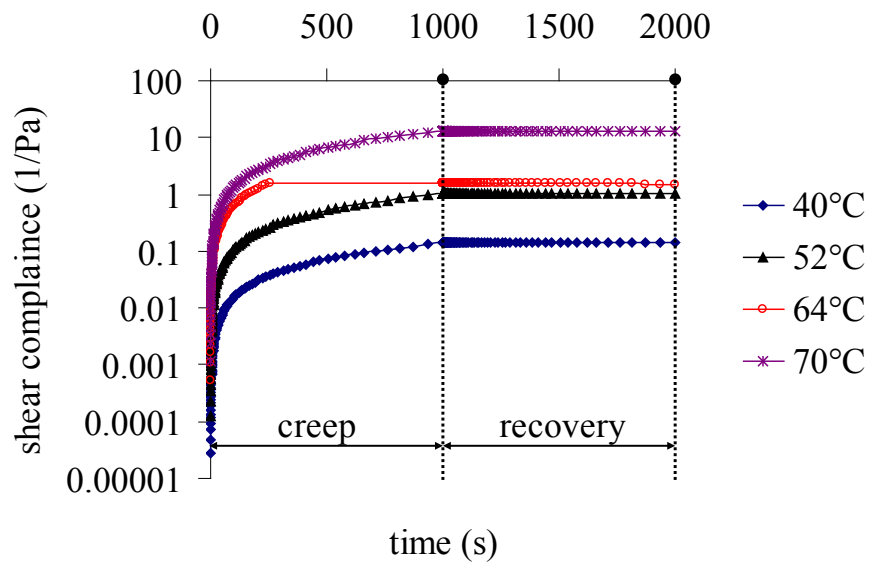
The test data was fitted with Burger's model using the procedure presented in the previous section. The calculated *AAEs* for creep and recovery tests are listed in Table 8.1. From the table, the following findings were observed:

(1) Burger's model can be utilized to fit creep as well as recovery data of both the binder and mastic, where the average errors of the creep section are 3.53%, 5.28% and 8.02% for the three materials, and the values are 0.69%, 1.286% and 1.80% for the recovery section.

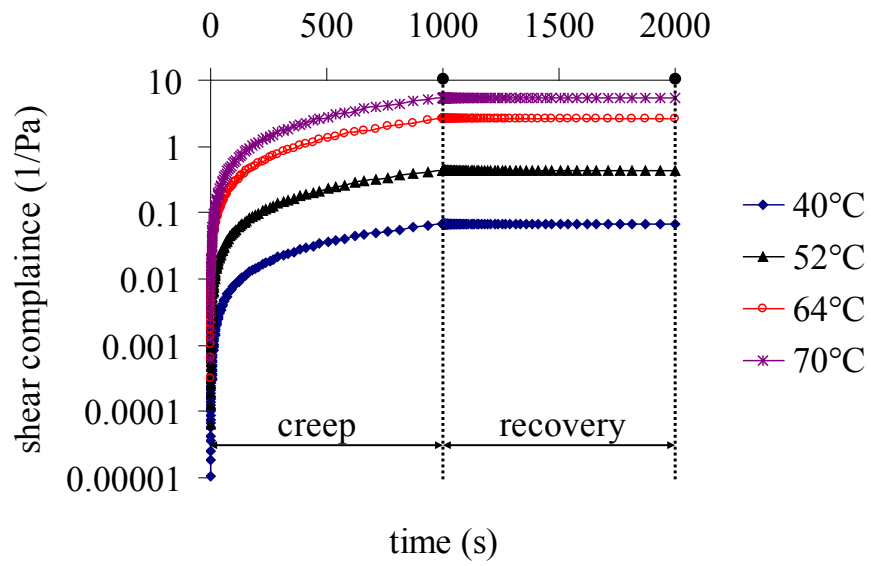
(2) The *AAEs* of asphalt binder are smaller than those of the two mastics, while mastic-100 has the *AAEs* larger than those of mastic-200. The reason is DSR test specimen of mastics is so thin that minerals in specimen have little room to deform, especially for larger-size minerals (mastic-100).

With the fitted Burger's model parameters listed in Table 8.2, three sections of the total strain,  $\varepsilon_v$ ,  $\varepsilon_e$ ,  $\varepsilon_d$ , are calculated, where  $\varepsilon_v$  represents the viscous flow and the sum of  $\varepsilon_e$  and  $\varepsilon_d$  represents the elasticity. The ratio of the viscous flow to the elasticity ( $\kappa$ ) is expressed in Equation 8.20.

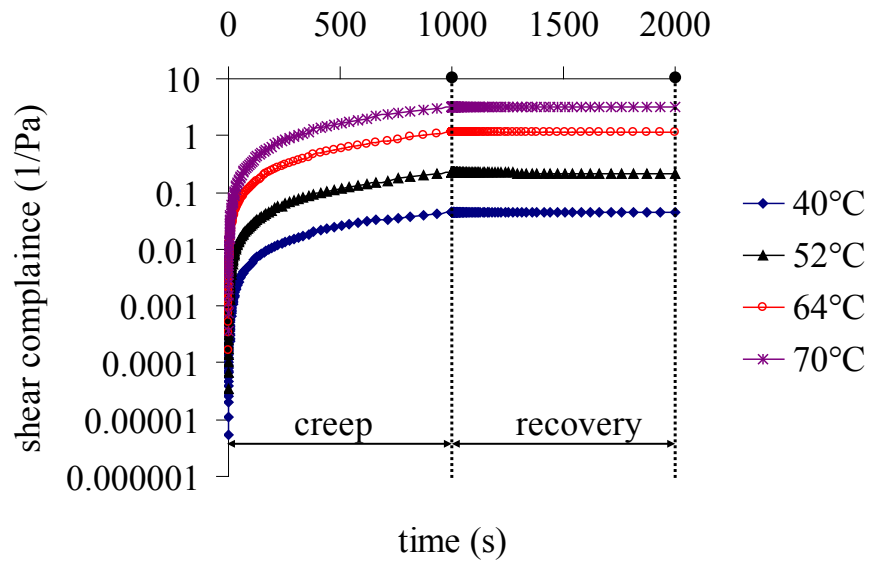
$$\kappa = \frac{\varepsilon_v}{\varepsilon_e + \varepsilon_d} \tag{8.20}$$



(a) Binder PG64-28



(b) Mastic-200



(c) Mastic-100

Figure 8.2 Shear compliances vs. time of the binder and mastics

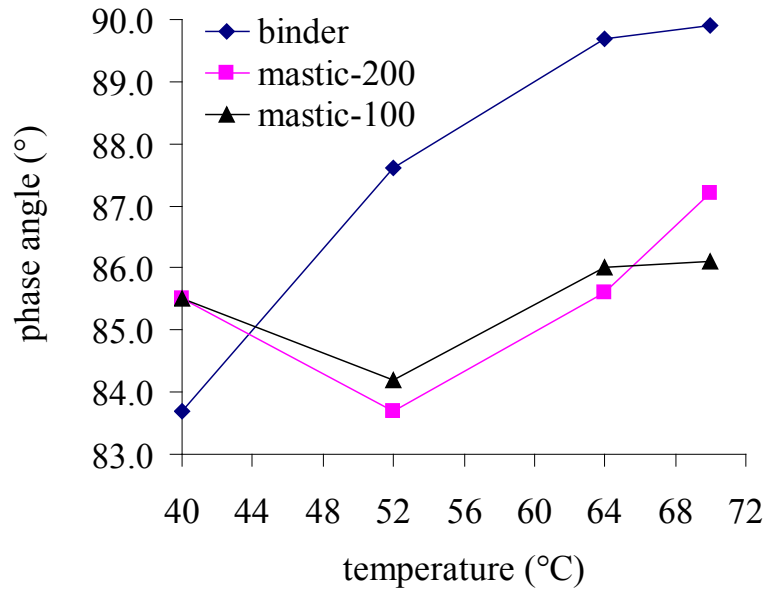


Figure 8.3 Phase angles vs. temperatures of the binder and mastics

**Table 8.1**  
**Average absolute errors (AAEs) for fitting creep-recovery test datum (%)**

Items		Temperature (°C)			
		40	52	64	70
Original Binder	Creep	3.47	2.73	5.22	3.88
	Recovery	0.51	0.42	1.89	0.35
Mastic-100	Creep	9.97	9.68	8.59	3.13
	Recovery	1.92	2.87	1.09	0.58
Mastic-200	Creep	6.46	8.07	3.68	2.15
	Recovery	1.53	1.84	0.39	0.32

**Table 8.2**  
**Burger's model parameters under creep-recovery tests**

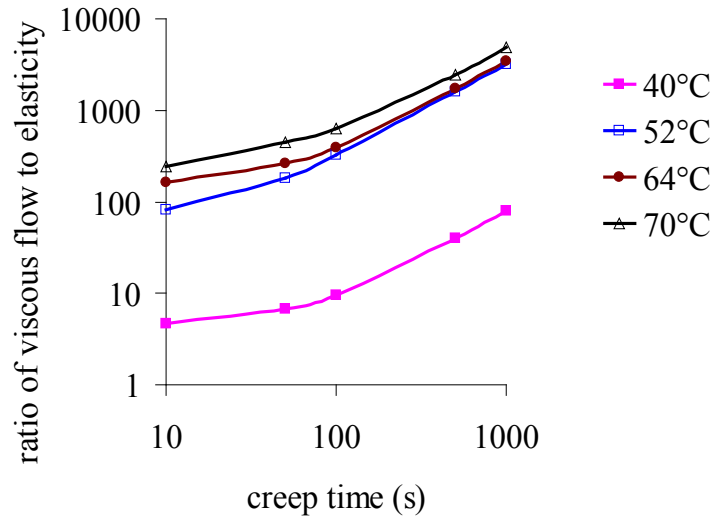
Items		Temperature (°C)			
		40	52	64	70
Binder	EM (Pa)	161,036	35,881	17,477	4,589
	$\eta$ M (Pa.s)	7,228	973	163	76
	EK (Pa)	583	3,448	576	408
	$\eta$ K (Pa.s)	31,779	84,026	27,945	28,354
Mastic-200	EM (Pa)	498,630	97,943	53,393	14,341
	$\eta$ M (Pa.s)	14,512	2,266	382	182
	EK (Pa)	16,155	1,965	1,351	893
	$\eta$ K (Pa.s)	70,312	3,348	574	419
mastic-100	EM (Pa)	17,792,839	215,851	39,524	377,051
	$\eta$ M (Pa.s)	21,259	4,437	879	309
	EK (Pa)	17,406	2,205	1,042	889
	$\eta$ K (Pa.s)	37,396	6,382	748	567

The ratio of the viscous flow to the elasticity at the four temperatures are calculated and plotted in Figure 8.2. The following findings were observed:

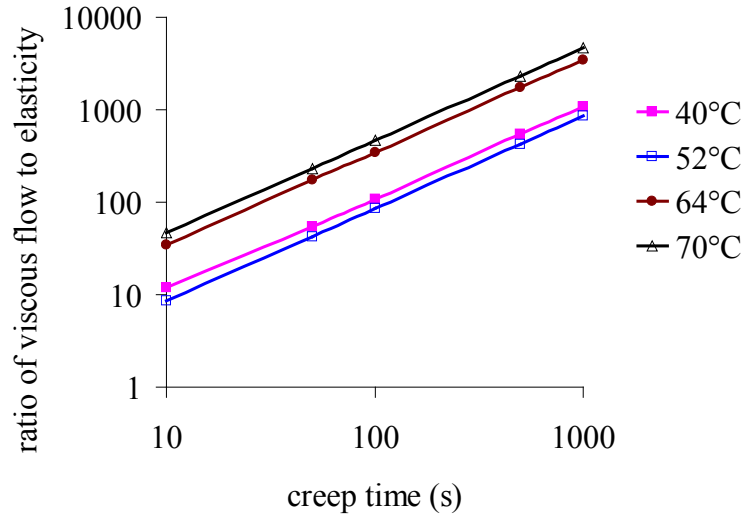
- (1) With creep time increasing, the ratios increase. Therefore, compared with the elastic properties, the viscous flow behaviors increase with creep time increase.
- (2) Compared with the elasticity, the viscous flow is more important for the asphalt binder and mastics, where when creep time increases from 10 to 1000 seconds and the temperatures range from 40°C to 70°C, the ratios,  $\kappa$ , range from 4.7 to 4943 for the asphalt binder, from 8.5 to 4623 for mastic-200 and from 5.1 to 2869 for mastic-200.

Therefore, when the creep time is 10 seconds, the viscous flow can account more than 82.5%, 87.9% and 83.6% of the total deformation (sum of viscous flow and elasticity) for the binder, mastic-200 and mastic 100. When the creep time reach 1000 seconds, the viscous flow accounts more than 99.9% for both the binder and mastics. Therefore, with the creep time increasing, the asphalt binder and mastics are going to flow and its elasticity can be neglected. The same conclusion also can be obtained from the raw creep-recovery data as shown in Figure 8.2, where the recovery strain is very small compared with the strain in creep section.

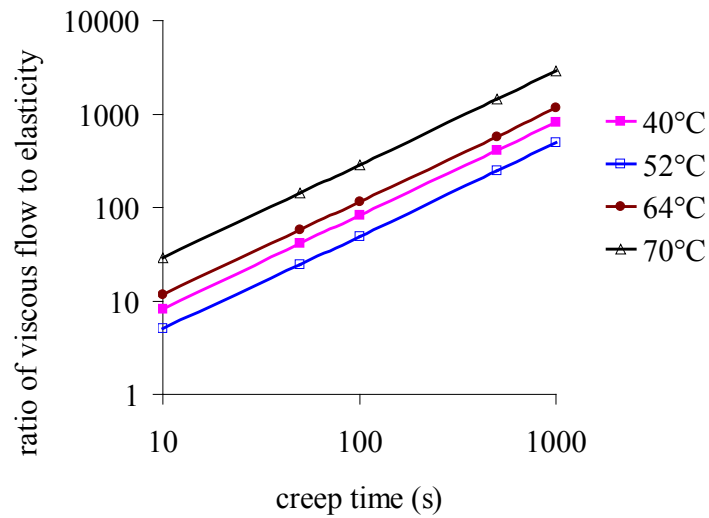
(3) With the temperature increasing, the ratios of the viscous flow to the elasticity increase for the asphalt binder, while the ratios decrease and increase for the two mastic. This finding is consistent with the phase angles as shown in Figure 8.3. The reason is that the tangent of a phase angle is the ratio of storage and loss moduli which approximately represent the viscous flow and elasticity of asphalt materials.



(a) Binder PG64-28



(b) Mastic-200



(c) Mastic-100

**Figure 8.4 Ratio of the viscous flow to the elasticity vs. creep time of binder and mastics**

## 8.6. Summary and Conclusions

Burger's model is simple, but it can be used to represent the properties of asphalt materials. This paper derives the constitutive equations of Burger's model under creep-recovery test condition, and proposes a procedure to fit creep-recovery data with the Burger's model. Creep-recovery data of the asphalt binder PG64-28 and its two mastics (mastic-100 and mastic-200) is processed with the procedure and the ratios of the viscous

flow to the elasticity are calculated with the fitted Burger's model parameters. Then, with the calculated ratios, the viscoelastic behaviors of the asphalt binder and mastics are analyzed. Finally, the following findings were observed:

- 1) Burger's model can be utilized to fit creep-recovery data of both the binder and mastics, where the average errors of the creep section are 3.53%, 5.28% and 8.02% for the three materials, and the values are 0.69%, 1.286% and 1.80% for the recovery section.
- 2) Errors of asphalt binder are smaller than those of the two mastics, while mastic-100 has the errors larger than those of mastic-200.
- 3) Compared with the elastic properties, the viscous flow behaviors increase with creep time increase.
- 4) Compared with the elasticity, the viscous flow is more important for the asphalt binder and mastics. Especially at a larger creep time (more than 1000s), the asphalt binder and mastics are going to flow and its elasticity can be neglected, where the viscous flow accounts more than 99.9%.

## **8.7. Acknowledgements**

This material is based in part upon work supported by the National Science Foundation under Grant CMMI 0701264. Any opinions, findings, and conclusions or recommendations expressed in this material are those of the author's and do not necessarily reflect the views of the National Science Foundation. The authors also acknowledge Dr. Xianguang Hu, former visiting scholar at the Transportation Material Research Center at Michigan Technological University for performing the preliminary lab testing of the materials.



# Chapter 9. Discrete Element Modeling through User-written C++ Codes<sup>8</sup>

## 9.1. Abstract

Compared with an embedded programming language “FISH” within the Particle Flow Code (PFC), the user-written C++ code is an optional feature in the PFC. This optional feature is an advanced application and can improve simulation speeds. In this paper, the user-written C++ codes for two and three dimensional models were developed. The discrete element simulation of asphalt mixtures were conducted with user-written C++ codes along with FISH programs. The simulation results from the two methods were compared. It was found that the user-written C++ program can speed up discrete element simulation, where the speed ratios (C++/FISH) are from 2.34 to 4.95 and the averaged value is 3.74.

## 9.2. Introduction

An asphalt mixture is composed of asphalt, graded aggregates, and air voids. The overall macro-mechanical behaviors of the asphalt mixture are determined by the micromechanics within the cementitious particulate system. Based on the heterogeneous multiphase nature of the asphalt material, it appears that a micromechanical model is more suitable to properly characterize such a material. In recent years, a number of research studies on micromechanical analysis of asphalt mixtures have been conducted using discrete element models. Among the studies, the digital samples of asphalt mixtures were built with the highly idealized model (Adhikari et al. 2008c; Collop et al. 2007; Collop et al. 2006a), randomly created polygon or polyhedron model, and image-based model (Abbas et al. 2007; Buttlar and You 2001; Tian et al. 2007a; Tian et al. 2007b; You and Buttlar 2004; You and Buttlar 2005; 2006). The discrete element mechanical models included the elastic contact model (Buttlar and You 2001; Collop et al. 2007; Dai and You 2007; You and Buttlar 2004; You and Buttlar 2005; 2006), the bilinear cohesive model (Kim and Buttlar 2005), and the time-dependent viscoelastic contact model (Collop et al. 2007); (Abbas et al. 2007; Abbas et al. 2005; Chang and Meegoda 1997b; Liu et al. 2007). With the digital samples and the corresponding micromechanical models, the DE modeling was conducted to predict the stiffness (or modulus) (Dai and You 2007; Liu and You 2008; You and Buttlar 2004; You and Buttlar 2005) and fatigue properties of asphalt mixtures (Carmona et al. 2007). Although many studies on discrete element simulation of asphalt mixtures have been very successful, the following issues have to be considered: 1) on one hand, in order to represent the accurate geometrical characteristics of asphalt mixtures, the discrete elements should be as small as possible, which increases the total number of discrete elements and slows down computation

---

<sup>8</sup>Full text reprinted with permission from ASCE: “Speed up Discrete Element Simulation of Asphalt Mixtures with User-written C++ Codes” by Yu Liu and Zhanping You, 2008, Proceedings of the 2008 Airfield and Highway Pavements Conference, pp. 64-72, Copyright © 2008, ASCE. See Copyright clearance in Appendix A.

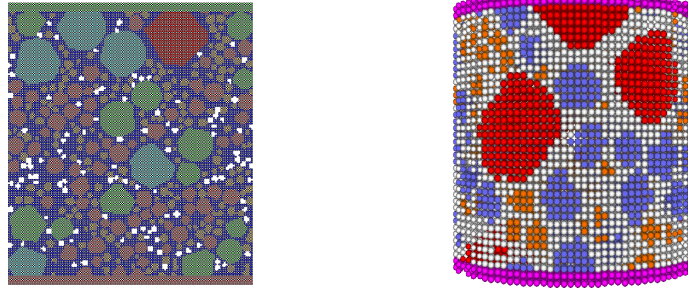
speeds, and; 2) on the other hand, in order to simulate the visco-elastic behaviors of asphalt mixtures, the real physical time has to be considered, which makes discrete element simulation very time-consuming. For example, simulation for a typical dynamic modulus test using elastic models can be conducted within several days, while the viscoelastic model simulation needs several months or more. To solve these two issues, the following approaches can be considered: (1) use advanced computers or supercomputers; (2) a newly developed programming method, and; (3) time-temperature superposition. This paper presents a methodology to speed up viscoelastic simulation of asphalt mixtures by developing programs with user-written C++ code which is an optional feature of Particle Flow Codes in two Dimensions and three Dimensions (PFC2D/3D).

### **9.3. Discrete Element Package: Particle Flow Codes**

Particle Flow Codes in two Dimensions and three Dimensions (PFC2D/3D) was commonly used in the literatures cited above. The internal standard codes in PFC2D/3D are written with the C++ programming language. FISH is a programming language embedded within PFC2D/3D for users to write their own programs. FISH programs are written as a text file and called by PFC2D/3D standard command. Functions and variables in the FISH program can be utilized as the standard commands and variables of PFC2D/3D. Because functions or variables in FISH are not written in the C++ programming language, they have to be interpreted and compiled before they can be executed. Therefore, it is very time-consuming in the situation where many PFC variables and functions must be manipulated and fed back to PFC2D/3D during computation time. In addition to FISH, user-written C++ code is an optional feature in PFC2D/3D, which allows users to write their programs in the C++ language and then create private PFC2D/3D executables. Because user-written C++ functions can have access to many variables or functions in the source program of PFC2D/3D, they can be used instead of FISH program to speed up execution considerably. Before applying the user-written C++ code, however, knowledge on the codes within the PFC2D/3D and C++ programming skills are necessary. Therefore, the user-written code is not commonly used even though it can speed up computation considerably. Simulation of asphalt mixtures are very time-consuming as discussed above: viscoelastic simulations take a few months or more with FISH programs. In order to speed up simulation, this paper develops discrete element simulation programs in the C++ programming language instead of FISH.

### **9.4. User-written C++ Code for Discrete Element Modeling**

With the optional feature (user-written C++ code), private PFC2D and PFC3D executables were created and named with PFC2D\_user 3.10 and PFC3D\_user 3.10. These two executables can be regarded as the user-developed version of PFC2D/3D which are more powerful than PFC2D/3D: they have both user-defined and PFC2D/3D functions. In this research, the following user-developed functions were added in the executables: (1) build digital samples; (2) define material properties, and; (3) apply loading conditions.



(a) 2D Model from PFC2D\_user 3.10 (b) 3D Model from PFC3D\_user 3.10

**Figure 9.1. Digital samples of asphalt mixture with user-written C++ code**

### 9.4.1. Build Digital Samples

The asphalt mixture was regarded as a composite of asphalt mastics (asphalt binder plus fine aggregates), coarse aggregates, and air voids in this study. The microstructures of asphalt mixtures were rebuilt with discrete elements (disks for 2D) or balls for 3D):

- (1) Rectangular or cylinder region filled with discrete elements was employed to represent an asphalt mixture sample.
- (2) Irregular polygons (2D) or polyhedrons (3D) were randomly created according aggregate gradation.
- (3) Discrete elements within the irregular polygons or polyhedrons were bonded together to simulate coarse aggregates, where the interactions between discrete elements were represented with the elastic contact models.
- (4) Discrete elements out of the irregular polygons or polyhedrons were bonded together to simulate the two-phase system: asphalt mastic plus air voids. The interactions between discrete elements were simulated with viscoelastic contact models.
- (5) Asphalt mastic and air voids were separated by removing discrete elements randomly to form air voids.

The detailed procedure to build the digital sample of asphalt mixtures is included in the previous paper. The final digital samples as shown in Figure 9.1 were created with the private PFC2D and PFC3D executables: PFC2D\_user 3.10 and PFC3D\_user 3.10, respectively. Compared with the FISH program, the computation speed was not obviously improved in this case. The reason is that only several functions were manipulated during computation time.

### 9.4.2. Defining Material Properties

Within the private PFC2D and PFC3D executables, four kinds of interactions within the asphalt mixtures were considered: interactions between aggregates, within aggregates, within asphalt mastics and between aggregates and the mastic. The contact-stiffness

model, the contact-bond model, the slip model, and the Burger's contact model (Adhikari et al. 2008b; Itasca Consulting Group 2004a; b) were applied to build the constitutive behaviors at each contact: the contact-stiffness model was employed to represent the interaction between or within aggregates, and the Burger's contact model was employed to characterize the interactions within asphalt mastic or between the mastic and aggregates. The contact-bond model was employed to represent the tensile strength between discrete elements and the slip model was activated when the slip exists at the contact points. Among these four models, Burger's model is an alternative model and the other three models are built-in models (Itasca Consulting Group 2004a; b). Parameters of built-in models are properties of each discrete element which are constants during simulation. An alternative model associates its parameters directly with the contacts. Therefore, when using an alternative model, such as the Burger's contact model herein, one furthermore consideration is the way in which the model is installed at a new contact. Usually, FISHcall is set so that the creation of a new contact will automatically trigger the calling of a FISH function which installs the Burger's contact model dynamically. In this research, instead of FISHcall, a CPPcall is set to trigger the calling of a user-defined C++ function for installing the Burger's contact model at a new created contact. Both FISHcall and CPPcall are methods in FISH and user-written C++ programs to call a specific function when particular events occur. When a new contact was created in this study, a defined function 'catch-HMACmodel' was called to update the contact model properties. If new contacts are created frequently during the simulation of an asphalt mixture, the defined function has to be called frequently. The difference between FISHcall and CPPcall is that FISHcall is applied to call a FISH function which has to be interpreted and compiled before execution and CPPcall is to call a C++ function. Therefore, by using CPPcall, the private PFC2D/3D executables can speed up computation, especially in the simulation where the contacts are frequently updated.

### **9.4.3. Loading Conditions**

In the current version of the private PFC2D/3D executables, three loading conditions are included: the uniaxial creep-recovery, ramp, and dynamic modulus tests. As shown in Figure 9.1, two loading platens were employed to apply loading conditions: on the top platen, the constant or ramp or cyclic load was applied, and the bottom one was fixed in all directions. Within the executables, the loading values and directions of the applied stress are controlled by program and updated at each iterative step by applying CPPcall to trigger the calling of C++ functions just before motion calculation, which can speed up discrete element modeling of asphalt mixtures.

## **9.5. Laboratory Tests and Discrete Element Simulation**

Laboratory tests developed in previous research work (You and Buttlar 2006) were employed. The asphalt mixture specimens were compacted in a Superpave gyratory compactor to a target air void level of 4% by volume, with a nominal maximum aggregate size of 19mm as shown in Table 9.1. The sand mastic had a nominal maximum aggregate size of 1.18-mm, which came from the mixture's aggregate gradation by eliminating all the aggregate particles larger than 1.18mm except the asphalt. The sand mastic had around 14% asphalt content by weight. The uniaxial compression test was

conducted to obtain the dynamic modulus and phase angles for mastics, aggregate (stones), and mixtures. The test procedure and the results of the mastics and mixtures were listed in previous research work (Dai and You 2008; You and Buttlar 2006). The aggregates test procedure and results were listed in a recent paper. Dynamic moduli and phase angles were measured at 0°C with four frequencies, 0.1, 1, 5, and 10Hz, and the results are listed in Table 9.2. Then the laboratory test results were fitted with Burger’s model and the fitted Burger’s model parameters are listed in Table 9.3.

Uniaxial dynamic modulus tests were simulated using the DE model built above and the corresponding loading condition, and the predicted modulus and phase angles were calculated. The predicted results and those from the lab were compared in the previous research, the errors of predicted modulus and phase angles are both less than 10%.

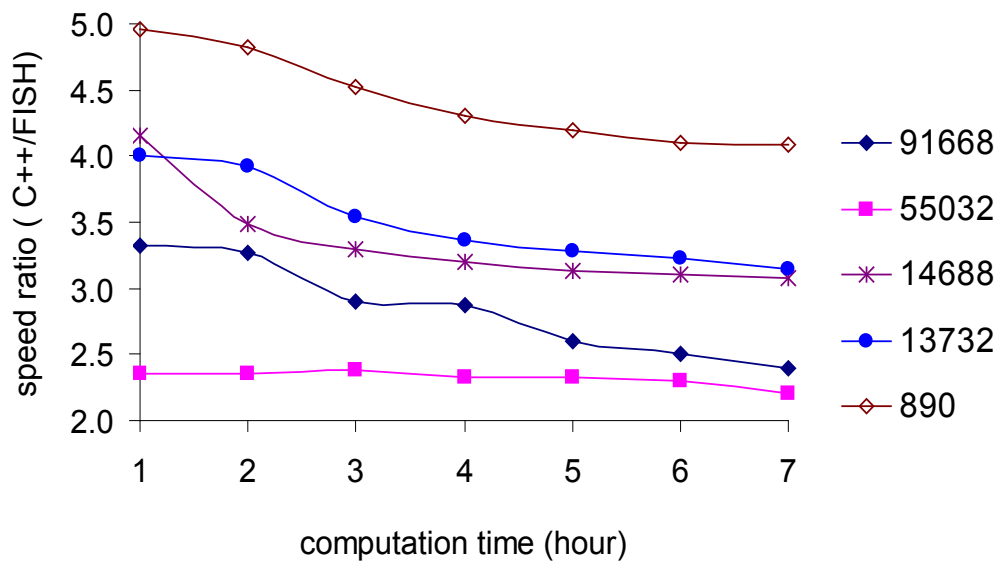


**Figure 9.2 Speed ratio vs. loading time for 5 samples (legend shows the number of discrete elements)**

**Table 9.1  
Gradation of the asphalt mixture (Dai and You 2008; Liu and You 2008; You and Buttlar 2006)**

Coarse Aggregates							
Size/mm	25-19	19-12.5	12.5-9.5	9.5-4.75	4.75-2.36	2.36-1.18	<1.18
Mass (%)	1.1	21.4	9.1	12.2	10	14.5	31.7
Volume (%)	0.94	18.24	7.76	10.40	8.52	12.36	27.02
	Asphalt Content			Air Voids		Mastic Content	-
Mass (%)	4.80			0		36.50	-
Volume (%)	10.77			4		41.78	-

**Table 9.2**  
**Laboratory test results of aggregates, asphalt mastic and mixture**

Loading Frequency (Hz)		0.1	1	5	10
Dynamic Modulus (GPa) (Dai and You 2008; Liu and You 2008; You and Buttlar 2006)	Mastic	4.40	6.19	8.69	9.86
	Mixture	10.62	14.67	17.67	20.08
Phase Angles (°C)	Mastic	38.93	28.80	24.50	28.65
	Mixture	23.24	20.54	18.16	16.87
Young's Modulus (GPa) (Dai and You 2007a)	Aggregates	55.50			

**Table 9.3**  
**Burger's model parameters fitted using lab data**

Burger's model parameters	Frequency (Hz)			
	0.1	1	5	10
$E_1$	901	901	901	901
$\eta_1$	607	607	607	607
$E_2$	3.77	5.64	8.07	8.88
$\eta_2$	3.66	0.41	0.011	0.0067

## 9.6. Timing Test: Comparison between C++ and FISH Codes

This section presents a timing test of C++ program (the private PFC2D/3D executables) by comparing with the similar FISH program. Nine different sizes of asphalt mixture digital samples were built, which consist of discrete elements ranging from 890 to 91,668. Discrete element modeling under cyclic loads was conducted on the nine samples, where both C++ and FISH programs were applied. The speed ratios of the C++ program to the FISH program (C++/FISH) were calculated during computation time which is consumed by a computer to finish a specified simulation task. The speed ratio vs. computation time is plotted in Figure 9.2 where the results of five samples were used and the other four samples have similar results. The average speed ratio of 7 hours' computation time vs. sizes of nine samples is plotted in Figure 9.3. The conclusions were observed as follows:

- 1) Speed ratios (C++/FISH) decrease with computation time increasing. The reason is that discrete elements within the digital samples tend to be stabilized and few contacts need to be updated with computation time increasing. As a result, the FISHcall or CPPcall will not be triggered and the advantage of C++ program is not obvious.
- 2) With the sizes of samples (numbers of discrete elements within the samples) increasing, speed ratios decrease and then increase. The reason for the decreasing of the speed ratio is that the smaller samples are not easy to stabilize and new contacts are created frequently. As a result, smaller samples have larger speed ratios. The

reason for the speed ratios increasing is that the larger samples have more contacts than the smaller samples, where there are more probabilities to create new contacts in a larger sample. As a result, larger speed ratios were observed when the sample sizes were large enough.

- 3) The average speed ratio is 3.74, ranging from 2.34 to 4.95.

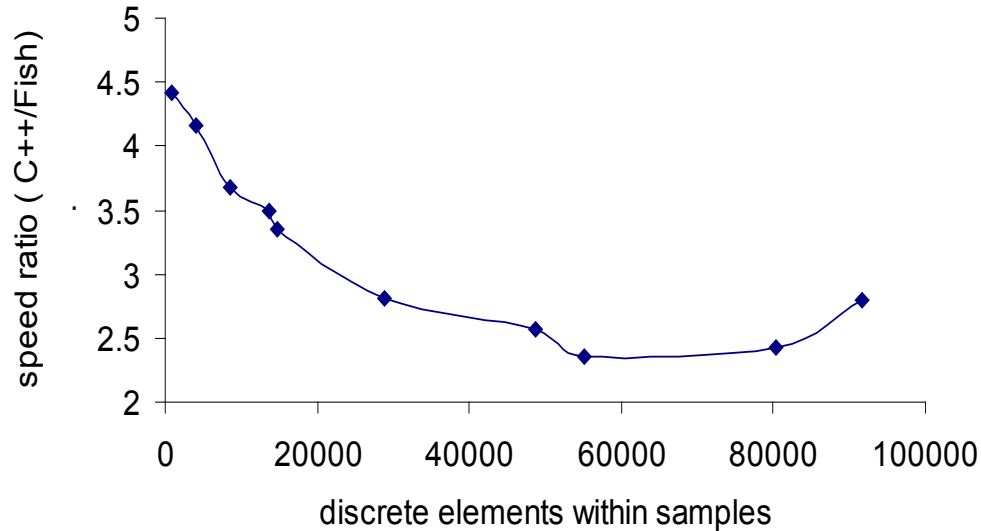


**Figure 9.3 Average speed ratio of 7 hours' loading simulation time vs. sizes of samples**

## 9.7. Summary and Conclusions

In the discrete element models of asphalt mixtures simulation, the computation speed is a key issue which has to be considered especially for viscoelastic simulation of asphalt mixtures. The objective of this research is to speed up computation by developing discrete element simulation program with an optional feature of PFC2D/3D—user-written C++ code. The private PFC2D/3D executables were developed with the user developed programs in C++ programming language. Timing tests were conducted by running C++ and FISH programs and comparing their results. The following conclusions were observed:

- 1) With the user-written C++ codes, discrete element modeling of asphalt mixtures can be sped up, where the speed ratio (C++/FISH) is from 2.34 to 4.95 while the average value is 3.74.
- 2) With the computation time increasing, the discrete elements in the digital samples tend to be stabilized and few contacts need to be updated. As a result, the user-defined C++ functions are not triggered frequently, which causes the speed ratios decrease with computation time increasing.

- 3) The smaller samples are not easy to stabilize and, new contacts can be created frequently, while larger samples with more discrete elements have more probabilities to create new contacts. Therefore, for models with large number of discrete elements, the speed ratios decrease in general, but increase when the number reaches a certain value.

## **9.8. Acknowledgements**

This material is based in part upon work supported by the National Science Foundation under Grant CMMI 0701264. Any opinions, findings, and conclusions or recommendations expressed in this material are those of the author's and do not necessarily reflect the views of the National Science Foundation.



# Chapter 10. Accelerated Discrete Element Modeling of Dynamic Modulus Tests with the Frequency-temperature Superposition Principle<sup>9</sup>

## 10.1. Abstract:

This chapter presents a methodology to reduce the computation time for discrete element (DE) modeling of asphalt based materials based on the frequency-temperature superposition principle. Laboratory tests of dynamic modulus of asphalt sand mastics and asphalt mixtures were conducted at four temperatures  $-5^{\circ}\text{C}$ ,  $4^{\circ}\text{C}$ ,  $13^{\circ}\text{C}$ ,  $21^{\circ}\text{C}$  and four frequencies 1Hz, 5Hz, 10Hz, 25Hz, respectively. The test results of the asphalt sand mastic were fitted with the Burger's model in order to obtain the micro parameters for DE models. In order to reduce the computation time of the DE modeling, the regular loading frequencies were amplified to virtual frequencies. Simultaneously, the Burger's model parameters (micro parameters in DEM) of asphalt sand mastic at the regular frequencies were modified to those at the virtual frequencies based on the frequency-temperature superposition principle. Since the virtual frequencies were much larger than the regular frequencies, the computation time can be significantly reduced by conducting the DE modeling with the virtual frequencies and the corresponding modified Burger's model parameters. The modeling work which took several months or years using the traditional methods only took a few hours or less in this study.

## 10.2. Introduction

Discrete element (DE) method is one of the commonly used numerical methods for analysis and simulation of asphalt materials. Both mechanical and geometrical models have been developed and applied to analyze and predict asphalt mix basic properties with DE method. Microfabric DE model (MDEM) is one of DE mechanical models. It was used to predict the stiffness of an asphalt mixture with the property parameters of its phase constituents (Buttlar and You 2001; You and Buttlar 2004; You and Buttlar 2006). With the MDEM, the time-independent elastic behaviors of asphalt mixtures can be simulated and predicted. Obviously, it is very difficult to simulate the viscoelastic behaviors with MDEM. To address this issue, viscoelastic DE models based on Burger's model were employed recently. With this kind of viscoelastic DE models, the uniaxial and triaxial creep and dynamic tests were simulated in the previous studies (Abbas et al. 2007; Collop et al. 2007; Collop et al. 2006a; Liu et al. 2009; Liu et al. 2007; Liu and You 2008). According to recent studies (Liu et al. 2009; Liu and You 2008), the errors between prediction from DE model and measurement in the laboratory were within 10% for dynamic moduli and phase angles of asphalt mixes. The prediction errors can be

---

<sup>9</sup>Full text reprinted with permission from ASCE: "Accelerated Discrete Element Modeling of Asphalt-based Materials with the Frequency-temperature Superposition Principle" by Yu Liu and Zhanping You, 2011, Journal of Engineering Mechanics, Posted ahead of print in November 2010, Finally published in May 2011, Vol. 137, No. 5, pp. 355-365, Copyright © 2010, ASCE. See Copyright clearance in Appendix A.

decreased by improving the geometric and mechanical models. For example, the generalized Maxwell model, the generalized Kelvin model, or more complicated viscoelastic models may more accurately represent the asphalt material behaviors. In addition to the two commonly used mechanical models, Bilinear fracture DE model was also implemented to address asphalt mix fracture properties (Kim and Buttlar 2005). It was stated that the bilinear fracture DE model had a significant potential to aid the understanding of fracture behavior in asphalt concrete (Kim and Buttlar 2005).

To represent the geometric properties of asphalt concrete, the highly idealized model, the user-defined irregular shape model, and the image-based model were developed and implemented. The highly idealized model comprises single-sized spherical particles which are randomly created (Collop et al. 2007; Collop et al. 2006a). With user-defined irregular shape model, aggregate shapes were simulated with polygons or polyhedrons in two-dimensional (2D) or three-dimensional (3D) models, while their distribution and sizes are controlled by the user-defined statistical parameters (Liu and You 2008; Liu and You 2009; Tian et al. 2007a; Tian et al. 2007b). The image-based model is built by utilizing image analysis techniques which captures the mixture microstructure. Usually, the 2D image-based DE models were utilized in the previous studies (Abbas et al. 2007; Buttlar and You 2001; Dai and You 2007; You and Buttlar 2006). Recently, 3D image-based models were also developed and used in several studies (Adhikari 2008; You et al. 2009; You 2008). Therefore, the accurate aggregate shapes, positions and distribution of asphalt and air voids can be represented with an image-based model. A disadvantage of this model, however, is that it is lab-dependent: a mixture specimen should be prepared and image-processing must be utilized to build the image-based model.

By summarizing studies in the past decades, several mechanical and geometric models have been developed and implemented in modeling the elastic, viscoelastic, and fracture behaviors of asphalt concrete. The following findings were observed from the previous literatures cited above: (1) Both the elastic and viscoelastic models were verified by comparing the numerical results with those from the experimental tests. The errors between the prediction and measurement of asphalt concrete modulus were within 10%. (2) Preliminary study was given to the bilinear fracture model, but the validation of this kind of model is expected. (3) Simulation results from the image-based model and the user-defined irregular shape model were significantly close for prediction of asphalt concrete dynamic modulus and phase angles. (4) Modeling with a viscoelastic DE model was very time-consuming. Sometimes, it needs several weeks or months with a 2D model, and years with a 3D model. Obviously, it is a challenging problem for the implementation of DE modeling of asphalt concrete.

To reduce computation time, the user-written C++ codes were used in the previous study (Liu et al. 2008). Although the computation time were reduced by 2 to 5 times with this technique, it was still difficult to implement a large DE model to simulate asphalt concrete viscoelastic behavior. Therefore, a new technique is expected to address this particular issue.

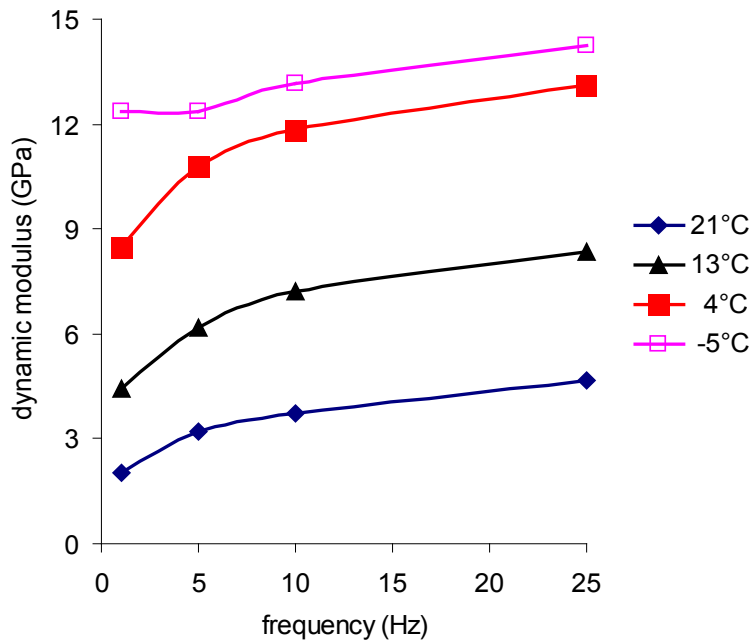
### 10.3. Objectives and Scopes

The main objective of this study is to apply the frequency-temperature superposition to the DE model of asphalt-based materials for reducing the computation time. In order to achieve the objective, the relevant tasks are as follows:

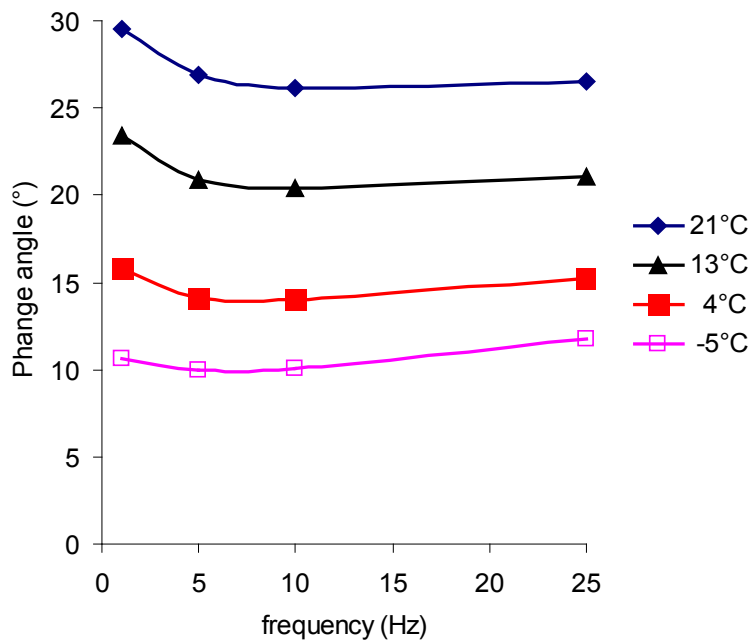
- 1) Conduct experimental tests and determine the Burger's model parameters  
Dynamic modulus tests of an asphalt mixture and its asphalt sand mastic (fines, fine aggregates and asphalt binder) were conducted at four temperatures (i.e., -5 °C, 4°C, 13 °C, 21 °C) and four frequencies (i.e., 1Hz, 5Hz, 10Hz, 25Hz). The Burger's model parameters of the asphalt sand mastic were determined using a newly developed technique.
- 2) Develop a Method to reduce the Computation time for the DE modeling based on frequency-temperature superposition under sinusoidal loads  
A methodology was presented to reduce the computation time for the DE modeling of asphalt based materials using the frequency-temperature superposition principle. The real loading frequency was amplified to a virtual frequency, which allows the Burger's model parameters of asphalt sand mastic at regular frequencies to be modified. The amplified frequency and the modified Burger's model parameters were used in the DE modeling to reduce the computation time.
- 3) Conduct the 2D DE modeling of asphalt sand mastic
- 4) Predict dynamic behaviors of asphalt concrete with the 2D & (3D DE models
- 5) Evaluate the computation time for the viscoelastic DE modeling.

**Table 10.1**  
**Aggregate gradation for asphalt mixture**

Size	Passing (%)	Retained (%)
19	100	
12.5	98.7	1.3
9.5	86.5	12.2
4.75	71.8	14.7
2.36	51.4	20.4
1.18	36.1	15.3
0.6	25.5	10.6
0.3	14.7	10.8
0.15	7.7	7
0.075	5.4	2.3
PAN	0	5.4



(a) Dynamic moduli



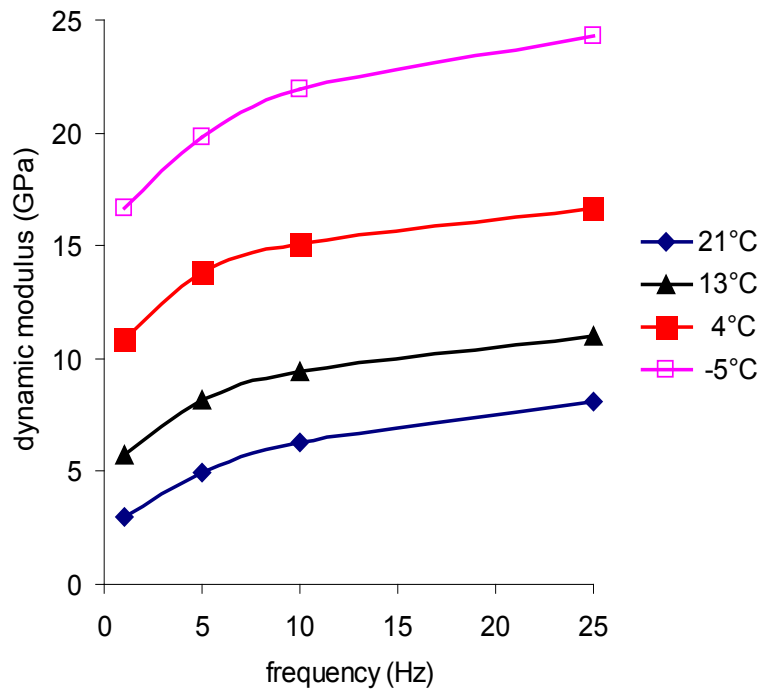
(b) Phase angles

Figure 10.1 Dynamic moduli and phase angles from measurement of asphalt mastic

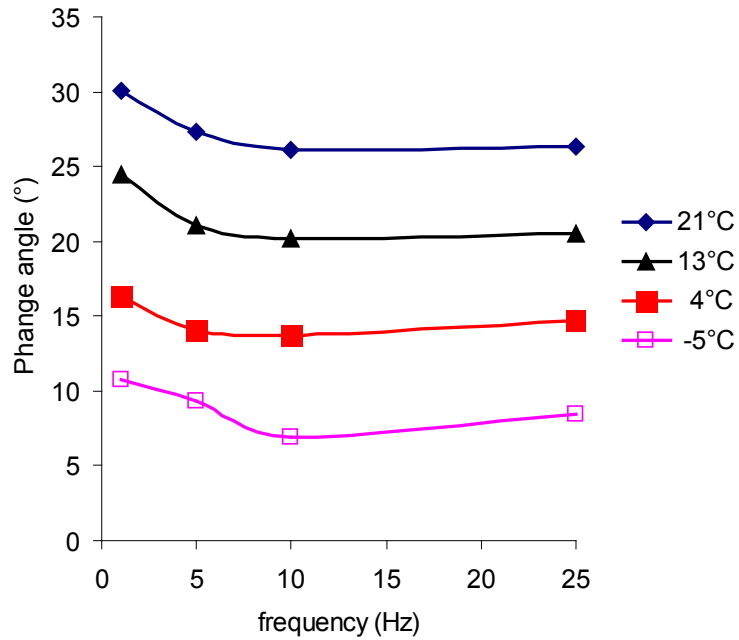
## 10.4. Experimental Tests and Burger's Model Parameters

### 10.4.1. Dynamic Modulus Test

In order to provide the input parameters and validate the DE modeling results, dynamic modulus tests of asphalt based materials were conducted. The asphalt mixture used in this study was from a Michigan highway field project, with a nominal maximum aggregate size of 19 mm and an asphalt content of 5.59% by mass (or 12.54% by volume). The aggregate gradation is listed in Table 10.1. Mineral fillers and fine aggregates in asphalt sand mastic came from the mixture's aggregate gradation by extracting all the coarse aggregates (bigger than 2.36 mm). Both asphalt mixture and mastic specimens were compacted in the Superpave gyratory compactor to their targeted air voids: 3.5% for mastic and 4.0% for mixture (both by volume). Uniaxial dynamic modulus tests of the asphalt mastic and mixture were conducted under haversine loading conditions. The dynamic moduli and phase angles were measured at four temperatures (i.e., -5 °C, 4°C, 13 °C, 21 °C) and four frequencies (1Hz, 5Hz, 10Hz, 25Hz) as plotted in Figures 1~2.



(a) Dynamic moduli



(b) Phase angles

**Figure 10.2 Dynamic moduli and phase angles from measurement of asphalt mixture**

### 10.4.2. Burger's Model Parameters under Sinusoidal Loads

According to the National Cooperative Highway Research Program (NCHRP) Report 465(Witczak et al. 2002), the stress-to-strain relationship under a continuous sinusoidal loading for linear viscoelastic materials is defined by a complex number called the complex modulus ( $E^*$ ). The dynamic modulus,  $|E^*|$ , is defined as the absolute value of  $E^*$ . Mathematically,  $|E^*|$  can be expressed with the maximum (i.e., peak) dynamic stress ( $\sigma_0$ ) and the peak recoverable strain ( $\epsilon_0$ ):

$$|E^*| = \frac{\sigma_0}{\epsilon_0} \quad 10.1$$

The phase angle,  $\phi$ , is the angle by which the recoverable strain ( $\epsilon_0$ ) lags behind the dynamic stress ( $\sigma_0$ ). It is an indicator of the viscous properties of the material being evaluated. The relationship between ( $E^*$ ),  $|E^*|$ , and  $\phi$  can be expressed as

$$E^* = |E^*| \cos(\phi) + |E^*| \sin(\phi) \quad 10.2$$

Although a dynamic modulus test in the laboratory is conducted under a combined loading of sinusoidal, creep, and ramp loads, only the sinusoidal stress and its

corresponding strain are used to calculate the dynamic modulus and phase angle according to the NCHRP Report 465(Witczak et al. 2002):

1) The stress in a real dynamic modulus test is:

$$\sigma(t) = a \cos(\omega t) + b \sin(\omega t) + \sigma_l(t) = \sqrt{a^2 + b^2} \sin(\omega t - \delta_\sigma) + \sigma_l(t) \quad 10.3$$

Where a, b are constant,  $\sigma_l(t)$  is non-cyclic loads including creep and ramp loads.

2) The strain response in a dynamic modulus test is:

$$\varepsilon(t) = A \cos(\omega t) + B \sin(\omega t) + \varepsilon_l(t) = \sqrt{A^2 + B^2} \sin(\omega t + \delta_\varepsilon) + \varepsilon_l(t) \quad 10.4$$

Where A, B are constants and  $\varepsilon_l(t)$  is a non-cyclic strain response.

3) Dynamic modulus and phase angles are calculated as:

$$|E^*| = \frac{\sqrt{a^2 + b^2}}{\sqrt{A^2 + B^2}} \quad 10.5$$

$$\phi = \delta_\varepsilon - \delta_\sigma \quad 10.6$$

Theoretically, any two-parameter linear viscoelastic mechanical model, such as Maxwell model, Kelvin model, is sufficient to fit the dynamic modulus,  $|E^*|$ , and phase angle,  $\phi$ , at a specific frequency. It can be explained as follows: the measured  $|E^*|$  and  $\phi$  in equations 10.5 and 10.6 can be formulated with two constants of Maxwell or Kelvin model. As a result, two equations are obtained where only the two constants are unknown. Then, the two constants can be easily solved with the two equations. The major limitation to using a two-parameter model, however, is that it is difficult to represent material behaviors under other loading conditions, such as creep and ramp loads in a real dynamic modulus test of asphalt based materials. For example, the Kelvin model is more suitable to represent creep and retardance behaviors, while Maxwell model, however, is suitable for stress relaxation. Therefore, although both Kelvin and Maxwell models are equivalent in simulating dynamic modulus and phase angle, they are definitely different in fitting creep, retardance, or relaxation. In order to represent material behaviors under more complex loading conditions, combinations of the two simple mechanical elements (Maxwell or Kelvin) are usually considered, such as the Burger's model, Generalized Maxwell model and Generalized Kelvin model. The Burger's model is the simplest combination whereby a Maxwell element and a Kelvin element are connected in series as shown in Figure 10.3.

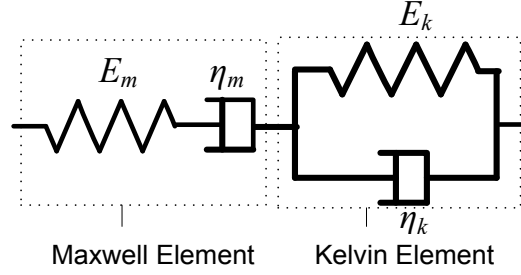


**Figure 10.3 Burger's model**

In this study, the Burger's model is selected to simulate asphalt-based materials. To fit a real dynamic modulus test with the Burger's model and determine model parameters, two steps are necessary:

1) Analytical solution for fitting dynamic behaviors with the Burger's model

In this step, only the dynamic load is considered, and the measured  $|E^*|$  and  $\phi$  can be related to the Burger's model parameters in Equation 10.7 and 10.8 according to the viscoelastic theory (Malkin and Isayew 2006). Obviously, with these two equations, the four Burger's model parameters cannot be determined. It was noted, however, that Equation (7) and (8) can be written in the form of Equations 10.9 and 10.10. Therefore, the four Burger's model parameters may be demonstrated in the M-K circles shown in Figure 10.4.

$$\frac{\cos(\phi)}{|E^*|} = \frac{1}{E_m} + \frac{E_k}{E_k^2 + \omega^2 \eta_k^2} \quad 10.7$$

$$\frac{\sin(\phi)}{|E^*|} = \frac{1}{\omega \eta_m} + \frac{\omega \eta_k}{E_k^2 + \omega^2 \eta_k^2} \quad 10.8$$

$$\left( \frac{1}{E_m} - \frac{\cos(\phi)}{|E^*|} \right)^2 + \left( \frac{1}{\omega \eta_m} - \frac{\sin(\phi)}{|E^*|} \right)^2 = \frac{1}{R_k^2} \quad 10.9$$

$$E_k^2 + (\omega \eta_k)^2 = R_k^2 \quad 10.10$$

Supposing  $R_k$  and  $\phi_k$  are given, then, the four Burger's model parameters can be determined by using the M-K circles.

$$E_k = R_k \cos(\phi_k) \quad 10.11$$

$$\eta_k = \frac{R_k \sin(\phi_k)}{\omega} \quad 10.12$$



$$E_m = \frac{|E^*| R_k}{R_k \cos(\phi) - |E^*| \cos(\phi_k)} \quad 10.13$$

$$\eta_m = \frac{|E^*| R_k}{\omega [\sin(\phi) R_k - |E^*| \sin(\phi_k)]} \quad 10.14$$

Mathematically,  $\phi_k$  can be any angle ranging from 0 to 90°. Considering the physical meaning of  $\phi_k$ , it is a phase angle from the Kelvin element that is a part of the Burger's model. Thus,  $\phi_k$  is one portion of  $\phi$ :  $0 \leq \phi_k \leq \phi$ . Because  $E_m$  and  $\eta_m$  are positive from Equations 10.13 and 10.14,  $R_k \geq |E^*|$ .

By summarizing, to analytically fit the material dynamic behaviors with the Burger's model, three steps are needed:

- 1) Selection of  $\phi_k$  with  $0 \leq \phi_k \leq \phi$ .
- 2) Selection of  $R_k$  with  $R_k \geq |E^*|$
- 3) Substitution of the  $\phi_k$  and  $R_k$ ; then, the four Burger's model parameters can be determined analytically with Equations 10.11 and 10.14. If any of the four Burger's model parameters are infinite, re-selection of  $R_k$  is done.

2) Fit the dynamic modulus testing data with the Burger's model

As demonstrated in Step 1), there are many solutions to fit the dynamic behaviors by setting different values of  $\phi_k$  and  $R_k$ , and all of them are equivalent under pure sinusoidal loading conditions. The real dynamic modulus test, however, involves not only the sinusoidal stress, but also constant and ramp stresses. Different values of  $\phi_k$  and  $R_k$  may reflect different loading conditions under constant and ramp stresses. The optimum values of  $\phi_k$  and  $R_k$  were achieved in this study through comparing the predicted and measured strains. When the minimum of the sum of square errors (SSE) (Nemat-Nasser and Okada) was observed, the corresponding values of  $\phi_k$  and  $R_k$  were considered as the optimum. The predicted strains were achieved with the Burger's model parameters using an equation provided in the previous study (Liu et al. 2009). Figure 10.5 shows the procedure for determination of the Burger's model parameters by fitting dynamic modulus testing data.

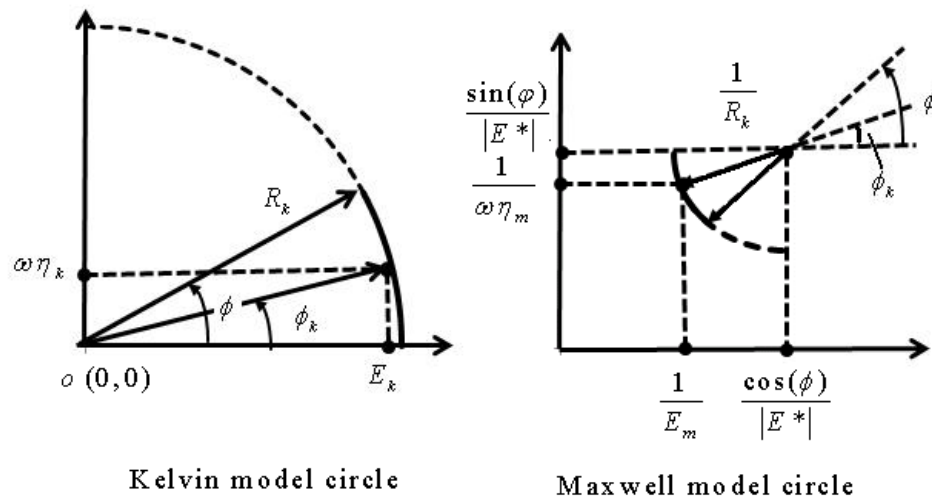


**Figure 10.4 M-K circle to determine Burger's model parameters**

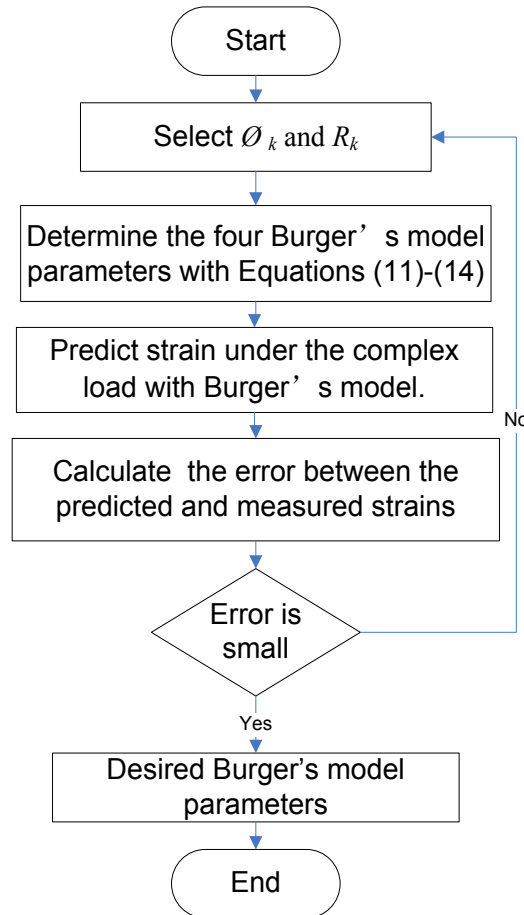


**Figure 10.5 Procedure to determine Burger's model parameters under a real dynamic modulus test loading condition**

It should be noted herein that a DE model simulates material behaviors using microscopic parameters. The constitutive model is represented by contact models at contacts of discrete elements. Different contact models represent different interactions in the microstructure of the target material (Liu et al. 2009). It is easy to understand that a DE model with one-dimensional (1D) inputs is able to address a 2D or 3D problem. Therefore, the 1D Burger's model in the Figure 10.3 could simulate the 3D viscoelastic problems as demonstrated in the subsequent sections. Readers may find more details in the references (Itasca Consulting Group 2008b; Liu et al. 2009).

## 10.5. Methodology: Application of Frequency-Temperature Superposition

The frequency-temperature superposition principle states that the behaviors of a time-dependent material are dependent on temperatures and loading frequencies. The effects of temperatures and frequencies can be equivalently and mathematically expressed as

$$E(\omega_1, T_1) = E(\omega_2, T_2) \quad 10.15$$

In Equation 10.15,  $E$  represents a time-dependent property, such as dynamic modulus and phase angle;  $\omega_1$  and  $T_1$  represent the angular frequency and the loading temperature in the laboratory test, while  $\omega_2$  and  $T_2$  represent the reference temperature and the reduced frequency at the reference temperature.

Traditionally, the frequency-temperature superposition principle was used for building master curves of dynamic modulus for analyzing or predicting asphalt mix properties (Daniel and Lachance 2005; Gahvari 1997; Kim et al. 2006; Kim et al. 2004). To build a master curve, a reference temperature was selected and the shifting factors of the other temperatures were calculated to move the regular testing data into a smooth master curve. Several techniques have been developed to calculate the shifting factors as demonstrated in the references (Gurjar et al. 1996; Pellinen et al. 2004).

Instead of calculating shift factors and constructing master curves, this study herein presents a new way to use the principle. Followed is the methodology which consists of three steps as demonstrated below:

(1) Amplify the regular loading frequency by multiplying it with a coefficient,  $\xi$ .

The frequency in the laboratory test,  $\omega_1$ , was amplified up to  $\omega_2$  by multiplying it with a coefficient,  $\xi$ :

$$\omega_2 = \xi\omega_1 \quad 10.16$$

Instead of using  $\omega_1$ ,  $\omega_2$  would be used in the DE modeling, which allows the computation time to be significantly saved. For example, when  $\xi = 1000$ , the DE modeling which usually took 1000 days could be finished in a single day.

- (2) Modify the Burger's model parameters based on the frequency-temperature superposition principle.

Traditionally, temperatures have to be directly involved in calculating the shifting factors (Gurjar et al. 1996; Pellinen et al. 2004) for building a master curve. In the newly developed approach herein, however, temperatures  $T_1$  and  $T_2$  were not directly involved in the calculation of the amplified coefficient,  $\xi$  which has the similar meaning of the shifting factor. Instead, the temperatures were reflected in modifying the Burger's model parameters based on the frequency-temperature superposition as demonstrated below:

Since the spring elements in the Burger's model are independent on temperatures and loading frequencies. Therefore, the viscosities of the two dashpots in the Burger's model represent effects of temperatures or loading frequencies. For instance,  $\eta_m(T_1)$  and  $\eta_k(T_1)$  represent the time-dependent properties at  $T_1$ , while  $\eta_m(T_2)$  and  $\eta_k(T_2)$  represent the time-dependent properties at  $T_2$ . Therefore, the frequency-temperature superposition principle in Equation 10.15 can be equivalently expressed in a new formulation below:

$$E(\omega_1, \eta_m(T_1), \eta_k(T_1)) = E(\omega_2, \eta_m(T_2), \eta_k(T_2)) \quad 10.17$$

By applying the principle in Equation 10.17 to Equations 10.7 and 10.8, it is easily achieved that:

$$\eta_M(T_2) = \frac{\omega_1}{\omega_2} \eta_M(T_1) = \frac{\eta_M(T_1)}{\xi} \quad 10.18$$

$$\eta_k(T_2) = \frac{\omega_1}{\omega_2} \eta_k(T_1) = \frac{\eta_k(T_1)}{\xi} \quad 10.19$$

- (3) Conduct the DE modeling with the amplified frequency and the modified Burger's model parameters.

As demonstrated in the two steps above, a time-dependent material property can be equivalently expressed with the Burger's model parameters at the regular temperature using the regular frequency and with the modified Burger's model parameters using the amplified frequency. The relationship between the two sets of the Burger's model parameters are expressed in Equations 10.18 and 10.19. It was the amplified frequency and the modified Burger's model parameters that this study has utilized to reduce the computation time for the DE modeling.

## 10.6. Simulation of Asphalt Mastic Using the 2D DE Model

In geometry, asphalt mastic was regarded as the homogeneous solid and the microstructure of fine aggregates and fines was ignored. Single-size discrete elements (disks with the radius of 0.2mm) were created within a rectangular region (30mm×45mm) and bonded together. The Burger's model was applied to simulate the

viscoelastic behaviors of an asphalt mastic specimen. The uniaxial dynamic modulus tests were simulated under the real loading condition as mentioned in the previous section. The real loading frequencies used in the laboratory were 1Hz, 5Hz, 10Hz and 25Hz. The Burger's model parameters were determined by fitting the original dynamic modulus test results of asphalt mastic and the fitted results are listed in Table 10.2. It should be noted that the spring parameters  $E_m$ ,  $E_k$  are usually considered as constants at different frequencies for a specific temperature, but they were slightly different in this study due to non-cyclic loads ( constant and ramp stresses).

In order to reduce the computation time, the real loading frequencies were amplified with  $\xi=50, 100, 500, 1000, 2500, 5000, 25000$ . The determined Burger's model parameters in Table 10.2 were modified using the Equations 10.18 and 10.19. Then, the DE simulation was conducted with the amplified frequencies and the modified model parameters. The average stress and strain were outputted during the simulation as shown in Figure 10.6. In Excel sheets, the output stress and strain were fitted in Equations 10.3 and 10.4, while the dynamic modulus and phase angle were calculated with Equation 10.5 and 10.6. The dynamic modulus from the DE prediction and the measurement are compared well as seen in Figure 10.7a, and the phase angles from the DE prediction and the measurement are compared well as seen in Figure 10.7b. In order to evaluate the quality of the dynamic modulus and phase angles, the relative error between the DE prediction and the measurement of dynamic modulus and phase angles were calculated with Equation as follows,

$$Error = \frac{|E^*|_{Lab} - |E^*|_{DEM}}{|E^*|_{Lab}} \quad 10.20$$

The calculated errors vs. the amplified frequencies are plotted in Figure 10.7c and 7d. The following findings were observed that:

- 1) When the amplified frequencies are less than 25KHz, (i.e.,  $\xi \leq 1,000$  for 25Hz,  $\xi \leq 2,500$  for 10Hz,  $\xi \leq 5,000$  for 5Hz, and  $\xi \leq 25,000$  for 1Hz), both the calculated dynamic moduli and phase angles of the four temperatures and frequencies are very close to those measured in the laboratory. The errors are within 8%, and most of them range from 0.05% to 4%.
- 2) When the amplified frequencies are larger than 25 KHz, the errors for both dynamic moduli and phase angles are relatively high, with some being larger than 15%. The larger errors were due to the following reasons: (a) under the lower loading frequencies or quasistatic condition, the mass inertia of viscoelastic material can be ignored. When the applied frequencies are so high that the mass inertia has to be considered, the DE modeling errors may increase. (b) As mentioned above, in addition to the dynamic load, non-cyclic loads, such as constant and ramp loads were also involved. Only the dynamic load, however, was considered when the frequencies were amplified and the Burger's model parameters were modified.

**Table 10.2**  
**The fitted Burger's model parameters of asphalt mastic**

Temperature	Frequency	$E_m$	$\eta_m$	$E_k$	$\eta_k$
(°C)	(Hz)	(GPa)	(GPa.s)	(GPa)	(GPa.s)
21	25	37.59	3.81	4.58	0.02
	10	25.51	3.60	3.77	0.03
	5	16.27	3.06	3.40	0.07
	1	6.84	5.65	2.24	0.27
13	25	9.69	14.90	4.67	0.14
	10	8.89	11.63	6.87	0.30
	5	6.77	55.70	1.11	0.55
	1	5.02	54.82	1.01	1.82
4	25	24.75	55.83	34.91	0.28
	10	18.26	112.03	12.95	1.08
	5	16.87	81.93	14.66	1.95
	1	13.10	323.84	5.97	7.14
-5	25	33.11	141.00	42.57	0.15
	10	21.47	173.02	48.77	1.25
	5	18.65	327.73	22.26	3.12
	1	18.67	1007.35	18.94	14.92

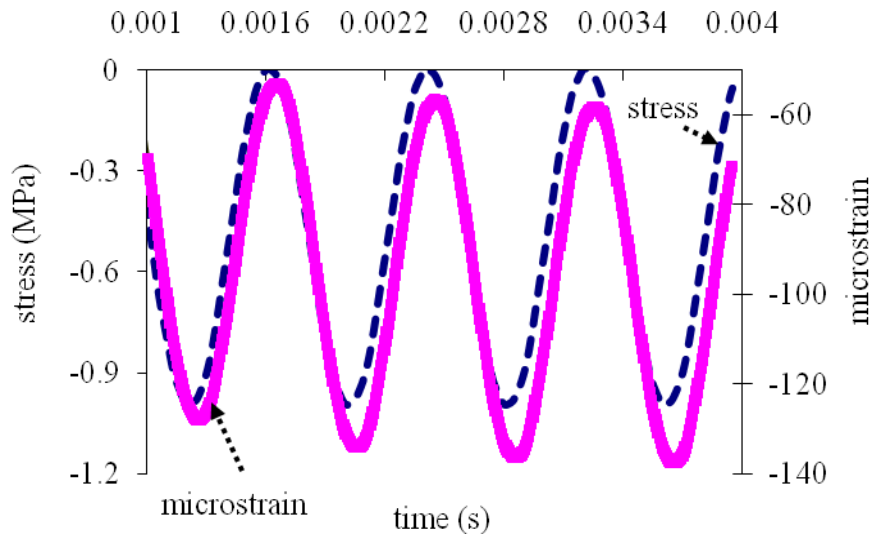
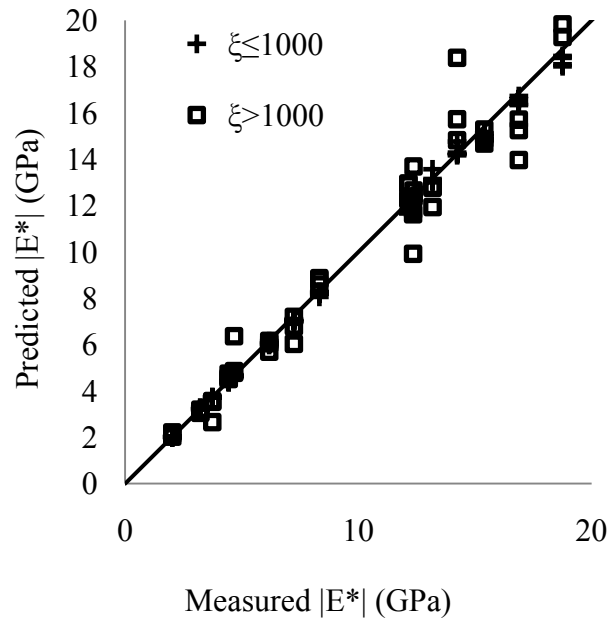
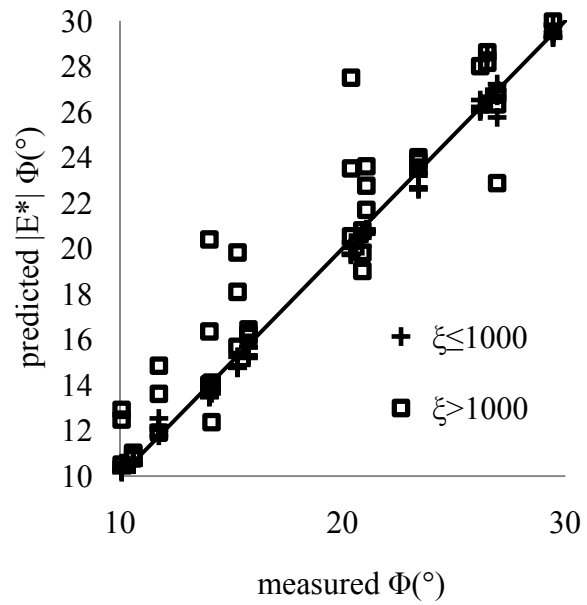


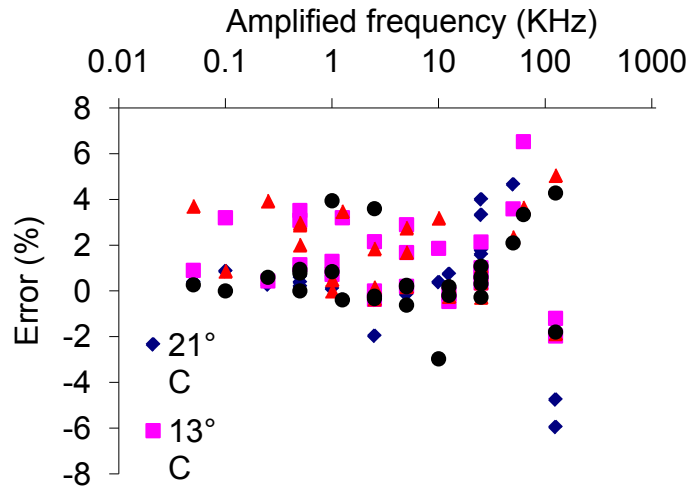
**Figure 10.6 Stress & strain vs. time curve from a simulation output data**



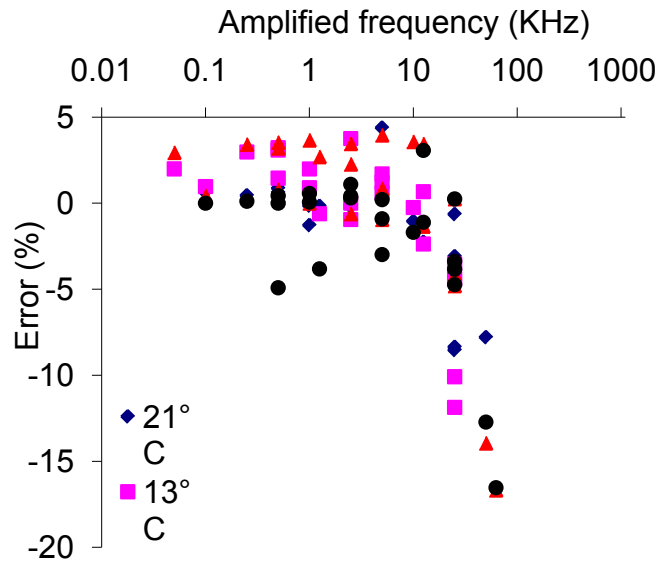
(a) Prediction vs. measurement for dynamic modulus



(b) Prediction vs. measurement for phase angle



(c) Errors for Dynamic modulus vs. amplified frequency



(d) Errors for Phase angle vs. amplified frequency

**Figure 10.7 Comparison between prediction and measurement of dynamic moduli and phase angles**

### 10.7. Predict Dynamic Behaviors of Asphalt Mixture

As discussed in the literatures cited in the introduction section, many researchers have focused their studies on DE modeling of asphalt mixtures. Due to the limitation of the



computation time, only 2D models were used and calibrated with the limited laboratory tests. As shown in the previous section, the frequency-temperature superposition is valid for the DE modeling of asphalt mastic when the amplified frequencies are less than 25,000Hz for asphalt mastic. Therefore, with the frequency-temperature superposition, the DE modeling of asphalt mastic can be expedited by 1,000 (for 25Hz) to 25,000 (for 1Hz) times, meaning one hour with the newly developed technique can be equivalent to 2.85 years with the traditional methods for the DE modeling at a lower frequency (1Hz). Obviously, the new technique is a good way to overcome the computation time limitation of the DE viscoelastic modeling. This section presents 2D and 3D DE viscoelastic modeling of asphalt mixture with the frequency-temperature superposition and compares the results from 2D and 3D models.

## 10.8. Geometric and Mechanical Models

In geometry, the microstructure of a cylinder asphalt mix specimen was rebuilt with randomly created model presented in the previous research studies (Liu and You 2008; Liu and You 2009). According to these studies, single-size discrete elements (0.5mm for 3D model and 0.2mm for 2D model) are created and bonded to simulate the asphalt mastic within the specimen. Aggregates are simulated with the randomly created irregular-shape clusters which consist of many discrete elements bonded together. The inter-spaces between aggregates are filled with asphalt mastic and air voids. The distributions of the phase constituents (asphalt mastic, aggregates and air voids) in a mixture digital sample are considered by setting different random speeds. By default, the random speed equals 10,000. Different values can be specified, but the specified value is recommended to be of the same magnitude as the default value (Itasca Consulting Group 2008a; b). Figure 10.8 shows one example of the asphalt mixture microstructure model with the default random seed value.

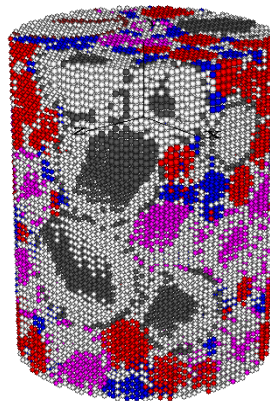


**Figure 10.8 Example of asphalt mixture microstructure (the white elements represent the asphalt sand mastic while the others represent coarse aggregates of different sizes)**

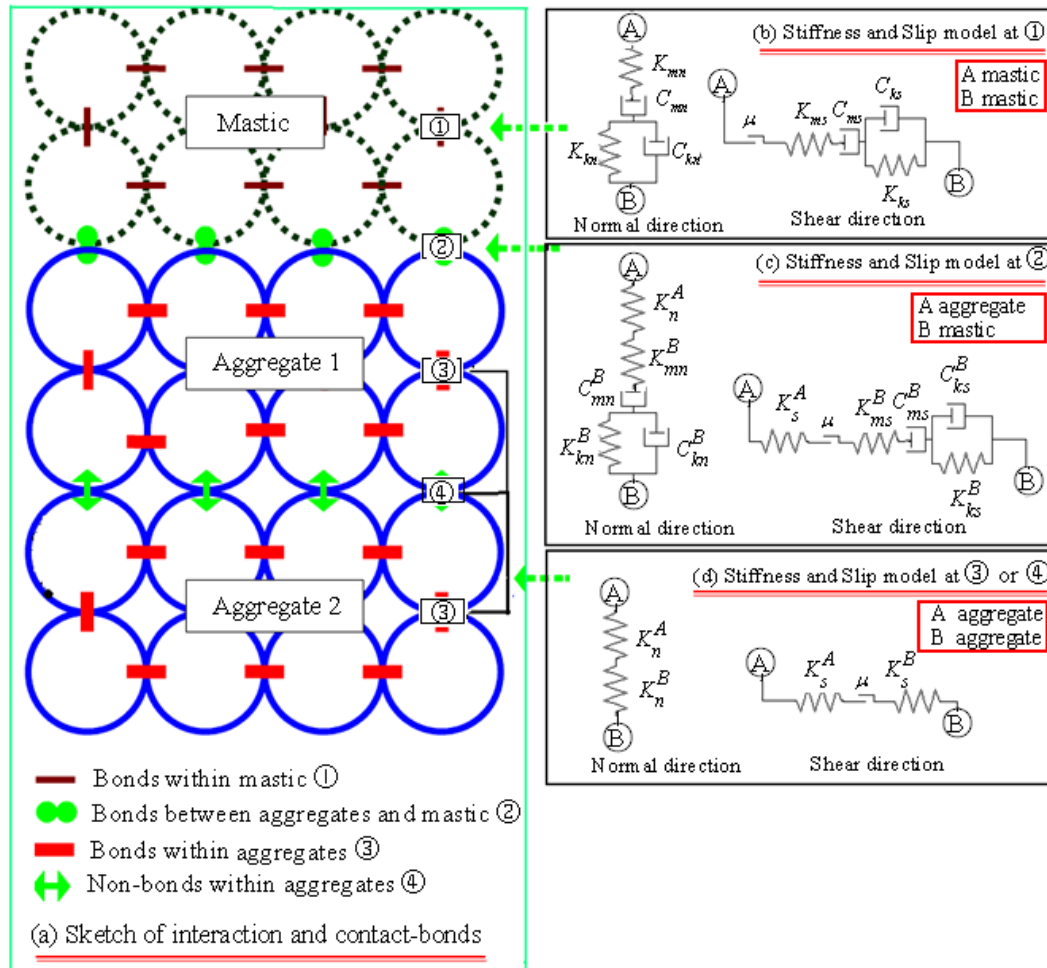


**Figure 10.9 Configuration of the DE viscoelastic model (Liu et al. 2009)**

The mechanical model was provided in the previous study (Liu et al. 2009). Figure 10.9 shows the configuration of the viscoelastic DE model. The viscoelastic behaviors of asphalt mastic are simulated with the Burger's model shown in the Figure 10.3, while the elastic behaviors between aggregates and within aggregates are simulated with the linear elastic model. Burger's model parameters are listed in Table 10.2, while the linear elastic parameters of aggregates were provided in the previous study (Liu et al. 2009). To accelerate the DE modeling, the amplified coefficients are 250, 500 1000 and 5000 for the real frequencies of 25Hz, 10Hz, 5Hz, and 1Hz. Therefore, the amplified frequencies are 6.25KHz for the real frequency of 25Hz, 5KHz for the other real frequencies.

### 10.8.1. DE Modeling with Different Random Seeds

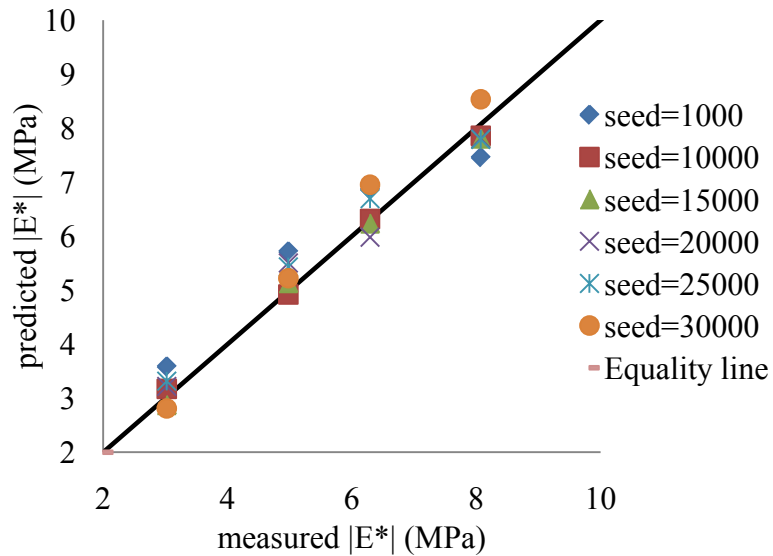
In order to investigate the effects of the random speeds on the DE modeling results of asphalt mixtures, six replicates of 3D asphalt mixture models were built with 6 different random seeds which were 1,000, 10,000, 15,000, 20,000, 25,000, 30,000, respectively. The Burger's model parameters at a temperature of 21°C were utilized. The outputs and calculation of dynamic modulus and phase angles are similar with those of asphalt mastic

provided in the previous section. The prediction errors of dynamic moduli and phase angles vs. the random seeds of the six replicates are plotted in Figure 10.10. The following findings were observed:

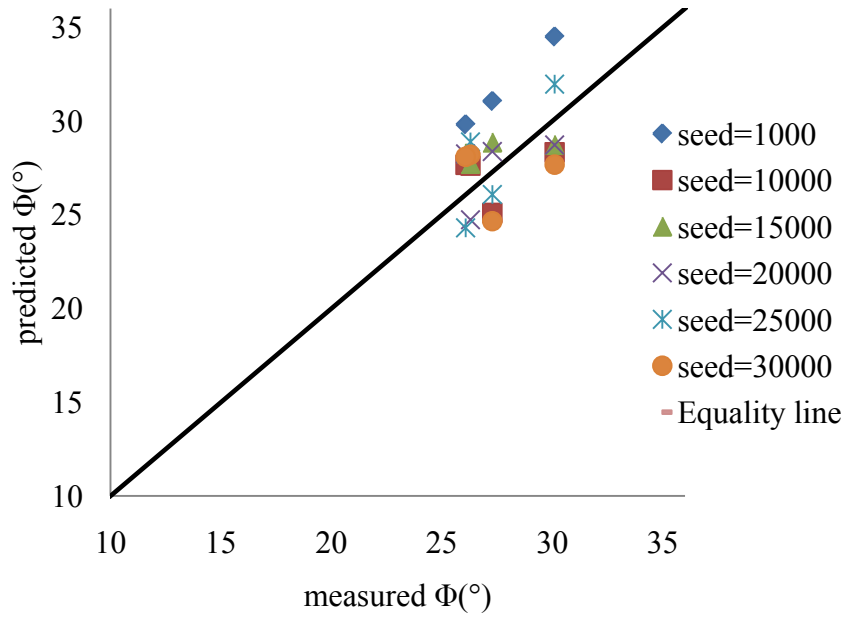
- 1) When the random seed is equal to 10,000 (default value), dynamic moduli of all the frequencies have minimum errors, while the phase angles of 25Hz and 10Hz also have minimum errors. Errors of phase angles at the other two frequencies (5Hz and 1Hz) are 7.99% and 5.79%, respectively.
- 2) When the random seeds are larger than 10,000 and of the same magnitude as 10,000, all the errors are within 10% and the maximum differences of the errors are 9.4% for dynamic modulus and 5.63% for phase angles.
- 3) When the random seed is 1,000, which is of different magnitude than the default value (10,000), the errors are relatively larger. The maximum errors are 18.65% for dynamic modulus and 14.38% for phase angle, while the minimum errors are 7.6% and 7.33%, respectively.

Followed are recommendations for selecting the random seeds:

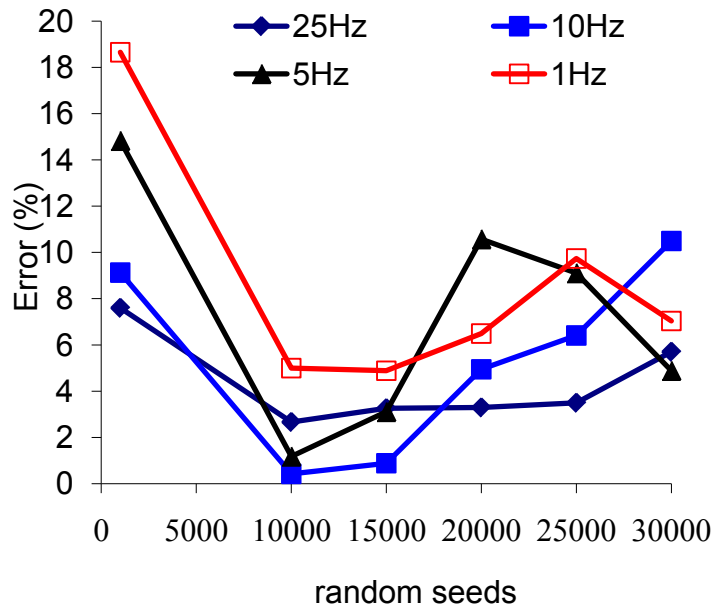
- 1) If the DE modeling of asphalt mixtures is conducted with only one replicate, the default random seed should be utilized.
- 2) If the DE modeling is conducted with more than one replicate, the random seeds should be of the same magnitude as the default value including the default value.



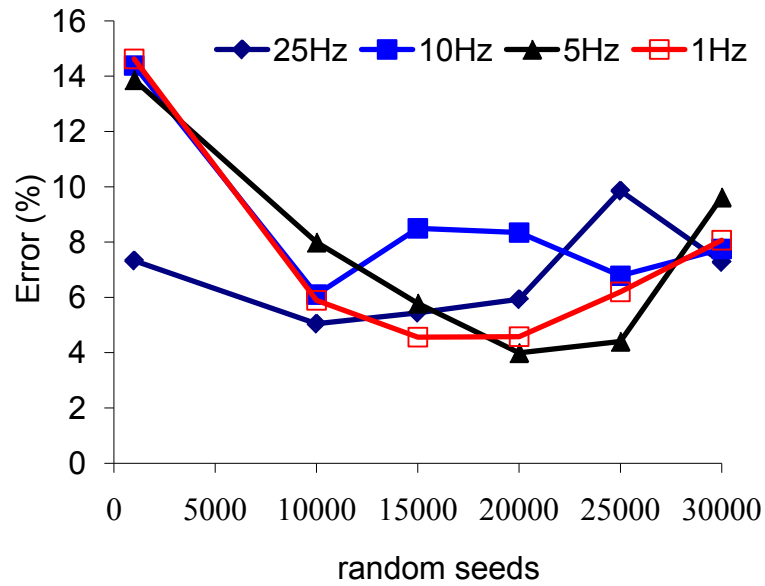
(a) Prediction vs. measurement for dynamic modulus



(b) Prediction vs. measurement for phase angles



(c) Errors vs. random seeds for dynamic modulus



(d) Errors vs. random seeds for phase angle

**Figure 10.10 Comparison between prediction and measurement of different random seeds**

### 10.8.2. Predict Dynamic Behaviors with 2D and 3D DE Models

This DE modeling of asphalt mixtures with 2D and 3D models was conducted under sinusoidal loads at  $-5^{\circ}\text{C}$ ,  $4^{\circ}\text{C}$ ,  $13^{\circ}\text{C}$ ,  $21^{\circ}\text{C}$  with the amplified frequencies. The default random seed was applied to build the microstructures of the asphalt mix. With the outputted stresses and strains, the dynamic moduli and phase angles were calculated and plotted in Figure 10.11. The average error of each temperature was calculated by dividing the sum of the errors of the four frequencies at this temperature with 4.0. The calculated average errors are listed in Table 10.3. The following findings were observed:

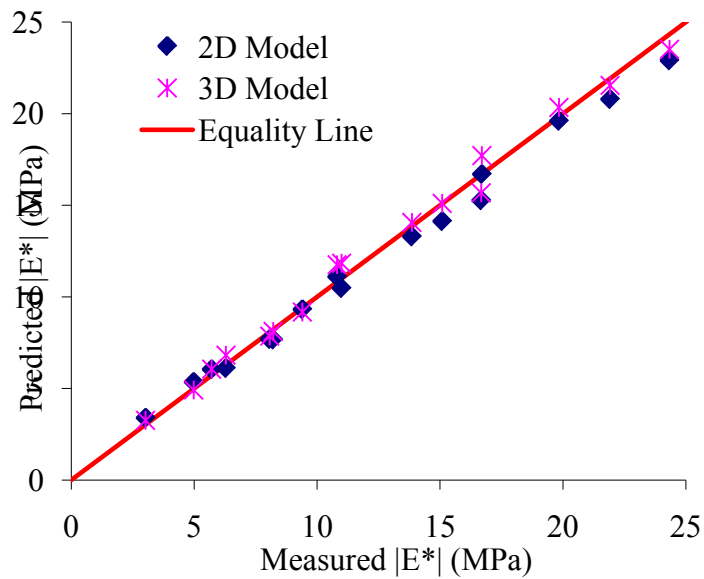
- 1) Both 2D and 3D modeling results are close to those measured in the laboratory: the average errors for dynamic modulus are 1.4% and -1.22%, while the average errors for phase angles are -3.23% and 0.82%;
- 2) Compared with dynamic moduli measured in the laboratory, those predicted with the 3D model are slightly higher (the average error is -1.22%) while those from the 2D model are slightly lower (the average error is 1.40%);
- 3) Compared with phase angles measured in the laboratory, those predicted with 3D model slightly lower (the average error is 0.82%) while those from 2D model are slightly higher (the average error is -3.23%).

Therefore, for prediction of dynamic moduli and phase angles, both 2D and 3D models can get reasonable results. Compared with 3D models, one advantage of 2D models is their reduced computation time. The disadvantage of 2D models, however, is that they

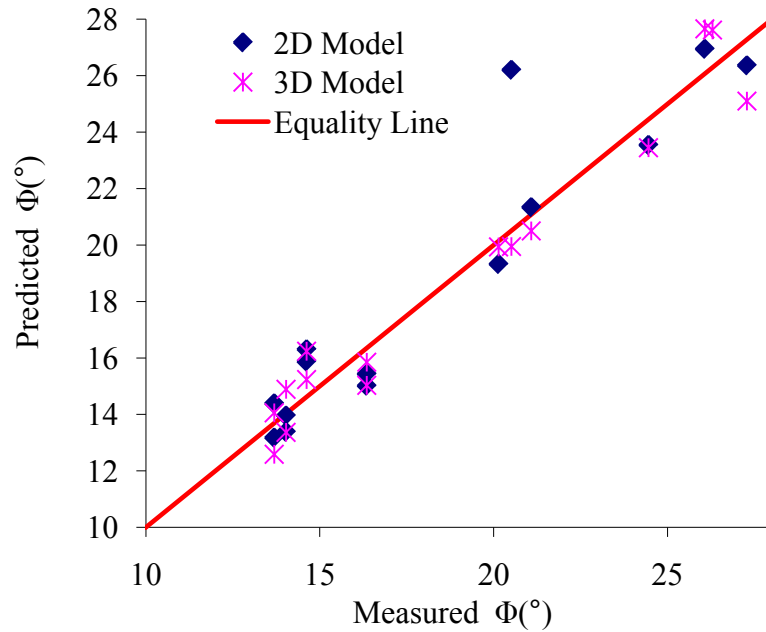
cannot represent the microstructures of asphalt mixtures well, as pointed out by previous studies. When the DE modeling at a larger strain level is conducted, the interlocks among aggregates cannot be well provided with 2D models, which may result in an unrealistic result. The disadvantage of 3D models is that they are time-consuming, but they can characterize well the internal structures of asphalt mixtures and give more reliable results.

**Table 10.3**  
**Average Errors of dynamic moduli and phase angles**

Temperatures °C	Dynamic moduli (%)		Phase angles (%)	
	2D	3D	2D	3D
21	-3.08	-0.39	-6.97	0.69
13	1.61	-2.51	-5.31	2.65
4	4.04	-1.08	-1.99	1.48
-5	3.05	-0.88	1.35	-1.53
Averaged	1.40	-1.22	-3.23	0.82



(a) Dynamic modulus:  $|E^*|$



(b) phase angle:  $\phi$

Figure 10.11 2D and 3D modeling vs. laboratory results of asphalt mixture

### 10.9. Computation Time for Viscoelastic DE Modeling

The DE method is a dynamic iterative method that works by successively solving Newton’s second law (law of moment) for each particle (discrete element) and applying the force-displacement law for each contact between particles. Usually thousands of iterative steps are needed to achieve the final results. The displacements, velocities and contact-forces of particles are updated after each iterative step. As defined in the previous section, the time-step,  $t_{del}$ , is the real physical time per iterative step. The real-physic time ( $t$ ) for a given project is the accumulative physical time after many iterative steps as expressed in Equation 10.21.

$$t_{physic} = t_{del} \times N_{step} \tag{10.21}$$

Where the  $t_{physic}$  is the real physical time;  $N_{step}$  is the number of the iterative steps.

Computation time is another concept in the DE modeling. It is the accumulative time of DE programs on a special computer. Different from the real physical time coded for the specified simulation time, the computation time is dependent on the numbers of discrete elements in the DE models and the computer performance. The DE modeling with larger models and a slower computer consumes more time, and vice versa. The real physical time, however, is independent on these factors. For example, the physical time of the DE modeling at 0.1Hz is 10 seconds for each loading period. The computation time can be calculated in Equation 10.22.

**Table 10.4**  
**Computation times for the 2D and 3D DE models with traditional method**

frequency	physical time ( $t_{physic}$ )	time-step		iterative steps		computation speed ( $V_{comp}$ )		computation time ( $t_{comp}$ )	
		( $t_{del}$ )		( $N_{step}$ )		(s/step)		(days)	
		(10 <sup>-8</sup> s/step)		(10 <sup>6</sup> )					
(Hz)	(s)	2D	3D	2D	3D	2D	3D	2D	3D
25	0.2	1.63	2.96	12.3	6.8	0.046	0.711	6.6	55.6
10	0.5	1.63	2.96	30.8	16.9	0.046	0.711	16.4	139
5	1	1.63	2.96	61.5	33.8	0.046	0.711	32.8	278
1	5	1.63	2.96	307.7	168.9	0.046	0.711	163.2	1390

$$t_{comp} = V_{comp} \times N_{step} \quad 10.22$$

Where  $t_{comp}$  is the computation time and  $V_{comp}$  is the computation speed of a given computer which is defined as the time per iterative step.

In this research study, a personal computer (Processor of Quad Core Extreme Edition) is utilized. The computation speed,  $V_{comp}$ , is 0.046 second per iterative step for the 2D DE model with 8,400 elements and 0.711 second per iterative step for the 3D DE model with 73,083 elements. The time-steps ( $t_{del}$ ) for the 2D and 3D simulation are  $1.63 \times 10^{-8}$  second/step and  $2.96 \times 10^{-8}$  second/step, respectively. Traditionally, the DE modeling was conducted to simulate the same frequencies used in the laboratory. The frequencies are from 1Hz to 25Hz in the laboratory, and therefore, the time per loading period is 0.04s to 1s. Supposing five loading periods are needed to get the reliable results,  $t_{physic}$  in Equation 10.21 should be from 0.2s to 5s. Then, the  $N_{step}$  is calculated in Equation 10.21 and the computation times are calculated by substituting  $N_{step}$  and  $V_{comp}$ , to Equation 10.22. The calculation and the final results are listed in Table 10.4. It was found that the computation times range from 6.6 to 163.2 days for the 2D model and from 55.6 to 1,390 days for the 3D model with traditional methods. Obviously, it is possible to conduct the DE simulation with the 2D model which takes a few days or months. But it becomes difficult or impossible with the 3D model which takes several years at a lower frequency (1Hz). If a larger sample or a frequency less than 1Hz is used, a longer time is needed. For example, the computation time for the 3D model is 13,900 days (i.e., more than 38 years) when the loading frequency is 0.1Hz.

In this study, the DE modeling was conducted under the amplified frequencies based on the frequency-temperature superposition principle. Since the amplified frequencies were



much larger than the regular frequencies, the computation time were significantly saved. For example, the amplified coefficients for both the 2D and 3D models are 1000 for the real frequency of 5Hz. As shown in Table 10.4, with the traditional methods, the computation time were 32.8 days and 278 days for 2D and 3D modeling at 5Hz. Now, the computation time is reduced to 0.0328 days and 0.278 days. Obviously, with the frequency-temperature superposition, the computation times of the viscoelastic DE simulation of asphalt mixtures are shortened significantly from several years to several hours.

## 10.10. Summary and Conclusions

In recent two decades, the DE method has been introduced to simulate asphalt-based materials. The DE viscoelastic geometric and mechanical models have been developed and validated, but the computation time was excessively long to fulfill modeling at regular frequencies (1~25Hz). In order to overcome this limitation, this research study develops a methodology to reduce the computation time by using the frequency-temperature superposition. The laboratory tests of asphalt mastic and mixture were conducted at  $-5^{\circ}\text{C}$ ,  $4^{\circ}\text{C}$ ,  $13^{\circ}\text{C}$ ,  $21^{\circ}\text{C}$  and 1Hz, 5Hz, 10Hz, 25Hz, respectively. A procedure was developed to fit the laboratory tests with the Burger's model. By using the frequency-temperature superposition, the normal loading frequencies in the laboratory tests were amplified and the fitted Burger's model parameters were converted into those at the amplified frequencies. The DE simulation of both asphalt mastic and mixture was conducted at the amplified frequencies by inputting the corresponding Burger's model parameters. The dynamic moduli and phase angles were calculated and compared with those measured in the laboratory. The following findings were observed:

- 1) When the amplified frequencies are less than 25KHz, the prediction results of asphalt mastic were very close to those measured in the laboratory. The errors are within 8%, and most of them range from 0.05% to 4%.
- 2) When the amplified frequencies are larger than 25KHz but less than 100KHz, the errors for both dynamic moduli and phase angles of asphalt mastic were relatively high. Some of them are larger than 15%.
- 3) Both the 2D and 3D results of asphalt mixes were close to those measured in the laboratory.
- 4) With the frequency-temperature superposition, the viscoelastic DE simulation of asphalt mixture takes less than one hour for the 2D model and several hours for the 3D model, which took several months or years with the traditional methods.
- 5) When the random seeds are equal to 10,000 (default value), or of the same magnitude of the default value, the errors of the predicted dynamic moduli and phase angles are relatively small.
- 6) Although the computation time can be reduced by amplifying real frequencies, the amplified frequencies should have their threshold values for a specific material. The reasons come from: (a) Under the lower loading frequencies or quasistatic condition, the mass inertia of viscoelastic material can be ignored. When the applied frequencies are so high that the mass inertia has to be considered, the DE modeling errors may increase. (b) In dynamic modulus tests, in addition to the dynamic load, constant and

ramp loads were also involved. In this study, however, only dynamic behaviors were considered when the frequencies were amplified and the Burger's model parameters were modified. The modified Burger's model parameters may change material behaviors under these non-cyclic loads.

### **10.11. Acknowledgements**

This material is based in part upon work supported by the National Science Foundation under grant 0701264. Any opinions, findings, and conclusions or recommendations expressed in this material are those of the author's and do not necessarily reflect the views of the National Science Foundation.

# Chapter 11. Discrete Element Simulation of Creep Tests using Time-Temperature Superposition<sup>10</sup>

## 11.1. Abstract

Microstructural-based discrete element (DE) models have been used for a better understanding of asphalt pavement concrete since the late 1990s. Most current studies have been done with two-dimensional (2D) models. Moreover, elastic models are primarily employed for simulation of an asphalt matrix's time-dependent behaviors. A 2D model is too simple to capture the complex microstructure of asphalt concrete, and an elastic model is not sufficient for simulating an asphalt matrix's viscoelastic behaviors. Therefore, it is necessary to consider a three-dimensional (3D) viscoelastic model for microstructural-based DE simulation of asphalt mixture behaviors. Currently, it is easy to build such a 3D microstructural-based DE viscoelastic model using the existing techniques presented in the previous studies. A major challenge however, is to reduce the computation time to run the 3D microstructural-based DE viscoelastic modeling process which is extremely time-consuming. The primary objective of this paper is to simulate and analyze creep responses of an asphalt mixture with a 3D microstructural-based DE viscoelastic model. A key task in this study is to develop an approach to reduce the computation time with the Time-Temperature Superposition (TTS) Principle. Using this developed approach, creep compliance tests of an asphalt mixture under temperatures of 0, -10, and -20°C, were simulated with a microstructural-based DE viscoelastic model. Additionally, a DE elastic model was also employed and compared with the viscoelastic model. It was observed that: 1) the computation time was reduced to several hours from several decades; 2) the DE viscoelastic model, the DE elastic model, and the experimental measurements yielded similar results.

## 11.2. Introduction

Asphalt Mixture is composed of graded aggregates, asphalt binder, and air voids. The aggregate sizes range from less than 0.075mm (passing the #200 sieve) to as large as 37.5mm (1.5 inches) in typical asphalt concrete mixtures. Additionally, aggregate particles in the mixture have complex morphological properties and arbitrary natures. Asphalt binder has a complex mechanical property, which depends on loading temperatures and testing times or frequencies. It is clearly important to build the relationship between the overall properties of an asphalt mixture and those of its phase constituents, which may help designers, engineers, or researchers to better understand the

---

<sup>10</sup>Full text reprinted with permission from ASCE: "Three-dimensional Microstructural-based Discrete Element Viscoelastic Modeling of Creep Compliance Tests for Asphalt Mixtures" by Zhanping You, Yu Liu, and Qingli Dai, 2009, Journal of Materials in Civil Engineering, Submitted 3 August 2009; accepted 30 December 2009; posted ahead of print 5 February 2010, Finally published in January 2011 Vol. 23, No. 1, pp. 79-87, Copyright © 2010, ASCE. See Copyright clearance in Appendix A.

mixture fundamental properties. As demonstrated in the past decades, the discrete element method (Nagel-Steger et al.) has been utilized for this purpose. An incomplete list of the researchers is provided in Table 10.1 with the key references. As reported in the previous studies listed in Table 11.1, several techniques have been used for reconstruction of asphalt mixture microstructures, while both DE elastic models and DE viscoelastic models have been employed for simulating time-dependent behaviors of asphalt mixtures. More details will be provided in the subsequent sections of this paper.

**Table 11.1**  
**An incomplete international review of the DEM study in pavement area**

Author(s) and Literatures	Key Studies
Rothenburg, L. Bogobowicz, A Hass, R. (Rothenburg et al. 1992)	Micromechanical modeling of asphalt concrete for studying pavement rutting problems
Chang and Meegoda (Chang and Meegoda 1997a; Chang and Meegoda 1999a)	DEM application on an asphalt mixture with a modified code
Buttlar and You (Buttlar and You 2001), You (You 2003)	Development of a micromechanical modeling approach for studying asphalt mixture stiffness using the discrete element method
Abbas and others (Abbas et al. 2007)	Simulation of the micromechanical behavior of asphalt mixtures based on the discrete element method
Fu (Fu 2005), Wang and others (Wang et al. 2007a)	Experimental quantification and discrete element modeling of micro-macro performances of granular materials using the x-ray tomography imaging techniques
Collop and others (Collop et al. 2004)	Modeling dilation in an idealized asphalt mixture using discrete element modeling
You and Buttlar (You and Buttlar 2002; You and Buttlar 2004; You and Buttlar 2005; 2006)	Stiffness prediction of hot mixture asphalt (HMA) through developing the microfabric discrete element modeling (MDEM): two-dimensional elastic model with optical scanned images
Adhikari, You, and others (Adhikari and You 2008; Adhikari et al. 2008a; Adhikari 2008; You et al. 2009; You 2008)	Microstructural-based modeling of an asphalt mixture with two-dimensional and three-dimensional DEM; X-ray computed tomography (or optical scanned image) was used for 3D models.
Liu, You, and others (Liu et al. 2009; Liu and You 2008; 2011a; Liu et al. 2008; Liu and You 2009)	Microstructural-based modeling of an asphalt mixture with a viscoelastic model and a user-defined mix structure.

In the past two decades, many studies have been done as shown in Table 11.1, although most of them were focused on prediction of macroscopic properties of an asphalt mixture from its constituent materials. Two-dimensional (2D) DE elastic models were primarily used in those previous studies. Due to the extremely long computation time, none of the current studies have reported simulation of asphalt mixture behaviors with a 3D microstructural-based DE viscoelastic model. Obviously, a 2D model is too simple to represent the complex morphological characteristics in a typical asphalt mixture, while a DE elastic model is not sufficient for modeling the time- and temperature-dependent behaviors of asphalt-based materials. Therefore, it is necessary to employ a 3D microstructural-based DE viscoelastic model for a better understanding of an asphalt mixture's behaviors.

### **11.3. Objective and Roadmap**

The primary objective of this paper is to simulate and analyze creep responses of an asphalt mixture with a 3D microstructural-based DE viscoelastic model. To achieve this objective, four tasks are essential. These tasks are discussed in four individual sections of this paper and include:

1) Reconstruction of the 3D microstructure of an asphalt mixture

The 3D microstructure of an asphalt mixture has been rebuilt from X-ray computed tomography (X-ray CT) images in the previous study (Adhikari 2008). In this 3D microstructure, the asphalt mixture was regarded as a composite of coarse aggregates (larger than 2.36mm), asphalt sand mastic, and air voids. Even though asphalt sand mastic is considered to be a fine mixture of fine aggregates (less than 2.36mm), fines, and asphalt binder, it was regarded as a homogenous phase in the asphalt concrete mixture. The technique in this task was completed in previous studies.

2) Discrete element micromechanical modeling

In order to simulate the interactions within the rebuilt microstructure of the asphalt mixture, a DE viscoelastic model was developed in the previous study (Liu et al. 2009).

Time-temperature superposition principle used in DE viscoelastic modeling

The Time-Temperature Superposition (TTS) Principle is typically used to build a master curve for experimental data analysis of asphalt-based materials (Pellinen and Witczak 2002; Stastna et al. 2006). This principle has been employed herein to reduce the computation time in a new form.

3) Creep responses from the DE viscoelastic model

Uniaxial creep compliance tests of the asphalt mixture were simulated with the 3D microstructural-based DE viscoelastic uniaxial loads. For the simulation, the rebuilt 3D microstructure of an asphalt mixture, the viscoelastic micromechanical model, and the TTS principle were used.

4) Comparative studies were also performed involving the following two tasks:

- a) Creep responses from a microstructural-based DE elastic model  
A DE elastic model has been developed in previous studies and reused in this study to simulate creep responses of an asphalt mixture similar to the one used in the DE viscoelastic model.
- b) Comparison and analysis  
The 3D microstructural-based viscoelastic and elastic model results, microstructural along with the experimental testing results were analyzed to identify the differences among them.

## 11.4. Reconstruction of an Asphalt Mixture Microstructure

To rebuild the microstructure of asphalt mixtures, three typical techniques were utilized in the previous studies as listed in Table 11.1: the highly-idealized model (Collop et al. 2007; Collop et al. 2006a), the randomly-created polyhedron model (Liu and You 2009), and the image-based model (Adhikari 2008). In the highly-idealized model, aggregates are simulated with discs in a 2D model or balls in a 3D model. In the randomly-created polyhedron model, aggregate particles are simulated with polyhedron particles which are randomly created. The greatest advantage of these two models is their laboratory independency, but they are not sufficient to accurately represent a specific mixture microstructure. To simulate an asphalt mixture's microstructure, an image-based model may be the best option. However, the laboratory dependency of an image-based model is a major limitation, because expensive laboratory equipment is needed. Furthermore, well-trained technicians are required to utilize the equipment and to process the output images. Moreover, this kind of model is only suitable for a specific mixture which has been available before running DE modeling. Therefore, an image-based model is commonly used for verifying a discrete element model as demonstrated in the previous studies (Adhikari 2008).

**Table 11.2**  
**Aggregate gradation**

Sieve size (mm)	25	19	12.5	9.5	4.75	2.36	1.18	0.6	0.3	0.15	0.075
Percentage passing (%)	100	98.9	77.5	68.4	56.2	46.2	31.7	20.8	12.6	8.3	5.6
Asphalt content	4.8% of the total mass of the mixture										
Air void content	4.0% of the total volume of the mixture										

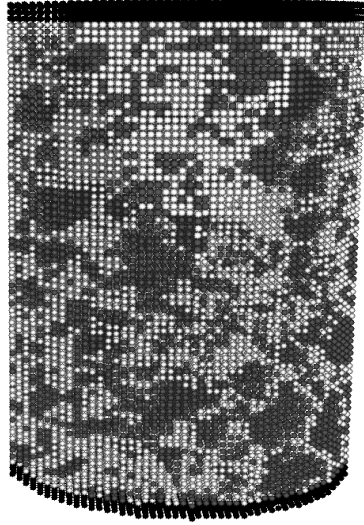


**Figure 11.1 Reconstructed three-dimensional microstructure of an asphalt mixture (dark-colored elements represent the upper and lower loading platens; white elements represent the asphalt sand mastic; grey elements symbolize mineral aggregates)**

As well known, the basic goal of a microstructural-based DE model is to conduct microscopic analysis for a better understanding of asphalt concrete micromechanics. Instead of focusing on the basic goal, this study is focused on verification of a 3D microstructural-based DE viscoelastic model in terms of simulating creep responses through comparative studies with experimental testing data and existing DE elastic modeling results. As a result, an image-based model was utilized in this study to accurately represent the 3D microstructure of a specific asphalt mixture. Volumetric parameters of the specific asphalt mixture are listed in Table 11.2, including gradation as well as the percentage of asphalt binder by mass and air voids by volume.

The X-ray CT images of this mixture were prepared by the Federal Highway Administration. From these X-ray CT images, the image-based model was built by reconstruction of the asphalt mixture microstructure with a digital image processing technique presented in the previous study (Adhikari 2008). According to the previous study, the coordinates of aggregates, mastic, and air voids were captured separately by processing the X-ray images. Then, the microstructure of the asphalt mixture was rebuilt using balls or spheres which were marked for identification. In this way, aggregates, asphalt sand mastic, and air voids can be distinguished in this subsequent process. Figure 11.1 displays the rebuilt mixture microstructure which consists of 148,200 discrete elements. In Figure 11.1, the dark-colored elements represent the upper and lower loading platens which are utilized for applying uniaxial loads. The white elements represent the asphalt sand mastic, while the grey elements symbolize mineral aggregates.

## 11.5. Discrete Element Micromechanical Models

As shown in Table 11.1, many studies have been done on discrete element modeling of asphalt mixtures. The micromechanical models which were used in the existing studies could be categorized into elastic and viscoelastic models. A typical elastic model is the one which was documented and used for predicting asphalt mixture stiffness by Buttlar and You in 2001 (Buttlar and You 2001b). Later, this model was also utilized by other researchers (Adhikari and You 2008; Adhikari et al. 2008a; Kim 2007; Kim et al. 2008; You and Buttlar 2006). A typical viscoelastic model is the one which was reported in a recent study (Liu et al. 2009). In this viscoelastic model, Burger's model was used to simulate the time-dependent behaviors of asphalt sand mastic, while an elastic model was used to replicate aggregates. The details were presented in the reference (Liu et al. 2009) and also will be briefly described below. In addition to the typical viscoelastic model, researchers simulated the asphalt mixture dynamic modulus with a similar viscoelastic model (Abbas et al. 2007). However, the details of this viscoelastic model were not fully documented. Therefore, in subsequent discussions in this paper, the DE viscoelastic model refers to the model presented in a recent study (Liu et al. 2009), while the DE elastic model is linked to the model used in a previous study by Buttlar and You (Buttlar and You 2001b).

As demonstrated in a recent study (Liu et al. 2009), a typical DE micromechanical model for asphalt concrete consists of three parts: a contact stiffness model, a slip model, and a contact-bond model. All three contact models describe the mechanical behaviors at a contact of two adjacent discrete elements. The contact stiffness model relates the contact forces at the contact point to the relative displacements of two contacting discrete elements. The other two contact models are used to consider the strength properties at the contact. The slip model represents the slip behaviors at the two contacting entities, while the contact-bond model is used to consider the tensile strength at the contact.

In the DE viscoelastic model, four contact models were used: the Burger's model, the linear elastic contact model, the slip model, and the contact-bond model. All of these contact models are available in the Particle Flow Code in three-dimensional (PFC3D) perspective (Itasca Consulting Group 2008b). The Burger's model and the linear elastic contact model were used as the contact stiffness models for asphalt sand mastic and aggregate particles, respectively. The slip model represents the slip behavior at the two contacting entities by enforcing a relation between shear and normal force. The contact-bond model can be envisioned as a pair of elastic springs which specify shear and normal tensile strength. Figure 11.2 shows the configuration of the DE viscoelastic model. Four contact interactions in the asphalt mixture microstructure are considered in this DE viscoelastic model including: between different aggregate particles, within a single aggregate particle, between an aggregate particle and asphalt sand mastic, and within the asphalt sand mastic. Each is addressed with a specific constitutive model which consists of a contact-stiffness model, a slip model, and a contact-bond model. Details are provided in the previous study (Liu et al. 2009).



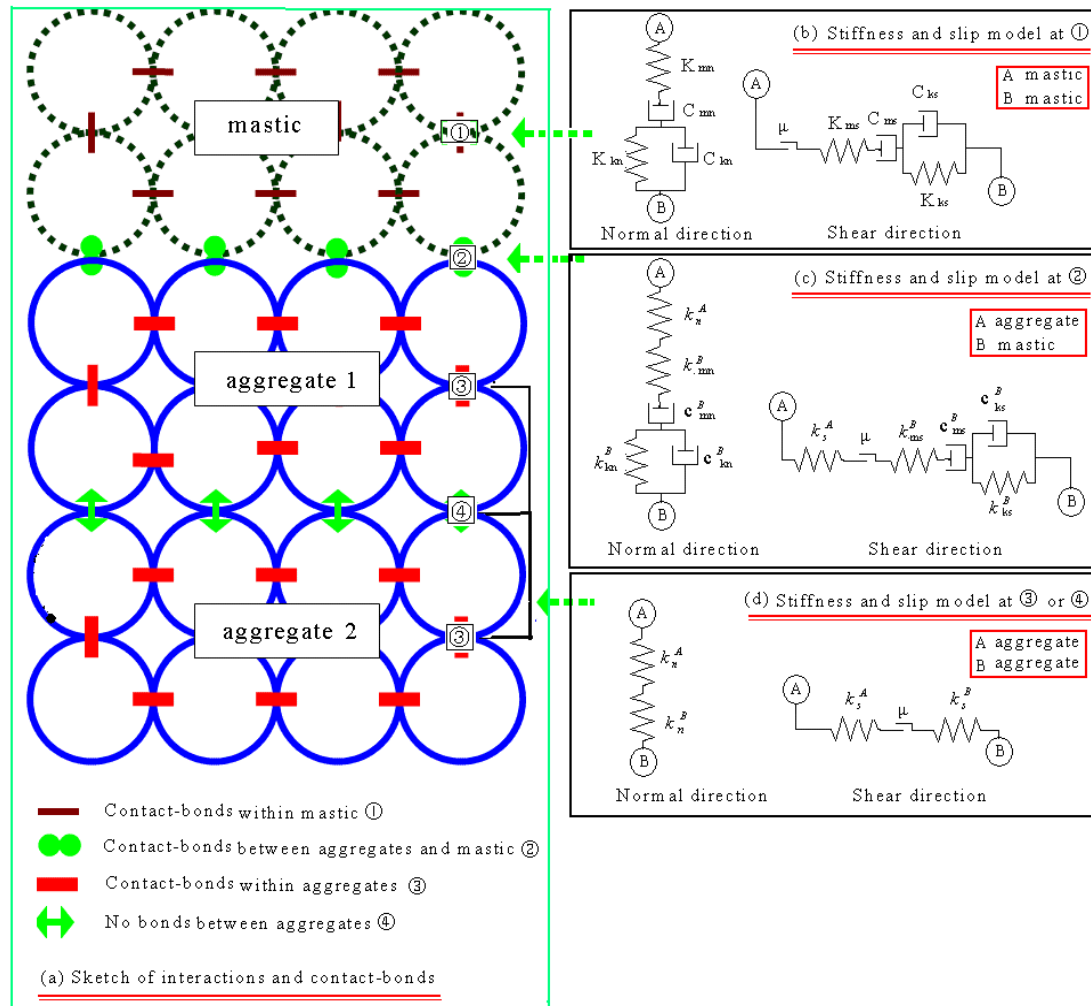


**Figure 11.2 Sketch of interactions and the corresponding constitutive models within the digital sample of asphalt mixtures (Liu et al. 2009)**

In the DE elastic model, however, the contact stiffness model is the linear elastic contact stiffness model instead of the Burger's model. Therefore, theoretically, this mechanical model can simulate only the elastic behaviors of a given material. In fact, this model has been used for simulating asphalt mixture time-dependent properties, such as dynamic modulus and creep stiffness (Dai and You 2007; You et al. 2009; You and Buttlar 2006). The underlying theory is that stiffness of an asphalt material is constant at a specific time and temperature even though its stiffness depends on loading times and temperatures. In other words, at a specific time and temperature, an asphalt material can be described with a linear elastic model. Figure 11.3 shows the methodology for predicting creep stiffness of an asphalt mixture with the DE elastic model at a specific time and temperature. When the temperature and loading time are different, the DE elastic model has to be iterated with a new input parameter at the new temperature and time.

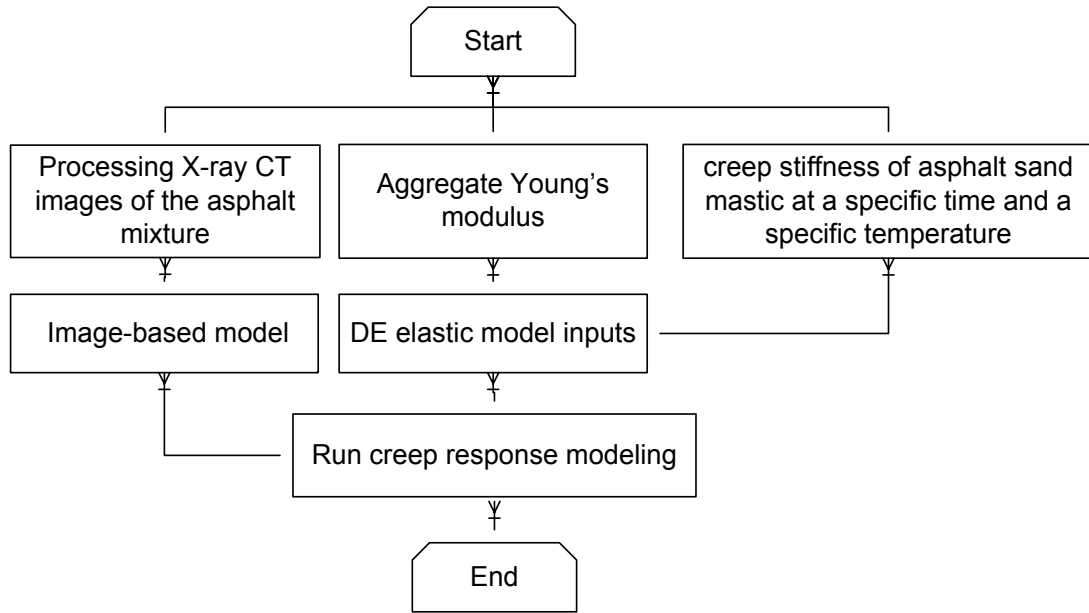


**Figure 11.3 Research methodology flow chart for modeling with the DE elastic model.**

## **11.6. Time-Temperature Superposition Used in the DE Viscoelastic Model**

With the DE viscoelastic model, real time-dependent behaviors of an asphalt mixture can be simulated. However, since real loading time is involved, it is very time-consuming to run the DE viscoelastic model without the TTS Principle. According to the previous study (Liu et al. 2009), it could take several weeks to run a 2D microstructural-based DE viscoelastic model if the real time, one second, is simulated. In the 2D model, a total of 9,540 discrete elements were included and a personal computer (processor of Quad Core Extreme Edition) was used for the 2D simulation. If the 3D microstructural-based model in Figure 11.1 is used, the computation time will be much longer. In order to reduce the computation time and make it possible to run a 3D microstructural-based DE viscoelastic model, this paper presents a technique which was derived on the basis of the TTS principle.

The underlying basis for the TTS principle is that there is a direct equivalency between time and temperature for a viscoelastic material. Hence, the loading time can be reduced by performing the laboratory tests at higher temperatures and then transposing (shifting) the resultant data to lower temperatures. This equivalency between time and temperature could be more clearly expressed through the use of Equations 11.1 and 11.2.

$$D(T, t) = D(T_r, t_r) \tag{11.1}$$

$$t = a_T t_r \quad 11.2$$

Where:

- $D(T,t)$  = creep compliance at the real temperature and loading time;
- $D(T_r,t_r)$  = creep compliance at the reference temperature and reduced loading time;
- $T, t$  = real temperature and loading time;
- $T_r, t_r$  = reference temperature and reduced loading time;
- $a_T$  = shifting factor.

The TTS Principle has been commonly used to build master curves for many years. Basically, the shifting factor,  $a_T$ , could be expressed with a function of temperatures  $T$  and  $T_r$  as demonstrated in the previous study (Basu et al. 2003). Therefore, when temperatures are given,  $a_T$  can be determined, and the original testing data may be shifted to those under the reference temperature and reduced loading time, which produces a smooth master curve. With such a master curve, the material parameter of interest at a given temperature could be estimated over a wide range of time scale (Rowe and Baumgardner 2007; Zanzotto and Stastna 1997). Instead of analyzing data with a master curve, this study seeks a method to reduce the computation time for the DE viscoelastic modeling. According to the viscoelastic theories (Malkin and Isayew 2006; Tschoegl 1989), creep compliance could be expressed on the basis of the Burger's model as:

$$D(T, t) = \frac{1}{E_m} + \frac{t}{\eta_m} + \frac{1}{E_k} (1 - e^{-\frac{E_k t}{\eta_k}}) \quad 11.3$$

Where:

$E_m, E_k$  = spring elements of the Maxwell element and Kelvin element, respectively;

$\eta_m, \eta_k$  = dashpot elements of the Maxwell element and Kelvin element, respectively;

The Burger's model parameters,  $E_m, E_k, \eta_m, \eta_k$ , in Equation 11.3 represent viscoelastic properties at the real testing temperature. For convenience, those Burger's model parameters are called "the real Burger's model parameters", since they are directly from the real testing data. If the temperature increases up to the reference temperature, the viscoelastic properties will be changed. Assuming  $E_m, E_k, \eta_{mr}, \eta_{kr}$  are the Burger's model parameters at the reference temperature, the creep compliance at the reduced time,  $t_r$ , can be calculated using Equation 11.4.

$$D(T_r, t_r) = \frac{1}{E_m} + \frac{t_r}{\eta_{mr}} + \frac{1}{E_k} (1 - e^{-\frac{E_k}{\eta_{kr}} t_r}) \quad 11.4$$

Where:

$\eta_{mr}, \eta_{kr}$  = dashpot elements in Burger's model at the reference temperature.

$t_r$  = reduced time, which can be determined from Equation 11.2.

Since the Burger's model parameters in Equation 11.4 represent the material properties under the reference temperature at the reduced time,  $t_r$ , they are named "the reference Burger's model parameters" for convenience. Although a specific material has different property values at the real and reference temperatures, the creep compliances at those two temperatures can be equivalent at different loading periods: the real time,  $t$ , and the reduced time,  $t_r$ , as demonstrated in Equations 11.1 through 11.4. By solving Equations 11.1 through 11.4, the reference Burger's model parameters can be expressed by the real Burger's model parameters as shown in the following two equations:

$$\eta_{mr} = \frac{\eta_m}{a_T} \quad 11.5$$

$$\eta_{kr} = \frac{\eta_k}{a_T} \quad 11.6$$

Traditionally, the real Burger's model parameters were used for DE viscoelastic simulation as demonstrated in the previous study. As a result, the creep compliance is a function of the real Burger's model parameters as well as the real time,  $t$ . Since the real time,  $t$ , was involved, the computation time was usually very long as demonstrated in the previous study (Liu et al. 2009). In this study, however, the reference Burger's model parameters were used. As a result, the same creep compliance is determined by the reference Burger's model parameters and the reduced time. Therefore, the computation time is dependent on the reduced time instead of the real time. Since the reduced time may be much smaller than the real time when the shifting factor is very large, the computation time is supposed to be reduced significantly.

## 11.7. Simulation of Creep Responses with the DE Viscoelastic Model

Based on the theory discussed in the previous section, the methodology of this study is shown in Figure 11.4 to simulate creep responses of an asphalt mixture. As shown in Figure 11.4, this methodology can be summarized in the following five steps:

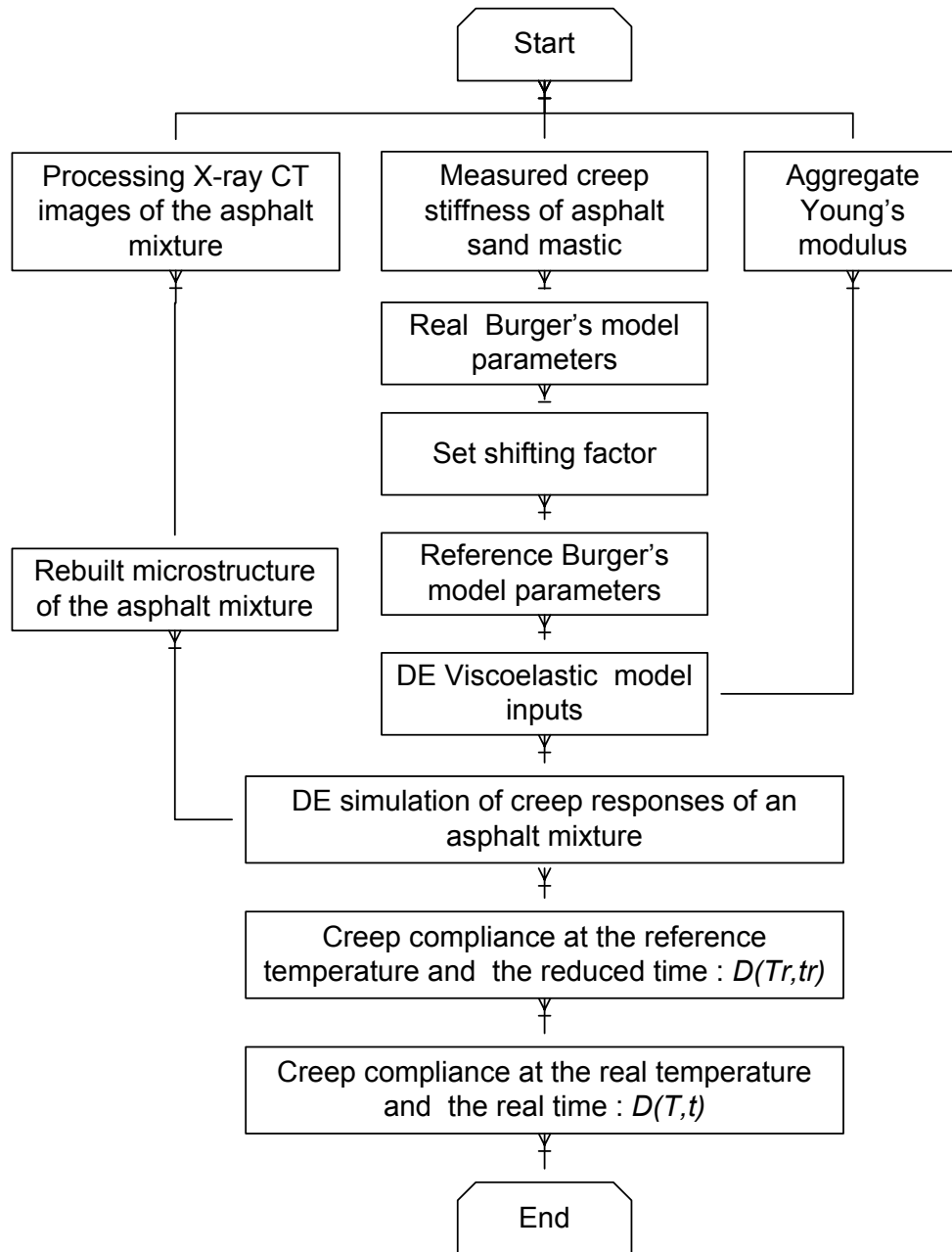


**Figure 11.4. Research methodology flow chart for modeling with the DE viscoelastic model**

1) Microstructure of an asphalt mixture and physical properties of its phase materials  
 The microstructure has been available as shown in Figure 11.1. Physical properties of the phase materials were also provided in the previous study (Dai and You 2007). The measured creep stiffness of the asphalt sand mastic is used as an input parameter as shown in Figure 11.5, while the input of Young's modulus of aggregates is 55.5GPa based on previous studies (You and Buttlar 2005; 2006).

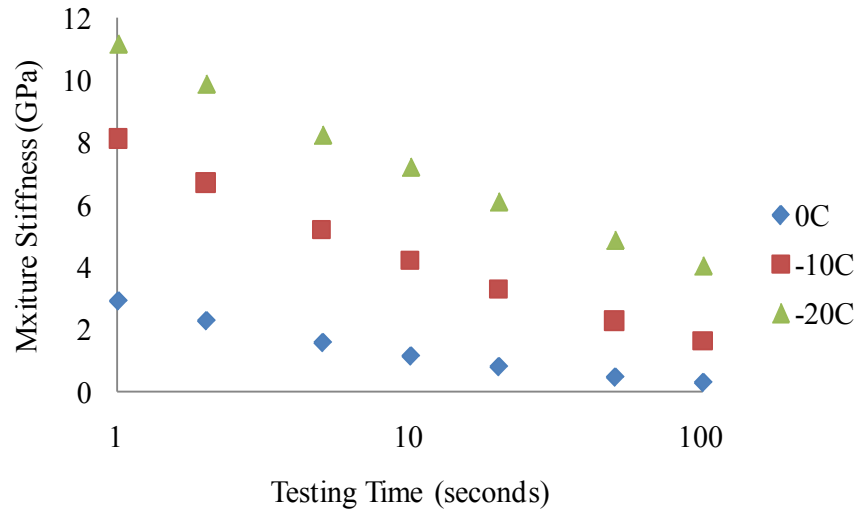


**Figure 11.5 Creep stiffness of the asphalt sand mastic**

**Table 11.3**

**Real Burger’s model parameters of the three temperatures in viscoelastic models**

	0 °C	-10 °C	-20 °C
$E_m$ (GPa)	430.9	508.4	566.7
$E_k$ (GPa)	1.8	5.4	8.3
$\eta_m$ (GPa)	35.0	201.9	600.8
$\eta_k$ (GPa)	2.2	5.5	6.6

2) Inputs of the DE viscoelastic micromechanical model

The inputs for the DE viscoelastic micromechanical model include Young’s modulus of aggregates and the reference Burger’s model parameters of asphalt sand mastic. The former is 55.5GPa, while the latter are determined in Equations 11.5 and 11.6 by shifting the real Burger’s model parameters with a shifting factor. The real Burger’s model parameters listed in Table 11.3 are determined by fitting the real creep compliance test data.

3) DE viscoelastic modeling of an asphalt mixture and results

After setting up the microstructure and the DE input model parameters, uniaxial creep compliance tests were simulated under a constant load. A constant load of 0.2MPa was applied to the top of the digital specimen in Figure 11.1 while its bottom remained fixed. During the simulation, creep stiffness values of the asphalt mixture were calculated by dividing the average stress by the average strain in the digital specimen at a specific loading time.

4) Creep stiffness of the reference temperature versus the reduced time

The final output of the DE viscoelastic modeling was a curve for the creep stiffness of the reference temperature versus the reduced time. Figure 11.7 shows three simulation results for real temperatures of 0,-10, and -20°C.

5) Creep stiffness of the real temperature versus the real time

The simulation results in Figure 11.7 were shifted back to those at the real temperature and the real time based on the TTS principle. The final results are shown in Figure 11.8.

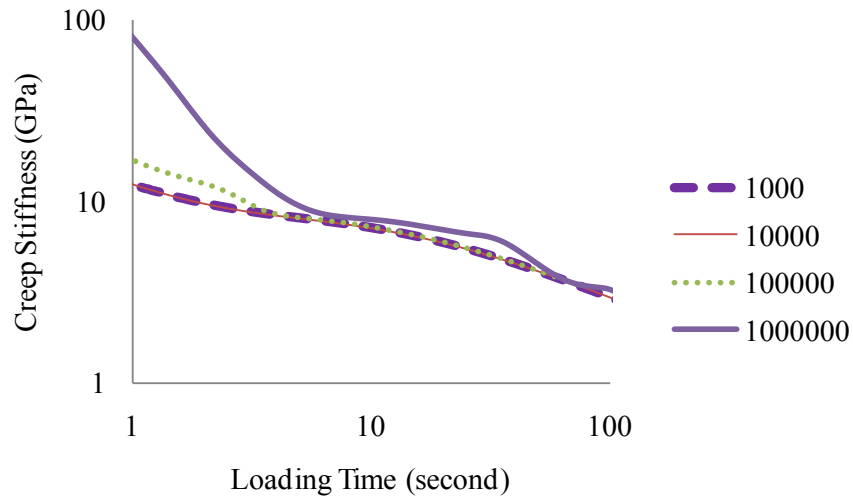


**Figure 11.6 Results of DE viscoelastic modeling with different shifting factors (the legends represent shifting factors, for example, 1000 means the shifting factor=1000)**

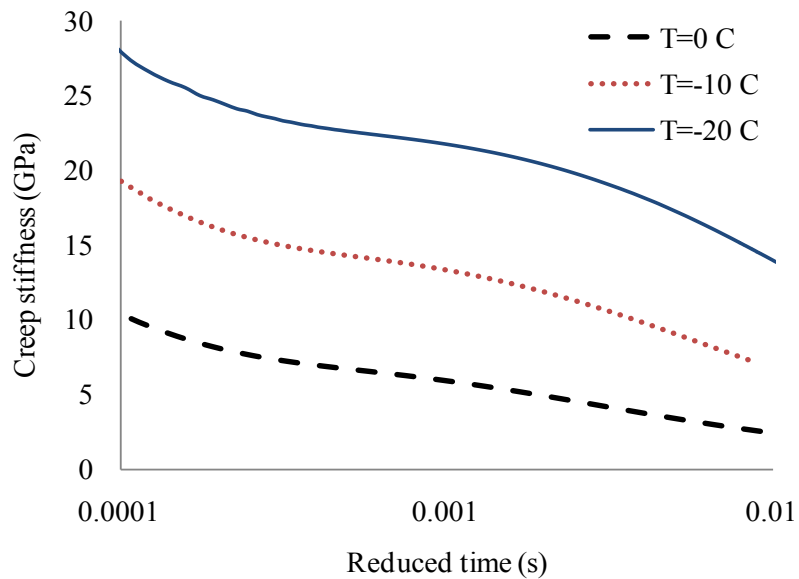


**Figure 11.7 Predicted creep stiffness at the reference temperature vs. the logarithmic reduced time ('T' in the legend is the real temperature, not the reference temperature)**

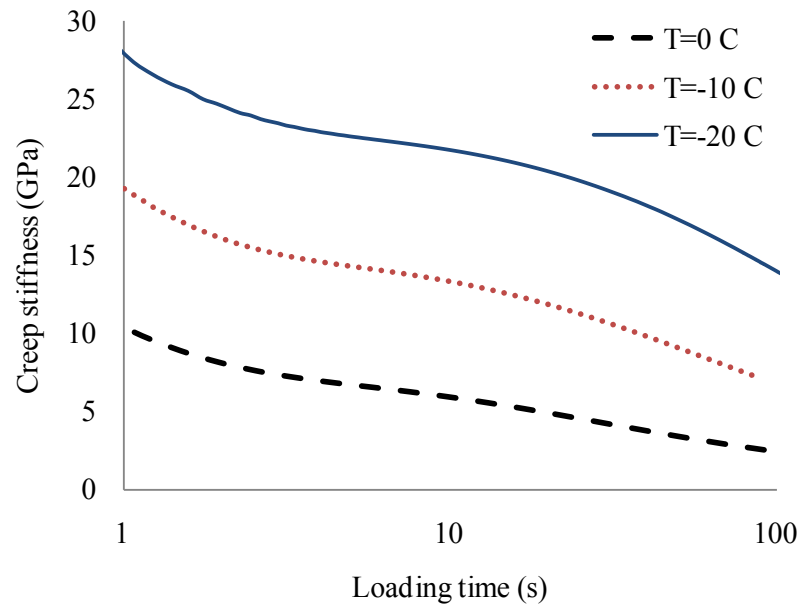


**Figure 11.8 Predicted creep stiffness at the real temperature vs. the logarithmic loading time**

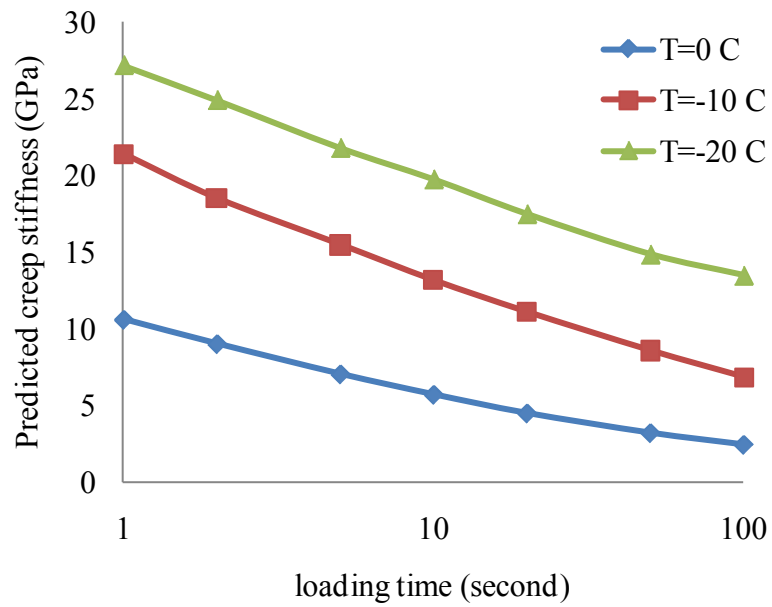


**Figure 11.9 Predicted creep stiffness vs. the logarithmic loading time**



## 11.8. Creep Response Simulation with Microstructural-based DE Elastic Model

For comparative study, the same microstructure of the asphalt mixture as shown in Figure 11.1 was used to simulate creep responses with the DE elastic model. As shown in Figure 11.3, aggregate Young's modulus and creep stiffness of asphalt sand mastic at a specific time and temperature are needed as input parameters. Upon completing the procedure in Figure 11.3, only one output, the predicted creep stiffness of an asphalt mixture at the specific temperature and time, could be obtained. To predict the mixture stiffness at other time periods and temperatures, the procedure in Figure 11.3 has to be iterated with new inputs of asphalt sand mastic at the corresponding temperatures and time periods. The input aggregate Young's modulus was 55.5GPa, while the creep stiffness values of asphalt sand mastic at various time periods and three temperatures are shown in Figure 11.5. With the methodology discussed above, the predicted creep stiffness versus the loading time is shown in Figure 11.9, which will be used for the comparative study in the following section.

## 11.9. Comparison and Analysis

As discussed in the previous sections, creep stiffness values of the asphalt mixture were predicted with both the DE elastic and viscoelastic models. The asphalt mixture stiffness values were also measured as demonstrated in the previous study (Dai and You 2007). The measured mixture stiffness values are shown in Figure 11.10. The stiffness values from the DE elastic model, the DE viscoelastic model, and laboratory measurement were compared as shown in Figure 11.11. It was observed that:

- 1) The predicted stiffness values from the DE viscoelastic model were very close to those from the DE elastic model;
- 2) Both the DE elastic and viscoelastic models tended to predict lower values of asphalt mixture creep stiffness when compared with the laboratory measurement;
- 1) Relatively large discrepancies existed between measurement and the prediction in Figure 11.11(b) and 11(c). These discrepancies may be attributed to two possible reasons:
  - 2) 10,000 has been calibrated for simulation at 0°C, but not at -10 and -20°C;
  - 3) The measured creep stiffness values at -10 and -20°C were questionable as shown in Figures 5 and 10.

It is clear that the stiffness values of asphalt concrete at -10 and -20°C are very close in Figure 11.10, but the corresponding stiffness values of the asphalt sand mastic at those two temperatures are quite different in Figure 11.5. Since the aggregate properties are independent of temperature, the measured stiffness values at -10 and -20°C in Figure 11.10 may be inaccurate if the data in Figure 11.5 is correct. These issues will be evaluated in the ongoing study at Michigan Technological University.

Prior to the study presented in this paper, simulation with a DE viscoelastic model was so time consuming that it was almost impossible to run a 3D microstructural-based DE viscoelastic model. A DE elastic model was an alternative in that situation. In order to

identify the efficiencies of these methods, they are compared in terms of computation time. In this study, 148,200 discrete elements were included to rebuild the mixture microstructure in Figure 11.1. A personal computer (Processor of Quad Core Extreme Edition) was used to conduct the DE simulations. The simulations were conducted under the default time-step ( $2.29 \times 10^{-8}$  seconds/ step). The details about the conception of time-step and calculation of the computation time were provided in the previous study (Liu et al. 2009). Table 11.4 shows the comparison of computation time: 1) It took half a day to finish the DE elastic modeling for each of the three temperatures; 2) It would take almost 31,000 days using the viscoelastic model without TTS; 3) It took about three days using the viscoelastic model with TTS. From Table 11.4, it is clear that the elastic model required less computation time than the viscoelastic model in this study. However, the viscoelastic model could provide a smooth curve instead of the discrete prediction points from the elastic model. With the TTS Principle, the computation time for the viscoelastic modeling was reduced from around 82 years (30,988.53 days) to three days without losing much accuracy. It should be noted that the results in Table 11.4 are dependent on digital sample sizes and capabilities of computers used in the simulation.

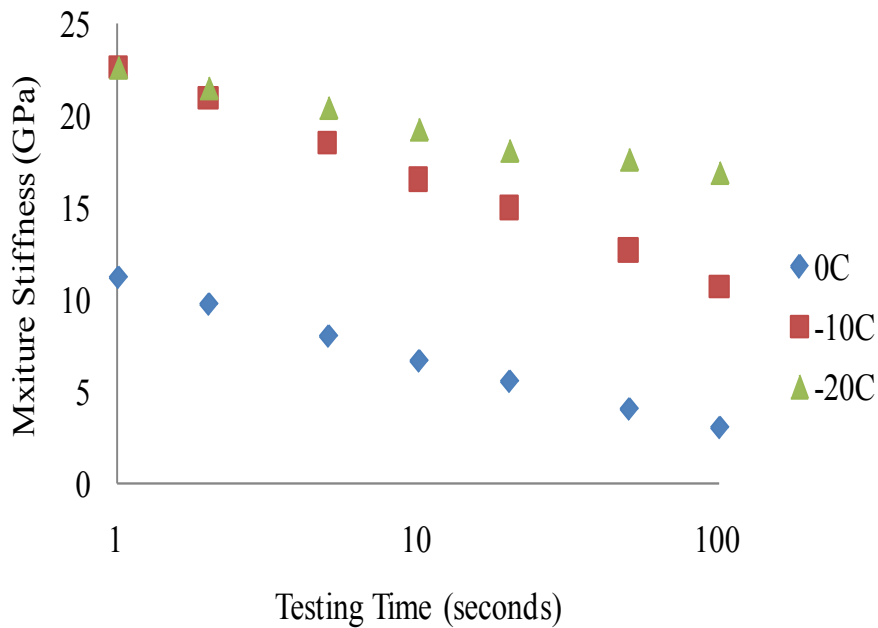
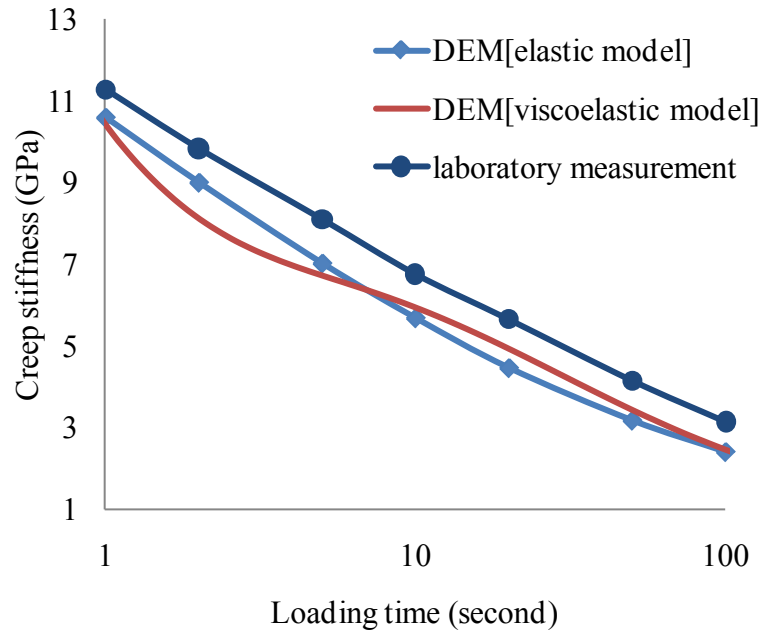
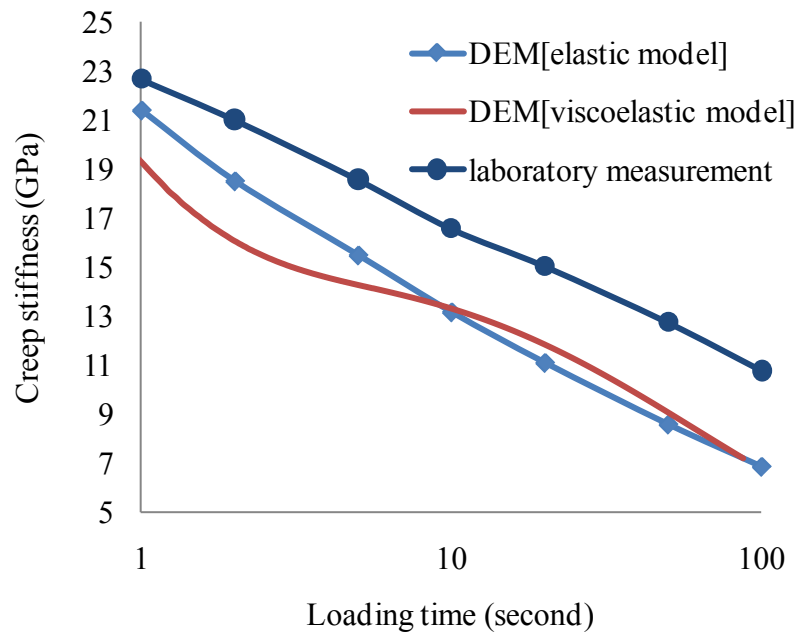


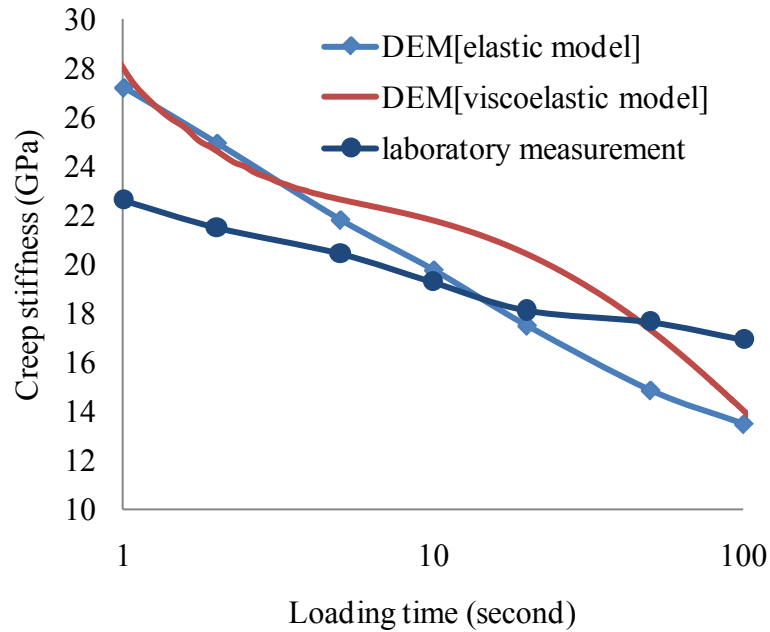
**Figure 11.10 Measured creep stiffness of the asphalt mixture vs. the logarithmic loading time**



(a) 0°C



b) -10°C



(c) -20°C

**Figure 11.11 Comparisons of DE modeling with the experimental measurements**

**Table 11.4  
Computation time comparison**

Model type	Computation time (days)		
	0°C	-10°C	-20°C
Elastic model	0.48	0.51	0.50
Viscoelastic model without TTS	30,988.53		
Viscoelastic model with TTS	3.10		

## 11.10. Summary and Conclusions

This study has presented a method for simulation of asphalt mixture creep compliance tests with a 3D microstructural-based DE viscoelastic model. An approach was presented on the basis of the TTS Principle to reduce the computation time. Additionally, a DE elastic model was also employed to simulate the same asphalt mixture tests for comparative study purposes. Finally, comparative studies were completed on the DE viscoelastic and elastic models in terms of prediction accuracy and efficiency. The following conclusions were observed:

- 1) The DE viscoelastic and elastic models yielded similar results in terms of the predicted asphalt mixture stiffness.
- 2) Both the DE elastic and viscoelastic models tended to predict lower values of asphalt mixture creep stiffness when compared to laboratory measurements.

- 3) With the TTS-based approach, the computation time could be significantly reduced for the simulation with the DE viscoelastic model. Computations that traditionally took many years could be completed within a few hours. Therefore, computation power is no longer an issue for viscoelastic modeling.

This study was focused on the TTS-based DE viscoelastic model for simulation of asphalt mixture time-dependent behaviors. The application of this study, however, is not limited to the prediction of creep stiffness. Ongoing research will apply this method for prediction of asphalt mixture rut depth.

## **11.11. Acknowledgments**

This material is based in part upon work supported by the National Science Foundation under grant 0701264. Any opinions, findings, and conclusions or recommendations expressed in this material are those of the author's and do not necessarily reflect the views of the National Science Foundation. The authors acknowledge the valuable discussions with Dr. William G. Buttlar at the University of Illinois in Urbana-Champaign. The authors are grateful for the assistance from Dr. Buttlar and Mr. Minkyum Kim in the preparation for laboratory testing at the University of Illinois in Urbana-Champaign.

# Chapter 12. Discrete Element Modeling of Asphalt Concrete Mixtures under Haversine Loading<sup>11</sup>

## 12.1. Abstract

Limited by the current computing power, it is impossible to simulate a full scale asphalt pavement with a three-dimensional (3D) microstructure-based discrete element (DE) model, when the time-dependent behaviors of the materials are considered. Researchers currently focus on modeling the microstructure of asphalt mixture materials and have not attempted pavement modeling. In addition, existing studies are limited to modeling asphalt mixtures without considering the time-dependent properties. In this paper, 3D DE models of asphalt mixtures under dynamic loads were developed with the assistance of X-ray Computed Tomography (X-ray CT). The time-dependent model was considered in the simulations. To shorten the computation, a frequency-temperature superposition technique was employed. X-ray CT images were used to reconstruct the microstructure of asphalt concrete, while a time-dependent model was built by taking into consideration micro-scale interactions within the models. Through this study, it was observed that the dynamic modulus and phase angles of asphalt mixtures could be well-predicted from the component properties of those mixtures. It is anticipated that the techniques developed in this study can be used to simulate full scale pavements when the computation power is available.

## 12.2. Introduction

Generally, three kinds of approaches have been used to understand mechanical behaviors within the asphalt mixture: experimental observation, analytical approach, and numerical modeling. Experimental observation is a direct and persuasive method, but the results are dependent on the boundary conditions which may include specimen size, geometry, and characteristics of the testing equipments. Analytical methods may provide accurate and useful benchmark solutions. However, those solutions are limited due to relatively simple boundary conditions and the highly simplified material properties. Numerical methods, such as the finite element method (FEM) and the discrete element method (DEM), can be applied to extend analytical methods for solving more complex boundary conditions and material characteristics. Therefore, many researchers have conducted their studies with FEM and DEM over the past decades. When compared with FEM, DEM was chosen in this study on the basis of the following reasons: 1) With FEM, expertise is required to address the discontinuities within the asphalt concrete, such as interfaces between aggregate particles and the asphalt matrix. Therefore, even though FEM can model discontinuities, it may require extra effort. DEM, however, can automatically satisfy

---

<sup>11</sup>Full text reprinted with permission from Hermès-Lavoisier: “Three-dimensional Discrete Element Simulation of Asphalt Concrete Subjected to Haversine Loading: An Application of the Frequency-Temperature Superposition Technique” by Zhanping You and Yu Liu, 2010, International Journal of Road and Pavement Design, Vol. 11, Issue 2, pp. 273-290, Copyright © 2010, RMPD. See Copyright clearance in Appendix A.

discontinuity at the interfaces (Kim 2007). 2) DEM uses a class of dynamically driven computational schemes which are built on the motion of contacting small elements. Therefore, even with simplified contact laws and a limited number of material parameters, discrete element (DE) modeling is able to simulate sophisticated material responses, such as larger strains, damage, and fracture. At least three kinds of models were developed with DEM: the elastic, viscoelastic, and bilinear cohesive models. In an elastic model, both aggregate and asphalt sand mastic (asphalt binder, fines, and fine aggregates) phases are simulated with elastic contact models. Even though an elastic model is unable to characterize material viscous behaviors, it can predict the stiffness of an asphalt mixture from its components as demonstrated in previous studies (Buttlar and You 2001; You et al. 2008c; You and Buttlar 2006). The major advantage of a viscoelastic model is that it can consider both elastic and viscous behaviors in asphalt concrete. The downfall is that it requires a longer time for calculation (Buttlar and You 2001; You et al. 2008c; You and Buttlar 2006). To shorten the computation time for a viscoelastic model, techniques have been developed in recent studies (Abbas et al. 2007; Liu et al. 2009). The studies found that computation time of viscoelastic DE simulation for asphalt mastic and mixtures can be significantly reduced with the developed techniques. For example, modeling work which took several months or years only takes a few hours or less by using the frequency-temperature superposition principle method (Liu and You 2011a; Liu et al. 2008). Additionally, the bilinear cohesive model was developed to model asphalt concrete fracture propagation (Liu and You 2011a).

**Table 12.1**  
**An incomplete summary of methodologies used in the studies with DEM**

		Elastic	Viscoelastic	Bilinear Cohesive
Idealized	2D	None	None	None
	3D	(Kim 2007; Kim et al. 2008)	(Collop et al. 2006a; Liu and You 2009; You et al. 2008b)	Not Available
Image-based	2D	(Collop et al. 2007; Collop et al. 2006a)	(Adhikari and You 2008; Buttlar and You 2001; You 2003; You et al. 2008d; You and Buttlar 2006)	(Abbas et al. 2007)
	3D	(Kim et al. 2008; Liu et al. 2009)	This paper	Not Available
Randomly-created	2D	(Adhikari and You 2008; Fu et al. 2008; Wang et al. 2007a; You et al. 2008c; You et al. 2008d)	(You et al. 2008b)	Not Available
	3D	(Liu and You 2008; 2011a; Liu et al. 2008)	(You et al. 2008b)	Not Available

It should be noted that a bilinear cohesive model could be integrated into elastic or viscoelastic models, but it was separated to distinguish itself from basic elastic or viscoelastic models. The reason is that the bilinear cohesive model has its own DE contact models (Kim 2007; Kim et al. 2008).

In terms of geometry, three kinds of models were developed to rebuild the microstructure of asphalt concrete: the idealized model, randomly-created irregular shape model, and image-based model. In an idealized model, aggregates were simulated with uniform balls. Therefore, many geometric properties, such as aggregate shape, gradations, orientations and angularities could not be characterized (Liu and You 2011a; Liu et al. 2008; Liu and You 2009). An image-based model is built from real images of an asphalt mixture. With current imaging techniques, such as X-ray Computed Tomography (X-ray CT), most of the real micro-structural features of asphalt concrete may be characterized (Collop et al. 2007). The main disadvantage is its laboratory dependency, including preparing the specimen and X-ray scanning. The randomly-created irregular shape model is a geometry model combining the idealized model and the image-based model: 1) it can represent some features of asphalt concrete micro-structure, such as aggregate shapes, orientations, angularities, gradation, distribution, and air voids; 2) it is laboratory independent.

A summary of the methodologies used in some previous studies is listed in Table 12.1. Many studies have been completed with elastic modeling. An advantage of elastic DE modeling is that it is less time-consuming. A disadvantage, however, is that it is unable to directly simulate time-dependent behaviors of asphalt materials. Quite the reverse is true for viscoelastic modeling. Although several researchers employed viscoelastic modeling in their studies, most of their works were done on the basis of 2D models. Many studies have been done to rebuild asphalt concrete microstructures. It was believed that a 3D image-based model could more accurately represent the real mix microstructure. Evidently, it is necessary to conduct DE viscoelastic modeling with realistic 3D microstructure-based models for better understanding of asphalt concrete mixtures. But few research efforts have been reported in this direction since it is too time-consuming to conduct such a DE modeling. This paper reports the authors' recent progress with the viscoelastic simulation of a 3D microstructure-based model.

### **12.3. Objectives and Scopes**

The objectives of this study are: 1) to provide three-dimensional (3D) discrete element (DE) models of asphalt mixtures under dynamic loads, and 2) to verify the DE modeling results by comparing them with experimental measurement. To achieve those two objectives, the 3D microstructure of an asphalt mixture was rebuilt from X-ray CT images, and the frequency-temperature superposition principle was applied to shorten the computation time. Uniaxial dynamic modulus testing results of asphalt sand mastic were utilized as viscoelastic parameters for the 3D DE modeling, while experimental testing results of an asphalt mixture were employed to verify the DE prediction. Details are provided in the subsequent sections.



## 12.4. Preliminary Studies

### 12.4.1. Reconstruction of Asphalt Mixture Microstructure

Researchers believed that larger sizes of coarse aggregate particles act as individual components while smaller sizes of fine aggregate particles, asphalt binder, and air voids act as an integrated component to interact with the coarse aggregate (Abbas et al. 2007; Masad 2004; Wang et al. 2007a; You and Adhikari 2008). Therefore, mineral aggregate can be divided into two parts: coarse aggregate particles and fine aggregate particles. The integrated component of asphalt binder and fine aggregate is called asphalt sand mastic in this study. 2.36 mm is selected as the cut-off size in this study, based on the following reasons: 1) The smallest coarse aggregate particle (2.36mm) can be simulated with the discrete elements whose radii are 0.5mm. 2) The maximum size of fine aggregate particles in the asphalt sand mastic is 2.36mm. The digital image processing technique has been developed to reconstruct the asphalt concrete microstructure in many studies (Li and Metcalf 2005b) using the X-ray CT imaging technique. To characterize the X-ray CT images of asphalt concrete, many studies have been done (Masad et al. 2005b; Wang et al. 2004; You et al. 2009).

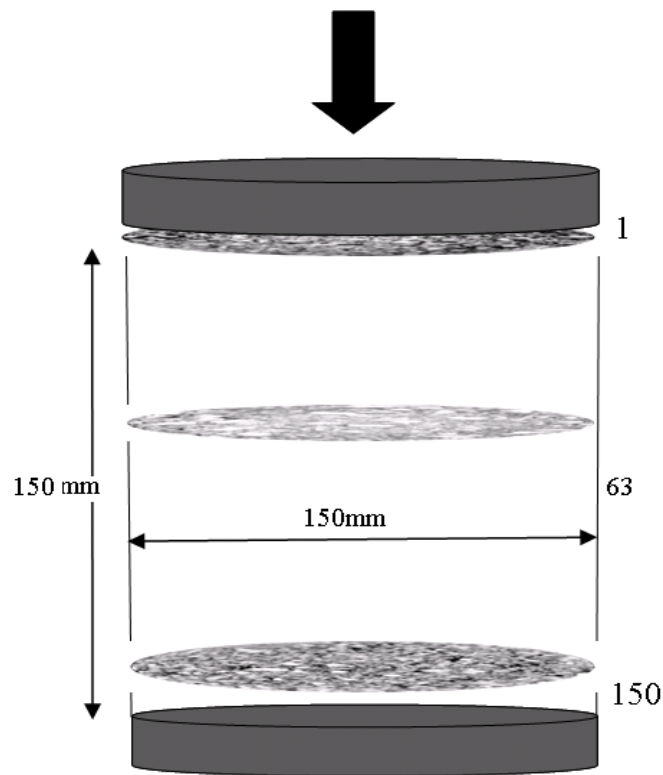


Figure 12.1. Three-dimensional visualization of X-ray Computed Tomography images

As shown in Figure 12.1, a total of 150 X-ray CT images were combined to reconstruct the 3D microstructure of an asphalt mixture specimen whose height and diameter were each 150mm. During the image processing, gray images were transferred into coarse aggregate (larger than 2.36mm), asphalt sand mastic, and air voids according to threshold segmenting of each representative volume element (RVE). More details on the imaging processing were provided in the preliminary study (Adhikari and You 2008; Masad et al. 2005b; Wang et al. 2004; You and Adhikari 2008).

After digital image processing, the coordinates of aggregates, mastic, and air voids were captured separately. Then, the microstructure of the asphalt mixture was built using balls or spheres which were marked for identification. In this way, aggregates, asphalt sand mastic, and air voids can be distinguished in this subsequent process. In the DEM simulation, uniaxial sinusoidal loading was applied as shown in the Figure 12.1. The top and bottom loading platens were used to apply the uniaxial loads, where the dynamic loading was applied on the top platen while the bottom platen remained fixed.

#### **12.4.2. Time-dependent Constitutive Model**

A viscoelastic constitutive model has been developed in the preliminary study (You et al. 2009). There were four types of contact interactions within the digital specimen, including contacts within asphalt mastic, within an aggregate, between an aggregate and mastic, and between two adjacent aggregates. At each contact within mastic or between aggregate and mastic, Burger's model was applied to characterize the relationship between the contact forces and relative displacements. At each contact between aggregates or within an aggregate, an elastic contact stiffness model was employed to relate the contact forces and relative displacements. Additionally, the strength property at each contact was addressed through assigning the slip model and a bonding model. In other words, the constitutive relation at each contact is composed of three contact models: the stiffness model, slip model, and bonding model. The stiffness model is used to relate the relative displacement and the contact force, and the slip model and the bonding models are used to address the strength properties at a contact. The DE model parameters are the properties at each contact which are out of reach of regular laboratory tests. Therefore, techniques are needed to relate the laboratory measurement to the DE model parameters. This kind of technique has been developed in the preliminary study. On the basis of this preliminary study, the input parameters can be calibrated from the laboratory measurement of the ingredients of the asphalt concrete, asphalt sand mastic and aggregates. As demonstrated in this preliminary study, the calibration process was conducted by comparing predicted values with the experimental data. Therefore, the input parameters for the time-dependent DE model were calibrated from the laboratory measurements. The input parameters include Burger's model parameters calculated from the dynamic moduli of sand mastic and Young's modulus of aggregates. Methodologies have been developed to determine Burger's model parameters from dynamic modulus testing data in the previous studies (Liu et al. 2009). Additional parameters include frictions and bonding strengths at contacts of discrete elements. Since the focus of this study is simulation of undamaged asphalt mixtures, larger values are given to those

parameters. In future studies, more realistic values of those parameters should be given for larger deformation or cracking problems.

### 12.4.3. Experimental Measurement

Uniaxial dynamic modulus tests of asphalt sand mastic and asphalt concrete were conducted on the Universal Testing Machine (UTM-100) according to AASHTO TP62-03. Superpave Performance Grade (PG) 64-28 binder was used and the nominal maximum aggregate size was 19mm for the asphalt concrete. The Superpave gyratory compactor was used to prepare asphalt concrete specimens with an asphalt content of 5.6% and a target air void level of 4.4%. The asphalt sand mastic consisted of fine aggregates (less than 2.36mm in diameter) and fines dispersed throughout the asphalt binder. The asphalt sand mastic was compacted on the cylindrical mold which had a height of 190mm and diameter of 76mm. The asphalt content in the asphalt sand mastic was 10.3% by weight and the air void level was assumed to be zero. The detailed procedure for uniaxial dynamic modulus tests of asphalt sand mastic and mixture were provided in previous studies (Liu et al. 2009; Liu and You 2008). The uniaxial dynamic modulus tests of asphalt sand mastic and asphalt mixture were conducted under the same conditions: four temperatures of -5, 4, 13, and 21°C and four frequencies of 1, 5, 10, and 25Hz. The experimental data of the asphalt sand mastic was utilized to determine the Burger's model parameters as inputs of the DE simulation. A previous study provides a detailed procedure for determining Burger's model parameters by using dynamic modulus testing data (Adhikari 2008; Liu et al. 2009; Liu and You 2011a; Liu et al. 2010). Experimental data of the asphalt mixture was used to verify the DE modeling results in this study.

### 12.4.4. Acceleration Techniques for DE modeling

In order to reduce the computation time, a technique was developed on the basis of frequency-temperature superposition from the previous study (Liu and You 2008). According to this previous study, the real (physical) loading frequency ( $\omega_1$ ) was amplified to a virtual (desired) frequency ( $\omega_2$ ). Then, in the subsequent process, the amplified frequency ( $\omega_2$ ) was used in the DE modeling to reduce the required computation time. To be equivalent, the material properties under the real temperature,  $T_1$ , should be modified into those under the desired temperature,  $T_2$ . Consequently, the Burger's model parameters (micro parameters in DEM) of asphalt sand mastic at regular frequencies were modified from  $\eta(T_1)$  to  $\eta(T_2)$  on the basis of frequency-temperature superposition. Equation 12.1 may help to clarify the frequency-temperature principle:

$$E(\omega_1, \eta_m(T_1), \eta_k(T_1)) = E(\omega_2, \eta_m(T_2), \eta_k(T_2)) \quad 12.1$$

Where:

$E$  = asphalt sand mastic properties, such as dynamic modulus or phase angle

$\omega_1, \omega_2$  = regular and amplified angular frequency

$T_1, T_2$  = Temperature before and after amplification of frequency

$\eta_m, \eta_k$  = Burger's model parameters

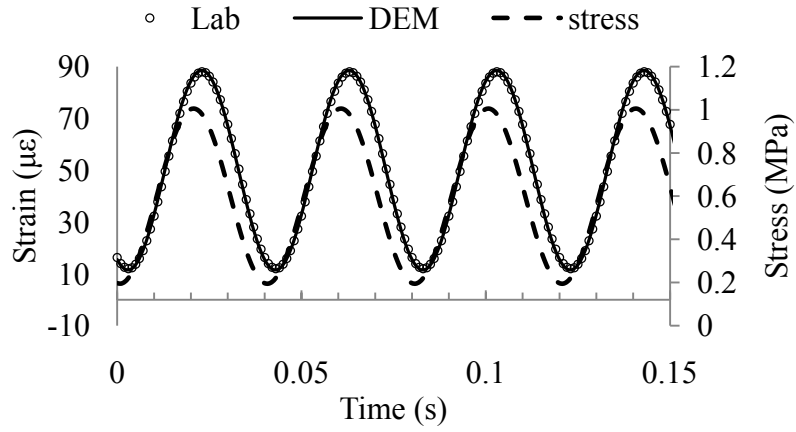
According to the previous study, the computation time of viscoelastic DE simulation of mixtures could be significantly reduced. For example, if the simulation was conducted using the traditional three-dimensional DE model under  $T_1=0^\circ\text{C}$ ,  $\omega_1=6.28$  radians per second,  $\eta_1=34.9\text{GP.s}$ ,  $\eta_2=2.0\text{GP.s}$ , it would take around three months to simulate a single cyclic load. When applying frequency-temperature superposition, however, the loading frequency can be amplified 1000 times, while mastic viscosities are reduced 1000 times. As a result,  $\omega_1=6280$  radians per second,  $\eta_1=0.0349\text{GP.s}$ , and  $\eta_2=0.002\text{GP.s}$ . The computation time is then reduced from three months to 2.16 hours. It should be noted that it is unnecessary to calculate the value of  $T_2$  which is represented by viscosities and not involved in the whole process.

## **12.5. Three-dimensional Discrete Element Modeling**

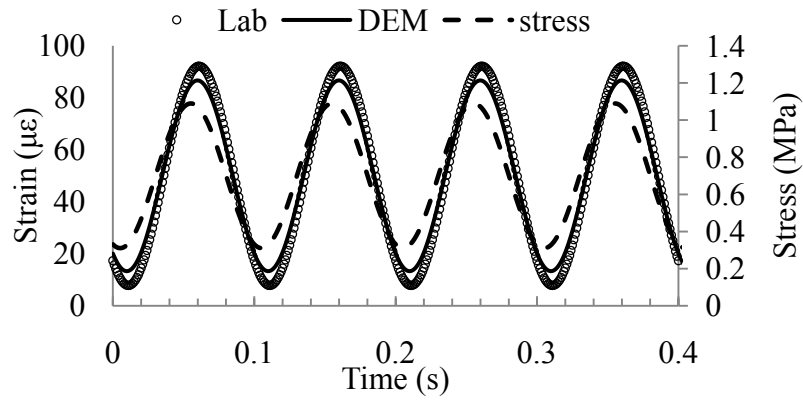
As mentioned above, the digital specimen of the asphalt mixture was prepared from X-ray CT images. The digital specimen is composed of 408,724 discrete elements and its height and diameter are 75mm and 50mm, respectively. Particle Flow Code in Three Dimensional (PFC3D) version 4.0 was used to run the DE modeling under uniaxial Haversine loads. Dynamic modulus tests with temperatures of -5, 4, 13, and  $21^\circ\text{C}$  were simulated. To decrease computation time, laboratory testing frequencies of 1, 5, 10, and 25Hz were multiplied by 5,000, 1,000, 2,500, and 1,000, respectively. In other words, 5,000, 5,000, 25,000, and 25,000Hz were used in simulation of dynamic modulus tests whose laboratory loading frequencies were 1, 5, 10, and 25Hz. Details about selection of the amplified frequencies will be provided in the next section of this paper.

### **12.5.1. Strain Responses under Dynamic Loading**

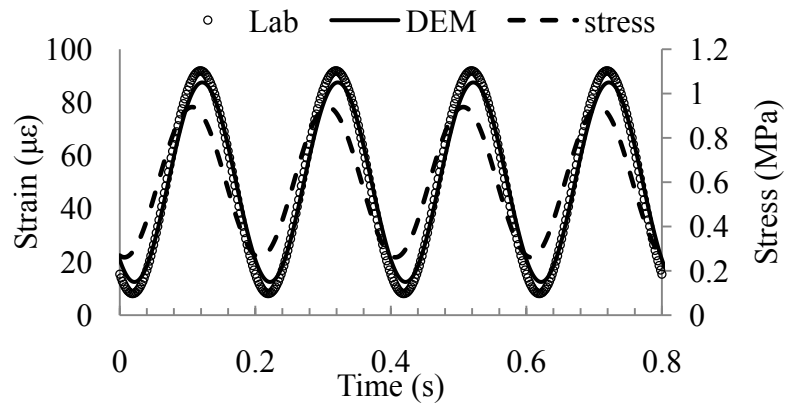
The laboratory measurement and DE prediction strain responses were compared with the same stress input. Since the loading frequencies were amplified in the DE simulation, strain responses of the DE simulation were reduced according to their corresponding laboratory testing frequencies. Then, both the reduced DE modeling strain responses and the laboratory testing strain responses are shown for  $13^\circ\text{C}$  in Figure 12.2. It was observed that the axial strain curves from DEM lagged slightly behind those from the laboratory tests, while their peaks were slightly lower than those from the laboratory tests. From the strain curves in Figure 12.2, the relative differences of the DEM prediction and the laboratory measurement were calculated in terms of strain response. The results revealed that the relative differences varied from 7.6% to 17.8%.



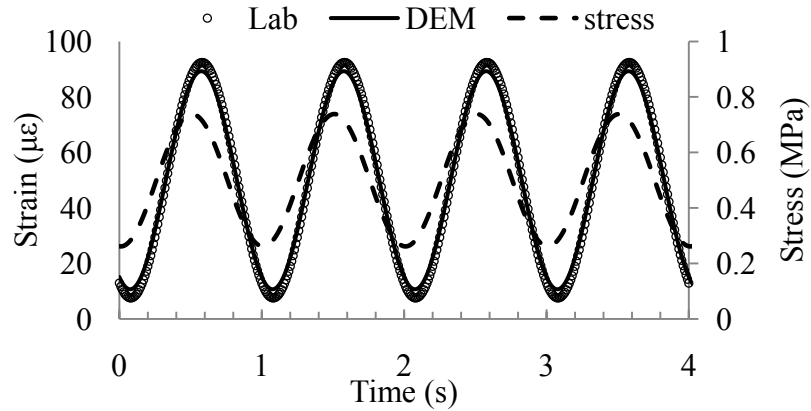
(a) 25Hz



(b) 10Hz



(c) 5Hz



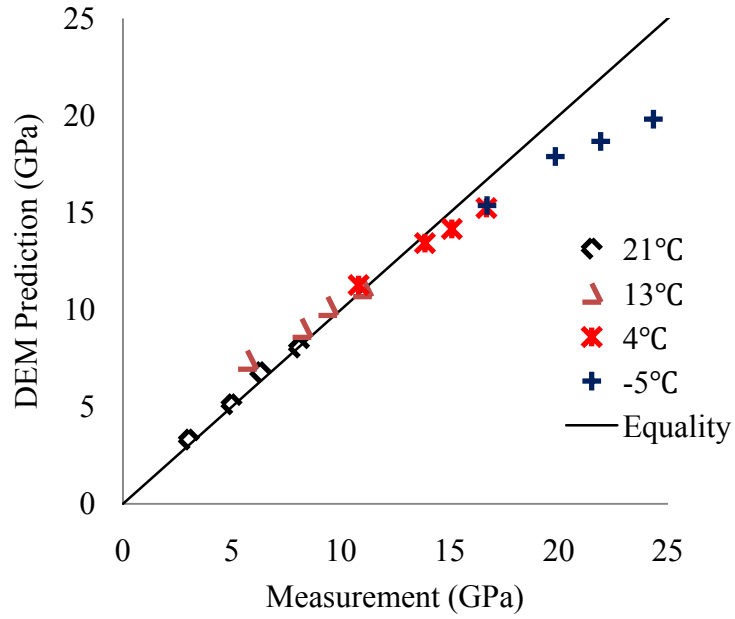
(d) 1Hz

**Figure 12.2. Strain responses of laboratory testing and DE modeling at 13°C (under an amplified frequency of 25000Hz)**

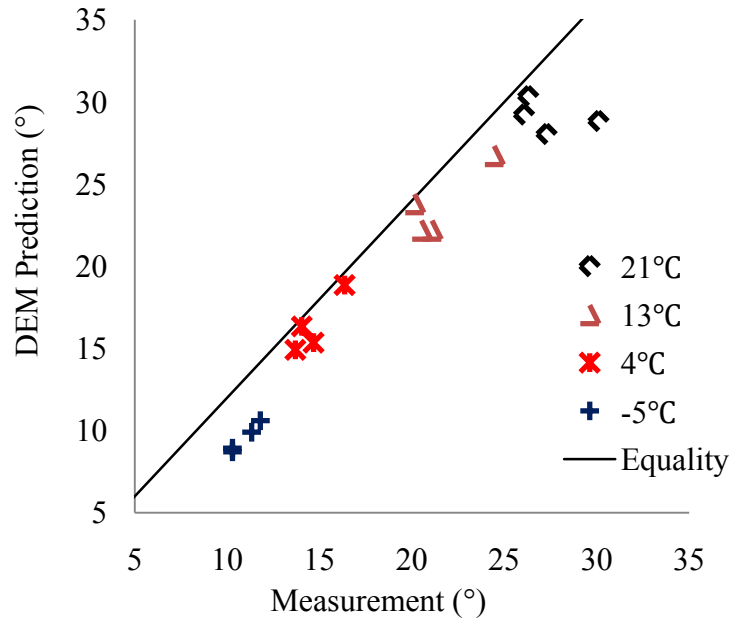
### 12.5.2. DE Prediction of Dynamic Modulus and Phase Angle

The dynamic modulus and phase angles were calculated from the recorded stress and strain histories during DE simulation. Figure 12.3 shows the comparison between the DE prediction and laboratory measurement in terms of dynamic modulus and phase angles. Both the dynamic moduli and phase angles predicted from DE simulation for each testing temperature are very close to the measurements for all the loading frequencies and testing temperatures. The average relative differences for the dynamic moduli and phase angles were 0.26% and 3%, respectively. Even though some individual relative differences were larger than 10%, most of them were less.

It is clear from Figure 12.3a that the predicted mixture dynamic moduli at -5°C are relatively lower than the laboratory measurements for that temperature. It may also be observed that the predicted mixture dynamic moduli for the other temperatures are nearly the same as the laboratory measurements. This could be attributed to the following two reasons: 1) the accuracies of dynamic modulus tests varied at different temperatures. Especially at a lower temperature, asphalt materials exhibit less time-dependent behaviors. 2) The DE simulation was conducted under the amplified frequencies instead of the regular frequencies. The details about the effects of amplified frequencies are provided in the subsequent section.



(a) Dynamic modulus



(b) Phase angle

**Figure 12.3. Dynamic Modulus and Phase Angle comparison between 3D prediction and the measurement (under an amplified frequency of 25000Hz)**

## **12.6. Sensitivity and Effects of DE Modeling under Amplified Frequencies**

### **12.6.1. Sensitivity Analysis of DE Modeling under Amplified Frequencies**

Under quasi-static conditions, mass inertia of viscoelastic materials can be ignored. The dynamic modulus testing conditions (loading frequencies ranging from 0.1 to 25Hz) can be considered as the quasi-static conditions. Therefore, under frequencies from 0.1 to 25Hz, the effects of mass inertia of asphalt and aggregates can be ignored, but these effects have to be taken into account when the frequencies are higher; the higher the loading frequency, the more the inertia affects the DEM simulation results. Use of high-frequency versus low-frequency dynamic loading may exaggerate the effects of mass inertia. Therefore, it is necessary to analyze sensitivity of DE modeling under amplified frequencies. Figure 12.4 shows results from sensitivity analysis of DE modeling at a temperature of 21°C. To conduct the sensitivity analysis, laboratory loading frequencies of 1, 5, 10, and 25Hz were amplified by different multiples. For example, three multiples of 100, 500, and 1,000 were given to the laboratory testing frequency of 25Hz. Thus, amplified frequencies of 2,500, 12,500, and 25,000Hz were used to simulate the dynamic modulus test for a given frequency of 25Hz. Figure 12.4 demonstrates that the predicted dynamic moduli increased as the amplified frequencies increased, even though they were expected to be constant. This is especially true for the frequencies of 1 and 5Hz.

Figure 12.5 shows the comparison of the predicted dynamic moduli with those from laboratory measurements. The curve “Predicted-high” was obtained from the DE modeling under high amplified frequencies of 25,000Hz. The curve “Predicted-low” was from the DE modeling under low amplified frequencies of 5,000, 5,000, 2,500, and 2,500Hz for the laboratory testing frequencies of 1, 5, 10, and 25Hz. It was discovered that dynamic moduli were over predicted with amplified frequencies. The prediction values were closer to the measurement at the low amplified frequencies.

Through sensitivity analysis, the aim is to determine reasonable amplified frequencies which could be used in the DE modeling. As discussed previously, a lower amplified frequency results in a better prediction but consumes more computation time. In this study, a four-step procedure was proposed to select a reasonable amplified frequency on the basis of the following two concerns: 1) to greatly reduce computation time; 2) to achieve reasonable accuracy. As shown in Figure 12.6, the four-step procedure is described as:

Step 1: a high amplified frequency and a low amplified frequency are determined. If the laboratory loading frequency is 25Hz, the 3D DE modeling will take around two years to complete, which is obviously too long. But several weeks may be acceptable even though it is still a long computation time. To reduce the computation time from around two years to several weeks, one could choose 2,500Hz instead of 25Hz to conduct the 3D DE modeling. If a computation time of several hours is desired, one could further increase the amplified frequency from 2,500 to 25,000Hz. The low and high amplified frequencies are 2,500Hz and 25,000Hz, respectively.



Step 2: a comparative study is conducted on the predicted dynamic moduli incorporating the low and high amplified loading frequencies. The relative difference between the predicted moduli is expressed as

$$\alpha = \frac{(E_h - E_l)}{E_h} \times 100\% \quad 12.2$$

Where:

$E_h$  = Predicted dynamic modulus under the high amplified frequency

$E_l$  = Predicted dynamic modulus under the low amplified frequency

$\alpha$  = Relative difference between  $E_h$  and  $E_l$

Step 3: If  $\alpha$  is larger than 5%, a lower value will be assigned to the high amplified frequency and step 2 will have to be repeated. It should be noted that the lower value of the high amplified frequency is larger than the low amplified frequency. For example, 12,500Hz may be selected to replace the high amplified frequency of 25,000Hz.

Step 4: The previous two steps are repeated till  $\alpha$  is less than 5%. Then, the final trial of the high amplified frequency is accepted as the DE modeling frequency. As shown in Figure 12.4, for curves of “25Hz” and “10Hz”, results at the three trial amplified frequencies are very close, therefore, the highest amplified frequency of 25,000Hz were selected as the loading frequency in the DE modeling of dynamic tests at 25Hz and 10Hz. For curves of “5Hz” and “1Hz”,  $\alpha$  is larger than 5% for each trial high amplified frequency. In this case, the low amplified frequency of 5,000Hz was selected as the loading frequency in the DE modeling of dynamic tests at 5Hz and 1Hz.

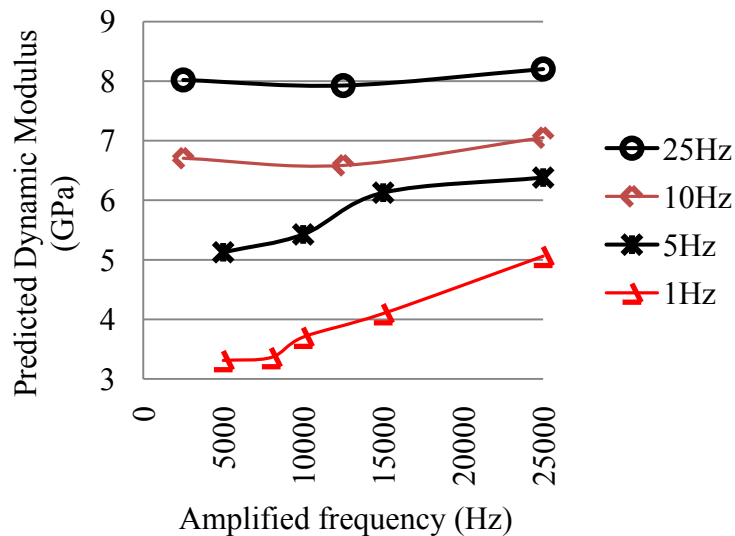


Figure 12.4. Predicted dynamic modulus vs. amplified frequencies at 21°C

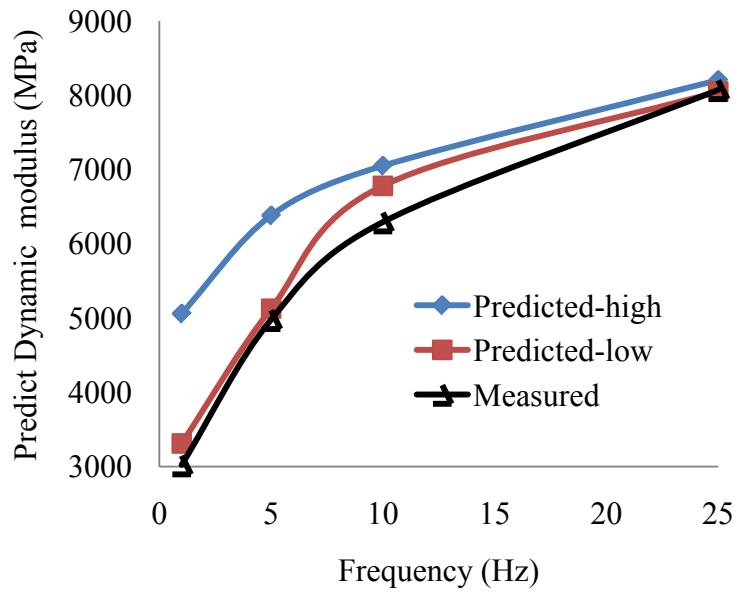


Figure 12.5. Comparison of predicted dynamic moduli with laboratory values at 21°C

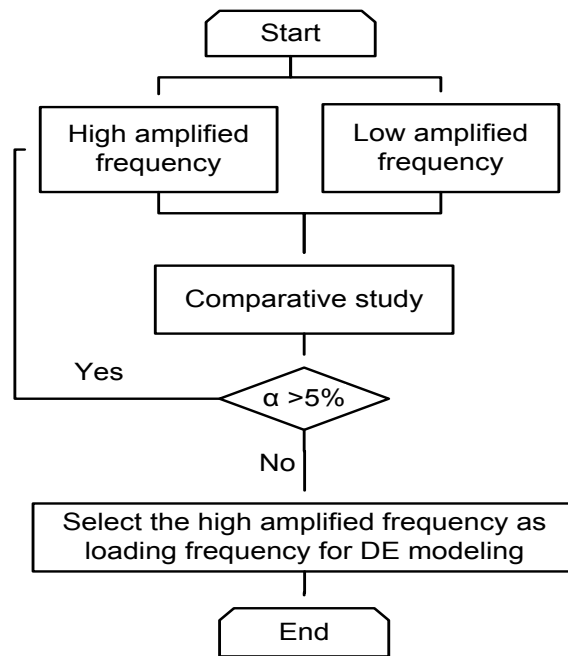


Figure 12.6. Sensitivity analysis of DE modeling under amplified frequencies

### 12.6.2. Computation Time of 3D DE Modeling

The discrete element method is a dynamic iterative method that works by successively solving Newton’s second law (law of moment) for each particle (discrete element) and

applying the force-displacement law for each contact between particles. The equations of motion are integrated in PFC3D using a centered finite-difference scheme. The computed solution produced by the centered finite-difference scheme will remain stable only if the time-step does not exceed the critical time-step that is related to the minimum Eigen-period of the total system (Liu and You 2011a). Usually, thousands of iterative steps are needed to achieve the final results. The displacements, velocities, and contact-forces of particles are updated after each iterative step. The time-step,  $t_{del}$ , is the true time per iterative step. The physical time ( $t$ ) for a given project is the accumulative physical time after many iterative steps as expressed in Equation 12.3.

$$t_{physic} = t_{del} \times N_{step} \quad 12.3$$

Where  $t_{physic}$  is the physical time and  $N_{step}$  is the number of the iterative steps.

Computation time is another key concept in DE modeling, which is the accumulative time of DE modeling computation on a special computer. Different from the physical time coded for the specified simulation time, the computation time is dependent on the number of discrete elements in a DE model and the computer performance. DE modeling with larger models and a slower computer consumes more time and vice versa. The real physical time, however, is independent of these factors. For example, the physical time of DE modeling at 10Hz is 0.1 seconds for each loading period. The computation time can be calculated using Equation 12.4:

$$t_{comp} = V_{comp} \times N_{step} \quad 12.4$$

Where  $t_{comp}$  is the computation time and  $V_{comp}$  is the computation speed of a given computer which is defined as the time per iterative step.

**Table 12.2**  
**Computational time required for DE modeling using laboratory frequencies**

Laboratory frequency (Hz)	Physical time ( $t_{physic}$ ) (s)	Time-step ( $t_{del}$ ) ( $10^{-8}$ s/step)	Iterative steps ( $N_{step}$ ) ( $10^{-6}$ )	Computation speed ( $V_{comp}$ ) (s/step)	Time consumed ( $t_{comp}$ ) (year)
25	0.20	3.28	6.10	8.72	1.69
10	0.50	2.96	16.89	8.72	4.67
5	1.00	2.56	39.06	8.72	10.80
1	5.00	2.33	214.59	8.72	59.34

In this research study, a personal computer (2.66GHz, 8MB L2 Cache, Intel® Core™ 2 Quad Extreme Processor) is utilized. The computation speed,  $V_{comp}$ , is 8.7 seconds per iterative step for the 3D DE model with 408,724 elements herein. The time-steps were automatically determined, which varied from  $2.23 \times 10^{-8}$  to  $3.28 \times 10^{-8}$  seconds per iterative step. With the traditional methods, DE modeling is conducted to simulate the same frequencies used in the laboratory. The frequencies range from 1 to 25Hz, and therefore, the time per loading period ranges from 0.04 to 1s. Suppose five loading periods are needed to obtain reliable results. Then,  $t_{physic}$  in Equation 12.3 should be from 0.2 to 5s. Next, the  $N_{step}$  is calculated in Equation 12.3 and the computation times are calculated by substituting  $N_{step}$  and  $V_{comp}$ , into Equation 12.4. The final results are listed in Table 12.2. It was found that the computation times range from 1.69 to 59.34 years for 3D modeling with the traditional method. Instead of the traditional method, the frequency-temperature superposition principle was used in this study to accelerate the DE modeling. Based on the frequency-temperature superposition, amplifying the regular frequencies by 1000 would reduce the computation time 1000 times. Therefore, using frequency-temperature superposition, the computation times could be from 0.00169 years (0.62 days) to 0.05934 years (22 days). As discussed in the previous section, the laboratory testing frequency of 1Hz could be amplified up to 5,000Hz. Thus, the maximum computation time of a DE modeling was 4.4 days in this study.

## 12.7. Summary and Conclusions

This study has provided a 3D viscoelastic DE modeling of an asphalt mixture under cyclic loads, where the dynamic modulus and phase angles of the asphalt mixture were predicted through inputting mechanical properties of its component materials. An image processing technique was used to rebuild the asphalt mixture structure from X-ray CT images, while Burger's model was used to characterize the time-dependent behaviors within the digital sample. The frequency-temperature superposition principle was applied to accelerate the computation time of the time-dependent modeling. Through this study, the following findings were observed:

- 1) Both dynamic moduli and phase angles were well-predicted under various frequencies and temperatures. The frequencies ranged from 1 to 25Hz, while temperatures ranged from  $-5^{\circ}\text{C}$  to  $21^{\circ}\text{C}$ . The average relative differences for dynamic moduli and phase angles from the measurement were 0.26 and 3%, respectively. Even though some individual predicted dynamic moduli and phase angles deviated from the measurement by more than 10%, most of the predicted results were very close to the measurements.
- 2) With frequency-temperature superposition, the DE modeling computation times were greatly reduced. Utilizing traditional methods, it took 1.69 to 59.34 years to complete 3D viscoelastic modeling of a dynamic modulus test. It was proven that the modeling could be completed within 4.4 days when applying frequency-temperature superposition.

In this study, the simulation of the asphalt concrete was based upon a small scale sample. With the developed methods as described in this paper, the simulation can be accelerated

significantly. It is anticipated that the techniques developed in this study can be used to simulate full scale pavements when the computation power is available.

## **12.8. Acknowledgments**

This material is based in part upon work supported by the National Science Foundation under grant 0701264. Any opinions, findings, and conclusions or recommendations expressed in this material are those of the author's and do not necessarily reflect the views of the National Science Foundation. The authors appreciate Dr. M. Emin Kutay for scanning the asphalt mixture specimens for the writers. The experimental work was completed in the Transportation Materials Research Center of Excellence at Michigan Technological University, which maintains the AASHTO Materials Reference Laboratory (AMRL) accreditation on asphalt and asphalt mixtures.

# Chapter 13. Discrete Element Simulation for Linking Aggregate Morphological Parameters to AC Creep Stiffness<sup>12</sup>

## 13.1. Abstract

Many studies have concluded that mineral aggregate properties such as sphericity and orientation play very important roles in determining asphalt concrete (AC) performance. Their observations of existing studies however, came from the combined effects of many factors such as air voids, aggregate gradations, asphalt binder properties, etc. The objective of this study is to investigate the isolated effects of aggregate sphericity and orientation angles on the creep stiffness of AC mixtures. Instead of using the traditional experiment-based methods, this study utilizes discrete element simulation of idealized AC mixtures. To build the AC microstructure, previously developed user-defined discrete element model was utilized; known as the rounded aggregate R model. The mechanical interactions in the digital specimens were simulated with the previously developed viscoelastic discrete element model. Through this study, it was observed that: 1) aggregate sphericity and orientation have significant impact on AC creep stiffness; 2) the effects of aggregate sphericity indices were correlated with that of aggregate orientation angles and vice versa.

## 13.2. Introduction

In a typical asphalt concrete (AC) mixture, mineral aggregate constitutes approximately 95% of the total weight and about 85% of the total volume. Due to its significant amount, mineral aggregate morphology characteristics, such as shape, fractured surface, texture, orientation, and size, were believed to have a dramatic influence on HMA performance and serviceability (Pan et al. 2005; 2006; Stakston et al. 2002). Through a comprehensive review of aggregate characteristics affecting pavement performance, researchers (Masad et al. 2005a) concluded that aggregate properties, such as shape, angularity, and texture play important roles in controlling the performance of HMA, hydraulic cement concrete mixtures, and unbound layers. Thus, a general agreement among worldwide research engineers has been achieved on the importance of aggregate characteristics in controlling mixture performances. Traditional mix design methods however, have focused on properties of the composite rather than the component materials (Leahy and McGennis 1999). Researchers in the Strategy Highway Research Program (SHRP) program realized the importance of constituent materials in AC mixtures, but their major target was the asphalt binder properties and their contributions to pavement performance. Instead of performing detailed investigations of aggregate contribution to pavement performance,

---

<sup>12</sup>Full text reprinted with permission from ASCE: “Discrete Element Simulation of Aggregate Sphericity and Orientation: An Approach to Improving the Understanding of Asphalt Concrete” by Yu Liu and Zhanping You, 2010, ICCTP 2010: Integrated Transportation Systems—Green, Intelligent, Reliable, Proceedings of the 10th International Conference of Chinese Transportation Professionals, pp. 3968-3976 Copyright © 2010, ASCE. See Copyright clearance in Appendix A

SHRP researchers surveyed pavement experts to determine which aggregate properties were most important. They then used the survey results to identify aggregate properties that needed to be drafted into the Superpave Specification System.

Even though mineral aggregate properties have not received enough emphasis in the practical mix design procedures, a considerable number of research studies have been done in investigating the effect of aggregates on mixture performances. Most of those studies were based on experimental tests. Experiment-based methods were direct and persuasive, but difficult to separate the desired impact factors from the others. As a result, observations from previous studies were sometimes conflicting. For example, researchers observed (Shklarsky and Livneh 1964) that crushed coarse aggregate did not significantly improve the asphalt mix properties. One researcher (Foster 1970) concluded that HMA mixtures containing crushed coarse aggregates showed no better performance than a mix with uncrushed aggregates. Researchers (Li and Kett 1967) concluded that flat and elongated particles could be permitted in a mixture without an adverse effect on its strength. Researchers (Huber et al. 1998) observed that: 1) the rate of rutting on a couch wheel tracker did not correlate well with the fine aggregate angularity (FAA); 2) rut depths measured on the asphalt pavement analyzer (APA) did not correlate well with the FAA; 3) dynamic modulus of mixtures measured on the Superpave shear tester did not vary with different FAA. However, researchers (Oduroh et al. 2000) argued that crushed coarse aggregate particles had a significant effect on HMA permanent deformation properties. Researchers (Asphalt-Institute 2001; Kandhal and Parker Jr 1998) found that flat or elongated particles are undesirable since they have a tendency to break during construction and under traffic loads. Researchers (Bennert et al. 2006) concluded that as the FAA increased, the APA rutting decreased. Researchers (Johnson et al. 2007) also observed that APA rutting resistance was significantly influenced by the aggregate blend FAA. Of course, there were other reasons for these conflicting findings. The authors believed that the major reason was the inability to isolate the effect of one aggregate characteristic from the others.

In recent decades, numerical models, such as discrete element (DE) and finite element (FE) models have been introduced to simulate AC mixtures (Buttlar and You 2001; Kose et al. 2000b; Liu et al. 2009; Meegoda and Chang 1994). The authors believed that either the FE or the DE models have the potential ability to isolate a desired aggregate factor from the other. Unfortunately, few existing studies have focused on this direction. The main objective of this study is to introduce an approach for analyzing the isolated effect of aggregate shape and orientation on the AC mixture creep stiffness. The aggregate shapes were represented by a sphericity (SP) index, which was defined according to the NCHRP Report 555 (Masad et al. 2007b). The aggregate orientation was defined with orientation angles, which were formed by rotating a standard axis-aligned ellipsoid around its three principal axes. A previously developed DE viscoelastic model was used to address the mechanical interactions within the specimens (Liu et al. 2009). The DE simulations of creep compliance tests were performed by inputting the Young's modulus of coarse aggregates and the Burger's model parameters of the asphalt sand mastic.

### 13.3. Discrete Element Models

To simulate the aggregate SP index and orientation angles, the recently developed user-defined model was utilized in this study. The model was named the DE R-Model, abbreviated form for the user-defined rounded aggregate model. The DE R-model was developed to highlight the effect of aggregate shapes and orientation angles (Liu and You 2011b), in which aggregate particles were simulated with ellipsoids whose orientation angles can be adjusted. Supposing  $a$ ,  $b$ , and  $c$  are the three radii of an ellipsoidal particle and  $a \geq b \geq c$ , the aggregate shape can be represented by defining the sphericity (SP) index (Masad et al. 2007b) below:

$$SP = \sqrt[3]{\frac{bc}{a^3}} \quad 13.1$$

Aggregate orientation was considered using three orientation angles:  $\alpha$ ,  $\beta$ , and  $\gamma$ . The three angles were defined by rotating the standard axis-aligned ellipsoid body around its three principal axes as shown in Figure

In this study, a total of 42 digital AC specimens were prepared. In order to highlight the two targeted aggregate characteristics, all the specimens had the same aggregate gradation, asphalt content, and air voids to highlight the two targeted aggregate characteristics. Furthermore, in order to avoid the combined effect from those two targeted characteristics, all the aggregate particles in each specimen have the same values of aggregate orientation angles and SP index. Figure 13.2 shows an example of the digital specimens.

The interactions in the digital specimens were addressed by employing the previously developed viscoelastic model (Liu et al. 2009). In the viscoelastic model, four contact models are used to describe the four interactions within an AC mixture. The four contact models are the Burger's model, the elastic contact-stiffness model, the contact-bond model, and the slip model, which are available in three-dimensional Particle Flow Code version 4.0 (PFC3D 4.0) (Itasca Consulting Group 2008b). The four interactions involved here are between an aggregate and the asphalt sand mastic, between two adjacent aggregate particles, within an individual aggregate particle, and within the asphalt sand mastic. The Burger's model and the elastic contact-stiffness model were the contact stiffness models for asphalt sand mastic and coarse aggregates, respectively, which were used to link the relative displacements and the contact forces at a contact. The other two contact models were used to characterize the strength properties at the contacts. The required mechanical inputs for the viscoelastic DE model included: the Young's modulus of coarse aggregates and the Burger's model parameters of asphalt sand mastic. Since the major goal of this study is to simulate aggregate shape and orientation, the same mechanical inputs were selected for the 42 digital specimens. Table 13.1 shows the mechanical inputs whose original experimental data was reported in the previous study (Dai and You 2007).



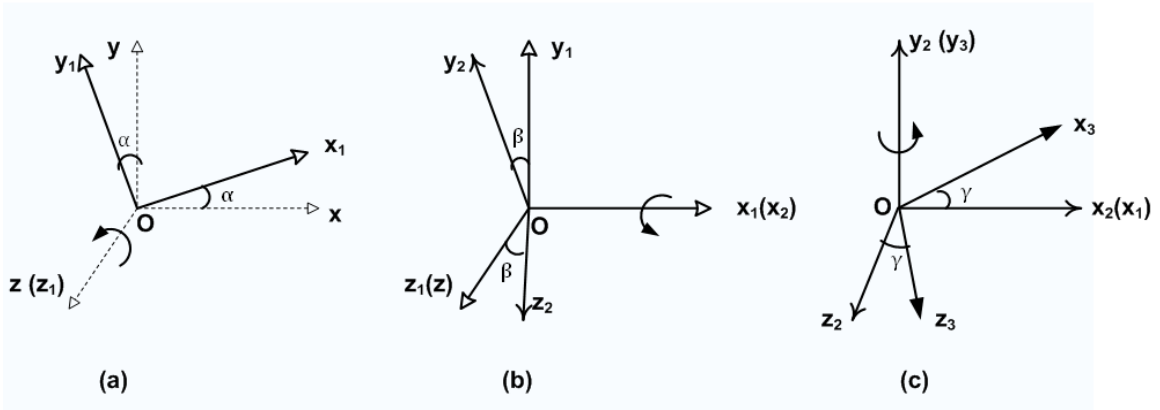


Figure 13.1 Definition of the three rotation angles:  $\alpha$ ,  $\beta$ , and  $\gamma$

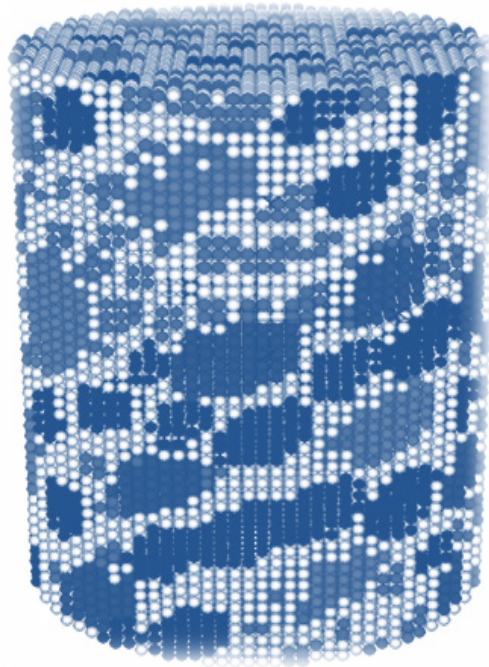


Figure 13.2 A DE R-model ( $SP=0.7$ ;  $\beta=0^\circ$ ,  $\gamma=0^\circ$ ,  $\alpha=30^\circ$ )

Table 13.1  
Inputs of the DE Viscoelastic Model Used In This Study

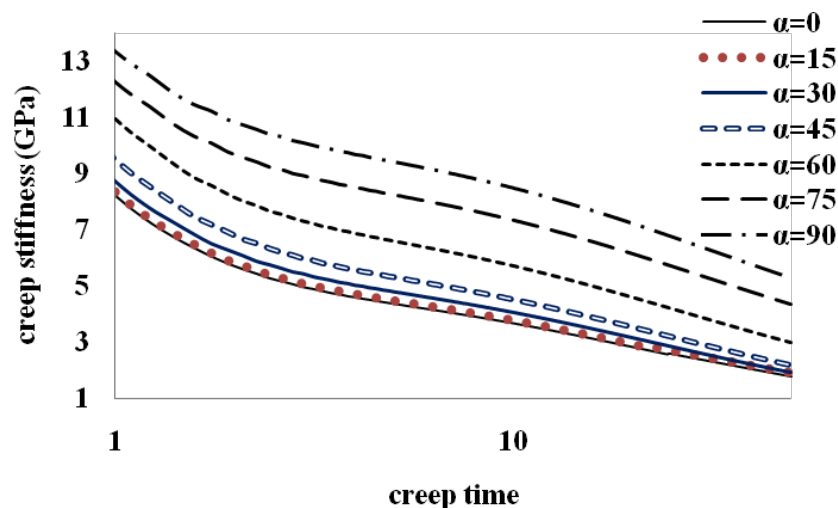
Aggregate	Young's modulus (GPa)			
	55.5			
Asphalt sand mastic	Burger's model parameters (GPa) at $0^\circ\text{C}$			
	$E_m$	$\eta_k$	$E_k$	$\eta_k$
	430.9	35.0	1.8	2.2

## 13.4. Creep Testing Simulation and Results

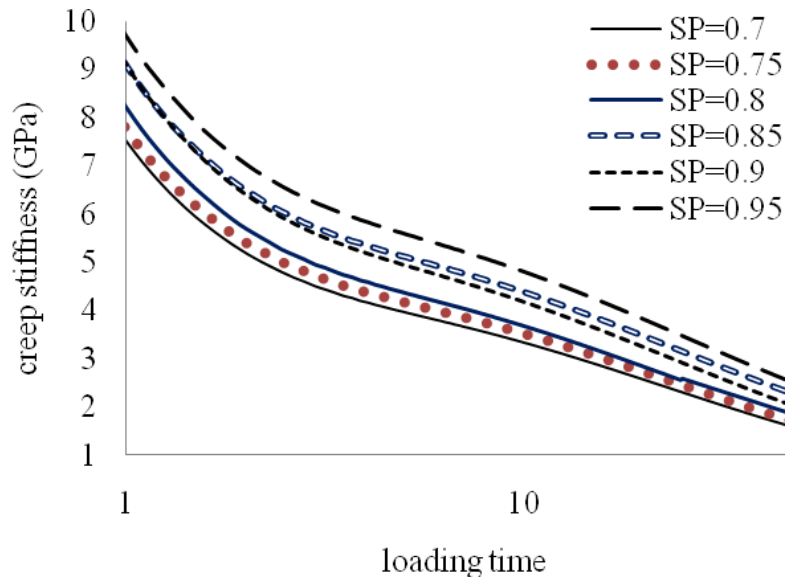
Creep compliance tests were simulated on the 42 digital specimens by applying uniaxial constant loads on the top end of each of them and with the bottom end fixed. The test duration was a maximum 50 seconds and the calculation of creep stiffness was recorded during the DE simulation. Some typical simulation results are shown in Figure 13.3.

Figure 13.3 (a) shows the typical results for the R-models with  $SP=0.8$  and  $\alpha=0\sim 90^\circ$ . Clearly, it could be concluded that: 1) creep stiffness significantly increased with  $\alpha$  values increasing; 2)  $\alpha=0^\circ$  and  $90^\circ$  are the lower and upper bounds of the creep stiffness. Similar conclusions were also reached for the other SP values ranging from 0.7 to 0.95. Coauthor Dai has conducted the isolated orientation effects of elliptical aggregates on the mixture damage behavior with a developed two-dimensional (2D) micromechanical finite element model (Dai and Sadd 2004). The findings from this study by using 3D micromechanical DE model have good agreements with the conclusions from 2D micromechanical FE simulations.

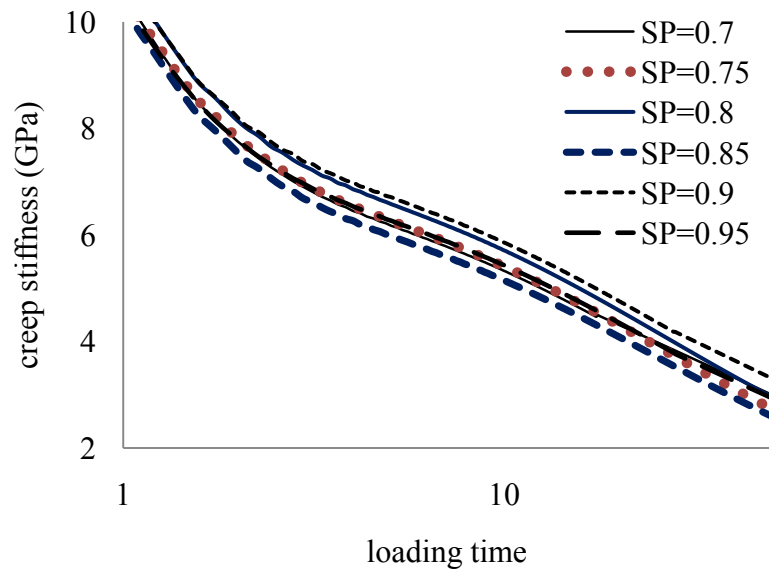
Figure 13.3(b), (c), and (d) show the typical outputs for the R-model with  $\alpha=0^\circ, 60^\circ, 90^\circ$ , and  $SP=0\sim 0.95$ . It was found that with the SP values increasing, the creep stiffness increased or decreased, which depended on the values of  $\alpha$  of the three observations: 1) when  $\alpha=0$ , creep stiffness increased with the SP values increasing; 2) when  $\alpha=90$ , creep stiffness decreased with the SP values increasing; 3) when  $\alpha=60$ , creep stiffness had received less influences from the SP values. It could also be concluded that 1) when  $\alpha<45$  or  $\alpha>60$ , SP values may have significant influence on the AC creep stiffness, while when  $45<\alpha<60$ , the SP values had insignificant impact on the AC creep stiffness; 2) when  $\alpha<45$ , creep stiffness increased with the SP values increasing; 3) when  $\alpha>60$ , creep stiffness decreased with the SP values increasing.



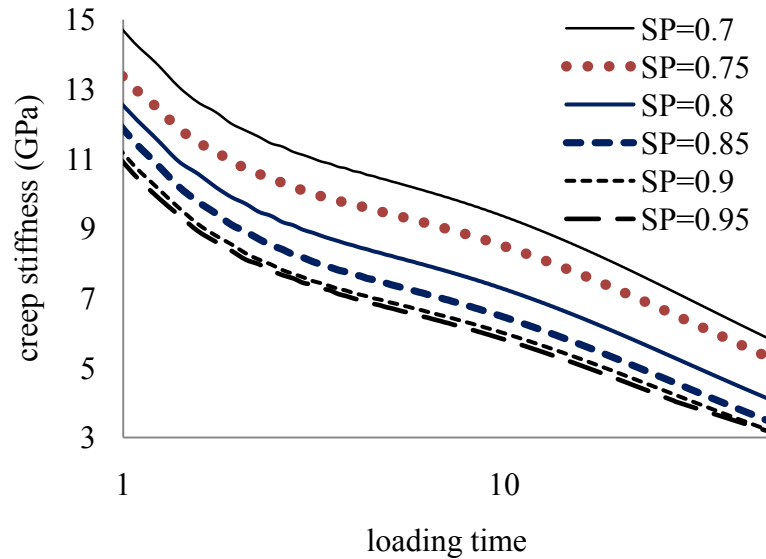
(a) R-models ( $SP=0.8$  and  $\alpha=0\sim 90^\circ$ )



(b) R-models (SP=0.7~0.95 and  $\alpha=0^\circ$ )



(c) R-models (SP=0.7~0.95 and  $\alpha=60^\circ$ )



(d) R-models (SP=0.7~0.95 and  $\alpha=90^\circ$ )

**Figure 13.3 Typical DE simulation results**

### 13.5. Conclusions

Although there has been a general understanding of aggregate effect on AC mixture performances, the major challenge of existing studies was how to isolate the effect of a specific aggregate characteristic from those of other impacting factors. This study presents a method to simulate creep tests of idealized HMA mixtures based on discrete element methods. A total of 42 idealized HMA specimens were specially built to model aggregate sphericity and orientation with simplified geometries. To minimize the influences from other factors, all the specimens had the same gradation, asphalt content, air voids, and mechanical inputs for the DE simulations. From this study, several interesting findings were observed as shown in the previous section in this paper:

- 1) Aggregate orientation angle ( $\alpha$ ) values significantly impacted the AC mixture creep stiffness. The AC creep stiffness increased with  $\alpha$  values increasing.  $\alpha=0^\circ$  and  $90^\circ$  were the lower and upper bounds of the AC stiffness. This conclusions agrees with an earlier micromechanical FE study (Dai and Sadd 2004).
- 2) Aggregate SP index values also greatly impacted the AC creep stiffness, but the stiffness values might increase or decrease, which was dependent on the  $\alpha$  values: a) when  $\alpha < 45$  or  $\alpha > 60$ , the SP values had significant influence on the AC creep stiffness, while when  $45 < \alpha < 60$ , the SP values had insignificant impact on the AC creep stiffness; b) when  $\alpha < 45$ , creep stiffness increased with the SP values increasing; c) when  $\alpha > 60$ , creep stiffness decreased with the SP values increasing.

As an initial attempt for investigating the isolated effect of aggregate properties using the discrete element method, the observations and conclusions in this study may be further

validated under more comprehensive aggregate packing, gradation, loading and temperature conditions.

### **13.6. Acknowledgements**

This material is based in part upon work supported by the National Science Foundation under grant 0701264. Any opinions, findings, and conclusions or recommendations expressed in this material are those of the authors and do not necessarily reflect the views of the National Science Foundation.

# Chapter 14. 3D Discrete Element Modeling for Stiffness of Sand Mastic versus Stiffness of Asphalt Binder<sup>13</sup>

## 14.1. Abstract

The main objective of this study is to predict and interpret the stiffness ratios of sand mastics to asphalt binder at a broad range of temperatures. Both fine and coarse sand mastics were studied using discrete element (DE) method. Twelve samples were prepared in this study, including six fine sand mastics, and six coarse sand mastics. The six fine sand mastics were prepared by blending fine sands (diameters ranging from 0.075mm to 0.3mm) with the 42.15%, 52.4%, 61.8%, 70.8%, 80.3%, 90% of asphalt binders by volume. The six coarse sand mastics were fabricated by blending coarse sands (diameters ranging from 0.3mm to 2.36mm) with the 42.15%, 52.4%, 61.8%, 70.8%, 80.3%, 90% of asphalt binders by volume. The previously developed DE model was employed to consider the interactions in the digital specimens of the 12 sand mastics. The DE simulations were conducted by varying the asphalt binder stiffness values with the constant stiffness value of sands. The stiffness ratios of mineral aggregates to asphalt binders were varied from 1 to  $1 \times 10^{10}$ . The outputs of the simulations were the predicted stiffness of the sand mastics. Finally, the outputs were analyzed to evaluate the impacts of asphalt binder stiffness values and volumetric fractions on the stiffness values of the asphalt sand mastics. Through this study, it was observed that 1) the DE simulation results agreed well with the micromechanical models; 2) the stiffness ratios of sand mastics to asphalt binders ranged from 1 to  $1.18 \times 10^9$  for fine sand mastics and from 1 to  $3.76 \times 10^8$  for coarse sand mastics.

## 14.2. Introduction

In the asphalt pavement industry, the current asphalt mix design methods are experience-based or empirical, which were developed based on the experimental testing results. In order to improve the fundamental understandings of asphalt concrete micromechanics, numerical methods, such as finite element (FE) method and discrete element (DE) method, have been developed, verified, and utilized to simulate asphalt concrete microstructure-based mechanics (Bahia et al. 1999; Buttlar and You 2001; Collop et al. 2006a; Kose et al. 2000a; Liu et al. 2009; Masad et al. 2007c). However, the majority of the models required asphalt sand mastic stiffness as inputs. The asphalt sand mastic herein was mixes of asphalt binders and mineral aggregates whose particle sizes ranged from less than 0.075mm up to 2.36mm. Currently, a few researchers (Buttlar and You 2001) measured asphalt sand mastic stiffness in the laboratory. The tests were performed

---

<sup>13</sup>Full text reprinted with permission from ASCE: “Stiffness of Sand Mastic versus Stiffness of Asphalt Binder using Three-dimensional Discrete Element Method” by Yu Liu, Zhanping You, and Qingli Dai, 2010, Pavements and Materials: Testing and Modeling in Multiple Length Scales, Proceedings of the Pavements and Materials: Characterization and Modeling Symposium at EMI 2010, pp: 54-65, Copyright © 2010, ASCE. See Copyright clearance in Appendix A.

at the relatively low temperatures ranging from  $-20^{\circ}\text{C}$  to  $21^{\circ}\text{C}$ . At higher temperatures, the asphalt sand mastics started to flow and were difficult to measure. As a result, most studies (Buttlar and You 2001; Liu et al. 2009; Liu and You 2009; You and Buttlar 2005) were limited at the low or moderate temperatures. Instead of performing experimental tests, researchers obtained the stiffness of the asphalt sand mastic through multiplying the measured asphalt binder stiffness by a factor of 30 (Abbas et al. 2007). In their study, the testing temperatures of asphalt binder ranged from  $7^{\circ}\text{C}$  to  $82^{\circ}\text{C}$ , while the sand particle sizes and volumetric fraction were not clearly stated. Clearly, at the low temperature, stiffness of mineral aggregate is close to that of asphalt binder, so the multiplying factor could be much smaller than 30, while at high temperatures, the factor may significantly increase.

Instead of studying on the asphalt sand mastics, many researchers (Buttlar et al. 1999; Delaporte et al. 2008; Hesp et al. 2002; Shashidhar and Shenoy 2002) focused on the mechanical properties of asphalt-mineral filler mastics. The mineral fillers were usually less than 0.075mm in their studies. The existing studies (Abbas et al. 2005; Buttlar et al. 1999; Hesp et al. 2002; Kim and Little 2004) usually emphasized the impacts of mineral fillers and tried to explore the relationship between the stiffness ratios of asphalt-mineral filler mastics to asphalt binder and the filler volumetric fractions. Researchers (Buttlar et al. 1999) utilized generalized self-consistent scheme (GSCS) to study the dynamic shear modulus ratios of asphalt mastic to asphalt binder. It was found that the modulus ratios were less than 9 when the binder modulus ranged from 0.001 to 1000 MPa. However, other researchers observed from experimental tests that the stiffness ratios could be larger than 100. Obviously, the GSCS was under-predict the stiffening impacts of mineral fillers since the complicated microstructures of the asphalt-mineral filler mastics were unable to be considered. Microstructure-based numerical models, such as discrete element models and finite element models, may provide more accurate prediction of asphalt sand mastics or asphalt-mineral filler mastics. Few studies, however, have focused on this area. Even though researchers (Abbas et al. 2005) have utilized discrete element models to simulate asphalt mastics, their focus was on the impacts from mineral filler volumetric fractions instead of those from the asphalt binders.

As mentioned above, although many excellent studies have been done on understanding asphalt mastic or sand mastic behaviors, more work is needed to understand the impacts of asphalt binder stiffness values and volumetric fractions on asphalt sand mastic stiffness values under a broad range of temperatures. Therefore, the main objective of this study is to evaluate stiffness of asphalt sand mastics vs. stiffness of asphalt binders using three-dimensional DE method. DE simulations of 12 sand mastics were performed under uniaxial constant loads. Both asphalt stiffness values and volumetric fractions were varied in the simulations. The DE models were introduced and the outputted results were discussed in the following sections.

### **14.3. Discrete Element Models Of Sand Mastics**

A total of 12 sand mastics were simulated in this study: Six of them were the fine sand mastics which were made by blending fine sands (particle sizes ranging from less than

0.075mm to 0.3mm) with 42.15%, 52.4%, 61.8%, 70.8%, 80.3%, and 90% of asphalt binders by volume. The other six were the coarse mastics which were made by blending the coarse sands (particle sizes ranging from 0.3mm to 2.36mm) with 42.15%, 52.4%, 61.8%, 70.8%, 80.3%, and 90% of the asphalt binders by volume. It should be mentioned herein that the asphalt binders in the coarse sand mastics could be pure asphalt, asphalt-miller filler mastics, or the fine sand mastics, while the asphalt binders in the fine sand mastics could be pure asphalt or asphalt miller filler mastics. The gradations of the coarse and fine sands are shown in Figure 14.1.

The 12 cylindrical specimens of the sand mastics were created using the previously developed three-dimensional (3D) model (Liu and You 2009), where coarse and fine sands were simulated with randomly-created polyhedron particles. The diameter and height of the cylindrical specimens were 6mm and 9mm for the coarse sand mastics, and 0.75mm and 1.1mm for the fine sand mastics. A total of 50,600 discrete elements were included in the coarse sand mastic specimens, while a total of 63,000 discrete elements were included in the fine sand mastic specimens. Figure 14.2 shows the examples of the coarse sand mastic samples with asphalt content of 42.15% and 70.8%, respectively. The fine sand mastics have the similar microstructures.

The mechanical interactions within the digital specimens were addressed using the previously developed DE model (Buttler and You 2001). Three contact models were employed in the DE model, namely the linear contact model, the slip model, and the contact-bond model. More details were provided in the references (Buttler and You 2001; Itasca Consulting Group 2008b). The DE model requires the following input parameters:

- 1) Stiffness values of both asphalt and sands
- 2) Tensile and shear strengths of asphalt and sand particles
- 3) Cohesive strengths at the interfaces between asphalt and sand particles
- 4) Friction coefficients between contacting discrete elements

The focus of this study is prediction of asphalt sand mastic stiffness at a strain level of about  $150\mu\epsilon$ . In the assumptions, the contact bonds were not allowed to break and the contacting elements were not supposed to slip from each other. Therefore, the extremely high values were given to the contact-bond strengths for the contact-bond model, and the friction was equal to 1 for the slip model. The stiffness values of both fine and coarse sands were the same and equal to 55GPa, while asphalt binder stiffness values were varied from 5.5Pa to 55GPa which represent the stiffness values of asphalt binder under the high temperatures and low temperatures, respectively. Table 14.1 shows the DE mechanical model inputs.



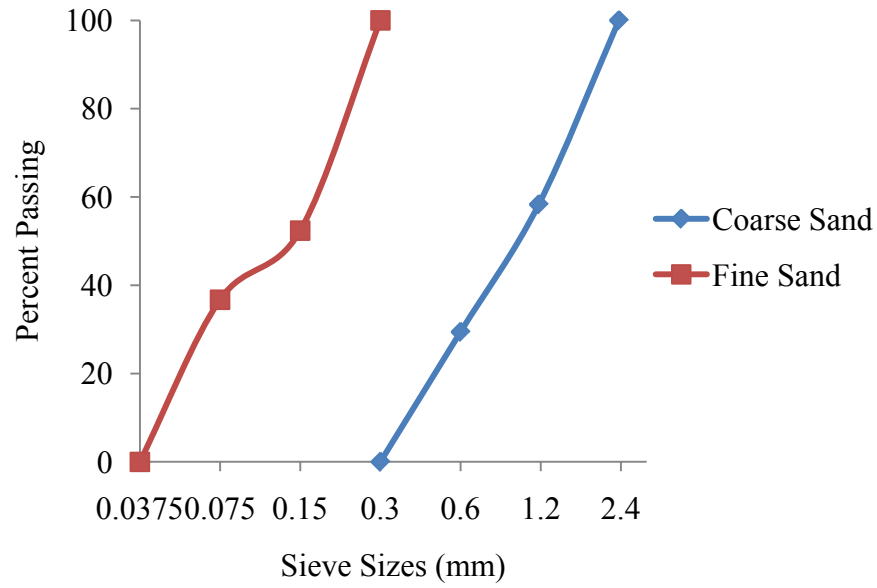


**Figure 14.1** Gradation graphs of coarse and fine sands

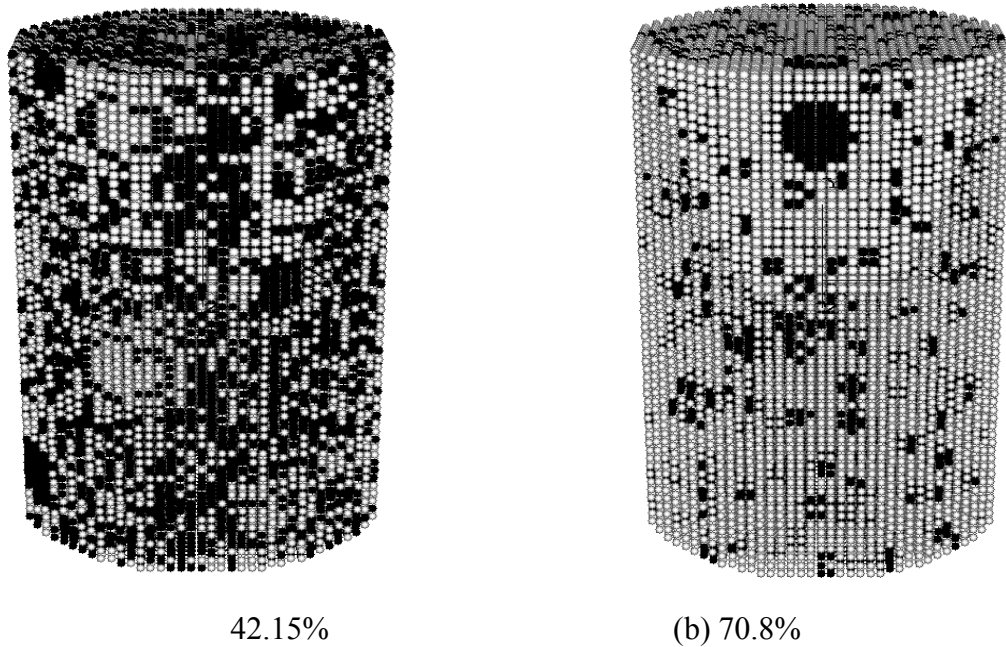


**Figure 14.2:** Examples of the digital coarse sand mastics

## 14.4. DE Simulation and Results

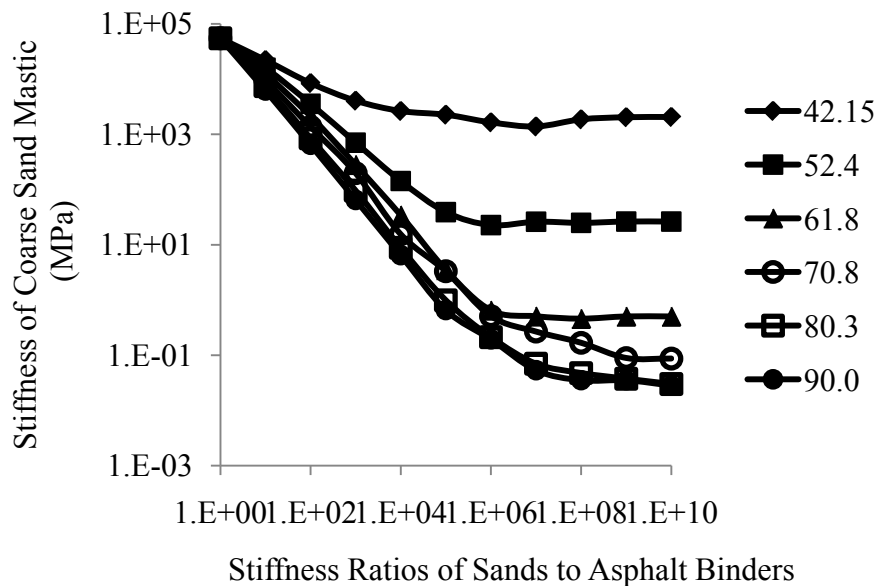
The DE simulations were performed by applying constant loads on the top of the digital specimens while the bottoms of those specimens were fixed. As mentioned in Table 14.1, the same stiffness value was given to both coarse and fine sands for all the simulations, while asphalt binders in the 12 sand mastics were assigned varied stiffness values. The

stiffness ratios of sands to asphalt binders ranged from 1 to  $10^{10}$ . Each DE simulation was completed when the strain reached  $150\mu\epsilon$ . Figure 14.3 shows the DE outputs of fine and coarse sand mastics.

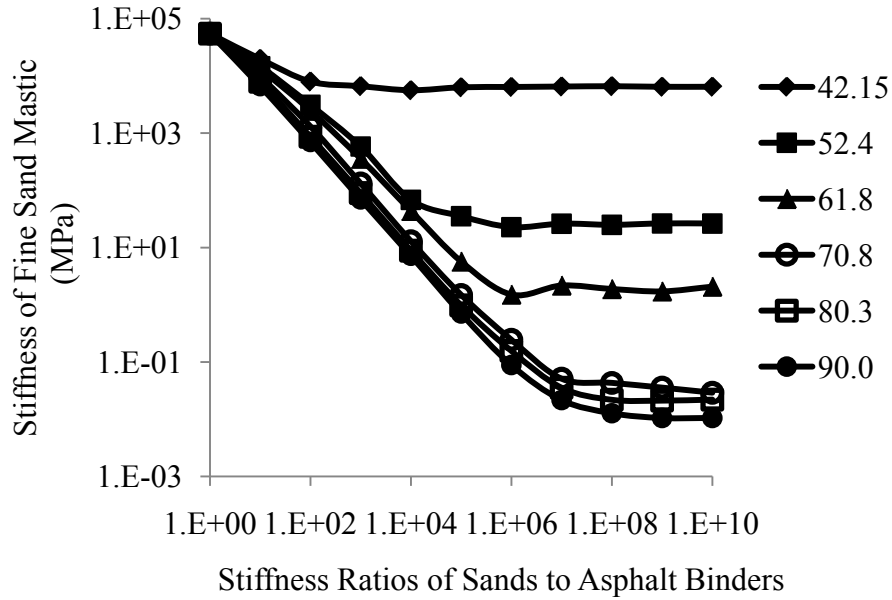
It was observed that 1) sand mastics' stiffness values decreased with the stiffness ratios of sands to asphalt increasing; 2) the sand mastic stiffness values decreased with the volumetric fractions of asphalt increasing; 3) Coarse sand mastics had similar stiffness values under the same asphalt stiffness values and volumetric fractions. 4) when the stiffness ratios of the sand to asphalt binder were larger than a specific value, the stiffness ratio values gave very slight impacts on the sand mastic stiffness values. For instance of the mastics with 42.15% asphalt content, the mastic stiffness values were almost the same when the stiffness ratios were larger than 10000.

**Table 14.1**  
**Inputs for the DE Model**

	Asphalt	Sands
Stiffness values	Range from 5.5Pa to 55GPa	55GPa
Tensile and shear strengths	10GPa	10GPa
Cohesive strengths at the interfaces	10GPa	
Friction coefficients	1	



(a) Coarse sand mastic



(b) Fine sand mastic

**Figure 14.3 Sand mastics stiffness VS. stiffness ratio of sands to asphalt (asphalt content: 42.15%, 52.4%, 61.8%, 70.8%, 80.3%, and 90%)**

## 14.5. Discussion: Micromechanical Basis

According to the micromechanical theory of two-phase composites (You and Buttlar 2004), asphalt mastic stiffness can be expressed as

$$E_m = E_b + (E_s - E_b) c_2 A_2 \quad 14.1$$

Where  $c_2$  is the volumetric friction of sand particles;  $A_2$  is the strain concentration factor of sand particles;  $E_m$ ,  $E_b$ , and  $E_s$  are the stiffness of the composite, the binder, and the sand particles, respectively. If the strain in sand particles is symbolized with  $\varepsilon_2$  the overall strain in the sand mastic is  $\bar{\varepsilon}$ , then the  $A_2$  can be defined in Equation 14.2

$$A_2 = \frac{\varepsilon_2}{\bar{\varepsilon}} \quad 14.2$$

If stiffness ratio of sand mastic to asphalt binder is defined in equation 14.3

$$SR_m = E_m / E_b \quad 14.3$$

And stiffness ratio of sands to asphalt binder is defined in Equation 14.4

$$SR_s = E_s / E_b \quad 14.4$$

Then, the Equation (1) can be written as

$$SR_m = 1 + (SR_s - 1)c_2 A_2 \quad 14.5$$

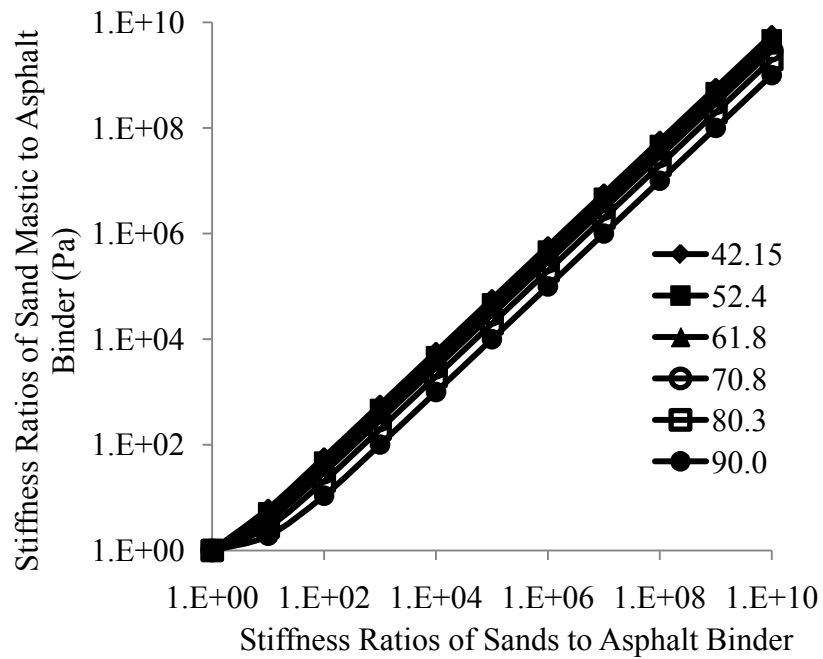
Basically, three categories of factors may impact  $A_2$ , namely the mechanical properties, volumetric fractions, and spatial distributions of asphalt and mineral aggregates as demonstrated in the previous study (Liu and You 2010). Herein, the mechanical properties are represented by the stiffness ratio of sands to asphalt,  $R_s$ . The volumetric fractions are represented by the volumetric fraction of sands,  $c_2$ . The spatial distributions can be represented by the distribution of sand particles in the 12 sand mastics. If the special spatial distribution of sand particles is given,  $A_2$  can be a function of  $R_s$  and  $c_2$ . Therefore, the Equation 14.5 can be rewritten as

$$SR_m = 1 + (SR_s - 1)c_2 f(SR_s, c_2) \quad 14.6$$

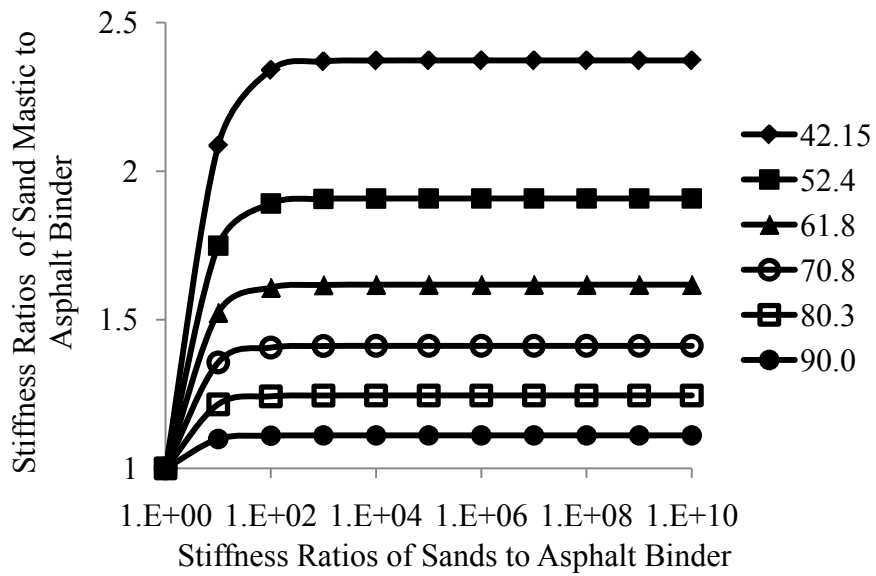
In the Equation 14.6,  $f(SR_s, c_2)$  is the function of  $SR_s$  and  $c_2$  which dependent on the spatial distributions of the sand particles. In other words, there are 12 different expressions of  $f(SR_s, c_2)$  for the 12 different digital sand mastics. The Voigt and Ruess models (Reuss 1929; Voigt 1889) represented two simplest geometrical distributions of the constituents in a two-phase composite, which were known as the upper and lower bounds of a two-phase mixture. Therefore, the upper and lower bounds of  $f(SR_s, c_2)$  can be derived from the Voigt and Ruess models. The upper bound is 1 while the lower bound is  $\frac{1}{c_2 + (1 - c_2)SR_s}$ . By substituting the upper and lower bounds of  $f(SR_s, c_2)$ , The

upper and lower bounds of  $SR_m$  can be predicted as shown in Figure 14.4. As shown in Figure 14.4 (a), the stiffness ratios of sand mastics to asphalt,  $SR_m$ , can range from 1 to  $5.79 \times 10^9$ , while from Figure 14.4(b), the stiffness ratios,  $R_m$  range from 1 to 2.4.

Theoretically, the  $SR_m$  for the two sand mastics should be between the upper and lower bounds shown in Figure 14.4. By analyzing the DE outputs in Figure 14.3, the  $SR_m$  for the 12 sand mastics were calculated and plotted in Figure 14.5. It was observed that the predicted  $SR_m$  ranged from 1 to  $1.18 \times 10^9$  for fine sand mastics, while  $SR_m$  ranged 1 to  $3.76 \times 10^8$  for coarse sand mastics. Clearly, the predicted results from DE models of coarse and fine sand mastics were between the upper and lower bounds which were from the upper and lower bound mix models. From Figure 14.5, it was also observed that the majority of the  $SR_m$  values were less than 100 even though a few of them could be as large as  $1.18 \times 10^9$  for the fine sand mastics and  $3.76 \times 10^8$  for the coarse sand mastics.

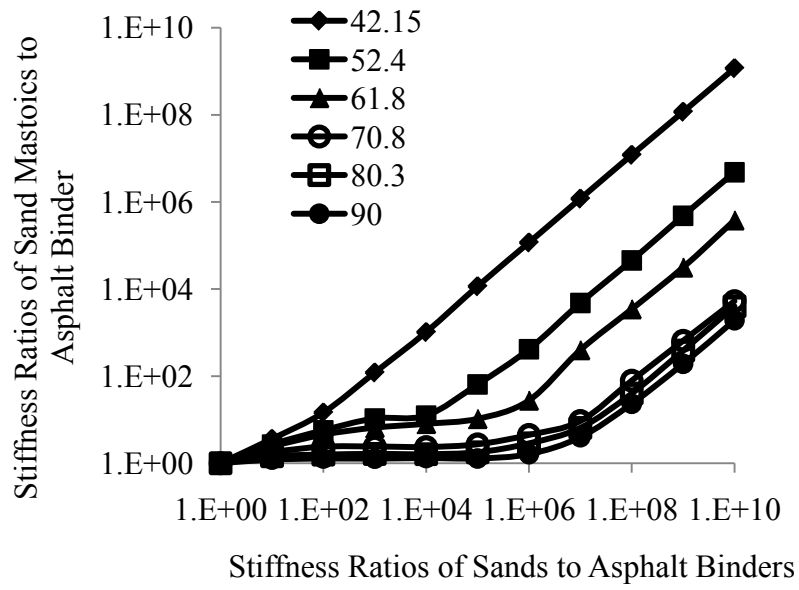


(a) The Voigt model (upper bound)

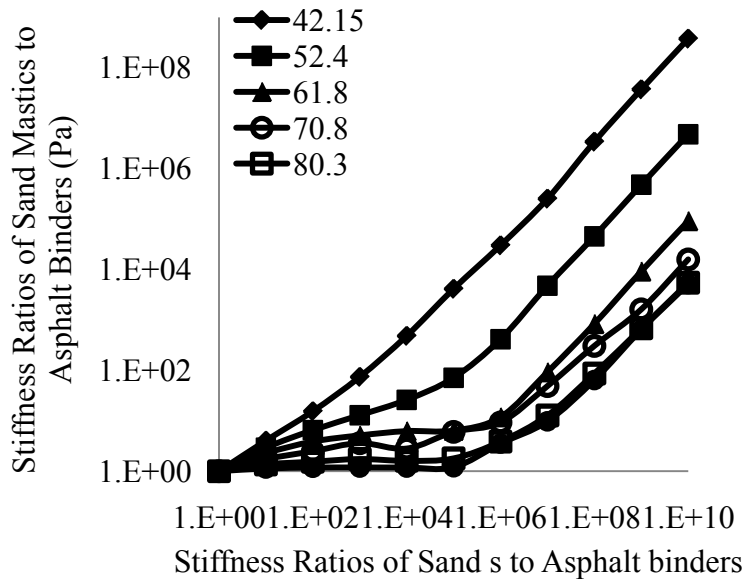


(b) The Ruess model (lower bound)

**Figure 14.4** Curves of  $R_m$  vs.  $R_s$  for the Voigt and Ruess models ( $R_m$  is the ratio of sand mastic to asphalt,  $R_s$  is the ratio of sands to asphalt)



(a) Fine sand mastics



(b) Coarse sand mastics

**Figure 14.5** Curves of stiffness ratios of sand mastics to asphalt vs. those of sands to asphalt.

## 14.6. Summary and Conclusion

A total of 12 sand mastics were studied using DE method. Through analyzing the DE outputs, the stiffness ratios of sand mastic to asphalt,  $SR_m$ , were evaluated when the stiffness ratio of sand particles to asphalt ranged from 1 to  $10^{10}$ . The goal of this study was to evaluate the impacts of asphalt stiffness and volumetric fractions on the asphalt mastic stiffness. Through this study, the following conclusions were observed:

- 1) The DE simulation results agreed well with the micromechanical models' solutions;
- 2) With the volumetric fractions of asphalt increasing, the stiffness ratio,  $SR_m$ , decreased dramatically;
- 3) The stiffness ratios,  $SR_m$ , could be as large as  $1.18 \times 10^9$  for the fine sand mastics and  $3.76 \times 10^8$  for the coarse sand mastics. But most of them were less than 100.

## 14.7. Acknowledgments

This material is based in part upon work supported by the National Science Foundation under grant 0701264. Any opinions, findings, and conclusions or recommendations expressed in this material are those of the author's and do not necessarily reflect the views of the National Science Foundation. The authors appreciate Dr. Xianguang Hu for the lab testing. The experimental work was completed in the Transportation Materials Research Center of Excellence at Michigan Technological University, which maintains the AASHTO Materials Reference Laboratory (AMRL) accreditation on asphalt and asphalt mixtures.

# Chapter 15. 3D DE Simulation to Formulate Asphalt Concrete Stiffness for Specific AC Microstructures<sup>14</sup>

## 15.1. Abstract

This study presents an approach to formulate asphalt concrete stiffness for specific microstructures. An asphalt concrete was designed on the basis of the Superpave mix design method. Its images were obtained from X-ray Computed Tomography (X-ray CT). Through processing those X-ray CT images, two-microstructure-based models, namely the Model-I and the Model-II were rebuilt on the basis of the discrete element (DE) method. In Model-I, no air void was included, while in Model-II, the air void level was 3.1%. The DE simulation of the asphalt concrete was conducted with those two models whose primary inputs were the stiffness values of both coarse aggregate and asphalt sand mastic. The asphalt sand mastic was defined as a sub-mix of fines, fine aggregate (less than 2.36mm), and asphalt binder. Through regression analysis of the DE simulation results, the asphalt concrete stiffness values were formulated into two analytical equations for Model-I and Model-II, respectively. A potential application of those two equations is to predict effective stiffness values of the asphalt concrete at various temperatures and different loading conditions. At the end of this study, an application example is provided. It was found that compared with the measured data, the formulated equation of Model-II could more precisely predict the asphalt concrete dynamic moduli at various temperatures and different frequencies than other models.

## 15.2. Introduction

Asphalt concrete is composed of asphalt binder and mineral aggregate as well as air voids. Asphalt binder can be considered as a binder agent to glue mineral aggregates into a dense mass, while aggregate particles can be regarded as a stone framework to contribute strength and toughness to the system. The property of asphalt concrete is affected by not only the individual components, but also their combined reaction within this system. Stiffness is one of the most important parameters of asphalt concrete. In the past one hundred years, a number of models have been developed for predicting asphalt concrete stiffness. Most of them could be categorized into three groups, namely experiment-based regression models, two-phase micromechanical models, and microstructure-based numerical models. The two most popularly used experiment-based regression models are the Witczak model (Dongre et al. 2005; Witczak and Fonseca 1996) and the Hirsch model (Al-Khateeb et al. 2006; Christensen et al. 2003). The shortcoming of an experiment-based regression models, however, is its laboratory dependency. First of all, a large number of laboratory tests are needed for model

---

<sup>14</sup>Full text reprinted with permission from ASCE: “Formulation of Asphalt Concrete Stiffness for Specific Microstructures Based on Discrete Element Method” by Yu Liu and Zhanping You, 2010, Paving Materials and Pavement Analysis (GSP 203), Proceedings of the 2010 GeoShanghai International Conference, pp. 135-417, Copyright © 2010, ASCE. See Copyright clearance in Appendix A



development or calibration. Secondly, its accuracy is dependent on the laboratory conditions and accuracy of the laboratory testing results. Also, it is only applicable at the conditions where it was developed.

Two-phase micromechanical models started about one hundred years ago. The earliest developers were Voigt (Voigt 1889) and Reuss (Reuss 1929). Subsequently, some other models were developed and used (Counto 1964; Dasgupta and Bhandarkar 1992; Hashin 1961; 1965; Hashin and Shtrikman 1963; Hirsch 1962; Paul 1960). According to the previous study (You and Buttlar 2004), all the existing two-phase micromechanical models could be formulated as

$$C = C^{(1)} + c_2 A_2 (C^{(2)} - C^{(1)}) \quad 15.1$$

where  $C^{(1)}$  and  $C^{(2)}$  are stiffness values of the phase 1 and the phase 2, respectively;  $C^*$  and  $c_2$  are the effective stiffness and volumetric fraction of the phase 2, respectively;  $A_2$  is the strain concentration factor of the phase 2. Evidently, it is  $A_2$  that has distinguished the existing two-phase micromechanical models. For example, for the Voigt model (Voigt 1889),  $A_2=1$ ; for the Reuss model (Reuss 1929),  $A_2 = C^{(1)} / (C^{(1)} + C^{(2)})$ . In fact, the existing two-phase micromechanical models were derived from their specific microstructures on the basis of solid mechanics. For example, Figure 15.1(a), (b), (c), and (d) shows the microstructures for the Voigt (Voigt 1889), the Reuss (Reuss 1929), the Hirsch (Hirsch 1962), and the Counto (Counto 1964) models, respectively. In other words, different microstructures have different formulations of  $A_2$ . Although those two-phase micromechanical models may provide useful benchmark solutions of asphalt concrete stiffness, they are limited to relatively simple microstructures and boundary conditions. Furthermore, air voids cannot be considered in those two-phase micromechanical models.

Microstructure-based numerical models, such as discrete element (DE) models (Liu et al. 2009; Liu and You 2009; You 2003) and finite element (FE) models (Dai and You 2007), are relatively new models. A major strong suit of a microstructure-based numerical model is that complex microstructures and micromechanics can be simulated under relatively complicated boundary conditions. It has some limitations for applying such a model for routine use to predict asphalt concrete stiffness since it is really time-consuming. For example, it took several weeks to predict the dynamic modulus of asphalt concrete with a two-dimensional viscoelastic DE model (Liu et al. 2009; Liu and You 2009). It would take much longer if a three-dimensional model was applied. Therefore, the authors believed that a microstructure-based numerical model is better suited for use as a research tool for investigating the fundamentals of asphalt mixtures rather than a routine method for prediction of stiffness. This study demonstrates the use of microstructure-based DE models as research tools.

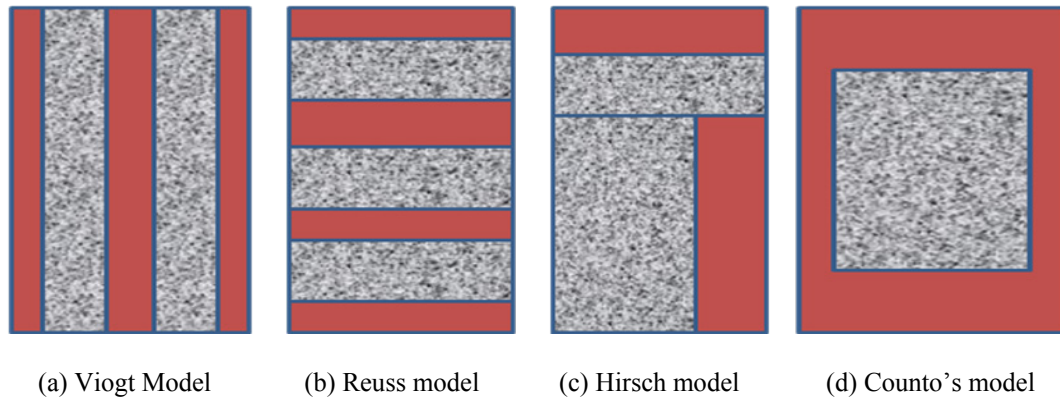


**Figure 15.1 Examples of microstructures for two-phase micromechanical models**

The objective of this study is to present a method for formulizing asphalt concrete stiffness with Equation 15.1. Instead of deriving  $A_2$  based on solid mechanical theories, microstructure-based DE simulation results were used to acquire the regression of  $A_2$ .

### 15.3. Microstructure-Based Discrete Element Models

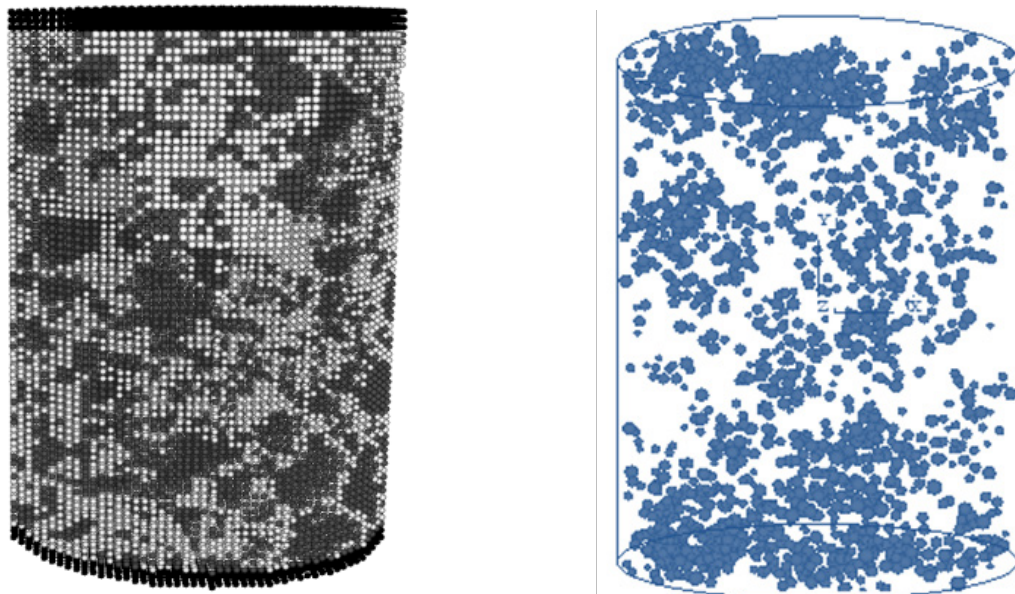
As is well known, asphalt concrete is a multi-phase system including coarse aggregate, fine aggregate, fines, asphalt binder, and air voids. Some researchers, however, believed that larger sizes of coarse aggregate particles act as individual components while asphalt binder, fine aggregate particles, fines, and air voids act as an integrated component to interact with the coarse aggregate (Li and Metcalf 2005a). Some other researchers believed that air voids should be an isolated phase paralleled with coarse aggregate and submix of fines, fine aggregates and asphalt binder (Shashidhar and Romero 1998a). In fact, air voids flow around in asphalt concrete and cannot be integrated with any component. The authors of this study believe asphalt concrete can be regarded as a three-phase system: air voids, coarse aggregates, and asphalt sand mastic. The asphalt sand mastic is a submix of fines, fine aggregates and binder. On the basis of the principle above, the major tasks for building a microstructure-based DE model of an asphalt concrete are as follows:

- 1) Acquire asphalt concrete X-ray Computed Tomography (X-ray CT) images
- 2) Process X-ray CT images with a technique developed in a previous study(Adhikari 2008).
- 3) Distinguish between coarse aggregate and asphalt sand mastic
- 4) Create a two-phase microstructure-based DE model
- 5) Create air voids by randomly deleting discrete elements from the two-phase model.

An asphalt concrete mixture was designed on the basis of the Superpave mix design method. The designed mineral aggregate gradation is shown in Table 15.1 and asphalt content is 5.59% by mass. The mineral aggregate was blended with the asphalt binder and compacted with Superpave Gyrotory Compactor (SGC) to 3.1% of air voids by volume. The images of the finished product were acquired from X-ray CT. With those X-ray CT images, two microstructure-based models were built, namely, Model-I and Model-II. The

Model-I was built by following steps one through four above, while the Model-II was built by following steps one through five. Therefore, the Model-I is a two-phase system without air voids. As shown in Figure 15. 2(a), a total of 148,200 discrete elements were used to build the Model-I, where dark-colored elements represent the upper and lower loading platens; white elements represent the asphalt sand mastic; and grey elements symbolize coarse aggregates. The Model-II is a three-phase system with 3.1% of air voids. The air void distribution is shown in Figure15. 2(b). It should be noticed herein that both the Model-I and the Model-II were from the same asphalt concrete. Therefore, the only difference between them is the air void content.

To address the interactions within the Model-I and the Model-II, a micromechanical model has been developed in a previous study(You 2003). According to the previous study (Liu et al. 2009), four interactions were addressed in the micromechanical model. They were interactions between coarse aggregate and asphalt sand mastic, between two adjacent coarse aggregate particles, within a coarse aggregate particle, and within the asphalt sand mastic. Four constitutive models were assigned to those four interactions. Each of them has three parts: contact-stiffness model, contact-bond model, and slip model. The contact stiffness model relates the relative displacements to the contact forces at a contacting point, while the other two contact models impart strength properties at the contact. Readers may refer to the previous study(You 2003) for more details.



(a) Reconstructed microstructure (b) air voids distribution in the microstructure

**Figure 15.2 Reconstructed three-dimensional microstructure and air void distribution**

**Table 15.1**  
**Aggregate Gradation**

<b>Sieve size (mm)</b>	19	12.5	9.5	4.75	2.36	1.18	0.6	0.3	0.15	0.075
<b>Percentage passing (%)</b>	100	98.7	86.5	71.8	51.4	36.1	25.5	14.7	7.7	5.4

## 15.4. Microstructure-Based Discrete Element Modeling

Figure 15.2(a) shows the loading setup for the microstructure-based DE modeling: the asphalt concrete specimen, either the Model-I or the Model-II, was loaded with the upper and lower loading platens. On the upper platen, a uniaxial constant load was applied while the lower platen remained fixed. The same mechanical inputs were utilized in the DE modeling with both the Model-I and the Model-II. The primary inputs include the Young's modulus for the coarse aggregate and the asphalt sand mastic. The Young's modulus of the coarse aggregate was set to 55GPa, while that of the asphalt sand mastic was varied from 0.0055GPa to 55GPa. The stiffness ratio,  $\alpha$ , is defined as the ratio of the asphalt sand mastic stiffness to the coarse aggregate stiffness. Therefore,  $\alpha$ , is equal to a value in the range from 0.00001 to 1. A total of 108 values were set to  $\alpha$ , which resulted in 108 outputs from the DE modeling with either the Model-I or the Model-II. The DE modeling results are plotted in FIGURE 15.3.

From the graph in FIG. 3, it is clear that the stiffness values from the Model-I were larger than those from Model-II. Especially when  $\alpha$  was larger than 0.1, the difference between the Model-I and the Model-II became larger. It was also noted that when  $\alpha$  was close to 1, the difference between the two models became smaller. The observations above could be explained below:

The Equation (1) can be equivalently expressed as

$$C^* = C^{(2)}[\alpha + c_2 A_2 (1 - \alpha)] \quad 15.2$$

When  $\alpha$  is smaller (less than 0.1),  $A_2$  plays a significant role in determining the effective stiffness. From the Figure 15.4 in the next section, the difference of  $A_2$  between the two models is larger. Therefore, the stiffness difference between the two models was also larger as observed above.

When  $\alpha$  is close to 1,  $A_2$  has an ignorable role in determining the effective stiffness. As mentioned above, air void is considered as one of the factors which may impact  $A_2$ . Therefore, the effects of air voids became smaller and the difference between the Model-I and the Model-II was smaller when  $\alpha$  was close to 1.

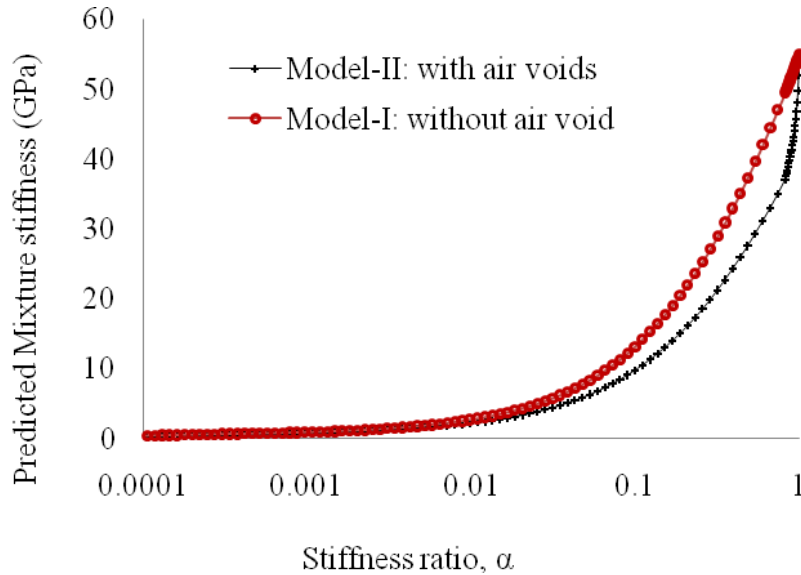


**Figure 15.3 DE modeling results of model-I and model-II**

## 15.5. Formulation of Asphalt Concrete Stiffness

As discussed in the introduction, Equation 15.1 is a universal solution to the effective stiffness of a two-phase system. The strain concentration factor,  $A_2$ , is the key parameter which is related to the microstructure of the two-phase system. In order to formulate the effective stiffness of a two-phase composite,  $A_2$  has to be determined. As demonstrated in the existing two-phase micromechanical models, formulations of  $A_2$  were derived on the basis of continuum solid mechanics for relatively simple microstructures.

Unfortunately, asphalt concrete has such complex microstructures that it is impossible to derive a solution for  $A_2$ . Therefore, this study presents an indirect method through regression analysis of the DE modeling results in Figure 15.3. In this indirect method, the asphalt concrete stiffness is formulated with Equation 15.1. To use Equation 15.1, the asphalt concrete was simplified into two phases. Phase 1 is the asphalt sand mastic, while phase 2 is the coarse aggregate. Therefore, the terms in Equation 15.1 could be interpreted as:

- $C^{(1)}$  = stiffness of the asphalt sand mastic
- $C^{(2)}$  = stiffness of the coarse aggregate
- $C^*$  = stiffness of the asphalt concrete;
- $c_2$  = volumetric fraction of the coarse aggregate
- $A_2$  = the strain concentration factor of the coarse aggregate

From Equation 15.1,  $A_2$  can be determined by using the following equation:

$$A_2 = \frac{C^* - C^{(1)}}{c_2(C^{(2)} - C^{(1)})}$$

15.3

In Equation 15.3,  $C^*$  is the predicted stiffness as shown in Figure 15.3, while  $C^{(2)}$  and  $C^{(1)}$  are inputs for the DE modeling.  $c_2$  may be calculated using the aggregate gradation in Table 15.1. In this study,  $c_2 = 0.417$ . Therefore, the values of  $A_2$  could be calculated with application of Equation (3), and they are plotted in Figure 15.4. From Figure 15.4, the following were observed:

- 1) For Model-I,  $A_2$  increases from 0 to 1 with the stiffness ratio,  $\alpha$  increasing from 0.00001 to 1. In Model-II, however,  $A_2$  increases and then decreases while  $\alpha$  increases from 0.00001 to 1.
- 2) For Model-I,  $A_2$  lies somewhere between the upper and lower bounds. For Model-II, however,  $A_2$  is within the two bounds when  $\alpha < 0.1$ , while the curve of  $A_2$  is below the lower bound when  $\alpha > 0.1$ .
- 3) For both Model-I and Model-II,  $A_2$  can be fitted with a 6-order polynomial function of  $\alpha$ . The  $R^2$  is very close to 1.

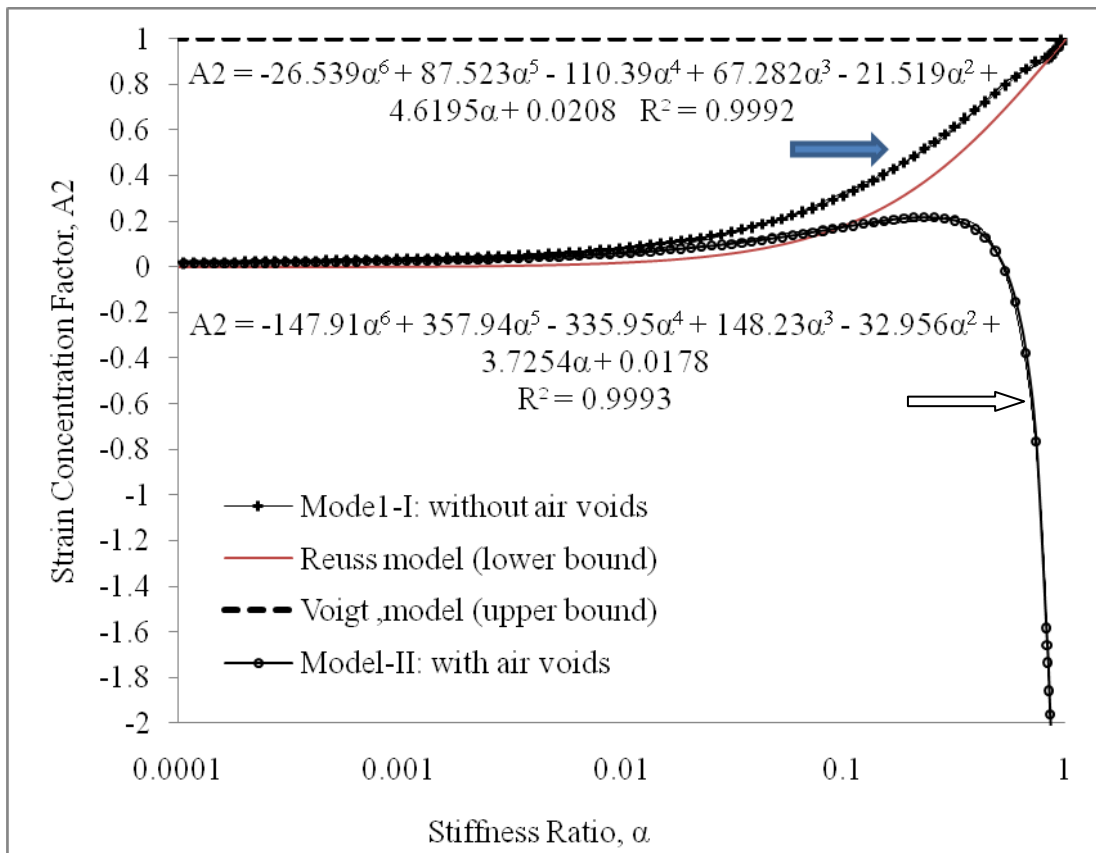


**Figure 15.4 Strain concentration factor versus stiffness ratio for various models**

Based on the findings above, it may be concluded that the stiffness of asphalt concrete could be formulated with Equation (1).  $A_2$  in Equation (1) is a function of the stiffness ratio,  $\alpha$ . For Model-I, the function is

$$A_2 = -26.539\alpha^6 + 87.523\alpha^5 - 110.39\alpha^4 + 67.282\alpha^3 - 21.519\alpha^2 + 4.6195\alpha + 0.0208 \quad 15.4$$

For the Model-II, the function is

$$A_2 = -147.91\alpha^6 + 357.94\alpha^5 - 335.95\alpha^4 + 148.23\alpha^3 - 32.956\alpha^2 + 3.7254\alpha + 0.0178 \quad 15.5$$

## 15.6. Example Application

A potential application of the formulations, such as Equations (4) and (5), is to predict the asphalt concrete stiffness under various temperatures and different loading conditions. This section presents an example application to demonstrate how to use the formulations. As discussed in the previous section, Equations (1), (4) and (5) are meant to be used for prediction of asphalt concrete stiffness. Therefore, four parameters are needed:  $C^{(1)}$ ,  $C^{(2)}$ ,  $c_2$ , and  $\alpha$ . In this example application,  $C^{(2)} = 55\text{GPa}$  and  $c_2 = 0.421$ . Uniaxial dynamic modulus tests of the asphalt sand mastic were measured under different temperatures and frequencies as shown in Table 15.2. Therefore,  $C^{(1)}$  could be any value in Table 15.2. And  $\alpha$  is determined by dividing  $C^{(1)}$  by  $C^{(2)}$ . An example calculation is shown below:

- At 25Hz and 4 °C,  $C^{(1)} = 13130\text{MPa}$  as shown in Table 15.2,  $C^{(2)} = 55000\text{MPa}$ ;
- The stiffness ratio  $\alpha = 13130/55000 = 0.2387$ ;
- $c_2 = 0.421$
- If the Model-I is used, from Equation (4),  $A_2 = 0.5169$ . Substitute  $A_2$  to the Equation (1), the predicted asphalt concrete stiffness  $C^* = 2224.3\text{ MPa}$
- If the Model-II is used, from Equation (5),  $A_2 = 0.20468$ . Substitute  $A_2$  to the Equation (1), the predicted asphalt concrete stiffness  $C^* = 16,738\text{ MPa}$

The uniaxial dynamic modulus tests of the asphalt concrete were also conducted under the same temperatures and frequencies. The results are listed in Table 15.3.

**Table 15.2**  
**Dynamic Modulus of the Asphalt Sand Mastic (MPa)**

frequency \ temperature	25 Hz	10 Hz	5 Hz	1 Hz	0.5 Hz	0.1 Hz
-5 °C	16,430	15,236	14,294	12,037	11,020	8,912
4 °C	13,130	11,814	10,775	8,490	7,442	5,490
13 °C	8,310	7,168	6,135	4,376	3,463	2,231
21 °C	4,685	3,752	3,240	2,035	1,533	9,49

**Table 15.3**  
**Dynamic modulus of the asphalt concrete (MPa)**

frequency \ temperature	25 Hz	10 Hz	5 Hz	1 Hz	0.5 Hz	0.1 Hz
-5 °C	24,335	21,917	19,839	16,704	15,302	12,193
4 °C	16,848	15,272	14,073	10,977	9,724	6,990
13 °C	11,062	9,234	8,046	5,448	4,336	2,596
21 °C	7,660	6,103	4,822	2,867	2,030	1,140

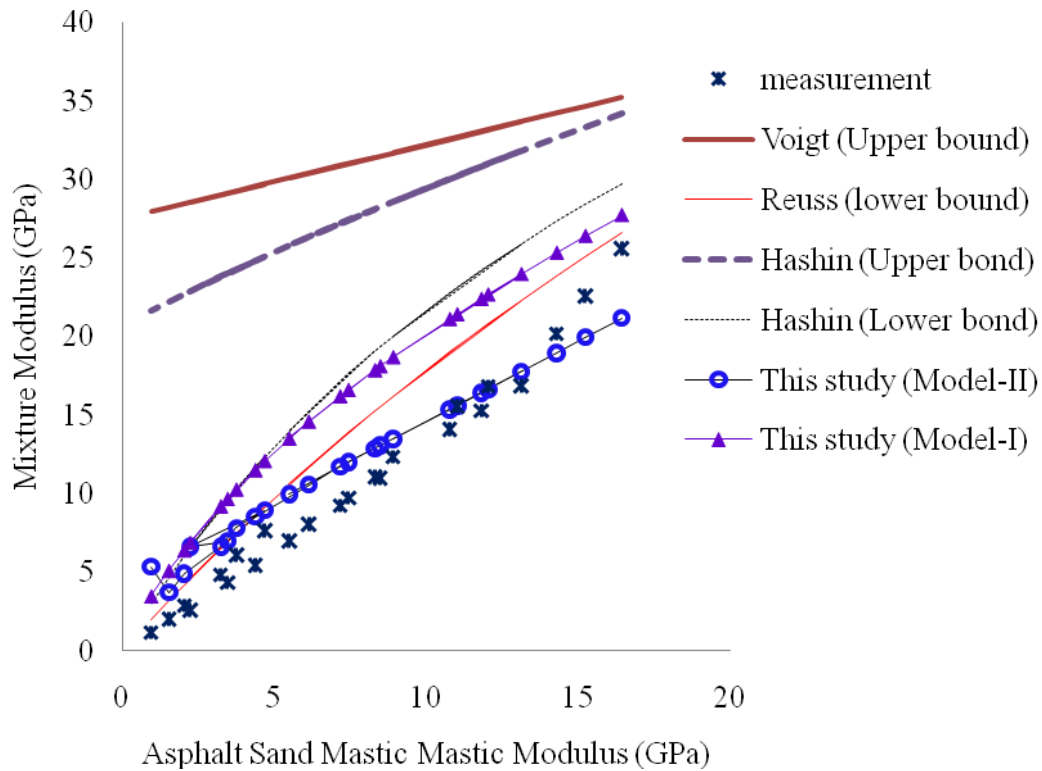


**Figure 15.5 Comparisons of different models as well as laboratory measurements**

At 25Hz and 4°C, the measured dynamic modulus of the asphalt concrete is 16,848MPa. If the Equation (5) is used to calculate  $A_2$ , the predicted stiffness (16,738 MPa) is very close to the measured value. If Equation (4) is used to calculate  $A_2$ , the predicted stiffness (2224.3 MPa) is much higher than the measured value. Figure 15.5 shows the comparisons of different methods for predicting asphalt concrete stiffness.



As shown in Figure 15.5, the methods include Model-I and Model-II used in this study as well as the Voigt, the Reuss, the Hashin (Hashin and Shtrikman 1963) models, and the laboratory measurements. The following findings were observed:

- 1) Both the measured stiffness values and predicted asphalt concrete stiffness from the Model-II are lower than those from the other models. This is due to the consideration of air voids in the Model-II and the actual samples.
- 2) Since no air voids were considered in Model-I of this study, the predicted stiffness is somewhere between the lower bound of the Reuss model and the lower bound of the Hashin model.
- 3) Compared with the results from the other micromechanical models, the predicted stiffness from Model-II is much closer to the measured value.

## 15.7. Conclusions

Due to the complex microstructural characteristics, it is impossible to derive an analytical solution of asphalt concrete effective stiffness. Therefore, this study has provided an indirect method to formulate asphalt concrete stiffness with specific microstructures. The universal formulation for predicting the effective stiffness of a two-phase composite was used in this study. But the key parameter, strain concentration factor of phase 2 ( $A_2$ ) was determined through regression analysis of microstructure-based DE simulation results. From this study, the following conclusions were made:

- 1)  $A_2$  can be a function of the stiffness ratio,  $\alpha$ . Different microstructures of asphalt concrete have different formulations. For the specific microstructure in this study,  $A_2$  could be expressed with a 6-order polynomial function of  $\alpha$  as shown in Figure 15.4.
- 2) Air voids have significant effects on  $A_2$ , especially when the stiffness ratio,  $\alpha$  is larger than 0.1.
- 3) Due to the effects of air voids, the measured dynamic modulus curve is lower than the lower bounds. The stiffness value of a two-phase composite is meant to fall somewhere between the upper and the lower bounds.
- 4) Since no air voids were considered in the Model-I of this study, the predicted stiffness is somewhere between the Reuss model and the lower bound of the Hashin model.
- 5) Compared with the other micromechanical models, the Model-II used in this study is much closer to the measurement in terms of dynamic modulus.

The goal of this study is to present the methodology and validate it using limited data. It should be noted herein that the DE modeling was conducted using the particular microstructure in Figure 15.2. Therefore, some observations and conclusions may be not applicable when the microstructure of asphalt mixture is different. However, by following the methodology presented in this paper, other asphalt mixtures can be easily modeled.

In the future, different AC microstructures will be used. By following the methodology presented in this chapter, links between  $A_2$  and microstructural parameters will be explored. Ultimately, the links will be used by engineers or designers to understand the relationship between mixture components and its mechanical performance parameters.

## **15.8. Acknowledgements**

This material is based in part upon work supported by the National Science Foundation under Grant CMMI 0701264. Any opinions, findings, and conclusions or recommendations expressed in this material are those of the authors' and do not necessarily reflect the views of the National Science Foundation.

# **Chapter 16. Discrete Element Models of Pavement under a Rolling Wheel**

## **16.1. Abstract**

A crucial step in the process of pavement design is to capture or accurately interpret mechanical responses of pavement layers under moving vehicles. In the currently used analytical solutions, both material properties and loading conditions are oversimplified. Experimental tests are expensive and time-consuming even though they could provide direct and persuasive results. Therefore, numerical methods become alternative for improving understandings of pavement materials under rolling wheels. This chapter presents several methods which are potential to be used for studying pavement responses under a rolling wheel, comparison between numerical simulation and the theoretical calculation, and numerical considerations. It was observed that the numerical results were comparable with the theoretical calculation.

## **16.2. Background**

A major function of pavement layers is to spread the vehicle load efficiently so that individual layers could not be overstressed and deteriorated prematurely. Theoretically, to design a pavement structure, the first important task is to understand the material responses of pavement layers under the transient loads generated by vehicles. Then, a designer could calculate the long term pavement performance in term of cracking and deformation through analysis of the material responses (stress or strain history). Finally, the designer could make a better decision on how to minimize the traffic disruption and maximize the pavement life. Obviously, the development of approaches for understanding pavement responses is a crucial step in the process of pavement design. Many excellent studies have been done in this area using experimental testing, computer simulation, and analytical approaches. Followed is a cursory review of the existing research efforts:

Barksdale (1971) investigated compressive stress pulse time in flexible pavement for use in dynamic testing. The shape and duration of the compressive stress pulse resulting at different depths beneath the surface are studied for several flexible pavement systems and for vehicle speeds varying between 1 and 45 mph. A comparison is made of the compressive stress pulses caused by a vehicle moving over a layered pavement system at a speed of 1 mph using both linear and nonlinear elastic finite element theory. The results show that the shape of the compressive stress pulse varies from approximately a sinusoidal one at the surface to more nearly a triangular pulse at depths below approximately the middle of the base.

Loulizi et al.(2002) investigated vertical compressive stress pulse in flexible pavements by analyzing the experimental data which was collected from the Virginia Smart Road tests. With those tests on the Virginia Smart Road, it was possible to capture pavement responses (the vertical compressive stress pulses) at different locations beneath the

pavement section. The pavement loads could come from a moving truck or the falling weight deflectometer (FWD). From their research, the following findings were observed that: 1) the measured normalized vertical compressive stress pulse could be formulated with a haversine or normalized bell-shape equation. The period of the Haversine equation was ranging from 0.02 to 1.0 seconds for a vehicle speed ranging from 70 km/h to 10 km/h and at the pavement depths from 40 mm to 597 mm. 2) the stress pulse generated by the FWD loading could be simulated with a haversine with a period of 0.03 s at any depth beneath the pavement surface. In the laboratory, however, the dynamic modulus testing frequency of hot-mix asphalt (HMA) is about 10Hz. In other words, the haversine loading period is about 0.1 second. As a typical viscoelastic material, asphalt concrete behaviors are relied on the loading time or loading frequency. Thus, in order to better simulate the field loading conditions generated by moving trucks with the FWD tests, the Haversine period of 0.1 seconds in the laboratory tests of HMA dynamic modulus was recommended to be reduced to 0.03 seconds.

Al-Qadi et al. (2004) presented an experimental approach using the Virginia Smart Road to investigate the influence of pavement instrumentation on understanding pavement performance. In their research, they described the pavement instrumentation at the Virginia Smart Road to measure flexible pavement responses, explained how the instrumentation was calibrated and installed, and introduced the instrumentation performance. They concluded that: 1) Instrumentation is a feasible tool to measure pavement response to loading; 2) High horizontal strains were produced during compaction of hot mix asphalt (HMA), especially when vibration is used; 3) The pavement response (the normalized vertical compressive stress pulse) under a moving vehicular load could be formulated with a haversine function; 4) Temperatures played a significant role in affecting both the measured vertical compressive stress and horizontal transverse strain beneath the HMA layers. 5) Vehicle speed significantly impacted the measured horizontal transverse strain and the loading pulse duration, but it gave no effect on the measured compressive vertical stress in pavement layers. 6) Tire pressure had little effect on both measured stress and strains at a pavement depth of 190mm.

Al-Qadi et al. (2008) developed a three-dimensional (3-D) finite element (FE) model for studying pavement responses under traffic loads. In their study, the FE model included the measured contact stresses at the tire-pavement interaction surface, the vehicular loads during the wheel continuously rolling on the pavement surface, and the viscoelastic properties of hot-mix asphalt (HMA). The following findings were observed: 1) The critical vertical shear strain was located at the upper 76 to 100 mm of the pavement surface and influenced by the three-dimensional tire-pavement contact stresses under each tire rib. 2) The total vehicular load was the primary factor to impact the tensile strain at the bottom of HMA. The vertical shear strain was considered as the primary factor for the fatigue cracking and primary rutting of HMA layers near the pavement surface. 3) Under the traffic loading of the wide-base tires, the bottom of HMA layer had the higher longitudinal tensile strain and the top of subgrade had higher compressive strain. Near the pavement surface, the vertical shear strains under the loading of wide-base tires were less than those under the loading of the dual-tire assembly.

Al-Qadi and Wang (2009) performed both accelerated pavement testing and finite element modeling to evaluate the full-depth pavement responses under various tire configurations. Followed are the findings: 1) The new generation of wide-base tire (455/50R22.5) caused much less fatigue damage compared with the first generation of wide-base tire (425/60R22.5). The FE model was successfully used to predict the pavement responses under a dual-tire assembly and the wide-based tire. 2) The FE was successful in predicting the pavement responses under a dual-tire assembly and the wide-based tire. 3) Thin and thick HMA pavements have different damage mechanism. The new generation of wide base tire caused less octahedral shear stress at the upper part of the HMA layer.

### **16.3. Problem Statement**

Obviously, the existing studies have contributed to understanding of pavement responses under traffic loads: The accelerated pavement testing results directly measured pavement compressive stress pulses, the FE modeling provided advanced understanding of the testing data, and the analytical approaches were usually integrated into FE models to interpret the theoretical basis. However, additional studies are still needed to address the following issues: 1) Most existing studies have emphasized compressive stress pulses and given less attention to other pavement responses, such as shear stress generated by frictional forces during pavement-vehicle interaction. 2) Frictional force between pavement and vehicle is obviously important, but few researchers have paid attentions to frictional force and its impact on pavement responses. 3) Obviously, vehicle motion features (Acceleration, deceleration, and steady moving) can give different impacts on pavement responses. However, few attentions have been paid in this area.

To solve those issues, there are three categories of approaches in general: experimental tests, theory-based analytical solutions, and numerical modeling. Analytical solutions, such as Boussinesq theory and Burmister's layered theory, are useful but too simple to fully interpret those existing problems. First of all, it is inadequate that the pavement response to dynamic loading is assumed to be elastic. Secondly, it is unrealistic to represent a moving vehicle as a quasi-static or static problem. Furthermore, it is inaccurate that the contact pressure between the vehicle wheel and the pavement surface is assumed as a single concentrated force or a circular uniform stress. Experimental tests are the most direct and persuasive approaches since the pavement responses could be directly measured. However, performing experimental tests are expensive and time-consuming. The testing results are the macro-scale responses of pavements which need to be further interpreted with analytical mechanical theories or the micro-scale or meso-scale analysis. Furthermore, the testing results are also influenced by many factors such as accuracy of testing equipments, testing conditions, and proficiency of the operators who perform the tests. Numerical models are useful, powerful, and important tools in understanding and interpreting complex science and engineering problems which are unable or difficult to be done with other approaches. As discussed in the background, few researchers employed DE models to simulate pavement rutting.

## **16.4. Objectives and Scope**

The objectives of this study are 1) to develop potential approaches for studying pavement material behaviors under a single rolling wheel; 2) to perform simple virtual tests and identify advantages and challenges of the developed models. It should be noted herein that this study will not provide comprehensive simulations which will be considered in the future studies. Although both finite element method and discrete element method are the two most commonly used numerical methods, DEM was selected in this study due to the following reasons: 1) In DEM, both static and dynamic systems are solved with the same dynamic scheme, which allows physical instability and path dependence to be tracked with numerical problems. 2) DEM is based on the explicit calculation, which allows nonlinear contact relations to be used without difficulty. 3) DEM is a discontinuum code, which makes the simulation of interaction between the wheel and the pavement surface more direct and intuitional.

## **16.5. DE Model for Asphalt Pavement Analyzer (APA)**

### **16.5.1. Geometry of the DE Model**

Figure 15.1 shows a procedure to generate the APA rutting testing mold and the two cylinder specimens. There are four steps:

#### **Step 1: Create Mesh**

Discrete elements are created in a rectangular box. The dimension of the box can be controlled by users. In this study, all the elements have the same radius and are uniformly distributed in the box. The users may use different ways to create elements for their own research purposes.

#### **Step 2: Create Mold**

The mold of the APA test is simulated with a clump which is a special element in PFC3D. Details about the clump logic are provided in Chapter 3 and PFC3D manual. The elements in the mesh box are categorized into three groups: mold, sample#1, and sample#2. To create the testing mold is to identify elements which belong to the mold and put them into the mold clump. It should be noted herein that elements of the two specimens should be removed if one intends to build AC microstructure. Before the elements are removed, their geometry and locations should be recorded.

#### **Step 3: Create Aggregates**

The recorded information of specimen elements is used to restore the removed elements in the step 2. Mineral aggregates will be added into the two specimens. There are various approaches to create aggregates as mentioned in the previous chapters including image-based models, user-defined models, and idealized models.

#### **Step 4: Build Rut Model**

The rut model is finalized by putting the two specimens with aggregates into the testing mold.

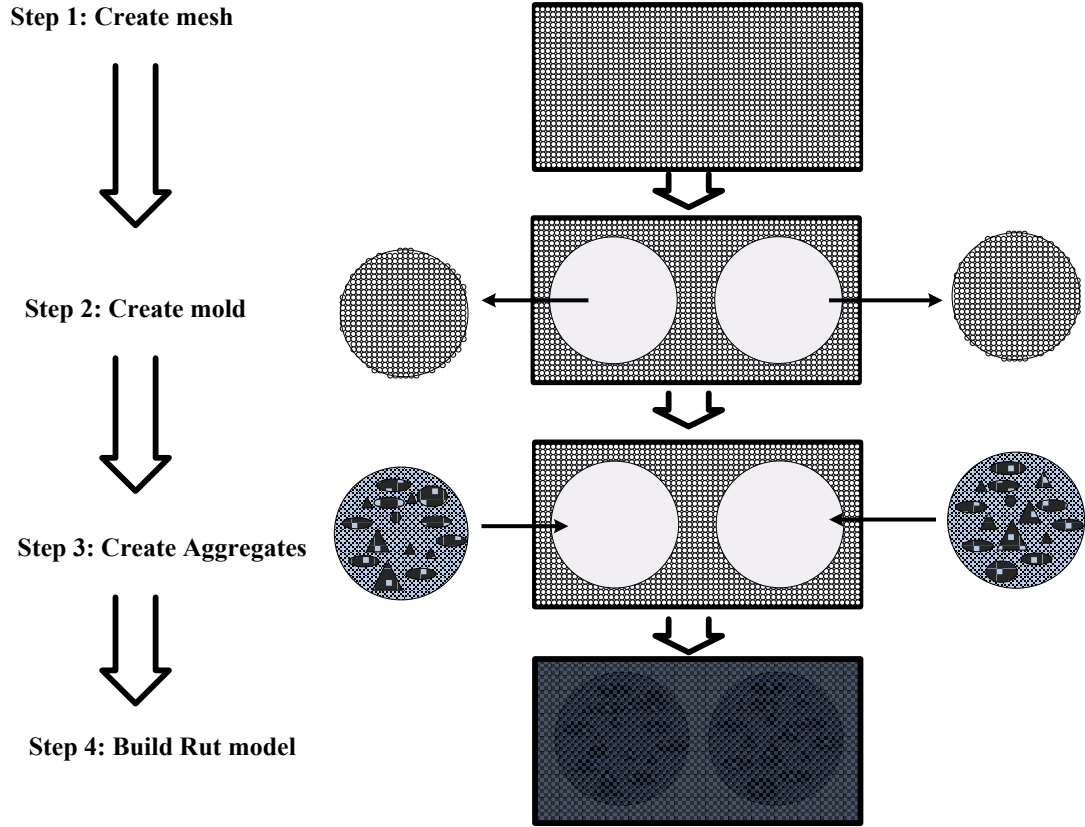


**Figure 16.1 APA Rutting-model Setting-up Demonstration**

### **16.5.2. Simulation of Wheel Loading**

In addition to the mold and specimens, it is important to simulate wheel loading conditions of APA tests. Figure 16.2 shows the APA rutting testing in laboratory. Obviously, wheels and hoses are components to apply the wheel loading. Figure 16.3 (a) shows the DE model with the wheel loading components considered. Figure 16.3(b) shows the contact forces generated in the simulation.

The motion of the wheel is controlled by apply an angular velocity and vertical compressive forces at the center of the wheel. The users can accelerate, decelerate, or keep the wheel steadily moving by controlling the applied angular velocity. They also can adjust apply the vertical force to simulate pavement responses under various traffic levels.

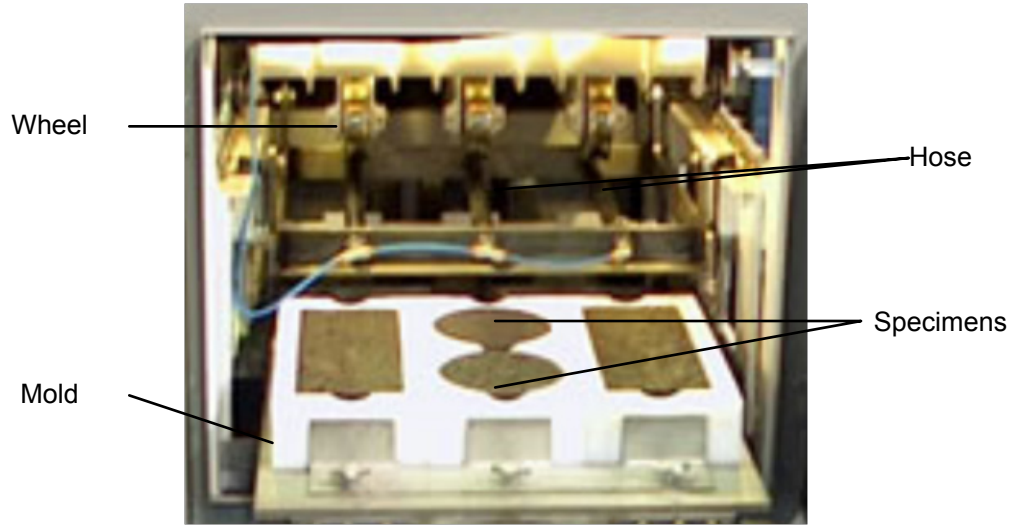
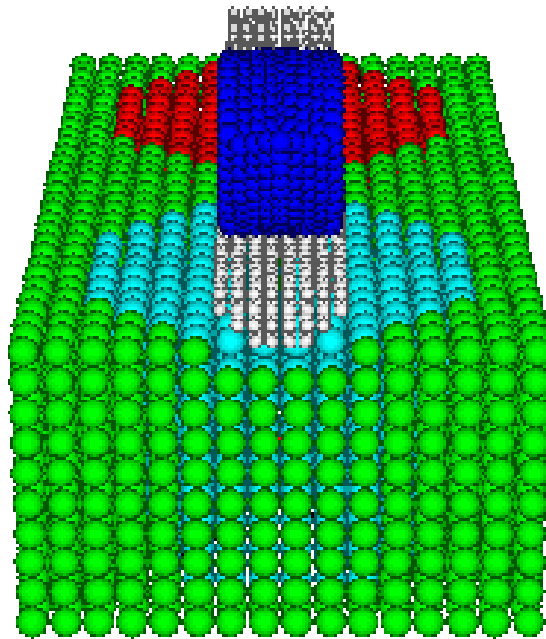
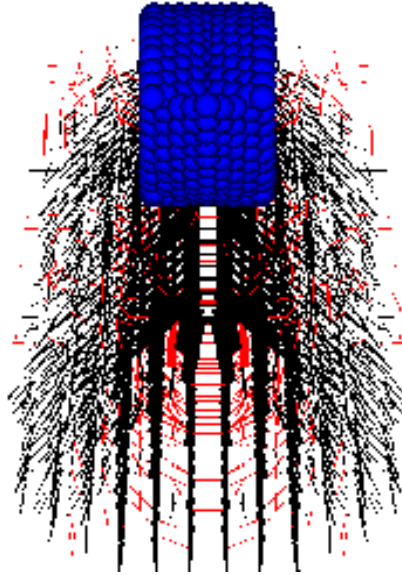


**Figure 16.2** APA rutting testing in laboratory



**(a)** DE model of APA rutting





(b) Contact forces under the rolling wheel

**Figure 16.3 APA Rutting-model and Contact Forces under the Rolling Wheel**

<p>A: Elastic Element B: Viscoelastic Element</p>
---

**Figure 16.4 Interaction between an elastic element and a viscoelastic element**

### 16.5.3. Mechanics in the APA Model

This section describes mechanical interactions in the model which include interactions between mold and specimens, wheel and hose, and hose and specimen as well as those within the specimens. As described in the previous studies (Liu et al. 2009; Liu and You 2009), there are at least four interactions in a AC specimens: interactions between aggregate particles, those between individual aggregate particles and asphalt mastic, those within an individual aggregate particle, and those within asphalt mastic.

Asphalt mastic is usually simulated with a viscoelastic model (the Burger's model in this study), mineral aggregate is simulated with a linear elastic model, the hose is simulated with a time-dependent model (the Burger's model in this study), the wheel is simulated with a linear elastic model, and the mold is simulated with a linear elastic model. The interaction between two linear elastic model can be regarded as the interaction between two springs in series, while the interaction between the linear elastic model and the Burger's model can be treated in a similar way (Liu et al. 2009). Figure 16.4 demonstrates the interaction between an elastic element (simulated with spring) and a viscoelastic element (simulated with the Burger's model) in normal and shear directions.

#### **16.5.4. Challenges in Simulating Rutting with the APA DE Model**

Even though the APA DE model and the corresponding PFC3D programming codes have been developed, they have not been applied to simulate AC rutting due to the following challenges:

- 1) It is a challenge to accurately simulate the hose. In the current model, the hose is simulated with a clump which is a rigid rod. In the reality, it is a soft rod. Therefore, further studies are needed to improve the current model.
- 2) It is a challenge to simulate microstructure-based AC specimens. Researchers have developed various approaches to reconstruct AC microstructures. But, it is very time consuming to run the APA model (with two AC specimens) in a personal computer.
- 3) It is a challenge to determine the mechanical inputs for the APA rutting simulation. Currently, the viscoelastic properties of asphalt mastic or sand mastic are required as inputs to simulate AC microstructure-based mechanics. It is very difficult to obtain high-temperature properties of asphalt sand mastic or mastic even though asphalt binder properties can be measured in Superpave binder laboratory.

### **16.6. DE Model of Pavement under a Rolling Wheel**

#### **16.6.1. Geometry of the DE Model**

Figure 16.5 shows the geometry of the DE model which consists of three parts: a wheel, a specimen, and a boundary. The wheel and boundary are simulated with clumps which have deformations only on the boundary elements. The specimen is simulated with bonded discrete elements. If one is interested in using asphalt concrete properties as inputting parameters, he/she does not need consider construction of the specimen's microstructure. Otherwise, the specimen's microstructure should be reconstructed with the existing or newly developed approaches and micromechanical inputs are needed.

In terms of dimensions, this model can be used to simulate APA rutting at laboratory level and perform full-scale pavement simulation at field-level. Therefore, both the wheel and specimen can be as large as its counterpart in the field or as small as its counterpart in the laboratory.

### **16.6.2. Simulation of Wheel Loading**

Similar with the APA model as discussed above, the motion of the wheel is controlled by apply an angular velocity and vertical compressive forces at the center of the wheel. The users can accelerate, decelerate, or keep the wheel steadily moving by controlling the applied angular velocity. They also can adjust apply the vertical force to simulate pavement responses under various traffic levels. Figure 16.6 shows an example of the simulation: the wheel is moving forth and forward. After many cycles, the rut was developed under the wheel.

### **16.6.3. Mechanics in the Rutting Model**

This section describes mechanical interactions in the model which include interactions between mold and specimens, those between wheel and specimen, and those within the specimens. As described in the previous studies, there are at least four interactions in an AC specimen: interactions between aggregate particles, those between individual aggregate particles and asphalt mastic, those within an individual aggregate particle, and those within asphalt mastic. Again, there are linear elastic contact models and viscoelastic contact models. Figure 16.4 demonstrates the interaction between an elastic element (simulated with spring) and a viscoelastic element (simulated with the Burger's model) in normal and shear directions.

### **16.6.4. Challenges in Applying the Rutting Model**

Similarly, even though the DE rutting model and the corresponding PFC3D programming codes have been developed, they have not been applied to solve any specific engineering or scientific problems due to the following challenges:

- 1) It is a challenge to perform a full-scale simulation of pavement section.
- 2) Figure 16.7 demonstrates a challenge when the rutting model was used to simulate pavement responses under the rolling wheel. As shown in the figure, several particles moved apart and flew around due to larger frictional forces generated during the wheel rolling.

The explanation why it happened in Figure 16.7 is followed: Each element (ball) at the pavement surface only has five contact points. Due to the large frictional force generated by wheel-pavement interaction, one or more of the five contacts may be broken. As a result, the element whose contact bonds were broken could not be balanced and moved apart. To solve this issue, the following new elements were introduced in this study as shown in Figure 16.8. Each of them is a clump which has deformation only at the boundary elements. Since the newly developed elements have more contacts, they are more stable than the traditional element (ball). Additionally, with the newly developed elements, the moment forces can be simulated with the simple contact-bond model.

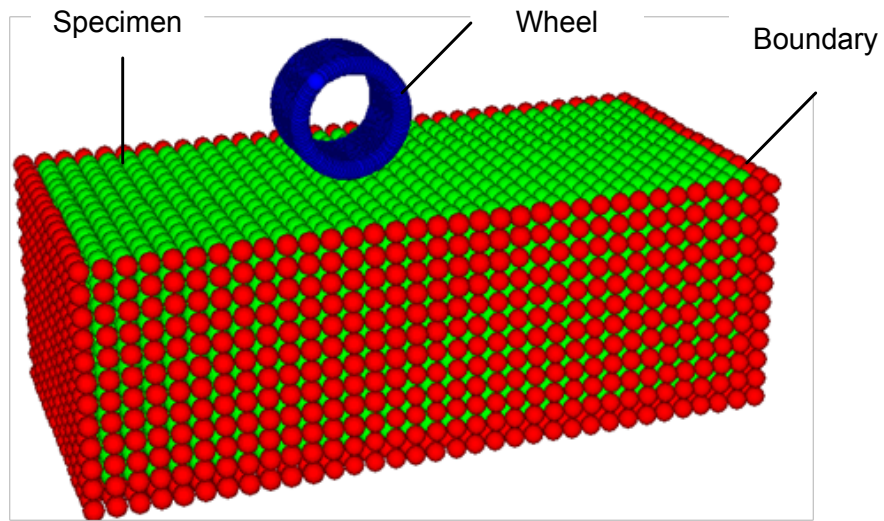


**Figure 16.5 DE model of pavement under a rolling wheel**

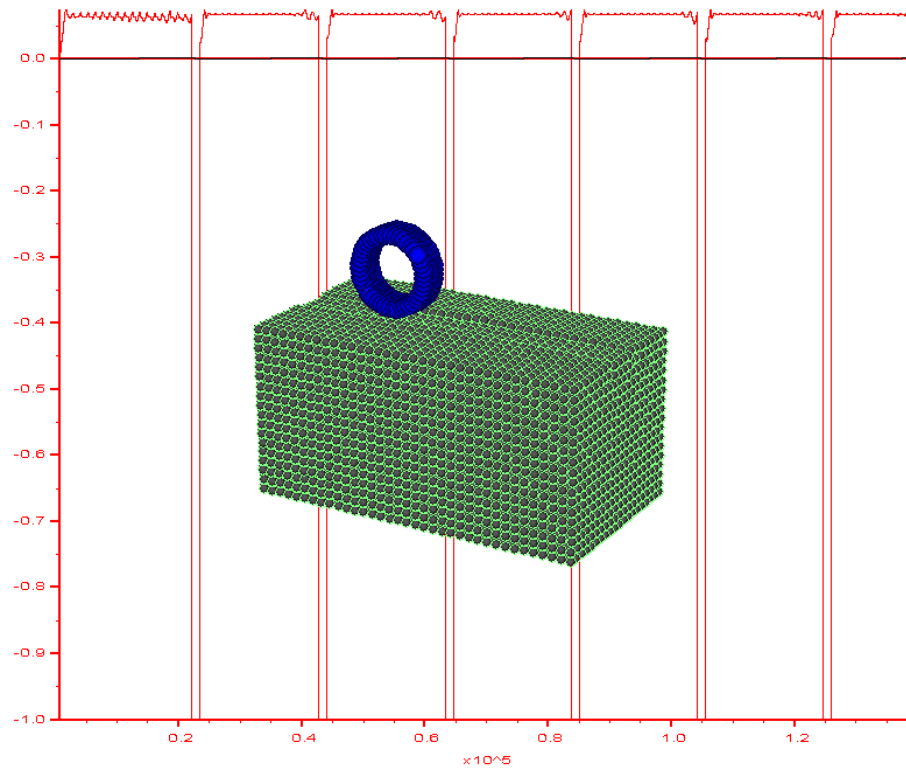


**Figure 16.6 Demonstration of rutting simulation under the rolling wheel: horizontal velocity vs. computational cycles**

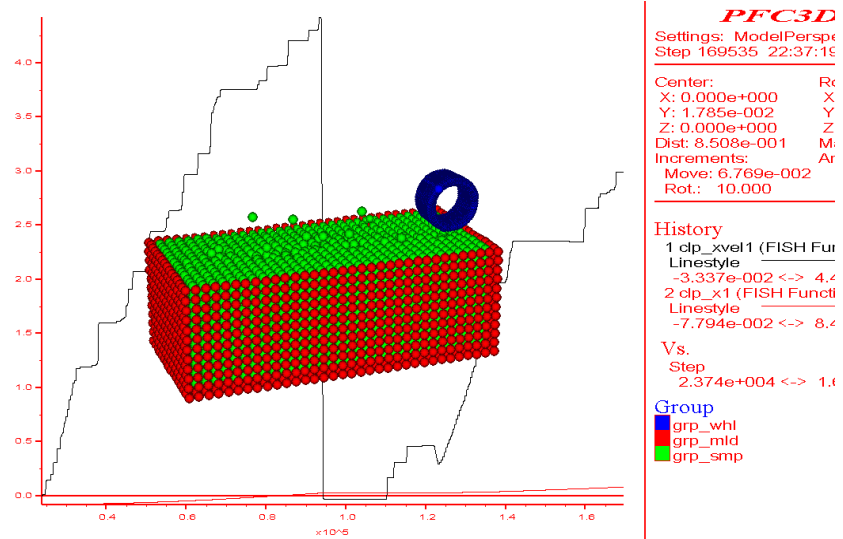
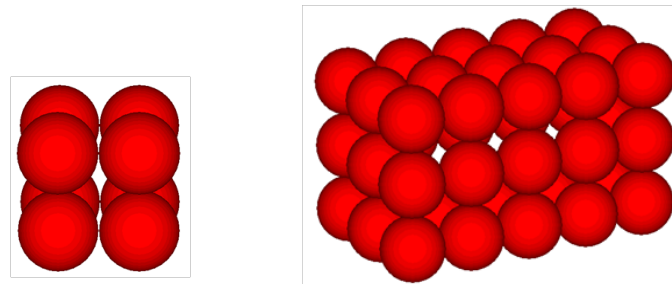
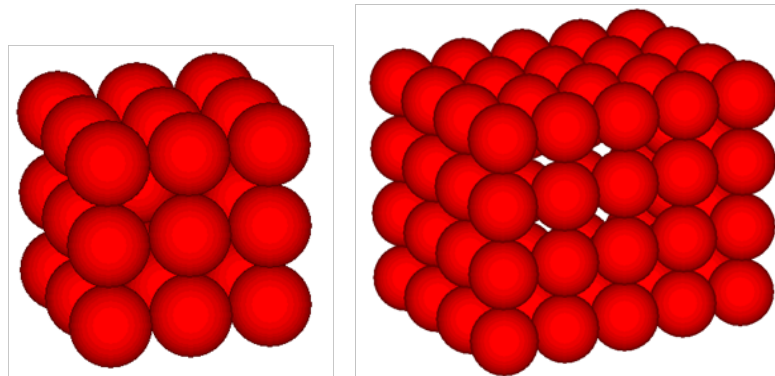


**Figure 16.7 Demonstration of a challenge in using the Rutting Model**



(a) 24-contacts Element

(b) 78-contacts Element



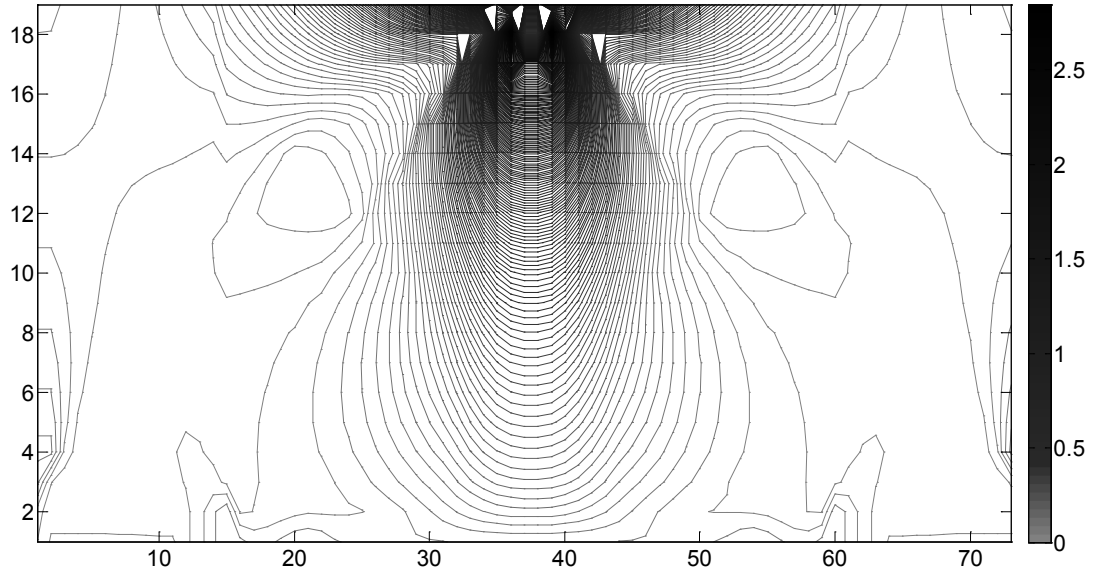
(a) 54-contacts Element

(b) 82-contacts Element

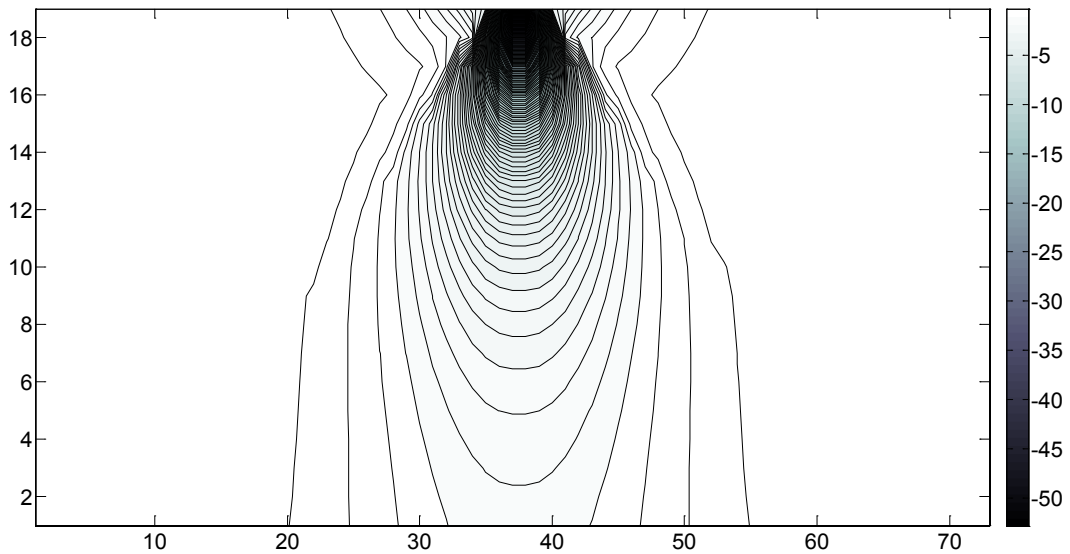
**Figure 16.8 Newly developed elements with more contacts**

## 16.7. Normal and Shear Forces under the Rolling Wheel

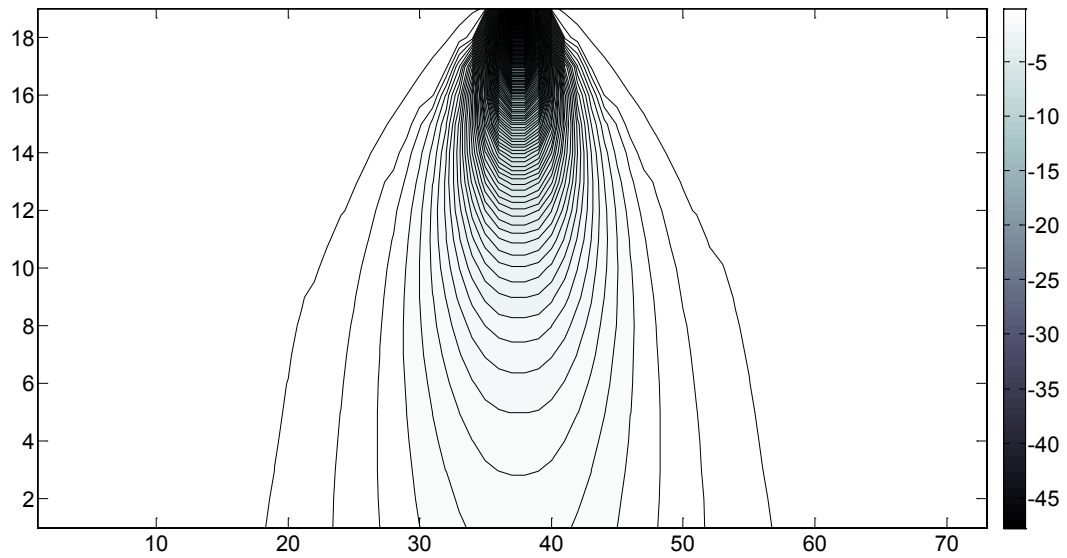
Figure 16.9 shows the stress contours of one typical simulation with the rutting model. Obviously, the stresses are concentrated near the location where the wheel loading is applied.



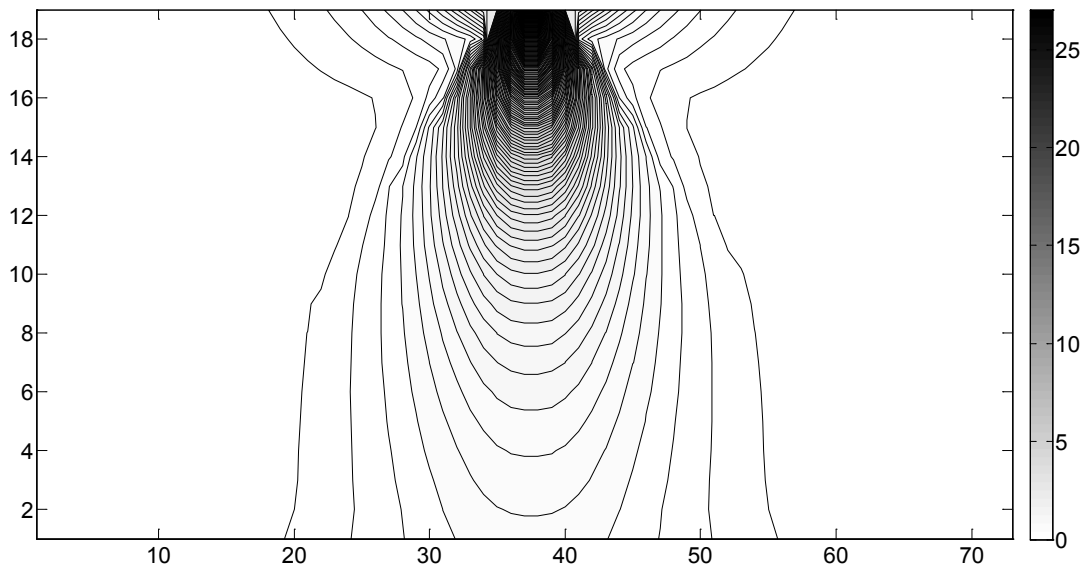
(a) Principal Stress  $\sigma_1$



(b) Principal Stress  $\sigma_3$



(c) Vertical Stress  $\sigma_y$



(d) Shear Stress  $\tau_{\max}$

**Figure 16.9 Stresses under the rolling wheel**

## 16.8. Comparison with Boussinesq Theory

In order to verify the DE models developed in this research, the DE simulation results were compared with those calculated with the Boussinesq theory as shown in Figure 16.10. In the figure, the numbers indicate the absolute error (AE) of the simulation results compared with the theoretical calculation.

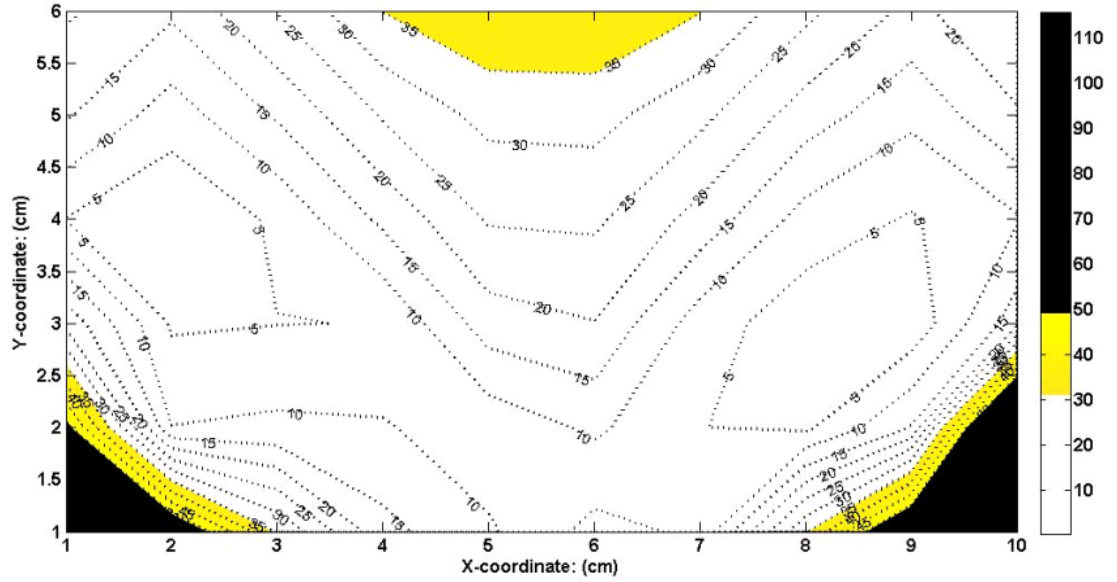


**Figure 16.10. Absolute error between the simulation results and those calculated from Boussinesq theory (Unit: %)**

$$AE = \frac{|\sigma_{model} - \sigma_{theory}|}{\sigma_{theory}} \times 100\% \quad 16.1$$

Obviously, the majority of the AEs are within 30% while the larger AEs exist at the locations under the wheel loading, the bottom corners of the sample. There are many reasons which might cause the errors between the theoretical calculation and simulation results. Followed are two of them:

- 1) One reason could be the effect of dimensions: In the DE simulation, the dimensions in the all the three directions are less than 10cm, while they are infinite in the Boussinesq theory.
- 2) Another reason could be the effect of difference in the loading conditions: In the Boussinesq theory, the load is a concentrated force, while in the DE model the load is a distributed load in certain area.

## 16.9. Impact of Stiffness Ratio on Poisson Ratio

There are many reasons which can impact Poisson ratio of a DE model. One of them is the ratio of the shear stiffness ( $K_s$ ) to the normal stiffness ( $K_n$ ):

$$\alpha = \frac{K_s}{K_n} \quad 16.2$$



In order to investigate the effect of the stiffness ratio on the Poisson's ratio, a triaxial test was simulated. The simulation was set-up as shown in Figure 16.11. A total of six walls were set up as loading boundaries to apply forces on the sample. The numbers in the figure indicate ID numbers of the six walls. The boundary loading conditions were applied by controlling the motion of the six walls. Figure 16.12 shows the three views of the testing specimen from different angles. It is easy to conclude that the specimen can be considered as an orthotropic material. According to the Hooke's Law, the following equation is suitable to this material.

$$\begin{bmatrix} \epsilon_{xx} \\ \epsilon_{yy} \\ \epsilon_{zz} \\ 2\epsilon_{yz} \\ 2\epsilon_{zx} \\ 2\epsilon_{xy} \end{bmatrix} = \begin{bmatrix} \frac{1}{E_x} & -\frac{\nu_{xy}}{E_x} & -\frac{\nu_{xz}}{E_x} & 0 & 0 & 0 \\ \frac{\nu_{yx}}{E_y} & \frac{1}{E_y} & -\frac{\nu_{yz}}{E_y} & 0 & 0 & 0 \\ -\frac{\nu_{zx}}{E_z} & -\frac{\nu_{zy}}{E_z} & \frac{1}{E_z} & 0 & 0 & 0 \\ 0 & 0 & 0 & \frac{1}{G_{yz}} & 0 & 0 \\ 0 & 0 & 0 & 0 & \frac{1}{G_{zx}} & 0 \\ 0 & 0 & 0 & 0 & 0 & \frac{1}{G_{xy}} \end{bmatrix} \begin{bmatrix} \sigma_{xx} \\ \sigma_{yy} \\ \sigma_{zz} \\ \sigma_{yz} \\ \sigma_{zx} \\ \sigma_{xy} \end{bmatrix} \quad 16.3$$

Additionally, there are the following assumptions:

$$\begin{aligned} \nu_{xy} &= \nu_{zy} = \nu_{hy} \\ \nu_{yx} &= \nu_{yz} = \nu_{hy} \\ \nu_{xz} &= \nu_{zx} = \nu_{hh} \end{aligned} \quad 16.4$$

As a result of Equation 16.3 and 16.4,

$$\begin{aligned} \epsilon_{xx} E_x &= \sigma_{xx} - \nu_{hy} \sigma_{yy} - \sigma_{zz} \nu_{hh} \\ \epsilon_{yy} E_y &= \sigma_{yy} - \nu_{yh} (\sigma_{xx} - \sigma_{zz}) \\ \epsilon_{zz} E_z &= \sigma_{zz} - \nu_{hy} \sigma_{yy} - \sigma_{xx} \nu_{hh} \end{aligned} \quad 16.5$$

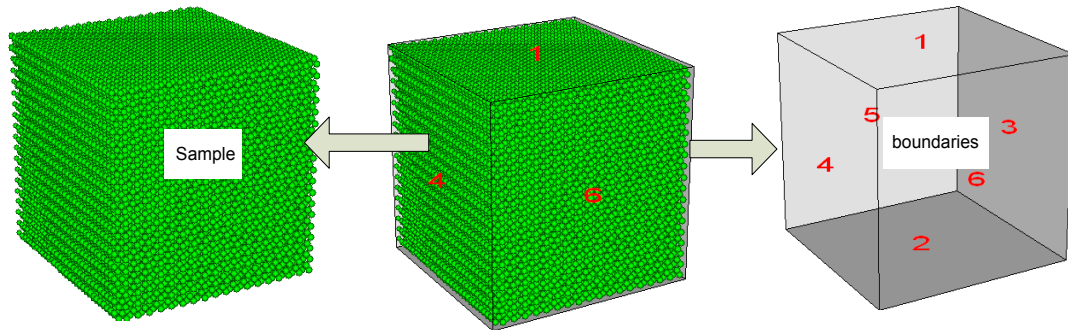
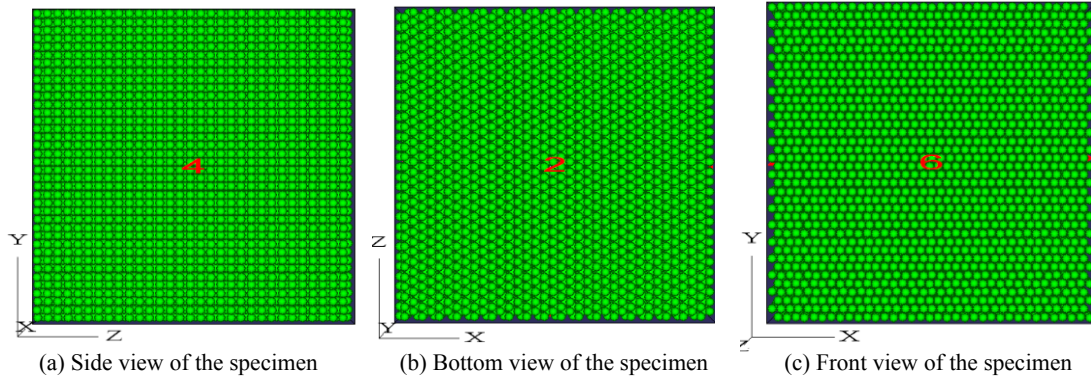
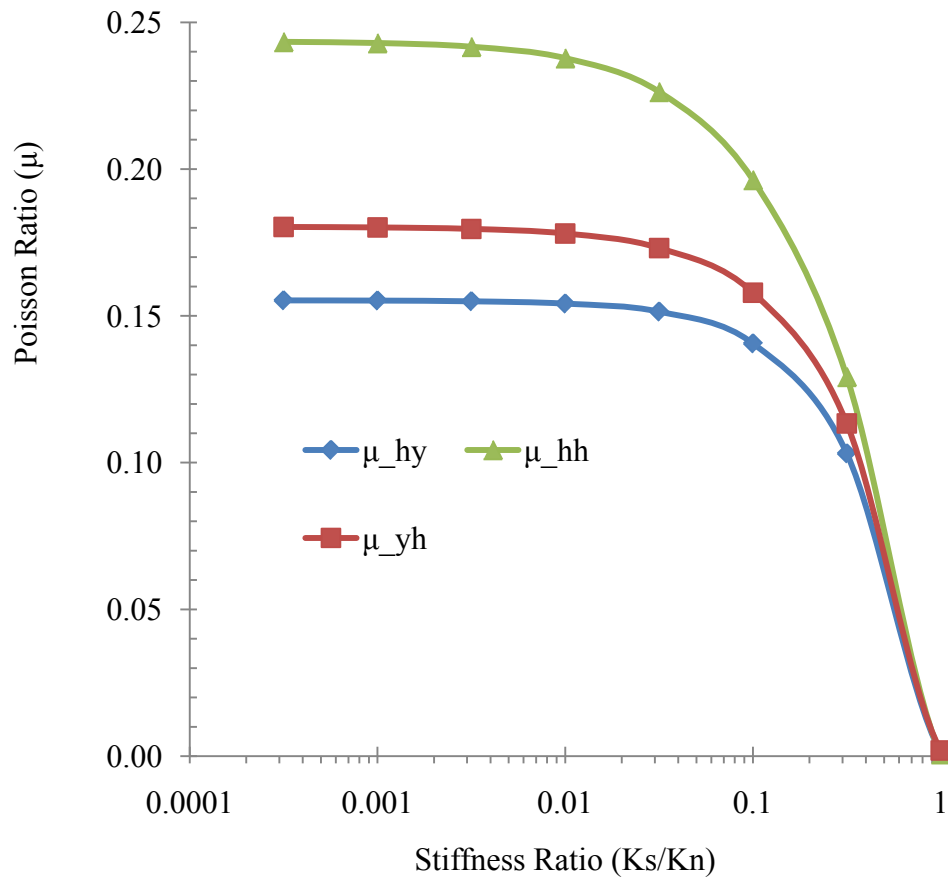


Figure 16.11 Setting-up for a triaxial test



**Figure 16.12 Views of the Testing Specimen from Different Angles**



**Figure 16.13 Poisson ratio vs. stiffness ratio**

**Table 16.1**  
**Loading conditions**

Loading Condition	Description	Calculation of Poisson Ratio
1	Fix walls 3 and 4 and move the other four walls to apply compressive loads.	$0 = \sigma_{xx}^{[1]} - \nu_{hy} \sigma_{yy}^{[1]} - \sigma_{zz}^{[1]} \nu_{hh}$ (16.6)
2	Fix walls 1 and 2 and move the other four walls to apply compressive loads.	$0 = \sigma_{yy}^{[2]} - \nu_{yh} (\sigma_{xx}^{[2]} + \sigma_{zz}^{[2]})$ (16.7)
3	Fix walls 5 and 6 and move the other four walls to apply compressive loads.	$0 = \sigma_{zz}^{[3]} - \nu_{hy} \sigma_{yy}^{[3]} - \sigma_{xx}^{[3]} \nu_{hh}$ (16.8)

**Note:** <sup>[1]</sup>, <sup>[2]</sup>, and <sup>[3]</sup> in Equations 16.6~ 16.8 indicate the loading conditions 1, 2, and 3.

In order to determine the Poisson's ratios, the following loading conditions are designed as shown in Table 16.1.

From Equation 16.7,

$$\nu_{yh} = \frac{\sigma_{yy}^{[2]}}{(\sigma_{xx}^{[2]} + \sigma_{zz}^{[2]})} \quad 16.9$$

From Equation 16.6 and 16.8,

$$\nu_{hh} = \frac{\sigma_{zz}^{[3]} / \sigma_{yy}^{[3]} - \sigma_{xx}^{[1]} / \sigma_{yy}^{[1]}}{\sigma_{xx}^{[3]} / \sigma_{yy}^{[3]} - \sigma_{zz}^{[1]} / \sigma_{yy}^{[1]}} \quad 16.10$$

$$\nu_{hy} = \frac{\sigma_{zz}^{[3]} / \sigma_{xx}^{[3]} - \sigma_{yy}^{[1]} / \sigma_{xx}^{[1]}}{\sigma_{yy}^{[3]} / \sigma_{xx}^{[3]} - \sigma_{zz}^{[1]} / \sigma_{xx}^{[1]}} \quad 16.11$$

Figure 16.13 shows the Poisson's ratio vs. stiffness ratio (Ks/Kn). From the figure, it was observed that 1)  $\nu_{hh} > \nu_{yh} > \nu_{hy}$ ; 2) Poisson's ratios slowly decreased when the value of stiffness ratio was less than 0.1, while they sharply decreased to zero when the value was larger than 0.1.

## 16.10. Summary

With the rapid development of computer technology, numerical methods become more and more popular in solving engineering problems. This chapter presents methods to

simulate pavement responses under a rolling wheel load using computer modeling technologies. Through this paper, it was observed that:

- 1) Even though it is possible to build computer-based modeling techniques, there are challenges to apply them for simulating their real counterparts.
- 2) From an example simulation, it was observed that the simulation results were comparable with the theoretical calculation.
- 3) Stiffness ratio ( $K_s/K_s$ ) had a significant impact on the calculated Poisson's ratio when its value was ranging from 0.1 to 1, while the impact was negligible when the stiffness ratio was less than 0.1.

# **Chapter 17. Modeling and Analysis of Dynamic Traffic Loads: An Idealized Discrete Element Model for Pavement-wheel Interaction<sup>15</sup>**

## **17.1. Abstract**

In order to design a long-lasting pavement, it is apparently important for pavement designers to understand the mechanism of the vehicular loading. The main objective of this paper is to present an idealized discrete element modeling of pavement-wheel interaction for better understanding traffic loading conditions. The idealized model consists of three parts: a smooth surface, a wheel, and a mass. The smooth surface simulates the pavement surface, while the wheel and mass represent a vehicle wheel and its corresponding mass, respectively. The mechanical behaviors at the interaction surface are simulated through an elastic contact model, a slip model, and a viscous contact damping model. Discrete Element simulation was performed through loading the wheel with a vertical force and a torsion moment at its center. As a result, the wheel was rotated and moved forward to simulate a vehicle running on the pavement surface. The average compressive and frictional forces were recorded during the wheel accelerating, steadily moving, and decelerating. Through analyzing the simulation results, It was found that 1) values of both compressive and frictional forces were not constant but vibrating around their average values; 2) the average frictional force was close to zero during the wheel steadily moving, while it was non-zero during its acceleration and deceleration; 3) damping ratio and peak rational velocities gave various effects on simulation results; 4) findings of this research were comparable with theoretical solutions and those of the finite element modeling in a previous study.

## **17.2. Background**

Apparently, traffic loading is one of the most important key aspects in pavement design. A running vehicle is a generator of traffic loads, while the pavement is the receiver. In order to build long-lasting pavements, it is necessary to interpret pavement-wheel interactions for better understanding traffic loading conditions. Followed is a discussion of research efforts which were made in the past decades.

Hegmon (1987) presented an overview of the interactions between vehicle tires and the pavement with the emphasis on highway safety. They pointed out that: 1) tire-pavement friction is important for traction and braking as well as directional stability of running vehicles. 2) It is difficult for one to predict the magnitude of tire-pavement friction which depends on so many variables. 3) Under certain driving conditions when the friction demand exceeds the available friction force, skidding, loss of vehicle control, and possibly an accident can happen.

---

<sup>15</sup>Full text of this chapter will be submitted for publication.

Markow et al (1988) analyzed the interactions between dynamic vehicle loads and highway pavements by developing analytic models. They pointed out that the existing mechanistic models for both flexible and rigid pavements retained a simplified and idealized depiction of tire loads, and none really incorporated a true representation of a moving, dynamic force along the pavement surface. They concluded that: 1) Fatigue damage due to dynamic moving loads in some rigid pavement slab locations was up to 40 percent greater than that due to static loads at the same locations; 2) the mid-slab regions were more sensitive to dynamics than the transverse joint. They also pointed out the importance of the vehicle itself in influencing dynamic pavement loads and recommended that the policies governing the maintenance and rehabilitation of highway infrastructure may need to look at the vehicle as well as the pavement or bridges.

Papagiannakis and Gujarathi (1995) presented a roughness model to investigate the influences of the pavement roughness on the interactions between the pavement and heavy vehicles. Both experimental and numerical results were analyzed. The experimental results were from the instrumented vehicle developed by the National Research Council of Canada while the numerical results were obtained from a quarter-vehicle simulation. It was found that the sprung mass vehicle acceleration was very important for addressing pavement-vehicle interaction since it could impact both pavement and vehicle damage as well as to ride quality and cargo damage.

Mamlouk (1996) performed both computer modeling and experimental tests to study effect of vehicle-pavement interaction. Their research target was to design a weigh-in-motion (WIM) equipment. They pointed out that the load applied by trucks on the pavement varied instantaneously due to road roughness, truck speed, suspension type, tire pressure as well as other factors. Multi-sensor WIM devices were capable of better representing the actual wheel load distribution due to the fact that they capture a large sample size from a variable population.

Sun and Deng (1998) considered dynamic vehicle-pavement interaction loads as two parts, namely moving loads or random loads. The Dirac-delta and Heaviside functions were employed to study the moving loads, while a quarter-truck vehicle model was used to simulate the random loads. They observed that the dynamic interaction loads were a constant mean Gaussian stationary ergodic process. The power spectral density of the process had a linear relation to that of pavement roughness.

Liu et al. (2000) presented a unified analytic framework to study responses of rigid pavements due to the vehicle-road interaction under a moving vehicle load. They believed that the newly developed framework could be applied to quantitatively understand the dynamic deflection and dynamic strains within a rigid pavement structure. From their research, it was observed that the surface roughness could significantly impact the dynamic responses of concrete slab.

Saleh et al (2000) proposed a mechanistic roughness model based on the vehicle-pavement interaction. The model was developed for flexible pavement design or evaluation with considering the relation between roughness and number of load

repetitions, axle load, and asphalt layer thickness. In the model, vehicle dynamics analysis was utilized to study the dynamic force profile and finite element structural analysis was employed to investigate the change of pavement surface roughness for each load repetition. The researchers believed that the developed mechanistic roughness performance model could be used 1) to estimate the 80-kN (18-kip) equivalent single-axle load for mixed traffic; 2) to design pavement.

Papagiannakis et al. (2007) interpreted dynamic interactions between axle loads of trucks and roughness profile of the pavement with a wavelet approach. An instrumented 5-axle semi-trailer truck was used to collect the experimental data. In the truck, an air suspension was equipped in the drive axles, while a rubber suspension was in the trailer axles. Through analyzing the experimental data with three-dimensional plots of relative energy versus load frequency versus roughness profile frequency, they concluded that the profile frequencies mainly influenced dynamic loads, depended on velocities of running trucks, and ranged from 0.65 to 3.76 cy/m.

Sun and Luo (2007) studied nonstationary dynamic pavement loads resulted from vibration of vehicles traveling at varying speed using a quarter-vehicle and a half-vehicle models. Time histories of dynamic coefficient corresponding to acceleration and deceleration were obtained numerically. The dynamic coefficient was defined as a ratio of the dynamic pavement load to the static load. It was found that: 1) when a vehicle accelerated, the dynamic coefficient fluctuated significantly at the beginning of the acceleration and then increased gradually. During the acceleration period, oscillation of dynamic coefficient was compressed to form a denser region near the end of acceleration period. The reversed phenomenon was observed when the vehicle decelerated. 2) during the acceleration and deceleration, the dynamic coefficient was distributed over a wide range of oscillation frequencies rather than concentrated at a particular frequency.

Kim and Tutumluer (2008) performed finite element analysis to study the multiple wheel-load interaction in flexible pavement. In their study, stress dependent resilient modulus models were successfully incorporated into the three-dimensional finite element-based mechanistic pavement analysis through a programmed user material subroutine in ABAQUS. Though analyzing the finite element simulation results, it was observed that pavement responses under multiple wheel loads were somewhat different from those obtained from the single wheel-load response superposition approach.

Li and Yang (2009) investigated dynamic interactions between heavy vehicles and the pavement with a three dimensional finite element model. According to their research observations, the dynamic vehicle-pavement interaction was a complex coupling action of several factors such as vehicle acceleration, suspension deformations, tire forces, and pavement responses. Thus, it was significantly important to simultaneously study both dynamic behaviors of running vehicles and the corresponding pavement responses.

Sawant (2009) and Sawant et al. (2010) analyzed dynamics of rigid pavement through studying the vehicle-pavement interaction. They pointed out that more and more research attentions had been put on the dynamics of pavements in order to improve the pavement

or runway design. In their study, based on the finite element method, they presented an improved solution for analyzing rigid pavements under moving vehicular or aircraft loads. In order to investigate the dynamic load-pavement interaction, the vehicle was modeled with the spring-dashpot unit. According to their research findings, velocities of aircraft had a significant influence on the pavement responses.

Shi and Cai (2009) presented a three-dimensional (3D) vehicle-pavement coupled model for studying dynamic pavement-interaction loads. In their study, both the vehicle vibration and pavement deformation were involved and the impact factors on pavement dynamics were analyzed. Those impact factors included pavement surface conditions, vehicle parameters, and driving velocities. Through this study, it was found that the vehicle dynamics under rough road conditions was much more significant than those under the static loads

Li et al (2009a; 2009b) performed dynamic analysis of an asphalt pavement due to vehicle-road interaction. This study was performed with a commercial finite element code (ANSYS program): 1) a moving vehicle was simulated with a "quarter-vehicle" model; 2) asphalt pavement was simulated with a three-dimensional model which was established based on the elastic layered theory. It was observed that 1) vehicle speeds have complicated impacts on pavement dynamic responses; 2) the pavement dynamic responses decreased with increasing tire stiffness, suspension stiffness, and suspension damping values of the moving vehicle.

Xia (2010) proposed a fully tire-pavement interaction finite element model that could effectively include the dynamic effect of tire rolling to the calculation of pavement response. The tire and the pavement were modeled as a finite strain hyperelastic material and the elastic material, respectively. Commercial finite element code, ABAQUS, was utilized in his study to perform several representative simulations. It was concluded that the tire/pavement interaction model could be used to predict pavement response and pavement damage due to fatigue cracking and rutting in the field of pavement engineering

Yang et al.(2010) presented a three-dimensional model for studying dynamic pavement-vehicle interaction. Both the Galerkin method and the quick direct integral method were involved in their study. A coupled system of vehicles, the pavement, and the foundation was used and its dynamic behaviors were studied. Through comparing the coupled system with the traditional pavement system and vehicle system, it was observed that the coupling action could impact on the vertical acceleration of vehicles, the suspension deformations, the tire forces, and the pavement displacements. Thus, the impacts of the coupling action were not negligible no matter whether the pavement surface is smooth or not. They believed that emphasis should be simultaneously put on the dynamics of both vehicle and pavement.

In summary of the existing research efforts, it was found that:



1) In terms of methodologies, there were three methods in the literatures to study the pavement-vehicle interaction, namely the experimental measurement, the analytical analysis, and the computer simulation. The majority of the literatures utilized computer simulation techniques to simulate the pavement-vehicle interaction and validated their simulation results with experimental data. Analytical equations were usually integrated into the computer models and few literatures utilized pure analytical analysis. Finite element codes, such as ANSYS and ABAQUS, were typically utilized to perform computer simulations.

2) In terms of research focuses, most studies was started from the model development, followed by prediction of the parameters of interest, and ended up with comparison between modeling results and those from experimental tests. Few attentions were paid to fundamental understanding of pavement-vehicle interactions.

3) Additionally, the majority of research efforts were developed based on the continuum mechanics. However, the pavement-vehicle interaction is a contacting problem whose contacting position is changing over time. Therefore, the existing continuum mechanical methods solved the pavement-vehicle interaction in an indirect manner instead of direct approach.

### **17.3. Objectives and Scopes**

As mentioned in the background, even though many research efforts have been made in the past decades, it is challenging to fully understand the mechanism underlying the pavement-vehicle interaction: 1) Even though tire-pavement friction is important to not only pavement performance but also highway safety, it is still challenging to predict the magnitude of tire-pavement friction. 2) There are many factors (such as road roughness, truck speed, suspension type, tire pressure, etc.) which can significantly impact tire-pavement interaction. Markow et al (1988) pointed out that not only pavement or bridge but also a running vehicle itself could influence dynamic pavement loads. It is extremely challenging to build a model which includes all the relevant factors. 3) The existing experimental testing approaches could provide accurate and persuasive results, but they are expensive, time-consuming, and challenging in interpreting the testing data. The exiting analytical approaches provided theory-based solutions of pavement-wheel interaction, but they were usually oversimplified. The finite element methods provided cheap and powerful approaches for improving understanding of pavement-wheel interaction and dynamic pavement responses. However, the continuum mechanics-based finite element models could predict and interpret the problems in an indirect manner.

The main objective of this study is to develop an idealized model for quantitatively studying pavement-wheel interaction in a direct manner. Different from the existing studies (eg. experimental tests, continuum-based modeling, and analytical solutions), this research employed the discrete element method (DEM) which was developed to seek solutions for interaction problems of individual entities. Therefore, simulation of the pavement-wheel interaction with DEM is direct and intuitional. In this study, the DEM will be used to simulate the pavement-wheel interactions under various conditions, such

as acceleration, deceleration, various traffic loads, various damping, various frictional coefficients, and various velocities. Experimental tests are not involved in this study due to the following reasons: 1) The accuracy of DEM in simulating contacting problems has been validated by many existing studies (Cundall and Strack 1979b; Hart et al. 1985; Huang et al. 2008; Kim and Choi 2008; Kim 2008; Taylor et al. 1985). 2) Instead of exactly and fully predict the actual pavement-wheel interaction for practical use, the goal of this research is to present a cross-section of the targeted problem for fundamental understanding of the problem. Compared with a complex model, the simple model of this research is easy to be understood and the modeling results can be applied to not only the pavement-wheel interaction problem but also many other engineering problems.

## 17.4. Discrete Element Model for Pavement-wheel Interaction

### 17.4.1. Hypotheses

As one can image, it is extremely difficult to fully simulate all aspects relevant to the pavement-wheel interaction in a single DEM model. First of all, limited by the current computational power, it is challenging to build a DEM model of a pavement section which needs millions of discrete elements. Secondly, it is still not feasible to accurately simulate texture of pavement surface using current discrete element modeling techniques. Thirdly, it is too complex to build a DEM model for exactly simulating a vehicle. Thus, this research was performed based on the following hypothesis:

- 1) The pavement surface can be simulated with an infinite wall which is a smooth plane with frictional and elastic properties.
- 2) The wheel can be simulated with a clump which is composed of slaved discrete elements (balls).
- 3) The damping system of a vehicle can be approximately simulated with the viscous damping model.
- 4) The selected values of the viscous damping model parameter (critical damping ratio) are reasonable.

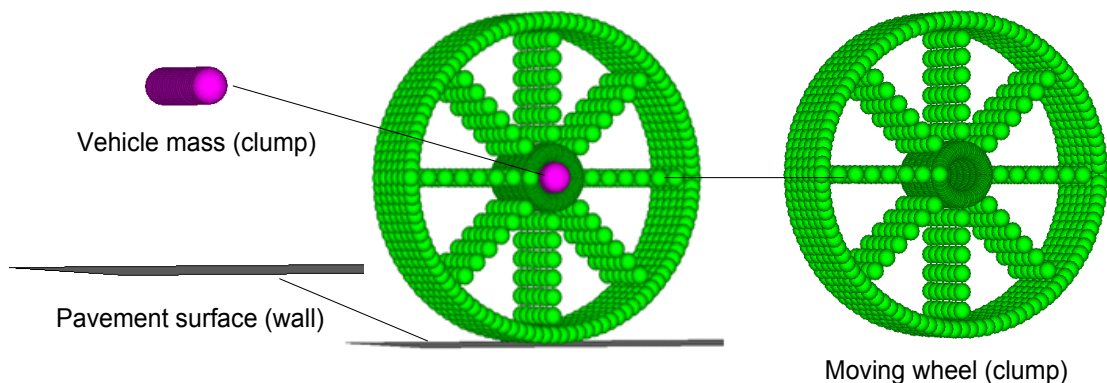


**Figure 17.1 Illustration of the idealized discrete element model**

### **17.4.2. Geometry of the DE Model**

The idealized discrete element model consisted of three parts as shown in Figure 17.1: a smooth surface to simulate the pavement surface, a moving wheel to simulate the vehicle wheel, and a mass to simulate the vehicle mass. The pavement smooth surface was simulated with a standard infinite wall, while the moving wheel and the vehicle mass were simulated with two individual clumps. Details about “wall” and “clump” logics can be found in the manual of Particle Flow Code in three-dimension (PFC3D). PFC3D is one of the most powerful discrete element codes. Since the standard infinite wall in PFC3D was absolutely smooth, the actual pavement roughness could not be exactly simulated in this research. However, this model allowed the authors of this paper to emphasize the other aspects relevant to pavement-wheel interaction without influence of pavement roughness variation. The frictional property at the pavement surface was simulated through setting a frictional coefficient of the infinite wall. In PFC3D, a clump can be considered as a special element which is created through modifying a group of slaved discrete elements (balls). A clump can also be regarded as a rigid body whose internal elements can be overlapped to any extent without causing larger internal contact forces. As shown in Figure 17.1, overlapped discrete elements were used in the two clumps in order to simulate the smooth interaction between the moving wheel and the vehicle mass. In order to simulate a moving and dynamic force along the pavement surface, mass of a running vehicle has to be considered in order to simulate the inertia force during the wheel acceleration or deceleration. As shown in the Figure 17.1, the mass of a running vehicle was concentrated into the center of the wheel and simulated with a special clump. Apparently, volume of the clump was much smaller than a real vehicle. Therefore, the density of the vehicle mass was larger than that of the rolling wheel.

### **17.4.3. Mechanical Model**

The mechanical model herein describes the force-displacement relations, frictional properties, and mechanical damping at contacting points in the discrete element model. The force-displacement relationships were simulated with a linear elastic contact stiffness model which was defined with normal stiffness ( $K_n$ ) and shear stiffness ( $K_s$ ). The frictional properties were simulated with a slip model which is defined with a frictional coefficient. Readers may refer to the previous research (Liu et al. 2009) and PFC3D manuals for more details about the linear elastic contact stiffness model and the slip model.

In PFC3D, the local damping is the most appropriate for discrete element simulation of quasi-static or static problems, but it is inappropriate for simulation of impacts between two particles or between particles and a wall. Therefore, the viscoelastic contact damping model was used in this study to simulate the mechanical damping. Two key parameters were used in this research to define the viscoelastic damping model. They are  $dmp\_yvis$  and  $dmp\_xvis$  which are critical damping ratios in the normal and shear directions, respectively. More details on the viscoelastic contact damping ratio are provided in the PFC3D manuals.

#### 17.4.4. Loading Conditions

As shown in Figure 17.2, a concentrated force and a torsion moment were applied at the center of the wheel. The concentrated force simulated the total weight carried by the wheel. The torsion moment was controlled to simulate motion features of the wheel. Figure 17.3 shows horizontal and rotational velocities of the wheel in a typical discrete element simulation. Evidently, the velocities linearly increased from 0 to its peak values at the beginning, then kept the peak values, and then decreased from its peak values to zero. In other words, the wheel accelerated, kept steadily moving, and decelerated along the pavement surface during the discrete element simulation.

In the reality, wheels of a running vehicle encounter not only the concentrated force and the torsion moment but also an inertia force during the wheel accelerating or decelerating. Therefore, not only traffic weight (the concentrated force) but also masses of the wheel and vehicle are also very important to correctly simulate the loading conditions of the wheel. As discussed in the next section of this paper, the inertia force was directly related to the frictional force at the pavement-wheel interaction surface.

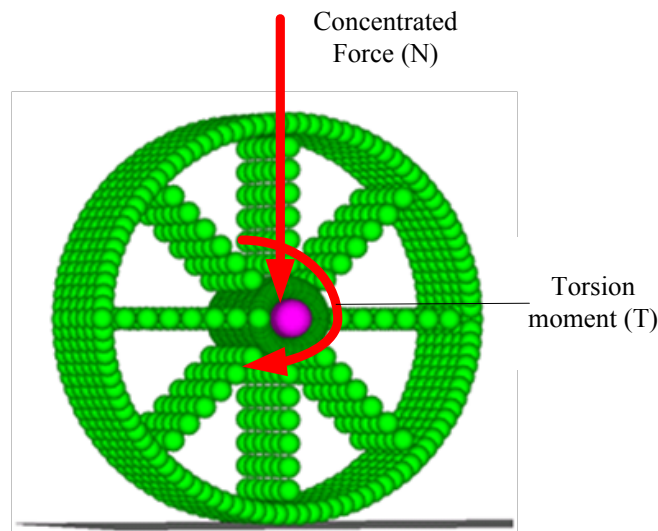
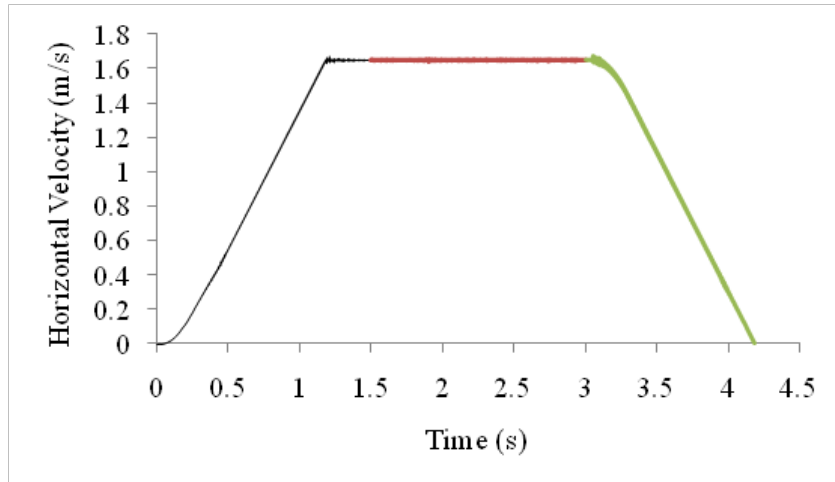
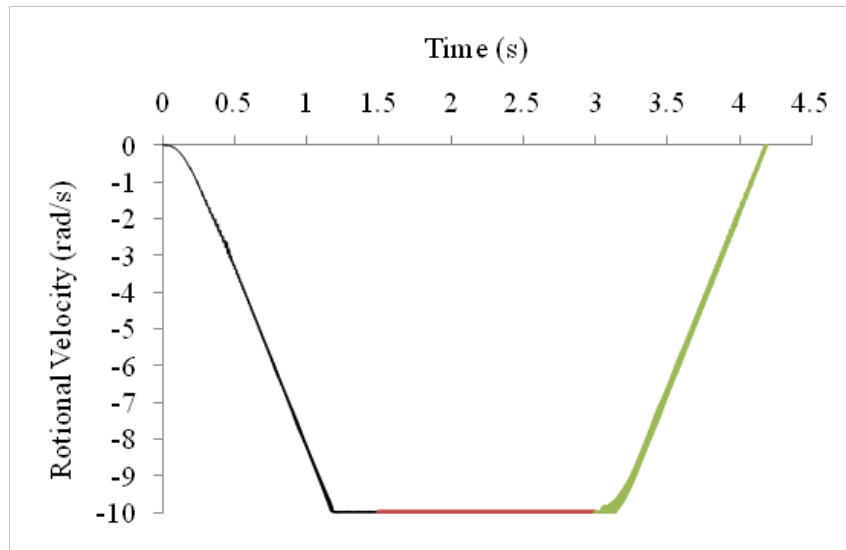


Figure 17.2 Typical motion feature of the rolling wheel



(a) Horizontal velocity vs. time



(b) Rotational velocity vs. time

**Figure 17.3 Typical motion feature of the rolling wheel (the different colors of the curves indicate that different motion features: acceleration, steadily moving, and deceleration)**

### **17.5. Discrete Element Simulation with different Critical Damping Ratio**

The critical damping ratios in the shear and normal directions are important parameters which may have significant impacts on the discrete element simulation results. Since the primary load was in the normal direction (vertical direction), this research mainly investigated influence of the critical damping ratio in the normal direction. A total of 10 simulations were performed by inputting various values of the critical damping ratio ( $dmp\_yvis$ ) in the normal direction. Table 1 shows the inputs for the 10 simulations.

Except the critical damping ratio in the normal direction, all the 10 simulations had the same geometry, mechanics, and loading conditions as shown in Table 1. For the geometry, a total of 1012 discrete elements were created to simulate the geometry of the wheel and 18 elements were used to simulate the vehicle mass. The total mass of the wheel and the vehicle mass was 1971.2Kg. It should be noted that the total weight carried by the wheel (19.712KN) was less than the concentrated force (100.0KN). The reason why the authors of this paper selected different values of the total weight and the concentrated force was to emphasize influence of the wheel and vehicle mass on the pavement-wheel interaction forces (normal force and frictional force).

The outputs of the discrete element simulation include horizontal and rotational velocities, vertical and frictional forces, and vertical velocity. Following paragraphs will discuss each of them.

**Table 17.1 Inputs for DEM simulation under different damping ratios**

Category	Input Variable	Meaning	Value
Geometry	whl_R (mm)	Wheel radius	150
	whl_W (mm)	Wheel width	120
	whl_brad (mm)	Radius of discrete elements:	15
Mechanics	whl_Ec (GPa)	Modulus of wheel	55
	whl_knos	Ratio of shear stiffness over normal stiffness	1
	whl_fric	Friction coefficient of the wheel	1
	wal_fric	Frictional coefficient of the infinite wall (pavement surface)	1
	wb_kratio	Ratio of wall stiffness over ball stiffness	1.2
	dmp_xvis	Shear critical damping ratio	0
	dmp_yvis	Normal critical damping ratio	ranging from 0 to 1.0
Loading	whl_dens (kg/m <sup>3</sup> )	Density of the running wheel	2600
	cwhl_dens (kg/m <sup>3</sup> )	Unit vehicle mass	7,600,000
	whl_yfmax (KN)	Concentrated force	100
	whl_zspc ( rad/s)	Controlled angular velocity	10

### 17.5.1. DEM Simulation Result: Horizontal and Angular Velocities

As discussed in the last section, the wheel rotated and moved along the pavement surface in acceleration, a constant velocity, and deceleration. Through analyzing the simulation results of the velocities under various values of the damping ratios, it was found:

- 1) All the simulations had the identical curves of the horizontal and angular velocities as shown in Figure 17.3. The horizontal and angular velocities linearly increased from 0 to its peak values in the beginning, and then kept constant, and then decreased from its peak values to 0.
- 2) The peak (or constant) horizontal and angular velocities are 1.65m/s and 10rad/s, respectively. From Table 1, the wheel radius is 150mm which is the distance from the wheel center to the center of the boundary elements. Therefore, the outermost radius of the wheel is 150mm+15mm=165mm. Evidently, if the horizontal velocity, angular velocity, and the outer radius of the wheel are symbolized with  $v_h$ ,  $\omega$ , and  $R_w$ , there is the following relation:

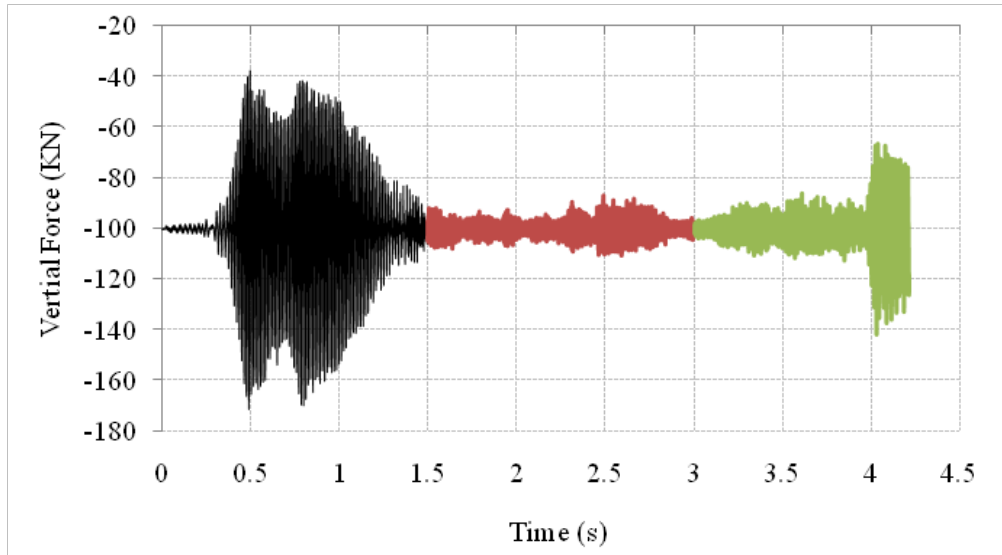
$$v_h = R_w \omega \quad 17.1$$

### 17.5.2. DEM Simulation Result: Vertical Compressive Force

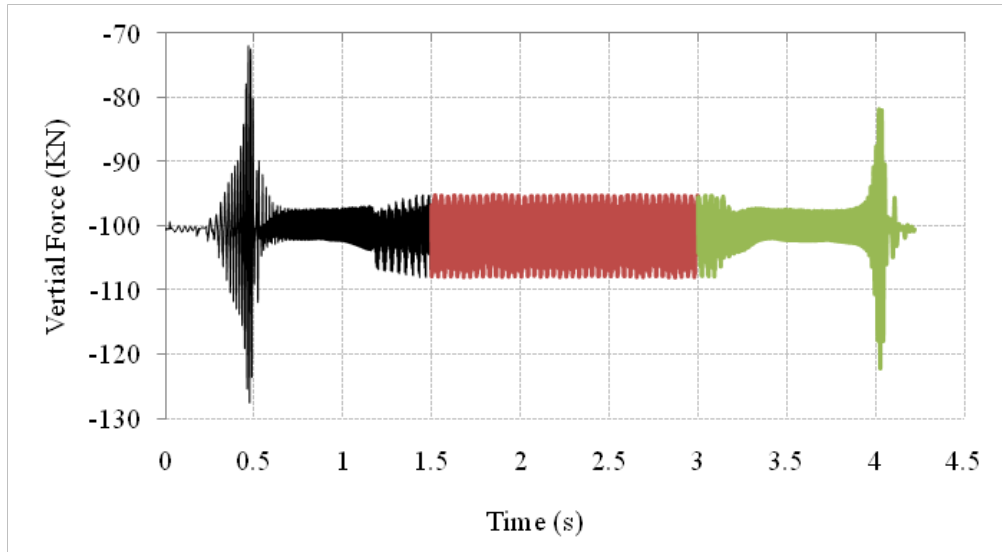
Figure 17.4 shows typical examples of recorded normal compressive forces along the pavement surface during the wheel acceleration, steady moving, and deceleration under the damping ratio of 0.0, 0.5, and 1.0. From this figure, the vertical compressive force was not constant, but oscillating around its average value. The oscillation amplitudes were various from time to time and dependent on damping ratios as well as wheel motion features:

- 1) First of all, increasing the damping ratio resulted in reducing the oscillation amplitudes of the compressive force for all the simulations. When the damping ratio was close to zero, the oscillating amplitude fluctuated from time to time and had no clear trends. When the damping ratio larger than 0.1, the oscillating amplitude had a clear trend: 1) during the wheel accelerating, the oscillating amplitude gradually increased to its peak value, then decreased to a certain value, and then increased at the end of the acceleration; 2) During the wheel decelerating, the reverse phenomenon was observed; 3) during the wheel steadily moving, the oscillating amplitude was constant.
- 2) Secondly, the wheel motion features gave apparent impacts on the compressive force. In other words, the wheel accelerating, steadily moving, and decelerating resulted in significant differences of the compressive force curves which were plotted in three different colors in Figure 17.4:
  - a) The compressive force oscillated around its average value, but the oscillating amplitudes during the wheel accelerating and decelerating were significantly larger than that during the wheel steadily moving.

- b) During the wheel accelerating or decelerating, the oscillating amplitudes fluctuated significantly, but the oscillating amplitudes during the wheel steadily moving was kept a constant.

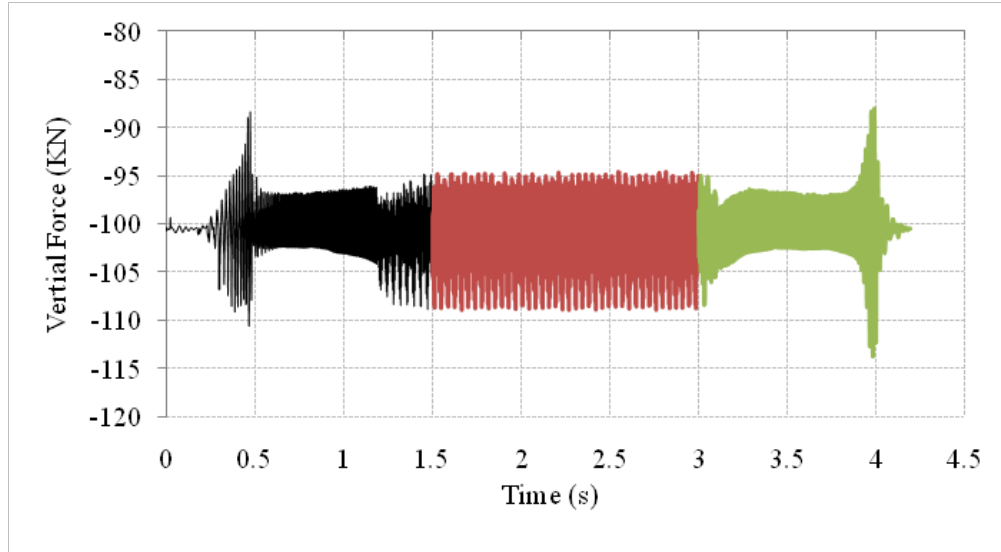


(a)  $dmp\_yvis=0$



(b)  $dmp\_yvis=0.5$





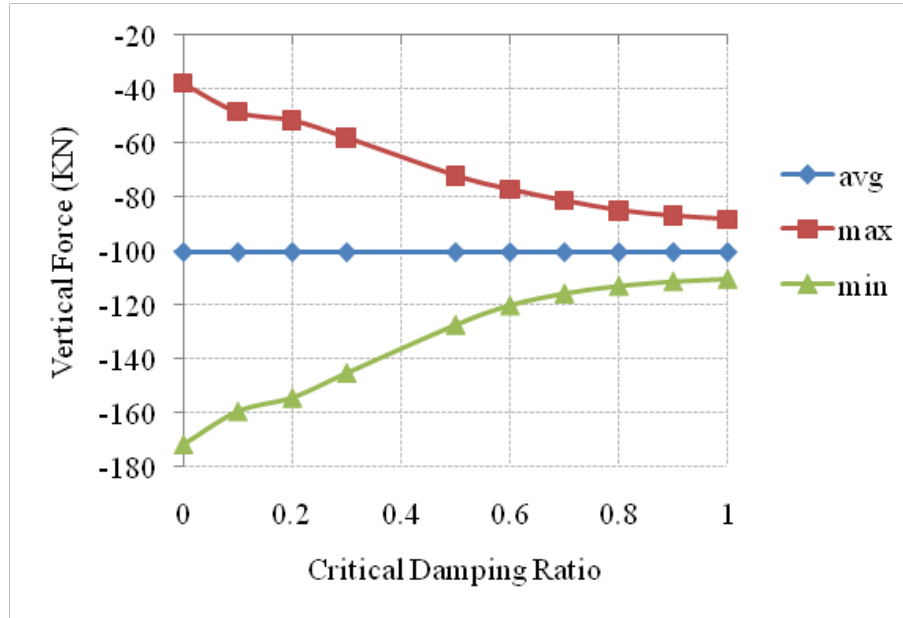
(c)  $dmp\_yvis=1.0$

**Figure 17.4 Vertical compressive force vs. loading time when the wheel rolling along pavement surface (peak rotational velocity=10rad/s; the different colors of the curves indicate that different motion features: acceleration, steadily moving, and deceleration)**

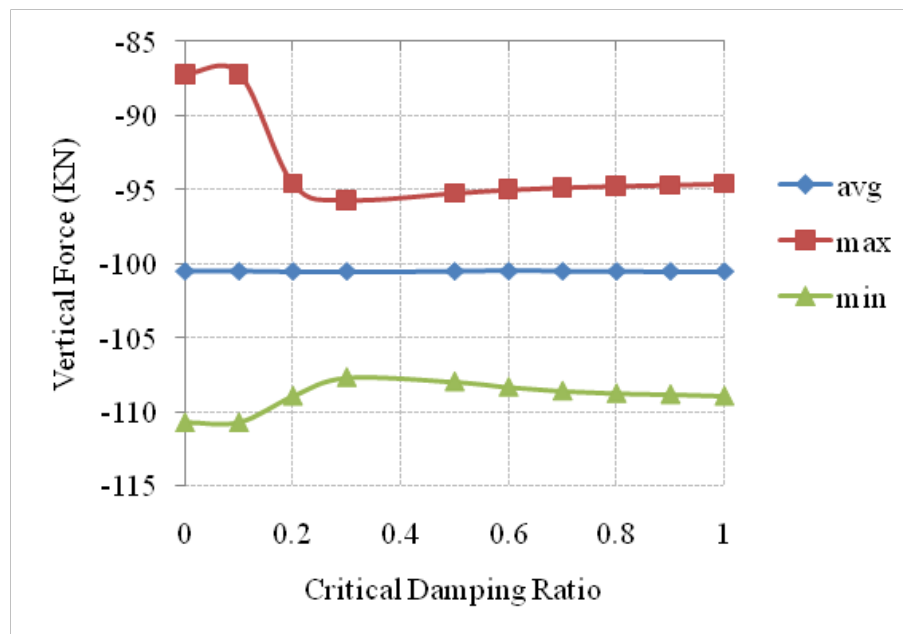
In order to further analyze the vertical compressive force as demonstrated in Figure 17.4, the discrete element simulation data was divided into three portions based on the wheel motion features: accelerating, steadily moving, and decelerating. From each portion of the data, the maximum, minimum, and average values were calculated and plotted in Figure 17.5. A dynamic coefficient of the vertical compressive force is defined as the ratio of its oscillating amplitude to its average value. For instance, the maximum and average of the compressive forces in Figure 17.5(a) are -40kN and -100kN at the critical damping ratio of 0.0, respectively. The oscillation amplitude is the difference between the average and the maximum or minimum:  $-40 - (-100) = -60$  kN. Thus, the dynamic coefficient is  $(-60 \text{ kN}) / (-100 \text{ kN}) = 60\%$ . From Figure 17.5, it was found that:

- 1) As the damping ratio was various from 0.0 to 1.0, the average vertical compressive force kept the same value of -100kN which was equal to the applied concentrated force. In other words, the discrete element simulation under various damping ratios resulted in the identical average value of the compressive force.
- 2) As the damping ratio was various from 0.0 to 1.0, the maximum and minimum values were not constant but dependent on the damping ratio and the wheel motion features.
  - a) During the wheel accelerating as shown in Figure 17.5(a), the maximum value decreased and the minimum value increased as the damping ratio increasing. Increasing the damping ratio from 0.0 to 1.0 resulted in a declined dynamic coefficient from up to 60% to 10%. The similar findings were found during the wheel decelerating as shown in Figure 17.5(c).

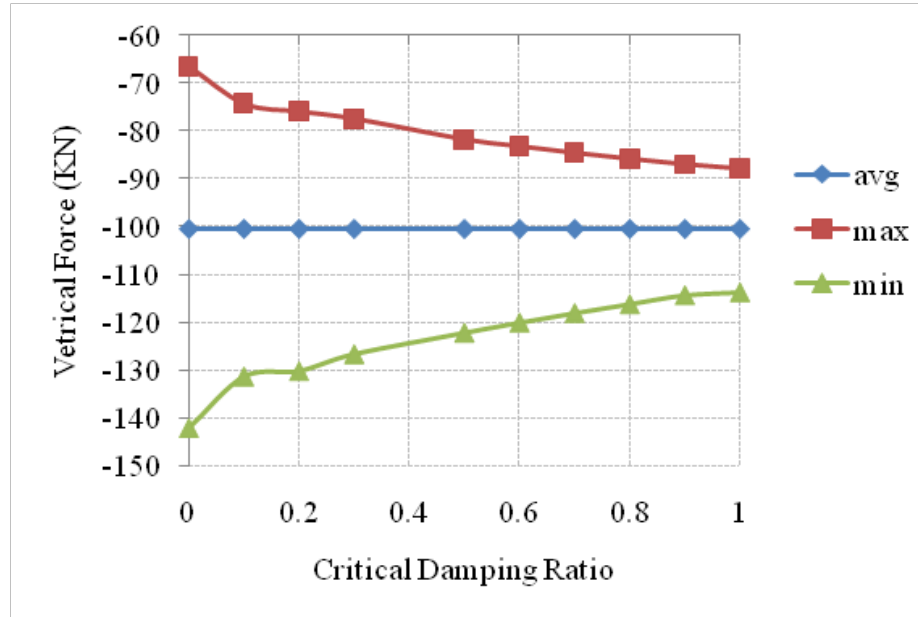
- b) During the wheel steadily moving as shown in Figure 17.5(b), the dynamic coefficient fluctuated from 10% to 5% at the critical damping ratio ranging from 0.0 to 0.2. When the damping ratio was larger than 0.2, the dynamic coefficient was about 5%.



(a) Accelerating



(b) Steadily moving



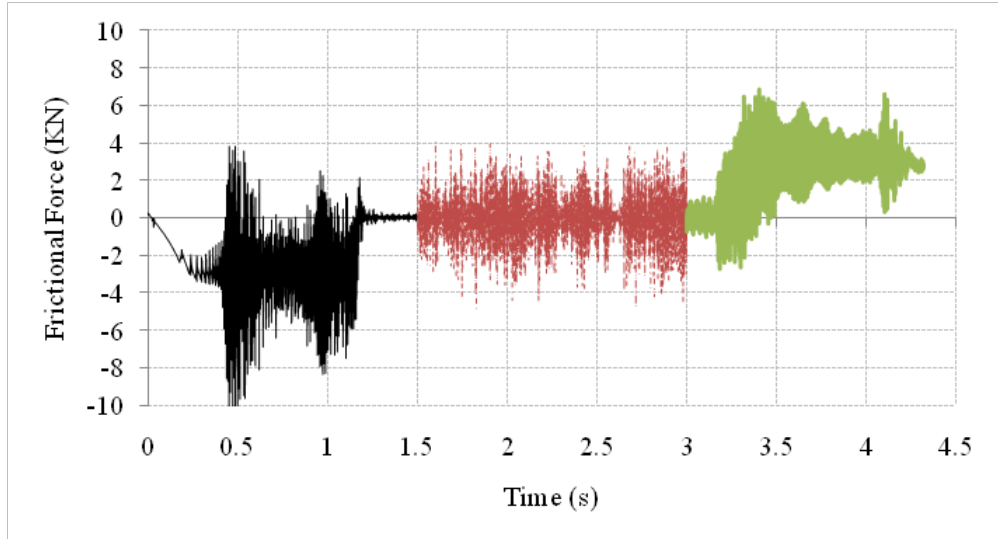
(c) Decelerating

**Figure 17.5 Average, maximum, and minimum values of the vertical force vs. critical damping ratio during the wheel accelerating, steadily moving, and decelerating**

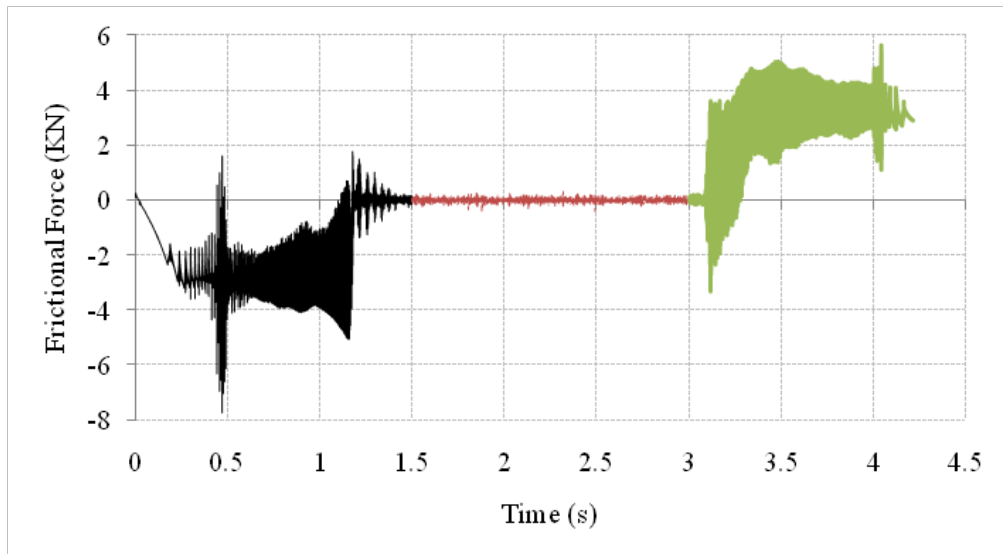
### 17.5.3. DEM Simulation Result: Contact Frictional Force

In order to demonstrate discrete element modeling output of the contact-frictional force, Figure 17.6 shows three examples of frictional forces along the pavement surface during the wheel acceleration, steady moving, and deceleration at the damping ratios of 0.0, 0.05, and 1.0. It was observed that:

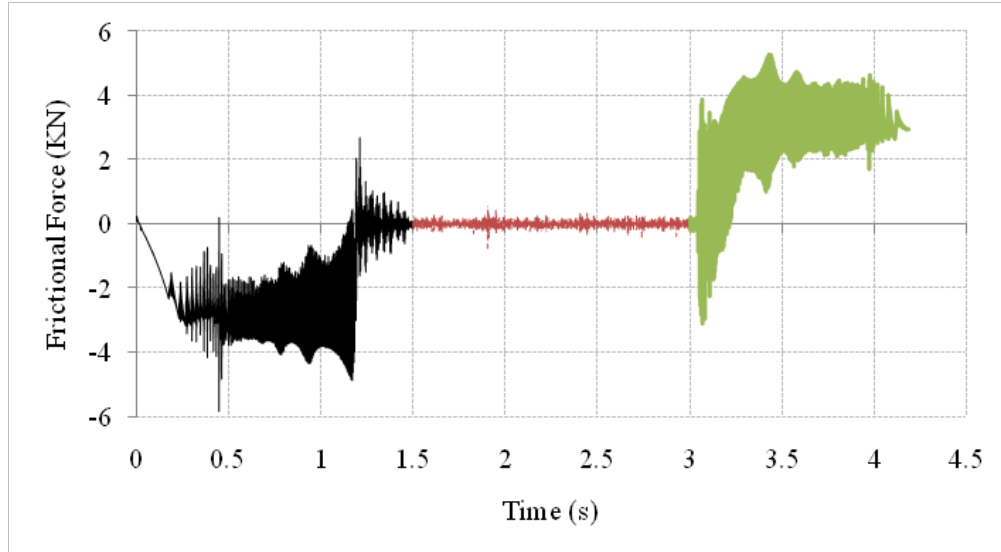
- 1) As shown in the figure, the average frictional force was close to zero during the wheel steadily moving along the pavement surface while it was non-zero value due to the inertia force during the wheel acceleration or deceleration. The frictional force under acceleration was opposite to that under deceleration.
- 2) The frictional force was not constant, but oscillating during the wheel moving along the pavement surface. The oscillation amplitude depended on values of the critical damping ratio and wheel motion features.



(a)  $dmp\_yvis=0$



(b)  $dmp\_yvis=0.5$



(c) dmp\_yvis=1.0

**Figure 17.6 Frictional force vs. loading time when the wheel rolling along pavement surface (peak rotational velocity=10rad/s; the different colors of the curves indicate that different motion features: acceleration, steadily moving, and deceleration)**

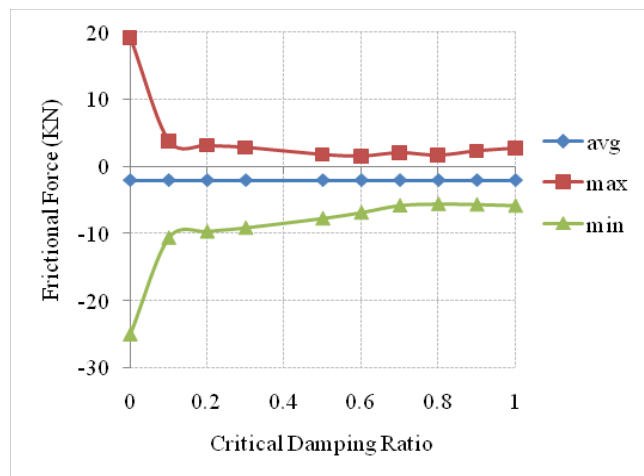
In order to further analyze the contact frictional force as demonstrated in Figure 17.4, the discrete element simulation data was divided into three portions based on the wheel motion features: accelerating, steadily moving, and decelerating. From each portion of the data, the maximum, minimum, and average values were calculated and plotted in Figure 17.7. It was found that:

- 1) The average values of the frictional force received no effect from the critical damping ratio, but they were different as the wheel motion features were different: the average value was -2.86kN, zero, and 2.83kN during the wheel accelerating, steadily moving, and decelerating. By analyzing the forces on the wheel, it should be noted that the wheel had only the frictional force in the horizontal direction. Therefore, the frictional force can be formulated as

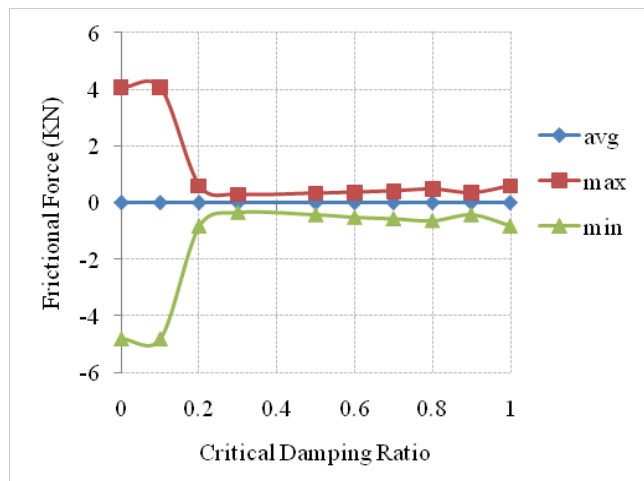
$$f = ma \quad 17.2$$

Where  $m$  is the total mass of the wheel and vehicle, while  $a$  is the acceleration ratio of the wheel.  $f$  is the frictional force. From Figure 17.3, the acceleration ratios during the wheel accelerating, steadily moving, and decelerating were  $1.5\text{m/s}^2$ ,  $0$ , and  $-1.5\text{m/s}^2$ . The total mass was  $1971.2\text{Kg}$  which was calculated from densities shown in Table 1. Therefore, the theoretical values of the friction force ( $f$ ) were  $2.95\text{KN}$ ,  $0$ , and  $-2.95\text{KN}$ . Since the frictional force along the pavement surface was opposite to that on the wheel. Therefore, the frictional force along the pavement surfaces was  $-2.95\text{KN}$ ,  $0$ , and  $2.95\text{KN}$ , respectively, during the wheel accelerating, steadily moving, and decelerating. Evidently, the predicted frictional force was slightly lower than its theoretical value.

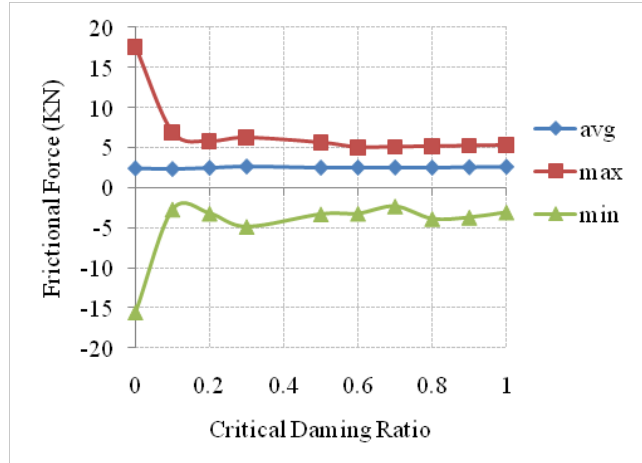
2) The maximum and minimum values of the frictional force received significant impacts of the damping ratio when it was less than 0.2, but negligible impacts when it was larger than 0.2. As shown in Figure 17.7 (a) and (c), increasing the damping ratio from 0.0 to 0.1 resulted in a sharp decrease of the maximum value and a sharp increase of the minimum value of the friction force. Then, the maximum and minimum values of the frictional force kept constant when the damping ratio was larger than 0.1. From Figure 17.7(b), increasing the damping ratio from 0.0 to 0.1 resulted in negligible changes of both the maximum and minimum values if the frictional force; then increasing the damping ratio from 0.1 to 0.2 resulted in a sharp decrease of the maximum value and a sharp increase of the minimum value; and then increasing the damping ratio from 0.2 to 1.0 resulted negligible impacts on the frictional force.



(a) Acceleration



(b) Steady Moving



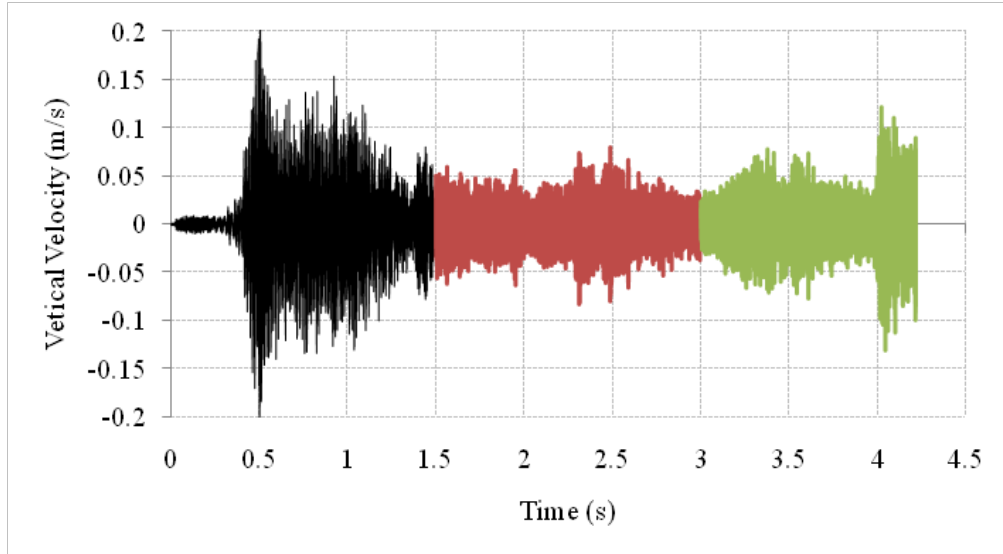
(c) Deceleration

**Figure 17.7 Average, maximum, and minimum values of the frictional force vs. critical damping ratio during the wheel accelerating, steadily moving, and decelerating**

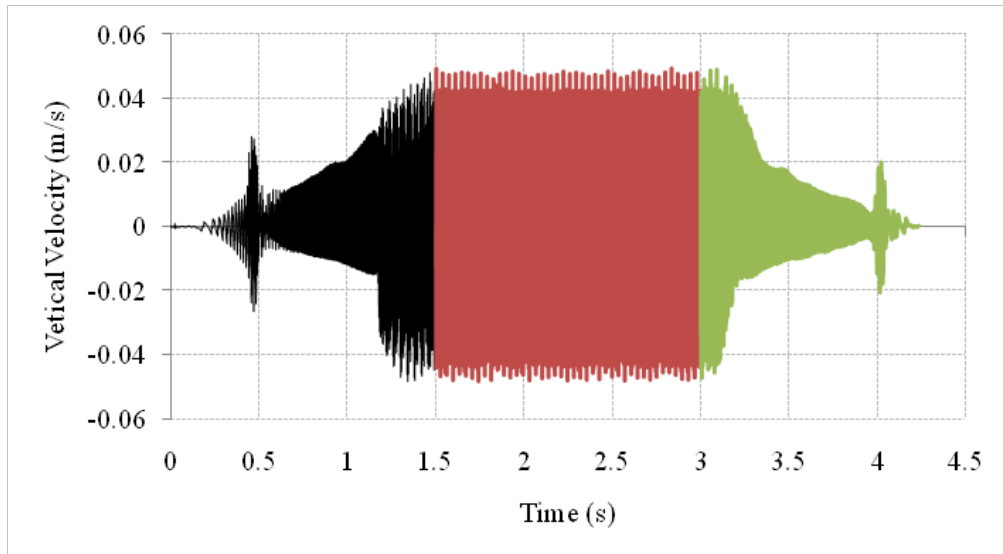
#### 17.5.4. DEM Simulation Result: Vertical Velocity of the Rolling Wheel

Vertical velocity is an important parameter which indicates vibration of the rolling wheel. Figure 17.8 shows three examples of the vertical velocity along the pavement surface during the wheel accelerating, steady moving, and decelerating. It was found that:

- 1) The vertical velocity oscillated around its average which was zero. The oscillating amplitude was dependent on the damping ratio and the wheel motion features. Increasing the damping ratio resulted in decreasing the oscillating amplitude. In other words, a larger damping ratio resulted in a less vibration of the rolling wheel.
- 2) As shown in Figure 17.8(a), the oscillating amplitude of the frictional force was changing from time to time and no clear trend was found as the damping ratio was close to 0.0. However, when the damping ratio became larger as shown in from Figure 17.8(b) and (c), a clear trend was found: a) the oscillating amplitude fluctuated in the beginning and increased to its peak value during the wheel accelerating; b) the peak value was unchanged during the wheel steadily moving; c) the phenomenon of the wheel decelerating was inverse to that of the wheel accelerating.

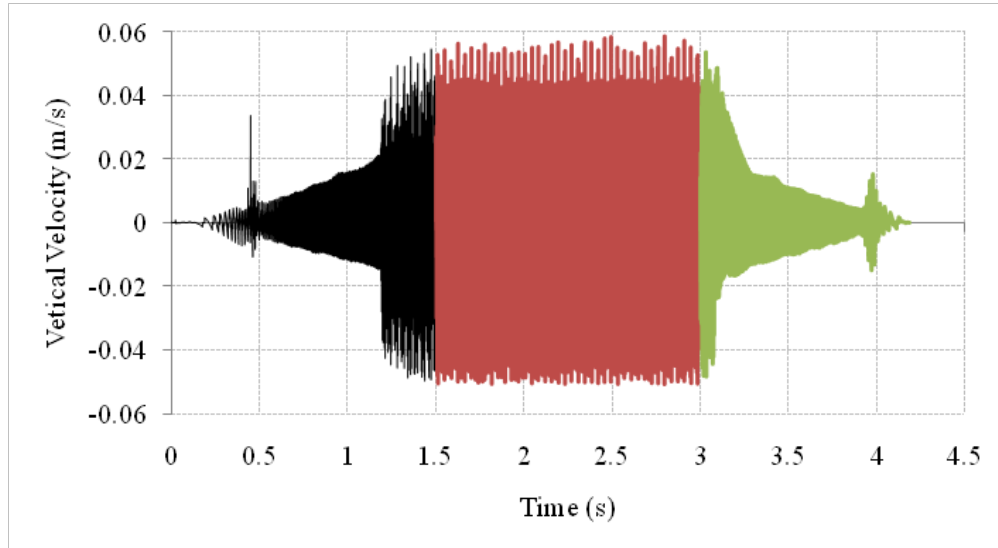


(a)  $dmp\_yvis=0.0$



(b)  $dmp\_yvis=0.5$



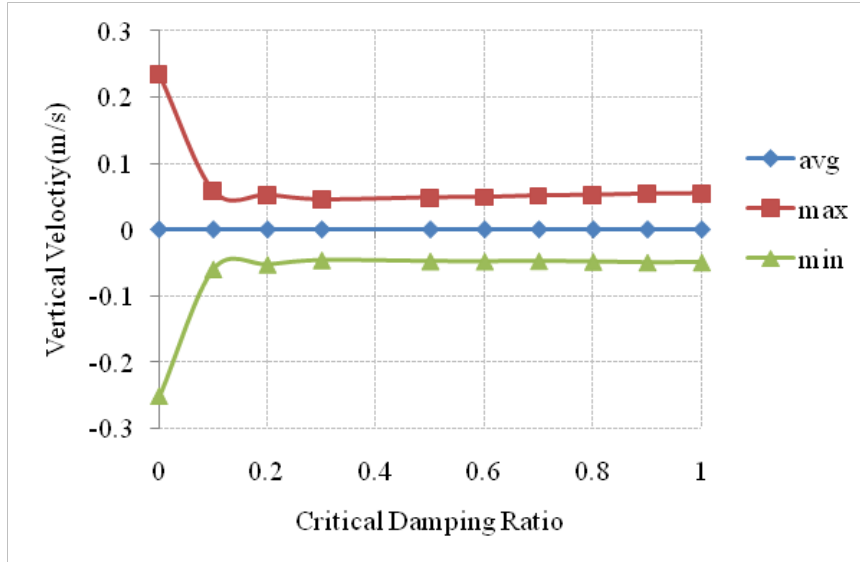


(c)  $dmp\_yvis=1.0$

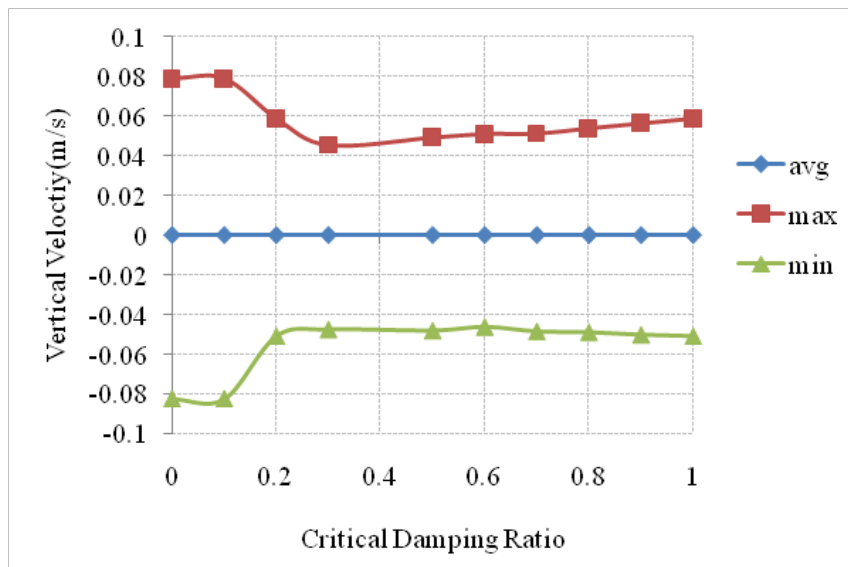
**Figure 17.8 Vertical velocity vs. loading time when the wheel rolling along pavement surface (peak rotational velocity=10rad/s; the different colors of the curves indicate that different motion features: acceleration, steadily moving, and deceleration)**

In order to further analyze the vertical velocity as demonstrated in Figure 17.8, the discrete element simulation data was divided into three portions based on the wheel motion features: accelerating, steadily moving, and decelerating. From each portion of the data, the maximum, minimum, and average values were calculated and plotted in Figure 17.9. The maximum oscillating amplitude of the vertical velocity is defined as the difference between the average and the maximum or minimum. It was found that:

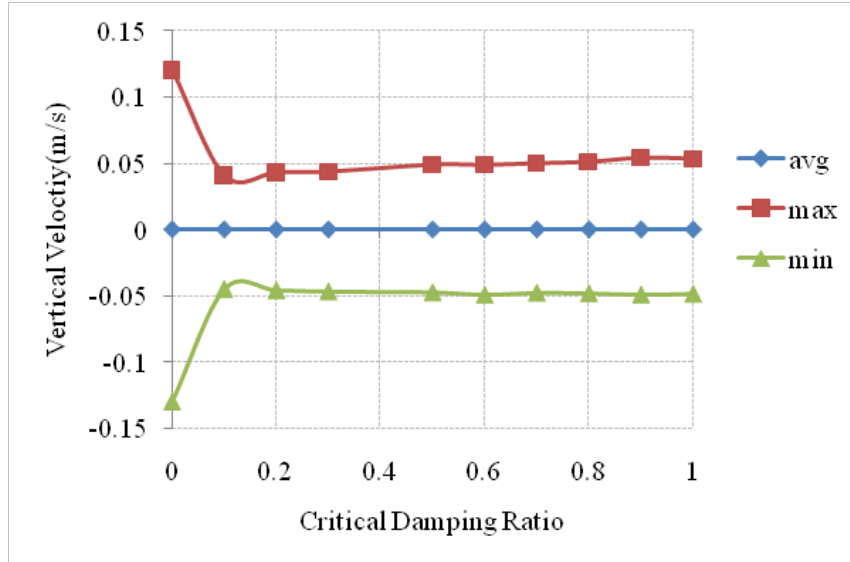
- 1) The average value of the vertical velocity was zero and independent on the damping ratio and the wheel motion features.
- 2) The maximum oscillating amplitude of the vertical velocity was non-zero and dependent on the damping ratio and the wheel motion features: a) the maximum oscillating amplitudes of the wheel accelerating or decelerating were much larger than those of the wheel steadily moving; b) increasing the critical damping ratio from 0.0 to 0.1 significantly impact the maximum oscillating amplitudes; c) Increasing the critical damping ratio from 0.1 to 1.0 resulted in negligible effects on the maximum oscillating amplitudes.



(a) Acceleration



(b) Steady Moving



(c) Deceleration

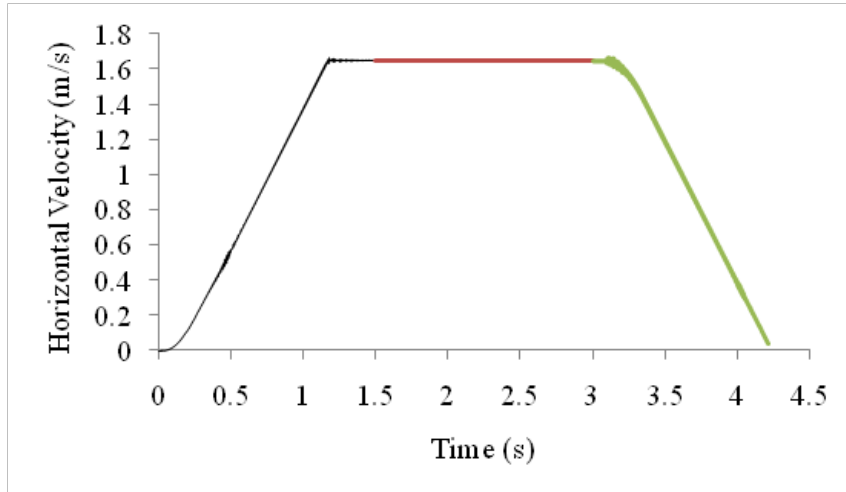
**Figure 17.9 Average, maximum, and minimum values of the vibration vs. critical damping ratio during the wheel accelerating, steadily moving, and decelerating**

## 17.6. Discrete Element Simulation under Various Rotational Velocities

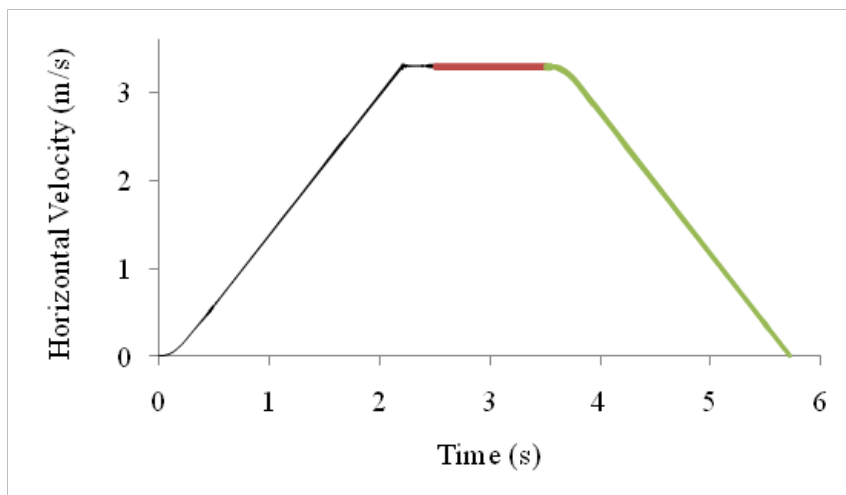
In the discrete element simulation presented in the previous section, the peak rotational velocity was 10rad/s. the peak rotational velocity here is referred to the constant rotational velocity in which the wheel kept steadily moving during the simulation. In the reality, the peak rotational velocity of a running vehicle can be 100rad/s or more. In order to investigate quantitative impacts of the peak rotational velocity on the wheel-pavement interaction forces, this section herein presents three discrete element simulations under various values of the peak rotational velocity of 10, 20, and 100rad/s, respectively. Additionally, the critical damping ratio was 0.5 and the other inputs were identical to those listed in the Table 1. The DEM simulation results are discussed as follows:

### 17.6.1. DEM Simulation Result: Horizontal Velocity

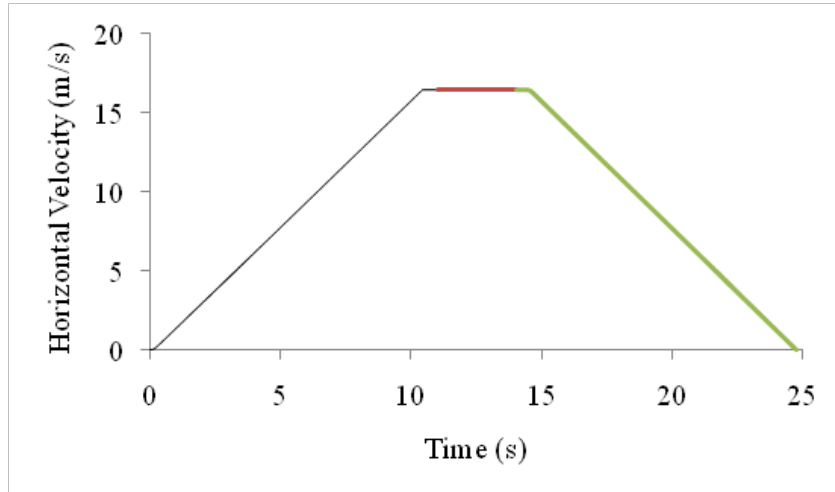
Figure 17.10 shows the horizontal velocity along the pavement surface vs. time for the three simulations. The horizontal velocities in Figure 17.10(a), (b), and (c) linearly increased in a ratio of  $1.5\text{m/s}^2$  at the beginning from 0.0 to its peak value, then the peak values were unchanged, and then decreased in a ratio of  $-1.5\text{m/s}^2$  from their peak values to zero. In other words, the wheel accelerated in a ratio of  $1.5\text{m/s}^2$  at the beginning, then kept steadily moving, and then decelerated in a ratio of  $1.5\text{m/s}^2$ .



(a) peak rotational velocity=10rad/s



(b) peak rotational velocity=20rad/s

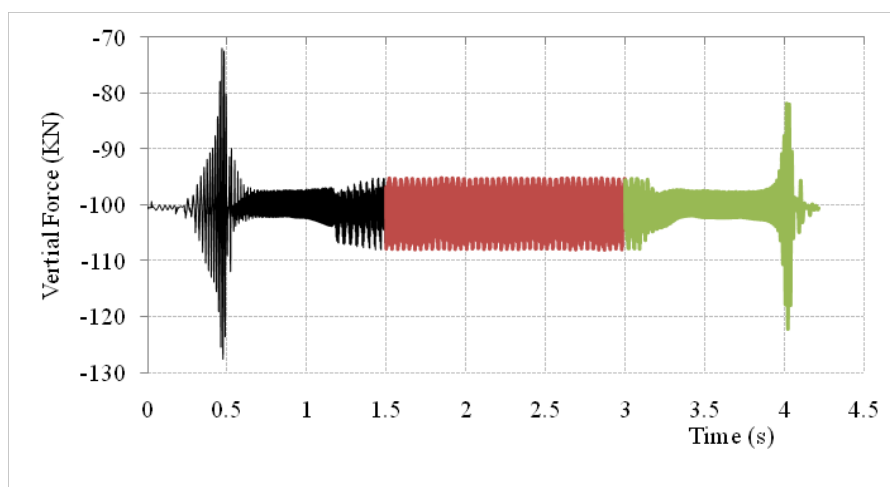


(c) peak rotational velocity=100rad/s

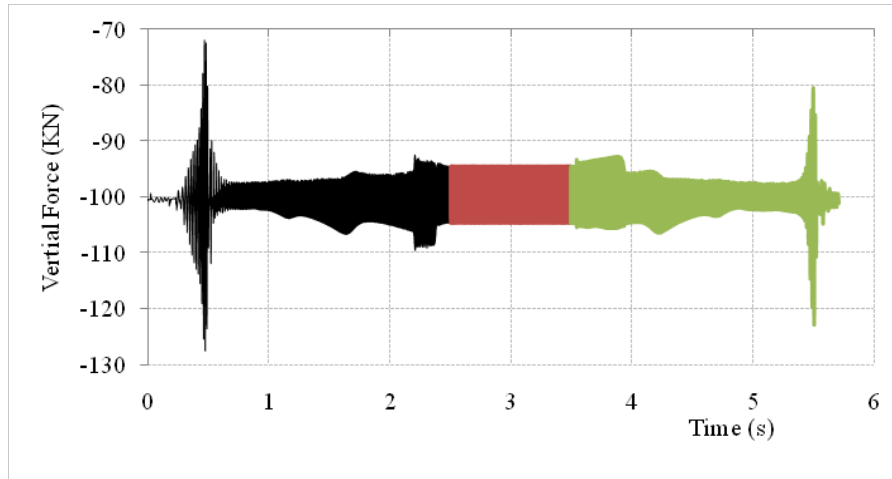
**Figure 17.10 Horizontal velocity vs. loading time when the wheel rolling along pavement surface (peak rotational velocity=10, 20, and 100rad/s and damping ratio=0.5; the different colors of the curves indicate that different motion features: acceleration, steadily moving, and deceleration)**

### 17.6.2. DEM Simulation Result: Vertical Compressive Force

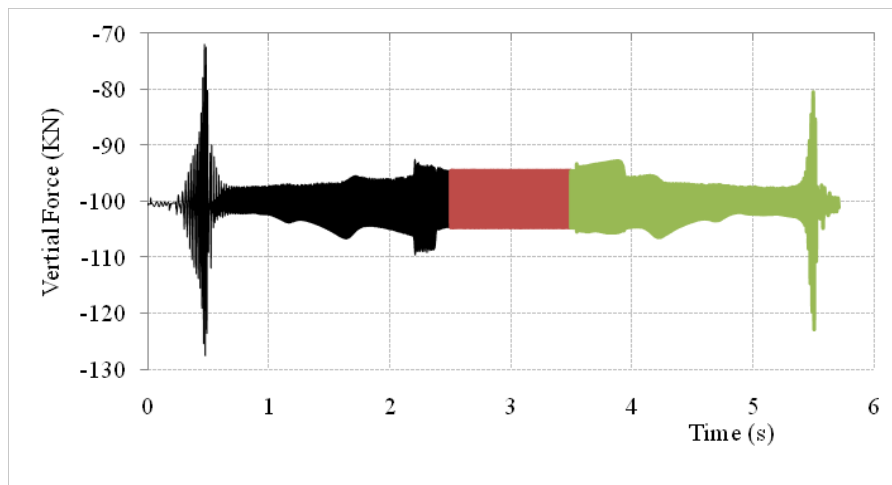
Figure 17.11 shows the compressive force along the pavement surfaces. It was found that: the vertical compressive forces in Figure 17.11 (a), (b), and (c) oscillated around its average value. It was noted that the oscillating amplitudes received negligible impacts when the peak rotational velocity increased from 10 to 100 rad/s. However, increasing the peak rotational velocity resulted in the increased oscillating frequency of the compressive force.



(a) peak rotational velocity=10rad/s



(b) peak rotational velocity=20rad/s



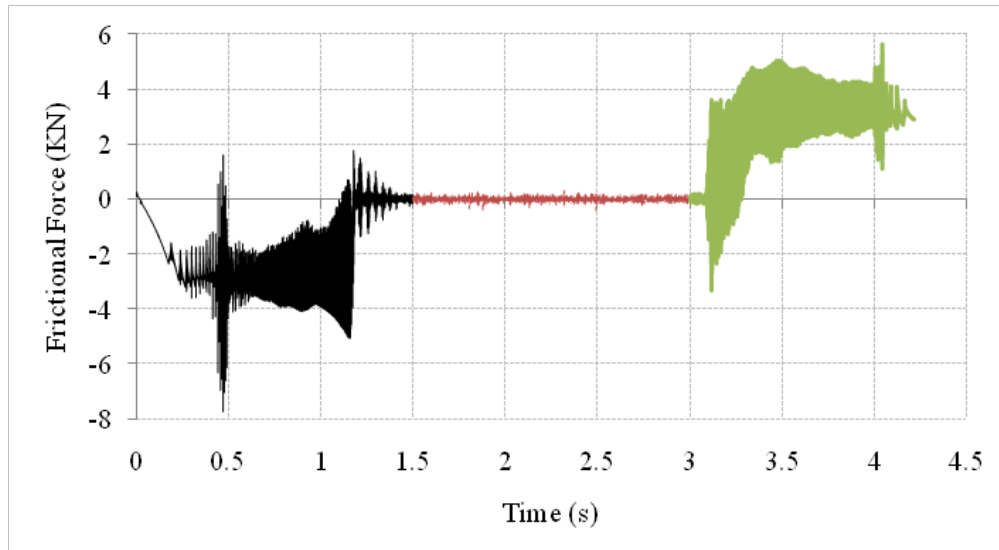
(c) peak rotational velocity=100rad/s

**Figure 17.11 Vertical compressive force vs. loading time when the wheel rolling along pavement surface (*peak rotational velocity=10, 20, and 100rad/s and damping ratio=0.5*; the different colors of the curves indicate that different motion features: acceleration, steadily moving, and deceleration)**

### 17.6.3. DEM Simulation Result: Frictional Force

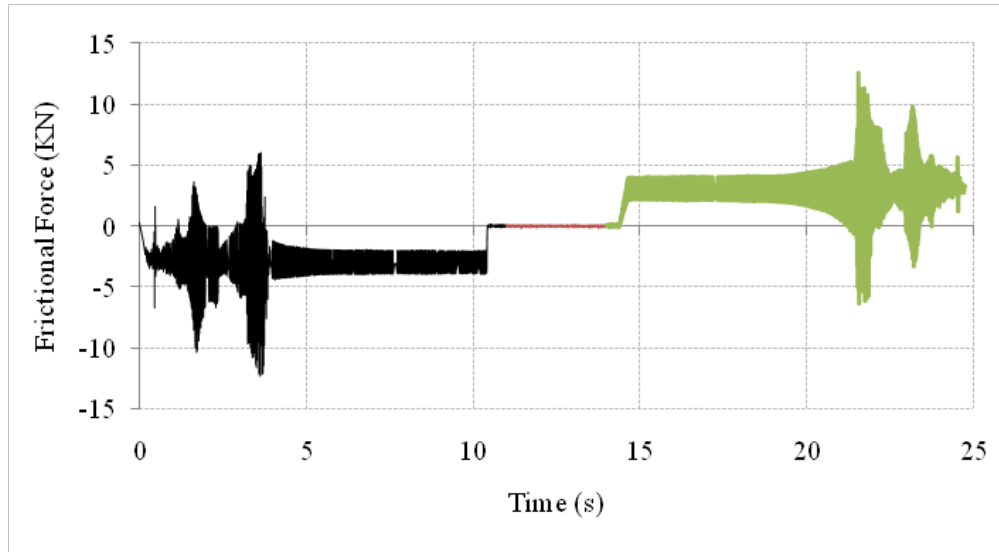
Figure 17.12 shows the frictional force along the pavement surface during the wheel moved on the pavement. It was found that: When the wheel moved along the pavement surface, the frictional forces in the three simulations oscillated among its average values. Increasing the peak rotational velocity from 10 to 100 rad/s resulted in the increased oscillating frequencies and amplitudes. It was noted that the average values of the frictional forces from the three simulations were identical. For instance, the average frictional force was -2.98KN, -2.99KN, and -3.01KN when the wheel accelerated to its

peak rotational velocity of 10, 20, and 100rad/s, respectively. The averaged frictional forces were 3.00kN, 3.01kN, and 2.99kN when the wheel decelerated from its peak rotational velocity of 10, 20, and 100rad/s, respectively. The averaged frictional forces were close to zero during the wheel kept steadily moving.



(a) peak rotational velocity=10rad/s

(b) peak rotational velocity=20rad/s



(c) peak rotational velocity=100rad/s

**Figure 17.12 Vertical compressive force vs. loading time when the wheel rolling along pavement surface (peak rotational velocity=10, 20, and 100rad/s and damping ratio=0.5; the different colors of the curves indicate that different motion features: acceleration, steadily moving, and deceleration)**

## 17.7. Summary and Conclusion

Dynamic forces under the vehicular wheels are apparently important in the pavement design. As is well-known, the dynamic forces come from the pavement-wheel interaction. This paper presents a discrete element modeling approach for studying the pavement-wheel interaction. Through this study, it was found that:

- 1) During the wheel moving along pavement surface, the contact forces (normal compressive force and the frictional forces) were not constant but oscillating around their average values.
- 2) Both the critical damping ratio and the wheel motion features significantly impacted the simulation results:
  - a) Increasing the damping ratio resulted in reducing the oscillating amplitudes.
  - b) Acceleration and deceleration resulted in fluctuation of the contact forces and the wheel velocities.
  - c) During the wheel steadily moving, the oscillating amplitudes of the contact forces and velocities were constant.
  - d) Acceleration and deceleration resulted in non-zero frictional forces while frictional force was zero during the wheel steadily moving along the pavement surface.

As mentioned at the beginning of this paper, it is very important but very challenging to fully understand the mechanism underlying the pavement-wheel interaction. This paper



presented a simplified discrete element modeling approach. More complex and realistic modeling approaches are desired in the future research through considering more realistic pavement surface roughness, contact models, and wheel configuration.

## References

- Abbas, A., Masad, E., Papagiannakis, T., and Harman, T. (2007). "Micromechanical modeling of the viscoelastic behavior of asphalt mixtures using the discrete-element method." *International Journal of Geomechanics*, 7(Compendex), 131-139.
- Abbas, A., Masad, E., Papagiannakis, T., and Shenoy, A. (2005). "Modelling asphalt mastic stiffness using discrete element analysis and micromechanics-based models." *International Journal of Pavement Engineering*, 6(2), 137-146.
- Abbas, A. R., Papagiannakis, A. T., and Masad, E. A. (2004). "Linear and nonlinear viscoelastic analysis of the microstructure of asphalt concretes." *Journal of Materials in Civil Engineering*, 16(2), 133-139.
- Aboudi, J. (1991). *Mechanics of Composite Materials: A Unified Micromechanical Approach*, Elsevier Science Publishing Company, New York.
- Adhikari, S., and You, Z. (2008). "Modeling of Hollow Cylindrical Asphalt Mixture Specimens." In: *Pavements and Materials*, Z. You, A. R. Abbas, and L. Wang, eds., ASCE, Minneapolis, Minnesota, 100-107.
- Adhikari, S., You, Z., Dai, Q., and Liu, Y. (2008a). "Investigation of the Air Void Effect on the Asphalt Mixture using 2D and 3D DEM." *First International FLAC/DEM Symposium on Numerical Modeling, Minneapolis, MN, USA*, 419-426.
- Adhikari, S., You, Z., Dai, Q., and Liu, Y. (2008b). "Investigation of the Air Void Effect on the Asphalt Mixture using 2D and 3D DEM." In: *First International FLAC/DEM Symposium on Numerical Modeling, Minneapolis, MN, USA*, 419-426.
- Adhikari, S., You, Z., and Kutay, M. E. (2008c). "Prediction of dynamic modulus of asphalt concrete using two-dimensional and three-dimensional discrete element modeling approach." American Society of Civil Engineers, New Orleans, LA, United states, 1020-1027.
- Adhikari, S. a. Y., Z., . (2008). "3D Microstructural Models for Asphalt Mixtures Using X-Ray Computed Tomography Images." *International Journal of Pavement Research and Technology*, 1 (3), 94-99.
- Al-Khateeb, G., Shenoy, A., Gibson, N., and Harman, T. (2006). *A New Simplistic Model for Dynamic Modulus Predictions of Asphalt Paving Mixtures*, Association of Asphalt Paving Technologists.
- Al-Qadi, I. L., Loulizi, A., Elseifi, M., and Lahouar, S. (2004). "The Virginia Smart Road: The Impact of Pavement Instrumentation on Understanding Pavement Performance." Association of Asphalt Paving Technologist, Baton Rouge, LA, United states, 427-465.
- Al-Qadi, I. L., and Wang, H. (2009). "Full-depth pavement responses under various tire configurations: Accelerated pavement testing and finite element modeling." Association of Asphalt Paving Technologist, Minneapolis, MN, United states, 721-759.
- Al-Qadi, I. L., Wang, H., Yoo, P. J., and Dessouky, S. H. (2008). "Dynamic analysis and in situ validation of perpetual pavement response to vehicular loading." *Transportation Research Record*(2087), 29-39.
- Anderson, D. A. (1971). "Mechanical Behavior of Asphalt-Mineral Powder Composites and Asphalt-Mineral Interaction," Purdue University.
- Anderson, D. A., Bahia, H. U., and Dongre, R. (1992). "Rheological properties of mineral filler-asphalt mastics and its importance to pavement performance." Publ by ASTM, San Diego, CA, USA, 131-153.

- Arambula, E., Masad, E., and Martin, A. E. (2007). "Influence of air void distribution on the moisture susceptibility of asphalt mixes." *Journal of Materials in Civil Engineering*, 19(8), 655-664.
- Asphalt-Institute. (2001). "Superpave Mix Design ", Asphalt Institute, Lexington, KY, 1-100.
- Bahia, H. U., and Kamel, N. I. (1994). "Rheological Evaluation of Engineered Asphalt Binders." ASCE, San Diego, CA, USA, 97-113.
- Bahia, H. U., Zhai, H., Onnetti, K., and Kose, S. (1999). "Non-linear Viscoelastic and Fatigue Properties of Asphalt Binders." *Asphalt Paving Technology 1999*, 68, p. 1-34.
- Barksdale, R. D. (1971). "Compressive stress pulse times in flexible pavements for use in dynamic testing." (34), 32-44.
- Basu, A., Marasteanu, M. O., and Hesp, S. A. M. (2003). "Time-Temperature Superposition and Physical Hardening Effects in Low-Temperature Asphalt Binder Grading." *Transportation Research Record*(1829), 1-7.
- Bennert, T. A., Maher, A., Bryant, M., and Smith, J. (2006). "Comparing Fine Aggregate Angularity with Aggregate and Hot-Mix Asphalt Performance Tests." *Transportation Research Board*, pp 79-89.
- Billiter, T. C., Davison, R. R., Glover, C. J., and Bullin, J. A. (1997). "Physical properties of asphalt-rubber binder." *Petroleum Science and Technology*, 15(3-4), 205-236.
- Bouldin, M., and Collins, J. (1990). "Influence of binder rheology on rut resistance of polymer modified and unmodified hot mix asphalt." Publ by ASTM, San Antonio, TX, USA, 50-60.
- Buttlar, W. G. (1995). "Relationships between Asphalt Binder and Mixture Stiffnesses at Low Temperature for Control of Thermal Cracking Pavement Performance," Pennsylvania State University, University Park.
- Buttlar, W. G., Bozkurt, D., Al-Khateeb, G. G., and Waldhoff, A. S. (1999). "Understanding asphalt mastic behavior through micromechanics." *Transportation Research Record*(1681), 157-169.
- Buttlar, W. G., and You, Z. (2001). "Discrete element modeling of asphalt concrete: Microfabric approach." *Transportation Research Record*(1757), 111-118.
- Carmona, H. A., Kun, F., Andrade, J. S., and Herrmann, H. J. (2007). "Computer simulation of fatigue under diametrical compression." *Physical Review E - Statistical, Nonlinear, and Soft Matter Physics*, 75(4), 046115.
- Chandan, C., Sivakumar, K., Masad, E., and Fletcher, T. (2004). "Application of imaging techniques to geometry analysis of aggregate particles." *Journal of Computing in Civil Engineering*, 18(1), 75-82.
- Chang, G. K., and Meegoda, J. N. (1997a). "Micromechanical Simulation of Hot Mixture Asphalt." *ASCE J. Engng. Mech.*, 123(5), 495-503.
- Chang, G. K., and Meegoda, J. N. (1999a). "Micro-mechanic Model For Temperature Effects of Hot Mixture Asphalt Concrete." *J. Trans. Res. Record National Research Council, Washington, D.C.*, 1687, 95-103.
- Chang, G. K., and Meegoda, J. N. (1999b). "Micromechanical model for temperature effects of hot-mix asphalt concrete." *Transportation Research Record*(1687), 95-103.
- Chang, K.-N. G., and Jay N, M. (1997). "Micromechanical Simulation of Hot Mix Asphalt." *Journal of Engineering Mechanics*, 123(5), 495-503.
- Chang, K. N., and Meegoda, J. N. (1997b). *Micromechanical simulation of hot mix asphalt*, American Society of Civil Engineers.
- Chen, J. S., Shiah, M. S., and Chen, H. J. (2001). "Quantification of coarse aggregate shape and its effect on engineering properties of hot-mix asphalt mixtures." *Journal of Testing and Evaluation*, 29(6), 513-519.

- Chen, Y.-C., and Hung, H.-Y. (1991). "Evolution of shear modulus and fabric during shear deformation." *Soils and Foundations*, 31(4), 148-160.
- Christensen, D. W., Jr., and Anderson, D. A. (1992). "Interpretation of dynamic mechanical test data for paving grade asphalt." Publ by Assoc of Asphalt Paving Technologists, St. Paul, MN, USA, Charleston, SC, USA, 67-116.
- Christensen, D. W., Pellinen, T., and Bonaquist, R. F. (2003). *Hirsch Model for Estimating the Modulus of Asphalt Concrete* Association of Asphalt Paving Technologists.
- Christensen, R. M. (1979). "Isotropic Properties of Platelet-Reinforced Media." *Journal of Engineering Materials and Technology, Transactions of the ASME*, 101(3), 299-303.
- Christensen, R. M., and Lo, K. H. (1979). "SOLUTIONS FOR EFFECTIVE SHEAR PROPERTIES IN THREE PHASE SPHERE AND CYLINDER MODELS." *Journal of the Mechanics and Physics of Solids*, 27(4), 315-330.
- Collop, A. C., McDowell, G. R., and Lee, Y. (2004). *Use of the distinct element method to model the deformation behavior of an idealized asphalt mixture*, Taylor & Francis Limited.
- Collop, A. C., McDowell, G. R., and Lee, Y. (2007). "On the use of discrete element modelling to simulate the viscoelastic deformation behaviour of an idealized asphalt mixture." *Geomechanics and Geoengineering*, 2(2), 77 - 86.
- Collop, A. C., McDowell, G. R., and Lee, Y. W. (2006a). "Modelling dilation in an idealised asphalt mixture using discrete element modelling." *Granular Matter*, 8(3-4), 175-184.
- Collop, A. C., McDowell, G. R., and Lee, Y. . (2007 ). "On the use of discrete element modeling to simulate the viscoelastic deformation behaviour of an idealized asphalt mixture " *Geomechanics and Geoengineering*, 2(2), 77 - 86
- Collop, A. C., McDowell, G.R., and Lee, Y. W. (2006b). "Modeling dilation in an idealised asphalt mixture using discrete element modeling " *Granular Matter*(Volume 8, Numbers 3-4 ), 175-184.
- Cook, R. (1974). *Concepts and applications of finite element analysis*(Book).
- Counto, U. J. (1964). "Effect of elastic modulus of aggregate on elastic modulus, creep and creep recovery of concrete." *Magazine of Concrete Research*, 16(48), 129-138.
- Cundall, P. A., and Strack, O. D. L. (1979a). "Development of Constitutive Laws for Soil Using The Distinct Element Method " *SAE Preprints*, 1, 289-298.
- Cundall, P. A., and Strack, O. D. L. (1979b). "Discrete numerical model for granular assemblies." *Geotechnique*, 29(1), 47-65.
- Dai, Q. (2009). "Prediction of Dynamic Modulus and Phase Angle of Stone-Based Composites using Micromechanical Finite Element Approach " *ASCE Journal of Materials in Civil Engineering*, in press.
- Dai, q. (2010). "Two- and three-dimensional micromechanical viscoelastic finite element modeling of stone-based materials with X-ray computed tomography images." *Construction and Building Materials*, 25(2), 1102-1114.
- Dai, Q., and Sadd, M. H. (2004). "Parametric Model Study of Microstructure Effects on Damage Behavior of Asphalt Samples." *International Journal of Pavement Engineering*, 5(1), 19-30.
- Dai, Q., and You, Z. (2007). "Prediction of creep stiffness of asphalt mixture with micromechanical finite-element and discrete-element models." *Journal of Engineering Mechanics*, 133(2), 163-173.
- Dai, Q., and You, Z. (2008). "Micromechanical finite element framework for predicting viscoelastic properties of asphalt mixtures." *Materials and Structures*, 41(6), 1025-1037.
- Dai, Q., You, Z., and Sadd, M. H. (2005). "A Micromechanical Viscoelasto-Plastic Model for Asphalt Mixture (presentation)." M. Eyad, P. P. Vassilis, and W. Linbing, eds., 2005 Joint ASME/ASCE/SES Conference on Mechanics and Materials (McMAT2005), American

Society of Civil Engineers, the American Society of Mechanical Engineers, and the Society of Engineering Science, Baton Rouge, Louisiana, June 1st -June 3rd, 2005

- Daniel, J. S., and Lachance, A. (2005). "Mechanistic and volumetric properties of asphalt mixtures with recycled asphalt pavement." *Transportation Research Record*(1929), 28-36.
- Dasgupta, A., and Bhandarkar, S. M. (1992). "Generalized self-consistent Mori-Tanaka scheme for fiber-composites with multiple interphases." *Mechanics of Materials*, 14(1), 67-82.
- Delaporte, B., Di Benedetto, H., Chaverot, P., and Gauthier, G. (2008). "Effect of ultrafine particles on linear viscoelastic properties of mastics and asphalt concretes." *Transportation Research Record*(2051), 41-48.
- Dickens, J. G., and Walker, P. J. (1996). "Use of distinct element model to simulate behaviour of dry-stone walls." *Structural Engineering Review*, 8(2-3), 187-199.
- Dobson, G. R. (1969). "DYNAMIC MECHANICAL PROPERTIES OF BITUMEN." 38 s Angees, 123-139.
- Dongre, R., Myers, L., #039, Angelo, J., Paugh, C., and Gudimettla, J. (2005). *Field Evaluation of Witczak and Hirsch Models for Predicting Dynamic Modulus of Hot-Mix Asphalt (With Discussion)*, Association of Asphalt Paving Technologists.
- Druta, C., Wang, L., Voyiadjis, G. Z., and Abadie, C. (2007). "Estimation of the stiffness of asphalt mastics using Hirsch model." American Society of Civil Engineers, Boulder, CO, United states, 33-44.
- Favier, J. F., Abbaspour-Fard, M. H., and Kremmer, M. (2001). "Modeling Nonspherical Particles Using Multisphere Discrete Elements." *Journal of Engineering Mechanics*, 127(10), 971-977.
- Foster, C. (1970). "Dominant effect of fine aggregate on strength of dense-graded asphalt mixes." 1-3.
- Fu, Y. (2005). "Experimental Quantification and DEM Simulation of Micro-Macro Behaviors of Granular Materials Using X-ray Tomography Imaging," Louisiana State University and Agricultural and Mechanical College.
- Fu, Y., Wang, L., Tumay, M. T., and Li, Q. (2008). "Quantification and simulation of particle kinematics and local strains in granular materials using X-ray tomography imaging and discrete-element method." *Journal of Engineering Mechanics*, 134(2), 143-154.
- Gahvari, F. (1997). "Effects of thermoplastic block copolymers on rheology of asphalt." *Journal of Materials in Civil Engineering*, 9(3), 111-116.
- Garboczi, E. J. (2002). "Three-dimensional mathematical analysis of particle shape using X-ray tomography and spherical harmonics: Application to aggregates used in concrete." *Cement and Concrete Research*, 32(10), 1621-1638.
- Garboczi, E. J., Cheok, G. S., and Stone, W. C. (2006). "Using LADAR to characterize the 3-D shape of aggregates: Preliminary results." *Cement and Concrete Research*, 36(6), 1072-1075.
- Giordano Jr, P., Barrot, D., Mease, P., Garrison, K., Mandayam, S., and Sukumaran, B. (2006). "An optical tomography system for characterizing 3D shapes of particle aggregates." Institute of Electrical and Electronics Engineers Computer Society, Houston, TX, United states, 125-127.
- Giuliani, F., and Merusi, F. (2009). "Flow characteristics and viscosity functions in asphalt binders modified by wax." *International Journal of Pavement Research and Technology*, 2(2), 51-60.
- Gurjar, A., Tang, T., Zollinger, D., and Slavick, K. (1996). "Age, deformation, and temperature effects of viscoelastic materials under large deformations." ASCE, New York, NY, USA, Washington, DC, USA, 1398-1407.

- Harold, L., and Quintus, V. (1991). *Asphalt-aggregate mixture analysis system: AAMAS*, National Research Council (U.S.). Transportation Research Board.
- Hart, R., Cundall, P. A., and Lemos, J. (1988). "Formulation of a Three-dimensional Distinct Element Model-Part II. Mechanical Calculations for Motion and Interaction of a System Composed of MANY Polyhedral Blocks." *International Journal of Rock Mechanics and Mining Sciences & Geomechanics Abstracts*, 25(3), 117-125.
- Hart, R. D., Cundall, P. A., and Cramer, M. L. (1985). "Analysis of a Loading Test on A large Basalt Block ", A. A. Balkema, Rotterdam, Neth, Rapid City, SD, USA, 759-768.
- Harvey, J., Mills, T., Scheffy, C., Sousa, J., and Monismith, C. L. (1994). "Evaluation of several techniques for measuring air-void content in asphalt concrete specimens." *Journal of Testing and Evaluation*, 22(5), 424-430.
- Harvey, J. T., and Tsai, B.-W. (1996). "Effects of asphalt content and air void content on mix fatigue and stiffness." *Transportation Research Record*(1543), 38-45.
- Hashin, Z. (1961). "Elastic moduli of heterogeneous materials." American Society of Mechanical Engineers (ASME), New York, NY, United States, 8.
- Hashin, Z. (1962). "The Elastic Moduli of Heterogeneous Materials." *Journal of Applied Mechanics*, 29, 143-150.
- Hashin, Z. (1965). "Viscoelastic behavior of heterogeneous media." *American Society of Mechanical Engineers -- Transactions -- Journal of Applied Mechanics*, 32(3), 630-636.
- Hashin, Z., and Shtrikman, S. (1963). "Variational approach to theory of elastic behaviour of multiphase materials." *Journal of Mechanics and Physics of Solids*, 11(2), 127-140.
- Hegmon, R. R. (1987). "Tire-Pavement Interaction." *Public Roads*, 51(1), 5-11.
- Hesp, S. A. M., Smith, B. J., and Hoare, T. R. (2002). "Effect of the filler particle size on the low and high temperature performance in asphalt mastic and concrete." Association of Asphalt Paving Technologist, Clearwater Beach, FL, United states, 492-508.
- Hill, R. (1952). "Elastic behaviour of crystalline aggregate." *Physical Society -- Proceedings*, 65(389A), 349-354.
- Hill, R. (1963). "Elastic properties of reinforced solids -- Some theoretical principles." *Journal of Mechanics and Physics of Solids*, 11(5), 357-372.
- Hirsch, T. J. (1962). "Modulus of elasticity of concrete affected by elastic moduli of cement paste matrix and aggregate." *American Concrete Institute -- Journal*, 59(3), 427-451.
- Huang, Z. Y., Yang, Z. X., and Wang, Z. Y. (2008). "Discrete element modeling of sand behavior in a biaxial shear test." *Journal of Zhejiang University-Science A*, 9(9), 1176-1183.
- Huber, G. A., and Heiman, G. H. (1987). *Effect of Asphalt Concrete Parameters on Rutting Performance: A Field Investigation (with discussion)* Association of Asphalt Paving Technologists.
- Huber, G. A., Jones, J. C., Messersmith, P. E., and Jackson, N. M. (1998). *Contribution of Fine Aggregate Angularity and Particle Shape to Superpave Mixture Performance*, Transportation Research Board.
- Idris, J., Verdel, T., and Al-Heib, M. (2008). "Numerical modelling and mechanical behaviour analysis of ancient tunnel masonry structures." *Tunnelling and Underground Space Technology*, 23(3), 251-263.
- Itasca Consulting Group. (2004a). "PFC 2D Version 3.1." Minneapolis, Minnesota 55415
- Itasca Consulting Group. (2004b). "PFC 3D Version 3.1." Minneapolis, Minnesota 55415
- Itasca Consulting Group. (2008a). "PFC 2D Version 4.0." Minneapolis, Minnesota 55415
- Itasca Consulting Group. (2008b). "PFC 3D Version 4.0." Minneapolis, Minnesota 55415
- Johnson, E., Li, X. J., Zofka, A., Marasteanu, M. O., and Clyne, T. R. (2007). "Investigation of Superpave fine aggregate angularity criterion for asphalt concrete." *Transportation Research Record*(1998), 75-81.

- Kandhal, P., and Parker Jr, P. (1998). "NCHRP Report 405: Aggregate Tests Related to Asphalt Concrete Pavement Performance in Pavements." *Transportation Research Board, Washington, DC*.
- Kelleher, E. S., and Markow, T. A. (2009). "Duplication, Selection and Gene Conversion in a *Drosophila mojavensis* Female Reproductive Protein Family." *Genetics*, 181(4), 1451-1465.
- Khalid, H. A., Walsh, C. M., Perez Jimenez, F. E., and Miro Recasens, J. R. (1998). "Rheological and mechanical characterization of aged and unaged porous asphalt binders." *Proceedings of the Institution of Civil Engineers: Transport*, 129(4), 240-246.
- Kim, H. (2007). "Investigation of Toughening Mechanisms in the Fracture of Asphalt Concrete using the Clustered Discrete Element Method," University of Illinois at Urbana-Champaign, Urbana.
- Kim, H., and Buttlar, W. G. (2005). "Micro mechanical fracture modeling of asphalt mixture using the discrete element method." American Society of Civil Engineers, Austin, TX, United States, 209-223.
- Kim, H., and Buttlar, W. G. (2009). "Discrete fracture modeling of asphalt concrete." *International Journal of Solids and Structures*, 46(13), 2593-2604.
- Kim, H., Wagoner, M. P., and Buttlar, W. G. (2008). "Simulation of fracture behavior in asphalt concrete using a heterogeneous cohesive zone discrete element model." *Journal of Materials in Civil Engineering*, 20(8), 552-563.
- Kim, H., Wagoner, M. P., and Buttlar, W. G. (2009a). "Micromechanical fracture modeling of asphalt concrete using a single-edge notched beam test." *Materials and Structures/Materiaux et Constructions*, 42(5), 677-689.
- Kim, H., Wagoner, M. P., and Buttlar, W. G. (2009b). "Rate-dependent fracture modeling of asphalt concrete using the discrete element method." *Canadian Journal of Civil Engineering*, 36(2), 320-330.
- Kim, M., and Tutumluer, E. (2008). "Multiple wheel-load interaction in flexible pavements." *Transportation Research Record*(2068), 49-60.
- Kim, S., and Choi, W. S. (2008). "Analysis of ball movement for research of grinding mechanism of a stirred ball mill with 3D discrete element method." *Korean Journal of Chemical Engineering*, 25(3), 585-592.
- Kim, Y.-R., Allen, D. H., and Little, D. N. (2005). "Damage-induced modeling of asphalt mixtures through computational micromechanics and cohesive zone fracture." *Journal of Materials in Civil Engineering*, 17(5), 477-484.
- Kim, Y. M. (2008). "A Granular motion simulation by discrete element method." *Journal of Mechanical Science and Technology*, 22(4), 812-818.
- Kim, Y. R., Lee, S. J., Seo, Y., and El-Haggan, O. (2006). "A mechanistic approach to determine price reduction factors for density-deficient asphalt pavements." American Society of Civil Engineers, Reston, VA 20191-4400, United States, Atlanta, GA, United States, 1018-1029.
- Kim, Y. R., and Little, D. N. (2004). "Linear viscoelastic analysis of asphalt mastics." *Journal of Materials in Civil Engineering*, 16(2), 122-132.
- Kim, Y. R., Seo, Y., King, M., and Momen, M. (2004). "Dynamic modulus testing of asphalt concrete in indirect tension mode." *Transportation Research Record*(1891), 163-173.
- Kose, S., Guler, M., Bahia, H., and Masad, E. (2000a). "Distribution of Strains Within Hot-Mix Asphalt Binders: Applying Imaging and Finite-Element Techniques." *Transportation Research Record: Journal of the Transportation Research Board*, 1728(-1), 21-27.
- Kose, S., Guler, M., Bahia, H. U., and Masad, E. (2000b). "Distribution of Strains within Hot-mix Asphalt Binders: Applying Imaging and Finite Element Techniques ", 21-27.

- Leahy, R., and McGennis, R. (1999). "Asphalt Mixes: Materials, Design and Characterization." *Journal of the Association of Asphalt Paving Technologists*, 68, 70-127.
- Li, H.-X., Suo, Z., and Wang, P.-M. (2008a). "Deformation and damage of bituminous mixtures with different air void." *Jianzhu Cailiao Xuebao/Journal of Building Materials*, 11(3), 306-310.
- Li, H., Yang, S.-P., and Li, S.-H. (2009a). "Dynamical analysis of an asphalt pavement due to vehicle-road interaction." *Zhendong yu Chongji/Journal of Vibration and Shock*, 28(4), 86-89+102.
- Li, H., Yang, S., and Li, S. (2009b). "Influence of vehicle parameters on the dynamics of pavement structure due to vehicle-road interaction." IEEE Computer Society, Zhangjiajie, Hunan, China, 522-525.
- Li, M. C., and Kett, I. (1967). "Influence of coarse aggregate shape on strength of asphalt concrete mixture." *Highway Research Record*, 178, 450-473.
- Li, S.-H., and Yang, S.-P. (2009). "Dynamical interaction between heavy vehicle and road pavement." *Zhendong yu Chongji/Journal of Vibration and Shock*, 28(6), 155-158.
- Li, X., Marasteanu, M. O., Williams, R. C., and Clyne, T. R. (2008b). "Effect of reclaimed asphalt pavement (proportion and type) and binder grade on asphalt mixtures." *Transportation Research Record*(2051), 90-97.
- Li, Y., and Metcalf, J. B. (2005a). *Two-Step Approach to Prediction of Asphalt Concrete Modulus from Two-Phase Micromechanical Models*, American Society of Civil Engineers.
- Li, Y., and Metcalf, J. B. (2005b). "Two-step approach to prediction of asphalt concrete modulus from two-phase micromechanical models." *Journal of Materials in Civil Engineering*, 17(4), 407-415.
- Liu, C., McCullough, B. F., and Oey, H. S. (2000). "Response of rigid pavements due to vehicle-road interaction." *Journal of Transportation Engineering*, 126(3), 237-242.
- Liu, Y., Dai, Q. L., and You, Z. P. (2009). "Viscoelastic Model for Discrete Element Simulation of Asphalt Mixtures." *Journal of Engineering Mechanics-Asce*, 135(4), 324-333.
- Liu, Y., Feng, S., and Hu, X. (2007). "Discrete Element Simulation of Asphalt Mastics Based on Burgers Model." *Journal of Southwest Jiaotong University*, 15(1), 20-26.
- Liu, Y., Li, H., Li, J., Zhou, Q., and Liu, G. (2004a). "UDEEC simulation on dynamic response of rock slope of huangmailing phosphorite mine under explosion." *Yanshilixue Yu Gongcheng Xuebao/Chinese Journal of Rock Mechanics and Engineering*, 23(21), 3659-3663.
- Liu, Y., and You, Z. (2008). "Simulation of cyclic loading tests for asphalt mixtures using user defined models within discrete element method." In: *GeoCongress 2008: Characterization, Monitoring, and Modeling of GeoSystems, March 9, 2008 - March 12, 2008*, American Society of Civil Engineers, New Orleans, LA, United states, 742-749.
- Liu, Y., and You, Z. (2010). "Formulization of Asphalt Concrete Stiffness for Specific Microstructures Based on Discrete Element Method." In: *Geoshanghai 2010: Paving Materials and Pavement Analysis B. Huang, E. Tutumluer, I. L. Al-Qadi, J. Prozzi, and X. Shu*, eds., American Society of Civil Engineers, Shanghai, China, 135-419.
- Liu, Y., and You, Z. (2011a). "Accelerated Discrete Element Modeling of Asphalt-Based Materials with the Frequency-Temperature Superposition Principle." *Journal of Engineering Mechanics*, 137(5), 355-365.
- Liu, Y., and You, Z. (2011b). "Discrete Element Modeling: Impacts of Aggregate Sphericity, Orientation, and Angularity on Creep Stiffness of Idealized Asphalt Mixtures." *Journal of Engineering Mechanics*, 137(4), 294-303.



- Liu, Y., You, Z., and Adhikari, S. (2008). "Speed up Discrete Element Simulation of Asphalt Mixtures with User-written C++ Codes." *ASCE Airfield and Highway Pavement Conference*, 64-72.
- Liu, Y., You, Z., Goh, S., and Mills-Beale, J. (2010). "A Post-processing Method for Dynamic Modulus Tests of Hot Mix Asphalt." *Journal of Material in Civil Engineering*, 22(7), 1-9.
- Liu, Y., and You, Z. P. (2009). "Visualization and Simulation of Asphalt Concrete with Randomly Generated Three-Dimensional Models." *Journal of Computing in Civil Engineering*, 23(6), 340-347.
- Liu, Y. Q., Li, H. B., Zhao, J., Li, J. R., and Zhou, Q. C. (2004b). "Udec simulation for dynamic response of a rock slope subject to explosions." *International Journal of Rock Mechanics and Mining Sciences*, 41(SUPPL 1), 2-23.
- Loulizi, A., Al-Qadi, I. L., Lahouar, S., and Freeman, T. E. (2002). "Measurement of vertical compressive stress pulse in flexible pavements - Representation for dynamic loading tests." *Pavement Management, Monitoring, and Accelerated Testing 2002*(1816), 125-136.
- Malkin, A. Y., and Isayew, A. I. (2006). "Rheology: Concepts, Methods, & Application." *Che Tec Publishing*, 59-60.
- Mamlouk, M. S. (1996). "Effect of vehicle-pavement interaction on weigh-in-motion equipment design." *Heavy Vehicle Systems*, 3(1-4), 306-332.
- Marasteanu, M. O., Basu, A., Hesp, S. A. M., and Voller, V. (2004). "Time-temperature superposition and AASHTO MP1a critical temperature for low-temperature cracking." *International Journal of Pavement Engineering*, 5(1), 31-38.
- Marasteanu, M., and Anderson, D. (1996). "Time-temperature dependency of asphalt binders-an improved model." Assoc of Asphalt Paving Technologists, Baltimore, MD, USA, 408-448.
- Markow, M. J., Hedrick, J. K., Brademeyer, B. D., and Abbo, E. (1988). "Analyzing the interactions between dynamic vehicle loads and highway pavements." *Transportation Research Record*(1196), 161-169.
- Masad, E. (2004). "X-ray computed tomography of aggregates and asphalt mixes." *Materials Evaluation*, 62(7), 775-783.
- Masad, E., Al-Rousan, T., Bathina, M., McGahan, J., and Spiegelman, C. (2007a). "Analysis of aggregate shape characteristics and its relationship to hot mix asphalt performance." *Road Materials and Pavement Design*, 8(2), 317-350.
- Masad, E., Al-Rousan, T., Button, J., Little, D., and Tutumluer, E. (2007b). "NCHRP Report 555: Test Methods for Characterizing Aggregate Shape, Texture, and Angularity." Transportation Research Board National Research, Washington DC.
- Masad, E., Al-Rousan, T., Button, J., Little, D., Tutumluer, E., and Urbana, I. (2005a). "Appendixes to NCHRP Report 555: Test Methods for Characterizing Aggregate Shape, Texture, and Angularity."
- Masad, E., Castelblanco, A., and Birgisson, B. (2006). "Effects of air void size distribution, pore pressure, and bond energy on moisture damage." *Journal of Testing and Evaluation*, 34(1), 15-23.
- Masad, E., Dessouky, S., and Little, D. (2007c). "Development of an elastoviscoplastic microstructural-based continuum model to predict permanent deformation in hot mix asphalt." *International Journal of Geomechanics*, 7(2), 119-130.
- Masad, E., Jandhyala, V. K., Dasgupta, N., Somadevan, N., and Shashidhar, N. (2002a). "Characterization of air void distribution in asphalt mixes using X-ray computed tomography." *Journal of Materials in Civil Engineering*, 14(2), 122-129.
- Masad, E., Muhunthan, B., Shashidhar, N., and Harman, T. (1999a). "Internal structure characterization of asphalt concrete using image analysis." *Journal of Computing in Civil Engineering*, 13(2), 88-95.

- Masad, E., Muhunthan, B., Shashidhar, N., and Harman, T. (1999b). "Quantifying laboratory compaction effects on the internal structure of asphalt concrete." *Transportation Research Record*(1681), 179-185.
- Masad, E., Saadeh, S., Al-Rousan, T., Garboczi, E., and Little, D. (2005b). "Computations of particle surface characteristics using optical and X-ray CT images." *Computational Materials Science*, 34(4), 406-424.
- Masad, E., and Somadevan, N. (2002). "Microstructural finite-element analysis of influence of localized strain distribution on asphalt mix properties." *Journal of Engineering Mechanics*, 128(10), 1106-1115.
- Masad, E., Somadevan, N., Bahia, H. U., and Kose, S. (2001). "Modeling and experimental measurements of strain distribution in asphalt mixes." *Journal of Transportation Engineering*, 127(6), 477-485.
- Masad, E., Tashman, L., Somedavan, N., and Little, D. (2002b). "Micromechanics-based analysis of stiffness anisotropy in asphalt mixtures." *Journal of Materials in Civil Engineering*, 14(5), 374-383.
- Meegoda, J. N., and Chang, K. G. (1994). "Modeling viscoelastic behavior of Hot Mix Asphalt (HMA) using discrete element methods." ASCE, San Diego, CA, USA, 804-811.
- Meegoda, J. N., and Chang, K. G. (1995). "Fundamental study on the discontinuities and heterogeneities of asphalt concrete." ASCE, Boulder, CO, USA, 465-468.
- Meegoda, N. J., and Chang, K.-n. G. (1993). "Novel approach to develop a performance based test for rutting of asphalt concrete." Publ by ASCE, Vicksburg, MS, USA, 126-140.
- Mohammad, L. N., Wu, Z., Zhang, C., Khattak, M. J., Abadie, C., and Hewitt, J. W. (2004). "Variability of air voids and mechanistic properties of plant-produced asphalt mixtures." *Transportation Research Record*(1891), 85-102.
- Mustoe, G. G. W., and Miyata, M. (2001). "Material Flow Analyses of Noncircular-Shaped Granular Media Using Discrete Element Methods." *Journal of Engineering Mechanics*, 127(10), 1017-1026.
- Nagel-Steger, L., Demeler, B., Meyer-Zaika, W., Hochdorffer, K., Schrader, T., and Willbold, D. (2009). "Modulation of aggregate size- and shape-distributions of the amyloid-beta peptide by a designed beta-sheet breaker." *Eur Biophys J*.
- Nemat-Nasser, S., and Okada, N. (1995). "Direct observation of deformation of granular materials through X-ray photographs." ASCE, New York, NY, USA, Boulder, CO, USA, 605-608.
- Newman, J. K. (1998). "Dynamic shear rheological properties of polymer-modified asphalt binders." *Journal of Elastomers and Plastics*, 30(3), 245-263.
- Ng, T.-T., and Dobry, R. (1994). "Numerical Simulations of Monotonic and Cyclic Loading of Granular Soil." *Journal of Geotechnical Engineering*, 120(2), 388-403.
- Nicholson, V. (1927). "Aggregate affects stability of asphalt mixtures." *Highway Engineer and Contractor*, 16(6), 43-47.
- Oduroh, P. K., Mahboub, K. C., and Anderson, R. M. (2000). *Flat and Elongated Aggregates in Superpave Regime*, American Society of Civil Engineers.
- Pan, T., and Tutumluer, E. (2005). "Imaging based evaluation of coarse aggregate size and shape properties affecting pavement performance." American Society of Civil Engineers, Austin, TX, United states, 33-47.
- Pan, T., and Tutumluer, E. (2006). "Evaluation of Visual Based Aggregate Shape Classifications Using the University of Illinois Aggregate Image Analyzer (UIAIA)." In: *Pavement Mechanics and Performance - GeoShanghai International Conference*, American Society of Civil Engineers, pp 203-211.
- Pan, T. Y., Tutumluer, E., and Carpenter, S. H. (2005). "Effect of coarse aggregate morphology on the resilient modulus of hot-mix asphalt." *Bituminous Paving Mixtures 2005*(1929), 1-9.

- Pan, T. Y., Tutumluer, E., and Carpenter, S. H. (2006). "Effect of coarse aggregate morphology on permanent deformation behavior of hot mix asphalt." *Journal of Transportation Engineering-Asce*, 132(7), 580-589.
- Papagiannakis, A. T., Abbas, A., and Masad, E. (2002). "Micromechanical analysis of viscoelastic properties of asphalt concretes." *Transportation Research Record*(1789), 113-120.
- Papagiannakis, A. T., and Gujarathi, M. S. (1995). "Roughness model describing heavy vehicle-pavement interaction." *Transportation Research Record*(1501), 50-59.
- Papagiannakis, A. T., Zelelew, H. M., and Muhunthan, B. (2007). "A wavelet interpretation of vehicle-pavement interaction." *International Journal of Pavement Engineering*, 8(3), 245-252.
- Paul, B. (1960). "Prediction of elastic constants of multiphase materials." *Metallurgical Society of American Institute of Mining, Metallurgical and Petroleum Engineers -- Transactions*, 218(1), 36-41.
- Pellinen, T. K., and Witczak, M. W. (2002). *Stress Dependent Master Curve Construction for Dynamic (Complex) Modulus (with discussion)*, Association of Asphalt Paving Technologists.
- Pellinen, T. K., Witczak, M. W., and Bonaquist, R. F. (2004). "Asphalt mix master curve construction using sigmoidal fitting function with non-linear least squares optimization." American Society of Civil Engineers, Reston, VA 20191-4400, United States, New York, NY., United States, 83-101.
- Reuss, A. (1929). "Calculation of flow limits of mixed crystals on basis of plasticity of monocrystals (Berechnung der Fließgrenze von Mischkristalle)." *Zeitschrift fuer Angewandte Mathematik und Mechanik*, 9(1), 49-58.
- Rothenburg, L., Bogobowicz, A., and Hass, R. (1992). "Micromechanical Modelling of Asphalt Concrete in Connection with Pavement Rutting Problems." In: *7th International Conference on Asphalt Pavements*, 230-245.
- Rowe, G. M., and Baumgardner, G. L. (2007). "Evaluation of the rheological properties and master curve development for bituminous binders used in roofing." *Journal of ASTM International*, 4(9).
- Sadd, M. H., Dai, Q., Parameswaran, V., and Shukla, A. (2003). "Simulation of Asphalt Materials Using Finite Element Micromechanical Model with Damage Mechanics." *Transportation Research Record*(1832), 86-95.
- Saleh, M. F., Mamlouk, M. S., and Owusu-Antwi, E. B. (2000). "Mechanistic roughness model based on vehicle-pavement interaction." *Transportation Research Record*(1699), 114-120.
- Sawant, V. (2009). "Dynamic analysis of rigid pavement with vehicle-pavement interaction." *International Journal of Pavement Engineering*, 10(1), 63-72.
- Sawant, V. A., Deb, K., and Patil, V. A. (2010). "Dynamic pavement-vehicle interaction of rigid pavement resting on two-parameter soil medium." American Society of Civil Engineers, Shanghai, China, 209-214.
- Schwartz, C. W., and Carvalho, R. L. (2007). "Evaluation of Mechanistic-Empirical Design Procedure." University of Maryland College Park.
- Schwartz, C. W., Gibson, N., and Schapery, R. A. (2002). "Time-temperature superposition for asphalt concrete at large compressive strains." *Transportation Research Record*(1789), 101-112.
- Sephehr, K., Svec, O. J., Yue, Z. Q., and El Hussein, H. M. (1994). "Finite element modelling of asphalt concrete microstructure." *Computational Mechanics Publ*, Udine, Italy, 225-225.
- Shashidhar, N., and Romero, P. (1998a). "Factors affecting the stiffening potential of mineral fillers." *Transportation Research Record*(1638), 94-100.

- Shashidhar, N., and Romero, P. (1998b). "Factors affecting the stiffening potential of mineral fillers." *Asphalt Mixture Components*(1638), 94-100.
- Shashidhar, N., and Shenoy, A. (2002). "On using micromechanical models to describe dynamic mechanical behavior of asphalt mastics." *Mechanics of Materials*, 34(10), 657-669.
- Shenoy, A., Stuart, K., and Mogawer, W. (2003). "Do Asphalt Mixtures Correlate Better with Mastics or Binders in Evaluating Permanent Deformation?" *Transportation Research Record*(1829), 16-25.
- Shi, X. M., and Cai, C. S. (2009). "Simulation of dynamic effects of vehicles on pavement using a 3D interaction model." *Journal of Transportation Engineering*, 135(10), 736-744.
- Shklarsky, E., and Livneh, M. (1964). "Use of gravels for bituminous paving mixtures." *Association of Asphalt Paving Technologists -- Proceedings*, 33, 584-610.
- Soleymani, H. R., Zhai, H., and Bahia, H. (2004). "Role of modified binders in rheology and damage resistance behavior of asphalt mixtures." *Transportation Research Record*(1875), 70-79.
- Souley, M., and Homand, F. (1996). "Stability of jointed rock masses evaluated by UDEC with an extended Saeb-Amadei constitutive law." *International Journal of Rock Mechanics and Mining Sciences*, 33(3), 233-244.
- Stakston, A. D., Bahia, H. U., and Bushek, J. J. (2002). "Effect of fine aggregate angularity on compaction and shearing resistance of asphalt mixtures." *Bituminous Paving Mixtures 2002*(1789), 14-24.
- Stastna, J., BAI, B., and Zanzotto, L. (2006). *Stiffness Master Curve Extensions of Polymer Modified Asphalt Binders and Mixes Based on Indirect Tensile Testing Results*, Polyscience Publications.
- Stephens, J. E., and Sinha, K. C. (1978). "Effect of Aggregate Shape on Bituminous Mix Character." *Association of Asphalt Paving Technologists -- Proceedings*, 47, 434-456.
- Stuart, K. D. (2002). *Understanding the Performances of Modified Asphalt Binder in Mixtures: High-temperature Characterization* Federal Highway Administration.
- Stuart, K. D., and Mogawer, W. S. (2002). *Understanding the Performance of Modified Asphalt Binders in Mixtures: Permanent Deformation Using A Mixture with Diabase Aggregate*, Federal Highway Administration.
- Sun, L., and Deng, X. J. (1998). "Predicting vertical dynamic loads caused by vehicle-pavement interaction." *Journal of Transportation Engineering-Asce*, 124(5), 470-478.
- Sun, L., and Luo, F. (2007). "Nonstationary dynamic pavement loads generated by vehicles traveling at varying speed." *Journal of Transportation Engineering*, 133(4), 252-263.
- Tanaka, K., and Mori, T. (1973). "Strength-differential effect in single crystal of martensite." *Scripta Metallurgica*, 7(3), 307-310.
- Tashman, L., Masad, E., Peterson, B., and Saleh, H. (2002). "Internal structure analysis of asphalt mixes to improve the simulation of superpave gyratory compaction to field conditions." Association of Asphalt Paving Technologist, Clearwater Beach, FL, United states, 605-645.
- Tayebali, A., Goodrich, J., Sousa, J., and Monismith, C. (1990). "Influence of the rheological properties of modified asphalt binders on the load deformation characteristics of the binder-aggregate mixtures." Publ by ASTM, San Antonio, TX, USA, 77-96.
- Taylor, R. P., Coleman, H. W., and Hodge, B. K. (1985). "Prediction of Turbulent Rough-Wall Skin Friction Using a Discrete Element Approach." *Journal of Fluids Engineering-Transactions of the Asme*, 107(2), 251-257.
- Tian, L., Liu, Y., Hu, X.-G., and Wang, B.-G. (2007a). "Random generation algorithm for simulation of polyhedral particles in asphalt mixture aggregate and its program." *Zhongguo Gonglu Xuebao/China Journal of Highway and Transport*, 20(3), 5-10.

- Tian, L., Liu, Y., and Wang, B.-g. (2007b). "3D DEM model and digital restructure technique for asphalt mixture simulation." *Journal of Chang'an University (Natural Science Edition)*, 27(4), 23-26.
- Tsai, B.-W., Monismith, C. L., Dunning, M., Gibson, N., D'Angelo, J., Leahy, R., King, G., Christensen, D., Anderson, D., Davis, R., and Jones, D. (2005). "Influence of asphalt binder properties on the fatigue performance of asphalt concrete pavements." Association of Asphalt Paving Technologist, Long Beach, CA, United states, 733-789.
- Tschoegl, N. W. (1989). "The Phenomenological Theory of Linear Viscoelastic Behavior: An Introduction." *Berlin Heidelberg in Germany : Spring-Verlag*.
- Tutumluer, E., Pan, T., and Carpenter, S. H. (2005). *Investigation of Aggregate Shape Effects on Hot Mix Performance Using an Image Analysis Approach*, University of Illinois, Urbana-Champaign, Federal Highway Administration.
- Vardakos, S. S., Gutierrez, M. S., and Barton, N. R. (2007). "Back-analysis of Shimizu Tunnel No. 3 by distinct element modeling." *Tunnelling and Underground Space Technology*, 22(4), 401-413.
- Vaswani, N. K., and Shukla, S. K. (1963). "Effect of mortar on stability of bituminous mixes." *Indian Roads Congress -- Journal*, 27(3), 343-353.
- Vavrik, W. R., Huber, G., Carpenter, S. H., and Bailey, R. (2002). "Bailey Method for Gradation Selection in Hot-mix Asphalt Mixture Design." Transportation Research Board, 39 p.
- Voigt, W. (1889). "The relation between the two elastic moduli of isotropic materials " In: *Annalen Der Physik und Chemie* W. annalen, ed., Ann Phys., Leipzig, 573-587.
- Walpole, L. J. (1966). "On bounds for the overall elastic moduli of inhomogeneous systems." *Journal of the Mechanics and Physics of Solids*, 14(3), 151-162.
- Wang, L., Park, J.-Y., and Fu, Y. (2007a). "Representation of real particles for DEM simulation using X-ray tomography." *Construction and Building Materials*, 21(2), 338-346.
- Wang, L., Park, J. Y., and Fu, Y. (2007b). "Representation of real particles for DEM simulation using X-ray tomography." *Construction and Building Materials*, 21(2), 338-346.
- Wang, L., Paul, H., Harman, T., and D'Angelo, J. (2004). "Characterization of Aggregates and Asphalt Concrete Using X-ray Computerized Tomography." *J. Assoc. Asphalt Paving Tech.*, 73(467-500).
- Wang, L., Zhang, B., Wang, D., and Yue, Z. (2007c). "Fundamental mechanics of asphalt compaction through FEM and DEM modeling." American Society of Civil Engineers, Boulder, CO, United states, 45-63.
- Wasage, T. L. J., Kazatchkov, I. B., Stastna, J., and Zanzotto, L. (2008). "Analysis of asphalt binder and mixture rutting potential from dynamic creep tests." *Proceedings, Annual Conference - Canadian Society for Civil Engineering*, 2, 946-955.
- Washington, D. W., and Meegoda, J. N. (2003). "Micro-mechanical simulation of geotechnical problems using massively parallel computers." *International Journal for Numerical and Analytical Methods in Geomechanics*, 27(14), 1227-1234.
- Witczak, M. W., and Fonseca, O. A. (1996). *Revised Predictive Model for Dynamic (Complex) Modulus of Asphalt Mixtures* REVISED PREDICTIVE MODEL FOR DYNAMIC (COMPLEX) MODULUS OF ASPHALT MIXTURES, Transportation Research Board.
- Witczak, M. W., Kaloush, K., Prellinen, T., El-Basyouny, M., and and Von Quintus, H. (2002). ""Simple Performance Test for Superpave Mix Design" , NCHRP Report 465," *Transportation Research Board, Washington, D.C.*
- Wu, T. T. (1966). "The Effect of Inclusion Shape on Elastic Moduli of a Two-phase Material." *The Effect of Inclusion Shape on Elastic Moduli of a Two-phase Material*, 2(1), 1-8.
- Xia, K. (2010). "A finite element model for tire/pavement interaction: Application to predicting pavement damage." *International Journal of Pavement Research and Technology*, 3(3), 135-141.

- Yang, S., Li, S., and Lu, Y. (2010). "Investigation on dynamical interaction between a heavy vehicle and road pavement." *Vehicle System Dynamics*, 48(8), 923-944.
- You, Z. (2003). "Development of a Micromechanical Modeling Approach to Predict Asphalt Mixture Stiffness Using Discrete Element Method," University of Illinois at Urbana-Champaign, published by UMI, a Bell & Howell Information Company, Ann Arbor, MI.
- You, Z. (2011). "Special Issue on Multiscale and Micromechanical Modeling of Asphalt Mixes." *Journal of Materials in Civil Engineering*, 23(1), 1.
- You, Z., and Adhikari, S. (2008). "Models for Asphalt Mixtures Using X-Ray Computed Tomography Images." *International Journal of Pavement Research and Technology*, 1(3), 94-99.
- You, Z., Adhikari, S., and Dai, Q. (2008a). "Air Void Effect on an Idealized Asphalt Mixture." *ASCE Geotechnical Special Publication 182: Pavements and Materials: Characterization, Modeling and Simulation, American Society of Civil Engineers (ASCE)*.
- You, Z., Adhikari, S., and Dai, Q. (2008b). "DEM Models of Idealized Asphalt Mixtures." In: *ASCE Geotechnical Special Publication (GSP 182): Pavements and Materials: Characterization, Modeling and Simulation*, Z. You, A. R. Abbas, and L. Wang, eds., American Society of Civil Engineers (ASCE), Blacksburg, VA, USA, 55-62.
- You, Z., Adhikari, S., and Dai, Q. (2008c). "Three-dimensional discrete element models for asphalt mixtures." *Journal of Engineering Mechanics*, 134(12), 1053-1063.
- You, Z., Adhikari, S., and Dai, Q. (2008d). "Two- and Three-Dimensional Discrete Element Models for Asphalt Mixtures." In: *ASCE Geotechnical Special Publication 182: Pavements and Materials: Characterization, Modeling and Simulation*; , American Society of Civil Engineers (ASCE), 118-127.
- You, Z., Adhikari, S., and Emin Kutay, M. (2009). "Dynamic modulus simulation of the asphalt concrete using the X-ray computed tomography images." *Materials and Structures/Materiaux et Constructions*, 42(5), 617-630.
- You, Z., Adhikari, S., and Dai, Q. (2008). "Three-Dimensional Discrete Element Models for Asphalt Mixtures." *Journal of Engineering Mechanics*, 134(12), 1053-1063.
- You, Z., and Buttlar, W. G. (2002). "Stiffness Prediction of Hot Mixture Asphalt (HMA) Based upon Microfabric Discrete Element Modeling (MDEM)." In: *Proc. of the 4th International Conference on Road & Airfield Pavement Technology*, People's Communications Publishing House Kunming, China, 409-417.
- You, Z., and Buttlar, W. G. (2004). "Discrete element modeling to predict the modulus of asphalt concrete mixtures." *Journal of Materials in Civil Engineering*, 16(2), 140-146.
- You, Z., and Buttlar, W. G. (2005). "Application of Discrete Element Modeling Techniques to Predict the Complex Modulus of Asphalt-Aggregate Hollow Cylinders Subjected to Internal Pressure." *Journal of the Transportation Research Board, National Research Council*, 1929, 218-226.
- You, Z., and Buttlar, W. G. (2006). "Micromechanical Modeling Approach to Predict Compressive Dynamic Moduli of Asphalt Mixture Using the Distinct Element Method." *Transportation Research Record: Journal of the Transportation Research Board, National Research Council, Washington, D.C.*(1970), 73-83.
- You, Z., and Dai, Q. (2007a). "Dynamic complex modulus predictions of hot-mix asphalt using a micromechanical-based finite element model." *Canadian Journal of Civil Engineering*, 34(12), 1519-1528.
- You, Z., and Dai, Q. (2007b). "A Review of Advances in Micromechanical Modeling of Aggregate-Aggregate Interaction in Asphalt Mixture." *Canadian Journal of Civil Engineering /Rev. can. génie civ.*, 34(2), 239-252.
- You, Z., Dai, Q., and Gurung, B. (2006). "Development and implementation of a finite element model for asphalt mixture to predict compressive complex moduli at low and intermediate

- temperatures." American Society of Civil Engineers, Baton Rouge, LA, United states, 21-28.
- You, Z., Liu, Y., and Qingli, D. (2011a). "Three-dimensional Microstructural-based Discrete Element Viscoelastic Modeling of Creep Compliance Tests for Asphalt Mixtures " *Journal of Materials in Civil Engineering*, 23(1), 79-81.
- You, Z. P., and Liu, Y. (2010). "Three-Dimensional Discrete Element Simulation of Asphalt Concrete Subjected to Haversine Loading An Application of the Frequency-Temperature Superposition Technique." *Road Materials and Pavement Design*, 11(2), 273-290.
- You, Z. P., Liu, Y., and Dai, Q. L. (2011b). "Three-Dimensional Microstructural-Based Discrete Element Viscoelastic Modeling of Creep Compliance Tests for Asphalt Mixtures." *Journal of Materials in Civil Engineering*, 23(1), 79-87.
- Yue, Z. Q., and Morin, I. (1996). "Digital image processing for aggregate orientation in asphalt concrete mixtures." *Canadian Journal of Civil Engineering*, 23(2), 480-489.
- Zanzotto, L., and Stastna, J. (1997). "Dynamic master curves from the stretched exponential relaxation modulus." *Journal of Polymer Science, Part B: Polymer Physics*, 35(8), 1225-1232.
- Zeilew, H. M., and Papagiannakis, A. T. (2010). "Micromechanical Modeling of Asphalt Concrete Uniaxial Creep Using the Discrete Element Method." *Road Materials and Pavement Design*, 11(3), 613-632.
- Zeng, M., and Huang, S.-C. (2006). "Characterizing the asphalt-aggregate mixtures using rheological properties of asphalt binders." *Journal of Testing and Evaluation*, 34(6), 471-476.
- Zhang, X., Last, N., Powrie, W., and Harkness, R. (1999). "Numerical modelling of wellbore behaviour in fractured rock masses." *Journal of Petroleum Science and Engineering*, 23(2), 95-115.
- Zhao, J., Chen, S.-G., Cai, J.-G., and Song, H.-W. (2002). "Simulation of blast wave propagation in jointed rock mass using UDEC." *Zhongguo Kuangye Daxue Xuebao/Journal of China University of Mining & Technology*, 31(2), 111-115.
- Zhao, X. B., Zhao, J., Cai, J. G., and Hefny, A. M. (2008). "UDEC modelling on wave propagation across fractured rock masses." *Computers and Geotechnics*, 35(1), 97-104.
- Zhao, Y., and Kim, Y. R. (2003). "Time-Temperature Superposition for Asphalt Mixtures with Growing Damage and Permanent Deformation in Compression." *Transportation Research Record*(1832), 161-172.
- Zhong, X., and Chang, C. S. (1999). "Micromechanical modeling for behavior of cementitious granular materials." *Journal of Engineering Mechanics*, 125(11), 1280-1285.
- Zhu, H., and Nodes, J. E. (2000). "Contact based analysis of asphalt pavement with the effect of aggregate angularity." *Mechanics of Materials*, 32(3), 193-202.

## Appendix A: Copyright Clearance

**ARTICLE 1:** Copyright Clearance of Published Conference Proceeding Paper “Review of Advances in Understanding Impacts of Mix Composition Characteristics on Asphalt Concrete (AC) Mechanics”, Taylor & Francis Journals

The full article has been used in Chapter 2 of this dissertation. The permission to reuse in dissertation is as follows:

RE: Reuse of the recently published paper

imap://email.mtu.edu:993/fetch?UID>/INBOX>54516?header=prir

**Subject:** RE: Reuse of the recently published paper  
**From:** "Lowe, Oliva" <Oliva.Lowe@informa.com>  
**Date:** Thu, 2 Jun 2011 11:12:47 +0100  
**To:** <yul@mtu.edu>

Our Ref: OL/GPAV/P4834

02.06.11

Dear Yu Liu,

Thank you for your correspondence requesting permission to reproduce the following material from our Journal in your thesis.

**'Review of Advances in Understanding Impacts of Mix Composition Characteristics on Asphalt concrete (AC) Mechanics'** by Yu Liu, Zhanping You, Qingali and Julian Mills-Beale *International Journal of Pavement Engineering* Vol. 12: 4 (2011).

We will be pleased to grant entirely free permission on the condition that you acknowledge the original source of publication and insert a reference to the Journal's web site:

<http://www.informaworld.com>

Thank you for your interest in our Journal.

Yours sincerely

Olivia Lowe  
Permissions Administrator  
Taylor & Francis Group  
Taylor & Francis Group is a trading name of Informa UK Limited, registered in England under no. 1072954

Visit <http://www.tandf.co.uk/eupdates> to receive email updates about journals, books and other news within your areas of interest.



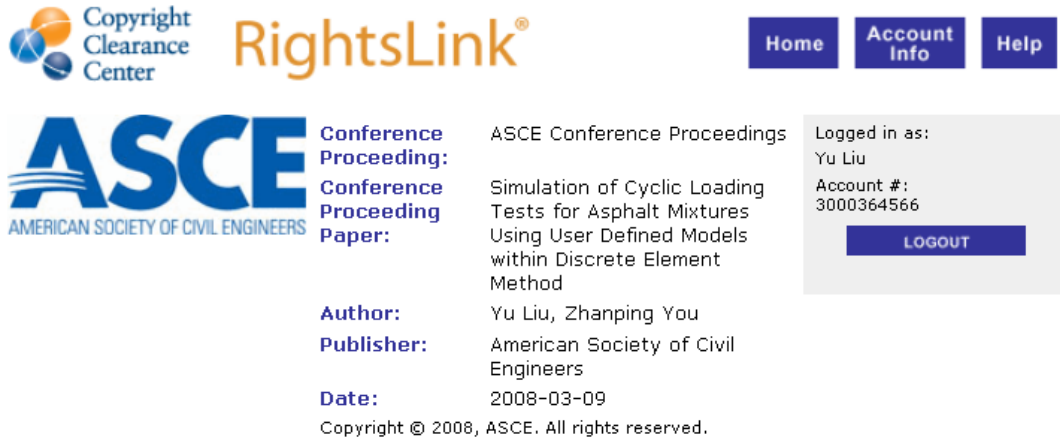
The mark of responsible forestry.

**P** Please don't print this e-mail unless you really need to.



**ARTICLE 2:** Copyright Clearance of Published Conference Proceeding Paper “Simulation of Cyclic Loading Tests for Asphalt Mixtures Using User Defined Models Within Discrete Element Method”, American Society of Civil Engineers (ASCE).

The full article has been used in Chapter 4 of this dissertation. The permission to reuse in dissertation is as follows:



The screenshot displays the Copyright Clearance Center RightsLink interface. At the top left is the Copyright Clearance Center logo. To its right is the RightsLink logo. Further right are three navigation buttons: Home, Account Info, and Help. Below the logos is the ASCE logo (American Society of Civil Engineers). To the right of the ASCE logo, the following information is displayed:

- Conference Proceeding:** ASCE Conference Proceedings
- Conference Proceeding Paper:** Simulation of Cyclic Loading Tests for Asphalt Mixtures Using User Defined Models within Discrete Element Method
- Author:** Yu Liu, Zhanping You
- Publisher:** American Society of Civil Engineers
- Date:** 2008-03-09

At the bottom of this section, it states: Copyright © 2008, ASCE. All rights reserved.

On the right side of the interface, there is a user login box. It shows: Logged in as: Yu Liu, Account #: 3000364566, and a LOGOUT button.

#### Permissions Request

As an ASCE author, you are permitted to reuse you own content for another ASCE or non-ASCE publication.

Please add the full credit line "With permission from ASCE" to your source citation. Please print this page for your records.

**Type of use:** Dissertation/Thesis

**Portion:** full article

**Format:** print and electronic

**Use of this content will make up more than 25% of the new work:** no

**Author of this ASCE work or ASCE will publish the new work:** yes

[BACK](#)


[CLOSE WINDOW](#)

Copyright © 2011 [Copyright Clearance Center, Inc.](#) All Rights Reserved. [Privacy statement.](#) Comments? We would like to hear from you. E-mail us at [customercare@copyright.com](mailto:customercare@copyright.com)

**ARTICLE 3:** Copyright Clearance of Published Journal Paper “Visualization and Simulation of Asphalt Concrete with Randomly Generated Three-Dimensional Models”, Journal of Computing in Civil Engineering, Vol. 23, No. 340, 2009, American Society of Civil Engineers (ASCE).


The full article has been used in Chapter 5 of this dissertation. The permission to reuse in dissertation is as follows:

---

**RightsLink**<sup>®</sup>

[Home](#)[Account Info](#)[Help](#)



**ASCE**  
AMERICAN SOCIETY OF CIVIL ENGINEERS

**Title:** Visualization and Simulation of Asphalt Concrete with Randomly Generated Three-Dimensional Models

**Author:** Yu Liu, Zhanping You P.E.

**Publication:** Journal of Computing in Civil Engineering

**Publisher:** American Society of Civil Engineers

**Date:** 10/15/2009

Copyright © 2009, ASCE. All rights reserved.

Logged in as:  
Yu Liu

Account #:  
3000364566

[LOGOUT](#)

#### Permissions Request

As an ASCE author, you are permitted to reuse you own content for another ASCE or non-ASCE publication.

Please add the full credit line "With permission from ASCE" to your source citation. Please print this page for your records.

**Type of use:** Dissertation/Thesis

**Portion:** full article

**Format:** print and electronic

**Use of this content will make up more than 25% of the new work:** no

**Author of this ASCE work or ASCE will publish the new work:** yes

[BACK](#)



[CLOSE WINDOW](#)


Copyright © 2011 [Copyright Clearance Center, Inc.](#) All Rights Reserved. [Privacy statement.](#)  
Comments? We would like to hear from you. E-mail us at [customer care@copyright.com](mailto:customer care@copyright.com)

**ARTICLE 4:** Copyright Clearance of Published Journal Paper “Discrete Element Modeling: Impacts of Aggregate Sphericity, Orientation, and Angularity on Creep Stiffness of Idealized Asphalt Mixtures”, Journal of Engineering Mechanics, Submitted 20 November 2009; accepted 24 September 2010; posted Ahead of print 27 October 2010, American Society of Civil Engineers (ASCE).

The full article has been used in Chapter 6 of this dissertation. The permission to reuse in dissertation is as follows:

---

HomeAccount InfoHelp



**Title:** Discrete Element Modeling: Impacts of Aggregate Sphericity, Orientation, and Angularity on Creep Stiffness of Idealized Asphalt Mixtures

**Author:** Yu Liu, Zhanping You

**Publication:** Journal of Engineering Mechanics

**Publisher:** American Society of Civil Engineers

**Date:** 10/27/2010

Copyright © 2010, ASCE. All rights reserved.

Logged in as:  
Yu Liu  
Account #:  
3000364566

[LOGOUT](#)

#### Permissions Request

As an ASCE author, you are permitted to reuse you own content for another ASCE or non-ASCE publication.

Please add the full credit line "With permission from ASCE" to your source citation. Please print this page for your records.

**Type of use:** Dissertation/Thesis

**Portion:** full article

**Format:** print and electronic

**Use of this content will make up more than 25% of the new work:** no

**Author of this ASCE work or ASCE will publish the new work:** yes

[BACK](#)

[CLOSE WINDOW](#)

**ARTICLE 5:** Copyright Clearance of Published Journal Paper “Viscoelastic Model for Discrete Element Simulation of Asphalt Mixtures”, Journal of Engineering Mechanics, Vol. 135, No. 324, 2009, American Society of Civil Engineers (ASCE).

The full article has been used in Chapter 7 of this dissertation. The permission to reuse in dissertation is as follows:



The screenshot displays the RightsLink interface. At the top left is the Copyright Clearance Center logo. To its right is the 'RightsLink' logo. Further right are three navigation buttons: 'Home', 'Account Info', and 'Help'. Below the Copyright Clearance Center logo is the ASCE logo (American Society of Civil Engineers). The main content area lists article details: Title: Viscoelastic Model for Discrete Element Simulation of Asphalt Mixtures; Author: Yu Liu, Qingli Dai, Zhanping You P.E.; Publication: Journal of Engineering Mechanics; Publisher: American Society of Civil Engineers. Below this is the copyright notice: Copyright © 2009, ASCE. All rights reserved. On the right side, there is a user information box showing 'Logged in as: Yu Liu' and 'Account #: 3000364566', with a 'LOGOUT' button below it.

#### Permissions Request

As an ASCE author, you are permitted to reuse you own content for another ASCE or non-ASCE publication.

Please add the full credit line "With permission from ASCE" to your source citation. Please print this page for your records.

**Type of use:** Dissertation/Thesis

**Portion:** full article

**Format:** print and electronic

**Use of this content will make up more than 25% of the new work:** no

**Author of this ASCE work or ASCE will publish the new work:** yes

[BACK](#)

[CLOSE WINDOW](#)

Copyright © 2011 [Copyright Clearance Center, Inc.](#) All Rights Reserved. [Privacy statement.](#)  
Comments? We would like to hear from you. E-mail us at [customercare@copyright.com](mailto:customercare@copyright.com)

**ARTICLE 6:** Copyright Clearance of Conference Proceeding Paper: “Determining Burger’s Model Parameters using Creep-recovery Testing Data”, 2008, American Society of Civil Engineers (ASCE).

The full article has been used in Chapter 8 of this dissertation. The permission to reuse in dissertation is as follows:



The screenshot shows the RightsLink interface. At the top left is the Copyright Clearance Center logo. To its right is the RightsLink logo. Further right are three navigation buttons: Home, Account Info, and Help. Below the logos is the ASCE logo (American Society of Civil Engineers). To the right of the ASCE logo is a list of article details: Conference Proceeding: Pavements and Materials: Modeling, Testing, and Performance (GSP 184); Conference Proceeding Paper: Determining Burger’s Model Parameters of Asphalt Materials Using Creep-Recovery Testing Data; Author: Yu Liu; Zhanping You; Publisher: American Society of Civil Engineers; Date: 2009. Below these details is the copyright notice: Copyright © 2009, ASCE. All rights reserved. On the right side of the interface, there is a user information box showing 'Logged in as: Yu Liu' and 'Account #: 3000364566', with a LOGOUT button below it.

**Permissions Request**

As an ASCE author, you are permitted to reuse you own content for another ASCE or non-ASCE publication.

Please add the full credit line "With permission from ASCE" to your source citation. Please print this page for your records.

**Type of use:** Dissertation/Thesis

**Portion:** full article

**Format:** print and electronic

**Use of this content will make up more than 25% of the new work:** no


**Author of this ASCE work or ASCE will publish the new work:** yes

[BACK](#) [CLOSE WINDOW](#)

Copyright © 2011 [Copyright Clearance Center, Inc.](#) All Rights Reserved. [Privacy statement.](#) Comments? We would like to hear from you. E-mail us at [customercare@copyright.com](mailto:customercare@copyright.com)

**ARTICLE 7:** Copyright Clearance of Conference Proceeding Paper “Speed Up Discrete Element Simulation of Asphalt Mixtures with User-written C++ Codes”, 2008, American Society of Civil Engineers (ASCE).

The full article has been used in Chapter 9 of this dissertation. The permission to reuse in dissertation is as follows:



The screenshot shows the Copyright Clearance Center RightsLink interface. At the top left is the Copyright Clearance Center logo. To its right is the RightsLink logo. Further right are three navigation buttons: Home, Account Info, and Help. Below the Copyright Clearance Center logo is the ASCE logo (American Society of Civil Engineers). To the right of the ASCE logo, the following details are listed:

- Conference Proceeding:** ASCE Conference Proceedings
- Conference Proceeding Paper:** Speed Up Discrete Element Simulation of Asphalt Mixtures with User-Written C Codes
- Author:** Yu Liu, Zhanping You
- Publisher:** American Society of Civil Engineers
- Date:** 2008-10-15

At the bottom of this section is the text: Copyright © 2008, ASCE. All rights reserved.

On the right side of the interface, there is a user login box. It displays: Logged in as: Yu Liu, Account #: 3000364566, and a LOGOUT button.

#### Permissions Request

As an ASCE author, you are permitted to reuse you own content for another ASCE or non-ASCE publication.

Please add the full credit line "With permission from ASCE" to your source citation. Please print this page for your records.

**Type of use:** Dissertation/Thesis

**Portion:** full article

**Format:** print and electronic

**Use of this content will make up more than 25% of the new work:** no

**Author of this ASCE work or ASCE will publish the new work:** yes

BACK

CLOSE WINDOW

Copyright © 2011 [Copyright Clearance Center, Inc.](#) All Rights Reserved. [Privacy statement.](#) Comments? We would like to hear from you. E-mail us at [customer@copyright.com](mailto:customer@copyright.com)

**ARTICLE 8:** Copyright Clearance of Published Journal Paper “Accelerated Discrete Element Modeling of Asphalt-based Materials with the Frequency-temperature Superposition Principle”, Journal of Engineering Mechanics, Submitted 24 November 2008; accepted 3 November 2010; posted ahead of print 5 November 2010, American Society of Civil Engineers (ASCE).

The full article has been used in Chapter 10 of this dissertation. The permission to reuse in dissertation is as follows:



The screenshot shows the RightsLink interface. At the top left is the Copyright Clearance Center logo. To its right is the RightsLink logo. Further right are three navigation buttons: Home, Account Info, and Help. Below the Copyright Clearance Center logo is the ASCE logo (American Society of Civil Engineers). To the right of the ASCE logo, the article details are listed: Title: Accelerated Discrete Element Modeling of Asphalt-Based Materials with the Frequency-Temperature Superposition Principle; Author: Yu Liu, Zhanping You; Publication: Journal of Engineering Mechanics; Publisher: American Society of Civil Engineers; Date: 11/05/2010. Below these details is the copyright notice: Copyright © 2010, ASCE. All rights reserved. On the right side of the interface, there is a user login box showing 'Logged in as: Yu Liu' and 'Account #: 3000364566', with a LOGOUT button below it.

#### Permissions Request

As an ASCE author, you are permitted to reuse you own content for another ASCE or non-ASCE publication.

Please add the full credit line "With permission from ASCE" to your source citation. Please print this page for your records.

**Type of use:** Dissertation/Thesis

**Portion:** full article

**Format:** print and electronic

**Use of this content will make up more than 25% of the new work:** no

**Author of this ASCE work or ASCE will publish the new work:** yes

[BACK](#)

[CLOSE WINDOW](#)

Copyright © 2011 [Copyright Clearance Center, Inc.](#) All Rights Reserved. [Privacy statement.](#)  
Comments? We would like to hear from you. E-mail us at [customercare@copyright.com](mailto:customercare@copyright.com)

**ARTICLE 9:** Copyright Clearance of Published Journal Paper “Three-Dimensional Microstructural-based Discrete Element Viscoelastic Modeling of Creep Compliance Tests for Asphalt Mixtures”, Journal of Materials in Civil Engineering, Vol. 23, No. 79, 2011 (Submitted 3 August 2009; accepted 30 December 2009; posted ahead of print 5 February 2010), American Society of Civil Engineers (ASCE).

The full article has been used in Chapter 11 of this dissertation. The permission to reuse in dissertation is as follows:



The screenshot shows the Copyright Clearance Center RightsLink interface. At the top left is the Copyright Clearance Center logo. To its right is the RightsLink logo. Further right are three navigation buttons: Home, Account Info, and Help. Below the logos is the ASCE logo (American Society of Civil Engineers). The main content area displays article details: Title: Three-Dimensional Microstructural-Based Discrete Element Viscoelastic Modeling of Creep Compliance Tests for Asphalt Mixtures; Author: Zhanping You P.E., Yu Liu, Qingli Dai; Publication: Journal of Materials in Civil Engineering; Publisher: American Society of Civil Engineers; Date: 02/05/2010. Below these details is a copyright notice: Copyright © 2010, ASCE. All rights reserved. On the right side, there is a user information box showing 'Logged in as: Yu Liu' and 'Account #: 3000364566', with a Logout button below it.

#### Permissions Request

As an ASCE author, you are permitted to reuse you own content for another ASCE or non-ASCE publication.

Please add the full credit line "With permission from ASCE" to your source citation. Please print this page for your records.

**Type of use:** Dissertation/Thesis

**Portion:** full article

**Format:** print and electronic

**Use of this content will make up more than 25% of the new work:** no

**Author of this ASCE work or ASCE will publish the new work:** yes

[BACK](#)

[CLOSE WINDOW](#)

Copyright © 2011 [Copyright Clearance Center, Inc.](#) All Rights Reserved. [Privacy statement.](#)  
Comments? We would like to hear from you. E-mail us at [customer@copyright.com](mailto:customer@copyright.com)



**ARTICLE 10:** Copyright Clearance of Published Journal Paper “Three-Dimensional Simulation of Asphalt Concrete Subjected to Haversine Loading: An Application of Frequency-temperature Superposition Technique”, Road Materials and Pavement Design, Vol. 11, Issue. 2, 2010, LAVOISIER.

The full article has been used in Chapter 12 of this dissertation. The permission to reuse in dissertation is as follows:



*Lavoisier*

## Road Materials and Pavement Design

Mr Yu LIU  
Depart of Civil & Environnemental  
Engineering  
Michigan Technological University

Cachan, 13 December 2010

Dear M. Liu,

In answer to your mail of December 13th, 2010, we have the pleasure to grant you the permission to reproduce the mentioned article:

“Three-dimensional Discrete Element Simulation of Asphalt Concrete Subjected to Haversine Loading: An Application of the Frequency-Temperature Superposition Technique”

by Zhan-ping You and Yu Liu published in the *International Journal of Road and Pavement Design* (Vol. 11, Issue 2, 2010, pp. 273-290.

In completely exceptional title, and as it is about educational purposes, we do not ask you for reproduction right, provided that you did not omit the exact references of the extract and to pass on to us two documentary evidences.

Sincerely yours

Editing Services

Hermès-Lavoisier

**ARTICLE 11:** Copyright Clearance of Conference Proceeding Paper “Discrete Element Simulation of Aggregate Sphericity and Orientation: An Approach to Improving the Understanding of Asphalt Concrete”, 2010, American Society of Civil Engineers (ASCE).

The full article has been used in Chapter 13 of this dissertation. The permission to reuse in dissertation is as follows:



The screenshot shows the Copyright Clearance Center RightsLink interface. At the top left is the Copyright Clearance Center logo. To its right is the RightsLink logo. Further right are three navigation buttons: Home, Account Info, and Help. Below the logo is the ASCE logo (American Society of Civil Engineers). To the right of the ASCE logo is a list of metadata for a conference proceeding: Conference Proceeding: ASCE Conference Proceedings; Conference Proceeding Paper: Discrete Element Simulation of Aggregate Sphericity and Orientation: An Approach to Improving the Understanding of Asphalt Concrete; Author: Yu Liu, Zhanping You; Publisher: American Society of Civil Engineers; Date: 2010-08-04. Below this is a copyright notice: Copyright © 2010, ASCE. All rights reserved. On the right side of the interface, there is a user login box showing 'Logged in as: Yu Liu' and 'Account #: 3000364566', with a LOGOUT button below it.

**Permissions Request**

As an ASCE author, you are permitted to reuse you own content for another ASCE or non-ASCE publication.

Please add the full credit line "With permission from ASCE" to your source citation. Please print this page for your records.

**Type of use:** Dissertation/Thesis

**Portion:** full article

**Format:** print and electronic

**Use of this content will make up more than 25% of the new work:** no

**Author of this ASCE work or ASCE will publish the new work:** yes

[BACK](#) [CLOSE WINDOW](#)

Copyright © 2011 Copyright Clearance Center, Inc. All Rights Reserved. [Privacy statement.](#) Comments? We would like to hear from you. E-mail us at [customercare@copyright.com](mailto:customercare@copyright.com)

**ARTICLE 12:** Copyright Clearance of Conference Proceeding Paper “Stiffness of Sand Mastic versus Stiffness of Asphalt Binder Using Three-Dimensional Discrete Element Method”, 2010, American Society of Civil Engineers (ASCE).

The full article has been used in Chapter 14 of this dissertation. The permission to reuse in dissertation is as follows:



The screenshot shows the Copyright Clearance Center RightsLink interface. At the top left is the Copyright Clearance Center logo. To its right is the RightsLink logo. Further right are three navigation buttons: Home, Account Info, and Help. Below the logos is the ASCE logo (American Society of Civil Engineers) and the text 'Conference Proceeding: ASCE Conference Proceedings'. The main title of the article is 'Stiffness of Sand Mastic versus Stiffness of Asphalt Binder Using Three-Dimensional Discrete Element Method'. Below the title are fields for Author (Yu Liu, Zhanping You, Qingli Dai), Publisher (American Society of Civil Engineers), and Date (2010-08-08). A copyright notice at the bottom reads 'Copyright © 2010, ASCE. All rights reserved.' On the right side, there is a user information box showing 'Logged in as: Yu Liu' and 'Account #: 3000364566', with a LOGOUT button below it.

**Permissions Request**

As an ASCE author, you are permitted to reuse you own content for another ASCE or non-ASCE publication.

Please add the full credit line "With permission from ASCE" to your source citation. Please print this page for your records.

**Type of use:** Dissertation/Thesis

**Portion:** full article

**Format:** print and electronic

**Use of this content will make up more than 25% of the new work:** no

**Author of this ASCE work or ASCE will publish the new work:** yes

[BACK](#) [CLOSE WINDOW](#)

Copyright © 2011 [Copyright Clearance Center, Inc.](#) All Rights Reserved. [Privacy statement.](#) Comments? We would like to hear from you. E-mail us at [customercare@copyright.com](mailto:customercare@copyright.com)

**ARTICLE 13:** Copyright Clearance of Conference Proceeding Paper “Formulization of Asphalt Concrete Stiffness for Specific Microstructures Based on Discrete Element Method”, 2010, American Society of Civil Engineers (ASCE).

The full article has been used in Chapter 15 of this dissertation. The permission to reuse in dissertation is as follows:



The screenshot displays the RightsLink interface. At the top left is the Copyright Clearance Center logo. To its right is the RightsLink logo. Further right are three navigation buttons: Home, Account Info, and Help. Below the logos is the ASCE logo (American Society of Civil Engineers). The main content area lists article details: Conference Proceeding: ASCE Conference Proceedings; Conference Proceeding Paper: Formulization of Asphalt Concrete Stiffness for Specific Microstructures Based on Discrete Element Method; Author: Yu Liu, Zhanping You; Publisher: American Society of Civil Engineers; Date: 2010-06-03. A copyright notice at the bottom of this section reads "Copyright © 2010, ASCE. All rights reserved." On the right side, a user information box shows "Logged in as: Yu Liu" and "Account #: 3000364566" with a LOGOUT button below.

#### Permissions Request

As an ASCE author, you are permitted to reuse you own content for another ASCE or non-ASCE publication.

Please add the full credit line "With permission from ASCE" to your source citation. Please print this page for your records.

**Type of use:** Dissertation/Thesis

**Portion:** full article

**Format:** print and electronic

**Use of this content will make up more than 25% of the new work:** no

**Author of this ASCE work or ASCE will publish the new work:** yes

BACK

CLOSE WINDOW

Copyright © 2011 [Copyright Clearance Center, Inc.](#) All Rights Reserved. [Privacy statement.](#)  
Comments? We would like to hear from you. E-mail us at [customer@copyright.com](mailto:customer@copyright.com)

## Appendix B: Computer Programs

### Computer Program 1: Randomly-generated Polygon Model for 2D Microstructure of AC Mixtures

This program was initially developed by Yu Liu in 2005 at Henan Transportation Research Institute. Thereafter, the program was modified by Yu Liu several times and last modified by Yu Liu in March 2011 at Michigan Technological University.. The primary purpose is to prepare digital samples for 2D DE simulation. The main program includes 18 files as shown below.

#### Archived files for the randomly-generated polygon model

File Names	Notes
2Dflt.FIS/2Dmd.FIS	Borrowed from PFC2D Fishtank
Public.FIS	Called by Gradballs.DVR or Matballs.DVR
Gradballs.DVR	Create Graded balls (Gradbal-spc.sav)
Matballs.DVR	Create Matrix balls (Matbal-spc.sav)
Server.DVR	Restore Gradbal-spc.sav and call Server.FIS in order to extract coordinates and radius of the graded balls. Those geometric information will be used for generating graded polygon particles.
Server.FIS	Called by Server.DVR
User.DVR	Generate Polygon particles (Random-spc.sav)
User.FIS	Called by User.DVR
Model.DVR	Restore Random-spc.sav and create MODEL_spc.sav
Model.FIS	Called by Model-1.DVR
Void_Gradballs.DVR	Restore Model_spc and create Graded balls which represent air voids (Voidbal-spc.sav)
Void_Gradballs.FIS	Called by Void_Gradballs.DVR
Void_Server.DVR	Restore Voidbal-spc.sav and call Void_Server.FIS in order to extract coordinates and radius of the graded balls. Those geometric information will be used for generating air voids.
Void_Server.FIS	Called by Void_server.DVR
Void_User.DVR	Generate AC microstructure with graded air voids (MODEL_-spc.sav)
Void_User.FIS	Called by Void_User.DVR

Followed is a representative portion of the program:

### **Function 1: Generation of Graded Balls from Public.FIS**

```
def bg_gradballs
;
; INPUT: bg_h - height of rectangle
;   bg_w - width of rectangle
;   bg_n - final porosity of sample
;   bg_rmin - minimum ball radius
;   bg_rmax - maximum ball radius
;
; --- Create the four confining walls
;
  bg_h = et2_ylen
  bg_w = et2_xlen
  bg_n = md_poros
  _tm_w_extend = 0.25
  _tm_makewalls
  command
    set extra ball 3
    endcommand
; --- Compute number of balls to generate
; using the expression:
;   
$$N = A(1 - n) / (\pi * Rbar^2) \quad (PFC2D)$$

;
  _xl = -0.5 * bg_w
  _xu = 0.5 * bg_w
  _yl = -0.5 * bg_h
  _yu = 0.5 * bg_h
  bvtol=bg_h*bg_w*( 1.0 - bg_n )
;create circles for minerals
loop i (1,grad_num)
  _gvol=bvtol*gb_ratio(i)
  o=out('it is creating balls for gradation '+string(i)+':')
  _rmin=gb_size(i)/2.0
  _rmax=gb_size(i)*gb_rzoom(i)/2.0
  av_rad=( _rmax+_rmin)/2.0
  _bvol=pi*av_rad^2.0
  b_num=int(_gvol/_bvol)+1
  n1=max_bid+1
  n2=max_bid+b_num
  _rmax =0.1*_rmax
  _rmin =0.1*_rmin
command
```

```

GENERATE x=(@_x1,@_xu) y=(@_y1,@_yu)&
        rad=(@_rmin,@_rmax) &
        id=(@n1,@n2) tries 200000
        prop dens 2600 range id @n1 @n2
end_command
    loop k (n1,n2)
        bp=find_ball(k)
            b_extra(bp,1)=i
            b_extra(bp,2)=gb_size(i)
        b_extra(bp,3)=gb_size(i)*gb_rzoom(i)
    endloop
endloop
; --- Determine radius multiplier, [_m], so that we
; achieve desired porosity, [bg_n].
;
_n0 = bg_poros
_m = ( (1.0 - bg_n) / (1.0 - _n0) )^(1.0/2.0)
loop i (1,2)
    _factor=@_m^0.5
command
    change rad mult @_factor
end_command
    tm_assemble_isopack
endloop
end

```

## **Function 2: Extraction of Geometry of Graded Balls from Server.FIS**

```

def convey_data
    oo = sopen(1,1); open data chunnel(1) for writing
    g_geo(1)=grad_num ; put grad_num to channel (1) and sent it to channel (4)
    oo = swrite(g_geo,1,1)
;track ball chain for transmitting data
bp=ball_head
; set isok and sent to channel (1)
isok=0
if bp # null then
    isok=1
endif
g_geo(1)=isok
oo = swrite(g_geo,1,1)
loop while bp # null
    bnext=b_next(bp)
        ;set g_geo() and set them to channel (1),6 total
        g_geo(1)=b_x(bp)
    endloop
end

```

```

g_geo(2)=b_y(bp)
g_geo(3)=b_rad(bp)
g_geo(4)=b_dens(bp)
    g_geo(5)=b_extra(bp,1)
    g_geo(6)=b_id(bp)
oo = swrite(g_geo,6,1)
    ; reset isok and sent it to channel (1)
    bp=bnext
    if bp = null then
        isok=0
    endif
    g_geo(1)=isok
    oo = swrite(g_geo,1,1)
endloop
end

```

### **Function 3: Generation of a Polygon Particle from User.FIS**

```

def df_clp
    clp_bnum=urand*5+4
    theta=theta+2*pi*urand
    theta0=theta
    loop _i (1,clp_bnum)
        _x1=_x0+clp_R*cos(theta)
        _y1=_y0+clp_R*sin(theta)
        del_theta=0
        s_ang1=spin_ang1*pi/180
        s_ang2=spin_ang2*pi/180
        loop while del_theta<s_ang1
            del_theta=pi*urand
            if del_theta>s_ang2 then
                del_theta=0.0
            endif
        endloop

        theta=theta+del_theta
        dtheta=theta-theta0
        if dtheta>2*pi then
            theta=theta0
            _i=clp_bnum+1
        endif
        _x2=_x0+clp_R*cos(theta)
        _y2=_y0+clp_R*sin(theta)
        _nx=_y1-_y2
        _ny=_x2-_x1
    command

```



```

        range name teprange line origin @_x1 @_y1 normal @_nx @_ny below &
                circle center _orx,_ory, radius _rad
        group clp_slav range teprange
    endcommand
endloop
command
    group myclp range group clp_slav not circle center _orx,_ory, radius _rad
endcommand
end

```

#### **Function 4: Create AC Microstructure with Polygon Particles from User.FIS**

```

def gen_polyclumps
    command
        prop color 0
    endcommand
    oo = sopen(0,1);open data chunnel(1) for reading
    oo = sread(sub_geo,1,1);receive grad_num by array g_geo(1)
    grad_num=sub_geo(1)
    oo = sread(sub_geo,1,1) ;receive isok from channel (1) by g_geo(1)
    isok=sub_geo(1)
    ;receive data from channel (1) to create clumps
    loop while isok # 0
        ;receive grad stlye from channel 1)
            oo = sread(sub_geo,6,1)
        _orx=sub_geo(1)
        _ory=sub_geo(2)
        _rad=sub_geo(3)
        _dens=sub_geo(4)
        _gindex=sub_geo(5)
        _aggid=sub_geo(6)
        _x0=_orx
        _y0=_ory
        clp_R=_rad
    command
        movie snap 1 file D:\SavesPFC\DEM_Models\2D_RC\veiw_2DRCmdl.avi
    endcommand
    df_clp
command
    prop n_bond 1e20 s_bond 1e20 color _gindex range group myclp
    prop dens @_aggid range group myclp
endcommand
if clp_flag=1
    command
        clump perm full on update_cycle 1 range group myclp
    endcommand

```

```

        endif
        command
            group delete myclp
        endcommand
        oo = sread(sub_geo,1,1)
        isok= sub_geo(1)
    endloop
    command
        group aggregates range color 1 grad_num
        group mastics range color 0
    endcommand
    loop i (1,grad_num)
        _goupnam='minerals_'+string(int(i))
        command
            group _goupnam owner aggregates range color i
        endcommand
    endloop
    bp=ball_head
    md_ac=0
    t_vol=0
    loop while bp # null
        t_vol=t_vol+pi*b_rad(bp)^2
        if b_color(bp)=0
            b_extra(bp,1)=2
            md_ac=md_ac+pi*b_rad(bp)^2
        else
            b_extra(bp,1)=1
            b_extra(bp,2)=b_dens(bp)
        endif
        ;b_extra(bp,2)='bdy_ball'
        bp=b_next(bp)
    endloop
    md_ac=md_ac/t_vol
    oo=sclose(1)
end

```

## Computer Program 2: Randomly-generated Polyhedron Model for 3D Microstructure of AC Mixtures

This program was initially developed by Yu Liu in 2006 at Henan Transportation Research Institute. Thereafter, the program was modified by Yu Liu several times and last modified by Yu Liu in March 2011 at Michigan Technological University. The primary purpose is to prepare digital samples for 3D DE simulation. The main program includes 18 files as shown below.

### Archived files for the randomly-generated polyhedron model

File Names	Notes
3Dflt.FIS/3Dmd.FIS	Borrowed from PFC3D Fishtank
Public.FIS	Called by Gradballs.DVR or Matballs.DVR
Gradballs.DVR	Create Graded balls (Gradbal-spc.sav)
Matballs.DVR	Create Matrix balls (Matbal-spc.sav)
Server.DVR	Restore Gradbal-spc.sav and call Server.FIS in order to extract coordinates and radius of the graded balls. Those geometric information will be used for generating graded polygon particles.
Server.FIS	Called by Server.DVR
User.DVR	Generate Polygon particles (Random-spc.sav)
User.FIS	Called by User.DVR
Model.DVR	Restore Random-spc.sav and create MODEL_spc.sav
Model.FIS	Called by Model-1.DVR
Void_Gradballs.DVR	Restore Model_spc and create Graded balls which represent air voids (Voidbal-spc.sav)
Void_Gradballs.FIS	Called by Void_Gradballs.DVR
Void_Server.DVR	Restore Voidbal-spc.sav and call Void_Server.FIS in order to extract coordinates and radius of the graded balls. Those geometric information will be used for generating air voids.
Void_Server.FIS	Called by Void_server.DVR
Void_User.DVR	Generate AC microstructure with graded air voids (MODEL_-spc.sav)
Void_User.FIS	Called by Void_User.DVR

Followed is a representative portion of the program:

### **Function 1: Generation of Graded Balls from Public.FIS**

```
def et3_gradballs
;
; ----- Generate initial particle assembly contained within six frictionless
; walls. Ball and wall material properties are not installed.
;
;
; INPUT: wlx, wly, wlz - specimen dimensions
;   _rmin    - minimum ball radius
;   _rmax    - maximum ball radius
;   _n       - target porosity
;   _ntries  - number of tries for the GENERATE command
;             (defaults to 125000)
;
; --- Compute number of balls to generate
; using the expression:
;   
$$N = 3V(1 - n) / (4\pi R_{bar}^3) \text{ (PFC3D)}$$

;
; grain_vol=wlx*wly*wlz*(1-@_n) ; the total volume of the grains in the assembly
; _xl = -0.5*wlx
; _xu = 0.5*wlx
; _yl = -0.5*wly
; _yu = 0.5*wly
; _zl = -0.5*wlz
; _zu = 0.5*wlz
; command
;   set extra ball 3
; endcommand
; loop i(1,grad_num)
;   _gvol=grain_vol*gb_ratio(i)
;   o=out('it is creating balls for gradation '+string(i)+':')
;   _rmin=gb_size(i)/2.0
;   _rmax=gb_size(i)*gb_rzoom(i)/2.0
;   av_rad=(_rmax+_rmin)/2.0
;   _bvol=(4.0/3.0)*pi*av_rad^3.0
;   b_num=int(_gvol/_bvol)+1
;   n1=max_bid+1
;   n2=max_bid+b_num
;   _rmax =0.1*_rmax
;   _rmin =0.1*_rmin
; command
;   print @n1,@n2 @gb_ratio(i) @gb_size(i) av_rad _rmax _rmin
;   GENERATE x=(@_xl,@_xu) y=(@_yl,@_yu) z=(@_zl,@_zu) &
```

```

        rad=(@_rmin,@_rmax) &
        filter=df_cylinder &
        id=(@n1,@n2) tries 200000 ;gauss
        prop dens 2600 range id @n1 @n2
    end_command
    loop k (n1,n2)
        bp=find_ball(k)
        b_extra(bp,1)=i
        b_extra(bp,2)=gb_size(i)
        b_extra(bp,3)=gb_size(i)*gb_rzoom(i)
    endloop
endloop
_m = ((1.0 - _n) / (1.0 - _et3_poros))^(1.0/3.0)
loop i (1,5)
    _factor=@_m^0.2
    command
        change rad mult @_factor
    endcommand
    et3_isopack
endloop
end

```

## **Function 2: Extraction of Geometry of Graded Balls from Server.FIS**

```

def convey_data

    oo = sopen(1,1); open data chunnel(1) for writing
    g_geo(1)=grad_num ; put grad_num to channel (1)
    oo = swrite(g_geo,1,1)
    ;track ball chain for transmitting data
    bp=ball_head
    ; set isok and sent to channel (1)
    isok=0
    if bp # null then
        isok=1
    endif
    g_geo(1)=isok
    oo = swrite(g_geo,1,1)
    loop while bp # null
        bnext=b_next(bp)
        ;set g_geo() and set them to channel (1),7 total
        g_geo(1)=b_x(bp)
        g_geo(2)=b_y(bp)
        g_geo(3)=b_z(bp)
        g_geo(4)=b_rad(bp)
        g_geo(5)=b_dens(bp)
        g_geo(6)=b_extra(bp,1)
        g_geo(7)=b_id(bp)
        oo = swrite(g_geo,7,1)
        ; reset isok and sent it to channel (1)
        bp=bnext
    endloop
end

```

```

        if bp = null then
            isok=0
        endif
        g_geo(1)=isok
        oo = swrite(g_geo,1,1)
    endloop
end

```

### **Function 3: Generation of a Polyhedron Particle from User.FIS**

```

def df_clp
    _num=urand*3+3
    s_num=0.0
    loop while s_num < _num
        cut_p=cut_percent
        if _rad<4.75e-3
            cut_p=0.3
        endif
        if _rad<2.36e-3
            cut_p=0.1
        endif
        if _rad<1.18e-3
            cut_p=0.0
        endif
        Rmin=(1-cut_p)*_rad
        Rmax=_rad
        f_R=Rmin ;+(Rmax-Rmin)*urand
        n_x=cos(pi*2.0*urand+s_num*0.1*pi)
        n_y=cos(pi*2.0*urand+s_num*0.1*pi)
        n_z=cos(pi*2.0*urand+s_num*0.1*pi)
        _mod=sqrt(n_x^2+n_y^2+n_z^2)
        _cosx=n_x/_mod
        _cosy=n_y/_mod
        _cosz=n_z/_mod
        _x=_orx+f_R*_cosx
        _y=_ory+f_R*_cosy
        _z=_orz+f_R*_cosz
        sph_rad=_rad-RegR_rad
        command
            range name teprange plane origin _x _y _z normal _cosx _cosy _cosz above &
                sphere center _orx _ory _orz radius sph_rad
            group clp_slav range teprange
        endcommand
        s_num=s_num+1
    endloop
command

```

```

        group myclp range group clp_slav not sphere center _orx _ory _orz radius sph_rad
    endcommand
end

```

#### **Function 4: Create AC Microstructure with Polyhedron Particles from User.FIS**

```

def gen_polyclumps
    command
        prop color 0
    endcommand
    oo = sopen(0,1);open data chunnel(1) for reading
    oo = sread(sub_geo,1,1);receive grad_num by array g_geo(1)
    grad_num=sub_geo(1)
    oo = sread(sub_geo,1,1) ;receive isok from channel (1) by g_geo(1)
    isok=sub_geo(1)
    ;receive data from channel (1) to create clumps
    loop while isok # 0
        ;receive grad stlye from channel 1)
            oo = sread(sub_geo,7,1)
            _orx=sub_geo(1)
            _ory=sub_geo(2)
            _orz=sub_geo(3)
            _rad=sub_geo(4)
            _dens=sub_geo(5)
            _gindex=sub_geo(6)
            _aggid=sub_geo(7)+1
            df_clp

        command
            prop dens @_aggid color _gindex range group myclp

        endcommand

        if _pfc_ver=4.0
            command
                clump add id _aggid range group myclp ;for PFC3D v 4.0
                ;print _aggid
                clump property color _aggid range id _aggid
                ;movie snap 1 file
                D:\SavesPFC\DEM_Models\3D_RC\veiw_3DRCmdl.avi
            endcommand
        else
            command
                clump id _aggid range group myclp ;for PFC3D v 3.1
                ;print _aggid
            endcommand
        end
    end
end

```

```

endif

command
  group delete myclp
endcommand
oo = sread(sub_geo,1,1)
isok= sub_geo(1)
endloop
command
  group minerals range color 1 grad_num
  group mastics range color 0
  range name agg-balls group minerals
  range name mastic-balls group mastics
endcommand
loop i (1,grad_num)
  _goupnam='minerals_'+string(int(i))
  command
    group _goupnam owner minerals range color i
  endcommand
endloop
oo=sclose(1)

md_ac=0
t_vol=0
bp=ball_head
loop while bp # null
  t_vol=t_vol+(4/3.0)*pi*b_rad(bp)^3
  if b_color(bp)=0
    b_extra(bp,1)=1;'bex_asp'
    md_ac=md_ac+(4/3.0)*pi*b_rad(bp)^3
  else
    b_extra(bp,1)=2;'bex_agg'
    b_extra(bp,2)=b_dens(bp)
  endif

  bp=b_next(bp)
endloop
md_ac=md_ac/t_vol
end

```



### Computer Program 3: Randomly-generated Ellipsoid Model for 3D Microstructure of AC Mixtures

This program was initially developed by Yu Liu in 2008 at Michigan Technological University for study aggregate morphological properties. Thereafter, the program was modified by Yu Liu several times and last modified by Yu Liu in March 2011 at Michigan Technological University. The primary purpose is to prepare digital samples for 3D DE simulation. The main program includes 22 files as shown below.

#### Archived files for the randomly-generated Ellipsoid model

File Names	Notes
3Dflt.FIS/3Dmd.FIS	Borrowed from PFC3D Fishtank
Public.FIS	Called by Matballs.DVR
Public-I.FIS/Public-II.FIS	Called by Gradballs-I.DVR/ Gradballs-II.DVR
Gradballs-I.DVR/ Gradballs-II.DVR	Create Graded balls (Gradbal-spc.sav)
Matballs.DVR	Create Matrix balls (Matbal-spc.sav)
Server.DVR	Restore Gradbal-spc.sav and call Server.FIS in order to extract coordinates and radius of the graded balls. Those geometric information will be used for generating graded polygon particles.
Server.FIS	Called by Server.DVR
User-I.DVR/User-II.DVR	Generate Polygon particles (Random-spc.sav)
User-I.FIS/ User-II.FIS	Called by User-I.DVR/User-II.DVR
Model.DVR	Restore Random-spc.sav and create MODEL_spc.sav
Model.FIS	Called by Model-I.DVR
Void_Gradballs.DVR	Restore Model_spc and create Graded balls which represent air voids (Voidbal-spc.sav)
Void_Gradballs.FIS	Called by Void_Gradballs.DVR
Void_Server.DVR	Restore Voidbal-spc.sav and call Void_Server.FIS in order to extract coordinates and radius of the graded balls. Those geometric information will be used for generating air voids.
Void_Server.FIS	Called by Void_server.DVR
Void_User.DVR	Generate AC microstructure with graded air voids (MODEL_spc.sav)
Void_User.FIS	Called by Void_User.DVR

Compared with computer program 2, this program has the following differences: 1) aggregate particles are simulated with ellipsoids instead of polyhedrons; 2) the digital sample of AC mixture is created in two steps. For example, there are two steps to create graded balls using Gradballs-I.DVR and Gradballs-II.DVR. Followed is a representative portion of the program:

### **Function 1: Extraction of Geometry of Graded Balls from Server.FIS**

```

def convey_data

oo = sopen(1,1); open data chunnel(1) for writing
g_geo(1)=grad_num ; put grad_num to channel (1) and sent it to channel (4)
oo = swrite(g_geo,1,1)

loop _i (1, grad_num)
    g_geo(_i)=gb_ratio(_i)
endloop
oo = swrite(g_geo,grad_num,1)

;track ball chain for transmitting data
bp=ball_head
; set isok and sent to channel (1)
isok=0
if bp # null then
    isok=1
endif
g_geo(1)=isok
oo = swrite(g_geo,1,1)
loop while bp # null
    bnext=b_next(bp)
    ;set g_geo() and set them to channel (1),7 total
    g_geo(1)=b_x(bp)
    g_geo(2)=b_y(bp)
    g_geo(3)=b_z(bp)
    g_geo(4)=b_rad(bp)
    g_geo(5)=b_dens(bp)
    g_geo(6)=b_extra(bp,1)
    g_geo(7)=b_id(bp)
    oo = swrite(g_geo,7,1)
    ; reset isok and sent it to channel (1)
    bp=bnext
    if bp = null then
        isok=0
    endif
    g_geo(1)=isok

```

```

        oo = swrite(g_geo,1,1)
    endloop
end

```

## **Function 2: Generation of an Ellipsoid Particle from User-I.FIS**

```

def agg_round
    range_element
    _x = fc_arg(1)
    _y = fc_arg(2)
    _z = fc_arg(3)
    _xx=(_x-_orx)*cos(_alpha)+(_y-_ory)*sin(_alpha)
    _yy=(_y-_ory)*cos(_alpha)-(_x-_orx)*sin(_alpha)
    _zzz=(_z-_orz)*cos(_beta)-_yy*sin(_beta)
    _xxxx=_xx*cos(_gama)-_zzz*sin(_gama)
    _yyyy=_yy*cos(_beta)+(_z-_orz)*sin(_beta)
    _zzzz=_zzz*cos(_gama)+_xx*sin(_gama)
    _dist = _xxxx^2/_a ^2+_yyyy^2/_b^2+_zzzz^2/_c^2
    if _dist > 1 then ; bp is not within the circle
        agg_round = 0
    end_if
end

```

```

def df_clp
    _num=urand*10+9
    s_num=0.0
    loop while s_num < _num
        cut_p=cut_percent
        if _rad<4.75e-3
            cut_p=0.3
        endif
        if _rad<2.36e-3
            cut_p=0.1
        endif
        if _rad<1.18e-3
            cut_p=0.0
        endif
        Rmin=(1-cut_p)*_rad
        Rmax=_rad
        f_R=Rmin+(Rmax-Rmin)*urand
        n_x=cos(pi*2.0*urand+s_num*0.1*pi)
        n_y=cos(pi*2.0*urand+s_num*0.1*pi)
        n_z=cos(pi*2.0*urand+s_num*0.1*pi)
        _mod=sqrt(n_x^2+n_y^2+n_z^2)
        _cosx=n_x/_mod
        _cosy=n_y/_mod
    endloop
end

```

```

        _cosz=n_z/_mod
        _x=_orx+f_R*_cosx
        _y=_ory+f_R*_cosy
        _z=_orz+f_R*_cosz
        sph_rad=_rad-RegR_rad
    command
        range name teprange plane origin _x _y _z normal _cosx _cosy _cosz above &
            sphere center _orx _ory _orz radius sph_rad
            group clp_slav range teprange
    endcommand
    s_num=s_num+1
endloop
command
    group myclp range group clp_slav not sphere center _orx _ory _orz radius sph_rad
endcommand
end

```

### **Function 3: Create AC Microstructure with Ellipsoid Particles from User-IFIS**

```

def gen_polyclumps
    cal_bvol
    oo = sopen(0,1);open data chunnel(1) for reading
    oo = sread(sub_geo,1,1);receive grad_num by array g_geo(1)
    grad_num=sub_geo(1)

    oo = sread(sub_geo,grad_num,1)
    loop _i (1, grad_num)
        gb_ratio(_i)=sub_geo(_i)*mv_bvol
    endloop

    oo = sread(sub_geo,1,1) ;receive isok from channel (1) by g_geo(1)
    isok=sub_geo(1)
    ;receive data from channel (1) to create clumps

    loop while isok # 0
        _nn=_nn+1
        ;receive grad stlye from channel 1)
        oo = sread(sub_geo,7,1)
        _orx=sub_geo(1)
        _ory=sub_geo(2)
        _orz=sub_geo(3)
        _rad=sub_geo(4)
        _dens=sub_geo(5)
        _gindex=sub_geo(6)
        _aggid=sub_geo(7)
        _aggcolor=_aggid-1
    endloop
enddef

```

```

; df_clp
_dl=2*_rad
_ds=sqrt(_sf/_Ris)*_sf*_dl
_di=_ds*_Ris
_a=_dl/2.0
_b=_di/2.0
_c=_ds/2.0
_vratio=(_a*_b*_c)/RegR_rad^3
if _vratio<8
    _b=_a
    _c=_a
    command
        print _vratio;_a _b _c
    endcommand
endif
if _a>2.0*RegR_rad
    _a=_a-RegR_rad
endif
if _b>2.0*RegR_rad
    _b=_b-RegR_rad
endif
if _c>2.0*RegR_rad
    _c=_c-RegR_rad
endif
_alpha=pi*2.0*urand
_beta=pi*2.0*urand
_gama=pi*2.0*urand
command
    range name temclp fish agg_round
    prop dens _aggid color _gindex range temclp
endcommand

if _pfc_ver=4.0
    command
        clump add id _aggid range temclp ;for PFC3D v 4.0
        clump prop color _aggcolor range id _aggid ;for PFC3D v
4.0
    endcommand
else
    command
        clump id _aggid range temclp ;for PFC3D v 3.1
    endcommand
endif

if _nn=1

```

```

else
    clp=clump_head
endif
clp=cl_next(clp)
endif
_bdv1=    gb_ratio(_gindex)
;if clp # null
    bp=cl_list(clp)
    loop while bp # null
        gb_ratio(_gindex)=gb_ratio(_gindex)-8.0*RegR_rad^3
        bp=b_cllist(bp)
    endloop
;endif
_bdv2=gb_ratio(_gindex)
if _bdv2<0
    command
        clump release id _aggid
        prop dens 0 color 0 range temclp
    endcommand
    if _bdv1>0
        _b=sqrt(3.0*_bdv1/(4.0*pi*_a))
        _c=_b
        command
            range name temclp fish agg_round
            prop dens _aggid color _gindex range temclp
        endcommand
        if _pfc_ver=4.0
            command
                clump add id _aggid range temclp                ;for
PFC3D v 4.0
                clump prop color _aggcolor range id _aggid      ;for
PFC3D v 4.0
            endcommand
        else
            command
                clump id _aggid range temclp                ;for PFC3D v 3.1
            endcommand
        endif
    endif
endif
command
    ;print _bdv1 _bdv2
    ;plot current 1
;movie          snap          1          file
C:\Users\yul\PhD_YuL_MTU\Saves\PFC3D\simulation_HMA\DEM_Model\Random_
Model\movie_3Dploygon_model.dcx

```

```

        endcommand
        oo = sread(sub_geo,1,1)
        isok= sub_geo(1)
    endloop
    command
        group minerals range color 1 grad_num
        group mastics range color 0
        range name agg-balls group minerals
        range name mastic-balls group mastics
    endcommand
    loop i (1,grad_num)
        _goupnam='minerals_'+string(int(i))
        command
            group _goupnam owner minerals range color i
        endcommand
    endloop
    oo=sclose(1)

    md_ac=0
    t_vol=0
    bp=ball_head
    loop while bp # null
        t_vol=t_vol+(4/3.0)*pi*b_rad(bp)^3
        if b_color(bp)=0
            b_extra(bp,1)=2
            md_ac=md_ac+(4/3.0)*pi*b_rad(bp)^3
        else
            b_extra(bp,1)=1
        endif
        b_extra(bp,3)=b_dens(bp)
        bp=b_next(bp)
    endloop
    md_ac=md_ac/t_vol
    loop _i (1, grad_num)
        gb_ratio(_i)=gb_ratio(_i)/mv_bvol
    endloop
end

```

## Computer Program 4: Viscoelastic DE Modeling of Dynamic /Creep Tests

This program was initially developed by Yu Liu in 2008 at Michigan Technological University for simulating dynamic/creep behaviors of AC materials. Thereafter, the program was modified by Yu Liu several times and last modified by Yu Liu in March 2011 at Michigan Technological University. The main program includes three files as shown below.

### Archived files for dynamic/creep simulation

File Names	Notes
Dynamic_Test.DVR	Main program for dynamic/creep simulation
Dynamic_Test.FIS	Called by Dynamic_Test.DVR
Dynamic_Burger_Set.DVR	Called by Dynamic_Test.DVR to provide inputs for performing the DE simulation.

There are different approaches to input viscoelastic parameters. For instance, users may consider using frequency-temperature superposition, time-temperature superposition, and other techniques.

### File 1: Dynamic Test.DVR

```
new
restore D:\SavesPFC\DEM_Models\3D_UD2\Voidmodel-spc.sav
SET echo off ; load support functions
  call DYNAMIC_TEST.FIS
  call DYNAMIC_Burgers_SET.DVR ;inputs of physical and mechanical parameters
SET echo off
config cppudm
model load udm_burger_32.dll
prop dens 2600
set bur_E1=@B_E1, bur_Y1=@B_Y1, bur_E2=@B_E2, bur_Y2=@B_Y2
fix x range brg_Bbdy
fix y range brg_Bbdy
fix z range brg_Bbdy
fix xspin range brg_Bbdy
fix yspin range brg_Bbdy
fix zspin range brg_Bbdy
prop xvcl 0 yvel 0 zvel 0 xspin 0 yspin 0 zspin 0
df_cmodel
```



```

;Apply dynamic loading
set pre_stress=2e4 del_stress=3.46e5 ;set applied stresses
set pre_time=0.00 loading_time=30 ;set computational time
set loading_freq=@loadfreq ;set loading frequency
set fishcall 0 dynamic_loading ;apply dynamic stress
set fishcall 0 get_ystrain ;calculate strain
set fishcall 8 catch_contact_model ;update contact model for PFC3D 4.0
;set fishcall 6 catch_contact_model ;update contact model for PFC3D 3.1

;Histories
hist reset
history nstep=100
reset_para
meas_circles
hist id 1 @cir_ystress
hist id 2 @cir_ystrain
hist id 3 @_dtime

;Plot graphs
plot create view_hist
plot set caption on
plot set background white
plot add hist -1 vs 3 skip 1 position 0.0 0.00 1.0 0.5 xlabel 'time(s)' ylab 'y_stress(Pa)
plot add hist -2 vs 3 skip 1 position 0.0 0.5 1.0 1.0 xlabel 'time(s)' ylab 'y_strain(N/A)
plot create view_velocity
plot set center (-0.05,0.03,0)
plot set rotation (110,30,0)
plot set title text 'view_velocity'
plot set background white
plot add velocity range brg_AGG
plot add fish smp_outline green
plot add hist -1 vs 3 skip 1 position 0.0 0.00 0.5 0.5 xlabel 'time(s)' ylab 'y_stress(Pa)
plot add hist -2 vs 3 skip 1 position 0.0 0.5 0.5 1.0 xlabel 'time(s)' ylab 'y_strain(N/A)
plot create view_displacement
plot set center (-0.05,0.03,0)
plot set rotation (110,30,0)
plot set title text 'view_displacement'
plot set background white
plot add displacement range brg_AGG
plot add fish smp_outline green
plot add hist -1 vs 3 skip 1 position 0.0 0.00 0.5 0.5 xlabel 'time(s)' ylab 'y_stress(Pa)
plot add hist -2 vs 3 skip 1 position 0.0 0.5 0.5 1.0 xlabel 'time(s)' ylab 'y_strain(N/A)

Plot create view_cforce
plot set center (-0.05,0.03,0)

```

```

plot set rotation (110,30,0)
plot set title text 'view_cforce btn agg and asphalt'
plot set background white
plot add cforce range rgc_aggasp
plot add hist -1 vs 3 skip 1 position 0.0 0.00 0.5 0.5 xlabel 'time(s)' ylab 'y_stress(Pa)'
plot add hist -2 vs 3 skip 1 position 0.0 0.5 0.5 1.0 xlabel 'time(s)' ylab 'y_strain(N/A)'
plot add fish smp_outline green

```

```

Plot create view_model2
plot set center (-0.05,0.03,0)
plot set rotation (110,30,0)
plot set title text 'view_model'
plot set background white
plot add ball white green red red
plot add hist -1 vs 3 skip 1 position 0.0 0.00 0.5 0.5 xlabel 'time(s)' ylab 'y_stress(Pa)'
plot add hist -2 vs 3 skip 1 position 0.0 0.5 0.5 1.0 xlabel 'time(s)' ylab 'y_strain(N/A)'

```

```

; Open and record AVI files
set plot avi size 1024 768
movie avi_open file D:\SavesPFC\DEM_APPS\3D_1\view_model.avi
movie avi_open file D:\SavesPFC\DEM_APPS\3D_1\view_his.avi
movie avi_open file D:\SavesPFC\DEM_APPS\3D_1\view_vel.avi
movie avi_open file D:\SavesPFC\DEM_APPS\3D_1\view_dis.avi
movie avi_open file D:\SavesPFC\DEM_APPS\3D_1\view_force.avi

movie step 1000 6 file D:\SavesPFC\DEM_APPS\3D_1\view_model.avi
movie step 1000 1 file D:\SavesPFC\DEM_APPS\3D_1\view_his.avi
movie step 1000 3 file D:\SavesPFC\DEM_APPS\3D_1\view_vel.avi
movie step 1000 4 file D:\SavesPFC\DEM_APPS\3D_1\view_dis.avi
movie step 1000 5 file D:\SavesPFC\DEM_APPS\3D_1\view_force.avi

```

```

;Activate dynamic modulus test simulation
SET md_run_name = 'D:\SavesPFC\DEM_APPS\3D_1\RESULTS'
set dt auto
dynamic_test

```

```

;close the AVI files
;NOTE: if the program is manually closed, please manually call the function below:
clos_AVIs

```

## **File 2: Dynamic Burger Set.DVR**

```

;parameters to define c_bond model for load platens
set p_Ec=99e9 ;-- contact modulus for load platens
;parameters to define contact between mineral fine balls
set f_Ec=56e9 ;-- contact modulus for mineral fine balls

```

```

set f_ksoverkn=1.0 ;--ratio of ks to kn
set f_fric=0.5
;parameters to define burgers models FHWA 19
set bur_fric=0.3
set bur_ksoverkn=1.0 ;bur_scale=1.0
set le_nbond=1e12
set le_sbond=1e12
set bur_nbond=1e12
set bur_sbond=1e12
; MTU Submix 5 AC=3.5%
def in_def
    xx=in(msg+'('+default:'+string(default)+'):')
    if type(xx)=3
        in_def=default
    else
        in_def=xx
    endif
end

def Bur_properties
    B_E1=121
    B_Y1=121
    B_E2=121
    B_Y2=121
    default=1.60
    msg='Input length of the equivalent beam (mm):Ebeam_len='
    Ebeam_len=in_def/1000.0

    default=1000
    msg='Input multiple coefficient: mult-coef='
    mult_coef=in_def
    default=25
    msg='Input laboratory test frequency: real_freq='
    real_freq=in_def
    loadfreq=real_freq*mult_coef

    _strs_scale=1
    if loadfreq>20000 then
        _strs_scale=5.6
    else
        if loadfreq>10000 then
            _strs_scale=3.6
        else
            if loadfreq>5000 then
                _strs_scale=1.6
            end
        end
    end
end

```

```

endif
endif
endif
;      21      C      100      -      200
if real_freq= 1      then
    B_E1=6.839732127e+9
    B_Y1=5.646486175e+9/mult_coef
    B_E2=2.239382927e+9
    B_Y2=0.269417135e+9/mult_coef
endif
if real_freq= 5      then
    B_E1=16.26688084e+9
    B_Y1=3.062743882e+9/mult_coef
    B_E2=3.400587209e+9
    B_Y2=0.065500401e+9/mult_coef
endif
if real_freq= 10     then
    B_E1=25.50727712e+9
    B_Y1=3.596282267e+9/mult_coef
    B_E2=3.771080866e+9
    B_Y2=0.033948182e+9/mult_coef
endif
if real_freq= 25     then
    B_E1=4.6e+9
    B_Y1=3.8e+9/mult_coef
    B_E2=34.73e+9
    B_Y2=1.0e+9/mult_coef
endif

_w=2*pi*loadfreq
_Jstar=sqrt(1/B_E1^2+1/(B_Y1*_w)^2+(1+2*(B_E2/B_E1+B_Y2/B_Y1))/(B_E2^2+(B_Y2*_w)^2))
Estar=1/_Jstar
_dstress=60e-6*Estar*_strs_scale
end
Bur_properties

```

### **File 3: Dynamic Test.FIS**

```

def _arrays
    Array et2_stress(2,2); yul_2DStrainTensor(2,2) yul_2DSTensor(2,2)
    Array A(2,2),et2_strainrate(2,2),B(2,2)
    bur_ksoverkn=0
    Array vpt1(dim)vpt2(dim)
end
_arrays

```

```

;INPUTs:
      ;udm_burger's Model Parameters: bur_E1, bur_Y1, bur_E2,
bur_Y2,@bur_nbond,@bur_sbond,@bur_fric
      ;Other Mechanical Parameters:f_Ec,p_Ec,f_fric,f_ksoverkn
      ;b_exatra(bp, 1)---1: aggregates, 2:asphalt,3:top_bdy, 4:bot_bdy
      ;Ebeam_len--distance between two adjacent elements

```

```

def df_cmodel
cp=contact_head
loop while cp # null
  _bp1=c_ball1(cp)
  _bp2=c_ball2(cp)
  ; if the first entity is asp
  if c_extra(cp,1)=4 ;asp-asp
      c_model(cp) = 'udm_burger'
      c_prop(cp,'bur_knk')=@bur_E2*Ebeam_len
      c_prop(cp,'bur_cnk')=@bur_Y2*Ebeam_len
      c_prop(cp,'bur_knm')=@bur_E1*Ebeam_len
      c_prop(cp,'bur_cnm')=@bur_Y1*Ebeam_len
      c_prop(cp,'bur_ksk')=@bur_E2*Ebeam_len*bur_ksoverkn
      c_prop(cp,'bur_csk')=@bur_Y2*Ebeam_len*bur_ksoverkn
      c_prop(cp,'bur_ksm')=@bur_E1*Ebeam_len*bur_ksoverkn
      c_prop(cp,'bur_csm')=@bur_Y1*Ebeam_len*bur_ksoverkn
      c_prop(cp,'bur_fric')=@bur_fric
      c_prop(cp,'bur_notension')=0.0
      c_nstrength(cp)=bur_nbond
      c_sstrength(cp)=bur_sbond
  endif
  if c_extra(cp,1)=3 ;agg-asp
      cvt_E1=2.0*(bur_E1*f_Ec)/(bur_E1+f_Ec)
      c_model(cp) = 'udm_burger'
      c_prop(cp,'bur_knk')=@bur_E2*Ebeam_len
      c_prop(cp,'bur_cnk')=@bur_Y2*Ebeam_len
      c_prop(cp,'bur_knm')=@cvt_E1*Ebeam_len
      c_prop(cp,'bur_cnm')=@bur_Y1*Ebeam_len
      c_prop(cp,'bur_ksk')=@bur_E2*Ebeam_len*bur_ksoverkn
      c_prop(cp,'bur_csk')=@bur_Y2*Ebeam_len*bur_ksoverkn
      c_prop(cp,'bur_ksm')=@cvt_E1*Ebeam_len*bur_ksoverkn
      c_prop(cp,'bur_csm')=@bur_Y1*Ebeam_len*bur_ksoverkn
      c_prop(cp,'bur_fric')=@bur_fric
      c_prop(cp,'bur_notension')=0.0
      c_nstrength(cp)=bur_nbond
      c_sstrength(cp)=bur_sbond
  endif
  if c_extra(cp,1)=5 ;smp-tbdy

```

```

        b_kn(_bp1)=2.0*p_Ec*Ebeam_len
        b_kn(_bp2)=2.0*p_Ec*Ebeam_len
        b_ks(_bp1)=f_ksoverkn*b_kn(_bp1)
        b_ks(_bp2)=f_ksoverkn*b_kn(_bp2)
            b_fric(_bp1)=f_fric
        b_fric(_bp2)=f_fric
        c_nstrength(cp)=le_nbond
        c_sstrength(cp)=le_sbond
    endif
    if c_extra(cp,1)=6 ;smp_bbdy
        b_kn(_bp1)=2.0*p_Ec*Ebeam_len
        b_kn(_bp2)=2.0*p_Ec*Ebeam_len
        b_ks(_bp1)=f_ksoverkn*b_kn(_bp1)
        b_ks(_bp2)=f_ksoverkn*b_kn(_bp2)
            b_fric(_bp1)=f_fric
        b_fric(_bp2)=f_fric
        c_nstrength(cp)=le_nbond
        c_sstrength(cp)=le_sbond

    endif
    ; if the first entity is agg
    if c_extra(cp,1)=2 ;agg-agg
        b_kn(_bp1)=2.0*f_Ec*Ebeam_len
        b_kn(_bp2)=2.0*f_Ec*Ebeam_len
        b_ks(_bp1)=f_ksoverkn*b_kn(_bp1)
        b_ks(_bp2)=f_ksoverkn*b_kn(_bp2)
            b_fric(_bp1)=f_fric
        b_fric(_bp2)=f_fric
        c_nstrength(cp)=0
        c_sstrength(cp)=0

    endif
    if c_extra(cp,1)=1 ;agg-in
        b_kn(_bp1)=2.0*f_Ec*Ebeam_len
        b_kn(_bp2)=2.0*f_Ec*Ebeam_len
        b_ks(_bp1)=f_ksoverkn*b_kn(_bp1)
        b_ks(_bp2)=f_ksoverkn*b_kn(_bp2)
            b_fric(_bp1)=f_fric
        b_fric(_bp2)=f_fric
        c_nstrength(cp)=le_nbond
        c_sstrength(cp)=le_sbond

    endif
    cp=c_next(cp)
endloop
end

```

```

;fishcall function to define contact parameters dynamically
;INPUTs:
      ;Burger's Model Parameters: bur_E1, bur_Y1, bur_E2,
bur_Y2,@bur_nbond,@bur_sbond,@bur_fric
      ;Other Mechanical Parameters:f_Ec,p_Ec,f_fric,f_ksoverkn
      ;b_exatra(bp, 1)---1: aggregates, 2:asphalt,3:top_bdy, 4:bot_bdy
      ;Ebeam_len

```

```

def catch_contact_model
  df_cextra
  br_n=br_n+1
  cp = fc_arg(0);
  bp1=c_ball1(cp)
  if pointer_type(c_ball2(cp))=100 then
    bp2=c_ball2(cp)
      ; if the first entity is asp
    if b_extra(bp1,1)=2 then
      if b_extra(bp2,1)=2
        c_model(cp) = 'udm_burger'
        c_prop(cp,'bur_knk')=@bur_E2*Ebeam_len
        c_prop(cp,'bur_cnk')=@bur_Y2*Ebeam_len
        c_prop(cp,'bur_knm')=@bur_E1*Ebeam_len
        c_prop(cp,'bur_cnm')=@bur_Y1*Ebeam_len
        c_prop(cp,'bur_ksk')=@bur_E2*Ebeam_len*bur_ksoverkn
        c_prop(cp,'bur_csk')=@bur_Y2*Ebeam_len*bur_ksoverkn
        c_prop(cp,'bur_ksm')=@bur_E1*Ebeam_len*bur_ksoverkn
        c_prop(cp,'bur_csm')=@bur_Y1*Ebeam_len*bur_ksoverkn
        c_prop(cp,'bur_fric')=@bur_fric
          c_prop(cp,'bur_notension')=0.0
          c_nstrength(cp)=bur_nbond
          c_sstrength(cp)=bur_sbond
        endif
      if b_extra(bp2,1)=1
        cvt_E1=2.0*(bur_E1*f_Ec)/(bur_E1+f_Ec)
        c_model(cp) = 'udm_burger'
        c_prop(cp,'bur_knk')=@bur_E2*Ebeam_len
        c_prop(cp,'bur_cnk')=@bur_Y2*Ebeam_len
        c_prop(cp,'bur_knm')=@cvt_E1*Ebeam_len
        c_prop(cp,'bur_cnm')=@bur_Y1*Ebeam_len
        c_prop(cp,'bur_ksk')=@bur_E2*Ebeam_len*bur_ksoverkn
        c_prop(cp,'bur_csk')=@bur_Y2*Ebeam_len*bur_ksoverkn
        c_prop(cp,'bur_ksm')=@cvt_E1*Ebeam_len*bur_ksoverkn
        c_prop(cp,'bur_csm')=@bur_Y1*Ebeam_len*bur_ksoverkn
        c_prop(cp,'bur_fric')=@bur_fric

```

```

        c_prop(cp,'bur_notension')=0.0
        c_nstrength(cp)=bur_nbond
        c_sstrength(cp)=bur_sbond
    endif
    if b_extra(bp2,1)=3
        b_kn(bp1)=2.0*p_Ec*Ebeam_len
        b_kn(bp2)=2.0*p_Ec*Ebeam_len
        b_ks(bp1)=f_ksoverkn*b_kn(bp1)
        b_ks(bp2)=f_ksoverkn*b_kn(bp2)
        b_fric(bp1)=f_fric
        b_fric(bp2)=f_fric
        c_nstrength(cp)=le_nbond
        c_sstrength(cp)=le_sbond
    endif
    if b_extra(bp2,1)=4
        b_kn(bp1)=2.0*p_Ec*Ebeam_len
        b_kn(bp2)=2.0*p_Ec*Ebeam_len
        b_ks(bp1)=f_ksoverkn*b_kn(bp1)
        b_ks(bp2)=f_ksoverkn*b_kn(bp2)
        b_fric(bp1)=f_fric
        b_fric(bp2)=f_fric
        c_nstrength(cp)=le_nbond
        c_sstrength(cp)=le_sbond
    endif
endif
; if the first entity is agg
if b_extra(bp1,1)=1 then
    if b_extra(bp2,1)=1 then
        b_kn(bp1)=2.0*f_Ec*Ebeam_len
        b_kn(bp2)=2.0*f_Ec*Ebeam_len
        b_ks(bp1)=f_ksoverkn*b_kn(bp1)
        b_ks(bp2)=f_ksoverkn*b_kn(bp2)
        b_fric(bp1)=f_fric
        b_fric(bp2)=f_fric
        if b_extra(bp2,2)=b_extra(bp1,2)
            c_nstrength(cp)=le_nbond
            c_sstrength(cp)=le_sbond
        endif
    endif
endif
if b_extra(bp2,1)=3 then
    b_kn(bp1)=2.0*p_Ec*Ebeam_len
    b_kn(bp2)=2.0*p_Ec*Ebeam_len
    b_ks(bp1)=f_ksoverkn*b_kn(bp1)
    b_ks(bp2)=f_ksoverkn*b_kn(bp2)
    b_fric(bp1)=f_fric

```



```

        b_fric(bp2)=f_fric
        c_nstrength(cp)=le_nbond
        c_sstrength(cp)=le_sbond
    endif
    if b_extra(bp2,1)=4 then
        b_kn(bp1)=2.0*p_Ec*Ebeam_len
        b_kn(bp2)=2.0*p_Ec*Ebeam_len
        b_ks(bp1)=f_ksoverkn*b_kn(bp1)
        b_ks(bp2)=f_ksoverkn*b_kn(bp2)
        b_fric(bp1)=f_fric
        b_fric(bp2)=f_fric
        c_nstrength(cp)=le_nbond
        c_sstrength(cp)=le_sbond
    endif
if b_extra(bp2,1)=2
                                cvt_E1=2.0*(bur_E1*f_Ec)/(bur_E1+f_Ec)
                                c_model(cp) = 'udm_burger'
c_prop(cp,'bur_knk')=@bur_E2*Ebeam_len
c_prop(cp,'bur_cnk')=@bur_Y2*Ebeam_len
c_prop(cp,'bur_knm')=@cvt_E1*Ebeam_len
c_prop(cp,'bur_cnm')=@bur_Y1*Ebeam_len
c_prop(cp,'bur_ksk')=@bur_E2*Ebeam_len*bur_ksoverkn
c_prop(cp,'bur_csk')=@bur_Y2*Ebeam_len*bur_ksoverkn
c_prop(cp,'bur_ksm')=@cvt_E1*Ebeam_len*bur_ksoverkn
c_prop(cp,'bur_csm')=@bur_Y1*Ebeam_len*bur_ksoverkn
c_prop(cp,'bur_fric')=@bur_fric
                                c_prop(cp,'bur_notension')=0.0
                                c_nstrength(cp)=bur_nbond
                                c_sstrength(cp)=bur_sbond
        endif
    endif
; if the first entity is top_bdy
if b_extra(bp1,1)=3 then
        b_kn(bp1)=2.0*p_Ec*Ebeam_len
        b_kn(bp2)=2.0*p_Ec*Ebeam_len
        b_ks(bp1)=f_ksoverkn*b_kn(bp1)
        b_ks(bp2)=f_ksoverkn*b_kn(bp2)
        b_fric(bp1)=f_fric
        b_fric(bp2)=f_fric
        c_nstrength(cp)=le_nbond
        c_sstrength(cp)=le_sbond
    endif
; if the first entity is bot_bdy
if b_extra(bp1,1)=4 then
        b_kn(bp1)=2.0*p_Ec*Ebeam_len

```

```

        b_kn(bp2)=2.0*p_Ec*Ebeam_len
        b_ks(bp1)=f_ksoverkn*b_kn(bp1)
        b_ks(bp2)=f_ksoverkn*b_kn(bp2)
            b_fric(bp1)=f_fric
        b_fric(bp2)=f_fric
        c_nstrength(cp)=le_nbond
        c_sstrength(cp)=le_sbond
    endif
endif
end

;INPUTs:
;xr, xl--coordinate of x in left and right points
;pre_stress--
;del_stress--equal to (peak stress-pre-stress)
;top_bnum--total amount of the balls in bdy_top
;pre_time--amount of time to pre-compress the digital sample

; NOTES:
def dynamic_loading

    pre_F=pre_stress*pi*mv_Rc^2
    pre_apf=pre_F/top_bnum
    del_F=del_stress*pi*mv_Rc^2
    del_apf=del_F/top_bnum
    if _dtime<pre_time then
        bal_apf=pre_apf
    else
        bal_apf=pre_apf+del_apf*(1+sin(2*pi*loading_freq*(time-ini_time)-1.5708))
    endif
    bp=ball_head
    loop while bp # null
        if b_extra(bp,1)=3 then
            b_yfap(bp)=-bal_apf
        endif
        bp=b_next(bp)
    endloop
end

; dynamic_test
;INPUTs:
;pre_time
;loading_time

def dynamic_test
    fname_out=in('Input <output file name>: fname_out=')
    fname_out=fname_out+'_dyn.out'

```

```

oo=out('pre_compressing test')
loop while _dtime<pre_time
  command
    cyc 1000
    hist write 1 2 vs 3 skip 10 file fname_out
  endcommand
endloop
md_tag_name = '-precompress'
md_save_state
oo=out('unloading test next')
oo=out('To continue dynamic loading test,please input [continue]!')
ini_time=time
_tt=pre_time+loading_time/5.0
loop while _dtime<_tt
  command
    cyc 1000
    hist write 1 2 vs 3 skip 10 file fname_out
    del_outbal
  endcommand
endloop
md_tag_name = '-loading1'
md_save_state
_tt=pre_time+2.0*loading_time/5.0
loop while _dtime<_tt
  command
    cyc 1000
    hist write 1 2 vs 3 skip 10 file fname_out
    del_outbal
  endcommand
endloop
md_tag_name = '-loading2'
md_save_state
_tt=pre_time+3.0*loading_time/5.0
loop while _dtime<_tt
  command
    cyc 1000
    hist write 1 2 vs 3 skip 10 file fname_out
    del_outbal
  endcommand
endloop
md_tag_name = '-loading3'
md_save_state
_tt=pre_time+4.0*loading_time/5.0
loop while _dtime<_tt
  command

```

```

        cyc 1000
        hist write 1 2 vs 3 skip 10 file fname_out
        del_outbal
    endcommand
endloop
md_tag_name = '-loading4'
md_save_state
_tt=pre_time+loading_time
loop while _dtime<_tt
    command
        cyc 1000
        hist write 1 2 vs 3 skip 10 file fname_out
        del_outbal
    endcommand
endloop
md_tag_name = '-loading5'
md_save_state
end

def reset_para
    @_theta=0.0
    @_time0=time
    @_step0=step
end

def _dtime
    _dtime=time-@_time0
end

def meas_circles
    meas_R=0.9*@mv_Rc;
    meas_yc=mv_top1-meas_R;
    command
        measure id 1 x 0 y @meas_yc z 0 radius @meas_R
    endcommand
    meas_yc=mv_bot2+meas_R;
    command
        measure id 2 x 0 y @meas_yc z 0 radius @meas_R
    endcommand
    meas_yc=(mv_top1+mv_bot2)/2;
    command
        measure id 3 x 0 y @meas_yc z 0 radius @meas_R
    endcommand
    madd1=find_meas(1)
    madd2=find_meas(2)

```

```

madd3=find_meas(3)
end

def cir_ystress
  oo=measure(madd1,1);
  oo=measure(madd2,1);
  oo=measure(madd3,1);
  cir_ystress=(m_s22(madd1)+m_s22(madd2)+m_s22(madd3))/3.0;
end
def get_ystrain
  oo=measure(madd1,2);
  oo=measure(madd2,2);
  oo=measure(madd3,2);
  cir_ystrain=cir_ystrain+tdel*(m_ed22(madd1)+m_ed22(madd2)+m_ed22(madd3)
)/3.0;
end

def del_outbal
  command
    delete ball range cylinder end1 (0,@mv_bot1,0) end2 (0,@mv_top2, 0)
rad @mv_RC not
  endcommand
end

def smp_outline
  plot_item
  _a=1.01*@mv_Rc
  _b=1.01*@mv_Rc
  theta=0
  vpt1(2)=@mv_top2
  vpt2(2)=@mv_bot1
  stat = set_line_width(0) ; thickest line
  loop while theta # 360
    vpt1(1)=_a*cos(pi*theta/180.0)
    vpt1(3)=_b*sin(pi*theta/180.0)
    vpt2(1)=_a*cos(pi*theta/180.0)
    vpt2(3)=_b*sin(pi*theta/180.0)
    if theta>180 then
      stat=set_dash_pattern(4)
    else
      stat=set_dash_pattern(0)
    endif
    if theta=180
      stat=set_dash_pattern(0)
    endif
  endif
end

```

```

        stat = move_to(vpt1)
        theta=theta+30
        vpt1(1)=_a*cos(pi*theta/180.0)
        vpt1(3)=_b*sin(pi*theta/180.0)
        vpt2(1)=_a*cos(pi*theta/180.0)
        vpt2(3)=_b*sin(pi*theta/180.0)
        stat = line_to(vpt1)
        stat = draw_line(vpt1,vpt2)
    endloop

    theta=0
    vpt1(1)=_a*cos(pi*theta/180.0)
    vpt1(3)=_b*sin(pi*theta/180.0)
    loop while theta # 360
        if theta>180 then
            stat=set_dash_pattern(4)
        else
            stat=set_dash_pattern(0)
        endif
        if theta=180
            stat=set_dash_pattern(0)
        endif
        vpt2(1)=_a*cos(pi*theta/180.0)
        vpt2(3)=_b*sin(pi*theta/180.0)
        stat = move_to(vpt2)
        theta=theta+30
        vpt2(1)=_a*cos(pi*theta/180.0)
        vpt2(3)=_b*sin(pi*theta/180.0)
        stat = line_to(vpt2)
    endloop
    theta=0
    vpt1(1)=_a*cos(pi*theta/180.0)
    vpt1(3)=_b*sin(pi*theta/180.0)
    vpt1(1)=0
    vpt1(3)=0
    ;stat=draw_circle(vpt1,@mv_Rc)
    vpt2(1)=0
    vpt2(3)=0
    ;stat=draw_circle(vpt2,@mv_Rc)
end

def clos_AVIs
    command
        movie avi_close file D:\SavesPFC\DEM_APPS\3D_1\view_model.avi
        movie avi_close file D:\SavesPFC\DEM_APPS\3D_1\view_his.avi










```

```
        movie avi_close file D:\SavesPFC\DEM_APPS\3D_1\view_vel.avi
        movie avi_close file D:\SavesPFC\DEM_APPS\3D_1\view_dis.avi
        movie avi_close file D:\SavesPFC\DEM_APPS\3D_1\view_force.avi
    endcommand
end
def in_def
    xx=in(msg+'('+default:'+string(default)+'):')
    if type(xx)=3
        in_def=default
    else
        in_def=xx
    endif
end
```

## Yu Liu's Vita

Yu Liu earned his B.S. in Structural Engineering and M.S. in Geotechnical Engineering at Henan University of Technology in 2002 and 2005, respectively. He worked at Henan Transportation Research Institute in China from May 2005 to May 2007 as a Civil Engineer. In May 2007, he came to the United States for his Ph.D. study in Civil Engineering at Michigan Technological University. He successfully defended his dissertation in May 2011 and his Ph.D. is to be awarded in September 2011. His doctoral research seeks computer modeling approaches for predicting and interpreting asphalt concrete materials. Due to his outstanding performance in his doctoral research program, he was awarded the Graduate Research Excellence Award, the Dean's Award for Outstanding Scholarship, and the Doctoral Finishing Fellowship in from 2010 to 2011 at Michigan Technological University.

His research interests are as follows: 1) Civil Engineering materials which may include Concrete, Asphalt, Granular base materials; 2) numerical methods which may include discrete element methods (DEM), finite element methods (FEM); 3) micromechanics which may include law of mix, composite mechanics, microstructure-based mechanics of random composites; 4) pavement material design which may include tests and data analysis of asphalt binder, aggregates, and mixtures; 5) soil mechanics/soil-structure interaction; 6) viscoelastic mechanics: Burger's model, Generalized Maxwell Model, General Kelvin Model; 7) application of computer modeling in education; 8) DEM-based virtual lab of random composites: Followed are movies to demonstrate his research interests (Please Connect to Internet to watch the movies):

- Microstructures of Asphalt Concrete:
  -  Computer-generated 3D model: [Link to Movie Here](#)
  -  Computer-generated 2D model: [Link to Movie Here](#)
- Dynamic Modulus Tests with FTS:
  -  Stress and Strain [Link to Movie1 Here](#) (alpha=1000), [Link to Movie2 Here](#) (alpha=100),
  -  Contact force between aggregates and asphalt mastic: [Link to Movie3 Here](#) (2D) [Link to Movie4 Here](#) (3D)
  -  Velocity of elements: [Link to Movie5 Here](#) (2D)
  -  Dynamic Modulus Tests without FTS: [Link to Movie Here](#)
- Creep Compliance Tests under Constant Loading:
  -  Stress and Strain: [Link to Movie1 Here](#)
  -  Contact force between aggregates and mastic: [Link to Movie3 Here](#) (3D)
  -  Velocity: [Link to Movie3 Here](#) (2D)
- Simulation of Pavement-vehicle Interaction [Link to Movie Here](#)
- Simulation of Rutting [Link to Movie1](#) (moving load), [Link to Movie2 Here](#) (constant load)
- Simulation of Beam-cracking [Link to Movie1 Here](#) (offset=0.5), [Link to Movie2 Here](#) (offset=0.7)



Yu Liu's Research was funded by National Natural Science Foundation of China (NSFC), U.S. National Science Foundation (NSF), and Federal Highway Administration (FHWA). His research work has been published in journals and conferences:

- 1) Liu, Y., You, Z., and Dai, Q.L. "Review of Advances in Understanding Impacts of Mix Composition Characteristics on Asphalt Concrete (AC) Mechanics" *Intl. J of Pavement Eng.* First published on: 13 June 2011(iFirst), Final published on Vol 12, No. 4 (2011)
- 2) Liu, Y., and You, Z. (2010) "Discrete Element Modeling Impacts of Aggregate Sphericity, Orientation, and Angularity on Creep Stiffness of Idealized Asphalt Mixtures" *J of Eng. Mechanics*. Posted ahead of print Oct. 27, 2010.
- 3) Liu, Y., and You, Z. "Accelerated Discrete Element Modeling of Asphalt Based Materials with the Frequency-temperature Superposition Principle." *J of Eng. Mechanics*. Posted ahead of print, 2010.
- 4) You, Z, Liu, Y., and Qingli, D. (2011). "Three-dimensional Micro structural-based Discrete Element Viscoelastic Modeling of Creep Compliance Tests for Asphalt Mixtures." *J. of Materials in Civil Eng.* 23(1), PP. 79-87
- 5) You, Z. and Liu, Y. (2010). Three-dimensional Discrete Element Simulation of Asphalt Concrete Subjected to Haversine Loading: An Application of Frequency-temperature Superposition Technique, *Intl. J. of Road Materials and Pavement Design*, 11( 2), pp. 273-290.
- 6) Liu, Y., You, Z., Goh, S., and Mills-Beale, J. (2010). "A Post-Processing Method for Dynamic Modulus Tests of Hot Mix Asphalt." *J. of Materials in Civil Eng.* 22(7), pp. 658-666.
- 7) Liu, Y., and You, Z. (2009). "Visualization and Simulation of Asphalt Concrete: a Randomly Generated 3D Model " *J of Computing in Civil Eng.* 23 (6), pp. 340-347.
- 8) Liu, Y., Dai, Q., and You, Z. (2009). "Viscoelastic Model for Discrete Element Simulation of Asphalt Mixtures." *J of Eng. Mechanics*, 135(4), 324-333.
- 9) Feng, S., Hu, X., and Liu, Y. (2008). "Numerical Analysis of Asphalt Mastics Based on Burger's Model with Discrete Element Method." *J of Pavement Base Eng.* (1).
- 10) Feng, S., Hu, X., and Liu, Y. (2008). "Numerical Analysis of Viscoelastic Materials Based on Discrete Element Method." *J.of Highway and Transportation Research and Development* 29(2), PP. 12-15.
- 11) Liu, Y., Feng, S., and Hu, X. (2007). "Discrete Element Simulation of Asphalt Mastics Based on Burgers Model." *J of Southwest Jiaotong University*, 15(1), pp.20-26.
- 12) Tian, L., Hu, X., and Liu, Y. (2007). "1134H1134HSectioned linear fitting method of parameters for asphalt mastics viscoelastic Burgers model (in Chinese)." *J of Traffic and Transportation Eng.*, 7(3), pp. 66-69.
- 13) Tian, L., Liu, Y., Hu, X., and Wang, B. (2007). "Random Generation Algorithm for Simulation of Polyhedral Particles in Asphalt Mixture Aggregate and Its Program (in Chinese)." *China J. of Highway and Transport* 20(3), pp. 5-10.
- 14) Tian, L., Liu, Y., and Wang, B. (2007). "3D DEM model and digital restructure technique for asphalt mixture simulation (in Chinese)." *J of Chang'an University (Natural Science Edition)*, 27(4), pp. 23-27.

- 15) Xiao, Z., Hu, X., and Liu, Y. (2007). "Discrete Element Method Analysis for Micro Structure of Asphalt Mixtures (in Chinese)." *Highway* (4), PP. 145-148.
- 16) Liu, Y., and You, Z. "Stiffness of Sand Mastic versus Stiffness of Asphalt Binder Using Three-dimensional Discrete Element Method" *ASCE The Engineering Mechanics Special Publication (EMSP)*, pp.54-65
- 17) Liu, Y., and You, Z. "Discrete Element Simulation of Aggregate Sphericity, Orientation, and Angularity: Improving Fundamental Understanding of Asphalt Concrete" *the 10th International Chinese Conference of Transportation Professionals (ICCTP 2010)*, August 4-8, 2010, Beijing, pp. 3968-3976.
- 18) Liu, Y. and Z. You (2010). "Formulization of Asphalt Concrete Stiffness for Specific Microstructures Based on Discrete Element Method". *ASCE Geo-shanghai 2010 (GSP 203)*, Shanghai, pp.135-419.
- 19) Liu, Y., and You, Z. (2008). "Determining Burger's Model Parameters of Asphalt Materials using Creep-recovery Data." *ASCE Geotechnical Special Publication Pavement Mechanics and Paving Materials*. PP. 26-36.
- 20) Liu, Y., and You, Z. (2008). "Simulation of Cyclic Loading Tests for Asphalt Mixtures using User Defined Models within Discrete Element Method." *ASCE GeoCongress 2008*, PP. 742-749.
- 21) Liu, Y., You, Z., and Adhikari, S. (2008b). "Speed up Discrete Element Simulation of Asphalt Mixtures with User-written C++ Codes." *ASCE Airfield and Highway Pavement Conference*, 64-72.
- 22) Adhikari, S., You, Z., Dai, Q., and Liu, Y. (2008). "Investigation of the Air Void Effect on the Asphalt Mixture using 2D and 3D DEM." *1<sup>st</sup> International FLAC/DEM Symposium on Numerical Modeling, Minneapolis, MN*, PP. 419-426.
- 23) Goh, S.W., Liu, Y., and You, Z. (2009). "Laboratory Evaluation of Warm Mix Asphalt Using Sasobit®", *The 8th International Conference on the Bearing Capacity of Roads, Railways, & Airfields*, pp.315-320
- 24) Hu, X., Feng, S., Liu, Y., And Tian, L.. "3-D Distinct Element Modeling for Viscoelastic Asphalt Mastics", *Transportation Research Board (in CD)*, Washington, DC, USA
- 25) Guan, J., Tian, L., and Liu, Y.. "Discrete Element Method and its Application in Asphalt Mixture". *in National Highway Technical Forum for Youths. 2005. Zhengzhou, Henan, in China.*
- 26) Hu, X., Liu, Y., and Tian, L.. "Discrete Element Simulation of Strength and Deformation of Graded Stone". *in National Highway Technical Forum for Youths. 2005. Zhengzhou, Henan,*